Arthritis & Rheumatology

An Official Journal of the American College of Rheumatology
www.arthritisrheum.org and wileyonlinelibrary.com

Cover design: Todd Machen

This journal is printed on acid-free paper.

Arthritis & Rheumatology

An Official Journal of the American College of Rheumatology
www.arthritisrheum.org and wileyonlinelibrary.com

VOLUME 73 • September 2021 • NO. 9

Systemic Sclerosis

Clinical Images

Gout

Letters

Cover image: The figure on the cover (from Fukuchi et al, pages 1683–1693) shows a confocal image of skin tissue from a patient with eosinophilic granulomatosis with polyangiitis. Immunofluorescence staining for eosinophil granule protein MBP (red), eosinophil cytoplasmic protein galectin-10 (green), and DNA (blue) indicated the presence of eosinophil ETosis–mediated eosinophil cytolysis.

In this Issue

Highlights from this issue of *A&R* | By Lara C. Pullen, PhD

Shared Immune Cell Signatures Can Be Used to Stratify Patients

Until now, patient stratification approaches in primary Sjögren's syndrome (SS) and systemic lupus erythematosus (SLE) have been primarily directed at cohorts of patients with the same diagnosis. p. 1626 In this issue, Martin-Gutierrez et al (p. 1626) describe an immune cell toolkit that may be useful in differentiating, with high accuracy, the immunologic profiles of patients with primary SS and patients with SLE. Such a toolkit could aid in achieving targeted therapeutic approaches.

The study included patients with well-controlled or mild-to-moderately active disease. As all the patients were women, the authors note that they were unable to evaluate the impact of high disease activity or severe flares on the identified immune signatures, and they were also unable to evaluate the influence of sex bias. Nevertheless, their analysis revealed 2 new disease endotypes, which were characterized by differential immune signatures that had a higher capacity for discriminating between patients than the immune signatures associated with the diagnostic label. The researchers report here, for the first time, that patients with primary SS and patients with SLE with low-to-moderate or no disease activity have very few significant differences in immunologic architecture.

The authors propose a new classification for patients with primary SS, those with SLE, and those with SLE/SS, and suggest that their findings may lead to a new stratification of patients with primary SS based on one of the 2 immune signatures derived from this analysis. The new findings also have implications for therapy, because, while several B cell–targeted biologic therapies have been separately investigated in patients with primary SS and patients with SLE, the only licensed anti–B cell biologic therapy for SLE (belimumab) is approved solely for patients with nonrenal SLE manifestations. These findings indicate that machine learning approaches can be used to select and validate patients for targeted therapeutic approaches including anti–B cell biologic therapy.

Association Between Gut Microbiota and Symptomatic Hand OA

Several studies have demonstrated that patients with inflammatory arthritis have a decreased relative abundance of the genus *Roseburia* in the gut microbiome. Moreover, researchers have proposed several biologic mechanisms linking the gut microbiome to systemic inflammation. For example, *Bilophila* member species have been shown to produce lipopolysaccharides that, in mouse models, promote intestinal barrier dysfunction, bile acid dysmetabolism, and inflammation. p. 1656

In this issue, Wei et al (p. 1656) describe results from their large, Chinese population-based study. The researchers' findings provide the first evidence that alterations in the composition of the gut microbiome among study participants with symptomatic hand osteoarthritis (OA) were associated with prevalent symptomatic hand OA. These alterations included, at the genus level, a low relative abundance of *Roseburia* combined with a high relative abundance of *Bilophila* and *Desulfovibrio*. The authors suggest that their population-based study should be generalizable to the entire Chinese population.

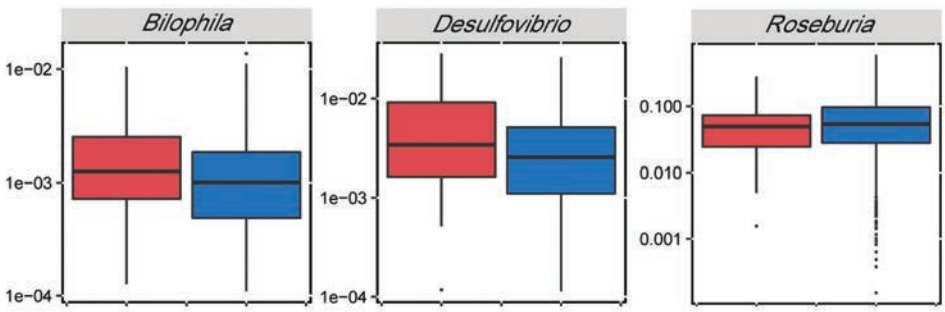

Figure 1. Differences in the composition of the gut microbiota at the genus level between individuals with symptomatic hand OA (n = 72) (red) and individuals without symptomatic hand OA (controls) (n = 1,316) (blue), after adjustments for age, sex, body mass index, alcohol consumption, and frequency of dietary intake of meat/eggs, dairy, and vegetables.

In their study, the investigators profiled the gut microbiomes using 16S rRNA gene sequencing. They acknowledge that, although this technology can identify microbial taxonomies and composition, it has only a limited ability to genetically identify specific species and strains. Nevertheless, the authors suggest that their findings may help other investigators understand the role of the microbiome in the development of symptomatic hand OA, as well as contribute to potential translational opportunities.

HCQ Not Associated with Significant Cardiovascular Risk

Rheumatologists prescribe hydroxychloroquine (HCQ) in recognition of its immunomodulatory, antiinflammatory, vasoprotective, and antithrombotic properties. Physicians have also prescribed HCQ with the intention of improving outcomes in patients with COVID-19. One (since retracted) study raised concerns, however, when it showed a higher risk of in-hospital mortality and ventricular arrhythmias in COVID-19 patients receiving HCQ. p. 1589 In this issue, Faselis et al (p. 1589) report that during the first year after the initiation of HCQ or another nonbiologic disease-modifying antirheumatic drug (DMARD), patients with rheumatoid arthritis (RA) have a low incidence of long QT syndrome and arrhythmia-related hospitalization. The investigators also found no evidence that HCQ was associated with a higher risk of adverse cardiovascular events or death.

The observational study measured 87 baseline characteristics for which treatment groups were balanced (HCQ group, n = 4,426; non-HCQ group, n = 4,426). Patients had a mean ± SD age of 64 ± 12 years; 14% were women and 28% were African American. The team documented 3 long QT syndrome events, 2 of which occurred in patients receiving HCQ. They also documented 56 arrhythmia-related hospitalizations, 30 of which occurred in the HCQ group. All-cause mortality was 144 in the patients in the HCQ group and 136 in the patients in the non-HCQ group. During the first 30 days of follow-up, the investigators identified 0 long QT syndrome events, 2 arrhythmia-related hospitalizations (none in the HCQ group), and 13 deaths (6 in the HCQ group).

The researchers found that <1% of patients with newly diagnosed RA had incident long QT syndrome or arrhythmia-related hospitalizations during the first 12 months after initiation of HCQ or another nonbiologic DMARD. Their results suggest that the overall incidence of long QT syndrome is extremely low and the risk for patients started on HCQ is not significantly higher. In addition, cardiovascular risk was not significantly higher in patients started on HCQ compared to those started on another nonbiologic DMARD.

Journal Club

A monthly feature designed to facilitate discussion on research methods in rheumatology.

Inclusion of Synovial Tissue–Derived Characteristics in a Nomogram for the Prediction of Treatment Response in Treatment-Naive RA Patients

Alivernini et al. *Arthritis Rheumatol.* 2021;92:1601–1613

Rheumatoid arthritis (RA) is characterized by a high degree of heterogeneity in terms of synovial tissue (ST) inflammation at disease onset, likely influencing the different treatment response rate among patients. Assessment of ST, despite having the potential to support the guidance of individual patient management, is not currently included in RA treatment recommendations.

Alivernini et al tested the diagnostic value of the Krenn synovitis score (KSS), a hematoxylin and eosin–based tool used to distinguish between low- and high-grade synovitis in ST samples obtained from minimally invasive ultrasound-guided biopsies in a large biologic sample data set of RA patients. The aim of the study was to test the diagnostic value of the KSS and ST cell composition, to identify pretreatment synovial biomarkers associated with disease characteristics, and to predict treatment response in treatment-naive RA.

This cross-sectional analysis of 1,015 patients undergoing ST biopsy revealed that KSS distribution and ST inflammation composition are contingent on disease phase in RA and other chronic inflammatory joint diseases. In particular, they found that KSS score is differentially distributed among inflammatory and noninflammatory joint disorders being increased in treatment-naive RA compared to other forms of inflammatory (i.e., PsA) or low-inflammatory joint diseases (i.e., OA), and contingent on the disease activity in RA. In treatment-naive RA, KSS score is influenced by symptom duration and autoantibody positivity; it was significantly higher in patients positive for anti–cyclic citrullinated protein antibody and/or rheumatoid factor and in patients whose ST was analyzed >3 months after symptom onset. Moreover, treatment-naive RA patients with a baseline KSS score of ≥5 had the lowest chance of achieving DAS28-based remission at 6 months compared to those with a KSS score of <5. Therefore, the authors developed a nomogram (subjected to 1,000 bootstrap resamples to assess predictive accuracy) that integrates the individual clinical and ST characteristics, enabling them to quantify the probability of first-line treatment success.

Questions

1. **What is currently known about ST analysis as a prognostic biomarker of treatment response in RA?**
2. **What is the correlation between H&E-based and immunohistochemical-based assessment of the degree of ST inflammation?**
3. **Is the identified cutoff value applicable to quantification of ST inflammation in every joint?**
4. **How did the developed nomogram perform? How does it compare with similar measures in the literature?**

Clinical Connections

Eosinophil ETosis–Mediated Release of Galectin-10 in EGPA

Fukuchi et al, *Arthritis Rheumatol* 2021;92:1683–1693

CORRESPONDENCE
Shigeharu Ueki, MD, PhD: shigeharu.ueki@gmail.com

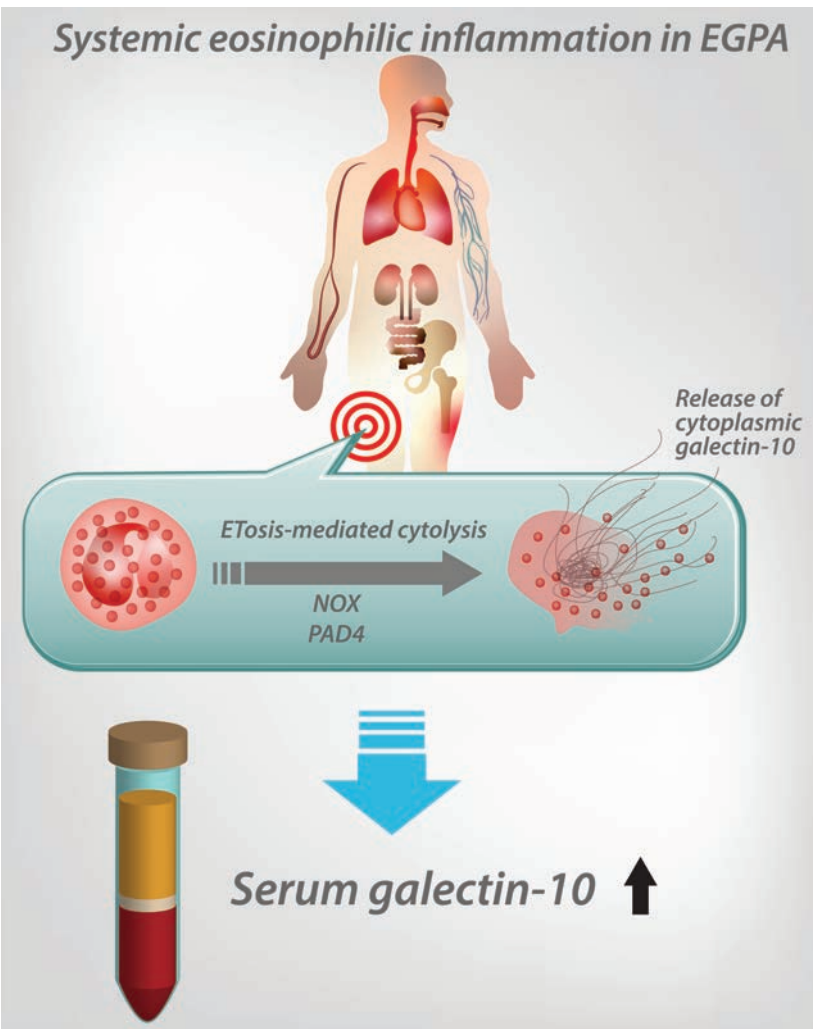

SUMMARY

Eosinophils are major inflammatory cells in the pathogenesis of eosinophilic granulomatosis with polyangiitis (EGPA). An active cytolytic cell death termed ETosis, which is characterized by the release of filamentous chromatin structures, has been recognized. Human eosinophil ETosis (EETosis) is dependent on NADPH oxidase (NOX) and peptidylarginine deiminase 4 (PAD4)–dependent histone citrullination. Fukuchi et al found that upon stimuli-induced EETosis, galectin-10, a nonsecreted protein that is highly abundant in eosinophil cytoplasm, is released extracellularly. Eosinophils infiltrating affected tissues from patients with EGPA undergo EETosis. Serum galectin-10 levels were increased in active EGPA but not in EGPA in remission, in patients with stable asthma, or in healthy controls. Galectin-10 levels positively correlated with disease activity in patients with EGPA. Serum interleukin-5 (IL-5) was significantly increased in active EGPA patients and positively correlated with galectin-10 levels. These data indicate that serum galectin-10 levels might reflect systemic occurrence of EETosis-mediated cytolysis and be a novel biomarker for EGPA.

KEY POINTS

- Stimuli-induced NOX and PAD4 activation acts as intracellular signaling that induces EETosis.
- EETosis is accompanied by the release of galectin-10 and is observed in diseased tissue from patients with EGPA.
- Serum galectin-10 levels are associated with disease activity and serum IL-5 in patients with EGPA.

Regulation of Monocyte Adhesion and Interferon Type I Signaling by CD52 in SSc Patients

Rudnik et al, *Arthritis Rheumatol* 2021;92:1720–1730

CORRESPONDENCE
Gabriela Kania, PhD: gabriela.kania@uzh.ch

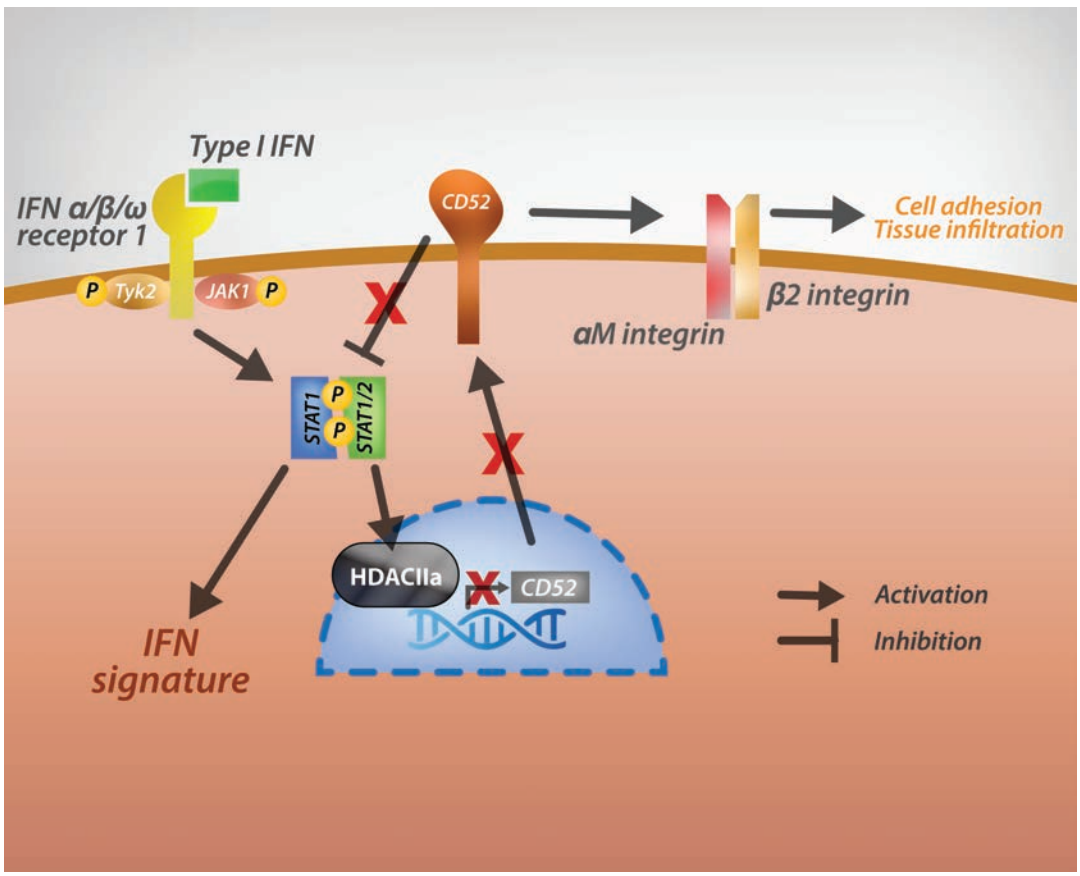

KEY POINTS

- SSc monocytes exhibit an activation phenotype with a predominance of induced adhesion.
- CD52 regulates integrin-dependent processes.
- CD52 influences type I IFN signaling.
- CD52 expression is regulated by inflammation-dependent mechanisms via JAK/STAT signaling.

SUMMARY

Infiltration of inflammatory cells into bodily organs (e.g., skin, lungs) is a major process leading to fibrosis, remodeling, and organ dysfunction in systemic sclerosis (SSc). Monocyte adhesion is a key process for cell infiltration; however, its pathomechanisms in SSc remain elusive. Rudnik et al investigated the role of CD 52 in monocyte adhesion and type I interferon (IFN) signaling in SSc patients. CD52 is a negative regulator of T cell receptor and NF-κB signaling. Upon stimulation with type I IFN, expression levels of CD52 decreased in a histone deacetylase type IIa–dependent manner. This resulted in the activation of integrin αM/β2 complex and enhanced monocyte adhesion. Additionally, deficiency of CD52 led to higher production of CXCL9, CXCL10, and STAT1 and development of the IFN signature. These data demonstrate new aspects of monocyte adhesion and proinflammatory type I IFN signaling in the context of SSc.

Arthritis & Rheumatology
Vol. 73, No. 9, September 2021, pp 1571–1573
DOI 10.1002/art.41801

American College of Rheumatology
Empowering Rheumatology Professionals

EDITORIAL

Few Adverse Cardiovascular Events Among Patients With Rheumatoid Arthritis Receiving Hydroxychloroquine: Are We Reassured?

Candace H. Feldman[1] and Mark S. Link[2]

Hydroxychloroquine (HCQ), an antimalarial agent, was first approved by the US Food and Drug Administration (FDA) for the treatment of rheumatic diseases in 1955 and has since become a crucial disease-modifying antirheumatic drug (DMARD). It is now a standard-of-care medication for the treatment of systemic lupus erythematosus (SLE) and part of the triple-therapy regimen for rheumatoid arthritis (RA). While risks of cardiotoxicity and specifically conduction abnormalities have been documented, they are thought to be rare. HCQ is known to block the rapid cardiac delayed-rectifier potassium current (I_{Kr}) channel, which may lead to a prolonged QT interval, which is a risk factor for torsades de pointes and sudden death (1,2). This effect is additive to other drugs that prolong the QT interval, and to congenital long QT syndrome.

HCQ was promoted as a treatment of severe acute respiratory syndrome coronavirus 2 (SARS–CoV-2), and among patients who were very ill and receiving HCQ, significant QT interval prolongation was observed, particularly when HCQ was used in combination with azithromycin (3). These data prompted an analysis of cardiac safety events linked to HCQ using the FDA Adverse Event Reporting System pharmacovigilance database, and there were multiple reports of cardiac arrhythmias and other cardiac conditions (4). A key limitation of these data, however, is that the baseline cardiovascular status and risk factors for these patients was not known. In addition, the number of exposures was unknown so that the prevalence of these toxicities could not be determined.

To date, rheumatologists have not routinely monitored the corrected QT (QTc) interval of patients receiving HCQ and, in general, have not hesitated to prescribe HCQ to patients with cardiac risk factors. In fact, studies among patients with SLE have shown HCQ to be potentially cardioprotective, with significantly reduced risk of coronary artery disease (5) and thrombosis (6). A recently published retrospective study examined QTc prolongation using electrocardiograms (EKGs) of 819 mostly male patients with rheumatic diseases treated with HCQ (2). The study demonstrated that 7% of patients had a QTc of 470–500 msec and 1.5% had a QTc of >500 msec. The authors also found that chronic kidney disease, history of atrial fibrillation, and heart failure were key risk factors for prolongation. Importantly, they also demonstrated that among the subset of patients with EKGs prior to initiating HCQ, there was a statistically significant mean increase in QTc of 7.6 msec, with nearly 4% demonstrating a >15% prolongation or a QTc of >500 msec. These findings, combined with data from pharmacovigilance studies and from patients with SARS–CoV-2, have appropriately prompted a critical reevaluation of the cardiovascular safety of HCQ among patients with rheumatic conditions.

In this issue of *Arthritis & Rheumatology*, Faselis et al (7) present cardiovascular outcome data from a retrospective, observational study of 8,852 US veterans with incident RA, comparing half who received HCQ to half who received another nonbiologic DMARD. Ideally, a randomized controlled trial would be conducted to ascertain adverse cardiovascular risk associated with HCQ use, with systematic collection of baseline cardiovascular risk factors, comorbidities, serial EKGs, and long-term EKG monitoring. However, with the urgent safety concerns raised in the COVID era, rigorous analyses of readily available data are needed to help guide current clinical practice.

The study by Faselis et al included a cohort of mostly male (86%) US veterans with a mean age of 64 years with newly diagnosed RA. Twenty-eight percent were African American and 10% were Hispanic. A significant percentage of the population had a history of cardiovascular disease. Patients who were prescribed HCQ (mean dosage ~370 mg/day) for the first time were compared to patients prescribed a nonbiologic DMARD; both groups were followed up for 12 months. Arrhythmogenic outcomes were

The content herein is solely the responsibility of the authors and does not necessarily represent the views of the funding sources.

Dr. Feldman's work was supported by the NIH (National Institute of Arthritis and Musculoskeletal and Skin Diseases grant K23-AR-071500).

[1]Candace H. Feldman, MD, ScD: Brigham and Women's Hospital, Boston, Massachusetts; [2]Mark S. Link, MD: UT Southwestern Medical Center, Dallas, Texas.

Dr. Feldman has received research support from Pfizer. No other disclosures relevant to this article were reported.

Address correspondence to Candace H. Feldman, MD, ScD, 60 Fenwood Road, Office 6016P, Boston, MA 02115. Email: cfeldman@bwh.harvard.edu.

Submitted for publication April 25, 2021; accepted in revised form May 4, 2021.

rare and did not differ significantly between the 2 groups. There were 3 documented episodes of long QT syndrome (0.03%), as determined by billing codes, 2 of which occurred in the HCQ group. In addition, there were 56 arrhythmia-related hospitalizations, 30 of which occurred among those treated with HCQ, with no significantly increased risk. There was no difference in all-cause mortality between the groups.

This study has a number of methodologic strengths. The authors designed the study to approximate a randomized controlled trial. To accomplish this, they used an active comparator design; patients receiving HCQ were compared with patients receiving nonbiologic DMARDs, drugs that are used relatively interchangeably for the treatment of RA. This design attempts to address confounding by indication by identifying 2 groups of patients who would receive medications for similar reasons, both measurable and unmeasurable (8). In addition, the authors used a new user design by comparing HCQ initiators to nonbiologic DMARD initiators. This allows for discrete periods for collection of baseline variables prior to medication use, and a follow-up period after initiation to assess outcomes, and allows early adverse events to be captured (8). This is in contrast to a prevalent user design, which may be biased toward individuals who "survived" on the drug because individuals with early events, for example, may discontinue treatment or die, thereby excluding them from the study cohort. In addition, the authors used propensity score matching to balance measured confounders between the 2 comparator groups. The cohort included patients with incident RA to minimize the possibility that duration of disease, as well as prior treatments, contributed to the outcomes of interest. The data set included claims data, medication refill data, and laboratory values, allowing for a robust set of measured potential confounders.

However, there were also limitations that should give clinicians pause in their desire to be entirely reassured by the findings. First, this study was restricted to the first year of HCQ treatment among patients with incident RA, and outcomes, as they were measured, were rare. It is not known whether longer duration of HCQ treatment, or of RA, may be associated with more cardiovascular events. In addition, outcomes presented in this study are limited to those identified by billing codes. EKGs were not collected at prespecified intervals for this cohort. If, in addition to billing codes, EKG and clinical note data were included, outcomes likely would have been higher. Billing codes have not been previously validated, meaning that the positive (or negative) predictive value of a diagnosis code of long QT syndrome is unknown. While all-cause mortality was considered, sudden cardiac death, which is an important outcome of interest when considering the consequences of prolonged QT intervals, could not be assessed.

The population studied was mostly male, which is not consistent with the demographic distribution of RA and thus may not be broadly generalizable to all patients with RA. In addition, QTc intervals are higher in women than in men, and QT prolongation is more common (9). A significant percentage of this cohort had underlying cardiovascular disease and while, on one hand, it is a "real world" cohort, it is also challenging to assess what may be a drug-related complication versus a preexisting condition. While propensity score matching minimizes the likelihood that cardiovascular conditions were significantly different between groups, residual unmeasured confounding likely remained. Further, this study was limited to RA patients and therefore findings may not be applicable to SLE patients, the most frequent HCQ utilizers, who may possess a different constellation of risk factors, concomitant medications, and comorbid conditions.

In addition, this study was conducted with an intent-to-treat design. This means that individuals who initiated HCQ were assumed to have continued HCQ throughout the follow-up period, and regardless of potential discontinuation, outcomes occurring in that group were attributed to HCQ exposure. It is well documented that there is a high rate of discontinuation of HCQ. An alternative and possibly better analysis would have been an as-treated analysis, in which medication refill data were used during the follow-up period to ensure that individuals were taking (or at least refilling) their drug throughout the time period leading up to the event. The authors did conduct an analysis examining 90-day adherence and did not find a difference between the arms when taking this into account. However, adherence data for the full 12-month follow-up period would have helped clarify the degree to which events could be attributed to the drug of interest.

Taking these limitations into account, the key question is whether clinicians can feel reassured by this study. Importantly, among nearly 9,000 individuals with incident RA, many with underlying cardiovascular disease, billing codes for long QT syndrome and arrhythmia-related hospitalizations were extremely rare, both among those receiving HCQ and those receiving other nonbiologic DMARDs during the first year of treatment. Certainly, further studies in cohorts that are diverse with respect to sex and race/ethnicity are needed to systematically collect EKG data longitudinally at prespecified intervals, and to account for HCQ dose, adherence, and duration of use. In addition, parallel studies among patients with SLE are necessary to understand whether the risk calculus is different. Overall, the results of this methodologically rigorous study suggest that HCQ administration among patients with RA is unlikely to be associated with a significant enough risk to dissuade clinicians from continuing to safely prescribe the medication. However, additional studies are essential to guide strategies for monitoring of QTc intervals, and to identify individuals at significantly higher risk of adverse outcomes for whom clinicians may consider avoiding HCQ.

AUTHOR CONTRIBUTIONS

Drs. Feldman and Link drafted the article, revised it critically for important intellectual content, and approved the final version to be published.

REFERENCES

1. World Health Organization. The cardiotoxicity of antimalarials: WHO Evidence Review Group meeting, 13–14 October 2016 Varembe Conference Centre, Geneva, Switzerland. March 2017. URL: https://www.who.int/malaria/mpac/mpac-mar2017-erg-cardiotoxicity-report-session2.pdf.
2. Hooks M, Bart B, Vardeny O, Westanmo A, Adabag S. Effects of hydroxychloroquine treatment on QT interval. Heart Rhythm 2020;17:1930–5.
3. Mercuro NJ, Yen CF, Shim DJ, Maher TR, McCoy CM, Zimetbaum PJ, et al. Risk of QT interval prolongation associated with use of hydroxychloroquine with or without concomitant azithromycin among hospitalized patients testing positive for coronavirus disease 2019 (COVID-19). JAMA Cardiol 2020;5:1036–41.
4. Singh AP, Tousif S, Umbarkar P, Lal H. A pharmacovigilance study of hydroxychloroquine cardiac safety profile: potential implication in COVID-19 mitigation. J Clin Med 2020;9:1867.
5. Yang DH, Leong PY, Sia SK, Wang YH, Wei JC. Long-term hydroxychloroquine therapy and risk of coronary artery disease in patients with systemic lupus erythematosus. J Clin Med 2019;8:796.
6. Kaiser R, Cleveland CM, Criswell LA. Risk and protective factors for thrombosis in systemic lupus erythematosus: results from a large, multi-ethnic cohort. Ann Rheum Dis 2009;68:238–41.
7. Faselis C, Zeng-Treitler Q, Cheng Y, Kerr GS, Nashel DJ, Liappis AP, et al. Cardiovascular safety of hydroxychloroquine in US veterans with rheumatoid arthritis. Arthritis Rheumatol 2021;73:1589–1600.
8. Yoshida K, Solomon DH, Kim SC. Active-comparator design and new-user design in observational studies [review]. Nat Rev Rheumatol 2015;11:437–41.
9. Imboden M, Swan H, Denjoy I, van Langen IM, Latinen-Forsblom PJ, Napolitano C, et al. Female predominance and transmission distortion in the long-QT syndrome. N Engl J Med 2006;355:2744–51.

American College of Rheumatology
Empowering Rheumatology Professionals

Arthritis & Rheumatology
Vol. 73, No. 9, September 2021, pp 1574–1578
DOI 10.1002/art.41765

NOTES FROM THE FIELD

Moving the Goalpost Toward Remission: The Case for Combination Immunomodulatory Therapies in Psoriatic Arthritis

Jose U. Scher,[1] Alexis Ogdie,[2] Joseph F. Merola,[3] and Christopher Ritchlin[4]

The challenge: a path to remission in psoriatic arthritis

Following the pivotal report that outlined unique disease features half a century ago (1), investigators in the field of psoriatic arthritis (PsA) have extrapolated clinical trial data and molecular insights from the more expansive experience in rheumatoid arthritis (RA). As a result, many of the diagnostic approaches, imaging modalities, therapeutics, and outcome measures paralleled (and at times became identical to) those developed for RA. This paradigm was reinforced 20 years ago when it was found that tumor necrosis factor inhibitors (TNFi) significantly improved signs and symptoms not only of RA, but also of PsA and psoriasis (2). However, and as practitioners familiarized themselves with its diagnosis and management, it became apparent that PsA was highly varied in presentation and clinical course. This heterogeneity and complexity are largely due to the interaction of multiple different tissue pathologies, orchestrated by an array of immune cells and molecular mediators (beyond TNF) not directly involved in RA pathogenesis. The revelation that psoriatic disease pathogenesis is orchestrated by the interleukin-23 (IL-23)/IL-17 axis, coupled with the domain approach to diagnostics and therapeutics, established PsA as markedly distinct from RA (3). Nonetheless, the therapeutic landscape and management strategies for both diseases remain remarkably analogous to date.

The arrival of monoclonal antibodies targeting IL-23 and IL-17 marked a transformative era characterized by extraordinary improvement in outcomes for patients with cutaneous psoriasis. Musculoskeletal responses to these same biologic therapies in PsA, however, did not significantly advance when compared to the American College of Rheumatology (ACR) composite outcomes reported in the first PsA TNFi trial in 2001 (2). Indeed, 12 agents (the TNF inhibitors etanercept, adalimumab, infliximab, golimumab, and certolizumab, the IL-17 inhibitors secukinumab and ixekizumab, the IL12/IL-23 inhibitor ustekinumab, the IL-23 inhibitor guselkumab, the phosphodiesterase 4 inhibitor apremilast, the CTLA4-Ig abatacept, and the JAK inhibitor tofacitinib) with remarkably similar levels of efficacy are currently approved by the US Food and Drug Administration for treatment of PsA. Importantly, and although still the benchmark for regulatory approval, the ACR criteria for 20% improvement (ACR20) (developed for RA) (4) as the primary end point is known to be clinically inadequate for most patients with PsA (5). Moreover, measures that resemble a state of low disease activity or remission, such as minimal disease activity (MDA), are achieved in a relatively small proportion of PsA patients, irrespective of the therapeutic agent (6). Taken together, these findings underscore the concept that there are multiple diverse pathways, cell types, and cytokines that promote and sustain synovio–entheseal disease and demand

Supported by National Institute of Arthritis and Musculoskeletal and Skin Diseases (NIAMS) grant R01-AR-074500-01A and the Riley Family Foundation. Dr. Scher's work was supported by the Snyder Family Foundation. Dr. Ritchlin's work was supported by NIAMS grant R01-AR-069000.

[1]Jose U. Scher, MD: New York University School of Medicine and NYU Langone Orthopedic Hospital, New York, New York; [2]Alexis Ogdie, MD, MSCE: University of Pennsylvania Perelman School of Medicine, Philadelphia; [3]Joseph F. Merola, MD, MMSc: Brigham and Women's Hospital and Harvard Medical School, Boston, Massachusetts; [4]Christopher Ritchlin, MD, MPH: University of Rochester School of Medicine and Dentistry, Rochester, New York.

Dr. Scher has received consulting fees from UCB, Janssen, AbbVie, Pfizer, Bristol Myers Squibb, Eli Lilly, and Novartis (less than $10,000 each) and from Sanofi (more than $10,000) and research support from Novartis, Janssen, UCB, and Pfizer. Dr. Ogdie has received consulting fees, speaking fees, and/or honoraria from AbbVie, Amgen, Bristol Myers Squibb, Celgene, Janssen, Eli Lilly, Novartis, Pfizer, and Corrona (less than $10,000 each). Dr. Merola has received consulting fees, speaking fees, and/or honoraria from Bristol Myers Squibb, AbbVie, Eli Lilly, Janssen, Sun Pharma, and Pfizer (less than $10,000 each) and from Novartis and UCB (more than $10,000 each). Dr. Ritchlin has received consulting fees from AbbVie, Amgen, Eli Lilly, Bristol Myers Squibb, Janssen, and Pfizer (less than $10,000 each) and from Novartis and UCB (more than $10,000 each).

Address correspondence to Jose U. Scher, MD, 333 East 38th Street, 4th Floor, New York, NY 10016 (email: jose.scher@nyulangone.org); or to Christopher Ritchlin, MD, MPH, AIR Division, 601 Elmwood Avenue, Box 695, Rochester, NY 14642 (email: Christopher_Ritchlin@URMC.Rochester.edu).

Submitted for publication December 7, 2020; accepted in revised form April 6, 2021.

new and fundamentally different treatment methodologies to achieve the depth of responses observed in psoriasis.

A new therapeutic paradigm: combining immunomodulatory drugs

In 1965, Emil Freireich and colleagues hypothesized that acute lymphocytic leukemia is best treated with combinations of drugs, each with a different mechanism of action, to decrease the chances of tumor resistance (7). After many experimental challenges, the group simultaneously administered methotrexate, vincristine, 6-mercaptopurine, and prednisone (i.e., the VAMP regimen), which induced long-term remissions in children with acute leukemia. They concluded that combinations of effective agents produce an additive increase in rates of complete remission that far exceed responses with single therapies. The premise of induction and maintenance of remission is a guiding principle that has successfully governed the approach to oncologic therapeutics ever since (8).

Support for a parallel approach to address chronic joint inflammation emerged based on the concept that multiple different cell lineages and disease pathways initiate and sustain joint inflammation and damage. To this end, RA investigators have tested combination strategies in recent decades, albeit with rather disappointing outcomes.

The original interest in combination anticytokine therapy originated from translational and clinical work showing that TNF, as well as IL-1, IL-6, and plasma cells, are pivotal in the development and maintenance of inflammatory arthritis (9). Murine models based on a combination strategy with proven efficacy paved the way for dual biologic treatment in human RA (10). The first such trial examined the potential for synergistic effects of combination therapy with etanercept (at full or half dose) and anakinra (11). Regrettably, no added efficacy was demonstrated compared to etanercept monotherapy and a higher overall incidence of serious adverse events and severe infections was observed, in an anakinra dose–dependent manner. These negative results were recapitulated with different combination strategies, including abatacept or rituximab in addition to etanercept (12,13), and were validated in a recent meta-analysis (14). Importantly, a bispecific TNF- and IL-17–targeted variable domain immunoglobulin (i.e., ABT-122) did not provide greater efficacy compared to adalimumab in RA, although, in contrast to previous combination strategies, major safety signals did not arise in these relatively small studies (15,16). In a subsequent trial, RA patients with inadequate response to certolizumab at 8 weeks were treated with bimekizumab (an IL-17A/F inhibitor) or placebo (17). The 28-joint Disease Activity Score response (18) was numerically greater in the combination treatment group without a clinically meaningful increase in safety signals, although the rate of treatment-emergent adverse events was twice as high.

Dual inhibition of IL-17 and TNF would be expected to be more effective in PsA than in RA based on the current disease paradigm, and a proof-of-concept study with ABT-122 was also performed in PsA patients with inadequate response to methotrexate (16). Intriguingly, and although ACR20 response was not different compared to that observed with adalimumab, the efficacy of ABT-122 based on the ACR50/ACR70 and the Psoriasis Area and Severity Index criteria for 75% improvement (PASI75)/PASI90 (19) was statistically significantly superior at several time points. These data, coupled with a safety profile comparable to that of adalimumab, provided rationale for the pursuit of further program development of ABT-122. The experience with this compound illustrates how a dual immunomodulatory strategy can concomitantly improve clinically relevant synovio–entheseal (e.g., ACR70) and skin (e.g., PASI90) outcomes in PsA patients without increased risk of infection. A variety of case reports have described significant clinical improvement with simultaneous use of TNFi and ustekinumab or guselkumab in 15 patients with recalcitrant PsA that was nonresponsive to multiple biologic disease-modifying antirheumatic drug (DMARD) monotherapy regimens (20). However, these patients had chronic, advanced disease and almost half of them developed infections. Moreover, the study was not blinded and may have been subject to publication bias.

Combinations with highest potential for increased efficacy and safety

Decisions regarding which combination(s) might yield an optimal balance of efficacy and safety in patients with PsA should be informed by our current understanding of the pathogenic mechanisms of the disease and synergistic effects, combined with data that might predict adverse events. Our emphasis is to consider the combination of 2 targeted anticytokines or a biologic with a targeted oral small molecule. This view is based on the experience that, unlike in RA, the use of methotrexate (21) or apremilast in randomized controlled trials or registry-based studies demonstrates no additional efficacy in PsA beyond that obtained with biologic monotherapy. Importantly, the improved safety profiles of newer, targeted second-generation biologics or targeted JAK inhibitors support the rationale for combination approaches that include IL-23i, IL-17i, or deucravacitinib, for example, with the expectation that patients would experience fewer adverse events than observed with historic combinations (TNFi with IL-1 or rituximab).

TNFi has demonstrated robust efficacy in the treatment of PsA. Yet, with IL-23i treatment, skin clearance rates increased to levels never before witnessed with first-generation biologics, while providing a remarkable safety profile coupled with infrequent dosing. It therefore stands to reason that combining these 2 classes with novel dosing provides an opportunity to optimize outcomes for both skin and synovio-entheseal components of psoriatic disease. This view is further supported by in vitro data demonstrating a synergistic effect of TNF and the IL-23/IL-17 axis on the enthesis

(22) and a deep suppression of cutaneous molecular pathways with IL-23i compared to other drug classes (23).

Finally, as an ever-increasing number of oral JAK inhibitors becomes available, it is intriguing to postulate combination strategies in PsA that include this class of drugs. Specific agents include nonselective JAK inhibitors (e.g., tofacitinib), and JAK1-selective inhibitors (e.g., upadacitinib), which have demonstrated TNFi-like efficacy in PsA.

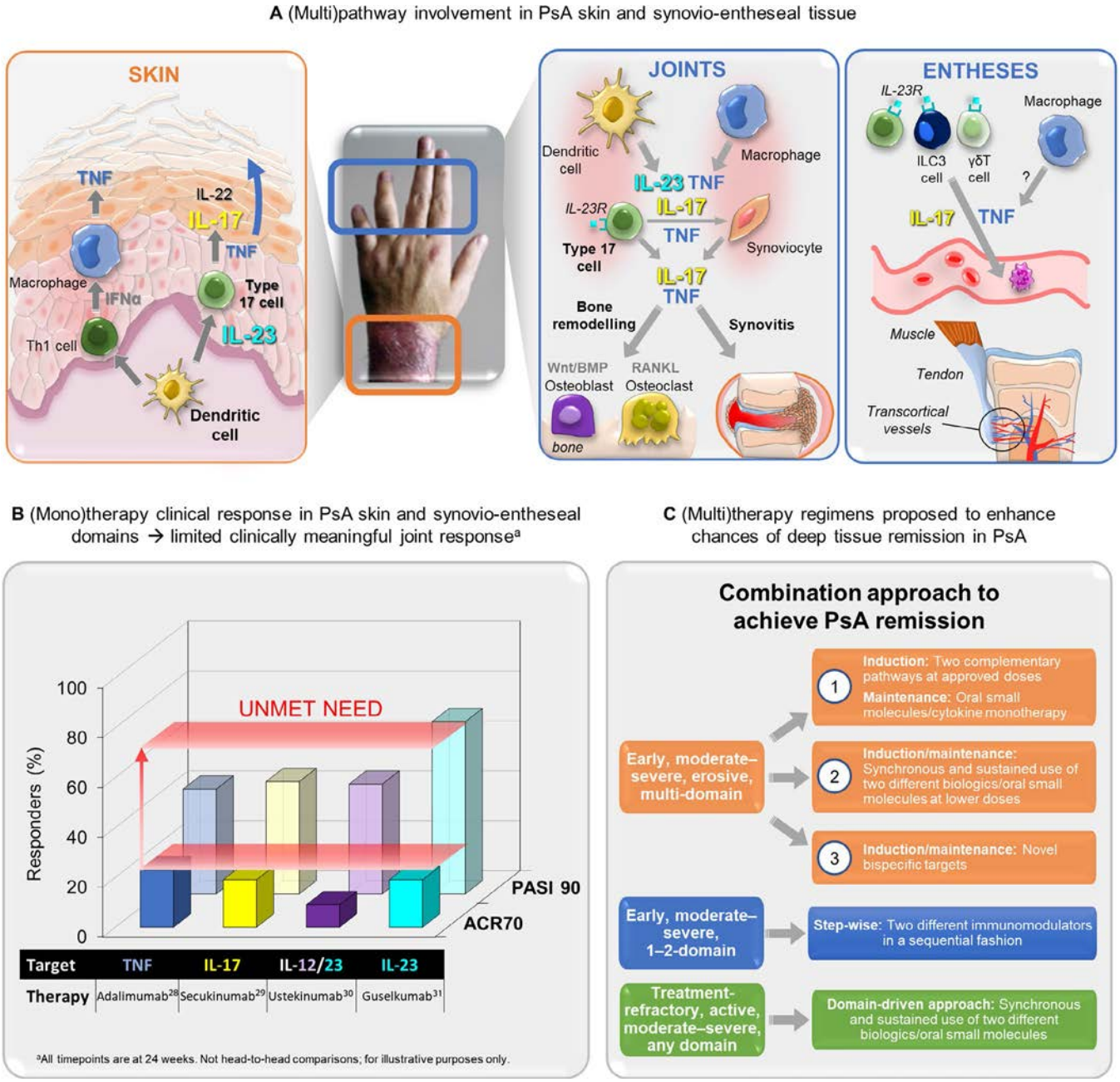

Figure 1. Psoriatic arthritis (PsA) pathogenesis and proposed treatment strategies. Unlike psoriasis and rheumatoid arthritis, the pathogenesis of PsA is orchestrated by a specific set of hyperactivated inflammatory pathways, with synergistic effects that cause damage in a variety of tissues, including skin, synovium, and entheses (**A**). Although monotherapy approaches blocking primarily tumor necrosis factor (TNF), interleukin-17 (IL-17), and IL-23 have led to extraordinary improvements in psoriatic skin inflammation, treatments targeting these same cytokines with monoclonal antibodies have not achieved parallel, clinically meaningful responses in synovio–entheseal outcomes (**B**). We propose an array of regimens combining multiple therapeutic strategies including dual cytokine blockade and/or combination with intracellular kinase inhibitors, with the ultimate goal of very low disease activity or even remission in patients with PsA (**C**). IFNα = interferon-α; IL-23R = IL-23 receptor; BMP = bone morphogenetic protein; ILC3 = group 3 innate lymphoid cells; PASI90 = Psoriasis Area and Severity Index criteria for 90% improvement; ACR70 = American College of Rheumatology criteria for 70% improvement (developed for RA).

Potential timing and dosing considerations

Insights gained from combination therapy in oncology are instructive. Examples include the timing of pathway-specific treatments and the concept that *order matters* (i.e., initial targeting of a tumor with chemotherapy allows for immunotherapies to become more effective). Mechanism also matters—allowing one therapy to open the tumor microenvironment may then allow a subsequent therapy to enter the tumor (24). Although parallel strategies may be effective in treating synovitis, studies exploring novel interventions in inflammatory arthritis are exceedingly rare.

Thus, prospective proof-of-concept studies are needed to test strategies in PsA that consider various dosages, sequence, and frequency of therapies. Several approaches are envisioned (Figure 1). For example, in early, moderate-to-severe, multidomain PsA, we propose a combination induction regimen using 2 complementary pathways at approved doses in order to induce rapid remission, followed by anticytokine (or oral small molecule) monotherapy for maintenance. Combinations of conventional synthetic DMARDs such as methotrexate, leflunomide, and sulfasalazine are problematic in PsA due to the high prevalence of obesity and fatty liver disease, while pulse steroids may trigger erythroderma during steroid taper. Other conceivable designs include the synchronous and sustained use of 2 different biologics (including novel bispecifics) at lower doses, or the administration of 2 different immunomodulators in an asynchronous manner.

Another intriguing possibility would entail a domain-driven approach in which, depending on the dominant clinical phenotype, a "background" drug can be used as monotherapy with the possibility of adding a second agent on an as-needed basis. This "boost" approach can be exemplified by the initiation of a TNFi or oral small molecule in an arthritis-predominant case, complemented with the use of a lower dose/less frequent IL-23i or IL-17i if and when there is a flare in the skin domain or full clearance is not achieved. Another important consideration with the domain-driven strategy is the differential timing of response for individual tissues, as skin response may be observed early, followed by improvement in joint symptoms, while reduction of enthesitis and nail symptoms may take place at later time points. With this in mind, targeting skin early, followed by addition of a second agent to target persistently active domains, may be a successful approach. An alternative strategy is to start with a combination of agents and then decrease or discontinue medications once significant responses in individual domains are achieved (25). Finally, if circulating, cutaneous, or synovial biomarkers to stratify heterogeneous subtypes could be identified, strategies to direct therapy combination, order, or dosing could be used to induce remission.

In pursuance of PsA remission: the way forward

There is mounting evidence supporting the notion that improved outcomes, and specifically remission, can be achieved in early and moderate-to-severe PsA. As the field prepares for clinical trials to address this unmet need, multiple elements are required for the planning and execution phases. Critically, relevant insights will be derived from similar efforts in inflammatory bowel diseases. The VEGA study, for example, is investigating the efficacy and safety of combination therapy with guselkumab and golimumab in moderate-to-severe active ulcerative colitis (26). Interestingly, this phase II proof-of-concept randomized trial compares dual blockade versus either agent as monotherapy, with remission outcomes assessed at 12 weeks. Regardless of efficacy, this is the first trial using this combination, and will provide highly relevant safety data to inform potential applicability in PsA. Importantly, the implementation of these more aggressive approaches should be paired with innovative trial designs that incorporate stringent composite end points that document remission in skin and synovio–entheseal domains as desired targets, including MDA/very low disease activity, Disease Activity in Psoriatic Arthritis score (27), and composite indices such as the ACR70 and PASI100. Concomitantly, and analogous to the positron emission tomography–computed tomography approach to surveillance in various solid tumors, the incorporation of novel imaging modalities (i.e., evaluation of subclinical changes on whole-body magnetic resonance imaging or musculoskeletal ultrasound) has potential to document the achievement of "deep tissue remission." Applying state-of-the-art immunophenotyping platforms and novel biomarkers will also be essential to characterize and understand the ideal order in which the specific pathways should be targeted to maximize the probability of long-term, deep remission.

We recognize that there may be other ways to enhance PsA response rates, including earlier initiation of biologic treatment, prevention strategies, and personalized medicine (i.e., biomarker-based therapeutic decision-making), all of which are also viable options. However, and based on the accumulated body of immunologic, molecular, and clinical evidence, we propose the hypothesis that PsA remission can best be achieved when diverse pathobiologic pathways are targeted with a combination approach comprising agents with distinct, but synergistic, mechanisms of action that counter inflammatory events in all affected domains. This approach has proven highly effective in patients with oncologic disease, which has many parallels with chronic immune-mediated inflammatory disorders. Rigorous proof-of-principle trials emphasizing both efficacy and safety (both short- and long-term) and coupled with state-of-the-art translational investigation should reveal whether these combination strategies can profoundly alter the current therapeutic paradigm in PsA and foster deep and long-lasting remission.

AUTHOR CONTRIBUTIONS

All authors were involved in drafting the article or revising it critically for important intellectual content, and all authors approved the final version to be published. Dr. Ritchlin had full access to all of the data in the study and takes responsibility for the integrity of the data and the accuracy of the data analysis.

Study conception and design. Scher, Ogdie, Merola, Ritchlin.
Acquisition of data. Scher, Ogdie, Merola, Ritchlin.
Analysis and interpretation of data. Scher, Ogdie, Merola, Ritchlin.

REFERENCES

1. Moll JM, Wright V. Psoriatic arthritis. Semin Arthritis Rheum 1973;3:55–78.
2. Mease PJ, Goffe BS, Metz J, VanderStoep A, Finck B, Burge DJ. Etanercept in the treatment of psoriatic arthritis and psoriasis: a randomised trial. Lancet 2000;456:385–90.
3. Ritchlin CT, Colbert RA, Gladman DD. Psoriatic arthritis [review]. N Engl J Med 2017;376:957–70.
4. Felson DT, Anderson JJ, Boers M, Bombardier C, Furst D, Goldsmith C, et al. American College of Rheumatology preliminary definition of improvement in rheumatoid arthritis. Arthritis Rheum 1995;38:727–35.
5. Ritchlin C, Scher JU. Strategies to improve outcomes in psoriatic arthritis [review]. Curr Rheumatol Rep 2019;21:72.
6. Zardin-Moraes M, da Silva AL, Saldanha C, Kohem CL, Coates LC, Henrique LR, et al. Prevalence of psoriatic arthritis patients achieving minimal disease activity in real-world studies and randomized clinical trials: systematic review with metaanalysis. J Rheumatol 2020;47:839–46.
7. Frei E III, Karon M, Levin RH, Freireich EJ, Taylor RJ, Hananian J, et al. The effectiveness of combinations of antileukemic agents in inducing and maintaining remission in children with acute leukemia. Blood 1965;26:642–56.
8. Chabner BA, Roberts TG. Chemotherapy and the war on cancer [review]. Nat Rev Cancer 2005;5:65–72.
9. McInnes IB, Schett G. Pathogenetic insights from the treatment of rheumatoid arthritis. Lancet 2017;389:2328–37.
10. Bendele AM, Chlipala ES, Scherrer J, Frazier J, Sennello G, Rich WJ, et al. Combination benefit of treatment with the cytokine inhibitors interleukin-1 receptor antagonist and PEGylated soluble tumor necrosis factor receptor type I in animal models of rheumatoid arthritis. Arthritis Rheum 2000;43:2648–59.
11. Genovese MC, Cohen S, Moreland L, Lium D, Robbins S, Newmark R, et al. Combination therapy with etanercept and anakinra in the treatment of patients with rheumatoid arthritis who have been treated unsuccessfully with methotrexate. Arthritis Rheum 2004;50:1412–9.
12. Weinblatt M, Combe B, Covucci A, Aranda R, Becker JC, Keystone E. Safety of the selective costimulation modulator abatacept in rheumatoid arthritis patients receiving background biologic and nonbiologic disease-modifying antirheumatic drugs: a one-year randomized, placebo-controlled study. Arthritis Rheum 2006;54:2807–16.
13. Greenwald MW, Shergy WJ, Kaine JL, Sweetser MT, Gilder K, Linnik MD. Evaluation of the safety of rituximab in combination with a tumor necrosis factor inhibitor and methotrexate in patients with active rheumatoid arthritis: results from a randomized controlled trial. Arthritis Rheum 2011;63:622–32.
14. Boleto G, Kanagaratnam L, Dramé M, Salmon JH. Safety of combination therapy with two bDMARDs in patients with rheumatoid arthritis: a systematic review and meta-analysis. Semin Arthritis Rheum 2019;49:35–42.
15. Genovese MC, Weinblatt ME, Mease PJ, Aelion JA, Peloso PM, Chen K, et al. Dual inhibition of tumour necrosis factor and interleukin-17A with ABT-122: open-label long-term extension studies in rheumatoid arthritis or psoriatic arthritis. Rheumatology (Oxford) 2018;57:1972–81.
16. Mease PJ, Genovese MC, Weinblatt ME, Peloso PM, Chen K, Othman AA, et al. Phase II study of ABT-122, a tumor necrosis factor– and interleukin-17A–targeted dual variable domain immunoglobulin, in patients with psoriatic arthritis with an inadequate response to methotrexate. Arthritis Rheumatol 2018;70:1778–89.
17. Glatt S, Taylor PC, McInnes IB, Schett G, Landewé R, Baeten D, et al. Efficacy and safety of bimekizumab as add-on therapy for rheumatoid arthritis in patients with inadequate response to certolizumab pegol: a proof-of-concept study. Ann Rheum Dis 2019;78:1033–40.
18. Prevoo ML, van 't Hof MA, Kuper HH, van Leeuwen MA, van de Putte LB, van Riel PL. Modified disease activity scores that include twenty-eight–joint counts: development and validation in a prospective longitudinal study of patients with rheumatoid arthritis. Arthritis Rheum 1995;38:44–8.
19. Fredriksson T, Pettersson U. Severe psoriasis—oral therapy with a new retinoid. Dermatologica 1978;157:238–44.
20. Thibodeaux Q, Ly K, Reddy V, Smith MP, Liao W. Dual biologic therapy for recalcitrant psoriasis and psoriatic arthritis. JAAD Case Rep 2019;5:928–30.
21. Mease PJ, Gladman DD, Collier DH, Ritchlin CT, Helliwell PS, Liu L, et al. Etanercept and methotrexate as monotherapy or in combination for psoriatic arthritis: primary results from a randomized, controlled phase III trial. Arthritis Rheumatol 2019;71:1112–24.
22. Bridgewood C, Watad A, Russell T, Palmer TM, Marzo-Ortega H, Khan A, et al. Identification of myeloid cells in the human enthesis as the main source of local IL-23 production. Ann Rheum Dis 2019;78:929–33.
23. Visvanathan S, Baum P, Vinisko R, Schmid R, Flack M, Lalovic B, et al. Psoriatic skin molecular and histopathologic profiles after treatment with risankizumab versus ustekinumab. J Allergy Clin Immunol 2019;143:2158–69.
24. Long KB, Gladney WL, Tooker GM, Graham K, Fraietta JA, Beatty GL. IFNγ and CCL2 cooperate to redirect tumor-infiltrating monocytes to degrade fibrosis and enhance chemotherapy efficacy in pancreatic carcinoma. Cancer Discov 2016;6:400–13.
25. Haberman RH, Castillo R, Scher JU. Induction of remission in biologic-naive, severe psoriasis and PsA with dual anti-cytokine combination. Rheumatology (Oxford) 2020 doi: 10.1093/rheumatology/keaa880. E-pub ahead of print.
26. Janssen Research & Development, LLC, sponsor. A study of efficacy and safety of combination therapy with guselkumab and golimumab in participants with moderately to severely active ulcerative colitis (VEGA). ClinicalTrials.gov identifier: NCT03662542; 2018.
27. Schoels MM, Aletaha D, Alasti F, Smolen JS. Disease activity in psoriatic arthritis (PsA): defining remission and treatment success using the DAPSA score. Ann Rheum Dis 2016;75:811–8.
28. Mease PJ, Gladman DD, Ritchlin CT, Ruderman EM, Steinfeld S, Choy EH, et al. Adalimumab Effectiveness in Psoriatic Arthritis Trial Study Group. Adalimumab for the treatment of patients with moderately to severely active psoriatic arthritis: results of a double-blind, randomized, placebo-controlled trial. Arthritis Rheum 2005;52:3279–89.
29. McInnes IB, Mease PJ, Kirkham B, Kavanaugh A, Ritchlin CT, Rahman P, et al. FUTURE 2 Study Group. Secukinumab, a human anti-interleukin-17A monoclonal antibody, in patients with psoriatic arthritis (FUTURE 2): a randomised, double-blind, placebo-controlled, phase 3 trial. Lancet 2015;386:1137–46.
30. Ritchlin C, Rahman P, Kavanaugh A, McInnes IB, Puig L, Li S, et al. PSUMMIT 2 Study Group. Efficacy and safety of the anti-IL-12/23 p40 monoclonal antibody, ustekinumab, in patients with active psoriatic arthritis despite conventional non-biological and biological anti-tumour necrosis factor therapy: 6-month and 1-year results of the phase 3, multicentre, double-blind, placebo-controlled, randomised PSUMMIT 2 trial. Ann Rheum Dis 2014;73:990–9.
31. Mease PJ, Rahman P, Gottlieb AB, Kollmeier AP, Hsia EC, Xu XL, et al. DISCOVER-2 Study Group. Guselkumab in biologic-naive patients with active psoriatic arthritis (DISCOVER-2): a double-blind, randomised, placebo-controlled phase 3 trial. Lancet 2020;395:1126–36.

Arthritis & Rheumatology
Vol. 73, No. 9, September 2021, pp 1579–1588
DOI 10.1002/art.41701

American College of Rheumatology
Empowering Rheumatology Professionals

Semaphorins: From Angiogenesis to Inflammation in Rheumatoid Arthritis

Jérôme Avouac,[1] Sonia Pezet,[2] Eloïse Vandebeuque,[3] Cindy Orvain,[2] Virginie Gonzalez,[2] Grégory Marin,[4] Gaël Mouterde,[5] Claire Daïen,[5] and Yannick Allanore[1]

Objective. To study the potential role of semaphorins in the pathogenesis of rheumatoid arthritis (RA).

Methods. Microarray experiments were performed on Affymetrix GeneChip Human Exon 1.0 ST arrays in RA endothelial cells (ECs) and control ECs derived from circulating progenitors. Expression of class 3 and class 4 semaphorins and their receptors in the serum of RA patients and healthy controls was assessed by immunohistochemical analysis in synovial tissue and by enzyme-linked immunosorbent assay.

Results. Microarray analysis revealed differential expression of class 3 and class 4 semaphorins and their receptors in RA ECs. Semaphorin 4A (SEMA4A), plexin D1, and neuropilin 1 messenger RNA (mRNA) levels were markedly increased in RA ECs by 1.75-, 2.21-, and 1.68-fold, respectively. Stimulation with tumor necrosis factor (TNF) led to a 2-fold increase in SEMA4A mRNA levels in RA ECs, and deficient SEMA4A expression modified RA EC angiogenic properties. Class 3 and class 4 semaphorins as well as their receptors were overexpressed in RA synovial tissue. A respective 1.30-fold increase and 1.54-fold increase in SEMA4A and SEMA3E, as well as a 24% decrease in SEMA3A, was observed in the serum of RA patients. Serum levels of SEMA4A, SEMA4D, and SEMA3A correlated with levels of inflammation and proangiogenic markers. In 2 independent cohorts of patients with low disease activity or with RA in remission, the presence of SEMA4A identified patients with residual disease activity.

Conclusion. Gene expression profiling of ECs identified class 3 and class 4 semaphorins as potential biomarkers and therapeutic candidates in RA, with confirmed overexpression in ECs, synovial vessels, and serum, and correlation with validated markers of inflammation and angiogenesis. Thus, semaphorins might be novel and appealing EC-derived inflammatory and proangiogenic targets in RA.

INTRODUCTION

Inflammatory diseases are associated with pathologic angiogenesis (1,2). The proposed mechanism for this association is the induction of angiogenesis by secreted mediators of tissue-infiltrating inflammatory cells (3,4). However, recent evidence has suggested primary involvement of angiogenesis in the onset of tissue inflammation, which occurs prior to inflammatory cell infiltration (5). Angiogenesis may precede leukocyte infiltration in experimental models of inflammatory diseases. These findings add to the accumulating evidence of the importance of endothelial function in the pathophysiologic processes of inflammation.

Rheumatoid arthritis (RA) is the most frequently observed inflammatory rheumatic disorder (6). The synovium is the affected tissue in the inflammatory process that may lead to irreversible damage of adjacent cartilage and bone. New blood vessel formation is an initial and critical event to stimulate the growth of the hyperplasic proliferative pathologic synovium. Increased vascular density results from the unrestrained activation of angiogenesis and vasculogenesis by inflammatory cytokines and growth factors synthetized from tissue infiltrating inflammatory cells, which lead to the uncontrolled formation of new blood vessels (1–4).

Endothelial cell (EC) activation, proliferation, and migration are critical for the formation of new blood vessels. We have developed

Supported by an internal grant from Hôpital Cochin as a part of Teaching, Research, Reference, and Innovation Missions (MERRI).

[1]Jérôme Avouac, MD, PhD, Yannick Allanore, MD, PhD: INSERM U1016, CNRS UMR8104, Institut Cochin, Université de Paris, Université Paris Descartes, Hôpital Cochin, AP-HP, Paris, France; [2]Sonia Pezet, RT, Cindy Orvain, PhD, Virginie Gonzalez, RT: INSERM U1016, CNRS UMR8104, Institut Cochin, Université de Paris, Université Paris Descartes, Paris, France; [3]Eloïse Vandebeuque, MD: Université de Paris, Université Paris Descartes, Hôpital Cochin, AP-HP, Paris, France; [4]Grégory Marin, PhD: Centre Hospitalier Universitaire de Montpellier, Montpellier, France; [5]Gaël Mouterde, MD, Claire Daïen, MD, PhD: Centre Hospitalier Universitaire de Montpellier, Université de Montpellier, Montpellier, France.

No potential conflicts of interest relevant to this article were reported.

Address correspondence to Jérôme Avouac, MD, PhD, Université de Paris, Service de Rhumatologie, Hôpital Cochin, 27 Rue du Faubourg St. Jacques, 75014 Paris, France. Email: jerome.avouac@aphp.fr.

Submitted for publication March 22, 2020; accepted in revised form February 16, 2021.

a relevant technique to obtain ECs in cell cultures derived from circulating endothelial progenitors (7,8). These cells represent valuable tools to study endothelial biologic processes since they have the phenotype of genuine ECs, display robust proliferative potential, exhibit in vitro angiogenic properties, and have the capacity to constitute and orchestrate vascular remodeling in vivo (7,9,10).

To better understand the involvement of angiogenesis and vasculogenesis in RA, we investigated the gene expression profile of RA and control circulating progenitor–derived ECs by comprehensive microarray analysis. This analysis revealed a semaphorin signature in RA ECs. The semaphorin family comprises a group of structurally similar molecules characterized by the presence of a Sema domain of ~500 amino acids. Semaphorins are expressed in a wide range of immune cells and have roles in various immune responses. In the context of RA, class 3 and class 4 semaphorins have been implicated in the regulation of T cell response, the promotion of synovial cell proliferation, or the induction of proinflammatory cytokine production by monocytes (11). However, their specific contribution to synovial neovascularization has not yet been studied. Thus, our aim was to investigate the relevance of semaphorins in RA vasculogenesis and synovial angiogenesis, as well as their merit as circulating markers reflecting disease-related joint/systemic inflammation and angiogenesis.

PATIENTS AND METHODS

Patient recruitment and synovial tissue samples. The present study included 200 patients who fulfilled the 2010 American College of Rheumatology/European Alliance of Associations for Rheumatology (EULAR) criteria for RA (12,13). The first set of 130 consecutive patients with RA, who were classified as the discovery cohort, was recruited from the rheumatology department at Cochin Hospital (Paris, France). A second prospective set of 70 patients with RA in remission or with low disease activity, who were classified as the replication cohort, was recruited from the rheumatology department at Lapeyronie Hospital (Montpellier, France). Patients in the replication cohort had a Disease Activity Score in 28 joints using the C-reactive protein level (DAS28-CRP) of <3.2 and no active synovitis (i.e., swollen and tender joints) detected by clinical examination at the inclusion visit. Treatment was kept unchanged (no tapering strategy), and patients were followed up for 12 months with visits performed regularly every 3 months.

The present study also included 30 age- and sex-matched control subjects recruited from the rheumatology department of Cochin Hospital (Paris, France). Synovial tissue from the knee joints of RA patients and control subjects was obtained in collaboration with the department of orthopedic surgery at Cochin Hospital (Paris, France). Detailed characteristics of the patients and control subjects are provided in Table 1. The number of samples used for each experiment is presented in Supplementary Table 1, available on the *Arthritis & Rheumatology* website at http://onlinelibrary.wiley.com/doi/10.1002/art.41701/abstract.

Table 1. Demographic features and clinical characteristics of the study population*

	Discovery cohort (Paris) (n = 130)	Replication cohort (Montpellier) (n = 70)
Demographic features		
Age, mean ± SD years	58.2 ± 12.9	59.6 ± 13.8
Female sex	111 (85.3)	53 (75.7)
Disease characteristics		
Disease duration, mean ± SD years	13.9 ± 11.2	8.6 ± 9.4
RF positivity	102 (78.5)	53 (75.7)
Anti-CCP2 antibody positivity	105 (80.8)	60 (85.7)
Erosions on hand/foot radiographs	79 (60.8)	37 (52.9)
Disease activity		
Tender joint count, mean ± SD	3.7 ± 4.9	0.5 ± 1.0
Swollen joint count, mean ± SD	4.0 ± 5.2	0.4 ± 0.8
DAS28 score, mean ± SD	3.52 ± 1.39	2.10 ± 0.70
DAS28 category		
<2.6	35 (26.9)	14 (82.3)†
2.6–3.2	21 (16.2)	3 (17.7)†
>3.2	74 (56.9)	0 (0)
>5.1	15 (11.5)	0 (0)
DAS28-CRP score, mean ± SD	3.02 ± 1.39	1.90 ± 0.59
DAS28-CRP category		
<2.6	43 (33.1)	64 (91.4)
2.6–3.2	30 (23.1)	6 (8.6)
>3.2	57 (43.8)	0 (0)
>5.1	14 (10.8)	0 (0)
ESR, mean ± SD mm/hour	19.6 ± 16.2	14.6 ± 11.0
ESR >28 mm/hour	29 (22.3)	3 (17.7)†
CRP, mean ± SD mg/liter	8.1 ± 21.2	5.6 ± 10.1
CRP >10 mg/liter	25 (19.2)	8 (11.4)
Ultrasound assessment		
Hand synovitis	76 (58.4)	49 (70)
Patients with grade ≥1 synovitis on PDUS		
Grade 1	51 (39.2)	49 (70)
Grade 2	34 (26.2)	27 (38.6)
Grade 3	16 (12.3)	0 (0)
Current treatment		
Glucocorticoids	87 (66.9)	24 (34.3)
Conventional DMARDs	118 (90.8)	63 (90)
Anti-TNF	26 (20)	30 (42.9)
Rituximab	27 (20.7)	0 (0)
Tocilizumab	12 (9.2)	10 (14.3)
Abatacept	8 (6.2)	5 (7.1)

* Except where indicated otherwise, values are the number (%). The study population also included 30 control subjects with a mean ± SD age of 59.4 ± 15.3 years, of whom 26 (86.7%) were female. RF = rheumatoid factor; anti-CCP2 = anti–cyclic citrullinated peptide 2; DAS28 = Disease Activity Score in 28 joints; DAS28-CRP = DAS28 using the C-reactive protein level; ESR = erythrocyte sedimentation rate; PDUS = power Doppler ultrasonography; DMARDs = disease-modifying antirheumatic drugs; anti-TNF = anti–tumor necrosis factor.
† Data were available for 17 patients.

All patients and controls provided written informed consent. The study was approved by the local institutional review boards in Paris and Montpellier, France (Comité de Protection des Personnes, Paris Ile de France 3 and Comité de Protection des Personnes Sud Méditerranée III).

Data collection. Review of medical files was systematically performed to collect patient history, current and past medication use, physical examination data, and results of laboratory tests. RA disease activity was evaluated by the DAS28 (14), using erythrocyte sedimentation rate (ESR) and CRP levels (15). Systematic radiographs of the hands and feet were used to assess the presence of erosions. Blood tests were performed on the morning of hospital visit, including complete blood cell count, Westergren ESR (considered elevated if >28 mm/hour), CRP concentration (considered elevated if >10 mg/liter), and serum creatinine concentration. Levels of rheumatoid factor (RF) and second-generation anti–cyclic citrullinated peptide 2 (anti-CCP2) antibodies were measured by enzyme-linked immunosorbent assay (ELISA).

Ultrasound assessment. Power Doppler ultrasonography (PDUS) examinations were performed with a multiplanar technique, as recommended by the EULAR guidelines for musculoskeletal ultrasound in rheumatology (16), with a 7–15 MHz linear array transducer (Toshiba Aplio) in Paris and a 12–18 MHz probe (Esaote MyLab 70) in Montpellier. Semiquantitative scales were used to score hypoechoic synovial hyperplasia and joint effusion (both assessed using grayscale ultrasound) and synovial vascularization (evaluated with power Doppler). Synovitis, indicated by the presence of synovial hyperplasia and the absence of joint effusion on PDUS, was scored in each joint according to the semiquantitative Outcome Measures in Rheumatology (OMERACT)–EULAR ultrasound composite PDUS scale (17). A global synovitis score, derived from the Global OMERACT-EULAR Synovitis Score (GOESS), was determined from the sum of the composite PDUS scores for all assessed joints and was calculated for 16 paired joints: both hands (metacarpophalangeal [MCP] joints 1–5 and proximal interphalangeal [PIP] joints 1–5), both wrists (radioulnar, mediocarpal, and radiocarpal joints), and both forefeet (metatarsophalangeal [MTP] joints 1–5), with a potential score range of 0–96 (18).

Cell culture. At the time of hospitalization, blood samples were obtained from the forearms of patients in a resting state, and 50 ml of heparinized blood was collected into tubes for laboratory testing and other routine analyses. Samples were immediately transported to the laboratory for testing. Cell culture methods have been described previously and were suitable to obtain and expand late outgrowth endothelial progenitor cell (EPC)–derived colonies (7). Blood mononuclear cell fraction was collected by Ficoll (Pancoll) density-gradient centrifugation and suspended in complete endothelial growth medium 2 (EGM-2; Lonza). Then, cells were seeded onto separate wells of a 12-well tissue culture plate precoated with type I rat tail collagen (BD Biosciences) and stored at a temperature of 37°C with an atmosphere consisting of 5% CO_2 in a humidified incubator. After 24 hours, nonadherent cells and debris were aspirated, adherent cells were washed once with phosphate buffered saline, and complete EGM-2 medium was added to each well. Medium was changed daily for 7 days, and then every other day until the first passage. Colonies of ECs generally appeared between 8 and 26 days of culture and were identified as well-circumscribed monolayers of cells with a cobblestone appearance. After the third passage, endothelial phenotyping was confirmed by flow cytometry, and ECs were then suspended in fetal bovine serum supplemented with 20% DMSO, frozen in liquid nitrogen, and stored until used (7). In a subset of experiments, RA ECs were stimulated with 50 ng/ml of tumor necrosis factor (TNF) or 100 ng/ml of interleukin-6 (IL-6; Miltenyi Biotec) for 6 hours.

Microarray analysis. Microarray analysis was performed on 29 samples from the Paris cohort (discovery cohort) obtained from 18 RA patients and 11 control subjects (Supplementary Table 1, available on the *Arthritis & Rheumatology* website at http://onlinelibrary.wiley.com/doi/10.1002/art.41701/abstract). Affymetrix Microarray technology was used to analyze gene expression levels (Affymetrix GeneChip Human Exon 1.0 ST Arrays). Labeling and microarray processing were performed according to the manufacturer's protocol (8,9). These procedures are described in detail in the Supplementary Methods, available on the *Arthritis & Rheumatology* website at http://onlinelibrary.wiley.com/doi/10.1002/art.41701/abstract. All data obtained by microarray analysis have been deposited on the GEO Omnibus site with accession no. GSE121894 (https://www.ncbi.nlm.nih.gov/geo/query/acc.cgi?acc=GSE121894).

Quantitative reverse transcription–polymerase chain reaction (RT-PCR). Total RNA isolation was performed using an RNeasy Mini kit (Qiagen) according to the manufacturer's protocol. First-strand complementary DNA was synthesized from 500 ng of total RNA using random primers and 200 units/μl of Superscript II reverse transcriptase (Invitrogen). Quantitative PCR was performed on a 7300 Real-Time PCR system (Applied Biosystems). We used primer sequences to detect the genes for semaphorin 4A (SEMA4A) (Hs00223617_m1), SEMA4D (Hs00925667_m1), SEMA3A (Hs00173810_m1), SEMA3E (Hs00180842_m1), plexin D1 (PLXND1) (Hs00892410_m1), vascular endothelial growth factor A (VEGF-A) (Hs00900054_m1), vascular cell adhesion molecule 1 (VCAM-1) (Hs00365486_m1), intercellular adhesion molecule 1 (ICAM-1) (Hs00277001_m1), and neuropilin 1 (NRP-1) (Hs00826128_m1) (all inventoried by Applied Biosystems). Levels of messenger RNA (mRNA) were normalized to the levels of human HPRT1 (Hs99999909_m1) and GAPDH (Hs02786624_m1).

Western blot analysis. For Western blot analyses, 20 μg of protein was loaded onto 10% polyacrylamide gels, and then transferred to PVDF membranes (PerkinElmer Life Sciences). Membranes were blocked in 5% milk for 1 hour and immunoblotted with monoclonal or polyclonal antibodies directed against SEMA4A (R&D Systems), SEMA4D (Abcam), SEMA3A (Abcam), SEMA3E (Novus Biologicals), PLXND1 (Abcam), and

NRP-1 (Abcam) at a 1:1,000 dilution each or against SEMA3E (Novus Biologicals) at a 1:750 dilution. Protein bands were detected with Amersham ECL Prime Western blotting detection reagent (GE Healthcare Life Sciences). Signals from bands were quantified using Fusion FX7 system imaging (Vilber Lourmat).

Enzyme-linked immunosorbent assay (ELISA). Peripheral blood samples were obtained from patients for ELISA analyses, at the same time that blood was collected for routine analyses. The blood was stored in a Vacutainer tube and left undisturbed at room temperature, allowing for clot formation. Serum was obtained by centrifuging whole blood at 1,000–2,000*g* for 10 minutes in a refrigerated centrifuge. Serum concentrations of SEMA4A, SEMA4D, SEMA3A, and SEMA3E were measured by quantitative ELISAs (Cloud-Clone Corp [SEMA4A and SEMA4D] and Wuhan Fine Biotech [SEMA3A and SEMA3E]). Intraassay/interassay coefficients of variation, recovery, and linearity are provided for each marker in Supplementary Table 2, available on the *Arthritis & Rheumatology* website at http://onlinelibrary.wiley.com/doi/10.1002/art.41701/abstract.

Serum concentrations of VEGF, soluble TIE-2, angiopoietin 1, soluble VCAM-1, and interleukin-8 (IL-8; CXCL8) were measured in the discovery cohort by quantitative ELISAs (R&D Systems and RayBiotech) according to the manufacturer's recommendations, as previously described (19).

Immunohistochemical analysis. Paraffin-embedded synovial tissue sections were rehydrated, permeabilized, and stained overnight at 4°C, with primary antibodies directed against SEMA4A (R&D Systems), SEMA4D (Abcam), SEMA3A (Abcam), SEMA3E (Novus Biologicals), PLXND1 (Abcam), and NRP-1 (Abcam) at a 1:50 dilution each and against SEMA4D (Abcam) and NRP-1 (Abcam) at a 1:100 dilution each after antigen retrieval and blocking. Polyclonal antibodies (Dako) labeled with horseradish peroxidase were used as secondary antibodies for 1 hour at room temperature. Immunoreaction products were revealed using diaminobenzidine solution with the Liquid DAB+ Substrate Chromogen System (Dako). Samples were analyzed using the Lamina Multilabel Slides Scanner (PerkinElmer). The amount of immunoreactivity was quantified using ImageJ software (http://rsbweb.nih.gov/ij/docs/examples/stained-sections/index.html). Isotype controls for all immunohistochemistry stainings are shown in Supplementary Figure 1, available on the *Arthritis & Rheumatology* website at http://onlinelibrary.wiley.com/doi/10.1002/art.41701/abstract.

Immunofluorescence analysis. Paraffin-embedded synovial tissue sections obtained from RA patients and control subjects were rehydrated, permeabilized, and incubated after antigen retrieval and blocking with primary monoclonal antibodies directed against SEMA4A (R&D Systems), SEMA4D (Abcam), PLXND1 (Abcam), and NRP-1 (Abcam) at a dilution of 1:100 each and against SEMA3A (Abcam) and SEMA3E (Novus Biologicals) at a dilution of 1:50 each. Slides were then incubated with Alexa Fluor–conjugated secondary antibodies (Invitrogen) at a dilution of 1:200, and samples were analyzed using the Lamina Multilabel Slides Scanner (PerkinElmer).

Small interfering RNA (siRNA) transfection. Control siRNA (D-001810-10-05; On-Target Plus Non-Targeting Pool) or SEMA4A siRNA (L-015686-01-0005; On-Target Plus Human SEMA4A siRNA SMARTpool) (both On-Target Pools from Horizon Discovery) were used at a final concentration of 10 n*M*. RA ECs were transfected with siRNA successively on day 0 and day 1 using INTERFERin (Polyplus Transfection) according to the manufacturer's protocol. Forty-eight hours after PEC transfection, RNAs and proteins were extracted.

Assessment of tube formation. ECs were coated with 10 μl of Matrigel in an angiogenesis μ-Slide solution (ibidi) at a cell density of 10,000 cells per well. Tube formation was assessed at 2, 4, 6, and 8 hours by visual microscopy with an inverted microscope (Olympus). Different parameters of tube formation were analyzed by using the Angiogenesis analysis plug-in of Image J software.

Statistical analysis. Statistical analyses were conducted using GraphPad Prism 7.0a software. Unpaired *t*-tests were used to compare 2 different groups of samples. One-way analysis of variance with Tukey's multiple comparisons test was conducted to compare data among 3 or more independent groups. Spearman's rank correlation was used to summarize the strength and direction of the relationship between 2 variables.

RESULTS

Gene expression profiles of cultured ECs identifying a semaphorin signature in RA patients. Unsupervised analyses by hierarchical clustering was used to distinguish gene expression profiles between RA patients and healthy controls. Supervised analyses identified 879 differentially expressed genes in unstimulated RA ECs compared to cells obtained from healthy controls. In these genes, IPA revealed an enrichment of class 3, class 4, and class 5 semaphorins and their receptors in RA EPC-derived ECs (Supplementary Table 3, available on the *Arthritis & Rheumatology* website at http://onlinelibrary.wiley.com/doi/10.1002/art.41701/abstract). Semaphorins were then entered with a list of top differentially expressed genes and their upstream regulators, chosen according to their consistency score, resulting *P* values (<0.05), fold change, and IPA findings (Supplementary Table 4), into the biologic database STRING to construct a functional protein association network. This analysis revealed a cluster of genes centered by VEGF-A interacting with the semaphorin family (Supplementary Figure 2). We then selected the following 4 semaphorins and their receptors (SEMA3A, SEMA3E, SEMA4A, SEMA4D, NRP-1, and

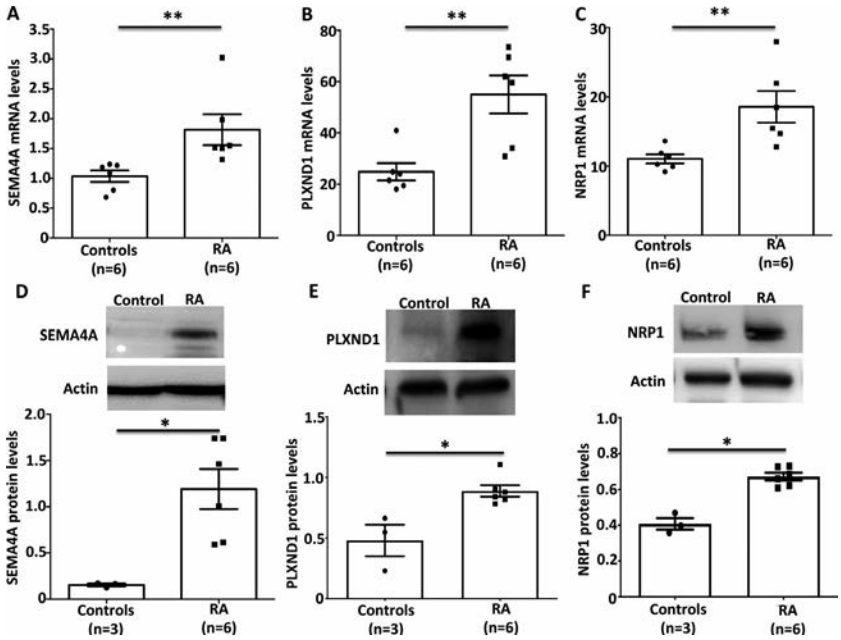

Figure 1. Expression of semaphorin 4A (SEMA4A) and its receptors in endothelial cells (ECs). **A**–**C**, Levels of SEMA4A (**A**), plexin D1 (PLXND1) (**B**), and neuropilin 1 (NRP-1) (**C**) mRNA, quantified by quantitative reverse transcription–polymerase chain reaction in rheumatoid arthritis (RA) and control ECs. **D**–**F**, Top, Western immunoblotting for (SEMA4A (**D**), PLXND1 (**E**), and NRP-1 (**F**) proteins in cell extracts from cultured RA ECs. Representative results are shown. Bottom, Quantification of the immunoblotting results in RA patients (n = 6) and healthy controls (n = 3). Symbols represent individual subjects; bars show the mean ± SEM. * = $P < 0.05$; ** = $P < 0.01$, by Student's *t*-test.

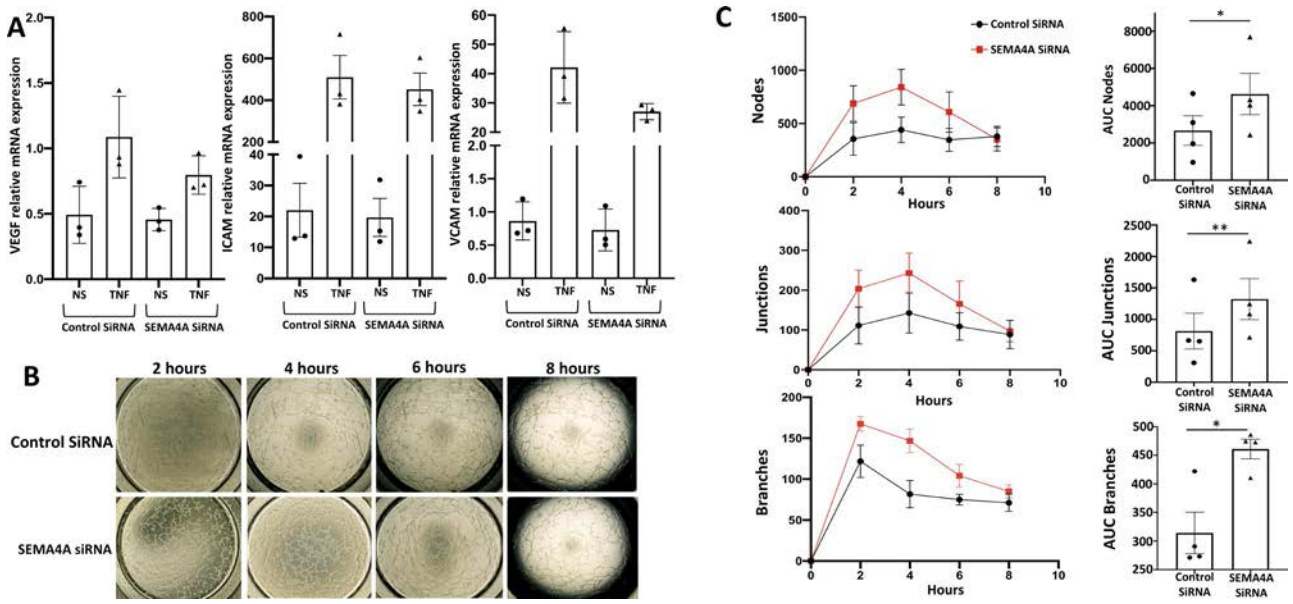

Figure 2. Effects of SEMA4A inhibition on angiogenic properties of ECs obtained from RA patients and transfected with SEMA4A small interfering RNA (siRNA). **A**, Levels of vascular endothelial growth factor (VEGF), intercellular adhesion molecule (ICAM), and vascular cell adhesion molecule (VCAM) mRNA expression, quantified by quantitative reverse transcription–polymerase chain reaction, in mock-transfected RA ECs (control siRNA) and SEMA4A-transfected RA ECs (SEMA4A siRNA) stimulated with 50 ng/ml of tumor necrosis factor (TNF) for 5 hours or left unstimulated (not stimulated [NS]). **B**, Representative images of tube formation at the indicated time points in mock-transfected and SEMA4A-transfected RA ECs. Original magnification × 4. **C**, Analysis of tube formation, measured as the number of nodes, junctions, and branches at the indicated time points in mock-transfected and SEMA4A-transfected RA ECs (left) and the area under the curve (AUC) for detection of tube formation using numbers of nodes, junctions, and branches in mock-transfected and SEMA4A-transfected RA ECs (right). In **A** and **C**, symbols represent individual subjects (n = 3 per group in **A**; n = 4 per group in **C**); bars show the mean ± SEM.* = P <0.05; ** = $P < 0.01$, by Student's *t*-test. See Figure 1 for other definitions. Color figure can be viewed in the online issue, which is available at http://onlinelibrary.wiley.com/doi/10.1002/art.41701/abstract.

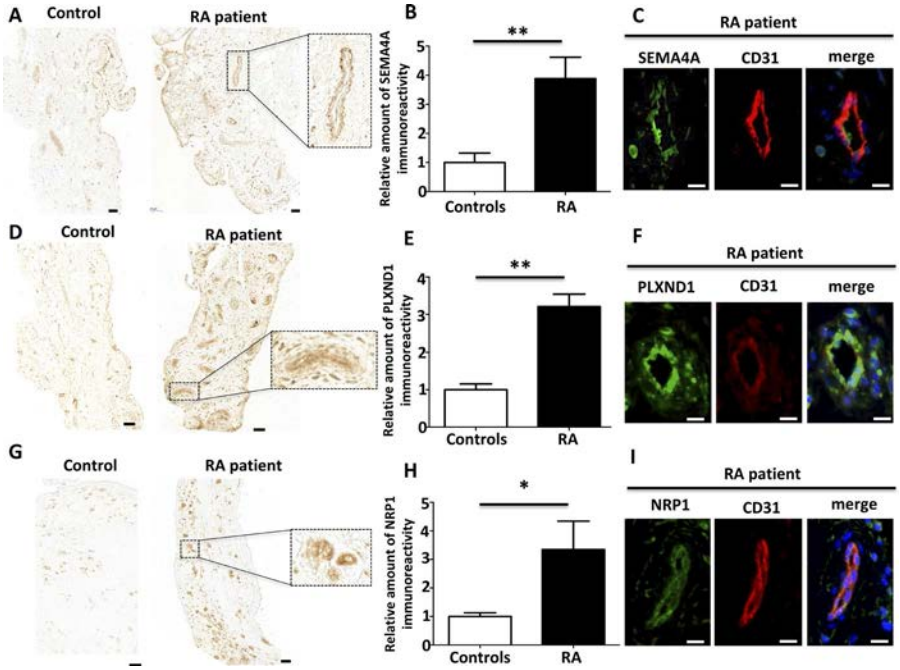

Figure 3. Synovial expression of SEMA4A and its receptors. **A**, **D**, and **G**, Representative immunohistochemical staining for SEMA4A (**A**), PLXND1 (**D**), and NRP-1 (**G**) in synovial tissue lesions from a patient with RA compared to synovial tissue from a healthy control. Bars = 50 μm. **Insets**, Higher-magnification views of the outlined areas. **B**, **E**, and **H**, Relative amount of immunoreactivity of SEMA4A (**B**), PLXND1 (**E**), and NRP1 (**H**) in ECs from 5 RA patients and 5 healthy controls, quantified using ImageJ software. Bars show the mean ± SEM. **C**, **F**, and **I**, Representative immunofluorescence staining for SEMA4A (**C**), PLXND1 (**F**), and NRP-1 (**I**) in ECs from a representative patient with RA. Bars = 20 μm. * = $P < 0.05$; ** = $P < 0.01$, by Student's *t*-test. See Figure 1 for definitions.

PLXND1) for further investigations of ECs, synovial tissue samples, and serum samples, based on a combination of *P* value (<0.05) and fold change (>1.5).

Increased expression of SEMA4A and its receptors in RA ECs. Quantitative RT-PCR confirmed a 1.75-fold increase in SEMA4A mRNA levels in unstimulated ECs from RA patients compared with controls ($P = 0.002$) (Figure 1A). Messenger RNA levels of the receptors PLXND1 (Figure 1B) and NRP-1 (Figure 1C) were also markedly increased by 2.21- and 1.68-fold in RA ECs compared to control cells ($P = 0.009$ and $P = 0.004$, respectively). The gene expression level of other semaphorins (SEMA3A, SEMA3E, and SEMA4D) was not significantly different between RA patients and controls (data not shown). In addition, the protein levels of SEMA4A and its receptors, NRP-1 and PLXND1, measured by Western blot analysis, were substantially increased in EC lysates obtained from RA patients when compared to those obtained from controls (Figures 1D–F).

SEMA4A is induced by TNF and displays both proangiogenic and antiangiogenic properties in RA ECs. Given the increased expression of SEMA4A in RA ECs, we next aimed to assess the regulation of its expression by inflammatory cytokines and its angiogenic properties in RA ECs. Messenger RNA levels of SEMA4A were increased by 209% following the stimulation of RA ECs with TNF ($P = 0.043$), but remained unchanged with IL-6 stimulation (Supplementary Figure 3 [http://onlinelibrary.wiley.com/doi/10.1002/art.41701/abstract]).

To assess whether decreased SEM4A expression may contribute to the angiogenic properties of RA ECs, we then transfected these cells with SEMA4A siRNA (Supplementary Figures 4A and B, available on the *Arthritis & Rheumatology* website at http://onlinelibrary.wiley.com/doi/10.1002/art.41701/abstract). RA ECs transfected with SEMA4A siRNA showed reduced sensitization to TNF. Indeed, the transfection of RA ECs with SEMA4A siRNA led to a 26% decrease in TNF-induced VEGF mRNA levels (Figure 2A). Consistent with this finding, SEMA4A knockdown resulted in an 11% and 35% reduction in TNF-dependent expression of the adhesion molecules ICAM-1 and VCAM-1, respectively (Figure 2A). Conversely, transfection of RA ECs with SEMA4A siRNA was associated with accelerated tube formation, with a higher number of nodes, junctions, and branches observed at 2, 4, and 6 hours (Figures 2B and C).

Synovial and circulating levels of semaphorins are elevated in patients with RA. A marked overexpression of SEMA4A (Figures 3A and B) and SEMA4D (Supplementary Figures 5A and B, available on the *Arthritis & Rheumatology* website at http://onlinelibrary.wiley.com/doi/10.1002/art.41701/abstract), SEMA3A (Supplementary Figures 5D and E), and SEMA3E (Supplementary Figures 5G and H) was observed in the synovial tissue of patients with RA, and the expression was prominent in immune cells and the vascular endothelium. Double labeling for CD31, as a marker

for vascular endothelium, and SEMA4A (Figure 3C), or SEMA4D (Supplementary Figure 5C), SEMA3A (Supplementary Figure 5F), or SEMA3E (Supplementary Figure 5I) confirmed endothelial expression of these semaphorins in lesional synovial tissue of RA patients. The expression of the receptors PLXND1 and NRP-1 was also strikingly increased in the synovial tissue of RA patients (Figures 3D, E, G, and H), and endothelial expression was confirmed by double labeling of these receptors with CD31 (Figures 3F and I).

After analysis of semaphorin expression in tissue samples, we assessed circulating levels of semaphorins in a cohort of 130 RA patients and 30 age and sex-matched controls. Levels of SEMA4A (mean ± SEM 65.92 ± 27.11 versus 51.16 ± 23.59 ng/ml; $P = 0.007$) (Figure 4A) and SEMA3E (1.21 ± 0.884 versus 0.78 ± 0.80 ng/ml; $P = 0.041$) (Figure 4D) were significantly increased in patients with RA compared to controls, and no difference was observed for SEMA4D (3.59 ± 7.39 versus 4.29 ± 10.19 ng/ml; $P = 0.331$) (Figure 4B). SEMA3A serum levels were markedly lower in patients with RA compared to control subjects (13.93 ± 5.69 versus 18.29 ± 6.69 ng/ml; $P < 0.001$) (Figure 4C).

Semaphorin levels correlate with validated markers of inflammation. *Class 4 semaphorins.* Serum levels of SEMA4A positively correlated with swollen joint count (r = 0.26, $P = 0.003$) (Figure 5A), global arthritis score assessed by PDUS (r = 0.21, $P = 0.030$) (Figure 5B), and CRP levels (r = 0.34, $P < 0.001$) (Figure 5C). Levels of SEMA4A positively correlated with DAS28 scores (r = 0.19, $P = 0.039$) (Figure 5D) and DAS28-CRP scores (r = 0.25, $P = 0.005$) (Figure 5F). Indeed, RA patients

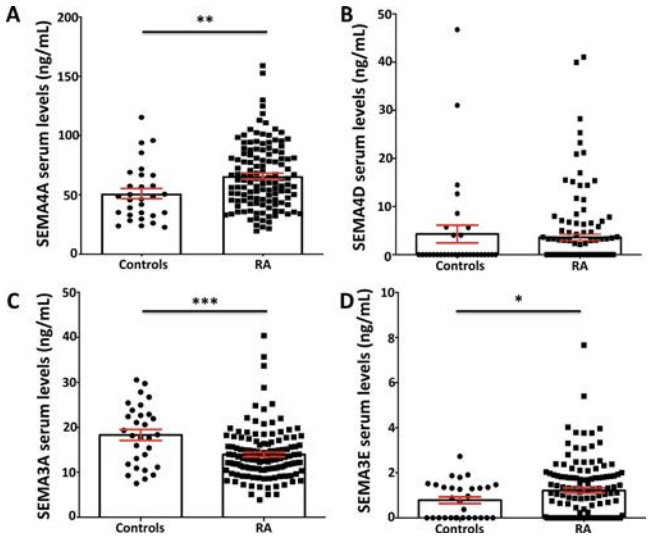

Figure 4. Serum concentrations of SEMA4A (**A**), SEMA4D (**B**), SEMA3A (**C**), and SEMA3E (**D**) in 30 healthy controls and 130 patients with RA from the discovery cohort. Symbols represent individual subjects; open bars indicate the mean, and the joined horizontal red lines show the SEM. * = $P < 0.05$; ** = $P < 0.01$; *** = $P < 0.001$, by Student's *t*-test. See Figure 1 for definitions. Color figure can be viewed in the online issue, which is available at http://onlinelibrary.wiley.com/doi/10.1002/art.41701/abstract.

with high disease activity, which was defined by a DAS28 or a DAS28-CRP score of >5.1, had increased serum concentrations of SEMA4A when compared to RA patients with moderate or low disease activity (Figure 5E and G). The diagnostic value of SEMA4A identifying patients with an "inflammatory profile" was defined by a sensitivity of 67%, a specificity of 89%, and an area under the curve (AUC) of 0.80 ($P < 0.001$), with 12 patients characterized as having an "inflammatory profile" who each had a DAS28 score of >3.2, CRP level of >10 mg/liter, and a global arthritis score assessed by PDUS of >7 (Figure 5H).

SEMA4D serum levels inversely correlated with global arthritis score assessed by PDUS (r = –0.24, $P = 0.013$) (Supplementary Figure 6A, available on the *Arthritis & Rheumatology* website at http://onlinelibrary.wiley.com/doi/10.1002/art.41701/abstract) and CRP levels (r = –0.24, $P = 0.005$) (Supplementary Figure 6B). Serum levels of SEMA4D inversely correlated with DAS28 scores (r = –0.21, $P = 0.017$) (Supplementary Figure 6C) and DAS28-CRP scores (r = –0.23, $P = 0.010$) (Supplementary Figure 6E). Patients with high disease activity (a DAS28 or a DAS28-CRP score of >5.1) were more likely to have decreased serum levels of SEMA4D (Supplementary Figures 6D and F).

Serum levels of SEMA4A were significantly decreased in patients treated with targeted biologic therapies compared to patients treated with conventional synthetic DMARDs only, independently of disease activity (Supplementary Figure 7A, available on the Arthritis & Rheumatology website at http://onlinelibrary.wiley.com/doi/10.1002/art.41701/abstract). Conversely, serum levels of SEMA4D were significantly increased in patients receiving targeted biologic therapies, especially in patients with low disease activity or disease in remission (DAS28 of ≤3.2) (Supplementary Figure 7B).

Class 3 semaphorins. Serum levels of SEMA3A inversely correlated with global arthritis scores assessed by PDUS (r = –0.22, $P = 0.022$), CRP levels (r = –0.22, $P = 0.012$), and with DAS28 scores (r = –0.18, $P = 0.042$). No correlation was observed between serum levels of SEMA3E and markers of inflammation.

Utility of semaphorins in detecting residual disease activity in patients with RA in remission or low disease activity. *Discovery cohort (Paris).* In the subset of 56 patients with RA in remission or low disease activity as defined by a DAS28 score of <3.2, serum levels of SEMA4A positively correlated with swollen joint counts (r = 0.40, $P = 0.002$) and DAS28-CRP score (r = 0.21, $P = 0.022$). Expression levels of SEMA4A and SEMA4D identified patients with infraclinical residual disease activity, defined by the persistence of synovial hyperemia detected in at least 1 joint, with a sensitivity of 57% and 78%, a specificity of 81% and 68%, and an AUC of 0.70 and 0.71 ($P = 0.008$ and $P = 0.012$) for SEMA4A and SEMA4D, respectively (Figure 5I and Supplementary Figure 6G).

Replication cohort (Montpellier). Semaphorin concentrations obtained in the replication cohort, which included 70 patients with RA in remission or low disease activity, are

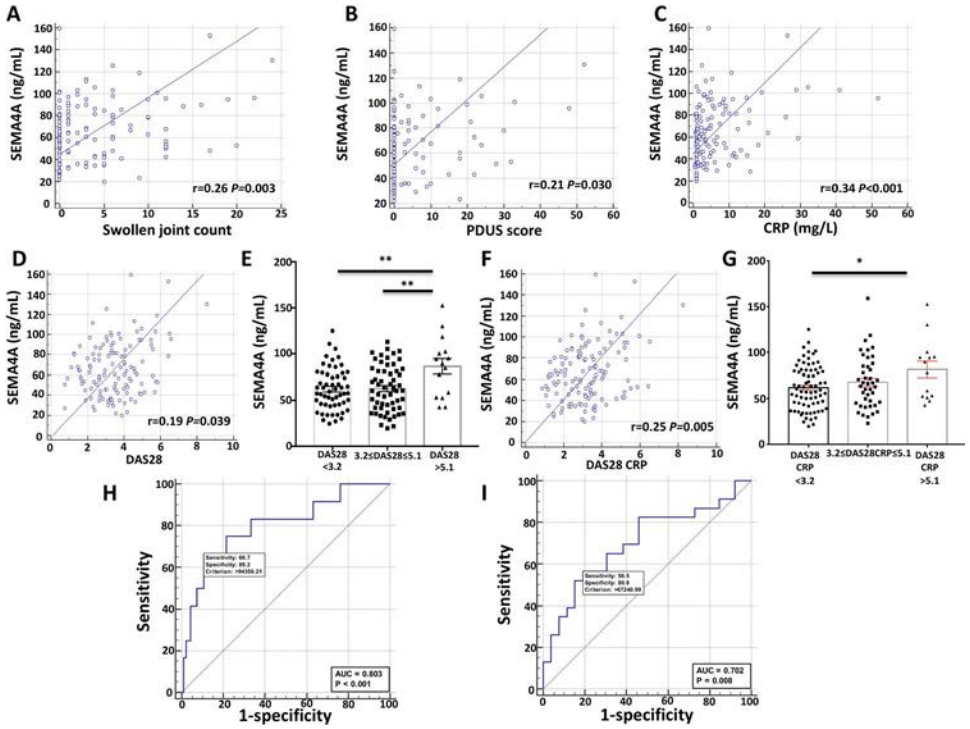

Figure 5. Correlation of semaphorin 4A (SEMA4A) serum concentrations with validated markers of disease activity. **A**–**D** and **F**, Correlations between serum levels of SEMA4A and swollen joint count (**A**), global arthritis score assessed by power Doppler ultrasonography (PDUS) (**B**), C-reactive protein (CRP) level (**C**), Disease Activity Score in 28 joints (DAS28) (**D**), and the DAS28 using the CRP level (DAS28-CRP) (**F**). **E** and **G**, Serum levels of SEMA4A in patients stratified by categories of scores on the DAS28 (**E**) and DAS28-CRP (**G**). **H**, Receiver operating characteristic (ROC) curve illustrating the diagnostic value of SEMA4A for the identification of patients with an "inflammatory profile" (n = 12 patients with a DAS28 score of >3.2, a CRP level of >10 mg/liter, and a global arthritis score of >7 assessed by PDUS). A global synovitis score of >7 corresponded to the 75th percentile value, and this cutoff provided the best sensitivity and specificity for active disease, as defined by a DAS28 score of >5.1. **I**, ROC curve illustrating the diagnostic value of SEMA4A for the identification of patients with persistence of synovial hyperemia detected in >1 joint. In **E** and **G**, symbols represent individual subjects; open bars indicate the mean, and the joined horizontal black or red lines show the SEM. * = $P < 0.05$; ** = $P < 0.01$, by Spearman's rank correlation test in **A**–**D** and **F**; by analysis of variance with Tukey's post hoc test for multiple comparisons in **E** and **G**. Color figure can be viewed in the online issue, which is available at http://onlinelibrary.wiley.com/doi/10.1002/art.41701/abstract.

presented in Supplementary Table 5 [http://onlinelibrary.wiley.com/doi/10.1002/art.41701/abstract]. A correlation was observed between baseline DAS28-CRP score and serum concentrations of SEMA4A (r = 0.24; $P = 0.004$). No association was seen between SEMA4A levels and the persistence of synovial hyperemia. In addition, SEMA4A levels were significantly higher at baseline in the 14 patients who did not maintain sustained remission during 12 months of follow-up as compared to patients who maintained sustained remission (DAS28 of <2.6) (mean ± SD 72.67 ± 25.59 ng/ml versus 59.63 ± 19.92 ng/ml; $P = 0.002$). Analysis of SEMA4D expression did not detect residual disease activity in the replication cohort, and analysis of SEMA3A or SEMA3E expression did not detect residual disease activity in either cohort.

Semaphorin levels correlate with validated markers of angiogenesis. In the Paris cohort, expression of SEMA4A positively correlated with serum levels of the proangiogenic markers VEGF (r = 0.19, $P = 0.042$), soluble TIE-2 (r = 0.19, $P = 0.046$), and IL-8 (r = 0.30, $P = 0.002$). Expression of SEMA3E only correlated with serum levels of soluble VCAM (r = 0.21, $P = 0.033$) (Supplementary Table 6 [http://onlinelibrary.wiley.com/doi/10.1002/art.41701/abstract]). No correlation with angiogenic markers was detected for SEMA4D or SEMA3A expression.

DISCUSSION

Semaphorins were originally identified as neural guidance molecules that lead neuronal axons to their appropriate targets (20). Since their initial characterization, however, the results of myriad studies have demonstrated that semaphorins, through interactions with their receptors, plexins and neuropilins, function in many physiologic and pathologic processes beyond neuronal guidance (11,21). Recently, the implication of semaphorins in the pathology of RA has been investigated, with class 3 being the most studied semaphorin family. However, their specific contribution in synovial neoangiogenesis has not yet been evaluated.

Our results provide the first experimental evidence of a transcriptional semaphorin signature in RA ECs, which, given the implication of this family in inflammation and angiogenesis, may

contribute to the activated and proangiogenic profile of these cells as recently described (22). Messenger RNA and protein levels of SEMA4A, PLXND1, and NRP1 were significantly increased in RA ECs and were overexpressed in the lesional tissue obtained from patients with RA, with prominent expression in the vascular endothelium. This finding is consistent with a previous observation by Wang et al of increased SEMA4A mRNA levels in the synovial tissue of RA patients, though Wang and colleagues did not conduct an analysis of SEMA4A-expressing cells (23). The present study provides insight about the function of SEMA4A in RA ECs. The precise role of SEMA4A in angiogenesis is considered a subject of controversy, as recent studies demonstrated either proangiogenic or antiangiogenic SEMA4A effects depending on the experimental settings (24), which is consistent with our findings. Indeed, SEMA4A invalidation was associated with increased tube formation in RA ECs, this antiangiogenic property being consistent with the previous description of a SEMA4A-induced suppression of VEGF-mediated EC migration and proliferation (25). Conversely, SEMA4A invalidation led to decreased mRNA levels of VEGF in RA ECs, which is consistent with the previous description of enhanced VEGF production by the SEMA4A–PLXND1 axis in different cell types (26).

In addition to EC and synovial tissue overexpression, we showed for the first time markedly increased serum SEMA4A concentrations in patients with RA. This finding is consistent with the Sema4A overexpression observed in the synovial fluid from a small group of 12 RA patients compared to a group of 12 osteoarthritis patients (23). Serum levels of SEMA4A correlated with multiple clinical, biologic, and PDUS markers of disease activity and angiogenesis, including the DAS28 and DAS28-CRP composite scores, which is consistent with the previously reported correlation between the presence of SEMA4A in synovial fluid and DAS28 scores that was observed in 12 RA patients (23). Beyond its potential implication in angiogenesis, SEMA4A may be directly implicated in the inflammatory process of the disease by its dual action on RA fibroblast-like synoviocytes (FLS). Indeed, SEMA4A was shown to induce IL-6 expression by RA FLS and to enhance the invasive ability of RA FLS by promoting the plexin D1–dependent expression of matrix metalloproteinase 3 (MMP-3) and MMP-9. In addition, autocrine Sema4A-plexin D1 signaling has been shown to act as a negative regulator of Th1 skewing and, conversely, as a key mediator in Th2 and Th17 differentiation (27).

We also demonstrate for the first time in 2 independent cohorts that SEMA4A may be a relevant marker of residual clinical disease activity and persistent synovial hyperemia in patients with disease in remission or patients with low disease activity, which is of importance to the clinician for the identification of patients who need continued treatment, as well as patients with disease activity in stringent clinical and infraclinical remission who would be candidates for treatment reduction.

SEMA4D, SEMA3A, and SEMA3E were also differentially expressed in the synovial tissue and/or in the serum of RA patients. SEMA4D has also been implicated in the pathogenesis of RA (28), and this semaphorin is thought to exacerbate the inflammatory responses of patients with RA via a positive feedback loop involving soluble SEMA4D, proinflammatory cytokines (IL-6 and TNF), and ADAMTS4. Treatment with an anti–SEMA4D antibody also prevented the development of arthritis in a collagen-induced arthritis mouse model (28). Negative correlations were observed between levels of SEMA4D and different markers of disease activity, which is in contrast to findings from a previous study that showed a positive correlation between serum levels of Sema4D and DAS28 scores (28). This discrepancy was not explained by the clinical characteristics of patients included in both studies, which were very similar. Opposite effects of SEMA4A and SEMA4D on properties of human umbilical vein ECs have been reported, although these 2 semaphorins share the PLXND1 receptor, suggesting potential competition for receptor binding between 2 semaphorins. This finding is supported by our data, which showed that markers of disease activity correlated positively with SEMA4A and negatively with SEMA4D and also demonstrated a significant reduction in serum concentrations of SEMA4A upon treatment with targeted biologic agents, contrasting with a significant increase in SEMA4D under the same conditions.

Discordant data have been reported regarding the expression and role of SEMA3A in RA. Decreased expression of SEMA3A has been shown to correlate with disease activity and the presence of histologic features of RA (29), which contrasts with the description of increased expression of Sema3A in RA patients, and has been shown to have a positive correlation with inflammatory factors, autoantibody production, and bone destruction (30). SEMA3A has been shown to induce the migration and invasive capacity of FLS (31), contrasting with the reduction in inflammation and progression of experimental autoimmune arthritis resulting from the administration of plasmid DNA encoding SEMA3A (32). Our data support a tissue specificity of SEMA3A expression, the levels of which are reduced in the serum of patients with RA, showing a correlation with markers of disease activity and an association with increased synovial tissue expression in patients with RA. SEMA3E has not yet been implicated in the pathogenesis of RA, whereas in other autoimmune diseases, including systemic sclerosis, overexpression of semaphorins has been observed in the skin and serum of patients (11).

In conclusion, gene expression profiling of ECs revealed semaphorins as potential biomarkers and therapeutic candidates in RA, and validation of their use as biomarkers in larger prospective cohorts is needed. More importantly, semaphorins contribute to complementary processes involved in the pathogenesis of RA. Therefore, targeting semaphorins might be a novel and appealing inflammatory and proangiogenic target in RA.

ACKNOWLEDGMENTS

We would like to thank Franck Lerourneur, Florent Dumont, and Sébastien Jacques for assistance with sequencing and the genomics

platforms, M. Favier for assistance with morphologic and histologic analyses, and P. Bourdoncle for help with cell imaging (INSERM U1016 and CNRS UMR8104, Institut Cochin, Paris, France).

AUTHOR CONTRIBUTIONS

All authors were involved in drafting the article or revising it critically for important intellectual content, and all authors approved the final version to be published. Dr. Avouac had full access to all the study data and takes responsibility for the integrity of the data and the accuracy of the data analysis.

Study conception and design. Avouac, Allanore.

Acquisition of data. Pezet, Vandebeuque, Orvain, Gonzalez.

Analysis and/or interpretation of data. Avouac, Pezet, Vandebeuque, Orvain, Marin, Mouterde, Daïen, Allanore.

REFERENCES

1. Leblond A, Allanore Y, Avouac J. Targeting synovial neoangiogenesis in rheumatoid arthritis [review]. Autoimmun Rev 2017;16:594–601.
2. Elshabrawy HA, Chen Z, Volin MV, Ravella S, Virupannavar S, Shahrara S. The pathogenic role of angiogenesis in rheumatoid arthritis. Angiogenesis 2015;18:433–48.
3. Szade A, Grochot-Przeczek A, Florczyk U, Jozkowicz A, Dulak J. Cellular and molecular mechanisms of inflammation-induced angiogenesis [review]. IUBMB Life 2015;67:145–59.
4. Szekanecz Z, Koch AE. Mechanisms of disease: angiogenesis in inflammatory diseases [review]. Nat Clin Pract Rheumatol 2007;3:635–43.
5. Riesner K, Shi Y, Jacobi A, Krater M, Kalupa M, McGearey A, et al. Initiation of acute graft-versus-host disease by angiogenesis. Blood 2017;129:2021–32.
6. Fries JF, Bloch DA. Mortality in rheumatoid arthritis patients [letter]. Ann Rheum Dis 1999;58:723–4.
7. Avouac J, Wipff J, Goldman O, Ruiz B, Couraud PO, Chiocchia G, et al. Angiogenesis in systemic sclerosis: impaired expression of vascular endothelial growth factor receptor 1 in endothelial progenitor–derived cells under hypoxic conditions. Arthritis Rheum 2008;58:3550–61.
8. Avouac J, Guignabert C, Hoffmann-Vold AM, Ruiz B, Dorfmuller P, Pezet S, et al. Role of stromelysin 2 (matrix metalloproteinase 10) as a novel mediator of vascular remodeling underlying pulmonary hypertension associated with systemic sclerosis. Arthritis Rheumatol 2017;69:2209–21.
9. Avouac J, Cagnard N, Distler JH, Schoindre Y, Ruiz B, Couraud PO, et al. Insights into the pathogenesis of systemic sclerosis based on the gene expression profile of progenitor-derived endothelial cells. Arthritis Rheum 2011;63:3552–62.
10. Kuwana M, Okazaki Y. Impaired in vivo neovascularization capacity of endothelial progenitor cells in patients with systemic sclerosis. Arthritis Rheumatol 2014;66:1300–5.
11. Nishide M, Kumanogoh A. The role of semaphorins in immune responses and autoimmune rheumatic diseases [review]. Nat Rev Rheumatol 2018;14:19–31.
12. Arnett FC, Edworthy SM, Bloch DA, McShane DJ, Fries JF, Cooper NS, et al. The American Rheumatism Association 1987 revised criteria for the classification of rheumatoid arthritis. Arthritis Rheum 1988;31:315–24.
13. Aletaha D, Neogi T, Silman AJ, Funovits J, Felson DT, Bingham CO III, et al. 2010 rheumatoid arthritis classification criteria: an American College of Rheumatology/European League Against Rheumatism collaborative initiative. Arthritis Rheum 2010;62:2569–81.
14. Van der Heijde DM, van 't Hof MA, van Riel PL, Theunisse LA, Lubberts EW, van Leeuwen MA, et al. Judging disease activity in clinical practice in rheumatoid arthritis: first step in the development of a disease activity score. Ann Rheum Dis 1990;49:916–20.
15. Avouac J, Meune C, Chenevier-Gobeaux C, Dieude P, Borderie D, Lefevre G, et al. Inflammation and disease activity are associated with high circulating cardiac markers in rheumatoid arthritis independently of traditional cardiovascular risk factors. J Rheumatol 2014;41:248–55.
16. Backhaus M, Burmester GR, Gerber T, Grassi W, Machold KP, Swen WA, et al. Guidelines for musculoskeletal ultrasound in rheumatology. Ann Rheum Dis 2001;60:641–9.
17. D'Agostino MA, Terslev L, Aegerter P, Backhaus M, Balint P, Bruyn GA, et al. Scoring ultrasound synovitis in rheumatoid arthritis: a EULAR-OMERACT ultrasound taskforce. Part 1. Definition and development of a standardised, consensus-based scoring system. RMD Open 2017;3:e000428.
18. D'Agostino MA, Boers M, Wakefield RJ, Hammer HB, Vittecoq O, Filippou G, et al. Exploring a new ultrasound score as a clinical predictive tool in patients with rheumatoid arthritis starting abatacept: results from the APPRAISE study. RMD Open 2016;2:e000237.
19. Leblond A, Pezet S, Trouvin AP, Elhai M, Gonzalez V, Allanore Y, et al. Linking systemic angiogenic markers to synovial vascularization in rheumatoid arthritis. PLoS One 2018;13:e0203607.
20. Kolodkin AL, Matthes DJ, Goodman CS. The semaphorin genes encode a family of transmembrane and secreted growth cone guidance molecules. Cell 1993;75:1389–99.
21. Gu C, Giraudo E. The role of semaphorins and their receptors in vascular development and cancer. Exp Cell Res 2013;319:1306–16.
22. Leblond A, Pezet S, Cauvet A, Casas C, Da Silva JP, Herve R, et al. Implication of the deacetylase sirtuin-1 on synovial angiogenesis and persistence of experimental arthritis. Ann Rheum Dis 2020;79:891–900.
23. Wang L, Song G, Zheng Y, Tan W, Pan J, Zhao Y, et al. Expression of semaphorin 4A and its potential role in rheumatoid arthritis. Arthritis Res Ther 2015;17:227.
24. Iyer AS, Chapoval SP. Neuroimmune semaphorin 4A in cancer angiogenesis and inflammation: a promoter or a suppressor? [review]. Int J Mol Sci 2018;20:124.
25. Toyofuku T, Yabuki M, Kamei J, Kamei M, Makino N, Kumanogoh A, et al. Semaphorin-4A, an activator for T-cell-mediated immunity, suppresses angiogenesis via Plexin-D1. EMBO J 2007;26:1373–84.
26. Meda C, Molla F, De Pizzol M, Regano D, Maione F, Capano S, et al. Semaphorin 4A exerts a proangiogenic effect by enhancing vascular endothelial growth factor-A expression in macrophages. J Immunol 2012;188:4081–92.
27. Carvalheiro T, Rafael-Vidal C, Malvar-Fernandez B, Lopes AP, Pego-Reigosa JM, Radstake T, et al. Semaphorin4A-plexin D1 axis induces Th2 and Th17 while represses Th1 skewing in an autocrine manner. Int J Mol Sci 2020;21:6965.
28. Yoshida Y, Ogata A, Kang S, Ebina K, Shi K, Nojima S, et al. Semaphorin 4D contributes to rheumatoid arthritis by inducing inflammatory cytokine production: pathogenic and therapeutic implications. Arthritis Rheumatol 2015;67:1481–90.
29. Takagawa S, Nakamura F, Kumagai K, Nagashima Y, Goshima Y, Saito T. Decreased semaphorin3A expression correlates with disease activity and histological features of rheumatoid arthritis. BMC Musculoskelet Disord 2013;14:40.
30. Gao H, Ma XX, Guo Q, Xie LF, Zhong YC, Zhang XW. Expression of circulating Semaphorin3A and its association with inflammation and bone destruction in rheumatoid arthritis. Clin Rheumatol 2018;37:2073–80.
31. Tang MW, Fernandez BM, Newsom SP, van Buul JD, Radstake T, Baeten DL, et al. Class 3 semaphorins modulate the invasive capacity of rheumatoid arthritis fibroblast-like synoviocytes. Rheumatology (Oxford) 2018;57:909–20.
32. Catalano A. The neuroimmune semaphorin-3A reduces inflammation and progression of experimental autoimmune arthritis. J Immunol 2010;185:6373–83.

Arthritis & Rheumatology
Vol. 73, No. 9, September 2021, pp 1589–1600
DOI 10.1002/art.41803

American College of Rheumatology
Empowering Rheumatology Professionals

Cardiovascular Safety of Hydroxychloroquine in US Veterans With Rheumatoid Arthritis

Charles Faselis,[1] Qing Zeng-Treitler,[2] Yan Cheng,[2] Gail S. Kerr,[3] David J. Nashel,[4] Angelike P. Liappis,[1] Amy C. Weintrob,[2] Pamela E. Karasik,[5] Cherinne Arundel,[1] Denise Boehm,[6] Michael S. Heimall,[6] Lawrence B. Connell,[7] Daniel D. Taub,[2] Yijun Shao,[2] Douglas F. Redd,[†] Helen M. Sheriff,[2] Sijian Zhang,[6] Ross D. Fletcher,[6] Gregg C. Fonarow,[8] Hans J. Moore,[9] and Ali Ahmed[10]

Objective. Hydroxychloroquine (HCQ) may prolong the QT interval, a risk factor for torsade de pointes, a potentially fatal ventricular arrhythmia. This study was undertaken to examine the cardiovascular safety of HCQ in patients with rheumatoid arthritis (RA).

Methods. We conducted an active comparator safety study of HCQ in a propensity score–matched cohort of 8,852 US veterans newly diagnosed as having RA between October 1, 2001 and December 31, 2017. Patients were started on HCQ (n = 4,426) or another nonbiologic disease-modifying antirheumatic drug (DMARD; n = 4,426) after RA diagnosis, up to December 31, 2018, and followed up for 12 months after therapy initiation, up to December 31, 2019.

Results. Patients had a mean ± SD age of 64 ± 12 years, 14% were women, and 28% were African American. The treatment groups were balanced with regard to 87 baseline characteristics. There were 3 long QT syndrome events (0.03%), 2 of which occurred in patients receiving HCQ. Of the 56 arrhythmia-related hospitalizations (0.63%), 30 occurred in patients in the HCQ group (hazard ratio [HR] associated with HCQ 1.16 [95% confidence interval (95% CI) 0.68–1.95]). All-cause mortality occurred in 144 (3.25%) and 136 (3.07%) of the patients in the HCQ and non-HCQ groups, respectively (HR associated with HCQ 1.06 [95% CI, 0.84–1.34]). During the first 30 days of follow-up, there were no long QT syndrome events, 2 arrhythmia-related hospitalizations (none in the HCQ group), and 13 deaths (6 in the HCQ group).

Conclusion. Our findings indicate that the incidence of long QT syndrome and arrhythmia-related hospitalization is low in patients with RA during the first year after the initiation of HCQ or another nonbiologic DMARD. We found no evidence that HCQ therapy is associated with a higher risk of adverse cardiovascular events or death.

INTRODUCTION

Hydroxychloroquine (HCQ) may prolong the QT interval, which in turn may increase the risk of torsade de pointes arrhythmias and sudden cardiac death (1). The evidence supporting this effect of HCQ in humans is primarily derived from occasional case reports (1). Chloroquine, the parent drug of HCQ and an antimalarial drug, is prescribed annually to several hundred million individuals worldwide without any surveillance reports of sudden unexpected death associated with its use (2).

The content of this article is solely the responsibility of the authors and does not necessarily represent the official views of the US Department of Veterans Affairs.

Dr. Ahmed's work was supported in part by the US Department of Veterans Affairs Office of Research and Development (grant IIR 17-095 from the Health Services Research and Development Service).

[1]Charles Faselis, MD, Angelike P. Liappis, MD, Cherinne Arundel, MD: Washington DC VA Medical Center, George Washington University, and Uniformed Services University, Washington, DC; [2]Qing Zeng-Treitler, PhD, Yan Cheng, PhD, Amy C. Weintrob, MD, Daniel D. Taub, PhD, Yijun Shao, PhD, Helen M. Sheriff, MD: Washington DC VA Medical Center and George Washington University, Washington, DC; [3]Gail S. Kerr, MD: Washington DC VA Medical Center, Georgetown University, and Howard University, Washington, DC; [4]David J. Nashel, MD: Washington DC VA Medical Center and Georgetown University, Washington, DC; [5]Pamela E. Karasik, MD: Washington DC VA Medical Center, Georgetown University, George Washington University, and Uniformed Services University, Washington, DC; [6]Denise Boehm, RN, Michael S. Heimall, MHA, MSS, FACHE, Sijian Zhang, MB, MS, MPH, Ross D. Fletcher, MD: Washington DC VA Medical Center, Washington, DC; [7]Lawrence B. Connell, MS: Providence VA Medical Center, Providence, Rhode Island; [8]Gregg C. Fonarow, MD: University of California, Los Angeles; [9]Hans J. Moore, MD: Washington DC VA Medical Center, George Washington University, Uniformed Services University, Georgetown University, and US Department of Veterans Affairs, Washington, DC; [10]Ali Ahmed, MD, MPH: Washington DC VA Medical Center, George Washington University, and Georgetown University, Washington, DC.

[†]Dr. Redd is deceased.

Drs. Faselis and Zeng-Treitler contributed equally to this work.

Dr. Fonarow has received consulting fees from Abbott, Amgen, AstraZeneca, Bayer, Edwards, Janssen, Medtronic, and Merck (less than $10,000 each) and from Novartis (greater than $10,000). No other disclosures relevant to this article were reported.

Address correspondence to Charles Faselis, MD, or Ali Ahmed, MD, MPH, Washington DC VA Medical Center, 50 Irving Street NW, Washington, DC 20422. Email: charles.faselis@va.gov or ali.ahmed@va.gov.

Submitted for publication July 27, 2020; accepted in revised form May 4, 2021.

However, controversies surrounding the now-revoked brief authorization for the limited, unapproved use of HCQ in patients with COVID-19 early in the pandemic have renewed concerns about its adverse cardiovascular effects (1,3). These concerns were further heightened by observational studies that suggested a higher risk of adverse cardiovascular events and mortality associated with HCQ use in hospitalized patients with COVID-19 (4–7). Because patients with rheumatic diseases are often treated with HCQ, they have been most affected by these controversies and concerns (8,9). The objective of the present study was to examine the cardiovascular safety of HCQ in US veterans with rheumatoid arthritis (RA) before the COVID-19 pandemic, emulating the design of a randomized controlled trial (RCT) (10).

PATIENTS AND METHODS

Data source. We used data from the US Department of Veterans Affairs (VA) national electronic health record archived by the Corporate Data Warehouse (CDW) and available via the VA Informatics and Computing Infrastructure workspace. These data sets contain extensive baseline and longitudinal information on demographic characteristics, clinical characteristics, treatment, and outcomes for >25 million veterans starting October 1, 1999. To ensure that a patient was a user of the VA health care system, we required each patient to have an outpatient health care visit to a VA medical facility in the 24 months prior to enrollment in the study. The study was exempted from review by the Institutional Review Board and approved by the Research and Development Committee of the Washington DC VA Medical Center.

RCT emulation. *Study population eligibility.* An RCT of HCQ in patients with RA will enroll patients with RA diagnosed by physical examination and laboratory markers such as rheumatoid factor (RF) and anti–citrullinated protein antibody (ACPA). To mimic that design, we identified all veterans in the VA CDW database between ages 18 and 100 years who had new International Classification of Diseases, Ninth Revision, Clinical Modification (ICD-9-CM) or ICD-10-CM codes of 714.0 or M05.9, respectively, for RA at ≥2 visits separated by ≥7 days between October 1, 2001 and December 31, 2017. RA was considered newly diagnosed if there was no record of ICD codes for RA in the 24 months preceding the first mention. We began our enrollment on October 1, 2001 to allow a 24-month window to verify prior RA from the CDW start date of October 1, 1999. This process yielded a total of 79,888 unique veterans with at least 2 instances of ICD codes for RA in their medical records (Figure 1).

We required these patients to have filled ≥1 prescription for a disease-modifying antirheumatic drug (DMARD), including HCQ, after the initial instance of ICD codes for RA. The addition of DMARD use to ICD codes in the algorithms for the diagnosis of RA has been shown to improve positive predictive value (11).

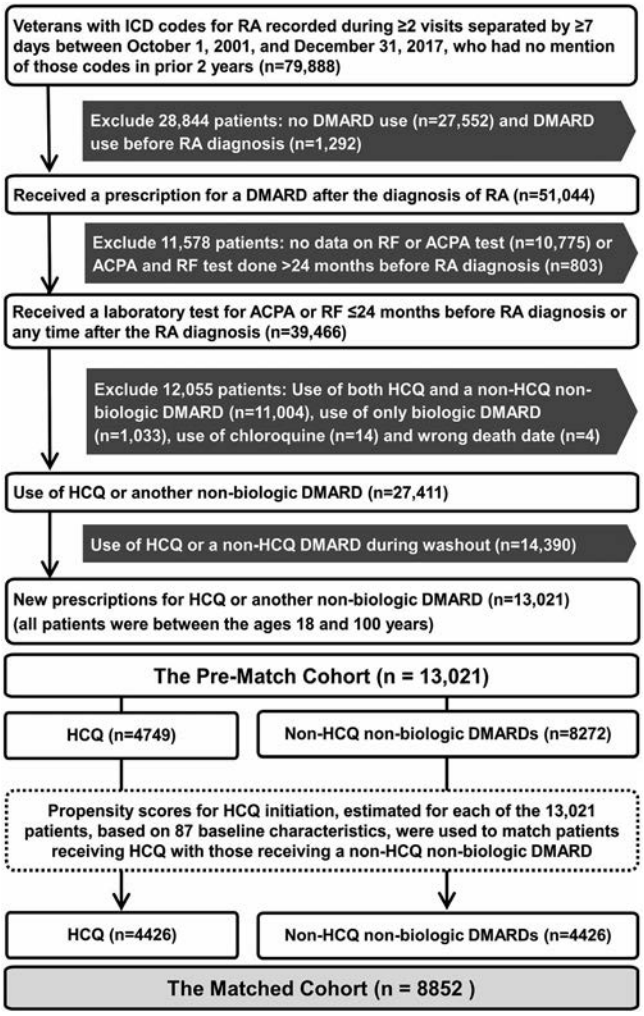

Figure 1. Flow chart showing the assembly of a matched cohort of US veterans newly diagnosed as having rheumatoid arthritis (RA) and started on hydroxychloroquine (HCQ) or another nonbiologic disease-modifying antirheumatic drug (DMARD). International Classification of Diseases, Ninth Revision, Clinical Modification (ICD-9-CM) code 714.0 and ICD-10-CM code M05.9 were used to identify US veterans with RA. RF = rheumatoid factor; ACPA = anti–citrullinated protein antibody.

Thus, we excluded 28,844 patients who never received a prescription for DMARDs (n = 27,552) or received one before the first ICD code for RA diagnosis was recorded (n = 1,292) (Figure 1). We then required every patient to have laboratory documentation of a test for either RF or ACPA done after the diagnosis of RA or within 24 months before the diagnosis. We excluded 11,578 patients who did not meet these criteria (Figure 1).

Active-comparator new-user design. Observational studies that compare prevalent users of a drug with nonusers of the drug are often confounded by selection and indication biases (10,12,13). These biases can be attenuated by using an active-comparator new-user design in which new users of a drug are compared with new users of another drug with a similar indication (13). Findings from observational studies based on a new-user

design have been shown to approximate those from RCTs (14,15). We used non-HCQ nonbiologic DMARDs as active comparators in the present study, since these drugs are often prescribed for the same indication as HCQ. Information about these drugs was obtained from VA CDW pharmacy files that contain detailed data on all prescription drugs (16). As such, from the cohort of 39,466 patients with ICD codes for RA who received DMARDs and were tested for ACPA or RF, we selected 27,411 patients who received a prescription for either HCQ or a non-HCQ nonbiologic DMARD after RA diagnosis, up to December 31, 2018 (Figure 1). We limited treatment initiation to December 31, 2018, to allow all patients to have a minimum follow-up of 12 months, up to December 31, 2019.

We then assembled a cohort of new users of HCQ or non-HCQ nonbiologic DMARDs by excluding patients who received prescriptions for these drugs during their respective washout periods preceding the first prescription (10). Patients were required to have ≥1 health care encounter during washout periods recorded to confirm that they did not receive these drugs. The duration of each drug's washout period was separately estimated as 5 times the elimination half-life of the drug (17), plus 90 days to account for the longest duration of a prior prescription. Using a terminal blood half-life of 40 days, we estimated the washout period for HCQ to be 290 days (18). After excluding 14,390 patients who received HCQ or a non-HCQ DMARD during the washout period, the final pre-match cohort consisted of 13,021 patients who received a new prescription for HCQ (n = 4,749) or another nonbiologic DMARD (n = 8,272) (Figure 1).

Outcome-blinded assembly of a balanced cohort. In an RCT of HCQ, all patients will have a 50% probability of receiving HCQ regardless of whether one receives it or not. In contrast, in the clinical practice setting, this probability would vary between 0 and 100% depending on many measured and unmeasured baseline characteristics that would be considered before initiating HCQ. This probability can be estimated as propensity scores using measured baseline characteristics and can be used to match patients started on HCQ and patients not started on HCQ (19,20). As 2 patients in an RCT, one receiving an active treatment and the other receiving placebo, will have the same 50% probability of receiving the drug but may not have similar baseline characteristics, 2 patients within a propensity score–matched pair with similar probabilities of receiving a drug may not have similar baseline characteristics. However, in a matched cohort the collective parity in the probability of receiving a drug ensures that patients receiving the drug and those not receiving the drug are balanced with regard to measured baseline characteristics. Another advantage of propensity score matching is that the process of assembling a balanced cohort is blinded with regard to the outcome as it would be in an RCT (21,22). Still, unlike in an RCT, the process cannot ensure balance with regard to unmeasured baseline characteristics. However, formal sensitivity analyses can determine whether significant associations observed in the matched cohort could be confounded by a potential unmeasured baseline characteristic (23).

We used a nonparsimonious multivariable logistic regression model to estimate propensity scores for the initiation of HCQ for each of the 13,021 patients in the pre-match cohort (Figure 1) (24,25). We used 87 baseline patient characteristics displayed in Table 1 as covariates in the model. Using a greedy matching algorithm, we matched 4,426 (93% of 4,749) patients started on HCQ with 4,426 patients started on a non-HCQ nonbiologic DMARD based on their propensity scores. Because propensity score models are sample-specific adjusters and are not intended to be used for out-of-sample prediction or estimation of coefficients, fitness and discrimination measures are not important for assessing the model's effectiveness (26–28). The propensity score model's appropriateness is assessed by comparing the distribution of the measured baseline characteristics between the 2 treatment groups in the matched cohort (26). As such, we estimated absolute standardized differences (ASDs) for all 87 baseline characteristics before and after matching (24,28). ASDs directly quantify bias in the means (or proportions) of baseline characteristics across the groups and are expressed as a percentage of the pooled standard deviation (26). Because unlike statistical tests of significance, ASDs are not affected by sample size, ASD values before and after matching are directly comparable (26). An ASD of 0% indicates no residual bias, and ASD values of <10% are considered inconsequential.

Study outcomes. Our primary outcomes of interest were incident long QT syndrome, arrhythmia-related hospitalization, and all-cause mortality. Secondary outcomes included all-cause hospitalization, the combined end point of arrhythmia-related hospitalization or all-cause mortality, and the combined end point of all-cause hospitalization or all-cause mortality. All outcomes were assessed for 12 months from the receipt of the first prescription and continued up to December 31, 2019, to allow at least 12 months of follow-up. A diagnosis of long QT syndrome was ascertained using ICD-9-CM code 426.82 or ICD-10-CM code I45.81. The ICD-9-CM and ICD-10-CM codes for arrhythmia-related hospitalizations are provided in Table 2. Data on death and time to death were collected from the Vital Status File in CDW that contains death dates for all VA beneficiaries and is updated quarterly. More than 98% of deaths in the VA data are confirmed by data in the National Death Index.

Statistical analysis. Baseline characteristics were compared between the 2 treatment groups using Pearson's chi-square and Wilcoxon's rank sum tests as appropriate. Associations between starting on HCQ and outcomes were assessed in the balanced matched cohort. Kaplan-Meier plots were generated to compare outcomes between the 2 treatment groups. Hazard ratios (HRs) and 95% confidence intervals (95% CIs) for outcomes associated with HCQ initiation were estimated using Cox

Table 1. Baseline characteristics of the patients with RA started on HCQ or a non-HCQ nonbiologic DMARD*

	Before propensity score matching (n = 13,021)			After propensity score matching (n = 8,852)		
	Non-HCQ DMARD (n = 8,272)	HCQ (n = 4,749)	ASD†	Non-HCQ DMARD (n = 4,426)	HCQ (n = 4,426)	ASD†
Age, mean ± SD years	64.3 ± 11.7	63.6 ± 12.1	6	63.9 ± 11.9	63.9 ± 12.0	0
Women	815 (9.9)	729 (15.4)	17	629 (14.2)	613 (13.8)	1
African American	2,106 (25.5)	1,352 (28.5)	7	1,229 (27.8)	1,221 (27.6)	0
Non-Hispanic ethnicity	7,433 (89.9)	4,267 (89.9)	0	3,986 (90.1)	3,969 (89.7)	1
Duration of RA, mean ± SD years	1.7 ± 2.9	2.4 ± 3.2	23	2.2 ± 3.3	2.2 ± 3.1	0
HCQ started during hospitalization	203 (2.5)	95 (2)	3	101 (2.3)	92 (2.1)	1
HCQ dosage, mean ± SD mg/day‡	–	372.3 ± 82.4	NA	–	372.6 ± 81.5	NA
Medical history						
Any hospitalization in past 12 months	1,136 (13.7)	702 (14.8)	3	631 (14.3)	641 (14.5)	1
Current smoker	1,719 (20.8)	1,131 (23.8)	7	1,029 (23.2)	1,018 (23)	1
Long QT syndrome	6 (0.1)	4 (0.1)	0	5 (0.1)	4 (0.1)	1
Atrial fibrillation	688 (8.3)	414 (8.7)	1	386 (8.7)	383 (8.7)	0
Other arrhythmias	1,837 (22.2)	1,099 (23.1)	2	1,018 (23)	1,001 (22.6)	1
Hypertension	6,159 (74.5)	3,467 (73)	3	3,258 (73.6)	3,255 (73.5)	0
Coronary artery disease	2,734 (33.1)	1,480 (31.2)	4	1,372 (31)	1,398 (31.6)	1
Acute myocardial infarction	684 (8.3)	357 (7.5)	3	338 (7.6)	335 (7.6)	0
Coronary artery bypass graft surgery	150 (1.8)	88 (1.9)	0	78 (1.8)	82 (1.9)	1
Percutaneous coronary intervention	437 (5.3)	229 (4.8)	2	218 (4.9)	214 (4.8)	0
Heart failure	827 (10)	468 (9.9)	0	444 (10)	437 (9.9)	1
Defibrillator use	88 (1.1)	48 (1)	1	53 (1.2)	45 (1)	2
Pacemaker use	180 (2.2)	115 (2.4)	2	115 (2.6)	106 (2.4)	1
Diabetes mellitus	2,613 (31.6)	1,358 (28.6)	7	1,255 (28.4)	1,289 (29.1)	2
Stroke	122 (1.5)	63 (1.3)	1	66 (1.5)	62 (1.4)	1
Peripheral arterial disease	1,297 (15.7)	755 (15.9)	1	704 (15.9)	715 (16.2)	1
Hypothyroidism	946 (11.4)	588 (12.4)	3	555 (12.5)	535 (12.1)	1
Lipid disorder	5,871 (71)	3,178 (66.9)	9	3,017 (68.2)	3,012 (68.1)	0
Liver disease	507 (6.1)	559 (11.8)	20	416 (9.4)	441 (10)	2
Renal failure/dialysis	752 (9.1)	524 (11)	6	469 (10.6)	468 (10.6)	0
Autoimmune disease	1,326 (16)	779 (16.4)	1	715 (16.2)	724 (16.4)	1
Chronic obstructive pulmonary disease	2,199 (26.6)	1,379 (29)	5	1,254 (28.3)	1,263 (28.5)	0
Asthma	888 (10.7)	556 (11.7)	3	510 (11.5)	512 (11.6)	0
Cancer	3,817 (46.1)	2,365 (49.8)	7	2,184 (49.3)	2,181 (49.3)	0
Anemia of chronic disease	220 (2.7)	174 (3.7)	6	147 (3.3)	144 (3.3)	0
Osteoarthritis	5,328 (64.4)	3,158 (66.5)	4	2,995 (67.7)	2,937 (66.4)	3
Depression	3,288 (39.7)	2,039 (42.9)	6	1,857 (42)	1,872 (42.3)	1
Dementia	141 (1.7)	96 (2)	2	83 (1.9)	83 (1.9)	0
Hyperkalemia	291 (3.5)	176 (3.7)	1	157 (3.5)	162 (3.7)	1
Hypokalemia	399 (4.8)	292 (6.1)	6	247 (5.6)	258 (5.8)	1
Hypomagnesemia	85 (1)	77 (1.6)	5	58 (1.3)	65 (1.5)	1
Hypocalcemia	52 (0.6)	24 (0.5)	2	27 (0.6)	23 (0.5)	1
Medication						
Biologic DMARDs	870 (10.5)	306 (6.4)	15	281 (6.3)	301 (6.8)	2
Azithromycin	209 (2.5)	109 (2.3)	2	114 (2.6)	108 (2.4)	1
Other antibiotics	386 (4.7)	206 (4.3)	2	202 (4.6)	192 (4.3)	1
Antifungal medications	192 (2.3)	100 (2.1)	1	98 (2.2)	96 (2.2)	0
Antipsychotics	39 (0.5)	24 (0.5)	0	26 (0.6)	23 (0.5)	1
Tricyclic antidepressants	364 (4.4)	208 (4.4)	0	194 (4.4)	196 (4.4)	0
Tetracyclic antidepressants	226 (2.7)	142 (3)	2	122 (2.8)	133 (3)	1
Atypical antidepressants	324 (3.9)	211 (4.4)	3	200 (4.5)	188 (4.2)	1
Antihistamines	857 (10.4)	472 (9.9)	1	433 (9.8)	446 (10.1)	1
Anticonvulsants	72 (0.9)	36 (0.8)	1	31 (0.7)	33 (0.7)	1
Amiodarone	51 (0.6)	31 (0.7)	0	35 (0.8)	31 (0.7)	1
Other antiarrhythmic drugs	79 (1)	48 (1)	1	47 (1.1)	47 (1.1)	0
Loperamide	75 (0.9)	40 (0.8)	1	35 (0.8)	37 (0.8)	1
Lithium	22 (0.3)	18 (0.4)	2	17 (0.4)	15 (0.3)	1
Diuretics	1,344 (16.2)	765 (16.1)	0	726 (16.4)	716 (16.2)	1
Sulfonylureas	387 (4.7)	202 (4.3)	2	186 (4.2)	197 (4.5)	1

(Continued)

Table 1. *(Cont'd)*

	Before propensity score matching (n = 13,021)			After propensity score matching (n = 8,852)		
	Non-HCQ DMARD (n = 8,272)	HCQ (n = 4,749)	ASD†	Non-HCQ DMARD (n = 4,426)	HCQ (n = 4,426)	ASD†
Steroids	1,462 (17.7)	704 (14.8)	8	652 (14.7)	674 (15.2)	1
Aspirin	970 (11.7)	562 (11.8)	0	546 (12.3)	528 (11.9)	1
Acetaminophen	2,111 (25.5)	1,165 (24.5)	2	1,108 (25)	1,092 (24.7)	1
NSAIDs	2,899 (35)	1,712 (36)	2	1,595 (36)	1,571 (35.5)	1
SSRI	1,164 (14.1)	699 (14.7)	2	639 (14.4)	643 (14.5)	0
SNRI	325 (3.9)	203 (4.3)	2	192 (4.3)	190 (4.3)	0
Methadone	109 (1.3)	72 (1.5)	2	66 (1.5)	68 (1.5)	0
Other opioids	1,679 (20.3)	964 (20.3)	0	875 (19.8)	891 (20.1)	1
Loratadine	479 (5.8)	330 (6.9)	5	292 (6.6)	294 (6.6)	0
Warfarin	374 (4.5)	190 (4)	3	177 (4)	181 (4.1)	0
Metformin	785 (9.5)	371 (7.8)	6	344 (7.8)	356 (8)	1
ACE inhibitors	2,025 (24.5)	1,034 (21.8)	6	1,006 (22.7)	984 (22.2)	1
Angiotensin receptor blockers	487 (5.9)	250 (5.3)	3	221 (5)	242 (5.5)	2
Beta blockers	1,994 (24.1)	1,108 (23.3)	2	1,037 (23.4)	1,038 (23.5)	0
Calcium channel blockers	1,169 (14.1)	710 (15)	2	682 (15.4)	662 (15)	1
Digoxin	136 (1.6)	50 (1.1)	5	42 (0.9)	50 (1.1)	2
Vital signs, mean ± SD						
Pulse, beats/minute	76.9 ± 14.1	76.3 ± 13.8	4	76.5 ± 13.8	76.3 ± 13.8	1
Systolic blood pressure, mm Hg	132.3 ± 17.0	131.9 ± 17.1	2	132.0 ± 16.8	132.0 ± 17.1	0
Diastolic blood pressure, mm Hg	75.7 ± 11.0	76.0 ± 10.8	3	75.9 ± 10.9	76.0 ± 10.8	1
Body mass index, kg/m^2	29.3 ± 5.9	29.0 ± 5.9	5	29.1 ± 5.8	29.1 ± 6.0	0
Laboratory values (serum/plasma)						
RF positive	8,210 (99.3)	4,697 (98.9)	4	4,384 (99.1)	4,382 (99)	0
ACPA positive	1,990 (24.1)	1,376 (29)	11	1,218 (27.5)	1,226 (27.7)	0
RF or ACPA positive	4,637 (56.1)	2,861 (60.2)	8	2,607 (58.9)	2,630 (59.4)	1
Erythrocyte sedimentation rate, mm/hour	32.3 ± 28.1	27.9 ± 24.4	17	27.8 ± 23.9	28.3 ± 24.7	2
C-reactive protein, mg/dl	2.4 ± 4.0	1.8 ± 3.7	16	1.8 ± 3.0	1.9 ± 3.8	3
Hemoglobin, gm/dl	13.6 ± 1.7	13.7 ± 1.7	6	13.7 ± 1.7	13.7 ± 1.7	0
White blood cells, 10^9/liter	8.0 ± 2.7	7.7 ± 3.5	10	7.8 ± 2.6	7.7 ± 3.6	3
Platelets, 10^9/liter	265.9 ± 93.6	247.2 ± 86.4	21	249.7 ± 81.5	249.4 ± 87.2	0
Glucose, mg/dl	114.7 ± 44.3	111.8 ± 40.3	7	112.4 ± 42.3	112.3 ± 40.6	0
Creatinine, mg/dl	1.0 ± 0.4	1.1 ± 0.5	22	1.0 ± 0.4	1.1 ± 0.4	3
Sodium, mEq/liter	138.9 ± 3.0	138.8 ± 2.9	3	138.9 ± 3.0	138.9 ± 2.9	0
Potassium, mEq/liter	4.2 ± 0.4	4.2 ± 0.4	0	4.2 ± 0.4	4.2 ± 0.4	0
Total cholesterol, mg/dl	172.4 ± 41.3	172.3 ± 41.5	0	173.3 ± 41.0	172.6 ± 41.4	2

* Except where indicated otherwise, values are the number (%). RA = rheumatoid arthritis; HCQ = hydroxychloroquine; DMARD = disease-modifying antirheumatic drug; NSAIDs = nonsteroidal antiinflammatory drugs; SSRI = selective serotonin reuptake inhibitor; SNRI = selective norepinephrine reuptake inhibitor; ACE = angiotensin-converting enzyme; RF = rheumatoid factor; ACPA = anti–citrullinated protein antibody.
† We estimated absolute standardized differences (ASDs) because unlike statistical tests of significance, ASDs are not affected by sample size, and as such, ASD values before and after matching are directly comparable. ASDs directly quantify bias in the means (or proportions) of baseline characteristics across the groups and are expressed as a percentage of the pooled standard deviation. The goal of propensity score matching is to achieve ASD values of <10% for all measured baseline characteristics, since at those values, any residual bias is considered inconsequential. An ASD of 0% indicates no residual bias.
‡ Not included in the propensity score model.

regression models. The proportional hazards assumption was assessed by visual examinations of the log (minus log) curves. All outcomes were compared at 30 days and after 12 months of follow-up. Time to event was calculated from baseline to the first instance of the codes for these events during the specified follow-up period (30 days or 12 months). For the mortality outcome, patients who did not die were censored at the study end (30 days or 12 months), and for non-mortality outcomes, patients who did not experience the outcome of interest were censored at study end (30 days or 12 months) or at the time of death, whichever occurred first.

Because none of the associations in the matched cohort were significant, formal sensitivity analyses using Rosenbaum's approach were not conducted (23). We conducted subgroup analyses to check for homogeneity of the associations in clinically relevant subgroups. Even though we were able to match 93% (4,426 of 4,749) of the patients in the HCQ group, only 54% (4,426 of 8,272) of the patients in the active comparator group were included in the matched cohort. Therefore, we also examined the association between HCQ initiation and outcomes in the pre-match cohort in a Cox regression model adjusted for propensity score.

Table 2. Outcomes according to treatment in a propensity score–matched cohort of patients with RA*

Outcomes by event type and follow-up duration	All patients (n = 8,852)	Non-HCQ DMARD (n = 4,426)	HCQ (n = 4,426)	HR associated with HCQ initiation (95% CI)
During the first 30 days of follow-up				
Long QT syndrome	0 (0.00)	0 (0.00)	0 (0.00)	–
Hospitalizations due to arrhythmias†	2 (0.02)	2 (0.05)	0 (0.00)	–
All-cause mortality	13 (0.15)	7 (0.16)	6 (0.14)	0.86 (0.29–2.55)
Hospitalizations due to all causes	174 (1.97)	87 (1.97)	87 (1.97)	1.00 (0.74–1.35)
Arrhythmia hospitalization or all-cause mortality	15 (0.17)	9 (0.20)	6 (0.14)	0.67 (0.24–1.87)
All-cause hospitalization or all-cause mortality	182 (2.06)	90 (2.03)	92 (2.08)	1.02 (0.77–1.37)
During the first 12 months of follow-up				
Long QT syndrome	3 (0.03)	1 (0.02)	2 (0.05)	2.00 (0.18–22.06)
Hospitalizations due to arrhythmias†	56 (0.63)	26 (0.59)	30 (0.68)	1.16 (0.68–1.95)
All-cause mortality	280 (3.16)	136 (3.07)	144 (3.25)	1.06 (0.84–1.34)
Hospitalizations due to all causes	1,246 (14.08)	650 (14.69)	596 (13.47)	0.92 (0.82–1.02)
Arrhythmia hospitalization or all-cause mortality	333 (3.64)	161 (3.64)	172 (3.89)	1.07 (0.86–1.33)
All-cause hospitalization or all-cause mortality	1,398 (15.79)	720 (16.27)	678 (15.32)	0.94 (0.85–1.04)

* Hazard ratios (HRs) were not significant for any outcome. Values are the number (%) of events. RA = rheumatoid arthritis; HCQ = hydroxychloroquine; DMARD = disease-modifying antirheumatic drug; 95% CI = 95% confidence interval.
† International Classification of Diseases, Ninth Revision, Clinical Modification (ICD-9-CM) codes for arrhythmia hospitalizations included 425.4, 425.5, 426, 426.1, 426.11, 426.12, 426.13, 426.3, 426.4, 426.5, 426.53, 426.54, 426.6, 426.7, 426.89, 427, 427.1, 427.2, 427.31, 427.32, 427.41, 427.5, 427.6, 427.61, 427.69, 427.81, 427.89, 427.9. ICD-10-CM codes for arrhythmia hospitalizations included I42.0, I42.7, I42.8, I42.9, I44.0, I44.1, I44.2, I44.39, I44.7, I45.10, I45.19, I45.2, I45.5, I45.81, I45.89, I46.9, I46.9, I47.1, I47.2, I48.0, I48.1, I48.19, I48.2, I48.20, I48.3, I48.4, I48.91, I48.92, I49.01, I49.01, I49.1, I49.2, I49.3, I49.5, I49.8, I49.9.

Finally, we assessed the impact of treatment adherence on the observed associations using several approaches. We estimated 90-day medication adherence using the proportion of days covered (PDC) approach and used a PDC of ≥80% as evidence of adequate adherence (29). PDC is calculated as the number of days "covered" by a prescription (e.g., 30 days or 90 days) divided by the total number of days intended to be covered (90 days in this case; examples provided in Table 3) (30). Patients in the HCQ and non-HCQ groups had a mean ± SD 90-day PDC of 68 ± 31% and 65 ± 30%, respectively ($P < 0.001$).

First, we examined the associations between HCQ initiation and 90-day outcomes in the 4,426 pairs of matched patients before and after adjusting for PDC as a continuous variable. Second, we examined these associations in patients who met the 80% PDC threshold for adequate adherence. Of the 8,852 matched patients, 3,856 (44%) had ≥80% PDC during the first 90 days of follow-up, of whom 2,061 (47% of 4,426) were in the HCQ group, and 1,795 (41% of 4,426) were in the non-HCQ group. Third, because these 3,856 patients (2,061 + 1,795) with a 90-day adherence of ≥80% are a subset of the balanced matched cohort of 8,852 patients, to examine these associations in a balanced cohort, we assembled a separate propensity score–matched balanced cohort of 2,988 patients. Finally, we examined the associations between HCQ initiation and outcomes in subgroups of patients who received a 90-day prescription. Of the 8,852 matched patients, 2,781 (31%) received a 90-day prescription, and of these 1,771 (40% of 4,426) were in the HCQ group and 1,010 (23% of 4,426) were in the non-HCQ group.

All statistical tests were 2-tailed and were conducted using SAS for Windows version 9.2. *P* values less than 0.05 were considered significant.

RESULTS

Baseline characteristics of the patients. Patients in the matched cohort (n = 8,852) had a mean ± SD age of 64 ± 12 years, 14% were women, and 28% were African American. Before matching, patients in the HCQ group had a longer mean duration of disease, and a lower proportion received biologic DMARDs (Table 1). After matching, ASDs for all 87 baseline characteristics were <4%, with 32 at 0% (Table 1), suggesting a balanced distribution between the 2 treatment groups. The mean ± SD daily dosages of HCQ before and after matching were 372 ± 82 mg and 373 ± 82 mg, respectively.

Long QT syndrome. Overall, 3 (0.03% of 8,852) matched patients had incident long QT syndrome during the first 12 months of follow-up, of which 2 (0.05% of 4,426) were in the HCQ group (Table 2). All 3 incidences of long QT syndrome occurred in the first 90 days (Table 3) and none during the first 30 days (Table 2).

Arrhythmia-related hospitalization. During 12 months of follow-up, arrhythmia-related hospitalizations occurred in 30 (0.68%) of 4,426 and 26 (0.59%) of 4,426 matched patients in the HCQ and other nonbiologic DMARD groups, respectively (HR associated with HCQ initiation 1.16 [95% CI 0.68–1.95]) (Table 2

Table 3. Ninety-day outcomes according to treatment in a propensity score–matched cohort of patients with RA, before and after accounting for 90-day adherence to HCQ treatment*

Outcomes by adherence	Overall	Non-HCQ DMARD	HCQ	HR associated with HCQ initiation (95% CI)
Propensity score–matched cohort†				
No. of patients	8,852	4,426	4,426	
Long QT syndrome	3 (0.03)	1 (0.02)	2 (0.05)	2.00 (0.18–22.06)
Hospitalizations due to arrhythmias‡	13 (0.15)	6 (0.14)	7 (0.16)	1.17 (0.39–3.47)
All-cause mortality	55 (0.62)	27 (0.61)	28 (0.63)	1.04 (0.61–1.76)
Hospitalizations due to all causes	446 (5.04)	220 (4.97)	226 (5.11)	1.02 (0.85–1.24)
Arrhythmia hospitalization or all-cause mortality	67 (0.76)	32 (0.72)	35 (0.79)	1.09 (0.68–1.77)
All-cause hospitalization or all-cause mortality	478 (5.40)	236 (5.33)	242 (5.47)	1.03 (0.86–1.23)
Patients with ≥80% adherence (PDC)§				
No. of patients	3,856	1,795	2,061	
Long QT syndrome	2 (0.05)	1 (0.06)	1 (0.05)	0.87 (0.06–13.94)
Hospitalizations due to arrhythmias‡	5 (0.13)	2 (0.11)	3 (0.15)	1.31 (0.22–7.83)
All-cause mortality	24 (0.62)	11 (0.61)	13 (0.63)	1.03 (0.46–2.30)
Hospitalizations due to all causes	179 (4.64)	79 (4.40)	100 (4.85)	1.11 (0.82–1.49)
Arrhythmia hospitalization or all-cause mortality	29 (0.75)	13 (0.72)	16 (0.78)	1.07 (0.52–2.23)
All-cause hospitalization or all-cause mortality	194 (5.03)	86 (4.79)	108 (5.24)	1.10 (0.83–1.46)
Propensity score–matched cohorts of patients with ≥80% adherence (PDC)¶				
No. of patients	2,988	1,494	1,494	
Long QT syndrome	1 (0.03)	1 (0.07)	0 (0.00)	–
Hospitalizations due to arrhythmias‡	4 (0.13)	2 (0.13)	2 (0.13)	1.00 (0.14–7.10)
All-cause mortality	17 (0.57)	9 (0.60)	8 (0.54)	0.89 (0.34–2.31)
Hospitalizations due to all causes	133 (4.45)	69 (4.62)	64 (4.28)	0.93 (0.66–1.30)
Arrhythmia hospitalization or all-cause mortality	21 (0.70)	11 (0.74)	10 (0.67)	0.91 (0.39–2.14)
All-cause hospitalization or all-cause mortality	141 (4.72)	71 (4.75)	70 (4.69)	0.98 (0.71–1.37)
Patients who received a 90-day prescription				
No. of patients	2,781	1,010	1,771	
Long QT syndrome	0 (0.00)	0 (0.00)	0 (0.00)	–
Hospitalizations due to arrhythmias‡	3 (0.11)	1 (0.10)	2 (0.11)	1.15 (0.10–12.63)
All-cause mortality	16 (0.58)	4 (0.40)	12 (0.68)	1.72 (0.55–5.32)
Hospitalizations due to all causes	109 (3.92)	35 (3.47)	74 (4.18)	1.21 (0.81–1.82)
Arrhythmia hospitalization or all-cause mortality	19 (0.68)	5 (0.50)	14 (0.79)	1.60 (0.58–4.45)
All-cause hospitalization or all-cause mortality	121 (4.35)	39 (3.86)	82 (4.63)	1.21 (0.83–1.77)

* Hazard ratios (HRs) were not significant for any outcome. Values are the number (%) of events. RA = rheumatoid arthritis; HCQ = hydroxychloroquine; DMARD = disease-modifying antirheumatic drug; 95% CI = 95% confidence interval.
† Propensity score–matched cohort as shown in Table 2. These associations did not change when adjusted for proportion of days covered (PDC) as a continuous variable.
‡ See Table 2 for ICD-9 codes for arrhythmia hospitalizations.
§ The PDC was calculated as the number of days "covered" by a medication dispensed to a patient divided by the total number of days intended to be covered. For example, if a patient receives a 90-day prescription on day 1, his or her 90-day PDC will be 100% (90/90 = 1.00). Similarly, if a patient receives a 30-day prescription on day 1 and refills on days 31 and 61, he or she will also have a 90-day PDC of 100% (90/90 = 1.00). However, if a patient receiving a 30-day prescription on day 1 misses the first refill on day 31 and gets the second refill on day 65, then the total days covered would be 55 days (30 + 0 + 25) with a 90-day PDC of 61% (65/90 = 0.61). Similarly, if a patient receiving a 30-day prescription on day 1 received the first refill on day 16 and the second refill on day 61, then the total days covered would be 75 days (30 + 30 – 15 + 30) with a 90-day PDC of 83% (75/90 = 0.83).
¶ The propensity score model included all 87 variables listed in Table 1, plus the PDC as a continuous variable.

and Figure 2). Of the 56 arrhythmia-related hospitalizations, 13 (23%) occurred during the first 90 days and 2 (3.57%) during the first 30 days, and neither were associated with HCQ initiation (Tables 2 and 3).

All-cause mortality. All-cause mortality occurred in 144 (3.25%) of 4,426 and 136 (3.07%) of 4,426 matched patients in the HCQ and non-HCQ nonbiologic DMARD groups, respectively (HR associated with HCQ initiation 1.06 [95% CI 0.84–1.34]) (Table 2 and Figure 2). Thirty-day and 90-day mortality occurred in 13 and 55 patients, respectively, and neither was associated with HCQ initiation (Tables 2 and 3).

Combined end point of arrhythmia-related hospitalization or all-cause mortality. The initiation of HCQ was not associated with the 12-month combined end point of arrhythmia-related hospitalization or all-cause mortality (HR 1.07 [95% CI

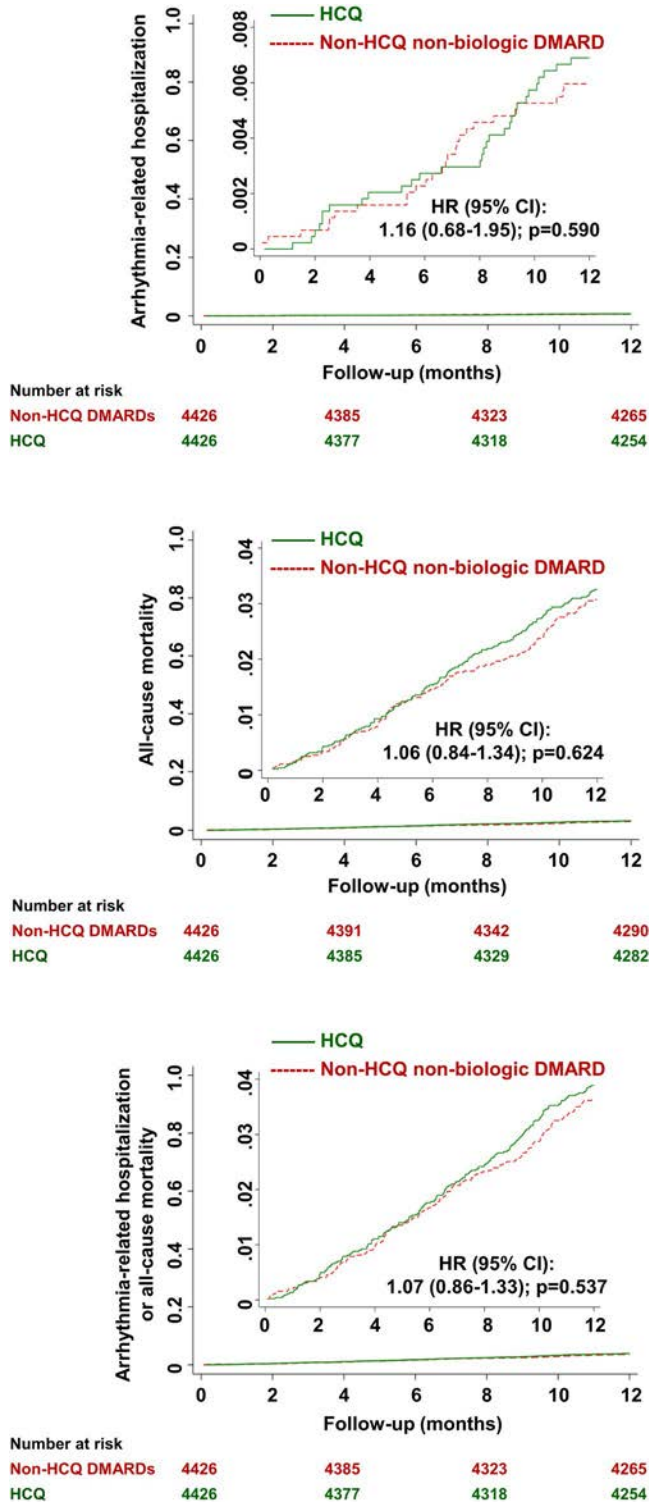

Figure 2. Kaplan-Meier plots for arrhythmia-related hospitalization, all-cause mortality, and the combined end point of arrhythmia-related hospitalization or all-cause mortality in patients with rheumatoid arthritis started on hydroxychloroquine (HCQ) or another nonbiologic disease-modifying antirheumatic drug (DMARD). Hazard ratios (HRs) and 95% confidence intervals (95% CIs) are based on Cox proportional hazards models, with the other nonbiologic DMARD group as the reference.

0.86–1.33]) (Table 2). There were 15 and 67 combined end point events during the first 30 and 90 days, respectively, but no association with HCQ initiation (Tables 2 and 3). HCQ initiation had no association with the combined end point of all-cause hospitalization or all-cause mortality (Tables 2 and 3).

Subgroup analyses. There was no evidence of heterogeneity in the association of HCQ initiation with the 12-month combined end point of arrhythmia-related hospitalization or total mortality in any of the clinically relevant subgroups examined (Figure 3).

Propensity score–adjusted associations in the pre-match cohort. None of the propensity score–adjusted associations between HCQ initiation and 12-month outcomes in the pre-match cohort was significant except for all-cause hospitalization (HR 0.90 [95% CI 0.82–0.99]; $P = 0.031$), which was consistent with that in the matched cohort (HR 0.92 [95% CI 0.82–1.02]; $P = 0.120$) (Table 2).

Treatment adherence and outcomes in the matched cohort. HRs for 90-day long QT syndrome, arrhythmia-related hospitalization, and all-cause mortality associated with HCQ initiation were 2.00 (95% CI 0.18–22.06), 1.17 (95% CI 0.39–3.47), and 1.04 (95% CI 0.61–1.76), respectively (Table 3). These associations remained unchanged when adjusted for 90-day adherence as well as in subgroups with adequate 90-day adherence (Table 3).

DISCUSSION

In the present study, <1% of the patients with newly diagnosed RA had incident long QT syndrome or arrhythmia-related hospitalizations during the first 12 months after initiation of HCQ or another nonbiologic DMARD, and patients started on HCQ did not have a significantly higher risk of these events than those started on another nonbiologic DMARD. We also observed that HCQ initiation had no association with all-cause mortality or all-cause hospitalization. To the best of our knowledge, this is the largest observational comparative safety study of HCQ initiation in a propensity score–matched balanced cohort of patients with RA that provides new information about the cardiovascular safety of HCQ.

The findings of our study suggest that the overall incidence of long QT syndrome is extremely low and that the risk is not significantly higher in patients started on HCQ. HCQ prolongs the QT intervals by inhibiting the rapid cardiac delayed-rectifier potassium current (I_{Kr}) in cardiac cells (1,31). However, the association between long QT syndrome and sudden death is complex, and all QT-prolonging drugs are not associated with sudden death. A sudden cardiac death autopsy study that adjudicated the cause of sudden death could not validate the association between

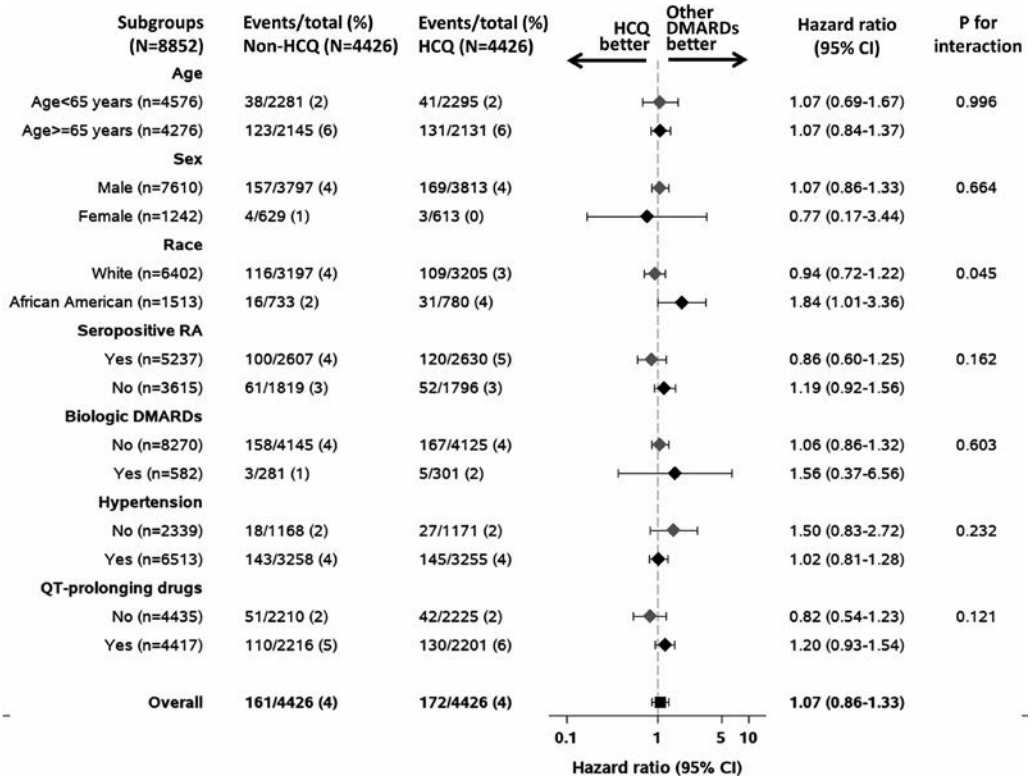

Figure 3. Forest plots showing hazard ratios for the combined end point of arrhythmia-related hospitalization or all-cause mortality during the first 12 months after initiation of hydroxychloroquine (HCQ), according to clinically relevant subgroups based on baseline characteristics in US veterans who were newly diagnosed as having rheumatoid arthritis (RA) and were not taking HCQ prior to diagnosis. Seropositive RA was defined as a positive result on a test for either rheumatoid factor or anti–citrullinated protein antibody. 95% CI = 95% confidence interval; DMARDs = disease-modifying antirheumatic drugs.

QT-prolonging drugs and sudden arrhythmic death (32). The lack of electrocardiographic confirmation of long QT syndrome may have underestimated incident long QT syndrome in our study, which in turn may have underpowered it to detect a significant risk difference. However, long QT syndrome is extremely rare. In one study of 2,000 elite athletes (mean age 20 years), 0.15% (3 of 2,000) had electrocardiographic evidence of heart rate–corrected QT values >0.500 msec, which is highly suggestive of long QT syndrome (33). The prevalence of long QT syndrome in our study was 0.10% (10 of 13,021), and the 12-month incidence was 0.03% (3 of 8,852). These lower estimates may, in part, be because long QT syndrome is less common in older men (34). Patients in our study had a mean age of 64 years, and 86% were men. Because HCQ is a slow-acting drug (18), it is possible that the incidence of long QT syndrome would be higher during more prolonged therapy.

HCQ is known for its immunomodulatory, antiinflammatory, vasoprotective, and antithrombotic properties (35). HCQ also suppresses Toll-like receptors (36), which have been shown to be activated in atherosclerosis in animal models and human studies (37). HCQ use has been associated with a lower risk of cardiovascular disease and diabetes mellitus in patients with RA (38) and a lower risk of death in SLE (8,39). Although patients with RA are at high risk of cardiovascular death, like those with SLE (40), we observed that HCQ use was not associated with a lower risk of all-cause mortality in patients with RA. It is possible that our use of other nonbiologic DMARDs as active comparators attenuated between-group mortality differences in our study. It is also possible that, unlike in patients with SLE in whom HCQ use is associated with a lower risk of death, HCQ use may not improve survival in patients with RA. One prior study that observed a lower risk of death associated with methotrexate use in patients with RA showed no such association with HCQ use (41).

Recent studies of the association of HCQ with outcomes have primarily been focused on hospitalized patients with COVID-19 (42–44). Two of those studies found no significant association with abnormal electrocardiographic findings or in-hospital mortality (42,43). The third study reported a higher risk of in-hospital mortality and ventricular arrhythmias in patients receiving HCQ but has since been retracted (44,45). Two recent RCTs of HCQ in patients with COVID-19 also found no association with mortality or cardiac arrhythmias (46,47). In another study of patients with RA without COVID-19, based on 14 sources of claims data or electronic medical records from 6 countries, including VA data for 32,028 veterans with RA taking HCQ alone, there was no evidence of a higher risk of short-term mortality (48). Primarily based on these findings, the COVID-19 clinical task force of the American College of

Rheumatology recommended that HCQ be temporarily withheld following COVID-19 infection "highlighting the potential for cardiotoxicity (primarily QT prolongation and arrhythmias) that could be heightened in the context of COVID-19 and the receipt of other QT-prolonging agents that are common among hospitalized patients" (49). Although we found no evidence of a higher risk of long QT syndrome associated with HCQ use, our subgroup analyses suggest a higher risk in those receiving other QT-prolonging drugs. However, results of subgroup analyses need to be interpreted with caution (50).

Adherence to HCQ therapy in patients with rheumatic diseases, including RA, is generally low (51,52). It has been reported that adherence may be further lowered due to perceived concerns surrounding its adverse cardiovascular effect in patients with COVID-19 (9). The findings of our study provide much-needed information for patients with RA about the cardiovascular safety of HCQ and suggest that these patients need not stop their HCQ based on the recent publicity. The findings of the present study also provide new information for clinicians that suggests that there is no need to avoid the use of HCQ when indicated in newly diagnosed patients with RA. Although our study was limited to patients with RA, these findings provide information about the safety of HCQ in those who might be taking the drug for other indications.

This study has some limitations. As in any observational study, residual bias or bias due to unmeasured confounders is possible. However, patients in our study were balanced with regard to 87 measured baseline characteristics, and the lack of significant associations precluded formal sensitivity analyses for potential confounding unmeasured baseline characteristics. The lack of a significant association also attenuates concerns about residual and unmeasured confounding. We did not have access to electrocardiograms, and it is possible that the incidence of QT prolongation was underestimated and/or misclassified. However, those would be expected to occur randomly in both treatment groups. The findings of the present study are based on male veterans with RA from before the COVID pandemic, which may limit generalizability, especially to patients with COVID-19.

In conclusion, the incidence of long QT syndrome and arrhythmia-related hospitalization during the first 12 months after initiation of a nonbiologic DMARD is infrequent in patients with RA, and the risk is not significantly higher in patients started on HCQ compared to those started on another nonbiologic DMARD. Although the very low incidence of long QT syndrome in our study is generally consistent with that reported in the literature, future studies need to replicate these findings with electrocardiographically adjudicated incident long QT syndrome events.

AUTHOR CONTRIBUTIONS

All authors were involved in drafting the article or revising it critically for important intellectual content, and all authors approved the final version to be published. Drs. Ahmed, Zeng-Treitler, Cheng, Shao and Zhang had full access to all of the data in the study and take responsibility for the integrity of the data and the accuracy of the data analysis.

Study conception and design. Faselis, Zeng-Treitler, Cheng, Kerr, Liappis, Shao, Redd, Sheriff, Zhang, Moore, Ahmed.

Acquisition of data. Faselis, Zeng-Treitler, Cheng, Shao, Redd, Sheriff, Zhang, Moore, Ahmed.

Analysis and interpretation of data. Faselis, Zeng-Treitler, Cheng, Kerr, Nashel, Liappis, Weintrob, Karasik, Arundel, Boehm, Heimall, Connell, Taub, Shao, Redd, Sheriff, Zhang, Fletcher, Fonarow, Moore, Ahmed.

REFERENCES

1. Roden DM, Harrington RA, Poppas A, Russo AM. Considerations for drug interactions on QTc interval in exploratory COVID-19 treatment. J Am Coll Cardiol 2020;75:2623–4.
2. World Health Organization. The cardiotoxicity of antimalarials: WHO Evidence Review Group meeting, 13–14 October 2016 Varembé Conference Centre, Geneva, Switzerland. March 2021. URL: https://www.who.int/malaria/mpac/mpac-mar2017-erg-cardiotoxicity-report-session2.pdf.
3. Bonow RO, Hernandez AF, Turakhia M. Hydroxychloroquine, coronavirus disease 2019, and QT prolongation [editorial]. JAMA Cardiol 2020;5:986–7.
4. Magagnoli J, Narendran S, Pereira F, Cummings TH, Hardin JW, Sutton SS, et al. Outcomes of hydroxychloroquine usage in United States veterans hospitalized with COVID-19. Med (N Y) 2020;1:114–27.
5. Bessiere F, Roccia H, Deliniere A, Charriere R, Chevalier P, Argaud L, et al. Assessment of QT intervals in a case series of patients with coronavirus disease 2019 (COVID-19) infection treated with hydroxychloroquine alone or in combination with azithromycin in an intensive care unit [letter]. JAMA Cardiol 2020;5:1067–9.
6. Mercuro NJ, Yen CF, Shim DJ, Maher TR, McCoy CM, Zimetbaum PJ, et al. Risk of QT interval prolongation associated with use of hydroxychloroquine with or without concomitant azithromycin among hospitalized patients testing positive for coronavirus disease 2019 (COVID-19). JAMA Cardiol 2020;5:1039–41.
7. Boseley S, Davey M. Covid-19: Lancet retracts paper that halted hydroxychloroquine trials. URL: https://www.theguardian.com/world/2020/jun/04/covid-19-lancet-retracts-paper-that-halted-hydroxychloroquine-trials. The Guardian. June 2020.
8. Guiding principles from the American College of Rheumatology for scarce resource allocation during the COVID-19 pandemic: the case of hydroxychloroquine. March 2020. URL: https://2plxya2ceafl3hs9qd35hk54-wpengine.netdna-ssl.com/wp-content/uploads/2020/03/ACR-Guiding-Principles-Scarce-Resource-Allocation-During-Covid-19.pdf.
9. Peschken CA. Possible consequences of a shortage of hydroxychloroquine for lupus patients amid the COVID-19 pandemic [editorial]. J Rheumatol 2020;47:787–90.
10. Danaei G, Rodriguez LA, Cantero OF, Logan R, Hernan MA. Observational data for comparative effectiveness research: an emulation of randomised trials of statins and primary prevention of coronary heart disease. Stat Methods Med Res 2013;22:70–96.
11. Barnado A, Casey C, Carroll RJ, Wheless L, Denny JC, Crofford LJ. Developing electronic health record algorithms that accurately identify patients with systemic lupus erythematosus. Arthritis Care Res (Hoboken) 2017;69:687–93.
12. Hernan MA, Alonso A, Logan R, Grodstein F, Michels KB, Willett WC, et al. Observational studies analyzed like randomized experiments: an application to postmenopausal hormone therapy and coronary heart disease. Epidemiology 2008;19:766–79.
13. Yoshida K, Solomon DH, Kim SC. Active-comparator design and new-user design in observational studies [review]. Nat Rev Rheumatol 2015;11:437–41.

14. Singh S, Moore H, Karasik PE, Lam PH, Wopperer S, Arundel C, et al. Digoxin initiation and outcomes in patients with heart failure (HFrEF and HFpEF) and atrial fibrillation. Am J Med 2020;133: 1460–70.
15. Fonarow GC, Masson R, Ahmed A. Reply: what is important for digoxin treatment in patients with heart failure [letter]. J Am Coll Cardiol 2019;74:2827–8.
16. Smith MW, Joseph GJ. Pharmacy data in the VA health care system [review]. Med Care Res Rev 2003;60 Suppl:92S–123S.
17. US Food and Drug Administration. CVM GFI #224 (VICH GL52) Bioequivalence: blood level bioequivalence study. December 2016. URL: https://www.fda.gov/regulatory-information/search-fda-guidance-documents/cvm-gfi-224-vich-gl52-bioequivalence-blood-level-bioequivalence-study.
18. Tett SE, Cutler DJ, Day RO, Brown KF. Bioavailability of hydroxychloroquine tablets in healthy volunteers. Br J Clin Pharmacol 1989;27:771–9.
19. Rosenbaum PR, Rubin DB. The central role of propensity score in observational studies for causal effects. Biometrika 1983;70: 41–55.
20. Rubin DB. Using propensity score to help design observational studies: application to the tobacco litigation. Health Serv Outcomes Res Methodol 2001;2:169–88.
21. Rubin DB. On principles for modeling propensity scores in medical research [editorial]. Pharmacoepidemiol Drug Saf 2004;13:855–7.
22. Austin PC, Stuart EA. Estimating the effect of treatment on binary outcomes using full matching on the propensity score. Stat Methods Med Res 2017;26:2505–25.
23. Rosenbaum PR. Sensitivity to hidden bias. In: Rosenbaum PR, editor. Observational studies. New York: Springer-Verlag; 2002. p. 105–70.
24. Arundel C, Lam PH, Gill GS, Patel S, Panjrath G, Faselis C, et al. Systolic blood pressure and outcomes in patients with heart failure with reduced ejection fraction. J Am Coll Cardiol 2019;73:3054–63.
25. Faselis C, Arundel C, Patel S, Lam PH, Gottlieb SS, Zile MR, et al. Loop diuretic prescription and 30-day outcomes in older patients with heart failure. J Am Coll Cardiol 2020;76:669–79.
26. Austin PC. Balance diagnostics for comparing the distribution of baseline covariates between treatment groups in propensity-score matched samples. Stat Med 2009;28:3083–107.
27. Ahmed MI, White M, Ekundayo OJ, Love TE, Aban I, Liu B, et al. A history of atrial fibrillation and outcomes in chronic advanced systolic heart failure: a propensity-matched study. Eur Heart J 2009;30: 2029–37.
28. Malik A, Masson R, Singh S, Wu WC, Packer M, Pitt B, et al. Digoxin discontinuation and outcomes in patients with heart failure with reduced ejection fraction. J Am Coll Cardiol 2019;74:617–27.
29. Hoque MR, Avina-Zubieta JA, De Vera MA, Qian Y, Esdaile JM, Xie H. Impact of antimalarial adherence on mortality among patients with newly diagnosed systemic lupus erythematosus: a population-based cohort study. Arthritis Care Res (Hoboken) 2021 doi: https://onlinelibrary.wiley.com/doi/10.1002/acr.24550. E-pub ahead of print.
30. Raebel MA, Schmittdiel J, Karter AJ, Konieczny JL, Steiner JF. Standardizing terminology and definitions of medication adherence and persistence in research employing electronic databases. Med Care 2013;51:S11–21.
31. Roden DM. Drug-induced prolongation of the QT interval. N Engl J Med 2004;350:1013–22.
32. Simpson TF, Salazar JW, Vittinghoff E, Probert J, Iwahashi A, Olgin JE, et al. Association of QT-prolonging medications with risk of autopsy-defined causes of sudden death. JAMA Intern Med 2020;180:698–706.
33. Basavarajaiah S, Wilson M, Whyte G, Shah A, Behr E, Sharma S. Prevalence and significance of an isolated long QT interval in elite athletes. Eur Heart J 2007;28:2944–9.
34. National Heart, Lung, and Blood Institute: National Institutes of Health. Long QT syndrome. URL: https://www.nhlbi.nih.gov/health-topics/long-qt-syndrome.
35. Schrezenmeier E, Dorner T. Mechanisms of action of hydroxychloroquine and chloroquine: implications for rheumatology [review]. Nat Rev Rheumatol 2020;16:155–66.
36. Kuznik A, Bencina M, Svajger U, Jeras M, Rozman B, Jerala R. Mechanism of endosomal TLR inhibition by antimalarial drugs and imidazoquinolines. J Immunol 2011;186:4794–804.
37. Edfeldt K, Swedenborg J, Hansson GK, Yan ZQ. Expression of Toll-like receptors in human atherosclerotic lesions: a possible pathway for plaque activation. Circulation 2002;105:1158–61.
38. Solomon DH, Massarotti E, Garg R, Liu J, Canning C, Schneeweiss S. Association between disease-modifying antirheumatic drugs and diabetes risk in patients with rheumatoid arthritis and psoriasis. JAMA 2011;305:2525–31.
39. Jorge A, McCormick N, Lu N, Zheng Y, Esdaile J, De Vera M, et al. Hydroxychloroquine and mortality among patients with systemic lupus erythematosus in the general population. Arthritis Care Res (Hoboken) 2020 doi: https://onlinelibrary.wiley.com/doi/10.1002/acr.24255. E-pub ahead of print.
40. Aviña-Zubieta JA, Choi HK, Sadatsafavi M, Etminan M, Esdaile JM, Lacaille D. Risk of cardiovascular mortality in patients with rheumatoid arthritis: a meta-analysis of observational studies. Arthritis Rheum 2008;59:1690–7.
41. Mikuls TR, Fay BT, Michaud K, Sayles H, Thiele GM, Caplan L, et al. Associations of disease activity and treatments with mortality in men with rheumatoid arthritis: results from the VARA registry. Rheumatology (Oxford) 2011;50:101–9.
42. Rosenberg ES, Dufort EM, Udo T, Wilberschied LA, Kumar J, Tesoriero J, et al. Association of treatment with hydroxychloroquine or azithromycin with in-hospital mortality in patients with COVID-19 in New York state. JAMA 2020;323:2493–502.
43. Geleris J, Sun Y, Platt J, Zucker J, Baldwin M, Hripcsak G, et al. Observational study of hydroxychloroquine in hospitalized patients with Covid-19. N Engl J Med 2020;382:2411–8.
44. Mehra MR, Desai SS, Ruschitzka F, Patel AN. Hydroxychloroquine or chloroquine with or without a macrolide for treatment of COVID-19: a multinational registry analysis [retracted in Lancet 2020;395:1820]. Lancet 2020 doi: 10.1016/S0140-6736(20)31180-6. E-pub ahead of print.
45. Mehra MR, Ruschitzka F, Patel AN. Retraction—Hydroxychloroquine or chloroquine with or without a macrolide for treatment of COVID-19: a multinational registry analysis. Lancet 2020;395:1820.
46. Horby P, Mafham M, Linsell L, Bell JL, Staplin N, Emberson JR, et al. Effect of hydroxychloroquine in hospitalized patients with COVID-19: preliminary results from a multi-centre, randomized, controlled trial [preprint]. medRxiv 2020 doi: https://doi.org/10.1101/2020.07.15.20151852. E-pub ahead of print.
47. Skipper CP, Pastick KA, Engen NW, Bangdiwala AS, Abassi M, Lofgren SM, et al. Hydroxychloroquine in nonhospitalized adults with early COVID-19: a randomized trial. Ann Intern Med 2020;173: 623–31.
48. Lane JC, Weaver J, Kostka K, Duarte-Salles T, Abrahao MT, Alghoul H, et al. Risk of hydroxychloroquine alone and in combination with azithromycin in the treatment of rheumatoid arthritis: a multinational, retrospective study. Lancet Rheumatol 2020;2:e698–711.
49. Mikuls TR, Johnson SR, Fraenkel L, Arasaratnam RJ, Baden LR, Bermas BL, et al. American College of Rheumatology guidance

for the management of rheumatic disease in adult patients during the COVID-19 pandemic: version 3. Arthritis Rheumatol 2021;73: e1–12.

50. Rothwell PM. Subgroup analysis in randomised controlled trials: importance, indications, and interpretation. Lancet 2005;365: 176–86.
51. Marengo MF, Suarez-Almazor ME. Improving treatment adherence in patients with rheumatoid arthritis: what are the options? Int J Clin Rheumtol 2015;10:345–56.
52. Liu LH, Fevrier HB, Goldfien R, Hemmerling A, Herrinton LJ. Understanding nonadherence with hydroxychloroquine therapy in systemic lupus erythematosus. J Rheumatol 2019;46:1309–15.

Arthritis & Rheumatology
Vol. 73, No. 9, September 2021, pp 1601–1613
DOI 10.1002/art.41726

American College of Rheumatology
Empowering Rheumatology Professionals

Inclusion of Synovial Tissue–Derived Characteristics in a Nomogram for the Prediction of Treatment Response in Treatment-Naive Rheumatoid Arthritis Patients

Stefano Alivernini,[1] Barbara Tolusso,[2] Marco Gessi,[2] Maria Rita Gigante,[2] Alice Mannocci,[3] Luca Petricca,[2] Simone Perniola,[4] Clara Di Mario,[5] Laura Bui,[2] Anna Laura Fedele,[2] Annunziata Capacci,[2] Dario Bruno,[5] Giusy Peluso,[2] Giuseppe La Torre,[3] Francesco Federico,[2] Gianfranco Ferraccioli,[5] and Elisa Gremese[1]

Objective. This study applied a synovitis score obtained during routine care from ultrasound (US)–guided biopsies of synovial tissue (ST) in patients with rheumatoid arthritis (RA) and patients with other inflammatory and noninflammatory joint diseases to identify pretreatment synovial biomarkers associated with disease characteristics, and to integrate the findings into a multiparameter nomogram for use in baseline prediction of diagnosis and treatment response in treatment-naive rheumatoid arthritis (RA) patients.

Methods. The study enrolled a total of 1,015 patients with various autoimmune diseases (545 patients with RA, 167 patients with psoriatic arthritis [PsA], 199 patients with undifferentiated peripheral inflammatory arthritis [UPIA], 18 patients with crystal-induced arthritis, 26 patients with connective tissue diseases, and 60 patients with osteoarthritis [OA] [as part of the SYNGem cohort]). All patients underwent a US-guided ST biopsy at baseline, and patients were then stratified according to disease phase. The KSS, along with disease characteristics and clinical outcomes, were incorporated into a nomogram for prediction of achievement of clinical remission in RA patients who were previously naive to treatment. In patients in whom a treat-to-target strategy was applied, remission was defined as change in the Disease Activity Score in 28 joints (DAS28) at 6 months after treatment initiation.

Results. The KSS significantly differed among RA patients, as well as PsA patients and UPIA patients, when compared to OA patients. In RA, the KSS directly correlated with the DAS28 and was related to autoantibody positivity in treatment-naive RA patients. Moreover, at baseline, treatment-naive RA patients achieving 6-month remission according to DAS28 had a lower KSS, shorter duration of symptoms (very early RA [VERA]), and lower disease activity than treatment-naive RA patients not achieving remission according to DAS28. Results of logistic regression analysis identified the following synergistic predictive factors of achievement of DAS28-based disease remission at 6 months: having a short disease duration (VERA), not having high disease activity, and having a KSS of <5 at baseline. A nomogram integrating these baseline clinical and histologic characteristics in treatment-naive RA patients yielded an up to 81.7% probability of achieving 6-month remission according to the DAS28.

Conclusion. The KSS is a reliable tool for synovitis assessment on US-guided ST biopsy, contingent on the phase of the disease and the autoimmune profile of each patient. This tool could be integrated within a therapeutic response–predictive nomogram for the prediction of treatment response in RA patients who were previously naive to treatment.

Supported in part by the Italian Ministry of Health (Ricerca Finalizzata grant GR-2018-12366992).

[1]Stefano Alivernini, MD, PhD, Elisa Gremese, MD: Fondazione Policlinico Universitario Agostino Gemelli, IRCCS, and Università Cattolica del Sacro Cuore, Rome, Italy; [2]Barbara Tolusso, BSc, Marco Gessi, MD, Maria Rita Gigante, MD, Luca Petricca, MD, Laura Bui, BTech, Anna Laura Fedele, MD, Annunziata Capacci, MD, Giusy Peluso, MD, PhD, Francesco Federico, MD, PhD: Fondazione Policlinico Universitario Agostino Gemelli, IRCCS, Rome, Italy; [3]Alice Mannocci, PhD, Giuseppe La Torre, MD, PhD: Sapienza University of Rome, Rome, Italy; [4]Simone Perniola, MD: Fondazione Policlinico Universitario Agostino Gemelli, IRCCS, Rome, Italy, and University of Verona, Verona, Italy; [5]Clara Di Mario, BSc, Dario Bruno, MD, Gianfranco Ferraccioli, MD: Università Cattolica del Sacro Cuore, Rome, Italy.

No potential conflicts of interest relevant to this article were reported.

Address correspondence to Stefano Alivernini, MD, PhD, or Elisa Gremese, MD, Università Cattolica del Sacro Cuore, Fondazione Policlinico Universitario Agostino Gemelli, IRCCS, Largo A. Gemelli 1, 00168 Rome, Italy. Email: stefano.alivernini@unicatt.it or elisa.gremese@unicatt.it.

Submitted for publication June 17, 2020; accepted in revised form March 4, 2021.

INTRODUCTION

Rheumatoid arthritis (RA) is the most prevalent type of autoimmune arthritis, and it affects the synovial tissue (ST), leading to joint destruction. RA is characterized by a high degree of heterogeneity in terms of ST inflammation at disease onset, likely influencing the different treatment response rates among patients (1,2). Assessment of ST, despite having the potential to guide individual patients' disease management, is not currently included in RA treatment recommendations (3). However, a recent analysis of the Pathobiology of Early Arthritis Cohort demonstrated the ability to refine early clinical classification criteria using synovial pathobiologic markers (1). In particular, systematic assessment of the cellular and molecular characterization of ST from treatment-naive early RA patients revealed that discrete pathotypes mirror different ST transcriptomic signatures and prognostic profiles in RA, indicating that such an approach may be useful in deciding whether more aggressive treatment is needed (1,4).

To date, among the available scoring methods, the Krenn synovitis score (KSS) is a feasible hematoxylin and eosin (H&E)–based staining system that includes assessment of 3 histologic features, which enables discrimination between low- and high-grade synovitis in routine pathologic settings (5). Until now, the KSS has been applied mainly to ST biopsy specimens obtained during surgical procedures in patients with longstanding RA, whereas KSS scores assessed in ST biologic samples obtained from cross-sectional cohorts are lacking. In this context, minimally invasive ultrasound (US)–guided ST biopsy is a well-tolerated procedure for basic and translational studies of chronic inflammatory joint diseases, such as RA, that has been successfully applied, providing high-quality tissue samples regardless of disease stage (4,6,7).

The aims of this study were 1) to assess the diagnostic value of the KSS using ST samples obtained from minimally invasive US-guided biopsies in a large biologic sample data set of RA patients compared to patients with different inflammatory and noninflammatory joint diseases; 2) to identify pretreatment synovial biomarkers associated with specific disease characteristics; and 3) to predict treatment response in RA patients who were previously naive to treatment.

PATIENTS AND METHODS

Selection and management of patients. The study enrolled a total of 1,015 patients undergoing US-guided ST biopsy at the Fondazione Policlinico Universitario A. Gemelli IRCCS–Università Cattolica del Sacro Cuore, Division of Rheumatology (SYNGem cohort). At study entry, patients were categorized based on clinical diagnosis, as shown in Supplementary Figure 1A (available available on the *Arthritis & Rheumatology* website at http://onlinelibrary.wiley.com/doi/10.1002/art.41726/abstract). A total of 545 patients who fulfilled the 2010 European Alliance of Associations for Rheumatology (EULAR)/American College of Rheumatology (ACR) classification criteria for RA (8) (240 patients naive to treatment with conventional disease-modifying antirheumatic drugs [DMARDs], 213 patients resistant to conventional DMARDs, and 92 patients who had achieved sustained clinical remission and who were in remission based on the findings from US assessment of synovitis [7]), 167 patients who fulfilled the classification criteria for psoriatic arthritis (PsA) (103 patients naive to treatment with conventional DMARDs, 48 patients resistant to conventional DMARDs, and 27 who had achieved sustained clinical remission and who were in remission based on the findings from US assessment of synovitis [7,9]), 199 patients classified as having undifferentiated peripheral inflammatory arthritis (UPIA) (10), 18 patients with crystal-induced arthritis, 26 patients with connective tissue diseases (CTDs), and 60 patients with osteoarthritis. The clinical and laboratory parameters for the disease categories of enrolled patients are listed in Table 1. All treatment-naive RA patients were treated according to a treat-to-target strategy (11). Briefly, all treatment-naive RA patients began taking conventional DMARDs, such as methotrexate, at the maximum tolerated dosage (up to 20 mg/week) according to the recommendations for RA management (12) and were followed up every 3 months to record the DAS28-based disease remission rate after 6 months of follow-up (13). The study protocol was approved by the Ethics Committee of the Università Cattolica del Sacro Cuore (approval no. 6334/15). All subjects provided signed informed consent.

US assessment. At baseline, each patient underwent US assessment following the same protocol (13) using gray-scale and power Doppler sonography (PDS) of the biopsied joint. US assessment was performed by 2 rheumatologists experienced in US (MRG and LP), who were unaware of the clinical and laboratory findings. US was conducted using a commercially available real-time scanner (MyLabTwice from Esaote). ST hypertrophy was measured (in centimeters), and a semiquantitative scoring method, which consists of a 0–3 scale, was used to grade the severity of synovitis based on power Doppler signals, in which a score of 0 = no power Doppler, 1 = minimal power Doppler, 2 = moderate power Doppler, and 3 = severe power Doppler (10,14).

ST biopsy performance and KSS assessment. Each patient underwent US-guided knee ST biopsy following the published protocol (15,16). Using the US view, the best point of entrance for the biopsy needle was identified on the lateral margin of the suprapatellar recess. Each patient was provided with a face mask and cap, and the procedure was performed under sterile conditions. Skin was disinfected twice with iodine solution, starting from the point of needle entrance up to 25 cm proximally and distally. The skin, subcutaneous tissue, and joint capsule were anesthetized with 10 ml of 2% lidocaine. Next, a 14-gauge needle (Precisa 1410-HS Hospital Service Spa) was inserted into the

Table 1. Demographic and clinical characteristics of the study patients identified from the SYNGem cohort (n = 1,105)*

					RA (n = 545)			PsA (n = 167)		
	OA (n = 60)	Crystal-induced arthritis (n = 18)	CTD (n = 26)	UPIA (n = 199)	Treatment-naive (n = 240)	Resistant to conventional DMARDs (n = 213)	In remission (n = 92)	Treatment-naive (n = 103)	Resistant to conventional DMARDs (n = 48)	In remission (n = 27)
Female sex	52 (86.7)	7 (38.9)	25 (96.2)	151 (75.9)	188 (78.3)	181 (85.0)	69 (75.0)	66 (64.1)	30 (62.5)	13 (48.1)
Age, mean ± SEM years	65.43 ± 1.15	68.88 ± 3.06	54.88 ± 2.64	53.24 ± 0.88	55.68 ± 1.02	56.81 ± 0.90	57.83 ± 1.51	55.96 ± 1.34	56.71 ± 1.53	59.18 ± 1.97
Disease duration, mean ± SEM years	–	–	–	1.82 ± 0.11	1.21 ± 0.05	6.49 ± 0.34	9.47 ± 0.67	1.53 ± 0.15	3.67 ± 0.44	7.85 ± 0.63
RA status										
VERA	–	–	–	–	63 (26.3)	–	–	–	–	–
Early RA	–	–	–	–	84 (35.0)	–	–	–	–	–
Non–early RA	–	–	–	–	93 (38.8)	–	–	–	–	–
RA-specific antibodies	0 (0)	0 (0)	0 (0)	32 (16.1)	147 (61.3)	124 (58.2)	60 (65.2)	0 (0)	0 (0)	0 (0)
ACPAs	0 (0)	0 (0)	0 (0)	27 (13.5)	122 (50.8)	111 (52.1)	56 (60.9)	0 (0)	0 (0)	0 (0)
Titer, mean ± SEM IU/ml	–	–	–	12.00 ± 2.97	128.81 ± 19.50	125.75 ± 19.38	106.1 ± 223.4	0.17 ± 0.04	0.10 ± 0.00	0.10 ± 0.00
IgM-RF	0 (0)	0 (0)	0 (0)	10 (5.0)	106 (44.2)	87 (40.8)	41 (44.6)	0 (0)	0 (0)	0 (0)
Titer, mean ± SEM IU/ml	–	–	–	17.31 ± 4.99	72.09 ± 8.31	79.85 ± 10.34	74.5 ± 136.4	4.84 ± 2.29	1.55 ± 0.80	1.60 ± 1.5
IgA-RF	0 (0)	0 (0)	0 (0)	5 (2.5)	91 (42.7)	74 (34.7)	34 (37.0)	0 (0)	0 (0)	0 (0)
Titer, mean ± SEM IU/ml	–	–	–	5.14 ± 1.61	67.30 ± 9.17	51.78 ± 7.51	67.5 ± 138.7	2.73 ± 1.25	1.81 ± 1.34	1.50 ± 1.40
DAS28, mean ± SEM	–	–	–	3.96 ± 0.12	5.46 ± 0.08	5.47 ± 0.08	2.22 ± 0.03	–	–	–
Minimal disease activity	–	–	–	–	–	–	–	–	–	27 (100.0)
MTX dose up to 20 mg/week, mean ± SEM	–	–	–	–	–	16.81 ± 0.56	14.67 ± 0.47	–	15.45 ± 0.87	14.98 ± 0.86
Anti-TNF usage	–	–	–	–	–	–	92 (100.0)	–	–	27 (100.0)

* Except where indicated otherwise, values are the number (%) of patients. RA = rheumatoid arthritis; PsA = psoriatic arthritis; OA = osteoarthritis; CTD = connective tissue disease; UPIA = undifferentiated peripheral inflammatory arthritis; DMARDs = disease-modifying antirheumatic drugs; VERA = very early rheumatoid arthritis; ACPAs = anti–cyclic citrullinated protein antibodies; RF = rheumatoid factor; DAS28 = Disease Activity Score in 28 joints; MTX = methotrexate; anti-TNF = anti–tumor necrosis factor.

joint. Regions of synovial hypertrophy were identified under gray-scale guidance to ensure sampling of representative ST. As shown in Supplementary Figure 1A (available on the *Arthritis & Rheumatology* website at http://onlinelibrary.wiley.com/doi/10.1002/art.41726/abstract), all ST specimens obtained (at least 6–8 fragments) were fixed in 10% neutral buffered formalin, embedded in paraffin, sectioned at 3 μm, and stained with H&E as follows: sections were deparaffinized in xylene and rehydrated in a series of graded ethanol, stained in hematoxylin, and counterstained in eosin/phloxine. Finally, sections were dehydrated, cleared in xylene, and mounted with Bio Mount (Bio-Optica).

Slides were examined using a light microscope (Leica DM2000) by 2 trained pathologists (MG and FF) who were unaware of the patients' clinical and immunologic characteristics. Synovitis severity was graded according to 3 ST features (synovial lining cell layer, stromal cell density, and inflammatory infiltrates), each ranked on a scale where 0 = none, 1 = slight, 2 = moderate, and 3 = strong. The analysis was done manually and included assessment of the whole tissue sections (at least 2 sequential sections for each patient) (mean ± SEM number of sections 2.29 ± 0.10 sections), and the highest score obtained from the analysis was recorded. The values of the parameters were summed and interpreted as follows: a score of 0–1 = no synovitis, 2–4 = low-grade synovitis, and 5–9 = high-grade synovitis (5) (Supplementary Figures 1B and C, available on the *Arthritis & Rheumatology* website at http://onlinelibrary.wiley.com/doi/10.1002/art.41726/abstract).

Moreover, the presence or absence of lymphocytes, plasma cells, and mucin was assessed for each ST sample. Briefly, using a high-magnification field of the whole tissue section, cells were considered to be lymphocytes if they were as small as erythrocytes and consisted almost entirely of nuclei and had only minimal cytoplasm visible on deep staining with hematoxylin. Conversely, cells were defined as plasma cells if they were larger than lymphocytes, were a round-to-ovoid shape containing abundant cytoplasm with a pale perinuclear area corresponding to the Golgi apparatus, and had a round, eccentrically placed nucleus with coarse chromatin arranged in a clock face (art wheel) pattern (Supplementary Figures 2A and B, available on the *Arthritis & Rheumatology* website at http://onlinelibrary.wiley.com/doi/10.1002/art.41726/abstract). The microanatomic organization of ST inflammation was categorized into "aggregate" or "no aggregate" based on the presence of inflammatory cell aggregates within 2 sequential ST sections in the same patient: if no inflammatory cell aggregates were found in the whole tissue section, the synovitis pattern was defined as "no aggregate."

Finally, 97 ST samples obtained from treatment-naive RA patients were processed for pathotype assessment using immunohistochemical (IHC) analysis. This is described in the Supplementary Materials and Methods (available on the *Arthritis & Rheumatology* website at http://onlinelibrary.wiley.com/doi/10.1002/art.41726/abstract).

Statistical analysis. The statistical analysis was performed using SPSS version 20.0 and GraphPad Prism software packages. Categorical and quantitative variables were described using frequencies, percentages, and mean ± SEM. Demographic and clinical features were compared between patients using the nonparametric Mann-Whitney U test or chi-square test, as appropriate. Spearman's rank correlation test was used for assessment of correlation between variables in all analyses.

An exploratory univariate analysis was first conducted to assess adequate event frequency between the outcomes and the candidate prognostic factors. Univariate associations between candidate predictors and outcomes were assessed using multivariable logistic regression analyses. In particular, predictors with univariate associations ($P < 0.05$) were included in the multivariable model. Finally, a nomogram was built to distinguish between treatment-naive RA patients with the outcome (i.e., achievement of clinical remission at 6 months following treatment initiation, assessed according to the DAS28) and those without the outcome. The performance of the nomogram was assessed using discrimination and calibration analyses. The discriminative ability of the model was determined by the area under the receiver operating characteristic (ROC) curve, which ranged from 0.5 (no discrimination) to 1 (perfect discrimination). The calibration of the prediction model was performed using a visual calibration plot comparing the predicted and actual probability of remission. In addition, the nomogram was subjected to 1,000 bootstrap resamples for internal validation, to assess their predictive accuracies. The model was developed and validated.

All statistical analyses and generation of graphics were performed using the Regression Modeling Strategies package of R 3.5.3 (The R Foundation). For all analyses, P values less than 0.05 were considered significant, and all tests were 2-tailed, unless otherwise indicated.

RESULTS

Effect of disease phase on features of synovial inflammation in RA and other chronic inflammatory joint diseases. Table 1 shows the demographic and clinical characteristics of the 1,015 enrolled patients. As shown in Figure 1A, KSS category distribution was contingent on disease category in patients with inflammatory and noninflammatory joint diseases. In particular, treatment-naive RA patients had the highest rate of high-grade synovitis (54.6%) compared to OA patients (2.9%; $P < 0.0001$) (Figure 1B). Moreover, treatment-naive RA patients had higher KSS scores (mean ± SEM 4.81 ± 0.15) compared to UPIA patients (2.80 ± 0.14; $P < 0.001$), treatment-naive PsA patients (3.00 ± 0.17; $P < 0.001$), CTD patients (2.90 ± 0.50; $P < 0.001$), patients with crystal-induced arthritis (3.44 ± 0.42; $P = 0.01$), and OA patients (1.70 ± 0.15; $P < 0.001$) (Figure 1C).

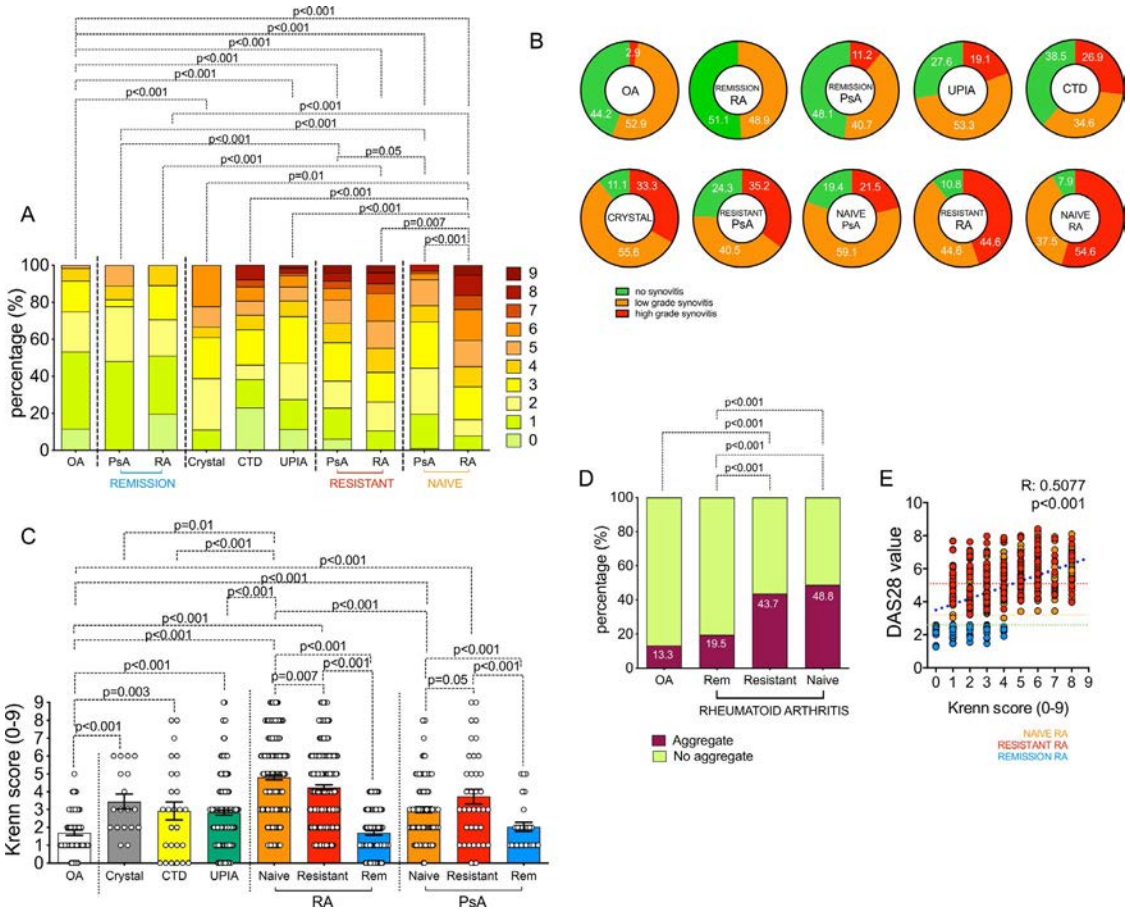

Figure 1. Degree of synovial tissue (ST) inflammation in relation to disease category among patients with inflammatory and noninflammatory joint conditions in the SYNGem cohort. **A**, Distribution of Krenn synovitis scores (KSS) according to disease category among patients with osteoarthritis (OA) (n = 60), patients who achieved sustained clinical remission (Rem) and ultrasound (US) imaging–based remission (psoriatic arthritis [PsA] n = 27, rheumatoid arthritis [RA] n = 92), patients with crystal-induced arthritis (n = 18), patients with connective tissue diseases (CTDs) (n = 26), patients with undifferentiated peripheral inflammatory arthritis (UPIA) (n = 199), patients resistant to treatment with conventional disease-modifying antirheumatic drugs (PsA n = 48, RA n = 47), and treatment-naive patients (PsA n = 103, RA n = 240). **B**, Degree of synovitis according to disease category. **C**, Distribution of mean KSS scores according to disease category. Each circle represents a single patient; values are the mean ± SEM. **D**, Follicular synovitis based on presence versus absence of inflammatory cell aggregates within 2 sequential ST sections from OA patients and RA patients stratified by disease category. **E**, Correlation between KSS scores and Disease Activity Scores in 28 joints (DAS28) in RA patients (n = 545) stratified by disease category.

Considering the different disease phases, the KSS was higher in treatment-naive RA patients (mean ± SEM 4.81 ± 0.15) and in RA patients resistant to conventional DMARDs (4.24 ± 0.15) compared to RA patients who had achieved sustained remission (1.69 ± 0.13; $P < 0.0001$, by analysis of variance [ANOVA]); similar findings were observed in PsA patients (treatment-naive PsA patients and PsA patients resistant to conventional DMARDs had scores of 3.00 ± 0.17 and 3.73 ± 0.42 in treatment-naive PsA patients and PsA patients resistant to conventional DMARDs, respectively, versus 2.04 ± 0.26 in PsA patients who had achieved sustained remission; $P = 0.0023$, by ANOVA) (Figure 1C). Moreover, considering the 3 subitems composing the KSS, treatment-naive RA patients had significantly higher KSS scores for synovial hyperplasia ($P = 0.0064$), stromal cell density ($P = 0.0366$), and inflammatory infiltrates ($P = 0.0235$) when compared to the KSS scores for these components in RA patients resistant to conventional DMARDs (Supplementary Figure 3A, available on the *Arthritis & Rheumatology* website at http://onlinelibrary.wiley.com/doi/10.1002/art.41726/abstract).

In analyzing the semiqualitative composition of the ST infiltrates, ST from treatment-naive RA patients was more likely to be enriched with plasma cells (65.4%), lymphocytes (95.0%), and mucin (87.1%) than ST from RA patients resistant to conventional DMARDs (56.3% plasma cells [$P < 0.0001$], 90.1% lymphocytes [$P < 0.0001$], 79.3% mucin [$P < 0.0001$]) and RA patients who had achieved sustained remission (26.1% plasma cells [$P < 0.0001$], 65.2% lymphocytes [$P < 0.0001$], and 68.5% mucin [$P < 0.0001$]) (Supplementary Figures 3B–D, available on the *Arthritis & Rheumatology* website at http://onlinelibrary.wiley.com/doi/10.1002/art.41726/abstract).

Moreover, in RA, the microanatomic organization of the ST inflammatory infiltrate was dependent on disease phase, and there was a significant reduction in the synovial inflammatory cell aggregate rate in RA patients who had achieved sustained remission (19.5%) compared to treatment-naive RA patients (48.8%; $P < 0.001$) or RA patients resistant to conventional DMARDs (43.7%; $P < 0.001$) (Figure 1D). Finally, analyzing the whole RA cohort (n = 545), the KSS of the biopsied joint directly correlated with the DAS28 at the time that the ST biopsy was performed ($P < 0.001$) (Figure 1E). Hence, results from the assessment of ST directly mirror the disease activity status across the whole disease course of RA.

Effect of US features on KSS in RA and other chronic inflammatory joint diseases. Assessment of synovial hypertrophy and findings from PDS of the biopsied joint were recorded for each patient and compared across different disease categories (Figure 2A). As shown in Figure 2B, treatment-naive RA patients had higher ST thickness than OA patients ($P < 0.001$). Moreover, ST hyperplasia was contingent on disease phase in both RA patients (mean ± SEM degree of synovial hypertrophy 1.10 ± 0.03 cm, 1.0 ± 0.02 cm, and 0.84 ± 0.02 cm in treatment-naive RA patients, RA patients resistant to conventional DMARDs, and RA patients in sustained remission, respectively; $P < 0.0001$ by ANOVA) and PsA patients (mean ± SEM 1.12 ± 0.04 cm, 1.15 ± 0.05 cm, and 0.90 ± 0.06 cm in treatment-naive PsA patients, PsA patients resistant to conventional DMARDs, and PsA patients in sustained remission, respectively; $P = 0.0112$ by ANOVA) (Figure 2B).

When considering the extent of disease activity in the ST samples, treatment-naive RA patients had a higher power Doppler score in the biopsied joint than that when compared to UPIA patients ($P < 0.001$), CTD patients ($P = 0.03$), and OA patients ($P < 0.001$), but the scores were similar to those of RA patients resistant to conventional DMARDs ($P = 0.27$) and patients with

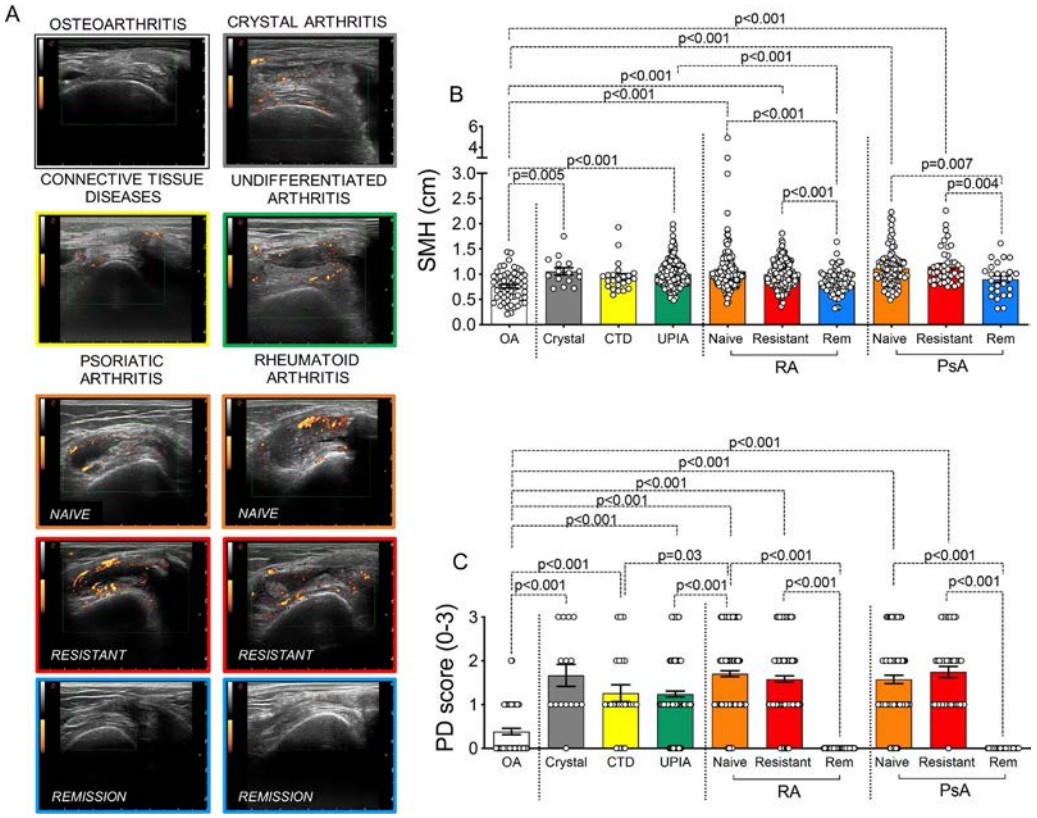

Figure 2. Features of US-assessed synovitis in relation to disease category among patients with RA and other chronic inflammatory joint diseases in the SYNGem cohort. **A**, Images from power Doppler sonography (PDS) assessment of knee ST from patients in each disease category. **B**, Distribution of the degree of synovial membrane hypertrophy (SMH), measured as ST thickness on PDS, in the biopsied joints of patients according to disease category. In treatment-naive RA patients, ST thickness was significantly higher than that in OA patients (mean ± SEM 1.10 ± 0.03 cm versus 0.75 ± 0.04 cm; $P < 0.001$), but did not differ from that in UPIA patients (1.01 ± 0.02 cm; $P = 0.1733$). **C**, Distribution of PD synovial hypertrophy scores in the ST biopsy samples from patients according to disease category. In treatment-naive RA patients, PD scores were significantly higher than those in UPIA patients (1.71 ± 0.10 versus 1.24 ± 0.07; $P < 0.001$), CTD patients (1.26 ± 0.19; $P = 0.03$), and OA patients (0.38 ± 0.07; $P < 0.001$), but were similar to that in RA patients resistant to treatment (1.58 ± 0.10; $P = 0.27$) and patients with crystal-induced arthritis (1.67 ± 0.25; $P = 0.88$). In **B** and **C**, each circle represents a single patient; values are the mean ± SEM. See Figure 1 for other definitions.

crystal-induced arthritis (P = 0.88). Additionally, the power Doppler score directly correlated with the KSS in the corresponding joint in the whole study cohort (P < 0.0001), as well as in RA patients (P < 0.0001), PsA patients (P = 0.002), and UPIA patients (P = 0.004) (Supplementary Figures 4A–D, available on the *Arthritis & Rheumatology* website at http://onlinelibrary.wiley.com/doi/10.1002/art.41726/abstract).

Effect of disease characteristics on KSS and synovial inflammation in treatment-naive RA patients. In stratifying treatment-naive RA patients (n = 240) based on demographic characteristics (age and sex), there were no significant differences in terms of KSS distribution (data not shown). However, when considering treatment-naive RA patients according to the time since the onset of symptoms to the time of ST biopsy, treatment-naive RA patients whose ST was biopsied within 3 months of joint symptom onset had lower KSS scores (mean ± SEM 4.11 ± 0.26) than RA patients whose ST was analyzed within 3–12 months (4.88 ± 0.26; P = 0.04) or >12 months (5.19 ± 0.23; P = 0.002) since symptom onset (Figures 3A–C). Moreover, treatment-naive RA patients whose ST was biopsied within 3 months of joint symptom onset had lower scores for synovial hyperplasia, stromal cell density, and inflammatory infiltrates (mean ± SEM 1.37 ± 0.12, 1.49 ± 0.10, and 1.26 ± 0.10, respectively) when compared to RA patients whose ST was biopsied >12 months since the onset of symptoms (mean ± SEM scores 1.79 ± 0.10, 1.81 ± 0.10, and 1.62 ± 0.10, respectively; P = 0.007, P = 0.01, and P = 0.01, respectively) (Figure 3D). However, the microanatomic organization of the synovial inflammatory infiltrates, in terms of the follicular structure, did not differ when comparing RA patients whose ST was biopsied within 3 months of the onset of joint symptoms (44.4%) and RA patients whose ST was biopsied within 3–12 months (47.6%; P = 0.740) or >12 months (52.7%; P = 0.332) since symptom onset (Figure 3E), as well as when comparing the percentages of plasma cells, lymphocytes, and mucin in the ST

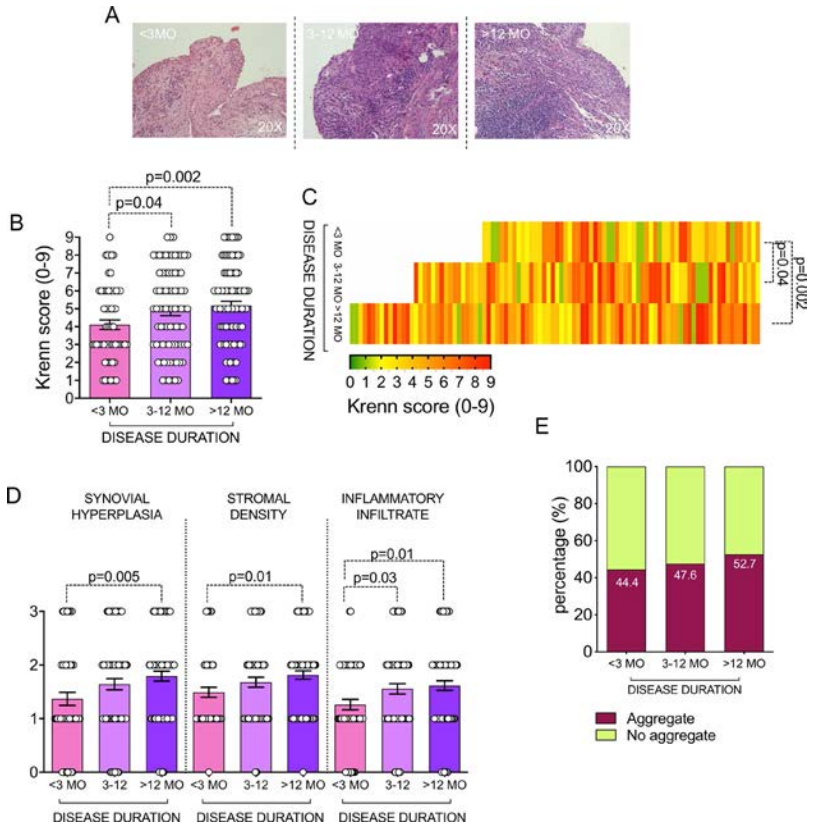

Figure 3. ST inflammation in relation to disease characteristics in treatment-naive RA patients. **A**, Hematoxylin and eosin staining of ST obtained using minimally invasive US-guided biopsy of the knees of treatment-naive RA patients. Each image shows a biopsy sample from an individual patient according to disease duration (time since symptom onset to time of biopsy <3 months [MO], 3–12 months, or >12 months). **B**, Distribution of mean KSS scores in treatment-naive RA patients according to disease duration. **C**, Heatmap showing distribution of KSS scores in treatment-naive RA patients according to disease duration. Each bar represents a single patient. **D**, Distribution of mean scores for subcomponents of the KSS (synovial hyperplasia, stromal cell density, and inflammatory infiltrates) in treatment-naive RA patients according to disease duration. In **B** and **D**, each circle represents a single patient; values are the mean ± SEM. **E**, Follicular synovitis based on presence versus absence of inflammatory cell aggregates in treatment-naive RA patients according to disease duration. See Figure 1 for other definitions.

(Supplementary Figures 5A–C, available on the *Arthritis & Rheumatology* website at http://onlinelibrary.wiley.com/doi/10.1002/art.41726/abstract). Finally, US features in treatment-naive RA patients did not differ based on the timeframe from joint symptom onset (Supplementary Figures 6A–B, available on the *Arthritis & Rheumatology* website at http://onlinelibrary.wiley.com/doi/10.1002/art.41726/abstract).

To determine whether the semiquantitative evaluation of the degree of synovitis using the KSS is representative of the cellular composition of synovial inflammation, 97 ST samples from treatment-naive RA patients were analyzed by IHC for the distribution of CD68, CD20, CD3, and CD138 cells (Supplementary Table 1, available on the *Arthritis & Rheumatology* website at http://onlinelibrary.wiley.com/doi/10.1002/art.41726/abstract), revealing that treatment-naive RA patients with a lympho-myeloid pathotype had the highest KSS scores (mean ± SEM 5.67 ± 0.26) compared to treatment-naive RA patients with a diffuse myeloid pathotype (4.06 ± 1.71; $P < 0.0001$) and those with a pauci-immune pathotype (2.30 ± 0.26; $P < 0.0001$) (Supplementary Figure 7A, available on the *Arthritis & Rheumatology* website at http://onlinelibrary.wiley.com/doi/10.1002/art.41726/abstract). Moreover, KSS-based evaluation of the degree of synovitis directly correlated with IHC-based synovitis assessment in terms of CD68, CD20, CD3, and CD138 IHC scores (Supplementary Figure 7B). Interestingly, ROC curve analysis revealed that a KSS of ≥6 had significant capacity to identify treatment-naive RA patients who were more likely to have a lympho-myeloid pathotype (51.0% sensitivity, 82.6% specificity; area under the curve [AUC] 0.79 [95% confidence interval (95% CI) 0.70–0.89] [$P < 0.0001$]). Conversely, a KSS of ≤2 had greater capacity to

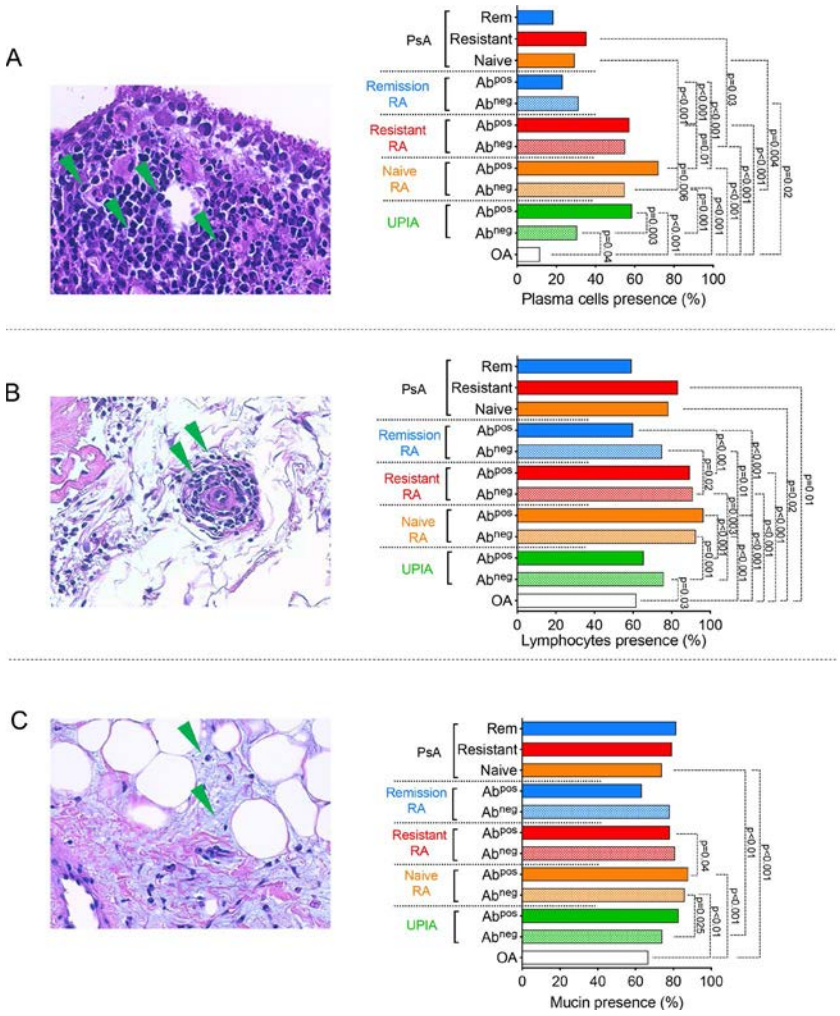

Figure 4. Composition of ST inflammation in relation to disease category and autoantibody status. **A–C**, Left, Hematoxylin and eosin (H&E) staining of ST obtained using minimally invasive US-guided biopsy of the knee. Images show ST from treatment-naive RA patients positive for ACPA and/or IgM/IgA–rheumatoid factor autoantibodies (Ab^{pos}), displaying enrichment of plasma cells (**A**) and infiltration of lymphocytes (**B**) and mucin (**C**) (indicated by **green arrowheads**). Original magnification × 40. Right, Results of H&E staining quantified as the percentage of plasma cells (**A**), lymphocytes (**B**), and mucin (**C**) among patients with PSA in each disease category, RA patients in each disease category stratified by autoantibody status, UPIA patients stratified by autoantibody status, and OA patients. See Figure 1 for other definitions.

identify treatment-naive RA patients were are more likely to have a pauci-immune pathotype (50.0% sensitivity, 96.5% specificity; AUC 0.09 [95% CI 0.02–0.17] [$P < 0.0001$]) (Supplementary Figures 7C and D).

Since autoantibody positivity was found to be related to the composition of ST inflammation in RA (17), the study cohort was stratified based on the presence of anti–cyclic citrullinated protein antibodies (ACPAs) and/or IgM–rheumatoid factor (IgM-RF) and IgA-RF at the time that ST biopsy was performed. Treatment-naive RA patients positive for ACPA and/or IgM/IgA-RF had higher KSS scores (mean ± SEM 5.05 ± 0.19) than RA patients negative for ACPA and/or IgM/IgA-RF (4.43 ± 0.22; $P = 0.04$) (Supplementary Figure 8A, available on the *Arthritis & Rheumatology* website at http://onlinelibrary.wiley.com/doi/10.1002/art.41726/abstract), and treatment-naive RA patients negative for ACPA and/or IgM/IgA-RF had significantly higher KSS scores (4.43 ± 0.22) compared to treatment-naive PsA patients (2.99 ± 0.17; $P < 0.0001$). Interestingly, treatment-naive RA patients positive for IgM/ ACPA and/or IgA-RF had significantly higher scores for inflammatory infiltrates (mean ± SEM 1.61 ± 0.07) compared to treatment-naive RA patients negative for ACPA and/or IgM/IgA-RF (1.35 ± 0.09; $P = 0.03$), whereas no significant difference in the scores for synovial hyperplasia or stromal cell density were observed between the positive and negative autoantibody groups (Supplementary Figures 8B–D). Moreover, the KSS directly correlated with plasma levels of ACPAs ($P = 0.016$), IgM-RF ($P = 0.009$), and IgA-RF ($P = 0.005$) in treatment-naive RA patients (Supplementary Figures 8E–G), whereas no significant differences were found in KSS scores in RA patients resistant to conventional DMARDs or in RA patients who had achieved sustained remission based on autoantibody positivity (Supplementary Figures 8A–D).

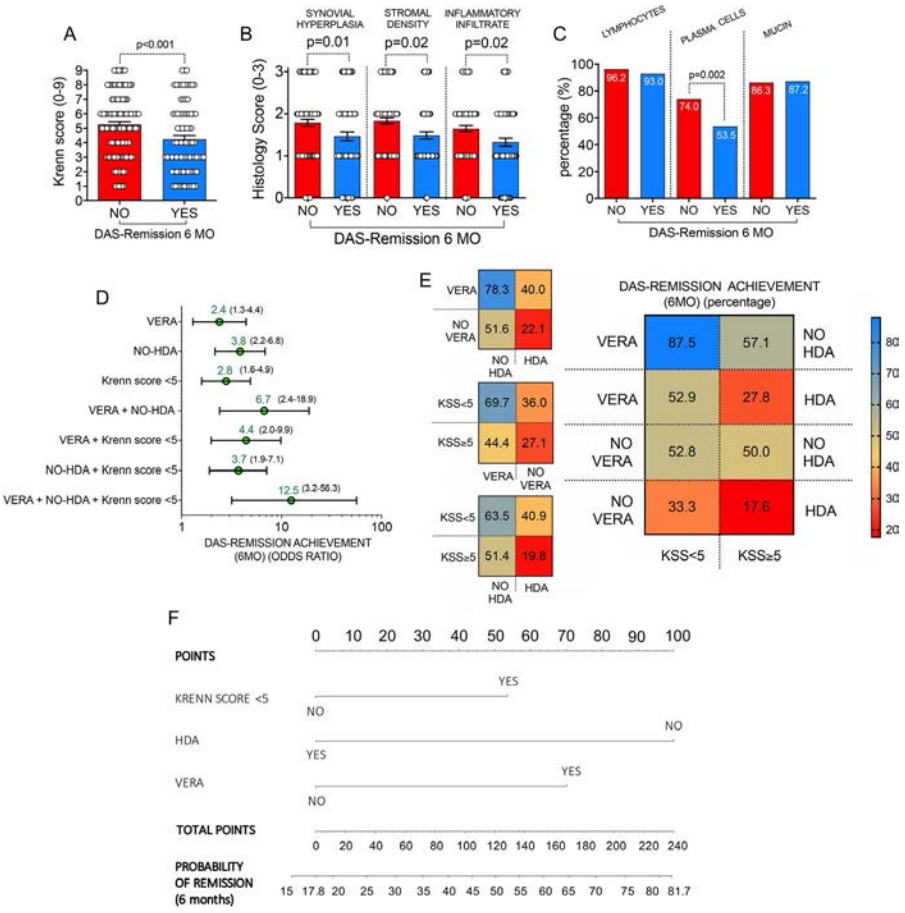

Figure 5. Nomogram for the prediction of early achievement of clinical remission based on the Disease Activity Score in 28 joints (DAS28) in treatment-naive RA patients. **A** and **B**, Distribution of mean KSS scores (**A**) and mean histology scores for subcomponents of the KSS (**B**) in treatment-naive RA patients based on achievement versus lack of achievement of DAS28-based clinical remission at 6 months (MO). Each circle represents a single patient; values are the mean ± SEM. **C**, Distribution of lymphocytes, plasma cells, and mucin presence in ST from treatment-naive RA patients based on presence versus absence of achievement of DAS28-based clinical remission at 6 months. **D** and **E**, Odds of achieving DAS28-based remission at 6 months (**D**) and percentage of patients achieving DAS28-based remission at 6 months (**E**) among treatment-naive RA patients according to different baseline characteristics, including presence versus absence of very early RA (VERA), presence versus absence of high disease activity (HDA), and a KSS score categorized as <5 versus ≥5. Values in **D** are the odds ratio (with 95% confidence interval) for achievement of DAS28-based remission at 6 months. **F**, Nomogram for the computation of the probability of achieving DAS28-based remission at 6 months in treatment-naive RA patients. See Figure 1 for other definitions.

In analyses of the composition of ST inflammatory infiltrates, ST from treatment-naive RA patients positive for ACPA and/or IgM/IgA-RF was enriched with plasma cells to a greater extent than ST from treatment-naive RA patients negative for ACPA and/or IgM/IgA-RF (72.1% versus 54.8%; $P = 0.006$) (Figure 4A). Conversely, no significant differences in terms of lymphocytes and mucin presence were found when RA patients were stratified based on presence versus absence of ACPA and/or IgM/IgA-RF (Figures 4B–C). Therefore, the timing of first medical referral, the autoimmune features, and the baseline disease burden significantly impact the degree of ST inflammation in treatment-naive RA patients.

Baseline KSS as a predictor of early achievement of DAS28-based remission in treatment-naive RA patients. Among the 240 enrolled treatment-naive RA patients, 217 (90.4%) reached at least 6 months of follow-up, of whom 86 (39.6%) achieved DAS28-based remission. A total of 23 patients (9.6%) were lost to follow-up. The baseline characteristics that were differentially distributed among treatment-naive RA patients based on achievement of DAS28-based remission at 6 months were investigated. The comparison revealed that DAS28 scores at baseline were lower in treatment-naive RA patients achieving DAS28-based remission at 6 months compared to those who did not achieve DAS28-based remission at 6 months (mean ± SEM 5.00 ± 0.12 versus 5.83 ± 0.10; $P < 0.001$), and patients in the remission group were more likely referred to a first medical evaluation within 3 months of symptom onset compared to patients in the no remission group (37.2% versus 19.8%; $P = 0.005$). In addition, the characteristics of the ST samples identified by US at baseline did not differ in treatment-naive RA patients with or without achievement of DAS28-based remission at 6 months (Supplementary Table 2. available on the *Arthritis & Rheumatology* website at http://onlinelibrary.wiley.com/doi/10.1002/art.41726/abstract). However, treatment-naive RA patients who achieved DAS28-based remission at 6 months had lower KSS scores at baseline (mean ± SEM 4.24 ± 0.25) than treatment-naive RA patients who did not achieve this outcome (5.26 ± 0.18; $P < 0.001$) (Figure 5A and Supplementary Table 2).

In considering the 3 components of synovial inflammation assessed in the KSS, scores for synovial hyperplasia, stromal cell density, and inflammatory infiltrates were significantly lower at baseline in treatment-naive RA patients achieving DAS28-based remission at 6 months compared to those who did not achieve DAS28-based remission at 6 months (mean ± SEM scores 1.47 ± 0.11, 1.49 ± 0.09, and 1.33 ± 0.10, respectively, in the remission group versus 1.79 ± 0.08, 1.83 ± 0.07, and 1.65 ± 0.07, respectively, in the no remission group; $P = 0.01$, $P = 0.02$, and $P = 0.02$, respectively) (Figure 5B). In addition, fewer ST samples from treatment-naive RA patients who achieved DAS28-based remission at 6 months were enriched with plasma cells at baseline compared to ST samples from RA patients who did not achieve 6-month DAS28-based remission (53.5% versus 74.0% of ST samples enriched with plasma cells; $P = 0.002$) (Figure 5C).

ROC curve analysis revealed that, compared to a KSS of ≥5, a KSS of <5 at baseline was more likely to identify treatment-naive RA patients who would achieve DAS28-based remission at 6 months (53.1% with KSS <5 versus 28.9% with KSS ≥5 achieving DAS28-based remission at 6 months; AUC 0.66 [95% CI 0.57–0.74] [$P = 0.001$]), with an odds ratio (OR) of 2.8 (95% CI 1.6–4.9) ($P < 0.001$); similar findings from ROC curve analyses were obtained in treatment-naive patients with very early RA (VERA) compared to those who did not develop VERA (non-VERA) (55.2% versus 34.0% achieving DAS28-based remission at 6 months; OR 2.4 [95% CI 1.3–4.4] [$P = 0.01$]) and in treatment-naive RA patients who did not have high disease activity at baseline compared to those who had high disease activity at baseline (58.6% versus 26.9% achieving DAS28-based remission at 6 months; OR 3.8 [95% CI 2.2–6.8] [$P < 0.001$]).

Both treatment-naive VERA patients and treatment-naive non-VERA patients with a KSS of <5 at baseline were more likely to achieve DAS28-based remission at 6 months compared to treatment-naive VERA patients and treatment-naive non-VERA patients with a KSS of ≥5 at baseline (42.2% of VERA patients and 44.4% of non-VERA patients achieving remission in the KSS <5 group versus 16.7% of VERA patients and 27.1% of non-VERA patients achieving remission in the KSS ≥5 group; $P = 0.011$ for VERA patients with KSS <5 versus VERA patients with KSS ≥5, $P = 0.01$ for non-VERA patients with KSS <5 versus non-VERA patients with KSS ≥5) (Figure 5D, Supplementary Figures 9A–D, and Supplementary Figures 10A and B, available on the *Arthritis & Rheumatology* website at http://onlinelibrary.wiley.com/doi/10.1002/art.41726/abstract). Interestingly, treatment-naive VERA patients with low-grade synovitis (KSS <5) and without high disease activity at baseline were more likely to achieve DAS28-based remission at 6 months than treatment-naive RA patients not fulfilling all these criteria (87.5% versus 17.6% achieving remission; OR 32.7 [95% CI 6.4–150.5] [$P < 0.0001$]) (Figure 5E).

Nomogram for the prediction of early achievement of DAS28-based remission in treatment-naive RA patients. Based on the variables incorporated into the final regression analysis, a nomogram was constructed including the 3 significant risk factors (having VERA, not having high disease activity at baseline, and having a KSS of <5) to predict the achievement of DAS28-based remission at 6 months in treatment-naive RA patients (Figure 5F). The value of each variable was given a score on the points scale axis. A total score was calculated by adding each single-point score and projecting the value of the "total points" score to the lower "probability" line. The nomogram was validated, and as shown in Supplementary Figure 11 (available on the *Arthritis & Rheumatology* website at http://onlinelibrary.wiley.com/doi/10.1002/art.41726/abstract), a calibration curve

confirmed that the probability of remission predicted by the nomogram was consistent with the actual probabilities.

DISCUSSION

This study is the first to apply semiquantitative assessment of ST inflammation to the largest available data set of ST samples at a single center (n = 1,015) obtained by minimally invasive US-guided biopsy from cross-sectional cohorts of patients with inflammatory diseases and patients with noninflammatory diseases who were stratified based on disease phase. The results of this study show that the KSS is a reliable tool to apply in the semiquantitative assessment of synovitis, not only in RA, but also in other different inflammatory and noninflammatory joint disorders. In particular, in treatment-naive RA patients, the KSS is contingent on patients' characteristics (i.e., autoantibody positivity), disease activity, and treatment response, and the integration of the KSS, at the time of the first medical evaluation, within a multiparametric nomogram enabled prediction of 6-month achievement of DAS28-based remission in up to 80% of treatment-naive RA patients.

Differential response rates to various therapies in RA may partially be a result of the high heterogeneity of the degree of inflammation of RA target tissue, the synovial membrane (18). In this context, at the ST level, treatment-naive RA patients may display 3 specific pathotypes in terms of the microanatomic organization of inflammation and the transcriptomic signature, which are directly linked to different clinical phenotypes, disease activity/severity, and response to treatment with conventional DMARDs (4). Moreover, using ST/peripheral blood paired samples, the ST immune response was shown to be associated with differential blood immune signals (19), and interestingly, the elevation of myeloid- and lymphoid-associated ST gene expression strongly correlates with conventional DMARD response in treatment-naive RA patients at 6 months (4).

The KSS has been previously developed and validated using ST surgery specimens, thereby enabling semiquantitative categorization of patients according to degrees of synovitis in large cohorts, including low- and high-grade synovitis in patients with longstanding RA and OA (5). The KSS may also reflect clinical disease activity in patients with longstanding RA (20). Additionally, synovitis semiquantification using H&E staining enabled the categorization of RA patients into different histologic subtypes (low, mixed, and high inflammation) that can predict ST genomic subtypes associated with disease-specific features (i.e., systemic inflammation and autoantibody positivity) (2).

Therefore, the semiquantitative assessment of ST inflammation using the KSS was included in the set of items for the analysis of synovial biopsy specimens in clinical practice and translational research from the EULAR Synovitis and Outcome Measures in Rheumatology ST Biopsy Groups (21). However, to date, despite being widely used in clinical and translational research, no studies have widely applied this tool for the semiquantitative assessment of inflammation in ST samples obtained using minimally invasive US-guided ST biopsies from cross-sectional cohorts (4,22). The findings from this study show that KSS scores are differentially distributed among inflammatory and noninflammatory joint disorders and are significantly increased in treatment-naive RA patients compared to patients with other forms of inflammatory diseases (i.e., PsA) or low-grade inflammatory joint diseases (i.e., OA) and is contingent on the disease phase mirroring the disease activity (i.e., DAS28) in RA.

Large cohort studies identified a 3-month window of opportunity as the time with the best therapeutic chance for a patient to achieve complete disease remission and stop bone damage in RA (23–26); however, no studies have explored the impact of joint symptom duration on ST inflammatory features in treatment-naive RA patients. In particular, in considering RA classification criteria, RA patients who fulfilled the ACR 1997 criteria for RA (27) had higher KSS scores than RA patients who fulfilled the 2010 ACR/EULAR criteria for RA (28) without any difference in terms of the frequencies of ST pathotypes, regardless of symptom duration (1). Our findings show that treatment-naive VERA patients (<3 months since symptom onset) have lower KSS scores than treatment-naive RA patients who were referred to a first medical evaluation >12 months since symptom onset, despite no differences in the microanatomic organization of the inflammatory infiltrate, suggesting that ST inflammation dynamically changes during the course of RA. These findings provide biologic support for early intervention in RA disease management aimed at achieving the highest possible remission rate (24) and suggest that ST analysis within 3 months of symptom onset is very likely the most informative time point to predict the future course of the disease.

In the context of biomarkers for RA patient stratification, ACPA and RF positivity can be used to identify RA patients with the highest likelihood of developing early bone erosions (29,30), chronic destructive disease (31,32), and extraarticular manifestations (33,34). IHC assessment showed that ST from treatment-naive RA patients positive for ACPAs is more enriched with B lymphocytes and lymphoid aggregates than ST from RA patients negative for ACPAs and is related to higher rate of erosive disease and a worse prognosis (17). In our study, H&E-based staining of ST revealed that the KSS is higher in patients positive for IgM/IgA-RF and/or ACPA than treatment-naive RA patients negative for IgM/IgA-RF and/or ACPA, which directly correlated with ACPA and IgM/IgA-RF plasma levels at the time that ST biopsy was performed. In addition, the systematic analysis of disease phase in cross-sectional RA cohorts showed that this difference is lost when considering RA patients resistant to conventional DMARDs and patients with RA in sustained remission. Moreover, at a treatment-naive stage, ST from RA patients positive for IgM/IgA-RF and/or ACPA was found to be more enriched with plasma cells than ST from RA patients negative for IgM/IgA-RF and/or ACPA, as previously described (35), supporting the reliability of this H&E-based scoring method.

Precision medicine is an approach to disease treatment that considers individual pathobiologic variability to more accurately predict which treatment strategies will be more successful in specific groups of patients. In this context, RA may be an ideal setting for patient stratification aimed at treatment optimization. In this study, we identified and validated a cutoff value of KSS scores based on which treatment-naive RA patients with ST with a KSS of <5 at the first medical evaluation are more likely to achieve DAS28-based remission at 6 months. These findings were confirmed even after patient stratification based on disease duration and activity, with both confirmed as prognostic factors of treatment success (24,36). Moreover, as is used in cancer and in other chronic inflammatory diseases (37,38), we developed the first multiparametric nomogram (SYNGem nomogram) that is able to easily predict the probability of early achievement of DAS28-based remission in treatment-naive RA patients at a first medical evaluation. Based on the proposed nomogram, treatment-naive RA patients without high disease activity, at a first medical evaluation within 3 months since the onset of joint symptoms, and with a KSS of <5 have an 81.7% probability of achieving DAS28-based remission at 6 months compared to treatment-naive RA patients who did not fulfill any of the above-mentioned criteria, whose probability of achieving DAS28-based remission drops to 17.8%. This easy tool may be useful for stratification of patients with early disease in clinical practice, in particular, in predicting whether treatment-naive patients with very early RA will require more intensive treatment, with the goal of optimization of disease management.

Despite being the first cross-sectional study to include ST samples collected using minimally invasive US-guided biopsy, the limitations of this study include the lack of information about the cell-specific contribution (i.e., myeloid and lymphoid) within ST inflammation, which could be solved by combining IHC staining (including staining of CD68, CD20, CD3, and CD138 cells) (1,4). The inclusion of IHC staining of these cells led to a better sensitivity and specificity than KSS scores when treating patients with longstanding RA taking immunosuppressants, representing a more functional synovitis evaluation (6,39). However, in this study, KSS-based assessment of synovitis was contingent on the synovial pathotype defined using IHC assessment, directly correlating with the IHC scores of all the cells identified as playing a role in synovial inflammation, including CD68, CD20, CD3, and CD138 cells (1). Therefore, despite the KSS, semiquantitative assessment of the degree of ST inflammation is simple, with high rates of interreader and intrareader agreement, and it is informative for predicting response to first-line therapy. In patients with more advanced clinical phases of RA, deeper analyses of immunomolecular functions and transcriptomic signatures could be helpful to define therapeutic strategies and interpret their outcomes.

In conclusion, the semiquantitative assessment of the degree of synovitis, using the H&E-based KSS method, is a reliable tool to apply to biologic samples obtained using a minimally invasive technique in the routine clinical care of RA. Additionally, synovitis assessment of treatment-naive RA patients at a first medical evaluation may help identify important disease characteristics for prognosis, and such an approach may be included in future multiparametric algorithms aimed at optimizing disease management.

ACKNOWLEDGMENT

We thank all patients who agreed to participate in our study.

AUTHOR CONTRIBUTIONS

All authors were involved in drafting the article or revising it critically for important intellectual content, and all authors approved the final version to be published. Dr. Alivernini had full access to all of the data in the study and takes responsibility for the integrity of the data and the accuracy of the data analysis.

Study conception and design. Alivernini, Tolusso, Gremese.

Acquisition of data. Alivernini, Gessi, Gigante, Petricca, Perniola, Di Mario, Bui, Fedele, Capacci, Bruno, Peluso, Gremese.

Analysis and interpretation of data. Alivernini, Tolusso, Gessi, Mannocci, La Torre, Federico, Ferraccioli, Gremese.

REFERENCES

1. Lliso-Ribera G, Humby F, Lewis M, Nerviani A, Mauro D, Rivellese F, et al. Synovial tissue signatures enhance clinical classification and prognostic/treatment response algorithms in early inflammatory arthritis and predict requirement for subsequent biological therapy: results from the pathobiology of early arthritis cohort (PEAC). Ann Rheum Dis 2019;78:1642–52.
2. Orange DE, Agius P, DiCarlo EF, Robine N, Geiger H, Szymonifka J, et al. Identification of three rheumatoid arthritis disease subtypes by machine learning integration of synovial histologic features and RNA sequencing data. Arthritis Rheumatol 2018;70:690–701.
3. Smolen JS, Landewé R, Bijlsma J, Burmester GR, Dougados M, Kerschbaumer A, et al. EULAR recommendations for the management of rheumatoid arthritis with synthetic and biological disease-modifying antirheumatic drugs: 2019 update. Ann Rheum Dis 2020;79:685–99.
4. Humby F, Lewis M, Ramamoorthi N, Hackney JA, Barnes MR, Bombardieri M, et al. Synovial cellular and molecular signatures stratify clinical response to csDMARD therapy and predict radiographic progression in early rheumatoid arthritis patients. Ann Rheum Dis 2019;78:761–72.
5. Krenn V, Morawietz L, Burmester GR, Kinne RW, Mueller-Ladner U, Muller B, et al. Synovitis score: discrimination between chronic low-grade and high-grade synovitis. Histopathology 2006;49:358–64.
6. Alivernini S, Bruno B, Tolusso B, Bui L, Petricca L, Gigante MR, et al. Differential synovial tissue biomarkers among psoriatic arthritis and rheumatoid factor/anti-citrulline antibody-negative rheumatoid arthritis. Arthritis Res Therapy 2019;21:116.
7. Alivernini S, Tolusso B, Petricca L, Bui L, Di Sante G, Peluso G, et al. Synovial features of patients with rheumatoid arthritis and psoriatic arthritis in clinical and ultrasound remission differ under anti-TNF therapy: a clue to interpret different chances of relapse after clinical remission? Ann Rheum Dis 2017;76:1228–36.
8. Aletaha D, Neogi T, Silman AJ, Funovits J, Felson DT, Bingham CO III, et al. Rheumatoid arthritis classification criteria: an American College of Rheumatology/European League Against Rheumatism collaborative initiative. Arthritis Rheum 2010;62:2569–81.

9. Taylor W, Gladman D, Helliwell P, Marchesoni A, Mease P, Mielants H, et al. Classification criteria for psoriatic arthritis: development of new criteria from a large international study. Arthritis Rheum 2006;54:2665–73.
10. Alivernini S, Tolusso B, Petricca L, Bui L, Di Mario C, Gigante MR, et al. Synovial predictors of differentiation to definite arthritis in patients with seronegative undifferentiated peripheral inflammatory arthritis: microRNA signature, histological, and ultrasound features. Front Med (Lausanne) 2018;5:186.
11. Smolen JS, Breedveld FC, Burmester GR, Bykerk V, Dougados M, Emery P, et al. Treating rheumatoid arthritis to target: 2014 update of the recommendations of an international task force. Ann Rheum Dis 2016;75:3–15.
12. Smolen JS, Landewé RB, Bijlsma JW, Burmester GR, Dougados M, Kerschbaumer A, et al. EULAR recommendations for the management of rheumatoid arthritis with synthetic and biological disease-modifying anti-rheumatic drugs: 2019 update. Ann Rheum Dis 2020;79:685–99.
13. Van Gestel AM, Prevoo ML, van 't Hof MA, van Rijswijk MH, van de Putte LB, van Riel PL. Development and validation of the European League Against Rheumatism response criteria for rheumatoid arthritis: comparison with the preliminary American College of Rheumatology and the World Health Organization/International League Against Rheumatism Criteria. Arthritis Rheum 1996;39:34–40.
14. Peluso G, Michelutti A, Bosello S, Gremese E, Tolusso B, Ferraccioli G. Clinical and ultrasonographic remission determines different chances of relapse in early and long standing rheumatoid arthritis. Ann Rheum Dis 2011;70:172–5.
15. Alivernini S, MacDonald L, Elmesmari A, Finlay S, Tolusso B, Gigante MR, et al. Distinct synovial tissue macrophage subsets regulate inflammation and remission in rheumatoid arthritis. Nat Med 2020;26:1295–306.
16. Michelutti A, Gremese E, Morassi F, Petricca L, Arena V, Tolusso B, et al. B-cell subsets in the joint compartments of seropositive and seronegative rheumatoid arthritis (RA) and no-RA arthritides express memory markers and ZAP70 and characterize the aggregate pattern irrespectively of the autoantibody status. Mol Med 2011;17:901–9.
17. Orr C, Najm A, Biniecka M, McGarry T, Ng CT, Young F, et al. Synovial immunophenotype and anti–citrullinated peptide antibodies in rheumatoid arthritis patients: relationship to treatment response and radiologic prognosis. Arthritis Rheumatol 2017;69:2114–23.
18. Pitzalis C, Kelly S, Humby F. New learnings on the pathophysiology of RA from synovial biopsies [review]. Curr Opin Rheumatol 2013;25:334–44.
19. Lewis MJ, Barnes MR, Blighe K, Goldmann K, Rana S, Hackney JA, et al. Molecular portraits of early rheumatoid arthritis identify clinical and treatment response phenotypes. Cell Rep 2019;28:2455–70.
20. Schmidt T, Najm A, Mussawy H, Burghardt R, Oehler N, Krenn V, et al. General synovitis score and immunologic synovitis score reflect clinical disease activity in patients with advanced stage rheumatoid arthritis. Sci Rep 2019;9:8448.
21. Najm A, Le Goff B, Orr C, Thurlings R, Cañete JD, Humby F, et al. Standardisation of synovial biopsy analyses in rheumatic diseases: a consensus of the EULAR Synovitis and OMERACT Synovial Tissue Biopsy Groups. Arthritis Res Ther 2018;20:265.
22. Slansky E, Li J, Haupl T, Morawietz L, Krenn V, Passiler F. Quantitative determination of the diagnostic accuracy of the synovitis score and its components. Histopathology 2010;57:436–43.
23. Bosello S, Fedele AL, Peluso G, Gremese E, Tolusso B, Ferraccioli G. Very early rheumatoid arthritis is the major predictor of major outcomes: clinical ACR remission and radiographic non-progression. Ann Rheum Dis 2011;70:1292–5.
24. Gremese E, Salaffi F, Bosello SL, Ciapetti A, Bobbio-Pallavicini F, Caporali R, et al. Very early rheumatoid arthritis as a predictor of remission: a multicentre real life prospective study. Ann Rheum Dis 2013;72:858–62.
25. Van der Linden MP, le Cessie S, Raza K, van der Woude D, Knevel R, Huizinga TW, et al. Long-term impact of delay in assessment of patients with early arthritis. Arthritis Rheum 2010;62:3537–46.
26. Lukas C, Combe B, Ravaud P, Sibilia J, Landewé R, van der Heijde D. Favorable effect of very early disease-modifying antirheumatic drug treatment on radiographic progression in early inflammatory arthritis: data from the Étude et Suivi des Polyarthrites Indifférenciées Récentes (Study and Followup of Early Undifferentiated Polyarthritis). Arthritis Rheum 2011;63:1804–11.
27. Arnett FC, Edworthy SM, Bloch DA, McShane DJ, Fries JF, Cooper NS, et al. The American Rheumatism Association 1987 revised criteria for the classification of rheumatoid arthritis. Arthritis Rheum 1988;31:315–24.
28. Aletaha D, Neogi T, Silman AJ, Funovits J, Felson DT, Bingham CO III, et al. 2010 rheumatoid arthritis classification criteria: an American College of Rheumatology/European League Against Rheumatism collaborative initiative. Arthritis Rheum 2010;62:2569–81.
29. Machold KP, Stamm TA, Nell VP, Pflugbeil S, Aletaha D, Steiner G, et al. Very recent onset rheumatoid arthritis: clinical and serological patient characteristics associated with radiographic progression over the first years of disease. Rheumatology (Oxford) 2007;46:342–9.
30. Syversen SW, Gaarder PI, Goll GL, Ødegård S, Haavardsholm EA, Mowinckel P, et al. High anti-cyclic citrullinated peptide levels and an algorithm of four variables predict radiographic progression in patients with rheumatoid arthritis: results from a 10-year longitudinal study. Ann Rheum Dis 2008;67:212–7.
31. Van der Woude D, Young A, Jayakumar K, Mertens BJ, Toes RE, van der Heijde D, et al. Prevalence of and predictive factors for sustained disease-modifying antirheumatic drug–free remission in rheumatoid arthritis: results from two large early arthritis cohorts. Arthritis Rheum 2009;60:2262–71.
32. Mjaavatten MD, Uhlig T, Haugen AJ, Nygaard H, Sidenvall G, Helgetveit K, et al. Positive anti-citrullinated protein antibody status and small joint arthritis are consistent predictors of chronic disease in patients with very early arthritis: results from the NOR-VEAC cohort. Arthritis Res Therapy 2009;11:R146.
33. Aubart F, Crestani B, Nicaise-Roland P, Tubach F, Bollet C, Dawidowicz K, et al. High levels of anti-cyclic citrullinated peptide autoantibodies are associated with co-occurrence of pulmonary diseases with rheumatoid arthritis. J Rheumatol 2011;38:979–82.
34. Alivernini S, Fedele AL, Cuoghi I, Tolusso B, Ferraccioli G. Citrullination: the loss of tolerance and development of autoimmunity in rheumatoid arthritis. Reumatismo 2008;60:85–94.
35. Rivellese F, Mauro D, Nerviani A, Pagani S, Fossati-Jimack L, Messemaker T, et al. Mast cells in early rheumatoid arthritis associate with disease severity and support B cell autoantibody production [review]. Ann Rheum Dis 2018;77:1773–81.
36. Gamboa-Cárdenas RV, Ugarte-Gil MF, Loreto M, Sacnun MP, Saurit V, Cardiel MH, et al. Clinical predictors of remission and low disease activity in Latin American early rheumatoid arthritis: data from the GLAFAR cohort. Clin Rheumatol 2019;38:2737–46.
37. Balachandran VP, Gonen M, Smith JJ, De Matteo RP. Nomograms in oncology: more than meets the eye. Lancet Oncol 2015;16: e173–80.
38. Guizzetti L, Zou G, Khanna R, Dulai PS, Sandborn WJ, Jairath V, et al. Development of clinical prediction models for surgery and complications in Crohn's disease. J Crohns Colitis 2018;12:167–77.
39. Najm A, Le Goff B, Venet G, Garraud T, Amiaud J, Biha N, et al. IMSYC immunologic synovitis score: a new score for synovial membrane characterization in inflammatory and non-inflammatory arthritis. Joint Bone Spine 2019;86:77–81.

Arthritis & Rheumatology
Vol. 73, No. 9, September 2021, pp 1614–1625
DOI 10.1002/art.41704

American College of Rheumatology
Empowering Rheumatology Professionals

Neutrophil Phospholipase Cγ2 Drives Autoantibody-Induced Arthritis Through the Generation of the Inflammatory Microenvironment

Krisztina Futosi, Orsolya Kása, Kata P. Szilveszter, and Attila Mócsai

Objective. Gain-of-function mutations and genome-wide association studies have linked phospholipase Cγ2 (PLCγ2) to various inflammatory diseases, including arthritis in humans and mice. PLCγ2-deficient (*Plcg2*$^{-/-}$) mice are also protected against experimental arthritis. This study was undertaken to test how PLCγ2 triggers autoantibody-induced arthritis in mice.

Methods. PLCγ2 was deleted from various mouse cellular lineages. Deletion efficacy and specificity were tested by immunoblotting and intracellular flow cytometry. Autoantibody-induced arthritis was triggered by K/BxN serum transfer. The role of neutrophil PLCγ2 was further investigated by analysis of the inflammatory exudate, competitive in vivo migration assays, and in vitro functional studies.

Results. PLCγ2 deficiency in the entire hematopoietic compartment completely blocked autoantibody-induced arthritis. Arthritis development was abrogated by deletion of PLCγ2 from myeloid cells or neutrophils but not from mast cells or platelets. Neutrophil infiltration was reduced in neutrophil-specific PLCγ2-deficient (*Plcg2*$^{\Delta PMN}$) mice. However, this was not due to an intrinsic migration defect since *Plcg2*$^{\Delta PMN}$ neutrophils accumulated normally when wild-type cells were also present in mixed bone marrow chimeras. Instead, the *Plcg2*$^{\Delta PMN}$ mutation blocked the accumulation of interleukin-1β, macrophage inflammatory protein 2 (MIP-2), and leukotriene B_4 (LTB_4) in synovial tissues and reduced the secondary infiltration of macrophages. These findings were supported by in vitro studies showing normal chemotactic migration but defective immune complex–induced respiratory burst and MIP-2 or LTB_4 release in PLCγ2-deficient neutrophils.

Conclusion. Neutrophil PLCγ2 is critical for arthritis development, supposedly through the generation of the inflammatory microenvironment. PLCγ2-expressing neutrophils exert complex indirect effects on other inflammatory cells. PLCγ2-targeted therapies may provide particular benefit in inflammatory diseases with a major neutrophil component.

INTRODUCTION

Phospholipase Cγ2 (PLCγ2) is a tyrosine kinase–activated PLC isoform primarily expressed in the hematopoietic system. Although the role of PLCγ2 is most prominent in B cells (1,2), it is also present in other lineages such as neutrophils (3,4), macrophages (1,5), mast cells (1,5), natural killer cells (1,6,7), platelets (1,8,9), and osteoclasts (10–12). PLCγ2 mediates signaling from diverse cell surface receptors including B cell receptors, Fc receptors (FcR), integrins, C-type lectins, and the collagen receptor glycoprotein VI (1–8,10,12,13).

PLCγ2 plays important roles in human autoimmune and inflammatory diseases. Deletion of late *PLCG2* exons causes an autosomal-dominant disease (PLCγ2-associated antibody deficiency and immune dysregulation [PLAID]) leading to high prevalence of various autoimmune diseases and antinuclear autoantibodies (14–16). Missense mutations in PLCγ2 trigger a distinct autosomal-dominant autoinflammatory disease (autoinflammation and PLAID

Supported by the Hungarian National Scientific Research Fund (NKFIH-OTKA grants KKP129954 and K119653 to Dr. Mócsai), the Hungarian National Research, Development, and Innovation Office (grant NVKP_16-2016-1-0039 to Dr. Mócsai), and the Hungarian Ministry of National Economy (grant VEKOP-2.3.2-16-2016-00002 to Dr. Mócsai). Dr. Futosi's work was supported by the Hungarian Academy of Sciences János Bolyai Research Scholarship and the New Excellence Program of the Hungarian Ministry of Human Capacities (grant ÚNKP-18-4-SE-43).

Krisztina Futosi, PhD, Orsolya Kása, MSc, Kata P. Szilveszter, MD, Attila Mócsai, MD, PhD: Semmelweis University School of Medicine, Budapest, Hungary.
Dr. Futosi and Ms Kása contributed equally to this work.
No potential conflicts of interest relevant to this article were reported.
Address correspondence to Attila Mócsai, MD, PhD, Semmelweis University School of Medicine, Department of Physiology, Tűzoltó utca 37-47, 1094 Budapest, Hungary. Email: mocsai.attila@med.semmelweis-univ.hu.
Submitted for publication April 10, 2020; accepted in revised form February 19, 2021.

[APLAID]) with blistering dermatitis, arthralgia, uveitis, and ulcerative colitis (17). Genetic studies have also linked *PLCG2* to inflammatory bowel disease (18), nephrotic syndrome (19), Alzheimer's disease (20), and dermatomyositis (21).

Several studies indicate the role of PLCγ2 in autoimmune and inflammatory diseases in experimental mice. Random mutagenesis generated 2 different gain-of-function mutations of *Plcg2* (*Ali5* and *Ali14*), triggering various forms of inflammatory diseases including arthritis, dermatitis, and glomerulonephritis (22,23). PLCγ2-deficient ($Plcg2^{-/-}$) animals were protected against autoantibody-induced (4,24) and antigen-induced arthritis (25). PLCγ2 is also involved in osteoclast biology, as indicated by osteoporosis in *Ali14* mice (23) and increased trabecular bone mass and defective osteoclast development in $Plcg2^{-/-}$ animals (10–12).

It is at present unclear in which cell type(s) PLCγ2 needs to be expressed during autoantibody-induced arthritis. Gain-of-function mutations in humans (14,17) and mice (22,23), as well as PLCγ2 deficiency in mice (1,2), indicate a prominent role for PLCγ2 in B cells. However, inflammatory changes in APLAID patients are dominated by a granulocytic infiltrate (17), and the autoinflammatory phenotype of *Ali5* mice also develops on the $Rag1^{-/-}$ background (22). Autoantibody-induced arthritis could also be triggered in $Rag1^{-/-}$ or B cell–deficient mice (26), suggesting a role for PLCγ2 in a non-lymphoid compartment.

A number of hematopoietic lineages including neutrophils (27–30), macrophages (31), platelets (32), and mast cells (33) have been implicated in autoantibody-induced arthritis (26). All of these lineages express and utilize PLCγ2 (1,3–5,8,9). However, it is unclear whether and how PLCγ2 expressed within these lineages contributes to arthritis development.

The studies described above prompted us to test the role of PLCγ2 in the autoantibody-induced K/BxN serum–transfer arthritis model in a lineage-specific manner, with further emphasis on the role of neutrophil PLCγ2. PLCγ2 expression in neutrophils, but not in mast cells or platelets, was critical for arthritis development, supposedly through the organization of the inflammatory process without a direct role in neutrophil migration.

MATERIALS AND METHODS

Animals. Mice carrying the $Plcg2^{tm1Jni}$ (referred to as $Plcg2^{-}$) (1) mutation inactivating the PLCγ2-encoding gene were kept in heterozygous form and bred to obtain $Plcg2^{-/-}$ animals. Lineage-specific deletion of PLCγ2 was achieved by crossing Vav1-Cre (34), LysM-Cre (35), MRP8-Cre (36), Mcpt5-Cre (37), or PF4-Cre (38) transgenic mice with animals carrying a floxed *Plcg2* ($Plcg2^{tm1Kuro}$, referred to as the $Plcg2^{flox}$) (2) allele to obtain Vav1-$Cre^{+}Plcg2^{flox/flox}$ (referred to as $Plcg2^{\Delta Haemo}$), LysM-$Cre^{+}Plcg2^{flox/flox}$ ($Plcg2^{\Delta Myelo}$), MRP8-$Cre^{+}Plcg2^{flox/flox}$ ($Plcg2^{\Delta PMN}$), PF4-$Cre^{+}Plcg2^{flox/flox}$ ($Plcg2^{\Delta Plt}$), and Mcpt5-$Cre^{+}Plcg2^{flox/flox}$ ($Plcg2^{\Delta MC}$) mice. CD18-deficient ($Itgb2^{tm2Bay/tm2Bay}$, referred to as $Itgb2^{-/-}$) mice (39) were obtained by crossing $Itgb2^{-/-}$ and $Itgb2^{+/-}$ mice. Mice carrying the KRN T cell receptor transgene (40) were maintained in heterozygous form. Mutant mice were obtained from James Ihle ($Plcg2^{-}$), Arthur Beaudet ($Itgb2^{-}$), Tomihiro Kurosaki ($Plcg2^{flox}$), Emmanuelle Passegue (MRP8-Cre), Axel Roers (Mcpt5-Cre), or Diane Mathis and Christophe Benoist (KRN), or were purchased from The Jackson Laboratory (Vav1-Cre, LysM-Cre, and PF4-Cre). All transgenic mice were backcrossed to the C57BL/6 genetic background for at least 6 generations. Genotyping was performed by allele-specific polymerase chain reaction. Wild-type control C57BL/6, NOD, and B6.SJL-$Ptprc^{a}$ mice were purchased from The Jackson Laboratory.

Mice were bred and maintained in individually sterile ventilated cages (Tecniplast) in a specific pathogen–free facility and transferred to a conventional facility for experiments. Animal experiments were approved by the Animal Experimentation Review Board of Semmelweis University.

For bone marrow transplantation, B6.SJL-$Ptprc^{a}$ (CD45.1) recipient mice were lethally irradiated with 11 Gy from a ^{137}Cs source using a GSM D1 irradiator, followed by intravenous injection of unfractionated donor mouse bone marrow cells. Four weeks after transplantation, peripheral blood samples were stained for Ly6G and CD45.2 (clones 1A8 and 104, respectively; both from BD Biosciences) and analyzed on a BD FACSCalibur flow cytometer as previously described (41).

K/BxN serum–transfer arthritis. KRN transgene–positive (arthritic) K/BxN mice and transgene-negative (nonarthritic) BxN mice were obtained as previously described (4,40), and their sera were pooled separately. Mice were randomly assigned to the arthritis group (~60% of mice) or the control group (~40%) and injected intraperitoneally with 300 μl K/BxN serum (arthritis group) or BxN serum (control group). Arthritis severity was assessed daily for 2 weeks by clinical scoring (0–1 = normal; 2–3 = mild arthritis; 4–6 = moderate arthritis; 7–10 = severe arthritis) and by measuring the ankle thickness using a spring-loaded caliper (Kroeplin) as previously described (4,42,43).

Cell culture and isolation. Neutrophils were freshly isolated from the bone marrow of mouse femurs and tibias by hypotonic lysis followed by Percoll (GE Healthcare) gradient centrifugation (42–44). For immunoblotting studies, cells were labeled with Ly6G antibodies and sorted on a BD FACSAria III cell sorter. Bone marrow–derived macrophages (BMMs) were cultured from bone marrow cells in the presence of murine macrophage colony-stimulating factor (PeproTech) as previously described (45). Platelets were freshly isolated from peripheral blood by mild centrifugation in the presence of heparin as previously described (46). Bone marrow–derived mast cells (BMMCs) were cultured from bone marrow cells in the presence of murine interleukin-3 (IL-3) and stem cell factor (both from PeproTech) as previously described (46). Their purity was tested by flow cytometry using an anti-FcεR antibody (clone MAR-1; eBioscience). Splenic B cells were labeled with B220 antibodies (clone RA3-6B2; BD Biosciences) and sorted on a BD FACSAria III cell sorter.

Immunoblotting and intracellular flow cytometry. For immunoblotting, neutrophils, BMMs, platelets, BMMCs, and B cells were lysed in a Triton X-100–based lysis buffer with protease and phosphatase inhibitors (46). Triton-soluble fractions were run on sodium dodecyl sulfate–polyacrylamide gel electrophoresis and immunoblotted using antibodies against PLCγ2 (Q-20) or β-actin (clone AC-74; Sigma-Aldrich) followed by peroxidase-labeled secondary antibodies (GE Healthcare) and development using an ECL system (GE Healthcare).

For intracellular flow cytometry, peripheral blood samples were stained for Ly6G, CD11b, and B220, followed by hypotonic lysis. Cells were fixed and permeabilized using an eBioscience kit and stained with anti-PLCγ2 (Q-20) and fluorescein isothiocyanate–labeled anti-rabbit antibodies.

Analysis of the inflammatory infiltrate. Mice were killed 5 days after serum transfer, and their front and hind paws were flushed with 1 ml phosphate buffered saline supplemented with 10 m*M* EDTA and 20 m*M* HEPES (pH 7.4). Infiltrating cells were identified by flow cytometry based on their forward-scatter/side-scatter profile and Ly6G, F4/80, and CD11b staining characteristics (clones 1A8, A3-1, or M1/70, respectively; BD BioSciences) as previously described (41).

Parallel measurements of neutrophil counts and hemoglobin concentration in the blood and synovial infiltrate revealed that not more than 6% of synovial neutrophils derived from the circulation after day 3, and this percentage was even <2% at clinical scores >4. IL-1β, macrophage inflammatory protein 2 (MIP-2), and leukotriene B_4 (LTB_4) levels in the cell-free supernatant of the synovial infiltrates were tested by enzyme-linked immunosorbent assay (ELISA; R&D Systems) as previously described (41).

Competitive in vivo migration experiments. Mixed bone marrow chimeras were used for in vivo competitive migration assay (41). CD45.1-expressing wild-type mouse bone marrow cells were mixed at 2:3 or 3:2 ratios with CD45.2-expressing wild-type, CD18-deficient (*Itg2b*$^{-/-}$), or *Plcg2*$^{\Delta PMN}$ mouse bone marrow cells, and were injected intravenously into lethally irradiated CD45.1-expressing recipient mice. Four weeks later, K/BxN serum transfer arthritis was induced in the chimeras (day 0). Peripheral blood samples were taken on days 0, 3, and 5. The mice were killed on day 5 and their synovial infiltrates were analyzed by flow cytometry, with additional labeling for CD45.2 (clone 104). Relative migration of CD45.2-expressing neutrophils (relative to CD45.1-expressing cells) was calculated as previously described (41).

In vitro neutrophil studies. Neutrophil assays were performed at 37°C in Hanks' balanced salt solution supplemented with 20 m*M* HEPES (pH 7.4). Transwell migration through fibrinogen-coated polycarbonate filters with 3-μm pore size (Corning) during a 60-minute incubation was tested as previously described (4,41,43,47). Chemoattractants included 100 ng/ml MIP-2 or 10-fold diluted synovial lavage fluid from wild-type mice 7 days after arthritis induction.

Immune complex–induced neutrophil responses were tested as previously described (41,43,47–49) using 20 μg/ml human serum albumin (HSA) with 1:400 anti-HSA ("strong" stimulation) or with 2-fold dilution of both reagents ("weak" stimulation; all reagents from Sigma-Aldrich). Respiratory burst was tested spectrophotometrically using 100 n*M* ferricytochrome c (Sigma-Aldrich). MIP-2 and LTB_4 production during a 6-hour period was determined by ELISA. Cell viability and the basal rate of apoptosis was tested by flow cytometry using Live/Dead and annexin V staining (both from Invitrogen) within the Ly6G-positive gate.

Statistical analysis. Experiments were performed the indicated number of times. Data are presented as the mean ± SEM from all independent in vitro experiments or from all individual mice tested. Statistical analyses were performed using StatSoft Statistica. Kolmogorov-Smirnov test for normality found mostly normal distribution of outcome parameters within groups. Competitive migration assays were analyzed by one-way analysis of variance (ANOVA). All other experiments were analyzed using two-way ANOVA, with treatment and genotype as the 2 independent variables. In the case of time courses, area under the curve (generated by adding together all outcome parameters for a given sample) as a simple measure of the response was used for statistical analysis. Reported *P* values refer to comparison of the indicated mutant genotype with parallel wild-type measurements. *P* values less than 0.05 were considered significant.

RESULTS

Abrogation of K/BxN serum–transfer arthritis upon complete or hematopoietic deletion of PLCγ2. We used the K/BxN serum–transfer model, a widely used model of autoantibody-induced arthritis in mice, to delineate the role of PLCγ2 in experimental arthritis. Arthritogenic (K/BxN) serum injection triggered robust arthritis in wild-type mice (Figures 1A–C). Consistent with prior reports (4,24), PLCγ2-deficient (*Plcg*$^{-/-}$) mice were completely protected against arthritis development ($P = 3.8 \times 10^{-10}$ and $P = 8.6 \times 10^{-5}$ for clinical score and ankle thickness, respectively, versus wild-type mice) (Figures 1A–C).

We next transplanted wild-type or *Plcg2*$^{-/-}$ mouse bone marrow cells into lethally irradiated wild-type or *Plcg2*$^{-/-}$ recipient mice. Arthritis development was completely abrogated in wild-type recipients transplanted with *Plcg2*$^{-/-}$ donor cells ($P = 2.2 \times 10^{-4}$ and $P = 0.0026$ for clinical score and ankle thickness, respectively, versus wild-type recipients transplanted with wild-type donor cells) (Figures 1D and E). In contrast, *Plcg2*$^{-/-}$ recipients transplanted with wild-type bone marrow cells developed robust arthritis comparable to that in similarly treated wild-type recipients ($P = 0.20$ and 0.17 for clinical score and ankle thickness,

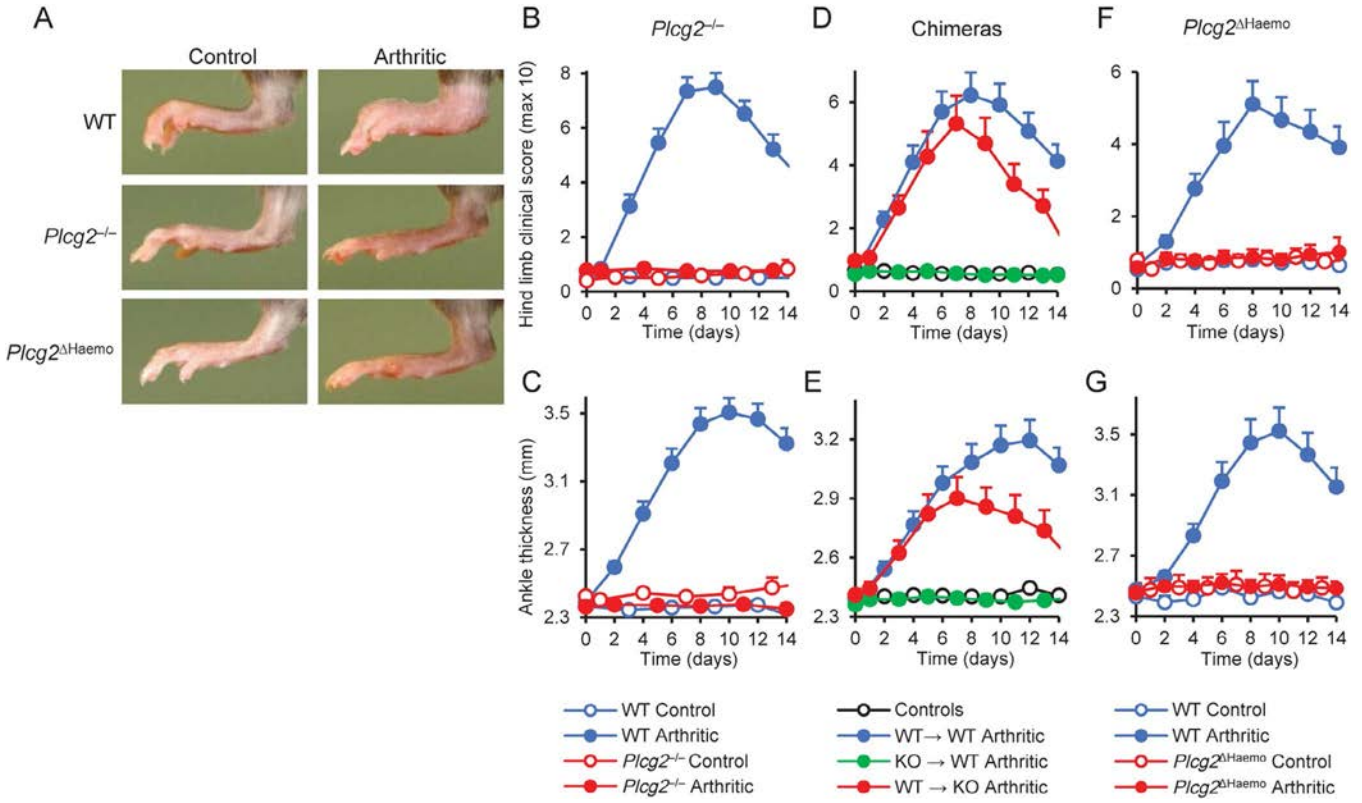

Figure 1. Autoantibody-induced arthritis requires phospholipase Cγ2 in the hematopoietic system. Wild-type (WT) mice, *Plcg2*$^{-/-}$ mice, and *Plcg2*$^{\Delta Haemo}$ mice or bone marrow chimeras were injected with BxN (control) or K/BxN (arthritogenic) serum intraperitoneally on day 0. **A**, Arthritis development in the hind limb of a mouse from each strain, representative of 4–11 control serum–treated mice and 11–16 arthritogenic serum–treated mice per group from at least 4 independent experiments **B**, **D**, and **F**, Clinical score in the hind limb in *Plcg2*$^{-/-}$ mice (**B**), bone marrow chimeras (**D**), and *Plcg2*$^{\Delta Haemo}$ mice (**F**). **C**, **E**, and **G**, Ankle thickness in *Plcg2*$^{-/-}$ mice (**C**), bone marrow chimeras (**E**), and *Plcg2*$^{\Delta Haemo}$ mice (**G**). In **D** and **E**, bone marrow chimeras were generated by transplanting WT or *Plcg2*$^{-/-}$ bone marrow cells into WT recipient mice (labeled WT→WT and knockout [KO]→WT, respectively) or WT bone marrow cells into *Plcg2*$^{-/-}$ recipient mice (labeled WT→KO). In **B**–**G**, values are the mean ± SEM. Values for all control samples were combined in **D** and **E**. Color figure can be viewed in the online issue, which is available at http://onlinelibrary.wiley.com/doi/10.1002/art.41704/abstract.

respectively) (Figures 1D and E), although they tended to show a faster recovery during the second week of the experiment.

We also generated mice with Cre/lox–mediated conditional deletion of PLCγ2 from the entire hematopoietic compartment. The resulting Vav1-Cre^{+}*Plcg2*$^{flox/flox}$ (*Plcg2*$^{\Delta Haemo}$) mice were also completely protected against K/BxN serum–transfer arthritis ($P = 5.0 \times 10^{-4}$ and $P = 7.3 \times 10^{-4}$ for clinical score and ankle thickness, respectively, versus wild-type mice) (Figures 1A, F, and G). Taken together, these findings indicate that autoantibody-induced arthritis requires PLCγ2 expression within the hematopoietic compartment.

PLCγ2 expression in hematopoietic lineages. PLCγ2 has been shown to be expressed and functionally important in a number of different hematopoietic lineages (1–9). Consistent with the results of those studies, in the present study PLCγ2 was detected in lysates of freshly isolated bone marrow neutrophils, peripheral blood platelets, or splenic B cells, or in in vitro differentiated primary BMMs or BMMCs from wild-type mice (Figures 2A–E). Importantly, no PLCγ2 was detected in similar cells from *Plcg2*$^{-/-}$ animals (Figures 2A–E).

Efficacy and specificity of lineage-specific PLCγ2 deletion. To test the role of PLCγ2 in autoantibody-induced arthritis in more detail, we generated several further lineage-specific PLCγ2-deficient mouse strains. These included PLCγ2 deletion in multiple (though not all) myeloid-lineage cells (LysM-Cre^{+}*Plcg2*$^{flox/flox}$; referred to as *Plcg2*$^{\Delta Myelo}$), neutrophils (MRP8-Cre^{+}*Plcg2*$^{flox/flox}$; *Plcg2*$^{\Delta PMN}$), platelets (PF4-Cre^{+}*Plcg2*$^{flox/flox}$; *Plcg2*$^{\Delta Plt}$), or mast cells (Mcpt5-Cre^{+}*Plcg2*$^{flox/flox}$; *Plcg2*$^{\Delta MC}$).

We next tested PLCγ2 expression in various lineages from the mutants listed above by immunoblotting (Figures 2A–E). PLCγ2 was absent from all *Plcg2*$^{-/-}$ and *Plcg2*$^{\Delta Haemo}$ samples. PLCγ2 expression was strongly reduced in *Plcg2*$^{\Delta Myelo}$ BMMs but was normal in *Plcg2*$^{\Delta PMN}$, *Plcg2*$^{\Delta Plt}$, and *Plcg2*$^{\Delta MC}$ BMMs (Figure 2A). PLCγ2 expression was greatly reduced in *Plcg2*$^{\Delta Myelo}$ and *Plcg2*$^{\Delta PMN}$ neutrophils but was normal in *Plcg2*$^{\Delta Plt}$ and *Plcg2*$^{\Delta MC}$ neutrophils (Figure 2B). PLCγ2 was nearly absent from *Plcg2*$^{\Delta Plt}$ platelets but was present at normal levels in *Plcg2*$^{\Delta Myelo}$, *Plcg2*$^{\Delta PMN}$, and *Plcg2*$^{\Delta MC}$ platelets (Figure 2C). PLCγ2 expression was partially reduced in *Plcg2*$^{\Delta MC}$ BMMCs but not in *Plcg2*$^{\Delta Myelo}$, *Plcg2*$^{\Delta PMN}$, or *Plcg2*$^{\Delta Plt}$ BMMCs (Figure 2D). None of the mutations

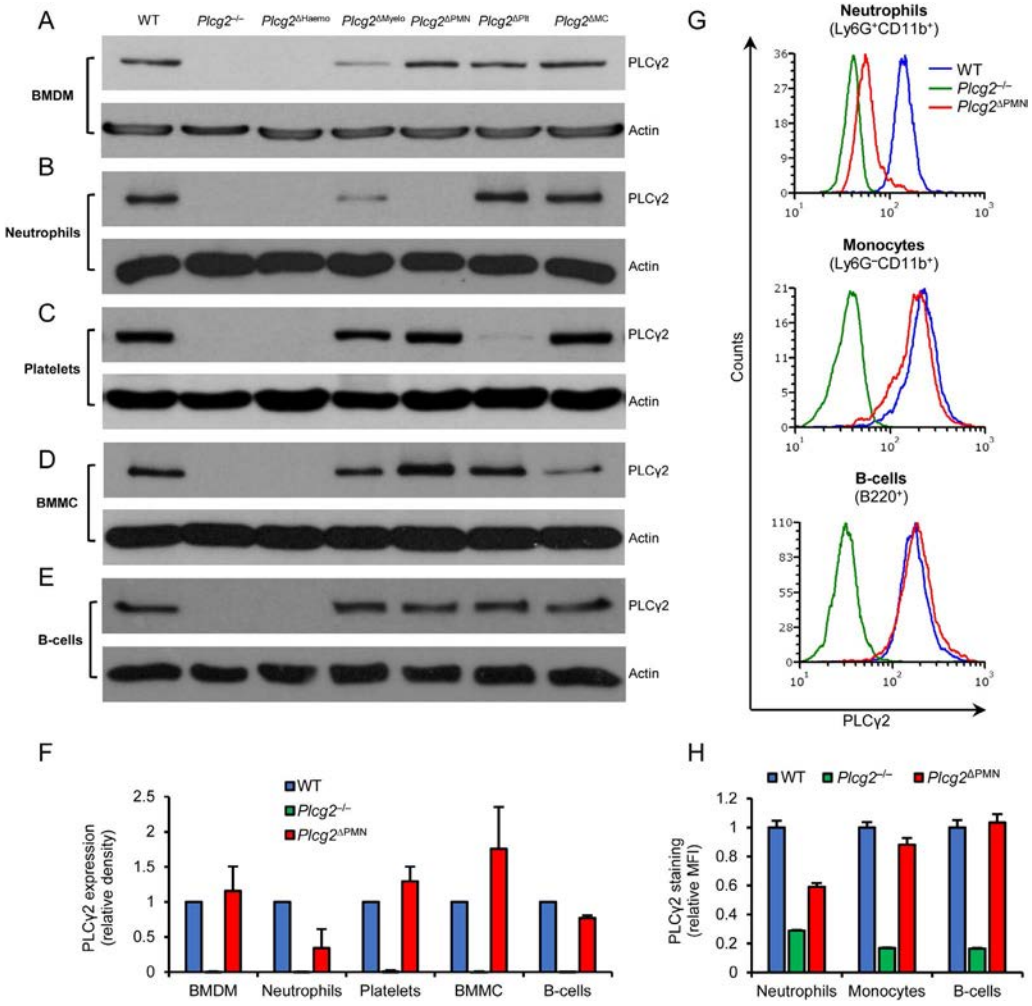

Figure 2. Efficacy and specificity of lineage-specific phospholipase Cγ2 (PLCγ2) deletion in mice. The efficacy and specificity of lineage-specific deletion was tested by immunoblotting or intracellular staining in flow cytometry. **A**–**E**, Immunoblotting of whole cell lysates of bone marrow–derived macrophages (BMMs) (**A**), neutrophils (**B**), platelets (**C**), bone marrow mast cells (BMMCs) (**D**), and splenic B cells (**E**) from wild-type (WT) mice and mice with the indicated PLCγ2 mutations, against PLCγ2 or actin (as a loading control). Results are representative of 2–3 independent experiments. **F**, Densitometric analysis of immunoblots for PLCγ2 expression in different cell subsets from WT, *Plcg2*$^{-/-}$, and *Plcg2*$^{\Delta PMN}$ mice. Bars show the mean ± SEM (n = 2–3 independent experiments). **G** and **H**, Representative histograms (**G**) and relative mean fluorescence intensity (MFI) values (**H**) from flow cytometric analysis of intracellular PLCγ2 expression in circulating neutrophils, monocytes, and B cells. Results in **G** are representative of 2–3 individual mice per group from 3 independent experiments. Bars in **H** show the mean ± SEM (n = 2–3 individual mice per group from 3 independent experiments). Color figure can be viewed in the online issue, which is available at http://onlinelibrary.wiley.com/doi/10.1002/art.41704/abstract.

(except *Plcg2*$^{-/-}$ and *Plcg2*$^{\Delta Haemo}$) affected PLCγ2 expression in B cells (Figure 2E). Densitometric analysis (Figure 2F) of cells from *Plcg2*$^{-/-}$ and *Plcg2*$^{\Delta PMN}$ mice (which are the main subjects of our study) confirmed the complete absence of PLCγ2 from all *Plcg2*$^{-/-}$ cells ($P = 2.3 \times 10^{-11}$ to 2.3×10^{-8} versus wild-type cells), and a strong but incomplete deletion of PLCγ2 from *Plcg2*$^{\Delta PMN}$ neutrophils ($P = 0.033$), without a substantial deletion in other lineages ($P = 0.026$ for B cells and $P = 0.15$–0.67 for the other lineages versus wild-type cells). Results of additional densitometric analyses are available upon request from the corresponding author.

We also performed intracellular staining of PLCγ2 in circulating neutrophils, monocytes, and B cells from wild-type, *Plcg2*$^{-/-}$, and *Plcg2*$^{\Delta PMN}$ mice (Figures 2G and H). Compared to the wild-type cells, PLCγ2 staining was strongly reduced in all *Plcg2*$^{-/-}$ cells ($P = 4.0 \times 10^{-8}$ to 1.1×10^{-6}). *Plcg2*$^{\Delta PMN}$ neutrophils showed strongly (though incompletely) reduced PLCγ2 expression ($P = 1.9 \times 10^{-6}$), while monocytes ($P = 0.065$) and B cells ($P = 0.68$) were not affected. These results confirmed the strong and specific, though incomplete, deletion of PLCγ2 from *Plcg2*$^{\Delta PMN}$ neutrophils.

Abrogation of K/BxN serum–transfer arthritis upon myeloid-specific deletion of PLCγ2. To test the effect of conditional PLCγ2 deletion, we first subjected *Plcg2*$^{\Delta Myelo}$ mice to K/BxN serum–transfer arthritis. *Plcg2*$^{\Delta Myelo}$ mice did not show visible signs of arthritis (Figure 3A), and quantitative analysis revealed nearly complete protection of *Plcg2*$^{\Delta Myelo}$ mice

against arthritis development ($P = 1.5 \times 10^{-14}$ and $P = 5.6 \times 10^{-10}$ for clinical score and ankle thickness, respectively, versus wild-type mice) (Figures 3B and C). In an assay of articular function (testing how long the mice were able to hold on to the bottom of a wire grid; data available upon request from the corresponding author), most arthritogenic serum–treated wild-type mice fell off the grid within a few seconds, whereas similarly treated *Plcg2*$^{\Delta Myelo}$ mice were able to hold on to the grid similar to control serum–treated animals ($P = 3.7 \times 10^{-5}$). These results indicate a critical role for PLCγ2 expression within myeloid lineage cells.

Neutrophil-specific PLCγ2 deletion protects mice against arthritis. Analysis of the effects of PLCγ2 deletion from the neutrophil compartment revealed no visible signs of K/BxN serum–transfer arthritis in *Plcg2*$^{\Delta PMN}$ animals (Figure 3A) and strong protection of *Plcg2*$^{\Delta PMN}$ mice in quantitative studies ($P = 7.4 \times 10^{-9}$ and $P = 3.5 \times 10^{-4}$ for clinical score and ankle thickness, respectively, versus wild-type mice) (Figures 3D and E). Arthritogenic serum–treated *Plcg2*$^{\Delta PMN}$ mice were able to hold on to the bottom of a wire grid, indicating protection against arthritis-induced loss of articular function ($P = 0.017$) (data available upon request from the corresponding author). These results suggest that PLCγ2 expression within neutrophils is critical for autoantibody-induced arthritis.

Function of PLCγ2 in platelets or mast cells is dispensable with regard to arthritis development. Platelets (32) and mast cells (33) have also been implicated in the development of autoantibody-induced arthritis. Therefore, we generated and tested mice with platelet-specific (*Plcg2*$^{\Delta Plt}$) or mast cell–specific (*Plcg2*$^{\Delta MC}$) PLCγ2 deletion.

The *Plcg2*$^{\Delta Plt}$ mutation failed to block visible signs of K/BxN serum–transfer arthritis (Figure 3A), and this was also confirmed by quantitative analyses ($P = 0.77$ and $P = 0.85$ for clinical score and ankle thickness, respectively, versus wild-type mice) (Figures 3F and G). Similarly, no visible protection was observed in *Plcg2*$^{\Delta MC}$ animals (Figure 3A), and no such protection was revealed during quantitative analyses either ($P = 0.91$ and $P = 0.95$ for clinical score and ankle thickness, respectively, versus wild-type mice) (Figures 3H and I). Therefore, PLCγ2 within platelets or mast cells is likely not critical for arthritis development in our model.

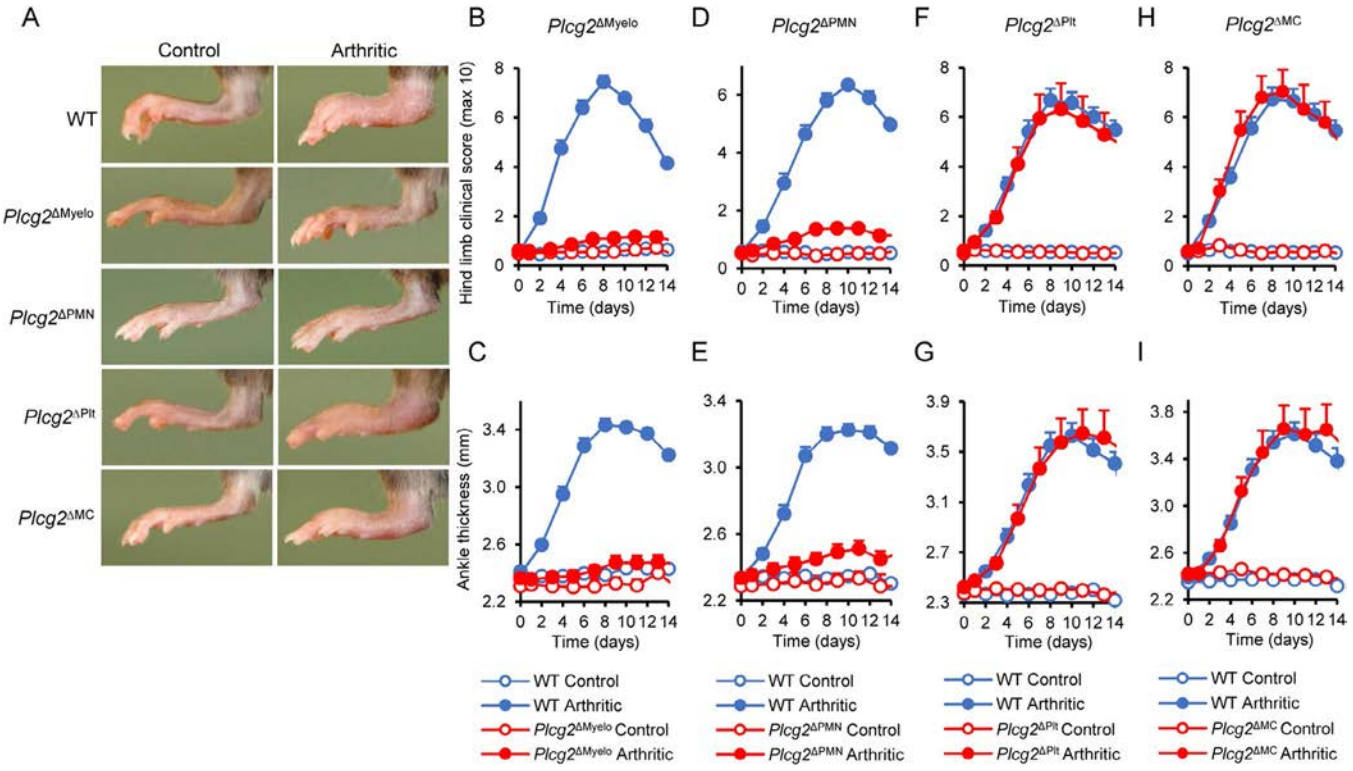

Figure 3. Myeloid- or neutrophil-specific deletion of phospholipase Cγ2 abrogates arthritis development. Wild-type (WT), *Plcg2*$^{\Delta Myelo}$, *Plcg2*$^{\Delta PMN}$, *Plcg2*$^{\Delta Plt}$, and *Plcg2*$^{\Delta MC}$ mice were injected with BxN (control) or K/BxN (arthritogenic) serum intraperitoneally on day 0. **A**, Arthritis development in the indicated mouse strains. **B**, **D**, **F**, and **H**, Clinical score in the hind limbs in *Plcg2*$^{\Delta Myelo}$ (**B**), *Plcg2*$^{\Delta PMN}$ (**D**), *Plcg2*$^{\Delta Plt}$ (**F**), and *Plcg2*$^{\Delta MC}$ (**H**) mice. **C**, **E**, **G**, and **I**, Ankle thickness in *Plcg2*$^{\Delta Myelo}$ (**C**), *Plcg2*$^{\Delta PMN}$ (**E**), *Plcg2*$^{\Delta Plt}$ (**G**), and *Plcg2*$^{\Delta MC}$ (**I**) mice. Values are the mean ± SEM (n = 6–15 control serum–treated mice and 12–29 arthritogenic serum–treated mice per group from 4 independent experiments in **B** and **C**; 11–17 control and 23–26 arthritogenic serum–treated mice per group from 6 independent experiments in **D** and **E**; 10–13 control and 13–34 arthritogenic serum-treated individual mice per group from at least 5 independent experiments in **F** and **G**; and 8–12 control and 11–33 arthritogenic serum–treated mice per group from at least 4 independent experiments in **H** and **I**).

Neutrophil-specific PLCγ2 deletion blocks leukocyte infiltration. To test how neutrophil PLCγ2 contributes to autoantibody-induced arthritis, we analyzed leukocyte infiltration into the synovial tissue. As shown in Figure 4A, K/BxN serum–transfer arthritis triggered robust infiltration of neutrophils into the synovial tissue, whereas hardly any neutrophils appeared in *Plcg2*$^{\Delta PMN}$ mice ($P = 7.6 \times 10^{-4}$). Interestingly, the *Plcg2*$^{\Delta PMN}$ mutation also abrogated accumulation of monocyte/macrophages in the synovial tissue of arthritogenic serum–injected mice ($P = 0.0010$ and $P = 5.8 \times 10^{-4}$ for Ly6G–F4/80+ and Ly6G–CD11b+ cells, respectively) (Figures 4B and C). Therefore, neutrophil PLCγ2 is critical for the accumulation of both neutrophils and monocyte/macrophages at the site of inflammation.

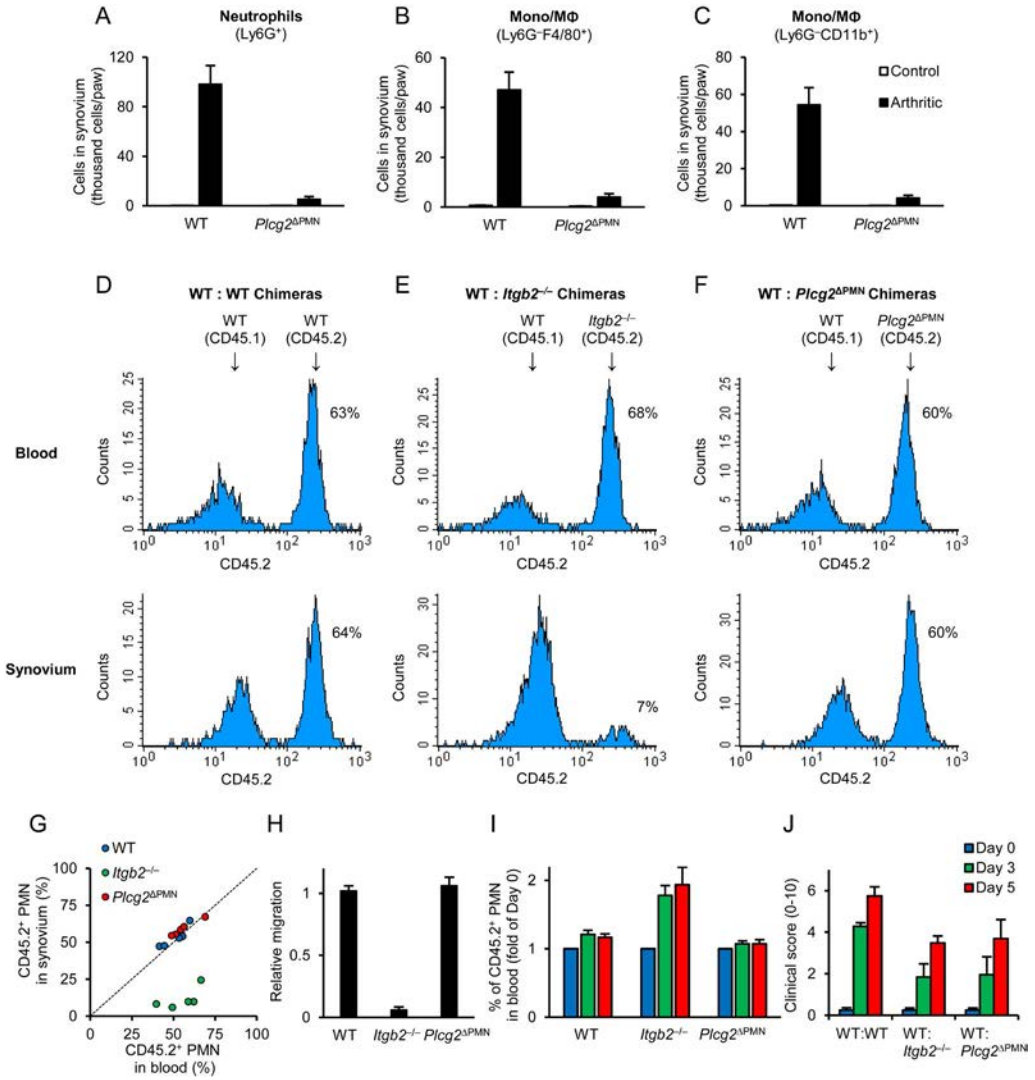

Figure 4. Accumulation of myeloid cells at the site of inflammation. Wild-type (WT) and *Plcg2*$^{\Delta PMN}$ mice (**A**–**C**) and chimeras of bone marrow from CD45.1-expressing WT and CD45.2-expressing WT, CD18-deficient (*Itgb2*$^{-/-}$), or *Plcg2*$^{\Delta PMN}$ hematopoietic cells (**D**–**J**) were subjected to K/B×N serum–transfer arthritis. **A**–**C**, In vivo accumulation of neutrophils (**A**), Ly6G–F4/80+ monocyte/macrophages (Mono/Mϕ) (**B**), and Ly6G–CD11b+ monocyte/macrophages (**C**) in WT and *Plcg2*$^{\Delta PMN}$ mice, determined by flow cytometric analysis on day 5. Bars show the mean ± SEM (n = 5–6 control and 10–12 arthritic mice per group from 5 independent experiments). **D**–**F**, CD45.2 expression in neutrophils in blood and synovial infiltrate from chimeras with mixed bone marrow cells from a CD45.1-expressing WT mouse and a CD45.2-expressing WT mouse (WT:WT chimeras) (**D**), a CD45.1-expressing WT mouse and a CD45.2-expressing CD18-deficient mouse (WT:*Itgb2*$^{-/-}$ chimeras) (**E**), and a CD45.1-expressing WT mouse and a CD45.2-expressing *Plcg2*$^{\Delta PMN}$ mouse (WT:*Plcg2*$^{\Delta PMN}$ chimeras) (**F**), determined by flow cytometric analysis on day 5. Results are representative of 5 independent experiments. **G**, Correlation between the percentage of CD45.2-expressing polymorphonuclear neutrophils (PMNs) in the synovial infiltrate (day 5) and percentage of CD45.2-expressing PMNs in the peripheral blood (average of days 0, 3, and 5) in the indicated mixed bone marrow chimeras, determined by flow cytometric analysis. **H**, Relative migration of CD45.2-expressing neutrophils in the indicated chimeras, determined by flow cytometric analysis. Data in **G** and **H** are derived from the same data set. **I** and **J**, Relative change in CD45.2-expressing neutrophils in the peripheral blood, determined by flow cytometric analysis (**I**), and clinical scores (**J**) in the indicated chimeras on days 0, 3, and 5. In **H**–**J**, bars show the mean ± SEM (n = 5 mice per group from 3 independent experiments). Color figure can be viewed in the online issue, which is available at http://onlinelibrary.wiley.com/doi/10.1002/art.41704/abstract.

Normal intrinsic migratory ability of *Plcg2*$^{\Delta PMN}$ neutrophils. The simplest explanation for the above findings would be a role for PLCγ2 in the transendothelial migration of neutrophils, a supposedly β_2 integrin–mediated process. To test that possibility, we compared the accumulation of wild-type and *Plcg2*$^{\Delta PMN}$ or CD18-deficient (*Itgb2*$^{-/-}$) neutrophils within the same individual mice using a competitive migration approach. To this end, lethally irradiated mice were transplanted with a mixture of bone marrow cells from a CD45.1-expressing wild-type mouse and a CD45.2-expressing wild-type mouse (WT:WT chimeras) (Figure 4D), CD18-deficient mouse (WT:*Itgb2*$^{-/-}$ chimeras) (Figure 4E), or *Plcg2*$^{\Delta PMN}$ mouse (WT:*Plcg2*$^{\Delta PMN}$ chimeras) (Figure 4F). Autoantibody-induced arthritis was then triggered (day 0), the clinical score (Figure 4J) was recorded and blood was taken on days 0, 3, and 5, and the mice were killed and their joint areas flushed on day 5. The percentage of CD45.2-expressing cells within the neutrophil compartment was then determined in all blood and synovial exudate samples by flow cytometry.

CD45.2 expression profiles in peripheral blood and synovial neutrophils of the mixed bone marrow chimeras described above are shown in Figures 4D–F. As expected, similar percentages of CD45.2 cells were observed in the peripheral blood and synovial tissue of WT:WT chimeras (Figure 4D). Consistent with the expected cell-autonomous requirement for CD18, the percentage of CD45.2 neutrophils was substantially lower in the synovial tissue than in the peripheral blood in WT:*Itgb2*$^{-/-}$ chimeras (Figure 4E). Importantly, no difference between the percentage of the CD45.2 cells in the peripheral blood and the synovial infiltrate was observed in WT:*Plcg2*$^{\Delta PMN}$ chimeras (Figure 4F), providing evidence against a cell-autonomous migration defect of *Plcg2*$^{\Delta PMN}$ neutrophils.

Results of all such mixed chimera experiments are summarized in Figures 4G and H. While the data points representing individual WT:WT and WT:*Plcg2*$^{\Delta PMN}$ chimeras lined up on a diagonal 45-degree axis (indicating similar ratios in the blood and the synovium), WT:*Itgb2*$^{-/-}$ chimeras showed a substantially lower percentage of CD45.2 (*Itgb2*$^{-/-}$) neutrophils in the synovium than in the peripheral blood, indicating a cell-autonomous migration defect of *Itgb2*$^{-/-}$ but not *Plcg2*$^{\Delta PMN}$ neutrophils. Relative migration calculated from the same data (Figure 4H) revealed a dramatically reduced accumulation of *Itgb2*$^{-/-}$ ($P = 3.8 \times 10^{-7}$) but normal accumulation of *Plcg2*$^{\Delta PMN}$ ($P = 0.93$) neutrophils.

Analysis of blood samples alone (Figure 4I) (additional data are available upon request from the corresponding author) revealed that the percentage of CD45.2-expressing circulating neutrophils remained stable during the course of the above experiments in WT:WT chimeras, whereas it increased significantly in WT:*Itgb2*$^{-/-}$ chimeras ($P = 0.043$) but not in WT:*Plcg2*$^{\Delta PMN}$ chimeras ($P = 0.75$). These results again suggested that *Plcg2*$^{\Delta PMN}$ neutrophils, but not *Itgb2*$^{-/-}$ neutrophils, were able to leave the circulation during arthritis.

Requirement of neutrophil PLCγ2 for the generation of the inflammatory microenvironment. A possible explanation for the defective neutrophil accumulation in intact *Plcg2*$^{\Delta PMN}$ mice (Figure 4A) despite apparently normal intrinsic migration of *Plcg2*$^{\Delta PMN}$ neutrophils (Figures 4D–I) and the defective accumulation of *Plcg2*$^{\Delta PMN}$ monocyte/macrophages (Figures 4B and C) which likely express normal PLCγ2 levels (Figures 2A and F–H) would be a role for neutrophil PLCγ2 in the generation of the inflammatory microenvironment. This was tested by measuring the levels of inflammatory mediators in the synovial tissue.

As shown in Figure 5A, arthritis induction triggered a robust accumulation of IL-1β in wild-type mice, whereas no such response was observed in *Plcg2*$^{\Delta PMN}$ mice ($P = 0.0045$). Similarly, MIP-2 chemokine levels were strongly increased in wild-type but not *Plcg2*$^{\Delta PMN}$ animals ($P = 0.0019$) (Figure 5B). Finally, autoantibody-induced arthritis led to the accumulation of LTB_4 in wild-type but not *Plcg2*$^{\Delta PMN}$ mice ($P = 0.029$) (Figure 5C). Therefore, PLCγ2-expressing neutrophils likely contribute to the generation of the inflammatory microenvironment.

Normal in vitro migration of PLCγ2-deficient neutrophils. We also performed in vitro experiments to corroborate the in vivo findings described above. As shown in Figure 6A, both *Plcg2*$^{-/-}$ neutrophils ($P = 0.40$) and *Plcg2*$^{\Delta PMN}$ neutrophils

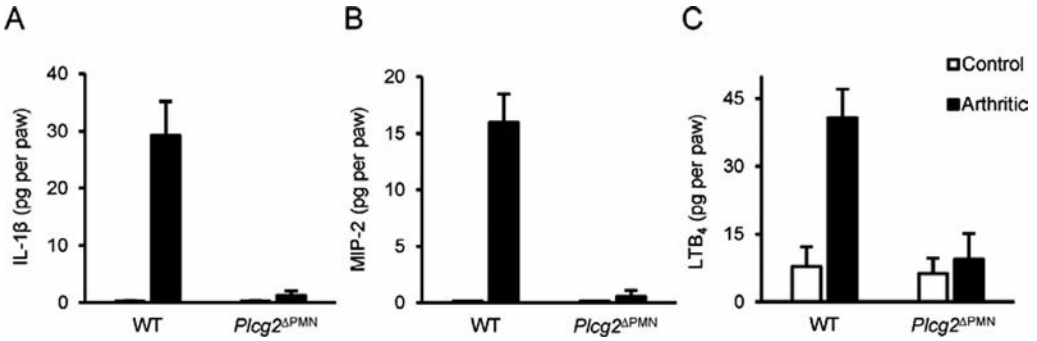

Figure 5. Neutrophil phospholipase Cγ2 (PLCγ2) is required for the generation of the inflammatory microenvironment. K/BxN serum–transfer arthritis was induced in wild-type (WT) and *Plcg2*$^{\Delta PMN}$ mice on day 0. The synovial area was flushed on day 5. Levels of interleukin-1 (IL-1β) (**A**), macrophage inflammatory protein 2 (MIP-2) (**B**), and leukotriene B_4 (LTB_4) (**C**) in cell-free supernatants of the synovial infiltrates are shown. Bars show the mean ± SEM (n = 3–6 control mice and 5–13 arthritic mice per group from at least 3 independent experiments.)

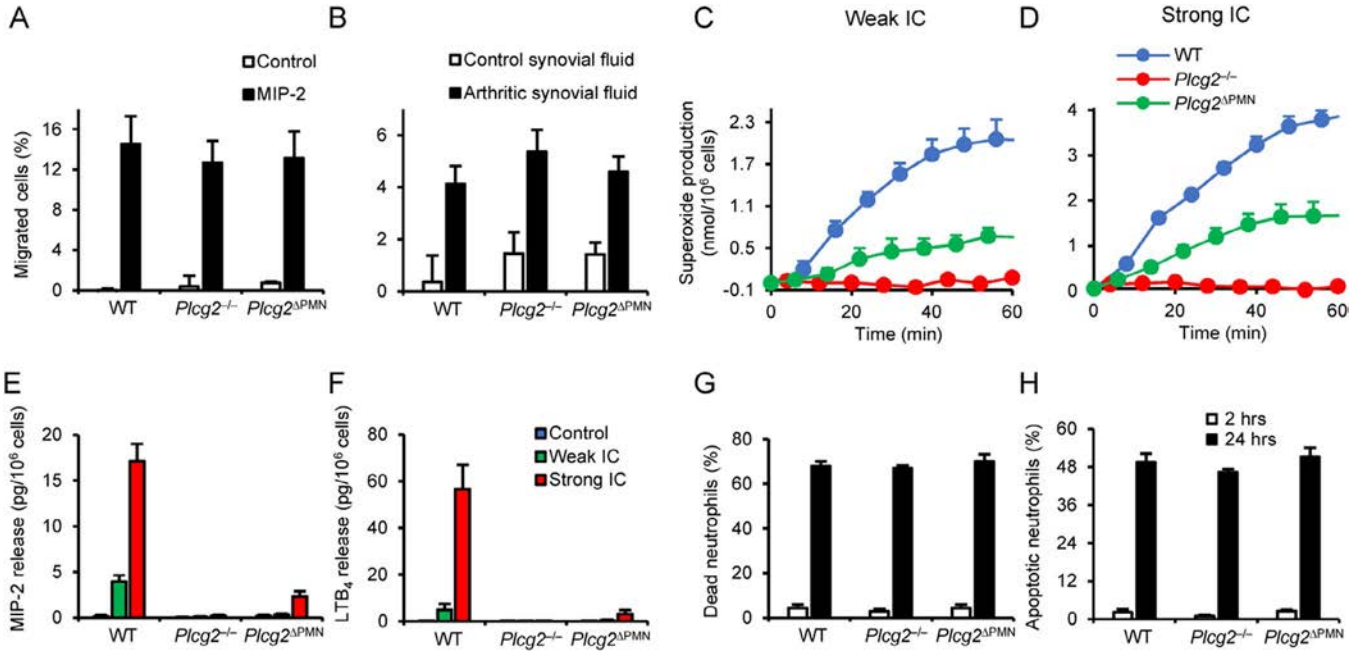

Figure 6. In vitro analysis of neutrophil function. **A** and **B**, In vitro migration of neutrophils isolated from wild-type (WT), *Plcg2*$^{-/-}$, and *Plcg2*$^{\Delta PMN}$ mice through fibrinogen-coated Transwell membranes toward 100 ng/ml macrophage inflammatory protein 2 (MIP-2) (**A**) or diluted synovial fluid from control serum–treated mice and arthritogenic serum–treated mice (**B**). **C** and **D**, Superoxide production of neutrophils plated on weakly (**C**) or strongly (**D**) activating immobilized immune complex (IC) surfaces. **E** and **F**, MIP-2 release (**E**) and leukotriene B4 (LTB_4) release (**F**) from neutrophils plated on weakly or strongly activating immobilized IC surfaces. **G** and **H**, Percentage of dead cells (**G**) and apoptotic cells (**H**) 2 and 24 hours after the isolation of neutrophils. Values are the mean ± SEM (n = 3 independent experiments). Color figure can be viewed in the online issue, which is available at http://onlinelibrary.wiley.com/doi/10.1002/art.41704/abstract.

(P = 0.41) migrated normally toward MIP-2 in a Transwell assay, similar to wild-type mouse cells. In addition, wild-type neutrophils migrated toward cell-free synovial infiltrates from arthritogenic serum–treated animals, and this response was also normal in *Plcg2*$^{-/-}$ (P = 0.94) and *Plcg2*$^{\Delta PMN}$ (P = 0.69) cells (Figure 6B). These results confirmed the normal intrinsic migratory ability of PLCγ2-deficient neutrophils.

Requirement of PLCγ2 for immune complex–induced neutrophil responses. We also plated neutrophils on immobilized IgG immune complexes, an in vitro surrogate of in vivo autoantibody deposition. We used two different conditions triggering different levels of cellular activation. As shown in Figures 6C and D, immune complexes triggered a robust respiratory burst from wild-type neutrophils, whereas *Plcg2*$^{-/-}$ neutrophils were completely protected ($P = 2.7 \times 10^{-8}$ versus wild-type) and *Plcg2*$^{\Delta PMN}$ neutrophils also showed a strongly reduced response ($P = 4.9 \times 10^{-4}$ versus wild-type).

As shown in Figure 6E, immune complex stimulation also triggered robust MIP-2 release from wild-type neutrophils, whereas *Plcg2*$^{-/-}$ neutrophils did not show any such response ($P = 6.8 \times 10^{-7}$), and *Plcg2*$^{\Delta PMN}$ neutrophils also showed a strong defect ($P = 4.2 \times 10^{-6}$). Similarly, wild-type neutrophils but not *Plcg2*$^{-/-}$ neutrophils ($P = 4.3 \times 10^{-5}$) showed robust LTB_4 release under these conditions (Figure 6F), and *Plcg2*$^{\Delta PMN}$ neutrophils were also strongly defective in this response ($P = 8.5 \times 10^{-5}$). These findings confirm the role of neutrophil PLCγ2 in the generation of the inflammatory microenvironment.

PLCγ2 deficiency does not affect neutrophil survival. Finally, we tested the effect of PLCγ2 deficiency on neutrophil survival and apoptosis. As shown in Figure 6G, approximately two-thirds of wild-type neutrophils died during a 24-hour in vitro culture period, which was not affected by the *Plcg2*$^{-/-}$ (P = 0.93) or *Plcg2*$^{\Delta PMN}$ (P = 0.80) mutations. Similarly, the majority of wild-type neutrophils were apoptotic by the end of the 24-hour culture period (Figure 6H), and similar levels were also observed in *Plcg2*$^{-/-}$ samples (P = 0.52) and *Plcg2*$^{\Delta PMN}$ samples (P = 0.75). Therefore, it is unlikely that the defective neutrophil accumulation in *Plcg2*$^{\Delta PMN}$ mice (Figure 4A) is due to a change in neutrophil survival.

DISCUSSION

Our experiments identified PLCγ2 expressed in neutrophils to be critical for autoantibody-induced arthritis (Figure 3) and the generation of the inflammatory microenvironment (Figures 5 and 6), with supposedly secondary defects in neutrophil and monocyte/macrophage accumulation (Figure 4).

Several different hematopoietic lineages have been implicated in autoantibody-induced arthritis (27–33). Of those, our results indicate a role for PLCγ2 expressed in neutrophils but not

in platelets or mast cells (Figure 3). However, care should be taken when interpreting results from lineage-specific conditional deletion approaches because of the limitation of the efficacy and specificity of those approaches. In particular, we cannot exclude the role of PLCγ2 in monocyte/macrophages because of the diversity of those cells and the lack of mouse strains with efficient but strictly monocyte/macrophage-specific Cre expression, and the confounding effect of Cre expression in neutrophils from the LysM-Cre promoter (Figure 2) (see also ref. 50). It should also be noted that *Plcg2*$^{\Delta PMN}$ mutants consistently showed less severe defects than *Plcg2*$^{-/-}$ ones both in vivo (compare Figures 1B and C and Figures 3D and E) and in vitro (Figures 6C–F). While this is likely due in part to the incomplete deletion of PLCγ2 from *Plcg2*$^{\Delta PMN}$ neutrophils (Figure 2), an additional factor may be the contribution of monocyte/macrophage PLCγ2 to arthritis development. In addition, though our results support a role of PLCγ2 in hematopoietic lineage(s) (Figures 1 and 3), we cannot exclude the additional role of PLCγ2 in nonhematopoietic lineage(s) either, especially given the somewhat faster recovery of *Plcg2*$^{-/-}$ recipients transplanted with wild-type bone marrow cells (Figures 1D and E).

CD18-deficient mice are protected against autoantibody-induced arthritis (42,51), and we hypothesized that defective CD18-dependent migration may also explain the phenotype of *Plcg2*$^{-/-}$ and *Plcg2*$^{\Delta PMN}$ animals. However, the different behavior of *Itgb2*$^{-/-}$ and *Plcg2*$^{\Delta PMN}$ neutrophils in mixed bone marrow chimera experiments (Figure 5) and the normal in vitro migration of *Plcg2*$^{-/-}$ and *Plcg2*$^{\Delta PMN}$ neutrophils (Figures 6A and B) suggest that PLCγ2-deficient neutrophils have normal migratory ability. Neutrophils also release proinflammatory mediators (52,53) and our findings indicate that neutrophil PLCγ2 is critical for this response (Figures 5 and 6C–F), therefore contributing to the generation of the inflammatory microenvironment during the amplification of arthritis. The defective accumulation of monocyte/macrophages at the inflammatory site in *Plcg2*$^{\Delta PMN}$ mice (Figures 4B and C) is likely due to secondary activation of macrophages by PLCγ2-expressing neutrophils. Those results indicate a master regulatory role for neutrophils during autoantibody-induced arthritis. Our results also suggest that PLCγ2-expressing neutrophils participate in feedback amplification loops by releasing mediators that attract further neutrophils to the inflammatory site (54). However, it is still unclear whether PLCγ2 participates in the accumulation of the first neutrophils during arthritis development.

Src family kinases, Syk, Vav family members, and SLP-76 (3,4,24,41,49,55) are likely upstream activators of PLCγ2. It would be reasonable to assume that this pathway acts downstream of β_2 integrins, which are also required for arthritis development (42,51). However, autoantibody-induced arthritis depends on lymphocyte function–associated antigen 1 (LFA-1) but not Mac-1 (51), whereas the molecules listed above have primarily been implicated in Mac-1–dependent functional responses (3,4,56,57), and the supposedly LFA-1–dependent accumulation of neutrophils is not affected by the *Plcg2*$^{\Delta PMN}$ mutation (Figure 4). An alternative explanation is that the role of PLCγ2 in arthritis is linked to its role in FcR signaling in neutrophils (4). The components downstream of PLCγ2 is less clear but may involve caspase recruitment domain 9–mediated NF-κB activation and chemokine/cytokine release (43), as well as LTB_4 production through PLCγ2-mediated Ca^{2+} signaling.

PLCγ2 has been implicated in a number of diseases ranging from immune dysfunction through autoimmune and autoinflammatory diseases to Alzheimer's disease (14–21). It is reasonable to assume that the pathways described in this article contribute to the pathogenesis of at least some of those diseases and possibly to other inflammatory diseases where the role of PLCγ2 has not yet been tested. Our results also suggest that targeting PLCγ2 may be particularly useful in inflammatory diseases with a substantial neutrophilic component.

ACKNOWLEDGMENTS

We thank Edina Simon, Nikolett Szénási, and Nóra Kiss for expert technical assistance; Judit Trendl and Lilla Tóth for help with experiments; Norbert Gyöngyösi for suggestions about statistical analyses; and James Ihle, Arthur Beaudet, Tomohiro Kurosaki, Emmanuelle Passegue, Axel Roers, Diane Mathis, and Christophe Benoist for transgenic animals.

AUTHOR CONTRIBUTIONS

All authors were involved in drafting the article or revising it critically for important intellectual content, and all authors approved the final version to be published. Dr. Mócsai had full access to all of the data in the study and takes responsibility for the integrity of the data and the accuracy of the data analysis.

Study conception and design. Futosi, Mócsai.
Acquisition of data. Futosi, Kása, Szilveszter.
Analysis and interpretation of data. Futosi, Kása, Szilveszter, Mócsai.

REFERENCES

1. Wang D, Feng J, Wen R, Marine JC, Sangster MY, Parganas E, et al. Phospholipase Cγ2 is essential in the functions of B cell and several Fc receptors. Immunity 2000;13:25–35.
2. Hashimoto A, Takeda K, Inaba M, Sekimata M, Kaisho T, Ikehara S, et al. Cutting edge: essential role of phospholipase Cγ2 in B cell development and function. J Immunol 2000;165:1738–42.
3. Graham DB, Robertson CM, Bautista J, Mascarenhas F, Diacovo MJ, Montgrain V, et al. Neutrophil-mediated oxidative burst and host defense are controlled by a Vav-PLCγ2 signaling axis in mice. J Clin Invest 2007;117:3445–52.
4. Jakus Z, Simon E, Frommhold D, Sperandio M, Mócsai A. Critical role of phospholipase Cγ2 in integrin and Fc receptor-mediated neutrophil functions and the effector phase of autoimmune arthritis. J Exp Med 2009;206:577–93.
5. Wen R, Jou ST, Chen Y, Hoffmeyer A, Wang D. Phospholipase Cγ2 is essential for specific functions of FcεR and FcγR. J Immunol 2002;169:6743–52.
6. Tassi I, Presti R, Kim S, Yokoyama WM, Gilfillan S, Colonna M. Phospholipase Cγ2 is a critical signaling mediator for murine NK cell activating receptors. J Immunol 2005;175:749–54.
7. Caraux A, Kim N, Bell SE, Zompi S, Ranson T, Lesjean-Pottier S, et al. Phospholipase Cγ2 is essential for NK cell cytotoxicity and innate immunity to malignant and virally infected cells. Blood 2006;107:994–1002.

8. Wonerow P, Pearce AC, Vaux DJ, Watson SP. A critical role for phospholipase Cγ2 in $\alpha_{IIb}\beta_3$-mediated platelet spreading. J Biol Chem 2003;278:37520–9.
9. Nonne C, Lenain N, Hechler B, Mangin P, Cazenave JP, Gachet C, et al. Importance of platelet phospholipase Cγ2 signaling in arterial thrombosis as a function of lesion severity. Arterioscler Thromb Vasc Biol 2005;25:1293–8.
10. Mao D, Epple H, Uthgenannt B, Novack DV, Faccio R. PLCγ2 regulates osteoclastogenesis via its interaction with ITAM proteins and GAB2. J Clin Invest 2006;116:2869–79.
11. Chen Y, Wang X, Di L, Fu G, Bai L, Liu J, et al. Phospholipase Cγ2 mediates RANKL-stimulated lymph node organogenesis and osteoclastogenesis. J Biol Chem 2008;283:29593–601.
12. Kertész Z, Győri D, Körmendi S, Fekete T, Kis-Tóth K, Jakus Z, et al. Phospholipase Cγ2 is required for basal but not oestrogen deficiency-induced bone resorption. Eur J Clin Invest 2012;42:49–60.
13. Faccio R, Cremasco V. PLCγ2: where bone and immune cells find their common ground. Ann N Y Acad Sci 2010;1192:124–30.
14. Ombrello MJ, Remmers EF, Sun G, Freeman AF, Datta S, Torabi-Parizi P, et al. Cold urticaria, immunodeficiency, and autoimmunity related to PLCG2 deletions. N Engl J Med 2012;366:330–8.
15. Aderibigbe OM, Priel DL, Lee CC, Ombrello MJ, Prajapati VH, Liang MG, et al. Distinct cutaneous manifestations and cold-induced leukocyte activation associated with PLCG2 mutations. JAMA Dermatol 2015;151:627–34.
16. Milner JD. PLAID: a syndrome of complex patterns of disease and unique phenotypes [review]. J Clin Immunol 2015;35:527–30.
17. Zhou Q, Lee GS, Brady J, Datta S, Katan M, Sheikh A, et al. A hypermorphic missense mutation in PLCG2, encoding phospholipase Cγ2, causes a dominantly inherited autoinflammatory disease with immunodeficiency. Am J Hum Genet 2012;91:713–20.
18. De Lange KM, Moutsianas L, Lee JC, Lamb CA, Luo Y, Kennedy NA, et al. Genome-wide association study implicates immune activation of multiple integrin genes in inflammatory bowel disease. Nat Genet 2017;49:256–61.
19. Gbadegesin RA, Adeyemo A, Webb NJ, Greenbaum LA, Abeyagunawardena A, Thalgahagoda S, et al. HLA-DQA1 and PLCG2 are candidate risk loci for childhood-onset steroid-sensitive nephrotic syndrome. J Am Soc Nephrol 2015;26:1701–10.
20. Sims R, van der Lee SJ, Naj AC, Bellenguez C, Badarinarayan N, Jakobsdottir J, et al. Rare coding variants in PLCG2, ABI3, and TREM2 implicate microglial-mediated innate immunity in Alzheimer's disease. Nat Genet 2017;49:1373–84.
21. Throm AA, Alinger JB, Pingel JT, Daugherty AL, Pachman LM, French AR. Dysregulated NK cell PLCγ2 signaling and activity in juvenile dermatomyositis. JCI Insight 2018;3:e123236.
22. Yu P, Constien R, Dear N, Katan M, Hanke P, Bunney TD, et al. Autoimmunity and inflammation due to a gain-of-function mutation in phospholipase Cγ2 that specifically increases external Ca^{2+} entry. Immunity 2005;22:451–65.
23. Abe K, Fuchs H, Boersma A, Hans W, Yu P, Kalaydjiev S, et al. A novel N-ethyl-N-nitrosourea–induced mutation in phospholipase Cγ2 causes inflammatory arthritis, metabolic defects, and male infertility in vitro in a murine model. Arthritis Rheum 2011;63:1301–11.
24. Cremasco V, Graham DB, Novack DV, Swat W, Faccio R. Vav/phospholipase Cγ2–mediated control of a neutrophil-dependent murine model of rheumatoid arthritis. Arthritis Rheum 2008;58:2712–22.
25. Cremasco V, Benasciutti E, Cella M, Kisseleva M, Croke M, Faccio R. Phospholipase Cγ2 is critical for development of a murine model of inflammatory arthritis by affecting actin dynamics in dendritic cells. PLoS One 2010;5:e8909.
26. Korganow AS, Ji H, Mangialaio S, Duchatelle V, Pelanda R, Martin T, et al. From systemic T cell self-reactivity to organ-specific autoimmune disease via immunoglobulins. Immunity 1999;10:451–61.
27. Wipke BT, Allen PM. Essential role of neutrophils in the initiation and progression of a murine model of rheumatoid arthritis. J Immunol 2001;167:1601–8.
28. Jonsson H, Allen P, Peng SL. Inflammatory arthritis requires Foxo3a to prevent Fas ligand-induced neutrophil apoptosis. Nat Med 2005;11:666–71.
29. Binstadt BA, Patel PR, Alencar H, Nigrovic PA, Lee DM, Mahmood U, et al. Particularities of the vasculature can promote the organ specificity of autoimmune attack. Nat Immunol 2006;7:284–92.
30. Csepregi JZ, Orosz A, Zajta E, Kása O, Németh T, Simon E, et al. Myeloid-specific deletion of Mcl-1 yields severely neutropenic mice that survive and breed in homozygous form. J Immunol 2018;201:3793–803.
31. Solomon S, Rajasekaran N, Jeisy-Walder E, Snapper SB, Illges H. A crucial role for macrophages in the pathology of K/BxN serum-induced arthritis. Eur J Immunol 2005;35:3064–73.
32. Boilard E, Nigrovic PA, Larabee K, Watts GF, Coblyn JS, Weinblatt ME, et al. Platelets amplify inflammation in arthritis via collagen-dependent microparticle production. Science 2010;327:580–3.
33. Lee DM, Friend DS, Gurish MF, Benoist C, Mathis D, Brenner MB. Mast cells: a cellular link between autoantibodies and inflammatory arthritis. Science 2002;297:1689–92.
34. De Boer J, Williams A, Skavdis G, Harker N, Coles M, Tolaini M, et al. Transgenic mice with hematopoietic and lymphoid specific expression of Cre. Eur J Immunol 2003;33:314–25.
35. Clausen BE, Burkhardt C, Reith W, Renkawitz R, Forster I. Conditional gene targeting in macrophages and granulocytes using LysMcre mice. Transgenic Res 1999;8:265–77.
36. Passegue E, Wagner EF, Weissman IL. JunB deficiency leads to a myeloproliferative disorder arising from hematopoietic stem cells. Cell 2004;119:431–43.
37. Scholten J, Hartmann K, Gerbaulet A, Krieg T, Muller W, Testa G, et al. Mast cell-specific Cre/loxP-mediated recombination in vivo. Transgenic Res 2008;17:307–15.
38. Tiedt R, Schomber T, Hao-Shen H, Skoda RC. Pf4-Cre transgenic mice allow the generation of lineage-restricted gene knockouts for studying megakaryocyte and platelet function in vivo. Blood 2007;109:1503–6.
39. Scharffetter-Kochanek K, Lu H, Norman K, van Nood N, Munoz F, Grabbe S, et al. Spontaneous skin ulceration and defective T cell function in CD18 null mice. J Exp Med 1998;188:119–31.
40. Kouskoff V, Korganow AS, Duchatelle V, Degott C, Benoist C, Mathis D. Organ-specific disease provoked by systemic autoimmunity. Cell 1996;87:811–22.
41. Kovács M, Németh T, Jakus Z, Sitaru C, Simon E, Futosi K, et al. The Src family kinases Hck, Fgr, and Lyn are critical for the generation of the in vivo inflammatory environment without a direct role in leukocyte recruitment. J Exp Med 2014;211:1993–2011.
42. Németh T, Futosi K, Hably C, Brouns MR, Jakob SM, Kovács M, et al. Neutrophil functions and autoimmune arthritis in the absence of p190RhoGAP: generation and analysis of a novel null mutation in mice. J Immunol 2010;185:3064–75.
43. Németh T, Futosi K, Sitaru C, Ruland J, Mócsai A. Neutrophil-specific deletion of the CARD9 gene expression regulator suppresses autoantibody-induced inflammation in vivo. Nat Commun 2016;7:11004.
44. Mócsai A, Zhang H, Jakus Z, Kitaura J, Kawakami T, Lowell CA. G-protein-coupled receptor signaling in Syk-deficient neutrophils and mast cells. Blood 2003;101:4155–63.

45. Csete D, Simon E, Alatshan A, Aradi P, Dobó-Nagy C, Jakus Z, et al. Hematopoietic or osteoclast-specific deletion of Syk leads to increased bone mass in experimental mice. Front Immunol 2019;10:937.
46. Németh T, Futosi K, Szilveszter K, Vilinovszki O, Kiss-Pápai L, Mócsai A. Lineage-specific analysis of Syk function in autoantibody-induced arthritis. Front Immunol 2018;9:555.
47. Futosi K, Németh T, Pick R, Vántus T, Walzog B, Mócsai A. Dasatinib inhibits proinflammatory functions of mature human neutrophils. Blood 2012;119:4981–91.
48. Jakus Z, Németh T, Verbeek JS, Mócsai A. Critical but overlapping role of FcγRIII and FcγRIV in activation of murine neutrophils by immobilized immune complexes. J Immunol 2008;180:618–29.
49. Jakus Z, Simon E, Balázs B, Mócsai A. Genetic deficiency of Syk protects mice from autoantibody-induced arthritis. Arthritis Rheum 2010;62:1899–910.
50. Abram CL, Roberge GL, Hu Y, Lowell CA. Comparative analysis of the efficiency and specificity of myeloid-Cre deleting strains using ROSA-EYFP reporter mice. J Immunol Methods 2014;408:89–100.
51. Watts GM, Beurskens FJ, Martin-Padura I, Ballantyne CM, Klickstein LB, Brenner MB, et al. Manifestations of inflammatory arthritis are critically dependent on LFA-1. J Immunol 2005;174:3668–75.
52. Mócsai A. Diverse novel functions of neutrophils in immunity, inflammation, and beyond. J Exp Med 2013;210:1283–99.
53. Németh T, Sperandio M, Mócsai A. Neutrophils as emerging therapeutic targets [review]. Nat Rev Drug Discov 2020;19:253–75.
54. Németh T, Mócsai A. Feedback amplification of neutrophil function. Trends Immunol 2016;37:412–24.
55. Futosi K, Mócsai A. Tyrosine kinase signaling pathways in neutrophils [review]. Immunol Rev 2016;273:121–39.
56. Mócsai A, Ligeti E, Lowell CA, Berton G. Adhesion-dependent degranulation of neutrophils requires the Src family kinases Fgr and Hck. J Immunol 1999;162:1120–6.
57. Mócsai A, Zhou M, Meng F, Tybulewicz VL, Lowell CA. Syk is required for integrin signaling in neutrophils. Immunity 2002;16:547–58.

Arthritis & Rheumatology
Vol. 73, No. 9, September 2021, pp 1626–1637
DOI 10.1002/art.41708

American College of Rheumatology
Empowering Rheumatology Professionals

Stratification of Patients With Sjögren's Syndrome and Patients With Systemic Lupus Erythematosus According to Two Shared Immune Cell Signatures, With Potential Therapeutic Implications

Lucia Martin-Gutierrez,[1] Junjie Peng,[1] Nicolyn L. Thompson,[1] George A. Robinson,[1] Meena Naja,[2] Hannah Peckham,[1] WingHan Wu,[1] Hajar J'bari,[3] Nyarko Ahwireng,[3] Kirsty E. Waddington,[1] Claire M. Bradford,[1] Giulia Varnier,[1] Akash Gandhi,[3] Rebecca Radmore,[3] Vivek Gupta,[3] David A. Isenberg,[2] Elizabeth C. Jury,[2] and Coziana Ciurtin[2]

Objective. Similarities in the clinical and laboratory features of primary Sjögren's syndrome (SS) and systemic lupus erythematosus (SLE) have led to attempts to treat patients with primary SS or SLE with similar biologic therapeutics. However, the results of many clinical trials are disappointing, and no biologic treatments are licensed for use in primary SS, while only a few biologic agents are available to treat SLE patients whose disease has remained refractory to other treatments. With the aim of improving treatment selections, this study was undertaken to identify distinct immunologic signatures in patients with primary SS and patients with SLE, using a stratification approach based on immune cell endotypes.

Methods. Immunophentyping of 29 immune cell subsets was performed using flow cytometry in peripheral blood from patients with primary SS (n = 45), patients with SLE (n = 29), and patients with secondary SS associated with SLE (SLE/SS) (n = 14), all of whom were considered to have low disease activity or be in clinical remission, and sex-matched healthy controls (n = 31). Data were analyzed using supervised machine learning (balanced random forest, sparse partial least squares discriminant analysis), logistic regression, and multiple *t*-tests. Patients were stratified by K-means clustering and clinical trajectory analysis.

Results. Patients with primary SS and patients with SLE had a similar immunologic architecture despite having different clinical presentations and prognoses. Stratification of the combined primary SS, SLE, and SLE/SS patient cohorts by K-means cluster analysis revealed 2 endotypes, characterized by distinct immune cell profiles spanning the diagnoses. A signature of 8 T cell subsets that distinctly differentiated the 2 endotypes with high accuracy (area under the curve 0.9979) was identified in logistic regression and machine learning models. In clinical trajectory analyses, the change in damage scores and disease activity levels from baseline to 5 years differed between the 2 endotypes.

Conclusion. These findings identify an immune cell toolkit that may be useful for differentiating, with high accuracy, the immunologic profiles of patients with primary SS and patients with SLE as a way to achieve targeted therapeutic approaches.

The views expressed in this article are those of the authors and not necessarily those of the NHS, the NIHR, or the Department of Health.

Supported by grants from Versus Arthritis (grants 21593 and 20164), Great Ormond Street Children's Charity, and the NIHR Biomedical Research Centres at Great Ormond Street Hospital (GOSH) and University College London Hospitals (UCLH). Ms Martin-Gutierrez's work was supported by The Dunhill Medical Trust (grant RPGF1902\117). Mr. Peng's work was supported by Versus Arthritis (grant 21226). Dr. Thompson's work was supported by a University College London (UCL) Division of Medicine PhD Studentship. Dr. Robinson's work was supported by LUPUS UK, Rosetrees Trust (grant M409), and Versus Arthritis (grant 21593). Ms Naja's work was supported by the NIHR UCLH Biomedical Research Centre (grant BRC525/III/CC/191350). Ms Peckham's work was supported by a Versus Arthritis PhD Studentship (grant 22203).

[1]Lucia Martin-Gutierrez, MSc, Junjie Peng, MSc, Nicolyn L. Thompson, PhD, George A. Robinson, PhD, Hannah Peckham, MSc, WingHan Wu, BSc, Kirsty E. Waddington, PhD, Claire M. Bradford, PhD, Giulia Varnier, MBBS: University College London, London, UK; [2]Meena Naja, MBBS, David A. Isenberg, MD, Elizabeth C. Jury, PhD, Coziana Ciurtin, PhD: University College London and University College London Hospitals, London, UK; [3]Hajar J'bari, BNS, Nyarko Ahwireng, BNS, Akash Gandhi, MBBS, Rebecca Radmore, MBBS, Vivek Gupta, MBBS: University College London Hospitals, London, UK.

Ms Martin-Gutierrez and Mr. Peng contributed equally to this work. Drs. Jury and Ciurtin contributed equally to this work.

No potential conflicts of interest relevant to this article were reported.

Address correspondence to Coziana Ciurtin, PhD, FRCP, University College London, Department of Rheumatology, 3rd Floor Central, 250 Euston Road, London NW1 2PG, UK. Email: c.ciurtin@ucl.ac. uk.

Submitted for publication October 2, 2020; accepted in revised form February 18, 2021.

INTRODUCTION

Primary Sjögren's syndrome (SS) and systemic lupus erythematosus (SLE) are chronic autoimmune rheumatic diseases that primarily affect women and that share common characteristics, including genetic, as well as clinical and serologic characteristics (1). Although significant progress has been made toward improving treatment and patient-related outcomes in primary SS and SLE, there is still a need for improvement in early diagnosis and adequate therapy monitoring, as well as new treatments for manifestations refractory to approved therapies and better strategies to address comorbidities (1).

Primary SS and SLE share etiopathogenic links. Both diseases are associated with a large number of major genetic susceptibility loci, such as HLA class II variants BLK, IRF5, and STAT4 (2–4), while neutrophil degranulation was identified as the most significantly enriched functional epigenetic pathway in both diseases (5). In addition, a gene expression meta-analytic strategy identified transcriptomic similarities comprising overexpressed genes related to interferon (IFN)–mediated signaling pathways as well as pathways mediated by other cytokines, and similar responses to viral infection (6). The IFN signature, defined as an increased expression of type I IFN–regulated genes, has been shown to be associated with increased disease activity in both SLE and primary SS (7,8). SLE and SS are also characterized by common environmental factors (9,10), aberrant B cell (11) and T cell activation (12,13), and autoantibody production (14,15), which are reflected in the similar therapeutic approaches (16,17).

However, the clinical evolution of both primary SS and SLE is difficult to predict, as patients present at different stages in the course of their disease with diverse clinical manifestations. This suggests that distinct pathways driving chronic inflammation and immune dysregulation in primary SS and SLE are activated at a certain point in the disease course (18,19). Therefore, recognizing the underlying molecular and cellular abnormalities characterizing patient-specific disease manifestations could identify markers for disease course prediction and tailored treatment strategies.

Previous efforts to stratify patients with SLE based on gene expression identified different mechanisms of disease progression, as well as distinct clinical manifestations (20,21). Similarly, research into stratification of patients with primary SS revealed distinct patient clusters driven by an association between activated CD4+ and CD8+ T cell signatures, disease activity and glandular inflammation (22), presence or absence of SSA/SSB antibodies, presence or absence of various HLA genetic markers (23), or distinctive clinical phenotypes (24). Recognizing that immune signatures, rather than the diagnostic label in certain patients, are likely to be more important in defining the disease, researchers recently proposed a molecular taxonomy–derived reclassification of autoimmune rheumatic diseases to reflect their pathogenesis and support better patient selection for clinical trials (the PRECISESADS project) (25).

Our hypothesis is that patients with primary SS and patients with SLE share immunologic features that span diagnostic boundaries, and recognition of these features could support the development of personalized medicine strategies and thus lead to better treatment selection. In particular, we suggest that stratification based on immune cell phenotype between certain groups of patients with primary SS and patients with SLE could support the implementation of similar therapeutic strategies (e.g., use of treatments licensed for SLE in patients with primary SS with similar immunologic makeup). Furthermore, we propose a new approach of including patients with an overlapping clinical phenotype and features of both diseases, such as patients with secondary SS associated with SLE (SLE/SS), which account for 14–17.8% of SLE patient cohorts (26,27).

Using machine learning approaches in a mixed cohort of patients with primary SS, those with SLE, and those with SLE/SS, we established 2 new disease endotypes based on peripheral blood immune signatures. Results were predictive of characteristic long-term disease activity and damage trajectories.

PATIENTS AND METHODS

Study subjects. Peripheral blood was obtained from patients with primary SS (n = 45), patients with SLE (n = 29), and patients with SLE and secondary SS (n = 14) who were recruited from the Autoimmune Rheumatic Diseases Clinic at the University College London Hospitals NHS Foundation Trust. Patients with primary SS or SLE/SS satisfied the American–European Consensus Group criteria for SS (28). All SLE patients fulfilled the revised Systemic Lupus International Collaborating Clinics (SLICC) criteria for SLE (29). Table 1 shows baseline clinical and demographic characteristics of the patient cohorts. Healthy controls with no symptoms of dryness (n = 31; mean age 44 years, range 20–77 years) were also recruited, matched for sex (all participants were women) and ethnicity. All subjects were enrolled in accordance with ethics regulations approved by the National Research Ethics Service Committee South East Coast–Surrey (reference no. 14/LO/2016) following written informed consent. Peripheral blood mononuclear cells (PBMCs) were isolated from peripheral blood using Ficoll-Hypaque density-gradient centrifugation. A detailed description of data collection methodology is available in the Supplementary Methods (available on the *Arthritis & Rheumatology* website at http://onlinelibrary.wiley.com/doi/10.1002/art.41708/abstract).

Flow cytometry. A total of 10^6 PBMCs were prelabeled with LIVE/DEAD Fixable Blue Dead Cell Stain (Invitrogen Life Technologies) before washing and resuspending in cell staining buffer (1% fetal bovine serum, 0.01% sodium azide) and surface staining for B cell and T cell subsets for 30 minutes at 4°C. Cells were fixed in 1% paraformaldehyde prior to analysis (See Supplementary Figure 1 for gating strategy, available on the *Arthritis & Rheumatology* website at http://onlinelibrary.wiley.com/doi/10.1002/art.41708/abstract). A minimum of 3×10^5 events were collected

Table 1. Demographic and baseline clinical characteristics of the patients with primary SS, patients with SLE, and patients with SLE/SS*

	Primary SS	SLE	SLE/SS	*P*†
No. of patients	45	29	14	–
Demographic characteristics				
Age, mean (range) years	59 (30–78)	48 (21–72)	55 (26–56)	0.003‡
Race/ethnicity, no.				
White	31	14	8	NS
Asian	9	6	3	NS
Black	5	7	3	NS
Other/unknown	0	2	0	–
Disease duration, mean (range) years	11.84 (3–33)	20.15 (0–39)	24.71 (9–38)	0.002‡
Laboratory markers				
WBC count, median (IQR) $\times 10^3$/mm^3 (normal 3–10)	4.92 (4.14–6.53)	5.59 (4.24–7.46)	5.645 (4.64–8.60)	NS
Neutrophils, median (IQR) $\times 10^9$/liter (normal 2.0–7.5)	2.965 (1.99–4.25)	3.42 (2.56–4.26)	3.55 (2.88–4.54)	NS
Lymphocytes, median (IQR) $\times 10^9$/liter (normal 1.2–3.65)	1.42 (1.11–1.79)	1.49 (1.01–2.22)	1.615 (1.30–2.31)	NS
Hgb, median (IQR) mg/liter (normal 115–155)	130 (120.0–134.2)	128 (123–140)	125.5 (114.7–136.0)	NS
Platelets, median (IQR) $\times 10^9$/liter (normal 150–400)	226.5 (213.5–273.0)	248 (213.5–297.0)	249 (233.0–278.5)	NS
ESR, median (IQR) mm/hour (normal 0–20)	14 (5.50–22.5)	16 (8–23)	24 (7.25–41.5)	NS
C-reactive protein level, median (IQR) gm/liter (normal 0–5 mg/liter)	1.4 (0.75–2.55)	2.4 (1.34–4.65)	3.1 (1.03–6.15)	NS
Complement C3 level, median (IQR) gm/liter (normal 0.9–1.8)	1.06 (0.91–1.26)	1 (0.86–1.28)	0.9 (0.83–1.14)	NS
IgG, median (IQR) gm/liter (normal 7–16)	14.19 (11.5–17.6)	12.6 (9.11–15.1)	18.53 (14.0–20.5)	NS
Anti-Ro/SSA positive, no. (%)	37 (82)	13 (45)	10 (71)	0.0033
Anti-La/SSB positive, no. (%)	24 (53)	5 (17)	4 (29)	0.0056
RF, no. (%)	27 (60)	2 (7)	3 (21)	<0.0001
Anti-dsDNA positive, no. (%)	2 (4)	11 (38)	6 (42)	0.007
Positive findings on salivary gland biopsy	10 (22)	NA	4 (29)	NS
Disease activity and damage scores				
SLEDAI-2K				
Median (IQR)	NA	2 (0–4)	2 (0–4)	NS
Mean (range)	NA	2.50 (0–10)	1.92 (0–4)	NS
SLICC/ACR damage index				
Median (IQR)	NA	0 (0–0.25)	1 (0–2)	0.0385
Mean (range)	NA	0.32 (0–2)	1.08 (0–4)	0.0385
ESSDAI				
Median (IQR)	1 (0–2.5)	NA	1.50 (0–3.5)	NS
Mean (range)	2.07 (0–18)	NA	2.67 (0–13)	NS
SSDDI				
Median (IQR)	1 (1–2)	NA	2 (1–2)	NS
Mean (range)	1.65 (0–8)	NA	1.58 (0–4)	NS
Treatments, no. (%)				
HCQ	24 (53)	21 (72)	2 (14)	0.0016
Prednisolone <10 mg/day	3 (7)	17 (59)	4 (29)	<0.0001
Prednisolone ≥10 mg/day	0 (0)	1 (3)	1 (7)	NS
AZA	1 (2)	6 (21)	3 (21)	0.0219
MMF	0 (0)	7 (24)	3 (21)	0.0026
MTX	2 (4)	1 (3)	1 (7)	NS
CYC	1 (2)	5 (17)	3 (21)	0.0367
RTX	0 (0)	4 (14)	0 (0)	0.0141
Time since last dose of RTX, mean (range) years	–	8 (4–16)	–	–

* All patients were women. NS = not significant; WBC = white blood cell; IQR = interquartile range; Hgb = hemoglobin; ESR = erythrocyte sedimentation rate; RF = rheumatoid factor; anti-dsDNA = anti–double-stranded DNA; NA = not applicable; SLEDAI-2K = Systemic Lupus Erythematosus Disease Activity Index 2000; SLICC/ACR = Systemic Lupus International Collaborating Clinics/American College of Rheumatology; ESSDAI = EULAR Sjögren's Syndrome Disease Activity Index; SSDDI = Sjögren's Syndrome Disease Damage Index; HCQ = hydroxychloroquine; AZA = azathioprine; MMF = mycophenolate mofetil; MTX = methotrexate; CYC = cyclophosphamide; RTX = rituximab.
† Except where indicated otherwise, *P* values are for comparisons among all 3 groups, determined using Kruskal-Wallis test or Mann-Whitney test and Dunn's test for multiple comparisons. *P* values less than 0.05 were considered significant.
‡ Patients with primary Sjögren's syndrome (SS) versus patients with systemic lupus erythematosus (SLE).

on an LSRII flow cytometer (Becton Dickinson), and data were analyzed using FlowJo software (Tree Star).

Statistical analysis. The study design and statistical analyses are summarized in Figure 1. Analysis of the demographic data was performed using GraphPad Prism software version 8. In each group, values are expressed as the mean and range or median and interquartile range, depending on data distribution, which was tested using the Kolmogorov-Smirnov test. Nonparametric 2-tailed Mann-Whitney test, Kruskal-Wallis test, and Dunn´s multiple comparison test were performed. Categorical variables were compared using chi-square tests. Correlation analyses of nonparametric data were performed using Spearman's correlation tests. *P* values less than 0.05 were considered significant. Data, including demographic data, immunophenotyping data, and longitudinal clinical data, were stored in Microsoft Excel.

The immunophenotyping data were compared between the different populations including healthy controls, those with SS, those with SLE, those with SLE/SS, and the stratified patient groups. Other statistical analyses were performed in R version 3.5.2 (https://www.R-project.org/).

Logistic regression for association analysis. The association between the immunophenotypes of 29 parameters and patient groups was assessed, adjusted for age and ethnicity. For each measurement, the odds ratio (OR) and the 95% confidence interval (95% CI) were determined, and the *P* value was calculated. Forest plots were produced with the ggplot2 package in R, with significant associations highlighted in red ($P < 0.05$).

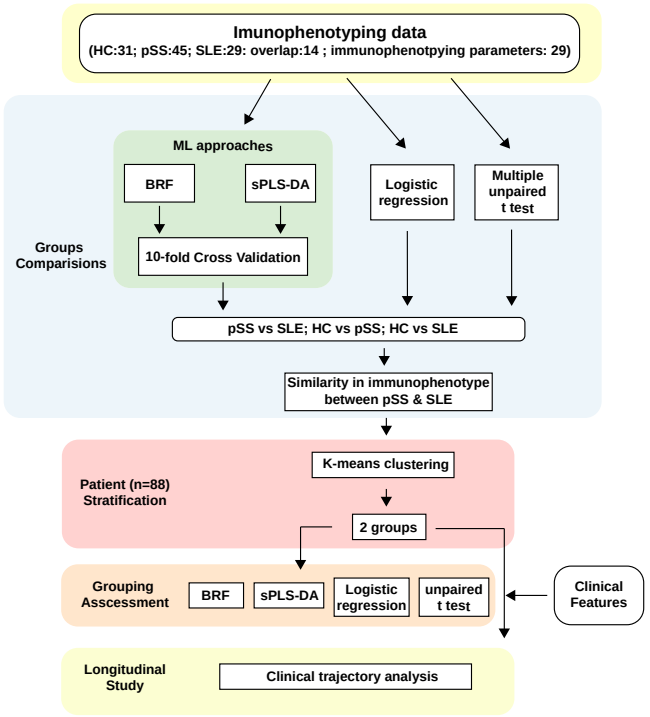

Figure 1. Flow diagram showing the statistical analyses in the study. HC = healthy control; pSS = primary Sjögren's syndrome; SLE = systemic lupus erythematosus; ML = machine learning; BRF = balanced random forest; sPLS-DA = sparse partial least squares discriminant analysis. Color figure can be viewed in the online issue, which is available at http://onlinelibrary.wiley.com/doi/10.1002/art.41708/abstract.

Machine learning approaches. Supervised machine learning approaches, balanced random forest plots, and sparse partial least squares discriminant analysis were applied for classification and parameter identification. A balanced random forest model was used for classification and variable selection using the randomForest package in R. A balanced random forest is an ensemble machine learning algorithm for classification, consisting of numerous decision trees that can increase model accuracy while minimizing the risk of model overfitting, which is often encountered in rare data sets from smaller cohorts; thus, this approach has been employed as a way to obtain validated data from smaller samples (30). Parameters were optimized for the best outcome in each model. A detailed description of the machine learning models and data analysis platforms is available in the Supplementary Methods (available on the *Arthritis & Rheumatology* website at http://onlinelibrary.wiley.com/doi/10.1002/art.41708/abstract).

Clinical trajectory analysis. The trajectories of patient clinical measures over time (expressed as visits/year; n = 5) are depicted by a spaghetti plot. The flow of the longitudinal data of patients (those with SS, those with SLE, and those with SLE/SS; n = 88) is shown in each plot, where each line represents one parameter from each patient. Smoothing lines were added to indicate the trend of patient groups as identified from K-means clustering analysis. Plots were produced using R package "ggplot2."

RESULTS

Similar immunologic architecture comprising a shared immune signature in patients with primary SS and patients with SLE. We compared routinely available clinical information from patients with primary SS, those with SLE, and those with SLE/SS to determine whether it could be used to identify similarities and differences between the patient groups irrespective of diagnosis (Table 1). Patients with primary SS were older (mean age 59 years, range 30–78 years) compared to patients with SLE (mean age 48 years, range 21–72 years) and patients with SLE/SS (mean age 55 years, range 26–56 years). All patients were women. Disease activity scores were not different between the patient groups when comparing the EULAR Sjögren's Syndrome Disease Activity Index (ESSDAI) (31) and Systemic Lupus Erythematosus Disease Activity Index 2000 (SLEDAI-2K) (32) scores, as applicable. Of note, the majority of patients included in this study had low or no disease activity. In comparing the SLICC/American College of Rheumatology

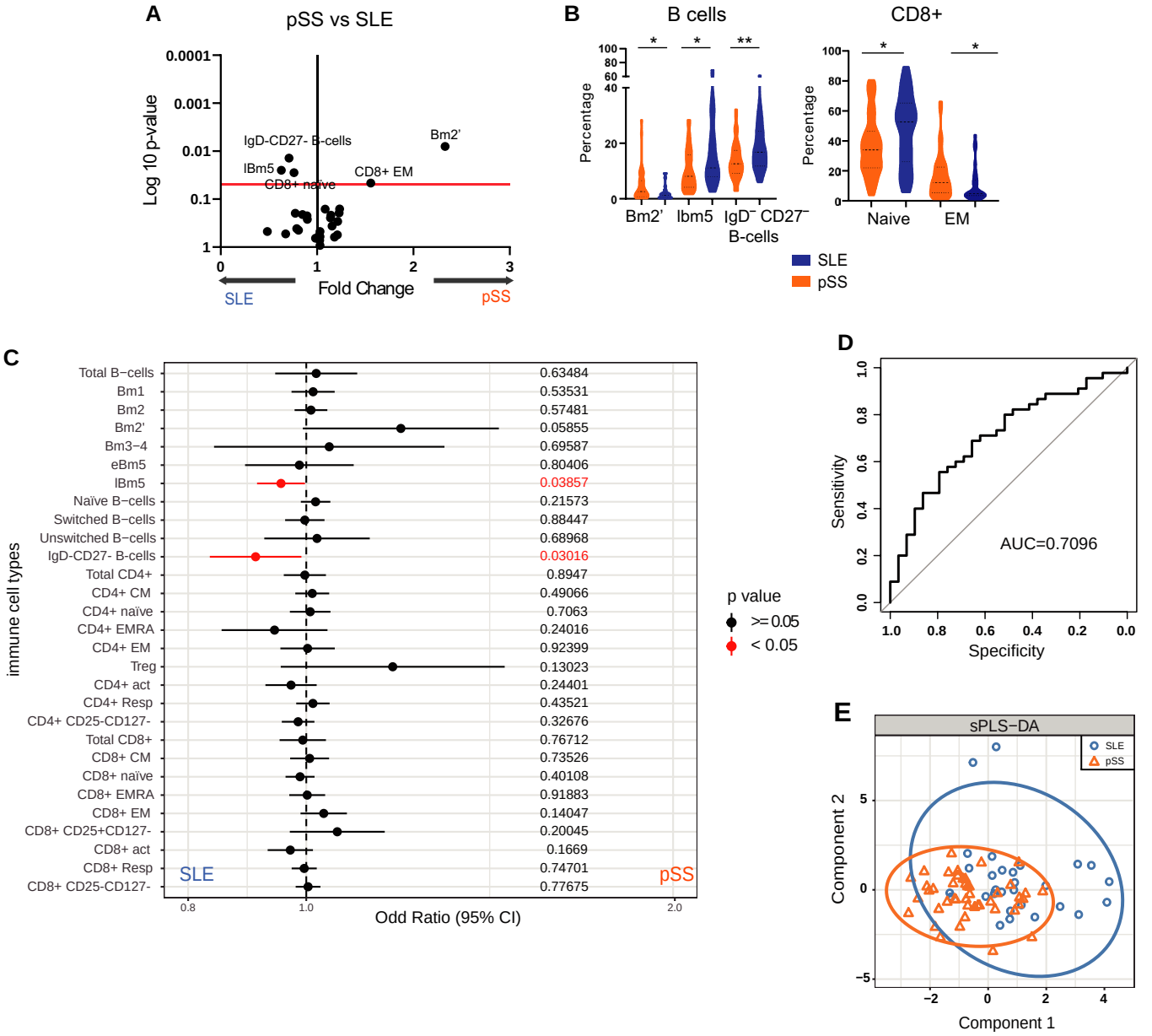

Figure 2. Immunologic architecture in patients with primary Sjögren's syndrome (pSS) and patients with systemic lupus erythematosus (SLE). **A**, Volcano plots showing differences in B and T cell subset frequencies (among 29 immune cell subsets) in patients with primary SS (n = 45) versus patients with SLE (n = 29) (more details in Supplementary Figure 1 [http://onlinelibrary.wiley.com/doi/10.1002/art.41708/ abstract]). Log_{10} *P* values were determined by unpaired t-test; horizontal line indicates the cutoff for a significant difference in fold change values. **B**, Violin plots showing percentages of immune cell subsets in patients with SLE and patients with primary SS. Data are the mean ± SEM. * = $P < 0.05$; ** = $P < 0.01$, by unpaired *t*-test. **C**, Forest plots showing odds ratios with 95% confidence intervals (95% CIs) for the differential frequencies of 29 immunologic parameters between patients with SLE and patients with primary SS, in a univariate logistic regression model adjusted for age and ethnicity. All patients were women. **D**, Area under the receiver operating characteristic curve (AUC) assessing performance of the balanced random forest model, adjusted for age and ethnicity, for distinguishing patients with SLE from patients with primary SS based on immune cell profiles. **E**, Sparse partial least squares discriminant analysis (sPLS-DA) assessing overlap of all 29 immune cell types between patients with primary SS and patients with SLE. Results are individual distribution points with confidence ellipses, in SLE (blue) and primary SS (orange). Bm = mature B; eBm5 = effector memory Bm5; IBM5 = late memory Bm5; CM = central memory T; EMRA = CD45RA+ effector memory T; TEM = effector memory T; CD4+ act = activated CD4+ T cells; CD8+ Resp = responder CD8+ T cells. Color figure can be viewed in the online issue, which is available at http://onlinelibrary.wiley.com/doi/10.1002/art.41708/abstract.

Damage Index (SDI) scores (33) between groups, patients with SLE/SS had increased SDI scores compared to SLE patients, whereas SDI scores were not significantly different between patients with primary SS and patients with SLE/SS.

The 3 patient groups were also strikingly similar in most other clinical and laboratory features, except in the comparison of disease duration, which was significantly longer in patients with SLE compared to patients with primary SS. Anti-Ro and

anti-La autoantibodies and rheumatoid factor were more common in patients with primary SS compared to patients with SLE. Frequency of treatment with conventional disease-modifying antirheumatic drugs differed significantly among the 3 patient populations. This reflects current practice: fewer patients with primary SS were treated with these agents, as the evidence of their efficacy is very limited. Only 14% of SLE patients had received rituximab 4–16 years before blood samples were collected.

To assess whether immune cell phenotyping could be used to stratify patients within the 3 different autoimmune diseases, 29 different B cell, CD4+ T cell, and CD8+ T cell subsets were examined (See Figure 1 for the analysis strategy and Supplementary Figure 1 for the gating strategies, available on the *Arthritis & Rheumatology* website at http://onlinelibrary.wiley.com/doi/10.1002/art.41708/abstract). As expected, patients with primary SS and patients with SLE had disrupted immune cell profiles compared to healthy controls, including alterations in both B cell and T cell subpopulation frequencies (Supplementary Figures 2A–F and Supplementary Figures 3A–F, available on the *Arthritis & Rheumatology* website at http://onlinelibrary.wiley.com/doi/10.1002/art.41708/abstract), which has also been reported in other studies (34,35).

However, when comparing the immune profiles of patients with primary SS and patients with SLE using a variety of statistical

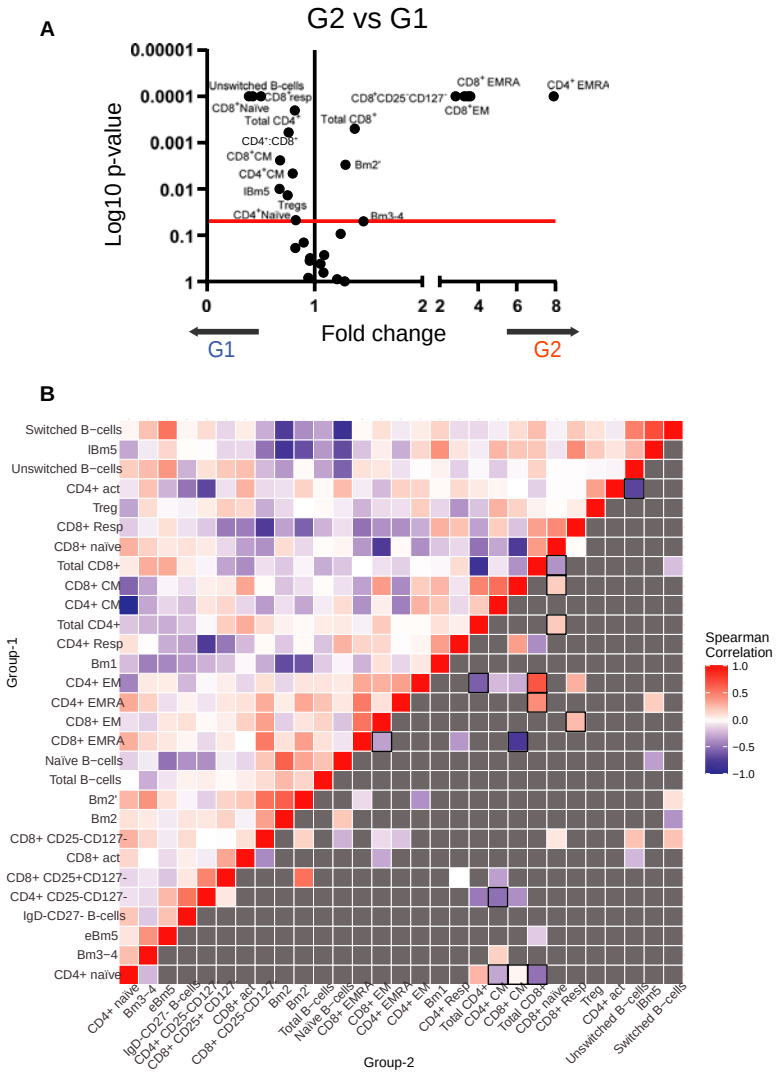

Figure 3. Differences in immunologic architecture between patients in group 1 (G1) and patients in group 2 (G2) based on multiple *t*-test comparisons. **A**, Volcano plots showing differences in B and T cell subset frequencies (among 29 immune cell subsets) in group 2 versus group 1. K-means cluster analysis was used to group all patients into 2 endotypes with distinct immune cell profiles. Log_{10} *P* values were calculated using unpaired *t*-test; horizontal line indicates the cutoff for significance. **B**, Correlation analyses of immunophenotype data from patients in group 1 and group 2. Colors in the heatmap represent Spearman's correlation coefficients for pairs of immune cell types (among 29 immunologic features) in group 1 (upper left) and group 2 (bottom right) (red = positive correlation; blue = negative correlation; dark gray = no significant difference compared to group 1). The intensity of the color is proportional to the strength of the correlation. Color boxes outlined in white indicate significantly different correlations in group 2 compared to group 1 at $P < 0.05$, while those outlined in black indicate significant differences at $P < 0.01$. See Figure 2 for other definitions.

and machine learning approaches, very few statistically significant differences were observed between the 2 cohorts (Figure 2). Only 5 of 29 immune cell subsets had differential frequencies between patients with primary SS and patients with SLE, as determined by the Mann-Whitney test, Kruskal-Wallis test, and a univariate logistic regression analysis: transitional mature B cells (Bm2′), late memory mature Bm5 cells, IgD–CD27– B cells, and CD8+ naive T and effector memory T (Tem) cells (Figures 2A–C). These findings were confirmed using machine learning approaches, with the optimized balanced random forest model showing a poor performance of these immune cell profiles in distinguishing between primary SS and SLE (area under the curve [AUC] 0.7096) (Figure 2D). Results from the sparse partial least squares discriminant analysis model showed a large overlap between the immune cell profiles of patients with primary SS and those with SLE (Figure 2E). Together, the results of these comprehensive comparison analyses suggest that while patients with SLE and those with SS had multiple significant immune phenotype differences compared to healthy controls, few statistically significant differences in the immune phenotype were observed between patients with SLE and those with SS, despite the patients having different clinical presentations and diagnoses.

Two groups of patients identified as having shared immune signatures across primary SS, SLE, and SLE/SS phenotypes irrespective of diagnosis. Based on the observed similarities of the immunologic architecture and the heterogeneous nature of the disease features of both primary SS and SLE, we hypothesized that immune-based subtypes could be shared between patients with primary SS, those with SLE, and those with SLE/SS. To investigate this, K-means clustering in an unsupervised machine learning algorithm was applied to the immunologic features of the combined patient cohorts (Supplementary Methods, available on the *Arthritis & Rheumatology* website at http://onlinelibrary.wiley.com/doi/10.1002/art.41708/abstract). Two distinct patient groups (defined by patient's immune cell profiles) were identified across the combined primary SS, SLE, and SLE/SS patient cohorts (Supplementary Figure 4, available at http://onlinelibrary.wiley.com/doi/10.1002/art.41708/abstract): group 1 (n = 49, including 24 with primary SS, 19 with SLE, and 6 with SLE/SS) and group 2 (n = 39, including 21 with primary SS, 10 with SLE, and 8 with SLE/SS).

Using the same approach for comparison analysis (as shown in Figure 1), multiple *t*-test comparisons of the B cell and T cell subsets revealed significantly different immune cell phenotype patterns with clear differentiation between the groups (Figure 3A and Supplementary Figure 5, available on the *Arthritis & Rheumatology* website at http://onlinelibrary.wiley.com/doi/10.1002/art.41708/abstract). Patients in group 1 had elevated frequencies of B cell subsets: late memory Bm5 cells and unswitched memory (IgD+CD27+) B cells, and T cell subsets: total CD4+, CD4+ naive, CD4+ central memory T (Tcm) cells, and regulatory, CD8+ naive, CD8+ Tcm, and responder (CD8+CD25–CD127+) T cells, as well as an elevated CD4+:CD8+ T cell ratio compared to patients in group 2. Frequencies of Bm2′ plasmablasts (Bm3–4), total CD8+, CD8+ Tem cells, CD4+ and CD8+ CD45RA+ effector memory T (Temra) (CD27–CD45RA+), and CD8+CD25–CD127– cells were significantly reduced in group 1 compared to group 2 (Figure 3A

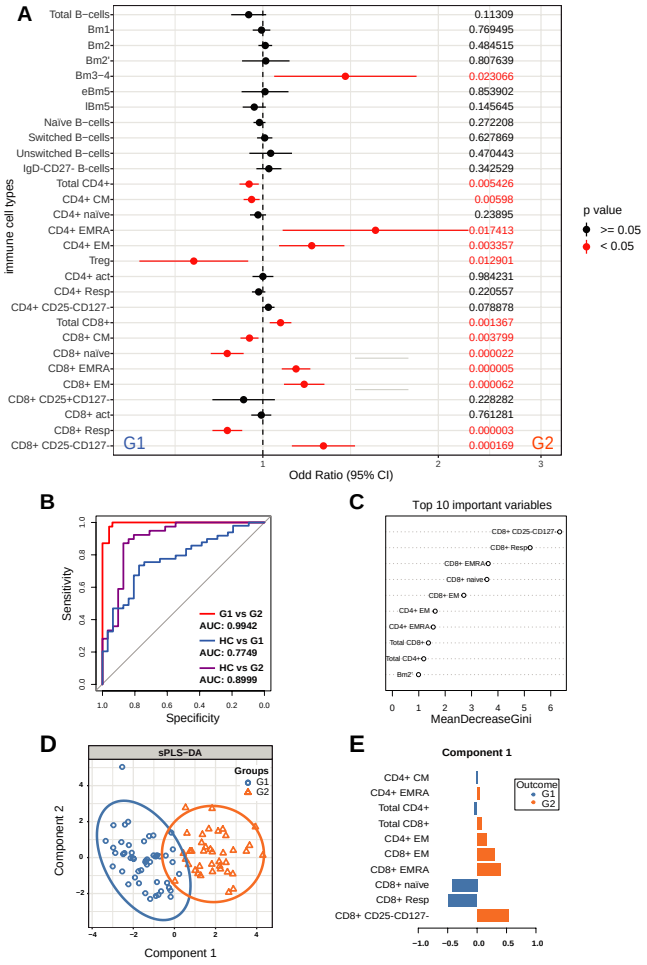

Figure 4. Differences in immunologic architecture between patients in group 1 (G1) and patients in group 2 (G2) based on univariate logistic regression analyses (adjusted for age and ethnicity). **A**, Forest plots show the odds ratios with 95% CIs for the associations of 29 immunologic parameters in group 1 and group 2. **B** and **C**, AUCs were calculated to assess performance of the balanced random forest model (adjusted for age and ethnicity) in distinguishing group 1 from group 2 patients and group 1 and group 2 patients from healthy controls (HC) (**B**). The top 10 variables contributing to the balanced random forest model are shown (**C**). The mean decrease in Gini measures the importance of each variable to the model, in that a higher score indicates a higher importance of the variable. **D**, Sparse partial least squares discriminant analysis with all 29 immune cell types was performed to validate the top hits from the predictive model. Results are shown as individual distribution points with confidence ellipses for group 1 (blue) and group 2 (orange). **E**, Factor-loading weights in component 1 are shown for the top 10 ranked immunologic parameters. Colors indicate the group with the maximal mean value. See Figure 2 for other definitions. Color figure can be viewed in the online issue, which is available at http://onlinelibrary.wiley.com/doi/10.1002/art.41708/abstract.

and Supplementary Figure 5, available on the *Arthritis & Rheumatology* website at http://onlinelibrary.wiley.com/doi/10.1002/art.41708/abstract). Furthermore, a correlation analysis of immune cell frequencies revealed significant differences in immune cell associations between group 1 and group 2 (Figure 3B).

To support these findings, a univariate logistic regression analysis was performed. Nearly half of the immune cell subsets (13 of 29) showed significant alterations in their frequencies between groups (Figure 4A). These results were further confirmed using machine learning approaches, in which the optimized balanced random forest model, with classifications assessed using 10-fold cross-validation, yielded an AUC of 0.9942 for distinguishing between the 2 patient groups (Figure 4B).

The top contributing immune features ranked using the mean decrease in Gini coefficient suggested a strong divergence of CD8+ T cell subsets between patients in group 1 and patients in group 2, including CD8+CD25–CD127–, CD8+ responder (CD127+CD25–), CD8+ Temra, CD8+ naive, CD8+ Tem, and total CD8+ T cells (Figure 4C). Balanced random forest classification models performed better when discriminating between group 2 and healthy controls (AUC 0.8999) compared to discriminating between group 1 and healthy controls (AUC 0.7749), suggesting that patients in group 2 had more aberrant immune cell profiles compared to healthy controls than did patients in group 1 (Figure 4B). Sparse partial least squares discriminant analysis also showed a clear separation between the 2 patient groups (Figure 4D) and identified similar immune cell subsets as being important in driving the group 1 stratification compared to group 2 (Figure 4E). Comparison of the results from multiple analysis approaches revealed that 8 immune cell subsets were common to all 4 analysis methods: total CD4+ and CD4+ Temra T cells, total CD8+ and CD8+ naive, Tem, Temra, responder T cells, and CD25–CD127– T cells (Supplementary Table 1, available on the *Arthritis & Rheumatology* website at http://onlinelibrary.wiley.com/doi/10.1002/art.41708/abstract).

Moreover, using these combined subsets maintained and slightly improved the performance of the model in differentiating between the groups (AUC 0.9979) compared to individual immune cell subsets alone (Supplementary Figures 6A–C, available at http://onlinelibrary.wiley.com/doi/10.1002/art.41708/abstract). In addition, the accuracy of the classification models was maintained at 96.16% in the 10-fold cross-validation analysis. Thus, despite patients with primary SS and those with SLE having low or no disease activity, these patients could still be stratified using their immune cell profile (Supplementary Table 2, available at http://onlinelibrary.wiley.com/doi/10.1002/art.41708/abstract). These

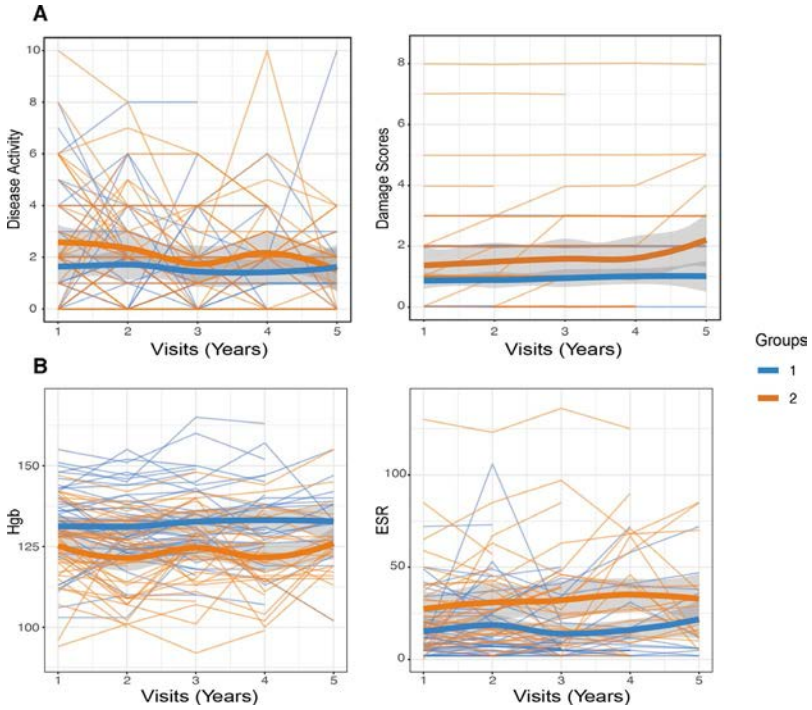

Figure 5. Differential clinical trajectories identified in patients in group 1 compared to those in group 2. Individual clinical trajectories across the 3 disease phenotypes were assessed as spaghetti plots, according to disease-specific activity scores (combined Systemic Lupus Erythematosus Disease Activity Index and EULAR Sjögren's Syndrome Disease Activity Index [31,32]; cutoffs for moderately active disease are similar) and damage scores (combined Systemic Lupus International Collaborating Clinics/American College of Rheumatology damage index and Sjögren's Syndrome Disease Damage Index [54]) (**A**) and laboratory markers, including hemoglobin (Hgb) level and erythrocyte sedimentation rate (ESR) (**B**), at 5 annual clinical encounters. Each line represents 1 patient. Smoothing lines were added to indicate the trend of individual clinical trajectories corresponding to patients in group 1 (blue) and those in group 2 (orange). 95% *t*-test–based confidence intervals for each group are shown (gray-shaded area).

findings suggest that differences in global immunologic features in these patients are a reflection of the underlying immunopathogenesis of shared pathogenesis, rather than being a reflection of the level of disease activity or the specific disease diagnosis.

Increased disease activity in patients in group 2. To assess whether the distinct immunologic profiles also reflect differences in clinical and disease features, laboratory markers (including anti-Ro and anti-La autoantibodies and rheumatoid factor), disease activity and damage scores, and treatments were compared between patients in group 1 and group 2 at the time of sample collection (Supplementary Table 3 and Supplementary Figure 7, available at http://onlinelibrary.wiley.com/doi/10.1002/art.41708/abstract). Patients from both groups had had similar disease outcomes and serologic biomarker levels overall, although patients in group 2 had a significantly elevated erythrocyte sedimentation rate (ESR), decreased hemoglobin (Hgb) levels, and increased ESSDAI scores compared to patients in group 1, suggesting that the disease state was more active at baseline in group 2, although disease activity was still predominantly low overall. In addition, frequencies of different therapies were not significantly different between SLE patients in group 1 and SLE patients in group 2 (SLE patients have more treatment options compared to the options available for patients with primary SS) (Supplementary Table 4, available at http://onlinelibrary.wiley.com/doi/10.1002/art.41708/abstract), thus suggesting that the identified immune cell signatures were not driven by differences in treatment, but rather could reflect the underlying disease pathogenesis.

To further investigate whether the grouping was clinically meaningful as a potential predictor of disease course, a wide range of clinical measurements were collected longitudinally at 5 subsequent annual encounters, including serologic markers and disease-specific outcome measures. Individual patients' disease trajectories for these assessments were compared between group 1 and group 2. Over the 5-year clinical encounter timeframe, patients in group 2 had overall higher disease activity compared to patients in group 1. Although, as expected, disease activity fluctuated over time in the SLE and SLE/SS patient groups (measured using the SLEDAI-2K), despite patients having low disease activity (SLEDAI-2K <3), there was a general trend toward more active SLE in group 2. The ESSDAI scores were characterized by less fluctuation over time and were marginally increased in the patients with primary SS and those with SLE/SS from group 2. Interestingly, all patients in group 2, irrespective of diagnosis, had increased SDI damage scores (Figure 5A and Supplementary Figure 8, available on the *Arthritis & Rheumatology* website at http://onlinelibrary.wiley.com/doi/10.1002/art.41708/abstract). Patients in group 2 overall also had decreased Hgb levels and elevated ESR, which corresponded to their slightly more increased disease activity (Figure 5B). No other laboratory biomarkers had the capacity to discriminate between patients in group 1 and group 2.

Correlations between immune cell subtypes and baseline clinical measurements. To assess whether the distinct immune cell profiles identified across the 3 disease phenotypes were associated with distinct clinical features, a correlation analysis was performed within the mixed patient population. Correlations between the immune cell frequencies and clinical characteristics of patients in each group were calculated using Pearson's correlation coefficients (Supplementary Figure 9, available on the *Arthritis & Rheumatology* website at http://onlinelibrary.wiley.com/doi/10.1002/art.41708/abstract). In concordance with the baseline immune cell phenotype characterization and trajectory analysis, ESR was significantly correlated with 4 CD8+ T cell subtypes, 3 CD4+ T cell subtypes, and 2 B cell subpopulations, which overlapped with the cell subsets driving the K-means clustering of patients in groups 1 and 2. Hgb level only correlated positively with the frequency of CD8+ Tcm cells in the mixed patient population. Disease damage scores across the mixed patient populations significantly correlated with CD8+ T cell frequencies, including CD8+CD25–CD127, CD8+ responder T cells, and CD8+ Temra cells, which were the top ranked immune features from the machine learning models.

DISCUSSION

We propose new classification for patients with primary SS, those with SLE, and those with SLE/SS based on unique peripheral blood immune signatures that are predictive of distinct long-term disease activity and damage trajectories in those with low or no disease activity. The 2 patient groups (endotypes) spanning the diagnostic boundaries we describe here are robust, as they have been derived from a complex analysis with several cross-validation steps.

Even if initial characterization of the 3 disease phenotypes included in our analysis showed differences in age and disease duration, as well as serologic markers and treatment, as previously reported in another study in patients with primary SS, those with SLE, and those with SLE/SS (36), we have shown for the first time that patients with primary SS and patients with SLE with low-to-moderate or no disease activity have very few significant differences in immunologic architecture. This comprised differences in 5 of 29 immune cell subsets, which included transitional Bm2′ cells, late memory Bm5 cells, IgD–CD27– B cells, and CD8+ naive and CD8+ Tem cells. Previous immunophenotyping studies in primary SS indicated a predominance of naive B cells, as well as lower frequencies and absolute numbers of memory B cells (37,38) and opposite trends in SLE (39), findings which were replicated in our study as well. The role of T cells in the pathogenesis of both primary SS (12) and SLE (13) has been established in the literature. SLE is associated with T cell functional alterations and increased effector and decreased regulatory T cell responses, while an

overall shift toward Th1 phenotype activation has been previously identified in primary SS.

Our analysis identified 2 new disease endotypes within our mixed cohort, which were characterized by differential immune signatures that had a higher capacity for discriminating between patients than the immune signatures associated with the diagnostic label (receiver operating characteristic curve 0.99 compared to 0.70). These findings highlight the shared immunopathogenic processes underlying primary SS and SLE manifestations that are likely to be more relevant for treatment selection strategies than basing treatment selection on disease diagnosis alone. In addition, the altered immune landscape associated with the 2 endotypes had predictive value for determining long-term disease trajectories related to disease activity and damage.

Previous patient stratification approaches in primary SS and SLE were mainly directed at cohorts of patients with the same diagnosis, despite the use of shared treatment strategies across many autoimmune rheumatic diseases. However, potential biomarkers shared by different autoimmune diseases have been described, including an expanded CD8+ memory T cell population associated with poor prognosis in both small vessel vasculitis and SLE (40) or elevated expression of genes related to CD8+ T cell responses, which correlated with poor prognosis in Crohn's disease and ulcerative colitis (41). This suggests that exploring biomarker commonalities within autoimmune diseases could expand the understanding of their potential shared pathogenic mechanisms. Prior efforts to elucidate the molecular heterogeneity of SLE revealed that IFN signatures are associated with disease activity (21,42) and the enrichment of neutrophil transcripts during the progression to active nephritis (21) also revealed transcriptional fingerprints that were shared across various autoimmune, inflammatory, and infectious diseases and were found to be associated with SLE disease progression (43). Our future studies will focus on exploring the role of these signatures in our patient groups.

Several B cell–targeted biologic therapies have been separately investigated in both patients with primary SS and patients with SLE (16,44). However, the only licensed anti–B cell biologic therapy for SLE (belimumab) is only approved for use in patients with nonrenal SLE manifestations (45) and has no proven clinical efficacy in primary SS, despite findings showing that this treatment normalizes the B cell frequency, phenotype, and function in patients with primary SS (46). Anti-CD20 monoclonal antibody therapy failed to meet the primary end point evaluated in randomized controlled trials in primary SS or SLE, despite being associated with some benefits (47,48) and being proven effective in other studies and case series (49–51). Exciting data have recently emerged regarding the potential clinical efficacy of a new biologic therapy for primary SS, ianalumab, which has a dual mode of action combining BAFF receptor inhibition and B cell depletion (52). Therefore, to date, the limited therapeutic success in primary SS and SLE emphasizes the need to rethink the way that treatment targets are selected, in order to pinpoint the role of shared pathogenic communalities across diseases, rather than selecting patients based on diagnostic labels or composite measures of disease activity.

The likely impact of our findings will include a new classification of patients with primary SS based on one of the two immune signatures derived from this analysis, using a simplified immunologic toolkit that includes the immune markers that drove patient clustering in group 1 compared to group 2. As patients included in group 1 had better outcomes based on disease trajectories, with no difference in medications used, and also had CD4+:CD8+ T cell ratios within normal range (compared to significantly increased ratios in group 2; $P < 0.0002$), we can hypothesize that patients with a group 2 immune signature across the 3 disease phenotypes could benefit from treatment with mycophenolate mofetil (which has been shown to restore the significantly lower CD4+:CD8+ T cell ratio associated with SLE in patients who responded to treatment with mycophenolate mofetil [53]). Also, since treatment with belimumab is associated with the depletion of naive and transitional B cells in patients with primary SS who responded to therapy (46), we could hypothesize that patients with primary SS stratified in group 1 are more likely to respond to belimumab, as they have an increased transitional B cell (Bm2′) signature.

Further research, including patient stratification, using the identified signatures to determine inclusion in interventional clinical trials of therapies that predominantly target B cells (rituximab, belimumab) compared to T cells (abatacept) is required to establish if the signatures we identified have predictive biomarker values for responses to certain therapies. In addition to stratifying patients for better treatment selection, our results can offer new therapeutic options for patients with primary SS who share immune signatures with selected SLE patients, by providing access to treatments licensed for use in SLE. This can lead to changes in clinical practice through the implementation of best-evidence personalized treatment strategies derived from interventional clinical trials using the stratification tool we are proposing here, to improve the benefit to the patient and justify access to existing SLE treatments for selected patients with primary SS.

Although patients included in our analysis have well-controlled or mild-to-moderately active disease, the disease trajectory analysis identified differences in accumulated damage over time between the 2 groups and higher ESSDAI scores in group 2, suggesting that closer monitoring may be required for patients with a group 2 immunologic signature. Investigating the immune signatures associated with various severe organ and system flares, as well as exploring the immune signatures present in target-organ tissue biopsy specimens, were beyond the scope of this study, as this would have introduced additional confounding factors and would have required a much larger sample size.

Our study has certain limitations: the patients were all women and all had well-controlled or mild-to-moderate disease

activity; therefore, we were unable to evaluate the influence of sex bias or the impact of high disease activity or severe flares on the identified immune signatures. This was an exploratory study; therefore, corrections for multiple comparisons were not performed so that potentially important markers would not have been excluded; thus, Type 1 family-wise errors could occur for some analyses. External validation will be required to assess whether the identified signatures can be reproduced in a study with a larger sample size, as well as to account for potential Type 1 family-wise errors and investigate whether other immune signatures, which this study had no statistical power to detect, could be identified. While in this study we stratified patients based on statistically significant differences in immune cell phenotype frequencies, functional experimental work is needed to categorically define whether patients in the stratified groups are immunologically similar, which will be the focus of future studies.

In conclusion, we propose the reclassification of patients with primary SS, patients with SLE, and patients with SLE/SS based on an immune cell toolkit comprising a limited immune cell set that can differentiate patients with high accuracy. Our results demonstrate that selection and validation of patients using machine learning approaches could be proven to be a suitable strategy to select patients for targeted therapeutic approaches.

ACKNOWLEDGMENTS

We thank Jamie Evans for expert support with the flow cytometry analysis and Eve McLoughlin for support with patient recruitment.

AUTHOR CONTRIBUTIONS

All authors were involved in drafting the article or revising it critically for important intellectual content, and all authors approved the final version to be published. Dr. Ciurtin had full access to all of the data in the study and takes responsibility for the integrity of the data and the accuracy of the data analysis.

Study conception and design. Martin-Gutierrez, Peng, Thompson, Robinson, Naja, Peckham, Wu, J'bari, Ahwireng, Waddington, Bradford, Varnier, Gandhi, Radmore, Gupta, Isenberg, Jury, Ciurtin.

Acquisition of data. Martin-Gutierrez, Peng, Thompson, Robinson, Isenberg, Jury, Ciurtin.

Analysis and interpretation of data. Martin-Gutierrez, Peng, Thompson, Robinson, Naja, Peckham, Wu, J'bari, Ahwireng, Waddington, Bradford, Varnier, Gandhi, Radmore, Gupta, Isenberg, Jury, Ciurtin.

REFERENCES

1. Pasoto SG, Adriano de Oliveira Martins V, Bonfa E. Sjögren's syndrome and systemic lupus erythematosus: links and risks [review]. Open Access Rheumatol 2019;11:33–45.
2. Nordmark G, Kristjansdottir G, Theander E, Eriksson P, Brun JG, Wang C, et al. Additive effects of the major risk alleles of IRF5 and STAT4 in primary Sjogren's syndrome. Genes Immun 2009;10:68–76.
3. Hom G, Graham RR, Modrek B, Taylor KE, Ortmann W, Garnier S, et al. Association of systemic lupus erythematosus with C8orf13-BLK and ITGAM-ITGAX. N Engl J Med 2008;358:900–9.
4. Lessard CJ, Li H, Adrianto I, Ice JA, Rasmussen A, Grundahl KM, et al. Variants at multiple loci implicated in both innate and adaptive immune responses are associated with Sjogren's syndrome. Nat Genet 2013;45:1284–92.
5. Imgenberg-Kreuz J, Almlof JC, Leonard D, Sjowall C, Syvanen AC, Ronnblom L, et al. Shared and unique patterns of DNA methylation in systemic lupus erythematosus and primary Sjogren's syndrome. Front Immunol 2019;10:1686.
6. Toro-Dominguez D, Carmona-Saez P, Alarcon-Riquelme ME. Shared signatures between rheumatoid arthritis, systemic lupus erythematosus and Sjogren's syndrome uncovered through gene expression meta-analysis. Arthritis Res Ther 2014;16:489.
7. Nezos A, Gravani F, Tassidou A, Kapsogeorgou EK, Voulgarelis M, Koutsilieris M, et al. Type I and II interferon signatures in Sjogren's syndrome pathogenesis: contributions in distinct clinical phenotypes and Sjogren's related lymphomagenesis. J Autoimmun 2015;63:47–58.
8. Crow MK. Type I interferon in the pathogenesis of lupus [review]. J Immunol 2014;192:5459–68.
9. Hanlon P, Avenell A, Aucott L, Vickers MA. Systematic review and meta-analysis of the sero-epidemiological association between Epstein-Barr virus and systemic lupus erythematosus. Arthritis Res Ther 2014;16:R3.
10. Nagata Y, Inoue H, Yamada K, Higashiyama H, Mishima K, Kizu Y, et al. Activation of Epstein-Barr virus by saliva from Sjogren's syndrome patients. Immunology 2004;111:223–9.
11. Dorner T, Giesecke C, Lipsky PE. Mechanisms of B cell autoimmunity in SLE [review]. Arthritis Res Ther 2011;13:243.
12. Singh N, Cohen PL. The T cell in Sjogren's syndrome: force majeure, not spectateur [review]. J Autoimmun 2012;39:229–33.
13. Mak A, Kow NY. The pathology of T cells in systemic lupus erythematosus [review]. J Immunol Res 2014;2014:419029.
14. Nocturne G, Mariette X. B cells in the pathogenesis of primary Sjogren syndrome [review]. Nat Rev Rheumatol 2018;14:133–45.
15. Shuai ZW, Huang Y, Zhang L, Cai J, Li M. Role of autoantibodies to various Ro60 epitopes in the decrease of lymphocytes seen in systemic lupus erythematosus and primary Sjogren's syndrome. Genet Mol Res 2015;14:10096–102.
16. Sada PR, Isenberg D, Ciurtin C. Biologic treatment in Sjogren's syndrome [review]. Rheumatology (Oxford) 2015;54:219–30.
17. Murphy G, Isenberg DA. New therapies for systemic lupus erythematosus: past imperfect, future tense [review]. Nat Rev Rheumatol 2019;15:403–12.
18. Fritzler MJ, Mahler M. Redefining systemic lupus erythematosus: SMAARTT proteomics [review]. Nat Rev Rheumatol 2018;14:451–2.
19. Voulgarelis M, Skopouli FN. Clinical, immunologic, and molecular factors predicting lymphoma development in Sjogren's syndrome patients. Clin Rev Allergy Immunol 2007;32:265–74.
20. Toro-Domínguez D, Martorell-Marugán J, Goldman D, Petri M, Carmona-Sáez P, Alarcón-Riquelme ME. Stratification of systemic lupus erythematosus patients into three groups of disease activity progression according to longitudinal gene expression. Arthritis Rheumatol 2018;70:2025–35.
21. Banchereau R, Hong S, Cantarel B, Baldwin N, Baisch J, Edens M, et al. Personalized immunomonitoring uncovers molecular networks that stratify lupus patients [published erratum]. Cell 2016;165:1548–50.
22. Mingueneau M, Boudaoud S, Haskett S, Reynolds TL, Nocturne G, Norton E, et al. Cytometry by time-of-flight immunophenotyping identifies a blood Sjogren's signature correlating with disease activity and glandular inflammation. J Allergy Clin Immunol 2016;137:1809–21.
23. Thorlacius GE, Hultin-Rosenberg L, Sandling JK, Bianchi M, Imgenberg-Kreuz J, Pucholt P, et al. Genetic and clinical basis for two distinct subtypes of primary Sjogren's syndrome. Rheumatology (Oxford) 2021;60:837–48.

24. Tarn JR, Howard-Tripp N, Lendrem DW, Mariette X, Saraux A, Devauchelle-Pensec V, et al. Symptom-based stratification of patients with primary Sjögren's syndrome: multi-dimensional characterisation of international observational cohorts and reanalyses of randomised clinical trials. Lancet Rheumatol 2019;1:e85–94.
25. Barturen G, Beretta L, Cervera R, van Vollenhoven R, Alarcon-Riquelme ME. Moving towards a molecular taxonomy of autoimmune rheumatic diseases [review]. Nat Rev Rheumatol 2018;14:180.
26. Alani H, Henty JR, Thompson NL, Jury E, Ciurtin C. Systematic review and meta-analysis of the epidemiology of polyautoimmunity in Sjogren's syndrome (secondary Sjogren's syndrome) focusing on autoimmune rheumatic diseases. Scand J Rheumatol 2018;47:141–54.
27. Yao Q, Altman RD, Wang X. Systemic lupus erythematosus with Sjogren syndrome compared to systemic lupus erythematosus alone: a meta-analysis. J Clin Rheumatol 2012;18:28–32.
28. Vitali C, Bombardieri S, Jonsson R, Moutsopoulos HM, Alexander EL, Carsons SE, et al, and the European Study Group on Classification Criteria for Sjögren's Syndrome. Classification criteria for Sjögren's syndrome: a revised version of the European criteria proposed by the American-European Consensus Group. Ann Rheum Dis 2002;61:554–8.
29. Petri M, Orbai AM, Alarcón GS, Gordon C, Merrill JT, Fortin PR, et al. Derivation and validation of the Systemic Lupus International Collaborating Clinics classification criteria for systemic lupus erythematosus. Arthritis Rheum 2012;64:2677–86.
30. Robinson GA, Peng J, Dönnes P, Coelewij L, Naja M, Radziszewska A, et al. Disease-associated and patient-specific immune cell signatures in juvenile-onset systemic lupus erythematosus: patient stratification using a machine-learning approach. Lancet Rheumatol 2020;2:e485–96.
31. Seror R, Ravaud P, Bowman SJ, Baron G, Tzioufas A, Theander E, et al, on behalf of the EULAR Sjögren's Task Force. EULAR Sjögren's Syndrome Disease Activity Index: development of a consensus systemic disease activity index for primary Sjögren's syndrome. Ann Rheum Dis 2010;69:1103–9.
32. Gladman DD, Ibanez D, Urowitz MB. Systemic Lupus Erythematosus Disease Activity Index 2000. J Rheumatol 2002;29:288–91.
33. Gladman D, Ginzler E, Goldsmith C, Fortin P, Liang M, Urowitz M, et al. The development and initial validation of the Systemic Lupus International Collaborating Clinics/American College of Rheumatology Damage Index for systemic lupus erythematosus. Arthritis Rheum 1996;39:363–9.
34. Verstappen GM, Kroese FG, Bootsma H. T cells in primary Sjögren's syndrome: targets for early intervention. Rheumatology (Oxford) 2019 doi: https://doi.org/10.1093/rheumatology/kez004. E-pub ahead of print.
35. Nagy G, Koncz A, Perl A. T- and B cell abnormalities in systemic lupus erythematosus [review]. Crit Rev Immunol 2005;25:123–40.
36. Manoussakis MN, Georgopoulou C, Zintzaras E, Spyropoulou M, Stavropoulou A, Skopouli FN, et al. Sjogren's syndrome associated with systemic lupus erythematosus: clinical and laboratory profiles and comparison with primary Sjogren's syndrome. Arthritis Rheum 2004;50:882–91.
37. Bohnhorst JO, Bjorgan MB, Thoen JE, Natvig JB, Thompson KM. Bm1-Bm5 classification of peripheral blood B cells reveals circulating germinal center founder cells in healthy individuals and disturbance in the B cell subpopulations in patients with primary Sjogren's syndrome. J Immunol 2001;167:3610–8.
38. Hansen A, Odendahl M, Reiter K, Jacobi AM, Feist E, Scholze J, et al. Diminished peripheral blood memory B cells and accumulation of memory B cells in the salivary glands of patients with Sjogren's syndrome. Arthritis Rheum 2002;46:2160–71.
39. Potter KN, Mockridge CI, Rahman A, Buchan S, Hamblin T, Davidson B, et al. Disturbances in peripheral blood B cell subpopulations in autoimmune patients. Lupus 2002;11:872–7.
40. McKinney EF, Lyons PA, Carr EJ, Hollis JL, Jayne DR, Willcocks LC, et al. A CD8+ T cell transcription signature predicts prognosis in autoimmune disease. Nat Med 2010;16:586–91.
41. Lee JC, Lyons PA, McKinney EF, Sowerby JM, Carr EJ, Bredin F, et al. Gene expression profiling of CD8+ T cells predicts prognosis in patients with Crohn disease and ulcerative colitis. J Clin Invest 2011;121:4170–9.
42. Petri M, Singh S, Tesfasyone H, Dedrick R, Fry K, Lal P, et al. Longitudinal expression of type I interferon responsive genes in systemic lupus erythematosus. Lupus 2009;18:980–9.
43. Chaussabel D, Quinn C, Shen J, Patel P, Glaser C, Baldwin N, et al. A modular analysis framework for blood genomics studies: application to systemic lupus erythematosus. Immunity 2008;29:150–64.
44. Fattah Z, Isenberg DA. Recent developments in the treatment of patients with systemic lupus erythematosus: focusing on biologic therapies [review]. Expert Opin Biol Ther 2014;14:311–26.
45. Weintraub B. Belimumab efficacy is 'mild' but market potential still great: anticipating US approval of the first lupus drug since 1957. BioDrugs 2011;25:203–5.
46. Pontarini E, Fabris M, Quartuccio L, Cappeletti M, Calcaterra F, Roberto A, et al. Treatment with belimumab restores B cell subsets and their expression of B cell activating factor receptor in patients with primary Sjogren's syndrome. Rheumatology (Oxford) 2015;54:1429–34.
47. Weidenbusch M, Rommele C, Schrottle A, Anders HJ. Beyond the LUNAR trial: efficacy of rituximab in refractory lupus nephritis [review]. Nephrol Dial Transplant 2013;28:106–11.
48. Brown S, Coy NN, Pitzalis C, Emery P, Pavitt S, Gray J, et al. The TRACTISS protocol: a randomised double blind placebo controlled clinical trial of anti-B cell therapy in patients with primary Sjogren's syndrome. BMC Musculoskelet Disord 2014;15:21.
49. Ramos-Casals M, Diaz-Lagares C, Soto-Cardenas MJ, Brito-Zeron P, Cuadrado MJ, Sanna G, et al. Rituximab therapy in lupus nephritis: current clinical evidence [review]. Clin Rev Allergy Immunol 2011;40:159–69.
50. Souza FB, Porfirio GJ, Andriolo BN, Albuquerque JV, Trevisani VF. Rituximab effectiveness and safety for treating primary Sjogren's syndrome (primary SS): systematic review and meta-analysis. PLoS One 2016;11:e0150749.
51. Meijer JM, Meiners PM, Vissink A, Spijkervet FK, Abdulahad W, Kamminga N, et al. Effectiveness of rituximab treatment in primary Sjogren's syndrome: a randomized, double-blind, placebo-controlled trial. Arthritis Rheum 2010;62:960–8.
52. Dorner T, Posch MG, Li Y, Petricoul O, Cabanski M, Milojevic JM, et al. Treatment of primary Sjogren's syndrome with ianalumab (VAY736) targeting B cells by BAFF receptor blockade coupled with enhanced, antibody-dependent cellular cytotoxicity. Ann Rheum Dis 2019;78:641–7.
53. Zhao L, Jiang Z, Jiang Y, Ma N, Wang K, Zhang Y. Changes in immune cell frequencies after cyclophosphamide or mycophenolate mofetil treatments in patients with systemic lupus erythematosus. Clin Rheumatol 2012;31:951–9.
54. Vitali C, Palombi G, Baldini C, Benucci M, Bombardieri S, Covelli M, et al. Sjögren's Syndrome Disease Damage Index and disease activity index: scoring systems for the assessment of disease damage and disease activity in Sjögren's syndrome, derived from an analysis of a cohort of Italian patients. Arthritis Rheum 2007;56:2223–31.

Arthritis & Rheumatology
Vol. 73, No. 9, September 2021, pp 1638–1645
DOI 10.1002/art.41735

American College of Rheumatology
Empowering Rheumatology Professionals

Association of Machine Learning–Based Predictions of Medial Knee Contact Force With Cartilage Loss Over 2.5 Years in Knee Osteoarthritis

Nicholas M. Brisson,[1] Anthony A. Gatti,[2] Philipp Damm,[3] Georg N. Duda,[3] and Monica R. Maly[4]

Objective. The relationship between in vivo knee load predictions and longitudinal cartilage changes has not been investigated. We undertook this study to develop an equation to predict the medial tibiofemoral contact force (MCF) peak during walking in persons with instrumented knee implants, and to apply this equation to determine the relationship between the predicted MCF peak and cartilage loss in patients with knee osteoarthritis (OA).

Methods. In adults with knee OA (39 women, 8 men; mean ± SD age 61.1 ± 6.8 years), baseline biomechanical gait analyses were performed, and annualized change in medial tibial cartilage volume (mm^3/year) over 2.5 years was determined using magnetic resonance imaging. In a separate sample of patients with force-measuring tibial prostheses (3 women, 6 men; mean ± SD age 70.3 ± 5.2 years), gait data plus in vivo knee loads were used to develop an equation to predict the MCF peak using machine learning. This equation was then applied to the knee OA group, and the relationship between the predicted MCF peak and annualized cartilage volume change was determined.

Results. The MCF peak was best predicted using gait speed, the knee adduction moment peak, and the vertical knee reaction force peak (root mean square error 132.88N; $R^2 = 0.81$, $P < 0.001$). In participants with knee OA, the predicted MCF peak was related to cartilage volume change ($R^2 = 0.35$, $\beta = -0.119$, $P < 0.001$).

Conclusion. Machine learning was used to develop a novel equation for predicting the MCF peak from external biomechanical parameters. The predicted MCF peak was positively related to medial tibial cartilage volume loss in patients with knee OA.

INTRODUCTION

Mechanical loading is implicated in the onset and progression of cartilage loss, a hallmark of knee osteoarthritis (OA) (1–7). Mechanical loads are theorized to be related to cartilage loss through their role in increasing compressive forces across joint surfaces (8). However, such a relationship has not yet been verified in patients with knee OA, since noninvasive, in vivo force measurement is not possible; direct measurement of knee contact forces is only possible using instrumented knee implants (9). Therefore, loads acting within native knees are estimated using musculoskeletal modeling from motion analysis data, or surrogate measures reflecting knee joint loading are calculated using inverse dynamics.

Key external biomechanical parameters used to describe loading across knee joint surfaces include the knee adduction moment (KAM), the knee flexion moment (KFM), the vertical knee reaction force (vKRF), gait speed, and measures of body size (height, body mass, and body mass index [BMI]). The KAM reflects

Dr. Brisson's work was supported by scholarships from the Canadian Institutes of Health Research Joint Motion Program and the Ontario Ministry of Training, Colleges, and Universities Ontario Graduate Scholarship Program. Dr. Gatti's work was supported by a scholarship from the Ontario Ministry of Training, Colleges, and Universities Ontario Graduate Scholarship Program and by The Arthritis Society, Canada (Doctoral Salary award). Dr. Damm's work was supported by Deutsche Arthrose-Hilfe eV, the DFG (Be 804/18-1 and Da 1786/5-1), the German Federal Ministry of Education and Research (BMBF workHealth grant 01EC1905D and OVERLOAD-PrevOP grant 01EC1408A), and the OrthoLoad Club, Germany. Dr. Duda's work was supported by the DFG (DU 298/25-1), the German Federal Ministry of Education and Research (BMBF OVERLOAD-PrevOP grant 01EC1408A), and the OrthoLoad Club, Germany. Dr. Maly's work was supported by the Canadian Institutes of Health Research (operating grant 102643 and a New Investigator Salary award), The Arthritis Society in partnership with the Canadian Institutes of Health Research Institute of Musculoskeletal Health and Arthritis (Career Development award), the Canadian Foundation for Innovation (Leaders Opportunity Fund 27501), and the Ministry of Research and Innovation (Ontario Research Fund).

[1]Nicholas M. Brisson, PhD: Charité–Universitätsmedizin Berlin, Berlin, Germany, and McMaster University, Hamilton, Ontario, Canada; [2]Anthony A. Gatti, PhD: McMaster University and NeuralSeg, Hamilton, Ontario, Canada; [3]Philipp Damm, PhD, Georg N. Duda, PhD: Charité–Universitätsmedizin Berlin, Berlin, Germany; [4]Monica R. Maly, PhD: McMaster University, Hamilton, Ontario, Canada, and University of Waterloo, Waterloo, Ontario, Canada.

Drs. Brisson and Gatti contributed equally to this work.

Dr. Gatti owns stock or stock options in NeuralSeg. No other disclosures relevant to this article were reported.

Address correspondence to Nicholas Brisson, PhD, Charité–Universitätsmedizin Berlin, Julius Wolff Institute, Philippstrasse 13, Haus 11, Raum 2.18, 10115 Berlin, Germany. Email: nicholas.brisson@charite.de.

Submitted for publication July 9, 2020; accepted in revised form March 11, 2021.

the distribution of load between medial and lateral knee compartments (10). The KFM provides insight into net muscle contraction across the knee (11). During the stance phase, the quadriceps produce an internal knee extension moment to counterbalance the external KFM, increasing compressive forces within the joint (1). The vKRF represents an equal and opposite vertical force acting between the tibia and femur, without accounting for muscle forces (12). Finally, although gait speed and measures of body size do not directly reflect joint loading, these are main effectors of the vertical ground reaction force (13), a primary determinant of the KAM, KFM, and vKRF (12,14,15).

Due to the theoretical relationship between mechanical loads and cartilage degeneration, and due to the high prevalence of tibiofemoral OA in the medial compartment (16), measurement and prediction of medial knee contact forces (MCFs) are of particular interest. Direct measurements in patients with instrumented tibial prostheses and estimates from tibiofemoral contact force models confirm correlations between external biomechanical parameters and MCFs during gait (9,10,17–22). In patients with instrumented knee implants, the KAM (9,17–19), vKRF (10), and gait speed (17) were independently positively associated with the MCF. Interestingly, combining the KFM with the KAM enabled more useful predictions of the MCF than when either variable was analyzed separately (9,18), supporting the notion that these variables collectively describe the knee loading environment (1,3,18). Furthermore, higher body mass and BMI were each associated with greater peak knee compressive forces in persons with knee OA (20–22).

Ample evidence links external gait measures to medial cartilage loss in knee OA. For instance, a higher KAM peak (3,4) and KAM impulse (4,6) at baseline predicted greater loss of medial knee cartilage over 1–5 years. A greater KFM peak at baseline was associated with reduced medial knee cartilage over 5 years (3). Furthermore, a higher BMI at baseline predicted greater medial knee cartilage loss over 2 years (23). Interestingly, the impact of a higher KAM peak and KAM impulse at baseline on medial knee cartilage loss over 2.5 years was amplified with increasing BMI (7). Conversely, no known work has examined the relationship between vKRF or gait speed and morphologic cartilage changes in knee OA, though their relationship with cartilage loss seems logical as these parameters directly influence knee load magnitudes. Since instrumented knee prostheses lack cartilage, MCF measurements acquired with such technology cannot be used to directly predict cartilage loss. Instead, biomechanical and/or statistical predictions of MCF can be developed in persons with instrumented prostheses and then validated in the population of interest (i.e., patients with knee OA).

A primary research goal is to confirm whether knee contact forces are in fact related to cartilage loss. Thus far, studies have examined the relationship between external knee loading variables as surrogates of contact forces and medial knee cartilage loss. To our knowledge, the relationship between the MCF (what the surrogate measures are said to represent) and cartilage loss has not yet been modeled directly. The purpose of the present study was to confirm the relationship between the predicted MCF peak during walking and changes in medial tibial cartilage volume over a period of 2.5 years in participants with clinical and radiographic knee OA. To accomplish this, we developed an equation to predict the MCF peak from external knee loading parameters using data from patients with instrumented tibial prostheses, which was then used to predict the MCF peak for a separate sample of participants with knee OA. It was hypothesized that a higher predicted MCF peak at baseline would be associated with greater cartilage volume loss in patients with knee OA.

PATIENTS AND METHODS

This analysis was performed using 2 data sets: 1 from participants with knee OA and 1 from patients with instrumented tibial prostheses. First, gait biomechanics and knee cartilage volume change were documented in a subset of participants with knee OA enrolled in a longitudinal, observational study. This study was approved by the Hamilton Integrated Research Ethics Board (no. 10-475). Second, gait biomechanics data from a sample of patients who received instrumented knee implants were used to derive a statistical model predicting the MCF peak. This study was approved by the ethics board of the Charité Universitätsmedizin Berlin (no. EA4/069/06) and registered at the German Clinical Trials Register (no. DRKS00000606; www.orthoload.com). This research was completed in compliance with the Declaration of Helsinki. All participants provided written informed consent.

Participants with knee OA. The knee OA cohort comprised a convenience sample of 64 adults with clinical knee OA, ages 40–70 years, who were recruited from local rheumatology and orthopedic clinics. Clinical knee OA was diagnosed according to the American College of Rheumatology criteria (24). Potential participants were excluded if they had other types of arthritis, past lower extremity joint injury and/or surgery, ipsilateral hip or ankle conditions (including OA), regular need for an adaptive walking aid, or lower extremity trauma or intraarticular therapies within 3 months prior to commencing the study. If participants had bilateral OA, the more symptomatic knee was studied.

At baseline, Kellgren/Lawrence (K/L) scores (25) were determined by an experienced radiologist using anteroposterior weight-bearing knee radiographs acquired in a standardized fixed-flexion position (26). These measurements have demonstrated moderate-to–very good interobserver reliability with intraclass correlation coefficients (ICCs) ranging between 0.51 and 0.89 (27). In addition, descriptive statistics were recorded, including sex, age, height, body mass, BMI, and anatomic knee alignment (28). In the current analysis, only participants with radiographic knee OA (i.e., K/L score ≥2) at baseline and those who had baseline and follow-up cartilage measurements were included (n = 47). There

were 39 women and 8 men included, with a mean ± SD age of 61.1 ± 6.8 years. Eighteen participants had a K/L score of 2, 18 participants had a K/L score of 3, and 11 participants had a K/L score of 4.

Cartilage morphology. At baseline and after ~2.5 years of follow-up, participants with knee OA underwent magnetic resonance imaging (MRI) of the study knee using the same 1T peripheral scanner (OrthOne; ONI Medical Systems). Participants underwent knee scans in the morning and were asked to minimize weight-bearing prior to MRI acquisition. For analysis of cartilage morphometry, MRI scans were acquired using a coronal, T1-weighted, fat-saturated, spoiled gradient-recalled acquisition in the steady-state sequence with an in-plane resolution of 0.3125 × 0.3125 mm and a slice thickness of 1.5 mm (60 msec repetition time, 12.4 msec echo time, 40° flip angle).

Medial tibial cartilage volume was determined using automated, atlas-based segmentations of MRI scans (Qmetrics) (29). Test–retest precision error for medial tibial cartilage volume using the same 1T scanner was 3.6% (30). Baseline and follow-up cartilage values were used to calculate annualized cartilage volume change (mm^3/year) for each participant using the following equation:

$$\Delta\, Cartilage/year = \frac{Cartilage\ volume\ at\ follow\text{-}up - cartilage\ volume\ at\ baseline}{No.\ of\ years\ between\ time\ points}.$$

Biomechanical assessment. Within 1 week of the baseline MRI, participants with knee OA underwent gait analyses to calculate 3-dimensional (3-D) knee kinematics and kinetics during self-paced barefoot walking. Active infrared markers, mounted in triads on rigid plates, were fixated to the sacrum, and lateral aspects of the mid-thigh, mid-shank, and foot of the study leg. Standard bony anatomic landmarks were digitized to create participant-specific rigid link-segment models of the pelvis and leg, as described previously (31). Marker trajectories were collected at 100 Hz with a 9-camera motion capture system (Optotrak Certus; Northern Digital). Kinetics were recorded synchronously at 1,000 Hz with a floor-embedded force platform (OR6-7-1000; AMTI). Data from 5 self-paced barefoot gait trials, in which the foot of the study leg landed fully on the force platform, were collected.

Gait data were processed with commercial software (Visual 3D; C-Motion). Marker trajectory and force plate data were filtered with a second-order, low-pass (6 Hz cutoff), bidirectional Butterworth filter (32). External knee moments and reaction forces were resolved in a 3-D floating axis coordinate system (33) using inverse dynamics (12). The following external biomechanical parameters, representing theoretically relevant potential predictors of MCF (9,10,17–22), were computed and extracted for 5 gait cycles and then averaged: gait speed, external KAM peak, external KAM impulse, external KFM peak, and vKRF peak. Given the importance of the first KAM and KFM peaks to the progression of cartilage loss in knee OA (3,6), and to ensure analysis of temporally matched outcomes between participants, the peak values for the kinetic outcomes (i.e., KAM, KFM, vKRF) were extracted from the first 50% of the stance phase. The KAM impulse, which captures both the magnitude and duration of load (34), was computed for the entire stance phase using trapezoidal integration of only positive values.

In vivo knee loads in patients with instrumented knee implants. To allow for predictions of the in vivo MCF peak, gait data were also acquired in a separate sample of patients with force-measuring tibial prostheses as a result of total knee arthroplasty to treat advanced OA (n = 9; 3 women, 6 men; mean ± SD age 70.3 ± 5.2 years) (9,17,35). Details of the design, calibration, and accuracy of the instrumented tibial tray have been reported elsewhere (36,37). Gait data were collected over 8 years (1–3 time points per participant); the earliest time point was 11.2 months after implantation. Marker trajectories (100 Hz or 120 Hz; Vicon), ground reaction forces (1,000 Hz or 960 Hz; AMTI), and internal knee implant kinetics (~100 Hz; Innex; Zimmer) were collected synchronously during barefoot walking at self-determined slow, natural, and fast walking speeds. A range of walking speeds was included to capture greater variability in MCF peaks and to allow for broader generalizability of the model. Marker trajectory and force plate data were processed using the same rigid link-segment model and processing parameters (i.e., filter, joint coordinate system, inverse dynamics) as described for the knee OA group, and the same descriptive statistics and external biomechanical parameters were computed. To enable prediction of the MCF peak from external parameters and to ensure temporal consistency with the extracted kinetic outcomes (i.e., KAM peak, KFM peak, vKRF peak), the first peak of the MCF was extracted from the measured in vivo loads for each trial. In total, 218 gait trials were analyzed, representing an average of 24.2 trials per participant (minimum 7, maximum 40).

Predictions of the MCF peak. The best combination of predictors of the measured MCF peak was determined in patients with instrumented knee implants using the machine learning method Least Absolute Shrinkage and Selection Operator (LASSO) regression (38,39). LASSO is a regularized form of least squares regression that uses a tunable parameter (λ). When the lambda value is set to 0, LASSO is equivalent to least squares regression; as the lambda value increases, unimportant beta coefficients are reduced to 0. Model selection was therefore simplified to identify the lambda value between 0 and 100 with the smallest out-of-sample root mean square error (RMSE) using leave-one-out cross-validation (38,39). In other words, the RMSE was assessed for the samples of data left out during each cross-validation step and represents the prediction error for data not used to fit the model. To prevent data leakage, cross-validation was performed at the participant level instead of at the trial level.

Table 1. Demographic, anthropometric, and gait data at baseline for the knee OA and instrumented knee implant groups*

	Knee OA (n = 47)	Knee implant (n = 9)	*P*
Female sex, no. (%)	39 (83)	3 (33)	0.001
Age, years	61.1 ± 6.8	70.3 ± 5.2	<0.001
Height, meters	1.63 ± 0.08	1.72 ± 0.04	0.002
Body mass, kg	76.1 ± 16.1	91.1 ± 12.5	0.010
BMI, kg/m^2	28.8 ± 5.8	30.8 ± 4.5	0.326
Coronal knee alignment, degrees	−2.3 ± 3.5†	2.4 ± 4.2‡	NA§
Gait speed, meters/second	1.17 ± 0.22	1.16 ± 0.11	0.350
KAM peak, Nm	25.03 ± 14.35	37.82 ± 13.53	0.017
KAM impulse, Nm × s	9.15 ± 6.58	15.72 ± 7.23	0.016
KFM peak, Nm	43.33 ± 18.09	30.78 ± 11.86	0.051
vKRF peak, N	749.64 ± 136.64	803.21 ± 113.79	0.275
Measured MCF peak, N	–	1,578.75 ± 264.21	–
Predicted MCF peak, N	1,355.25 ± 326.02	–	0.058¶

* Gait data are for overground barefoot walking trials performed at a self-selected, natural speed. Except where indicated otherwise, values are the mean ± SD. BMI = body mass index; NA = not applicable; KAM = knee adduction moment; KFM = knee flexion moment; vKRF = vertical knee reaction force; MCF = medial knee contact force.
† Anatomic tibiofemoral angle determined from weight-bearing anteroposterior knee radiographs acquired in a fixed-flexion position (see ref. 28). A negative value indicates valgus alignment.
‡ Mechanical tibiofemoral angle (hip-knee-ankle angle) determined from standing anteroposterior full-leg radiographs (see ref. 28). A positive value indicates varus alignment.
§ Knee alignment measurements were not compared statistically, because anatomic (knee osteoarthritis [OA] sample) and mechanical (knee implant sample) alignments are inconsistent with one another (see ref. 28).
¶ Versus measured MCF peak in the knee implant group.

Potential predictors included height, body mass, BMI, gait speed, KAM peak, KAM impulse, KFM peak, and vKRF peak, as well as the squared versions of each term and all possible 2-way interactions. To create the final model, predictors with non-zero beta coefficients at the optimal lambda values were fitted to the data from all 218 trials using least squares regression. To account for non-independence of repeated measurements, a cluster-robust variance matrix was used (40).

Predicted MCF model fit parameters, including the fitted beta coefficients, R^2, and RMSE, as well as the out-of-sample cross-validation RMSE, were calculated. In addition, simple linear regressions were run for each of the identified predictors to determine how well they individually predicted the MCF peak.

Statistical analysis. Descriptive statistics were calculated as the mean ± SD for continuous data and the number (percentage) for categorical data. Demographic, anthropometric, and overground, self-paced gait data were compared between the 2 groups (knee OA and instrumented knee implant) using independent sample *t*-tests. If assumptions of normality or homogeneity of variance were not met, a 2-sample Mann-Whitney U test was used. To determine whether cartilage volume changed from baseline to follow-up in participants with knee OA, a 1-sample *t*-test was used.

To determine the relationship between the predicted MCF peak and the change in medial tibial cartilage volume, a 2-step approach was used. First, predictions of the MCF peak were calculated for all participants with knee OA using the aforementioned equation generated in patients with instrumented knee implants. Second, the relationship between the predicted MCF peak and the annualized cartilage volume change was fitted using ordinary least squares regression.

To assess the fidelity of the MCF peak predictions in the knee OA group, and their relationship with cartilage change, additional analyses were performed. Reliability of the MCF peak predictions was determined using data from a subsample of knee OA patients (n = 40) for whom gait data were available from a second occasion ~6 months following the baseline assessment. Relative and absolute test–retest reliabilities were estimated using a Shrout and Fleiss type 2,1 ICC and the SEM, respectively. Furthermore, the predictive model of cartilage change was assessed for assumptions of linear regression, including linearity, normality of residuals, and homoscedasticity. Finally, a multivariate linear regression model between the identified predictors of the MCF peak and cartilage volume change was created. The goodness of fit of this multivariate model was compared to that of the MCF peak model using the likelihood ratio test. All data and statistical analyses were performed with StatsModels for Python 3.7 (41).

RESULTS

At baseline, the knee OA group had a higher proportion of women (P = 0.001), and patients with knee OA were on average younger (P < 0.001) than those in the instrumented knee implant group. Participants with knee OA also tended to be shorter (P = 0.002) and weigh less (P = 0.010) (likely attributable to the sex discrepancy between groups); however, the groups did not differ in BMI (P = 0.326). Demographic and anthropometric data as well as all tested biomechanical parameters for the knee OA group and the instrumented knee implant group are described in Table 1. The KAM peak (Δ = −12.79 Nm; P = 0.017) and KAM impulse (Δ = −6.57 Nm × s; P = 0.016) were lower in the knee OA group compared to the instrumented knee implant group. No between-group

Table 2. Final linear regression model to predict the measured MCF peak from external biomechanical gait outcomes in the patients with instrumented knee implants*

	β	SE	*P*
Intercept	−446.21	303.75	0.142
Gait speed, meters/second	398.06	67.90	<0.001
KAM peak, Nm	15.27	3.35	<0.001
vKRF peak, N	1.27	0.32	<0.001

* Final linear regression model included fit parameters of R^2 = 0.81 (P < 0.001), root mean square error (RMSE) = 132.88N, and cross-validation RMSE = 196.58N. MCF = medial knee contact force; KAM = knee adduction moment; vKRF = vertical knee reaction force.

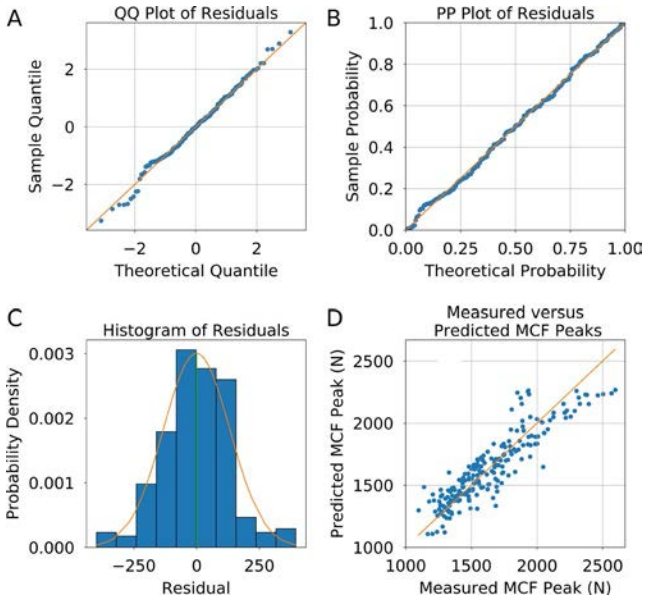

Figure 1. Visual assessment of model fit for the medial knee contact force (MCF) peak as predicted from external biomechanical gait outcomes. A Q–Q plot of residuals (**A**), a P–P plot of residuals (**B**), a histogram of residuals (**C**), and a scatterplot of measured versus predicted MCF peaks (**D**) are shown. For the Q–Q plot, P–P plot, and histogram, the solid orange line represents a theoretical normal distribution. For the Q–Q plot and P–P plot, limited deviation of the blue scatter points from the orange line indicates that the residuals follow a normal distribution. In the scatterplot of measured versus predicted MCF peaks, the orange line represents a 1:1 relationship between measured and predicted values; tighter fit of the scatter points indicates smaller error in the predicted MCF peak.

differences were observed for gait speed, KFM peak, vKRF peak, or measured/predicted MCF peak ($P > 0.05$).

In patients with instrumented knee implants, the identified parameters that best predicted the MCF peak using LASSO regression were gait speed, KAM peak, and vKRF peak. The optimal lambda value of the LASSO regression was 10.5. The linear model fit using the predictors identified from the LASSO analysis and all data from the 218 trials showed $R^2 = 0.81$ ($P < 0.001$) and RMSE = 132.88N (Table 2). Leave-one-out cross-validation showed that the model had an out-of-sample RMSE of 196.58N. Figure 1 shows a visual assessment of model fit for the predicted MCF peak model, including a Q–Q plot, a P–P plot, a histogram of residuals, and a plot of measured versus predicted MCF peaks. Simple linear regression of the identified predictors showed that they were each related to the MCF peak (gait speed $R^2 = 0.19$ [$P = 0.018$]; KAM peak $R^2 = 0.55$ [$P = 0.006$]; vKRF peak $R^2 = 0.49$ [$P = 0.025$]) (Table 3).

For the knee OA group, the mean ± SD follow-up time was 2.57 ± 0.53 years. Between baseline and follow-up assessments, medial tibial cartilage volume was reduced by a mean ± SD of 47.95 ± 65.72 mm^3/year ($P < 0.001$), which is equivalent to a mean ± SD of 2.63 ± 3.88% per year. The mean ± SD total change in cartilage volume over the duration of the study was 6.39 ± 9.41%, which was greater than the measurement error of 3.6%. No evidence of a ceiling effect on cartilage change was observed in participants with K/L grade–4 knees, as this subgroup experienced significant cartilage loss over the duration of the study ($P = 0.005$). Test–retest reliability estimates for the predicted MCF peak were as follows: ICC = 0.908 (95% confidence interval 0.833–0.950) and SEM = 102.48N, which is equivalent to 7.6% of the group mean. The predicted MCF peak was a significant predictor of annualized change in medial tibial cartilage volume over a period of 2.5 years (RMSE 52.60 mm^3/year; $R^2 = 0.35$, $\beta = -0.119$ [$P < 0.001$]) (Figure 2). An R^2 of 0.35 renders a Cohen's f^2 of 0.54, signifying a large effect of the MCF peak on cartilage loss (42). The multivariate model of cartilage volume change containing the 3 predictors of the MCF peak (gait speed, KAM peak, vKRF peak) produced an R^2 of 0.41 ($P < 0.001$); however, the goodness of fit was not different between the multivariate model and the single predictor (MCF peak) model ($P = 0.094$).

DISCUSSION

This study is the first to provide direct evidence that the MCF is positively related to loss of medial tibial cartilage volume in people with knee OA, supporting the notion that mechanical loading is a key contributor to structural disease progression. While direct measurement of knee contact forces in patients with instrumented tibial prostheses represents the gold standard for determining internal joint loads, such measurements are not possible in native knees. Accurate and reliable predictions of the MCF peak can be statistically modeled based on specific external biomechanical gait parameters obtained with motion analysis and inverse dynamics. The implication of a higher gait speed, KAM peak, and vKRF peak when increasing the compressive forces across the joint surfaces and ultimately contributing to cartilage

Table 3. Univariate linear regression models between each predictor of the MCF peak identified by LASSO regression (gait speed, KAM peak, vKRF peak) and the measured MCF peak in patients with instrumented knee implants*

	β	SE	*P*
Gait speed model†			
Intercept	894.57	174.58	<0.001
Gait speed, meters/second	643.98	216.17	0.003
KAM peak model‡			
Intercept	743.19	200.67	<0.001
KAM peak, Nm	22.43	6.13	<0.001
vKRF peak model§			
Intercept	74.82	548.80	0.892
vKRF, N	1.95	216.17	0.006

* LASSO = Least Absolute Shrinkage and Selection Operator (see Table 2 for other definitions).
† Gait speed model included fit parameters of $R^2 = 0.19$ ($P = 0.018$), RMSE = 275.86N, cross-validation RMSE = 330.97N.
‡ KAM peak model included fit parameters of $R^2 = 0.55$ ($P = 0.006$), RMSE = 206.60N, cross-validation RMSE = 268.33N.
§ vKRF peak model included fit parameters of $R^2 = 0.49$ ($P = 0.025$), RMSE = 218.29N, cross-validation RMSE = 311.14N.

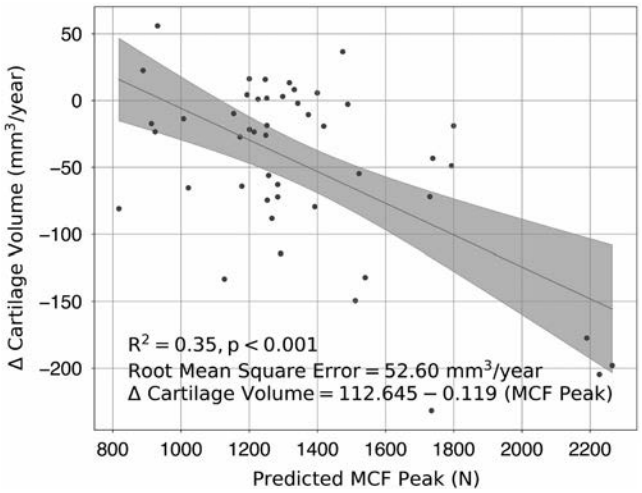

Figure 2. Predicted medial knee contact force (MCF) peak versus annualized change in medial tibial cartilage volume over 2.5 years in participants with knee osteoarthritis. The fitted model (diagonal line) and its 95% confidence band (shaded area) are overlaid on a scatterplot of individual observations (n = 47 subjects).

breakdown make these biomechanical parameters ideal targets for intervention. Strategies to reduce the magnitude of the MCF peak may curb the deleterious effects of knee biomechanics on the progression of cartilage loss in knee OA.

The predicted MCF peak explained 35% ($P < 0.001$) of the variance in 2.5-year changes in medial tibial cartilage volume. Prior studies have modeled the relationship between biomechanical outcomes (e.g., KAM) and medial tibial cartilage volume change; however, direct comparisons with the current model are not possible, because either the R^2 was not reported (6) or the model included multiple covariates (7). Instead, our multivariate analysis may provide insight into this. The multiple linear regression model of cartilage change that included the 3 predictors of the MCF peak (gait speed, KAM peak, vKRF peak) as individual variables yielded an R^2 of 0.41 ($P < 0.001$). It was expected that this multivariate model would yield a higher R^2 than that of the single predictor MCF peak model, because it is based on the same core predictors but has more degrees of freedom (3 versus 1). The greater degrees of freedom with the same inputs necessarily improve model flexibility and fit, thereby decreasing the RMSE and increasing the R^2. Nonetheless, the goodness of fit between the 2 models was not different. Therefore, the MCF peak model predicted cartilage loss in a way that was comparable to that of the best possible linear combination of the same core predictors, demonstrating good generalizability of the MCF peak prediction equation in the OA group. Ultimately, the fact that the measurement of interest (MCF peak) had the ability to predict the future outcome (cartilage loss) to which it is theorized to be related (8) provides predictive validity (43), a form of criterion validity, for the MCF peak equation.

In the current analysis, the MCF prediction model showed a positive relationship between all predictors and the MCF peak, explaining 81% of the variance. These findings, and those from the univariate regression analyses, corroborate findings from prior works in patients with instrumented knee implants. For instance, single-subject analyses that included different gait patterns (e.g., normal, medial thrust, walking poles) showed that the first KAM peak was independently associated with the first MCF peak ($R^2 = 0.57$) (18); the current study showed nearly the same strength of association ($R^2 = 0.55$). In a different analysis, the first vKRF peak predicted the first MCF peak ($R^2 = 0.38$) (10); a stronger association ($R^2 = 0.49$) between these variables was observed in the present study, which may be attributed to its larger sample size (n = 9 versus n = 1). The only known study examining the link between gait speed and the MCF was performed on baseline data from the same patients with instrumented knee implants included in the current analysis. In that study, gait speed explained 49% of the variance in the MCF peak during the early stance phase (17). The current study noted a weaker univariate association ($R^2 = 0.19$), likely because the MCF was analyzed as a discrete peak rather than continuous data (17). Ultimately, it seems intuitive that the MCF is best predicted by a combination of measures that reflect axial loading (vKRF), mediolateral force distribution (KAM), and a general mediator of knee loads (gait speed).

Joint contact forces have been predicted using 2 primary modeling methods: statistical and musculoskeletal. Statistical models predict measured contact forces from extracted biomechanical measurements, such as from patients with instrumented knee implants (9,10,17–19). For single-subject analyses of different gait patterns, the lowest reported RMSEs were 15% (10) and 32% body weight (18) for the first MCF peak. Alternatively, musculoskeletal models estimate the muscle forces necessary to generate the measured joint mechanics, resolving for physiologic joint loads (44–47). For example, using the common approach of minimizing the sum of muscle activations squared, an error of 40% body weight was obtained for the predicted first peak of the compressive joint reaction force (cJRF: compressive tibiofemoral load along the long axis of the tibia) during gait (47). By tuning muscle parameters of the same general model to match the peak cJRF*, lower errors were achieved (e.g., RMSE of 28% body weight over the entire gait cycle waveform) (44). More complex approaches have incorporated subject-specific musculoskeletal geometry, joint kinematics determined from fluoroscopy, and different electromyography-informed optimization methods to resolve muscle forces (45). These approaches, depending on the model and optimization used, yielded RMSEs from ~22% to 105% body weight (~150N to >700N) when predicting the MCF for the stance phase waveform. The current analysis yielded a cross-validation RMSE of 196.58N (22.0% body weight) and an RMSE of 132.88N (14.9% body weight) when tested on all participants used to fit the model. These errors are comparable to

*The authors tuned a set of muscle synergies which penalized individual muscles or groups of muscles using weighting constants. All possible weighting constants were tested, and the combination that produced the smallest compressive force with an error less than 20% was selected.

those from the aforementioned "best" statistical models (10,17) and the most complex musculoskeletal models (45).

However, when comparing the ability of models to predict their respective outcomes, factors other than reported errors must be considered. First, predictions from most statistical models and all musculoskeletal models referenced above were fitted and then tested on data from a single participant, likely resulting in overfit models. Given the rarity of the data and complexity involved in modeling, the analysis of a single participant is not surprising and represents unique, important data to advance the field. Second, while muscle parameter tuning can reduce model errors, this approach is only possible with data from instrumented prostheses (44,45). Without muscle tuning, RMSEs were relatively high at ~100% body weight for predictions of the entire MCF stance phase waveform (45). Third, the resources and competencies required for scaling musculoskeletal models, as well as collecting and analyzing medical imaging, fluoroscopy, and electromyography data are immense. Finally, no known comparable studies have performed any form of model validation. The comparable errors obtained in the present analysis using only motion capture data, model validation using both cross-validation and predictions of cartilage loss in persons with knee OA, the excellent reliability of the MCF predictions in the knee OA group, and the considerably lower barrier to implementation make using such a statistical equation to predict the MCF appealing.

This study had limitations. Most patients with knee implants were men, whereas most knee OA patients were women. Furthermore, the equation to predict the MCF peak was derived using gait data from 9 patients with total knee replacements. Yet, the observed relationship between the predicted MCF peak and cartilage volume loss in persons with knee OA provides criterion validity of the generated equation. In addition, the MCF prediction equation was based on barefoot gait data only, thereby limiting its generalizability to shod conditions. Finally, the knee OA sample comprised mostly older, overweight women with radiographic disease. Thus, the extent to which the association between the predicted MCF peak and cartilage loss can be extended to other populations is uncertain.

In conclusion, results from this study provide robust evidence supporting the role of higher MCFs in cartilage volume loss in persons with clinical and radiographic knee OA. Using gold standard measurements from patients with instrumented tibial prostheses, reliable, accurate, and generalizable predictions of the MCF peak were statistically modeled based on key external biomechanical gait parameters obtained with motion analysis and inverse dynamics. This work acts as a stepping stone toward confirming the theoretical relationship between the MCF and cartilage loss; with technological and analytical advancements, future studies can improve upon our predictions. Nonetheless, these findings underscore the notion that accurate knee load predictions can be obtained without the need for far more resource-intensive approaches. Strategies to reduce the MCF magnitude may aid in curbing structural disease progression associated with mechanical loading in knee OA.

ACKNOWLEDGMENTS

The authors would like to thank Emily Wiebenga and Christine Dibblee from the Mobilize Laboratory for helping with data collection, Leonie Krahl and Pedro Sequeira Delgado from the Julius Wolff Institute for helping with data processing, and all study participants for making this research possible.

AUTHOR CONTRIBUTIONS

All authors were involved in drafting the article or revising it critically for important intellectual content, and all authors approved the final version to be published. Dr. Brisson had full access to all of the data in the study and takes responsibility for the integrity of the data and the accuracy of the data analysis.

Study conception and design. Brisson, Gatti, Maly.
Acquisition of data. Brisson, Damm, Maly.
Analysis and interpretation of data. Brisson, Gatti, Duda, Maly.

ADDITIONAL DISCLOSURES

Author Gatti is the Founder of NeuralSeg Ltd., a provider of medical image analyses that support research conducted within academic and industry settings. NeuralSeg was not involved in the analysis of magnetic resonance imaging data in the current study.

REFERENCES

1. Creaby MW. It's not all about the knee adduction moment: the role of the knee flexion moment in medial knee joint loading [editorial]. Osteoarthritis Cartilage 2015;23:1–3.
2. Erhart-Hledik JC, Favre J, Andriacchi TP. New insight in the relationship between regional patterns of knee cartilage thickness, osteoarthritis disease severity, and gait mechanics. J Biomech 2015;48:3868–75.
3. Chehab EF, Favre J, Erhart-Hledik JC, Andriacchi TP. Baseline knee adduction and flexion moments during walking are both associated with 5 year cartilage changes in patients with medial knee osteoarthritis. Osteoarthritis Cartilage 2014;22:1833–9.
4. Chang AH, Moisio KC, Chmiel JS, Eckstein F, Guermazi A, Prasad PV, et al. External knee adduction and flexion moments during gait and medial tibiofemoral disease progression in knee osteoarthritis. Osteoarthritis Cartilage 2015;23:1099–106.
5. Miyazaki T, Wada M, Kawahara H, Sato M, Baba H, Shimada S. Dynamic load at baseline can predict radiographic disease progression in medial compartment knee osteoarthritis. Ann Rheum Dis 2002;61:617–22.
6. Bennell KL, Bowles KA, Wang Y, Cicuttini F, Davies-Tuck M, Hinman RS. Higher dynamic medial knee load predicts greater cartilage loss over 12 months in medial knee osteoarthritis. Ann Rheum Dis 2011;70:1770–4.
7. Brisson NM, Wiebenga EG, Stratford PW, Beattie KA, Totterman S, Tamez-Peña JG, et al. Baseline knee adduction moment interacts with body mass index to predict loss of medial tibial cartilage volume over 2.5 years in knee osteoarthritis. J Orthop Res 2017;35:2476–83.
8. Andriacchi TP, Mundermann A, Smith RL, Alexander EJ, Dyrby CO, Koo S. A framework for the in vivo pathomechanics of osteoarthritis at the knee. Ann Biomed Eng 2004;32:447–57.
9. Trepczynski A, Kutzner I, Bergmann G, Taylor WR, Heller MO. Modulation of the relationship between external knee adduction

moments and medial joint contact forces across subjects and activities. Arthritis Rheumatol 2014;66:1218–27.
10. Meyer AJ, D'Lima DD, Besier TF, Lloyd DG, Colwell CW, Fregly BJ. Are external knee load and EMG measures accurate indicators of internal knee contact forces during gait? J Orthop Res 2013;31:921–9.
11. Schipplein OD, Andriacchi TP. Interaction between active and passive knee stabilizers during level walking. J Orthop Res 1991;9:113–9.
12. Winter DA. Biomechanics and motor control of human movement. 4th ed. Hoboken (New Jersey): John Wiley & Sons; 2009.
13. Frederick EC, Hagy JL. Factors affecting peak vertical ground reaction forces in running. Int J Sport Biomech 1986;2:41–9.
14. Hall M, Wrigley TV, Metcalf BR, Hinman RS, Cicuttini FM, Dempsey AR, et al. Mechanisms underpinning the peak knee flexion moment increase over 2-years following arthroscopic partial meniscectomy. Clin Biomech 2015;30:1060–5.
15. Hunt MA, Birmingham TB, Giffin JR, Jenkyn TR. Associations among knee adduction moment, frontal plane ground reaction force, and lever arm during walking in patients with knee osteoarthritis. J Biomech 2006;39:2213–20.
16. Metcalfe AJ, Le Andersson M, Goodfellow R, Thorstensson CA. Is knee osteoarthritis a symmetrical disease? Analysis of a 12 year prospective cohort study. BMC Musculoskelet Disord 2012;13:153.
17. Kutzner I, Trepczynski A, Heller MO, Bergmann G. Knee adduction moment and medial contact force: facts about their correlation during gait. PLoS One 2013;8:e81036.
18. Walter JP, D'Lima DD, Colwell CW, Fregly BJ. Decreased knee adduction moment does not guarantee decreased medial contact force during gait. J Orthop Res 2010;28:1348–54.
19. Zhao D, Banks SA, Mitchell KH, D'Lima DD, Colwell CW, Fregly BJ. Correlation between the knee adduction torque and medial contact force for a variety of gait patterns. J Orthop Res 2007;25:789–97.
20. Messier SP, Beavers DP, Loeser RF, Carr JJ, Khajanchi S, Legault C, et al. Knee-joint loading in knee osteoarthritis: influence of abdominal and thigh fat. Med Sci Sport Exerc 2014;46:1677–83.
21. Messier SP, Pater M, Beavers DP, Legault C, Loeser RF, Hunter DJ, et al. Influences of alignment and obesity on knee joint loading in osteoarthritic gait. Osteoarthritis Cartilage 2014;22:912–7.
22. Harding GT, Dunbar MJ, Hubley-Kozey CL, Stanish WD, Wilson JL. Obesity is associated with higher absolute tibiofemoral contact and muscle forces during gait with and without knee osteoarthritis. Clin Biomech (Bristol, Avon) 2016;31:79–86.
23. Pelletier JP, Raynauld JP, Berthiaume MJ, Abram F, Choquette D, Haraoui B, et al. Risk factors associated with the loss of cartilage volume on weight-bearing areas in knee osteoarthritis patients assessed by quantitative magnetic resonance imaging: a longitudinal study. Arthritis Res Ther 2007;9:R74.
24. Altman R, Asch E, Bloch D, Bole G, Borenstein D, Brandt K, et al. Development of criteria for the classification and reporting of osteoarthritis: classification of osteoarthritis of the knee. Arthritis Rheum 1986;29:1039–49.
25. Kellgren JH, Lawrence JS. Radiological assessment of osteo-arthrosis. Ann Rheum Dis 1957;16:494–502.
26. Kothari M, Guermazi A, von Ingersleben G, Sieffert M, Block JE, Stevens R, et al. Fixed-flexion radiography of the knee provides reproducible joint space width measurements in osteoarthritis. Eur Radiol 2004;14:1568–73.
27. Wright RW, Ross JR, Haas AK, Huston LJ, Garofoli EA, Harris D, et al. Osteoarthritis classification scales: interobserver reliability and arthroscopic correlation. J Bone Joint Surg Am 2014;96:1145–51.
28. Chang CB, Choi JY, Koh IJ, Seo ES, Seong SC, Kim TK. What should be considered in using standard knee radiographs to estimate mechanical alignment of the knee? Osteoarthritis Cartilage 2010;18:530–8.
29. Tamez-Peña JG, Farber J, González PC, Schreyer E, Schneider E, Totterman S. Unsupervised segmentation and quantification of anatomical knee features: data from the Osteoarthritis Initiative. IEEE Trans Biomed Eng 2012;59:1177–86.
30. Inglis D, Pui M, Ioannidis G, Beattie K, Boulos P, Adachi JD, et al. Accuracy and test-retest precision of quantitative cartilage morphology on a 1.0 T peripheral magnetic resonance imaging system. Osteoarthritis Cartilage 2007;15:110–5.
31. Brisson NM, Stratford PW, Maly MR. Relative and absolute test–retest reliabilities of biomechanical risk factors for knee osteoarthritis progression: benchmarks for meaningful change. Osteoarthritis Cartilage 2018;26:220–6.
32. Robertson DG, Dowling JJ. Design and responses of Butterworth and critically damped digital filters. J Electromyogr Kinesiol 2003;13:569–73.
33. Wu G, Cavanagh PR. ISB recommendations for standardization in the reporting of kinematic data. J Biomech 1995;28:1257–61.
34. Thorp LE, Sumner DR, Block JA, Moisio KC, Shott S, Wimmer MA. Knee joint loading differs in individuals with mild compared with moderate medial knee osteoarthritis. Arthritis Rheum 2006;54:3842–9.
35. Bergmann G, Bender A, Graichen F, Dymke J, Rohlmann A, Trepczynski A, et al. Standardized loads acting in knee implants. PLoS One 2014;9:e86035.
36. Heinlein B, Graichen F, Bender A, Rohlmann A, Bergmann G. Design, calibration and pre-clinical testing of an instrumented tibial tray. J Biomech 2007;40:S4–10.
37. Bergmann G, Graichen F, Rohlmann A, Westerhoff P, Heinlein B, Bender A, et al. Design and calibration of load sensing orthopaedic implants. J Biomech Eng 2008;130:021009.
38. Hastie T, Tibshirani R, Friedman J. The elements of statistical learning: data mining, inference, and prediction. 2nd ed. New York: Springer; 2009.
39. James G, Witten D, Hastie T, Tibshirani R. An introduction to statistical learning: with applications in R. New York: Springer; 2013.
40. Cameron AC, Miller D. A practitioner's guide to cluster-robust inference. J Hum Resour 2015;50:317–72.
41. Seabold S, Perktold J. Statsmodels: econometric and statistical modeling with Python [abstract]. Presented at the 9th Python for Scientific Computing Conference, Austin, TX, June 28–July 3, 2010.
42. Cohen J. A power primer. Psychol Bull 1992;112:155–9.
43. Hulley SB, Newman TB, Cummings SR. Planning the measurements: precision, accuracy, and validity. In: Hulley SB, Cummings SR, Browner WS, Grady DG, Newman TB, editors. Designing Clinical Research. 4th ed. Philadelphia: Lippincott Williams & Wilkins; 2013. p. 32–42.
44. Steele KM, DeMers MS, Schwartz MS, Delp SL. Compressive tibiofemoral force during crouch gait. Gait Posture 2012;35:556–60.
45. Gerus P, Sartori M, Besier TF, Fregly BJ, Delp SL, Banks SA, et al. Subject-specific knee joint geometry improves predictions of medial tibiofemoral contact forces. J Biomech 2013;46:2778–86.
46. Walter JP, Kinney AL, Banks SA, D'Lima DD, Besier TF, Lloyd DG, et al. Muscle synergies may improve optimization prediction of knee contact forces during walking. J Biomech Eng 2014;136:0210311–9.
47. DeMers MS, Pal S, Delp SL. Changes in tibiofemoral forces due to variations in muscle activity during walking. J Orthop Res 2014;32:769–76.

Arthritis & Rheumatology
Vol. 73, No. 9, September 2021, pp 1646–1655
DOI 10.1002/art.41725

American College of Rheumatology
Empowering Rheumatology Professionals

Efficacy and Safety of Diclofenac–Hyaluronate Conjugate (Diclofenac Etalhyaluronate) for Knee Osteoarthritis: A Randomized Phase III Trial in Japan

Yoshihiro Nishida,[1] Kazuyuki Kano,[2] Yuji Nobuoka,[2] and Takayuki Seo[2]

Objective. To confirm the efficacy and safety of intraarticular (IA) injection of diclofenac covalently linked to hyaluronic acid (diclofenac etalhyaluronate [DF-HA]; ONO-5704/SI-613) in patients with knee osteoarthritis (OA).

Methods. In a phase III multicenter, randomized, double-blind, placebo-controlled trial, eligible subjects ages 40–75 years with symptomatic knee OA (Kellgren/Lawrence score of 2 or 3) were randomly assigned to receive IA injections of DF-HA 30 mg or placebo (citric acid–sodium citrate buffered solution; 1:1) once every 4 weeks for 20 weeks (a total of 6 injections). Subjects were followed up for 24 weeks. The primary end point was the mean change from baseline to 12 weeks in Western Ontario and McMaster Universities Osteoarthritis Index version 3.1 (WOMAC) pain subscale scores, measured on a 100-mm visual analog scale. Safety was evaluated by adverse event monitoring.

Results. All 440 subjects received investigational products (220 received placebo and 220 received DF-HA). The full analysis set and safety population comprised 438 subjects (220 in the placebo group and 218 in the DF-HA group) and 440 subjects, respectively. At 12 weeks, subjects receiving DF-HA showed significant improvement from baseline in the WOMAC pain subscale score (–23.2 mm) compared to subjects receiving placebo (–17.1 mm), with a difference of –6.1 mm (95% confidence interval –9.4, –2.8; $P < 0.001$). The difference between groups was significant as early as week 1, and a difference was maintained for 24 weeks, although the difference at week 24 was not significant. Anaphylactic reactions were observed in 2 subjects receiving DF-HA.

Conclusion. Our findings indicate that treatment with DF-HA results in significant improvement in the WOMAC pain subscale score compared to placebo over 12 weeks. Anaphylactic reactions were observed, and further safety evaluation is needed.

INTRODUCTION

Osteoarthritis (OA) is the most common degenerative joint disease, occurring frequently in the elderly (1). Current disease management mainly focuses on the treatment of symptoms (pain relief) to improve joint function and quality of life until the late stages of arthritis leading to knee replacement (2). The selection of knee OA treatment depends on disease severity, comorbidity, and patient preference (1,3–5). Main treatment options include conservative therapies such as exercise therapy, physiotherapy, and pharmacotherapy. Pharmacotherapies include oral or topical nonsteroidal antiinflammatory drugs (NSAIDs), selective cyclooxygenase 2 (COX-2) inhibitors, and intraarticular (IA) injection of glucocorticoids or hyaluronic acid (HA). NSAIDs are most commonly used for the symptoms of knee OA (6); however, upper and lower gastrointestinal (GI) tract disorders, adverse cardiovascular (CV) reactions, and renal dysfunction are associated with the long-term use of oral NSAIDs (7–10). Therefore, lower dosing of oral NSAIDs for a shorter period is recommended in patients at risk of these adverse events (1,4). In addition, topical NSAIDs are recommended for patients with knee OA who have these comorbid conditions (4).

Although IA injection of glucocorticoids or HA is used for the conservative treatment of knee OA, these agents are a subject

JAPIC identifier: JapicCTI-173537.
Supported by Seikagaku Corporation and Ono Pharmaceutical Company, Ltd.
[1]Yoshihiro Nishida, MD: Nagoya University Hospital, Nagoya, Japan; [2]Kazuyuki Kano, BSc, Yuji Nobuoka, MSc, Takayuki Seo, PhD: Seikagaku Corporation, Tokyo, Japan.
Dr. Nishida has received consulting fees, speaking fees, and/or honoraria from Eli Lilly, Kaken, Hisamitsu, Kyowa Hakko Kirin, and Asahi Kasei (less than $10,000 each) and from Seikagaku Corporation (more than $10,000) and has received research grants from Daiichi Sankyo, Chugai, Novartis, Pfizer, Eisai, and Zimmer Biomet. Mr Kano, Mr Nobuoka, and Dr. Seo own stock or stock options in Seikagaku Corporation.
Address correspondence to Yoshihiro Nishida, MD, Nagoya University Hospital, Department of Rehabilitation, Orthopaedic Surgery, 65 Tsurumai-cho, Nagoya 466-8560, Japan. Email: ynishida@med.nagoya-u.ac.jp.
Submitted for publication July 10, 2020; accepted in revised form March 4, 2021.

of controversy. IA glucocorticoids should be used for short-term pain relief because of their short-lived efficacy and safety issues (1,11–13). The benefits of HA have been reported in multiple studies, although there is conflicting data. Clinical and nonclinical reports suggest that IA HA has antiinflammatory and analgesic effects, suppresses joint cartilage degeneration, and normalizes synovial fluid. HA also functions as a lubricant due to its viscoelasticity (14,15). Nevertheless, treatment of knee OA with IA HA has not yet been established, and most guidelines do not currently recommend the use of IA HA based on poor evidence of its benefits (1,3,5).

In pursuit of OA treatments, Seikagaku Corporation developed a novel compound, diclofenac etalhyaluronate (DF-HA; ONO-5704/SI-613), which is DF covalently linked to HA. It is a high molecular weight fermented HA (600–1,200 kd) combining the purported advantages of IA HA injection and NSAIDs: antiinflammatory and analgesic effects, suppression of joint cartilage degeneration, and normalization of synovial fluid function (16,17). Compared with oral DF therapy, IA injection of DF-HA is thought to reduce systemic exposure to DF because the amount of DF released from DF-HA is ~3.5 mg/dose. Indeed, in rabbits with antigen-induced arthritis, systemic exposure to DF was much lower after a single effective IA dose of DF-HA than after a single effective oral dose of diclofenac sodium (16). Furthermore, the sustained release of DF from DF-HA after 1 injection into the joint tissue has potential analgesic effects lasting up to 28 days (16). The efficacy and safety of DF-HA in patients with knee OA was confirmed in a previous trial (18), in which patients who received a total of 3 injections of DF-HA, one every 4 weeks for 12 weeks, showed significant improvements in the Western Ontario and McMaster Universities Osteoarthritis Index 3.1 (WOMAC) (19) pain subscale score compared to patients who received placebo, with no major safety concerns.

We conducted a phase III trial to confirm the efficacy and safety of IA injection of DF-HA 30 mg every 4 weeks into the knee joint cavities of patients with knee OA. The primary objective was to verify the superiority of DF-HA over placebo by showing a greater change from baseline in the WOMAC pain subscale score over 12 weeks. The primary end point was the 12-week mean change from baseline in WOMAC pain subscale score to verify the results of the phase II trial. The secondary objective was to evaluate the safety of DF-HA when injected 6 times, once every 4 weeks, up to 24 weeks compared with placebo.

PATIENTS AND METHODS

Study design and characteristics of the subjects. A phase III multicenter, randomized, double-blind, placebo-controlled trial was performed at 50 sites in Japan. The study was conducted in accordance with the Declaration of Helsinki and the International Council for Harmonisation Guidelines for Good Clinical Practice and was approved by the institutional review boards at the central boards or at each local site. All subjects provided written informed consent.

Eligible subjects were ages 40–75 years and had knee OA (not secondary OA caused by trauma or another disease) with a Kellgren/Lawrence (K/L) grade of 2 or 3 diagnosed radiographically, pain for at least 1 year in the target knee, and a WOMAC pain subscale score and pain score on the 50-foot walking test of 50–90 mm (on a 100-mm visual analog scale [VAS]) in the target knee and ≤30 mm in the contralateral knee at the time of screening. Patients with lower extremity pain caused by other diseases; inflammation, infection, skin disease, or systemic disease at the target knee; body mass index (BMI) ≥35.0 kg/m^2, which indicates a high risk of complications; hypersensitivity to DF, HA, or acetaminophen; aspirin-induced asthma; surgical or invasive treatment within 1 year; or joint effusion removal within 7 days prior to screening were excluded.

Randomization and blinding. Subjects were allocated to receive either DF-HA (30 mg/3 ml in a prefilled syringe; Seikagaku Corporation) or placebo (citric acid–sodium citrate buffered solution [3 ml in a prefilled syringe; Seikagaku Corporation]) at a 1:1 ratio, and randomization was performed using an interactive web response system. Balance between the treatment groups at each site was achieved using a minimization method (20). Groups were stratified by K/L grade, mean baseline WOMAC pain subscale score, and sex.

Both treatments were clear, colorless, and identical in appearance; however, the force needed to inject them differed because DF-HA has a greater viscosity. To maintain blinding, an investigator other than the one who administered the injection performed all postinjection evaluations. Moreover, the investigator who administered the injection was prohibited from divulging information about the treatment to the investigators conducting the assessments or the subjects.

Procedures. Screening was conducted 1 week before randomization and on the day of randomization. The entire volume (3 ml) of study drug or placebo was injected IA into the target knee of each subject a total of 6 times, once every 4 weeks (at weeks 0, 4, 8, 12, 16, and 20). Although the administration method was not specified, IA injection was given by an orthopedist or a general physician who routinely performs IA injections, following the same procedure as in their normal clinical practice. The observation period began on the day of the first injection and ended at week 24. Efficacy and safety were assessed on the day of the first injection (week 0), and at weeks 1, 2, 4, 6, 8, 10, 12, 16, 20, and 24.

Analgesic agents (IA HA products, NSAIDs, glucocorticoids, opioid analgesics, and psychotherapeutic drugs), which are known to affect the underlying disease and its assessment, were prohibited from the specified washout period prior to the screening through the end of the study. Acetaminophen was provided for all subjects as a rescue medication from 7 days prior to screening

through the end of the study and permitted at a dosage of up to 3,600 mg/day but was proscribed starting 2 days before each visit.

Outcome measures. The primary outcome measure was the WOMAC pain subscale score, measured on a 100-mm VAS, and the primary end point was the mean change from baseline in WOMAC pain subscale score at 12 weeks. The secondary outcome measures were WOMAC index score (stiffness subscale score, physical function subscale score, and total score on a 100-mm VAS), pain score on a 100-mm VAS after a 50-foot walking test, daily pain score on an 11-point numerical rating scale as recorded in the subject's diary, rates of responders and strict responders according to the Outcome Measures in Rheumatology (OMERACT)–Osteoarthritis Research Society International (OARSI) response criteria (21), patient global assessment, physician global assessment, Medical Outcomes Study Short Form 36 (SF-36) health survey (22–24), EuroQol 5-domain (EQ-5D) (25), and acetaminophen consumption.

Safety was evaluated by monitoring treatment-emergent adverse events (TEAEs) after the initial injection, based on the definitions listed in Supplementary Table 1, available on the *Arthritis & Rheumatology* website at http://onlinelibrary.wiley.com/doi/10.1002/art.41725/abstract. AEs that led to study drug withdrawal were considered important AEs, while those that occurred at the injection site, and were associated with GI disorders, CV disorders, renal dysfunction, anaphylactic reaction, or hypersensitivity were considered AEs of special interest.

Clinical laboratory tests (hematology, blood biochemistry, and urine test), measurement of vital signs (body temperature, blood pressure, and pulse rate), examination of the target knee (for joint effusion, swelling, redness, and warmth) to assess the injection site reaction, and radiography, including anteroposterior standing, lateral standing, and patellar axial radiographs to observe structural changes (worsening) in the target knee (osteophytes, joint space narrowing, osteosclerosis, or deformity of epiphysis) were conducted based on the protocol at preinjection and at 24 weeks or at the time of study discontinuation. To prevent variations in evaluation at each site, instructions for radiography were distributed (Supplementary Table 2, available on the *Arthritis & Rheumatology* website at http://onlinelibrary.wiley.com/doi/10.1002/art.41725/abstract). Imaging evaluation was performed by the investigator. Findings that were judged by the investigator to be unfavorable or unintended were considered AEs.

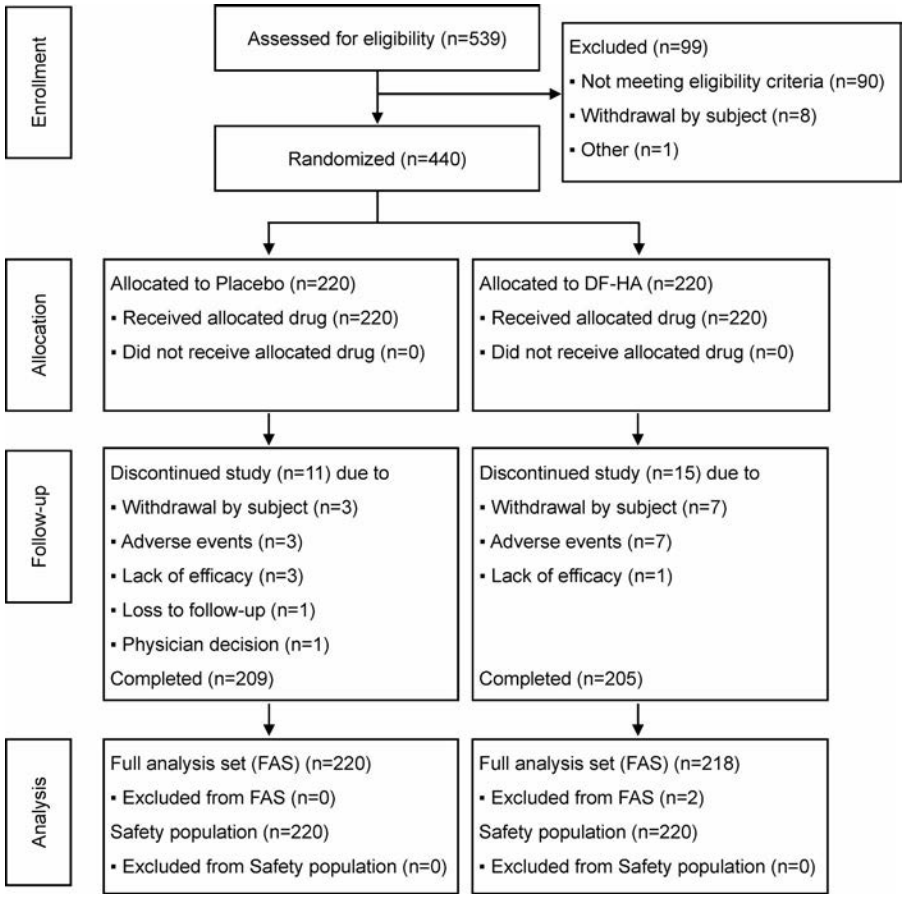

Figure 1. Disposition of the study subjects. Details are given according to the Consolidated Standards of Reporting Trials (CONSORT) statement for reporting randomized controlled trials. DF-HA = diclofenac etalhyaluronate.

Statistical analysis. We estimated that a sample size of 220 subjects per group would be needed to attain at least 90% power to detect a significant difference between groups with a 2-sided significance level of 5%, assuming that the difference between groups in the change from baseline in WOMAC pain subscale score was –7.5 mm, with an SD of 23 mm and a dropout rate of ~10% (18).

Efficacy analyses were conducted in the full analysis set, which included subjects who received ≥1 injection and were evaluated for efficacy. For the primary analysis, the mean change from baseline in the WOMAC pain subscale score over 12 weeks was analyzed using a mixed-effects model for repeated measures (MMRM) at each time point from weeks 1 through 12. The model included treatment group, time point, treatment group–by–time point interaction, baseline WOMAC pain subscale score, K/L grade, sex, and pooled site as fixed effects. The covariance structure was assumed to be unstructured. The Kenward-Roger method was used to calculate degrees of freedom. For the secondary analysis, the change from baseline in WOMAC pain subscale score at each time point of weeks 1 through 24 was compared between the groups using the same MMRM as used in the primary analysis. To evaluate the impact of missing data, a sensitivity analysis was conducted using the pattern-mixture model approach to multiple imputation under the missing-not-at-random assumption by creating control-based pattern imputation. Mean changes from baseline in WOMAC pain subscale score over 12 weeks in the subgroups were analyzed using the same MMRM model without K/L grade, sex, and pooled site.

Secondary continuous outcomes expected for EQ-5D and mean daily acetaminophen consumption were analyzed using the same MMRM as used for analyses of the primary outcome. The responder rate and strict responder rate were analyzed using a generalized estimating equation. The odds ratio over 12 weeks and at each time point were calculated using the model that included treatment group, time point, treatment group–by–time point interaction, baseline WOMAC pain subscale score, K/L grade, sex, and pooled site. The covariance structure was assumed to be unstructured. The change from baseline in the mean daily acetaminophen consumption at each time point was compared with that in the placebo group using Wilcoxon's rank sum test.

Responder analyses were performed post hoc to interpret clinically meaningful treatment benefits of group differences (26). These analyses were conducted using the percentages of subjects with an improvement in WOMAC pain subscale score from baseline of >20%, >30%, or >50%, who were considered to have clinically meaningful pain reduction, and subjects whose WOMAC pain subscale score reached <40 mm, <30 mm, or <20 mm based on different levels of response on ratings of treatment satisfaction at 1, 4, 12, and 24 weeks.

TEAEs and other safety outcomes were summarized in the safety population, which included subjects who received treatment at least once. The incidences of TEAEs were calculated for each treatment group. TEAEs were coded using the Medical Dictionary for Regulatory Activities (MedDRA) version 21.1. TEAEs associated with GI disorders, CV disorders, renal dysfunction, anaphylactic reaction, or hypersensitivity were categorized using a standardized MedDRA query.

SAS software, version 9.4 (SAS Institute) was used for all statistical analyses. *P* values less than 0.05 (2-sided) were considered significant.

RESULTS

Between March 24, 2017 and July 30, 2018, 539 subjects were screened (Figure 1). Of the 539 subjects, 440 were determined to be eligible for the study, randomized, and received treatment (220 received placebo and 220 received DF-HA). The safety

Table 1. Baseline characteristics of the subjects with knee OA*

	Placebo (n = 220)	DF-HA 30 mg (n = 218)
Age, years	62.4 ± 8.1	63.3 ± 8.7
Sex, no, (%) male/female	75 (34.1)/ 145 (65.9)	75 (34.4)/ 143 (65.6)
BMI, kg/m^2	25.61 ± 3.95	25.46 ± 3.75
Duration of current pain, weeks	268.3 ± 257.8	252.4 ± 262.0
K/L grade, no. (%)		
2	124 (56.4)	122 (56.0)
3	96 (43.6)	96 (44.0)
WOMAC pain score, mm†	65.2 ± 7.6	64.9 ± 7.9
WOMAC pain score category, no. (%)†		
<70 mm	163 (74.1)	162 (74.3)
≥70 mm	57 (25.9)	56 (25.7)
WOMAC stiffness score, mm†	57.5 ± 21.4	56.6 ± 20.9
WOMAC physical function score, mm†	61.3 ± 12.8	59.8 ± 12.8
WOMAC total score, mm†	61.8 ± 11.0	60.6 ± 11.3
50-foot walking test pain score, mm†	68.0 ± 7.6	68.0 ± 8.5
Daily pain score	6.69 ± 1.20‡	6.60 ± 1.27
Patient global assessment score, mm†	70.1 ± 12.7	69.7 ± 12.9
Physician global assessment score, mm†	62.5 ± 14.1	62.9 ± 14.0
SF-36 summary score		
MCS score	55.8 ± 8.3	55.4 ± 8.1
RCS score	45.1 ± 13.0	47.2 ± 13.1
PCS score	25.8 ± 10.5	25.9 ± 11.6
EQ-5D		
QOL score	0.6778 ± 0.1354	0.6906 ± 0.1254
VAS score	66.3 ± 16.2	67.0 ± 16.3
Daily acetaminophen dosage, mg/day	220.5 ± 390.0	230.2 ± 399.5

* Except where indicated otherwise, values are the mean ± SD. OA = osteoarthritis; DF-HA = diclofenac etalhyaluronate; BMI = body mass index; K/L = Kellgren/Lawrence; WOMAC = Western Ontario and McMaster Universities Osteoarthritis Index; SF-36 = Short Form 36; MCS = mental component summary; RCS = social role component summary; PCS = physical component summary; EQ-5D = EuroQol 5-domain; QOL = quality of life.
† On a 100-mm visual analog scale (VAS).
‡ Data were available for 219 patients.

population comprised 440 subjects (220 in the placebo group and 220 in the DF-HA group), and the full analysis set comprised 438 subjects (220 in the placebo group and 218 in the DF-HA group), which was the safety population minus 2 subjects who had no efficacy evaluation data. Demographic and other baseline characteristics were similarly distributed between the treatment groups (Table 1).

The least squares mean (LSM) change from baseline in the WOMAC pain subscale score at 12 weeks was –17.1 mm for placebo and –23.2 mm for DF-HA (Table 2). The difference in LSM between the groups was –6.1 mm (95% confidence interval [95% CI] –9.4, –2.8; $P < 0.001$), which demonstrates the superiority of DF-HA over placebo. Results of the MMRM sensitivity analysis using placebo multiple imputation were similar to the results of the primary analysis without imputation of missing data. Figure 2 shows forest plots of the difference in LSM between the groups and the 95% CI for all subjects and for subgroups of subjects. The change from baseline in WOMAC pain subscale score over 12 weeks was greater in all DF-HA subgroups than in all placebo subgroups. The between-group differences in LSM were similar for all subgroups.

Table 2 also shows the results of the secondary outcomes over 12 weeks. Significant differences were observed for all outcomes except for the mental component summary score and social role component summary score of the SF-36. OMERACT-OARSI responder analysis indicated that the responder and strict responder rates at week 12 were 63.7% for placebo versus 76.7% for DF-HA and 41.0% for placebo versus 54.3% for DF-HA, respectively (Supplementary Table 3, available on the *Arthritis & Rheumatology* website at http://onlinelibrary.wiley.com/doi/10.1002/art.41725/abstract). The odds ratios for achieving a response or a strict response at week 12 with DF-HA versus placebo were 1.69 (95% CI 1.24, 2.30; $P < 0.001$) and 1.74 (95% CI 1.25, 2.43; $P = 0.001$), respectively (Table 2).

Figure 3 shows the time course of the WOMAC pain subscale score, WOMAC function subscale score, and patient global assessment score, which improved after each DF-HA injection. The between-group difference was significant beginning at week 1, and a difference was maintained for 24 weeks, although the difference at week 24 was not significant. The between-group differences in LSM in WOMAC pain subscale score were –7.2 mm at week 1 (95% CI –10.5, –3.9; $P < 0.001$), –6.2 mm at week 4 (95% CI –9.9, –2.5; $P = 0.001$), –6.1 mm at week 12 (95% CI –10.3, –2.0; $P = 0.004$), and –4.0 mm at week 24 (95% CI –8.6, 0.5; $P = 0.082$) (Supplementary Table 4, available on the *Arthritis & Rheumatology* website at http://onlinelibrary.wiley.com/doi/10.1002/art.41725/abstract). Similar effects were observed for the secondary outcomes (Supplementary Tables 4–10, available on the *Arthritis & Rheumatology* website at http://onlinelibrary.wiley.com/doi/10.1002/art.41725/abstract).

Table 2. Primary and secondary outcomes at 12 weeks*

	LSM change from baseline (95% CI)		Difference (95% CI)	*P*
	Placebo	DF-HA		
Primary outcome				
WOMAC pain score, mm†				
Primary analysis	−17.1 (−19.8, −14.4)	−23.2 (−25.9, −20.4)	−6.1 (−9.4, −2.8)	<0.001
Sensitivity analysis	−17.2 (−19.9, −14.4)	−23.2 (−25.9, −20.4)	−6.0 (−9.3, −2.7)	<0.001
Secondary outcomes				
WOMAC stiffness score, mm†	−13.3 (−16.1, −10.5)	−17.9 (−20.7, −15.1)	−4.6 (−8.0, −1.2)	0.008
WOMAC physical function score, mm†	−13.2 (−15.8, −10.5)	−18.9 (−21.5, −16.2)	−5.7 (−8.9, −2.5)	<0.001
Total score	−14.0 (−16.6, −11.4)	−19.6 (−22.2, −16.9)	−5.6 (−8.7, −2.4)	<0.001
50-foot walking test pain score, mm†	−21.3 (−24.3, −18.2)	−28.1 (−31.1, −25.1)	−6.8 (−10.5, −3.2)	<0.001
Mean daily pain score	−1.20 (−1.41, −0.99)	−1.76 (−1.97, −1.55)	−0.56 (−0.82, −0.31)	<0.001
Patient global assessment score, mm†	−18.1 (−20.7, −15.4)	−24.6 (−27.2, −22.0)	−6.5 (−9.7, −3.3)	<0.001
Physician global assessment score, mm†	−16.4 (−18.6, −14.2)	−20.9 (−23.1, −18.7)	−4.5 (−7.2, −1.9)	<0.001
SF-36 summary score				
MCS	−0.1 (−1.0, 0.7)	0.5 (−0.3, 1.4)	0.6 (−0.4, 1.7)	0.209
RCS	2.5 (1.2, 3.8)	2.1 (0.8, 3.4)	−0.4 (−2.0, 1.1)	0.588
PCS	4.3 (3.0, 5.6)	5.9 (4.5, 7.2)	1.6 (0.0, 3.2)	0.049
OMERACT-OARSI response				
Responder‡	−0.11 (−0.36, 0.14)§	0.41 (0.15, 0.67)§	1.69 (1.24, 2.30)¶	<0.001
Strict responder#	−1.26 (−1.56, −0.97)§	−0.71 (−0.99, −0.43)§	1.74 (1.25, 2.43)¶	0.001

* OMERACT-OARSI = Outcome Measures in Rheumatology–Osteoarthritis Research Society International (see Table 1 for other definitions).
† On a 100-mm visual analog scale.
‡ Responders were defined as subjects with ≥20% improvement from baseline and an absolute change of ≥10 mm in ≥2 of the following 3 measures: WOMAC pain subscale score, WOMAC physical function subscale score, and/or patient global assessment score.
§ Values are the log odds (95% confidence interval [95% CI]).
¶ Values are the odds ratio (95% CI).
# Strict responders were defined as subjects with ≥50% improvement from baseline and absolute change of ≥20 mm in the WOMAC pain subscale score or WOMAC physical function subscale score.

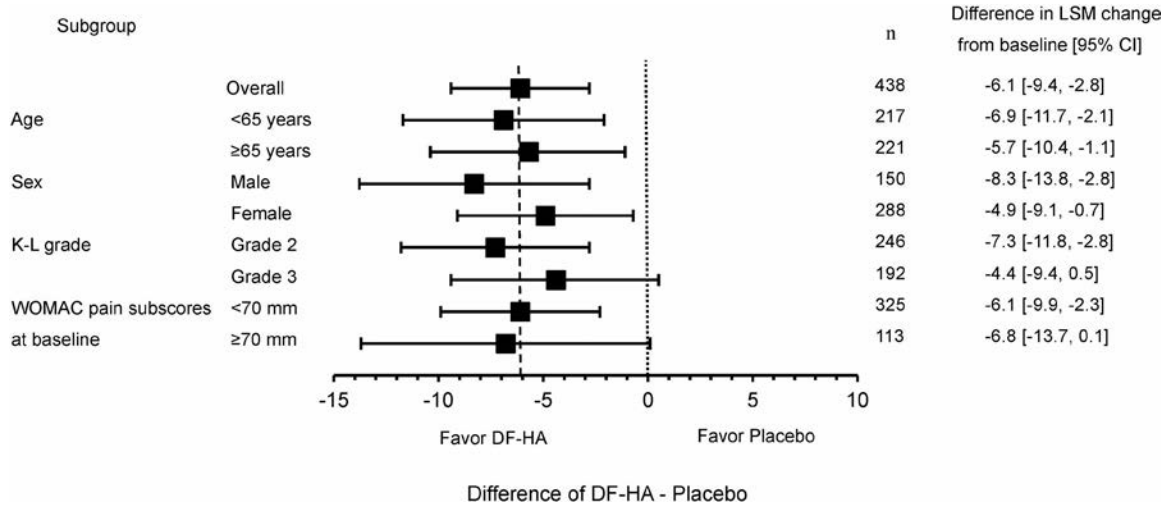

Figure 2. Forest plot showing the change from baseline over 12 weeks in Western Ontario and McMaster Universities Osteoarthritis Index (WOMAC) pain subscale score in the full analysis set (overall) and in the indicated subgroups of subjects with knee osteoarthritis receiving diclofenac etalhyaluronate (DF-HA) or placebo. Values are the least squares mean (LSM) change from baseline (95% confidence interval [95% CI]). Values were estimated using a mixed-effects model for repeated measures. K/L = Kellgren/Lawrence.

The OMERACT-OARSI response rates were higher in the DF-HA group than the placebo group at all time points until week 24. The response rates for placebo versus DF-HA were 26.9% versus 45.0% at week 1 and 71.8% versus 81.1% at week 24, and the response rates in each group increased after injection (Supplementary Table 3). The decrease from baseline in mean

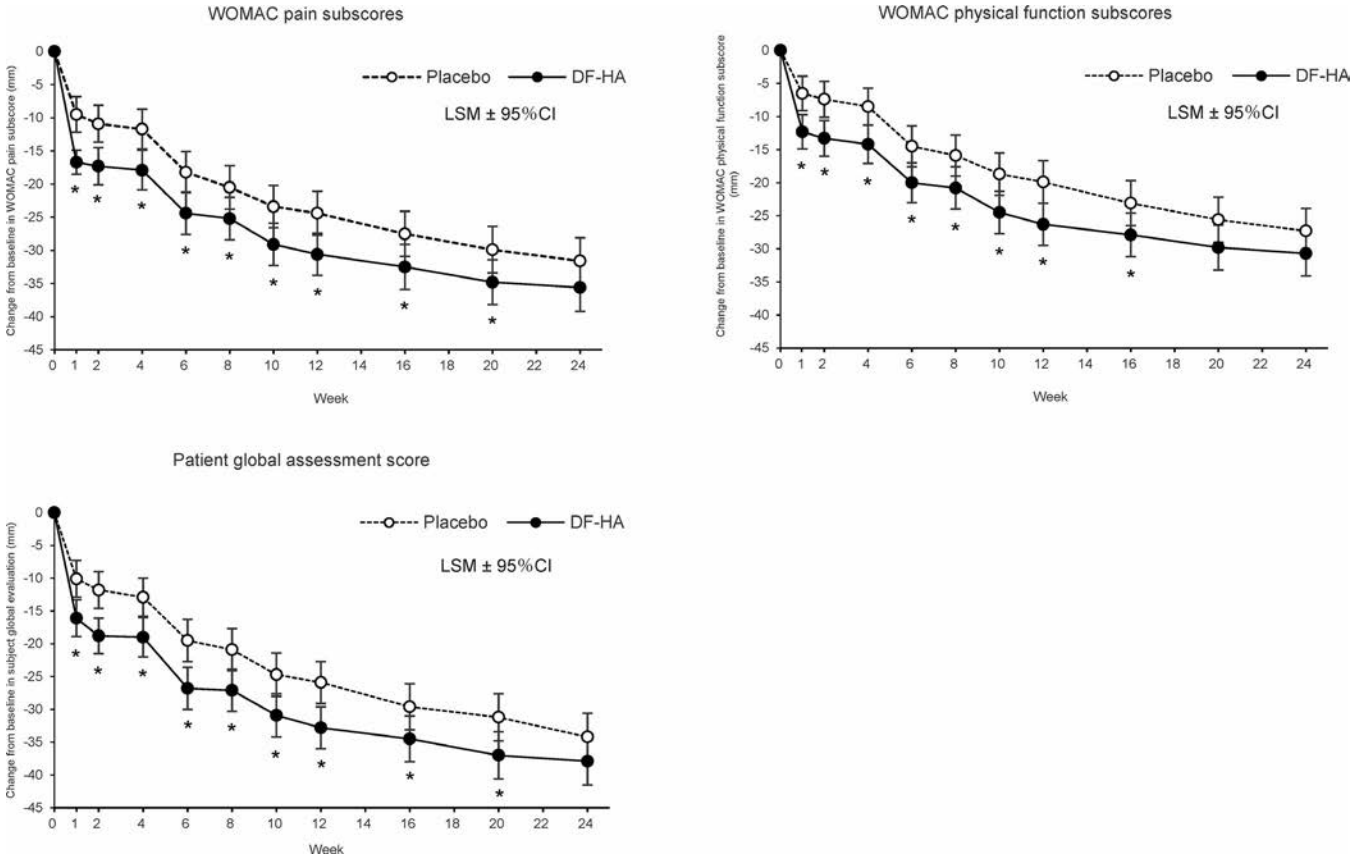

Figure 3. Time course of change from baseline in Western Ontario and McMaster Universities Osteoarthritis Index version 3.1 (WOMAC) pain subscale, WOMAC physical function subscale, and patient global assessment scores up to week 24 in the full analysis set of patients with knee OA receiving diclofenac etalhyaluronate (DF-HA) or placebo. Values are the least squares mean (LSM) change from baseline with 95% confidence interval (95% CI). * = $P < 0.05$ versus placebo.

daily acetaminophen consumption at each time point was greater in the DF-HA group than in the placebo group, and the difference was significant at all time points through week 12 (Supplementary Table 11, available on the *Arthritis & Rheumatology* website at http://onlinelibrary.wiley.com/doi/10.1002/art.41725/abstract).

Post hoc responder analyses showed that the DF-HA group had a higher proportion of subjects with improved pain than the placebo group at all cutoffs and time points in terms of the percentages of subjects with clinically meaningful pain reduction (improvement of >20%, >30%, or >50%), and subjects reporting different levels of response on ratings of treatment satisfaction (pain level of <40 mm, <30 mm, or <20 mm) (Supplementary Table 12, available on the *Arthritis & Rheumatology* website at http://onlinelibrary.wiley.com/doi/10.1002/art.41725/abstract). The proportions of subjects with improvement from baseline of >20%, >30%, and >50% at week 12 in the placebo group versus the DF-HA group were 66.5% versus 78.1%, 56.1% versus 71.0%, and 38.2% versus 51.9%, respectively, and the proportions of subjects with a pain level of <40 mm, <30 mm, and <20 mm at week 12 in the placebo group versus the DF-HA group were 49.5% versus 61.4%, 37.3% versus 48.6%, and 26.9% versus 38.1%, respectively (Supplementary Table 12, available on the *Arthritis & Rheumatology* website at http://onlinelibrary.wiley.com/doi/10.1002/art.41725/abstract).

Table 3 shows that the incidence of TEAEs was 126 (57.3%) in the placebo group and 134 (60.9%) in the DF-HA group. No severe TEAEs occurred in either group. The incidence of serious TEAEs was 1 (0.5%) in the placebo group and 5 (2.3%) in the DF-HA group. Serious TEAEs were nausea and vomiting in 1 subject in the placebo group and anaphylactic shock, anaphylactic reaction, autonomic seizure, unstable angina, and strabismus correction in 1 subject each in the DF-HA group. All serious TEAEs were moderate in severity and were resolved with complete recovery except for unstable angina (resolving). Anaphylactic shock and anaphylactic reaction occurred on the first day of DF-HA injection. The subject with anaphylactic shock was not hospitalized, and the subject with anaphylactic reaction was hospitalized. Anaphylactic shock and anaphylactic reaction were mitigated on the day the subjects received various antianaphylaxis therapies or medications and were resolved at 6 and 8 days after onset, respectively. Autonomic seizure was caused by pain during puncture and was judged to be a serious TEAE based on symptoms such as SpO_2 decline. Emergency treatment was performed, and recovery was confirmed 2 hours after the onset. Unstable angina and strabismus correction were judged to be serious TEAEs because of hospitalization for treatment (Supplementary Table 13, available on the *Arthritis & Rheumatology* website at http://onlinelibrary.wiley.com/doi/10.1002/art.41725/abstract).

TEAEs leading to study drug withdrawal were joint swelling and injection site pain in 1 subject each in the placebo group, and anaphylactic shock, anaphylactic reaction, and autonomic seizure (these 3 events were the serious TEAEs described above) in 1 subject each in the DF-HA group. The incidence of TEAEs of special interest at the injection site was 20 (9.1%) in the placebo group and 19 (8.6%) in the DF-HA group (Supplementary Table 14, available on the *Arthritis & Rheumatology* website at http://onlinelibrary.wiley.com/doi/10.1002/art.41725/abstract). The incidence of TEAEs associated with GI disorders was 1 (0.5%) in the DF-HA group and was not reported in the placebo group; the incidence of TEAEs associated with CV disorders was 3 (1.4%) in the placebo group and 7 (3.2%) in the DF-HA group; and the incidence of TEAEs associated with renal dysfunction was 1 (0.5%) in both groups (Supplementary Table 14, available on the *Arthritis & Rheumatology* website at http://onlinelibrary.wiley.com/doi/10.1002/art.41725/abstract). TEAEs associated with anaphylactic reaction and hypersensitivity were evaluated because serious TEAEs of anaphylaxis were observed in this study. The incidence of TEAEs associated with anaphylactic reaction was 6 (2.7%) in the placebo group and 4 (1.8%) in the DF-HA group, and the incidence of TEAEs associated with hypersensitivity was 12 (5.5%) in both groups (Supplementary Table 14). Overall, there was no clear between-group difference in the incidence of TEAEs.

Table 3. Overview of treatment-emergent adverse events*

	Placebo (n = 220)	DF-HA (n = 220)
All events	126 (57.3)	134 (60.9)
Severity of events		
Mild	107 (48.6)	114 (51.8)
Moderate	19 (8.6)	20 (9.1)
Severe	0 (0)	0 (0)
Death	0 (0)	0 (0)
Serious events	1 (0.5)	5 (2.3)
Events leading to study drug withdrawal	2 (0.9)	3 (1.4)
Common events (in ≥2% of patients)		
Nasopharyngitis	30 (13.6)	37 (16.8)
Eczema	2 (0.9)	5 (2.3)
Arthralgia	7 (3.2)	10 (4.5)
Back pain	7 (3.2)	7 (3.2)
Myalgia	1 (0.5)	5 (2.3)
Osteoarthritis	8 (3.6)	7 (3.2)
Injection site joint pain	6 (2.7)	6 (2.7)
Contusion	5 (2.3)	4 (1.8)
Ligament sprain	1 (0.5)	7 (3.2)
Events of special interest		
Events at injection site	20 (9.1)	19 (8.6)
Gastrointestinal disorders†	0 (0)	1 (0.5)
Cardiovascular disorders†	3 (1.4)	7 (3.2)
Renal dysfunction†	1 (0.5)	1 (0.5)
Anaphylactic reaction†	6 (2.7)	4 (1.8)
Hypersensitivity†	12 (5.5)	12 (5.5)

* Adverse events were classified based on the Medical Dictionary for Regulatory Activities (MedDRA) version. 21.1. Values are the number (%).

† Standardized MedDRA query (broad scope) term. The term "gastrointestinal disorders" indicates gastrointestinal perforation, ulceration, hemorrhage, or obstruction. "Cardiovascular disorders" indicates acute cardiac failure, ischemic heart disease, or cardiac arrhythmias. "Renal dysfunction" indicates acute renal failure or chronic kidney disease.

There were no noteworthy changes from baseline in laboratory values and vital signs. The percentage of subjects who experienced worsening from baseline on target knee examination was low for each outcome measure in both the placebo and DF-HA groups. The frequency did not increase with dose and was similar between groups (Supplementary Table 15, available on the *Arthritis & Rheumatology* website at http://onlinelibrary.wiley.com/doi/10.1002/art.41725/abstract). Some subjects were determined to have structurally "changed" (worsening) target knees on radiography, but there was no between-group difference (Supplementary Table 16, available on the *Arthritis & Rheumatology* website at http://onlinelibrary.wiley.com/doi/10.1002/art.41725/abstract).

DISCUSSION

We achieved the primary objective of a significant improvement in WOMAC pain subscale score in subjects receiving DF-HA compared to those receiving placebo for 12 weeks. Sensitivity analysis demonstrated the robustness of the results. Furthermore, the results were not influenced by demographic characteristics according to subgroup analysis, and there were no between-group differences in demographic or other baseline characteristics. Similar to the primary outcome, most of the secondary outcomes indicated the superiority of 12 weeks of treatment with DF-HA compared to placebo. These results confirmed the efficacy of DF-HA and reproduced the results of our previous phase II study (18).

According to Initiative on Methods, Measurement, and Pain Assessment in Clinical Trials (IMMPACT) recommendations (26), the clinical importance of a group difference should be evaluated by demonstrating a significant improvement in the primary end point relative to placebo, but also by multiple other factors. Responder analyses using the percentages of subjects with clinically meaningful pain reduction and subjects reporting different levels of response on ratings of treatment satisfaction are considered useful for interpreting between-group differences (26). In this study, when the percentages of subjects with improved pain at multiple cutoffs were compared between groups, they were higher in the DF-HA group than in the placebo group for all cutoffs at all time points. In addition, the OMERACT-OARSI response rate was higher in the DF-HA group than the placebo group at all time points. Improvement was demonstrated in ~50% of DF-HA–treated subjects at week 1, and this was extended to >80% of DF-HA–treated subjects at week 24.

Moreover, DF-HA improved pain as well as physical function and global assessment. In a clinical trial conducted in patients with knee OA, assessment of pain, physical function, and global function were important outcomes (27). DF-HA also improved the quality of life and decreased the use of acetaminophen as outcomes for chronic pain (28). These results suggest that DF-HA improves multiple symptoms including pain in knee OA. Of note, in the present study DF-HA decreased WOMAC pain subscale scores from as early as week 1, and this level of decrease was maintained for 4 weeks. This effect was extended to 24 weeks by injection once every 4 weeks.

However, WOMAC pain subscale scores were decreased from baseline after each injection in both the DF-HA and placebo groups, and there were many responders in the placebo group. These results may be explained by the placebo effect. The large placebo effects related to IA injection are likely to be caused by the invasiveness of the administrative procedure and the physiologic response to liquid injected into the articular cavity (29,30). In the present study, injections were administered frequently (6 times), which may have further increased the placebo effect (30). Indeed, a large placebo effect is always a concern in clinical trials using IA injection, and many trials in OA fail to show a significant difference between placebo and the study drug. In addition, the between-group difference in WOMAC pain subscale scores was not significant at week 24, which may result from floor effects as well as large placebo effects. As described above, some benefits of DF-HA were confirmed, but further studies are needed to evaluate their clinical importance.

Regarding safety, anaphylactic shock and anaphylactic reaction in 1 subject each were judged to be moderate and were resolved after pharmacotherapy. Because anaphylactic symptoms in response to DF-HA may not be ruled out for clinical use, careful monitoring and immediate treatment with established anaphylaxis therapies will be required. No clinically important GI- or CV-related TEAEs, which have been observed with oral NSAIDs and selective COX-2 inhibitors, or clinically important renal dysfunction, were observed in the DF-HA group. This promising safety profile may be related to the lower dose needed and reduced systemic exposure to DF that occurs when DF-HA is administered via injection.

In a previous phase II study, joint inflammation at the injection site was observed in 1 subject. Therefore, we performed examination of the target knee to evaluate the safety of injection into the local joint. No clinical issues were revealed on target knee examination, demonstrating that AEs similar to those in the previous study did not occur in the present study despite the larger number of DF-HA injections. No differences in the incidence of TEAEs at the injection site were observed between the treatment groups, whereas these local reactions have been reported for other HA preparations (31). Finally, no clinical issue was observed on radiography. Nevertheless, NSAIDs have been reported to be deleterious to joint cartilage (32). Although no particular concern was confirmed by the findings of this study, further studies are needed to determine the effects of DF-HA on joint cartilage, since DF-HA, after approval, would be the first IA preparation of NSAIDs to be injected into human knee cavities.

Some existing IA preparations are effective when injected once every 3 or 6 months. However, DF-HA requires repeated injections every 4 weeks to maintain efficacy. This is a limitation of the practical use of DF-HA. Furthermore, although not confirmed in this study, joint infection is a common risk of IA injection, and the risk is higher with more frequent administration compared with IA preparations administered once every 3 or 6 months. Given that serious

safety issues caused by DF-HA were confirmed in this study, it is necessary to compare the risk/benefit ratio with that of other IA preparations. In particular, a head-to-head study of DF-HA versus an approved HA is required to determine whether there is a great enough benefit of DF-HA to justify the monthly injection frequency versus the semiannual injection frequency of most HA preparations.

This study had some limitations. Data were collected from a limited population that only comprised Japanese patients, there were no data for the excluded patient population (e.g., patients with a BMI of ≥35.0 kg/m^2), no information was obtained on combinations with other analgesics because use of other analgesics was prohibited, and the study did not evaluate safety with regard to joint tissues, including joint cartilage. Active treatment–controlled clinical trials are needed to evaluate the clinical usefulness of DF-HA, and how long the effect of DF-HA lasts after IA treatment is stopped should be investigated in future clinical studies. Additional safety data are needed, since the number of subjects in this study was relatively small, and the long-term safety of DF-HA treatment exceeding 24 weeks should be determined because the treatment term may be longer in actual clinical practice than that assessed in this study. In addition, evaluation of safety with regard to the joint tissue including joint cartilage is needed, using imaging techniques other than radiography by a central measurement.

In conclusion, DF-HA, a conjugated compound with the advantages of IA HA and NSAIDs, promoted significant improvements in symptoms, with fast-acting, long-lasting efficacy in knee OA patients when injected once every 4 weeks. Anaphylactic reactions were observed, and further safety evaluation is needed. Although future studies are needed to further demonstrate its clinical usefulness, DF-HA is expected to be a novel therapeutic agent fulfilling an unmet need for pharmacotherapy for knee OA.

ACKNOWLEDGMENTS

The authors thank the patients who participated in the clinical trial, and also thank all study investigators, study coordinators, and other study personnel for their contributions to the study.

AUTHOR CONTRIBUTIONS

All authors were involved in drafting the article or revising it critically for important intellectual content, and all authors approved the final version to be published. Dr. Nishida had full access to all of the data in the study and takes responsibility for the integrity of the data and the accuracy of the data analysis.

Study conception and design. Nishida, Kano, Nobuoka, Seo.
Acquisition of data. Kano, Nobuoka.
Analysis and interpretation of data. Seo.

ROLE OF THE STUDY SPONSOR

Seikagaku Corporation facilitated the study design, data collection, data analysis, interpretation of the data, and the writing of the manuscript. Ono Pharmaceutical Company, Ltd. provided writing assistance for the manuscript. Seikagaku Corporation and Ono Pharmaceutical Company, Ltd. reviewed and approved the manuscript prior to submission. Publication of this article was contingent upon approval by Seikagaku and Ono Pharmaceutical Company, Ltd. Medical writing and editorial support were provided by Dr. Kazuyoshi Masuda (ASCA Corporation, Chuo-ku, Osaka, Japan) and funded by Seikagaku Corporation and Ono Pharmaceutical Company, Ltd.

REFERENCES

1. Kolasinski SL, Neogi T, Hochberg MC, Oatis C, Guyatt G, Block J, et al. 2019 American College of Rheumatology/Arthritis Foundation guideline for the management of osteoarthritis of the hand, hip, and knee. Arthritis Rheumatol 2020;72:220–33.
2. Roos EM, Arden NK. Strategies for the prevention of knee osteoarthritis [review]. Nat Rev Rheumatol 2016;12:92–101.
3. Hunter DJ, Bierma-Zeinstra S. Osteoarthritis [review]. Lancet 2019;393:1745–59.
4. Bannuru RR, Osani MC, Vaysbrot EE, Arden NK, Bennell K, Bierma-Zeinstra SM, et al. OARSI guidelines for the non-surgical management of knee, hip, and polyarticular osteoarthritis. Osteoarthritis Cartilage 2019;27:1578–89.
5. American Academy of Orthopaedic Surgeons. Treatment of osteoarthritis of the knee–2nd edition: evidence-based clinical practice guideline. May 2013. URL: https://www.aaos.org/globalassets/quality-and-practice-resources/osteoarthritis-of-the-knee/osteoarthritis-of-the-knee-2nd-editiion-clinical-practice-guideline.pdf.
6. Gore M, Tai KS, Sadosky A, Leslie D, Stacey BR. Use and costs of prescription medications and alternative treatments in patients with osteoarthritis and chronic low back pain in community-based settings. Pain Pract 2012;12:550–60.
7. Schaffer D, Florin T, Eagle C, Marschner I, Singh G, Grobler M, et al. Risk of serious NSAID-related gastrointestinal events during long-term exposure: a systematic review. Med J Aust 2006;185:501–6.
8. Bresalier RS, Sandler RS, Quan H, Bolognese JA, Oxenius B, Horgan K, et al. Cardiovascular events associated with rofecoxib in a colorectal adenoma chemoprevention trial. N Engl J Med 2005;352:1092–102.
9. Trelle S, Reichenbach S, Wandel S, Hildebrand P, Tschannen B, Villiger PM, et al. Cardiovascular safety of non-steroidal anti-inflammatory drugs: network meta-analysis. BMJ 2011;342:c7086.
10. Ungprasert P, Cheungpasitporn W, Crowson CS, Matteson EL. Individual non-steroidal anti-inflammatory drugs and risk of acute kidney injury: a systematic review and meta-analysis of observational studies. Eur J Intern Med 2015;26:285–91.
11. Deyle GD, Allen CS, Allison SC, Gill NW, Hando BR, Petersen EJ, et al. Physical therapy versus glucocorticoid injection for osteoarthritis of the knee. N Engl J Med 2020;382:1420–9.
12. McAlindon TE, LaValley MP, Harvey WF, Price LL, Driban JB, Zhang M, et al. Effect of intra-articular triamcinolone vs saline on knee cartilage volume and pain in patients with knee osteoarthritis: a randomized clinical trial. JAMA 2017;317:1967–75.
13. Kompel AJ, Roemer FW, Murakami AM, Diaz LE, Crema MD, Guermazi A. Intra-articular corticosteroid injections in the hip and knee: perhaps not as safe as we thought? Radiology 2019;293:656–63.
14. Ghosh P, Guidolin D. Potential mechanism of action of intra-articular hyaluronan therapy in osteoarthritis: are the effects molecular weight dependent? Semin Arthritis Rheum 2002;32:10–37.
15. Altman RD, Dasa V, Takeuchi J. Review of the mechanism of action for Supartz FX in knee osteoarthritis. Cartilage 2018;9:11–20.
16. Yoshioka K, Kisukeda T, Zuinen R, Yasuda Y, Miyamoto K. Pharmacological effects of N-[2-[[2-[2-[(2,6-dichlorophenyl)amino]phenyl]acetyl]oxy]ethyl]hyaluronamide (diclofenac etalhyaluronate, SI-613), a novel sodium hyaluronate derivative chemically linked with diclofenac. BMC Musculoskelet Disord 2018;19:157.

17. Kisukeda T, Onaya J, Yoshioka K. Effect of diclofenac etalhyaluronate (SI-613) on the production of high molecular weight sodium hyaluronate in human synoviocytes. BMC Musculoskelet Disord 2019;20:201.
18. Nishida Y, Kano K, Nobuoka Y, Seo T. Sustained-release diclofenac conjugated to hyaluronate (diclofenac etalhyaluronate) for knee osteoarthritis: a randomized phase 2 study. Rheumatology (Oxford) 2021;60:1435–44.
19. WOMAC. WOMAC 3.1 Knee and hip osteoarthritis index. URL: http://www.womac.com/womac/index.htm.
20. Pocock SJ, Simon R. Sequential treatment assignment with balancing for prognostic factors in the controlled clinical trial. Biometrics 1975;31:103–15.
21. Pham T, van Der Heijde D, Lassere M, Altman RD, Anderson JJ, Bellamy N, et al. Outcome variables for osteoarthritis clinical trials: the OMERACT-OARSI set of responder criteria. J Rheumatol 2003;30:1648–54.
22. Fukuhara S, Bito S, Green J, Hsiao A, Kurokawa K. Translation, adaptation, and validation of the SF-36 Health Survey for use in Japan. J Clin Epidemiol 1998;51:1037–44.
23. Fukuhara S, Ware JE Jr, Kosinski M, Wada S, Gandek B. Psychometric and clinical tests of validity of the Japanese SF-36 Health Survey. J Clin Epidemiol 1998;51:1045–53.
24. Fukuhara S, Suzukamo Y. Manual of SF-36v2 Japanese version, Kyoto: Institute for Health Outcomes and Process Evaluation Research, 2004.
25. Hurst NP, Kind P, Ruta D, Hunter M, Stubbings A. Measuring health-related quality of life in rheumatoid arthritis: validity, responsiveness and reliability of EuroQol (EQ-5D). Br J Rheumatol 1997;36:551–9.
26. Dworkin RH, Turk DC, McDermott MP, Peirce-Sandner S, Burke LB, Cowan P, et al. Interpreting the clinical importance of group differences in chronic pain clinical trials: IMMPACT recommendations. Pain 2009;146:238–44.
27. McAlindon TE, Driban JB, Henrotin Y, Hunter DJ, Jiang GL, Skou ST, et al. OARSI clinical trials recommendations: design, conduct, and reporting of clinical trials for knee osteoarthritis. Osteoarthritis Cartilage 2015;23:747–60.
28. Committee for Medicinal Products for Human Use. Guideline on the clinical development of medicinal products intended for the treatment of pain. European Medicines Agency. December 2016. URL: https://www.ema.europa.eu/en/documents/scientific-guideline/guideline-clinical-development-medicinal-products-intended-treatment-pain-first-version_en.pdf.
29. Finniss DG, Kaptchuk TJ, Miller F, Benedetti F. Biological, clinical, and ethical advances of placebo effects [review]. Lancet 2010;375:686–95.
30. Zhang W, Robertson J, Jones AC, Dieppe PA, Doherty M. The placebo effect and its determinants in osteoarthritis: meta-analysis of randomised controlled trials. Ann Rheum Dis 2008;67:1716–23.
31. Bannuru RR, Osani M, Vaysbrot EE, McAlindon TE. Comparative safety profile of hyaluronic acid products for knee osteoarthritis: a systematic review and network meta-analysis. Osteoarthritis Cartilage 2016;24:2022–41.
32. Brandt K. The role of analgesics in the management of osteoarthritis pain [review]. Am J Ther 2000;7:75–90.

Arthritis & Rheumatology
Vol. 73, No. 9, September 2021, pp 1656–1662
DOI 10.1002/art.41729

AMERICAN COLLEGE of RHEUMATOLOGY
Empowering Rheumatology Professionals

BRIEF REPORT

Association Between Gut Microbiota and Symptomatic Hand Osteoarthritis: Data From the Xiangya Osteoarthritis Study

Jie Wei,[1] Chenhong Zhang,[2] Yuqing Zhang,[3] Weiya Zhang,[4] Michael Doherty,[4] Tuo Yang,[5] Guangju Zhai,[6] Abasiama D. Obotiba,[4] Houchen Lyu,[7] Chao Zeng,[8] and Guanghua Lei[8]

Objective. Systemic inflammatory factors have been implicated in symptomatic hand osteoarthritis (OA). Gut microbiome dysbiosis promotes systemic inflammation. The aim of this study was to examine the association between the gut microbiome and the presence of symptomatic hand OA in a population-based study.

Methods. Study participants were subjects of the Xiangya Osteoarthritis Study, a community-based observational study conducted in the Hunan Province of China. Symptomatic hand OA was defined as the presence of both symptoms and radiographic OA in the same hand. The gut microbiome was analyzed using 16S ribosomal RNA gene sequencing in stool samples. We examined the relation of α-diversity, β-diversity, relative abundance of taxa, and potential bacterial functional pathways to symptomatic hand OA.

Results. A total of 1,388 participants (mean age 61.3 years, 57.4% women) were included in the study, of whom 72 had symptomatic hand OA (prevalence of symptomatic hand OA 5.2%). Beta-diversity of the gut microbiome, but not α-diversity, was significantly associated with the presence of symptomatic hand OA ($P = 0.003$). Higher relative abundance of the genera *Bilophila* and *Desulfovibrio* as well as lower relative abundance of the genus *Roseburia* was associated with symptomatic hand OA. Most functional pathways (i.e., those annotated in the KEGG Ortholog hierarchy) that were observed to be altered in participants with symptomatic hand OA belonged to the amino acid, carbohydrate, and lipid metabolic pathways.

Conclusion. This large, population-based study provides the first evidence that alterations in the composition of the gut microbiome were observed among study participants who had symptomatic hand OA, and a low relative abundance of *Roseburia* but high relative abundance of *Bilophila* and *Desulfovibrio* at the genus level were associated with prevalent symptomatic hand OA. These findings may help investigators understand the role of the microbiome in the development of symptomatic hand OA and could contribute to potential translational opportunities.

INTRODUCTION

Hand osteoarthritis (OA) is highly prevalent within middle-aged and older populations (1). Individuals with hand OA may experience pain and stiffness and develop structural joint damage, which can impair their ability to undertake activities of daily living (1). Results from previous studies have shown that symptomatic hand OA can have a clinical burden comparable to that of rheumatoid arthritis (2). Although the pathogenesis of hand OA remains largely unknown, systemic factors, including systemic

Supported by the National Natural Science Foundation of China (grants 81772413, 81702207, 81702206, 81930071, 81902265, and 82072502), the National Key Research and Development Project from the Ministry of Science and Technology of China (grant 2018YFB1105705), the Hunan Province Key Research and Development Program (grants 2018SK2070 and 2018SK2071), the Project Program of the National Clinical Research Center for Geriatric Disorders (grant 2020LNJJ03 to Xiangya Hospital), and the Hunan Province Science and Technology Program (grant 2019RS2010).

[1]Jie Wei, PhD: Health Management Center, Xiangya Hospital, Central South University, Changsha, China; [2]Chenhong Zhang, PhD: State Key Laboratory of Microbial Metabolism, School of Life Sciences and Biotechnology, Shanghai Jiao Tong University, Shanghai, China; [3]Yuqing Zhang, DSc: Division of Rheumatology, Allergy, and Immunology, Department of Medicine, Massachusetts General Hospital, and the Mongan Institute, Massachusetts General Hospital, Harvard Medical School, Boston, Massachusetts; [4]Weiya Zhang, PhD, Michael Doherty, MD, Abasiama D. Obotiba, MD: Academic Rheumatology, Clinical Sciences Building, University of Nottingham, City Hospital, Nottingham, and Arthritis Research UK Pain Centre, Nottingham, UK; [5]Tuo Yang, MD, PhD: Health Management Center, Xiangya Hospital, Central South University, Changsha, China, Academic Rheumatology, Clinical Sciences Building, University of Nottingham, City Hospital, Nottingham, UK, and Arthritis Research UK Pain Centre, Nottingham, UK; [6]Guangju Zhai, PhD: Discipline of Genetics, Faculty of Medicine, Memorial University of Newfoundland, St. John's, Newfoundland, Canada; [7]Houchen Lyu, MD, PhD: Department of Orthopedics, General Hospital of Chinese PLA, Beijing, and Department of Orthopaedics, Xiangya Hospital, Central South

inflammation, have been implicated as a potential risk factor for symptomatic hand OA (1,3).

Gut microbiome dysbiosis can lead to the dysregulation of various important physiologic functions, such as production of small molecules that interact with the host, synthesis of essential amino acids, and regulation of fat metabolism, which can in turn contribute to the development of systemic inflammation (4). Over recent decades, many studies have found that the gut microbiome and its metabolites play important roles in the pathologic development and progression of several systemic inflammatory diseases, including inflammatory bowel disease, inflammatory arthritis, multiple sclerosis, and systemic lupus erythematosus (4). However, to the best of our knowledge, no study has examined the association between the gut microbiome and hand OA. Elucidating this association would help clarify the role of the microbiome in the development of hand OA and contribute to potential translational opportunities for the prevention and treatment of this common condition.

To help fill this knowledge gap, we examined the association between the gut microbiome and prevalent symptomatic hand OA, using data collected from the Xiangya Osteoarthritis (XO) Study, a population-based observational study conducted among the residents of rural areas of China.

PATIENTS AND METHODS

Study participants. The XO Study is a population-based longitudinal study of the natural history of and risk factors for the development of OA in a rural area of China (ClinicalTrials.gov identifier: NCT04033757) (5). Participants in the XO Study were a randomly selected sample of residents age ≥50 years from rural mountainous villages in Longshan County in the Hunan Province. Specifically, for selection of the initial 14 communities, we first adopted a sampling method of probability proportionate to population size. All of the villages in the selected communities were then listed in a random order. The village-to-village recruitment began in the first village in the first community until the number of participants in that community met the predetermined quota. Eventually, a total of 25 rural mountainous villages in Longshan County were included in the XO Study. Of note, the XO Study includes 3 subcohorts (i.e., subcohorts I, II, and III), comprising participants recruited in 2015, 2018, and 2019, respectively.

The XO Study was approved by the Research Ethical Committee of Xiangya Hospital, Central South University (approval no. 201510506). All participants gave their written informed consent to participate in the studies.

Assessment of hand OA. Posteroanterior radiographs of both hands were obtained from each participant in the XO Study. Radiographs of the bilateral second to fifth distal interphalangeal joints, second to fifth proximal interphalangeal joints, first to fifth metacarpophalangeal joints, thumb interphalangeal joints, and thumb base (carpometacarpal) joints were graded using a modified Kellgren/Lawrence (K/L) scale for radiographic hand OA (6). All hand radiographs were read by a single musculoskeletal researcher (TY; an orthopedic surgeon who was the primary reader). With each new batch of radiographs (n = 50 films), we commingled 5 previously read radiographs to test intrarater reliability. For assessment of interrater reliability, another reader (ADO; a musculoskeletal imaging specialist) scored a selected subset of 30 films independently. Intra- and interrater reliabilities were assessed using kappa statistics with 95% confidence intervals (95% CIs). Radiographic hand OA was defined as the presence of a K/L radiographic severity grade of ≥2 in any of the joints of each hand (i.e., those joints listed above). The intrarater reliability for the identification of radiographic hand OA (presence versus absence) was a kappa of 0.91 (95% CI 0.83–0.99), and the interrater reliability was a kappa of 0.71 (95% CI 0.45–0.96).

Presence of hand symptoms was ascertained by noting the patient's response to the question, "On most days, do you have pain, aching, or stiffness in your left/right hand?" (7). Symptomatic hand OA was defined as the presence of both self-reported symptoms and radiographic OA in the same hand. Participants were defined as having symptomatic hand OA if they had symptomatic hand OA in at least one hand (7).

Stool sample collection and DNA extraction. Stool samples collected from the participants at the recruitment site were immediately frozen and transported on dry ice within 20 minutes. Samples were stored in freezers at a temperature of –80°C until analyzed. For DNA assessment, DNA was extracted from 200 mg of each stool sample using a Magen Hipure Soil DNA kit, according to the manufacturer's protocol. DNA was quantified using a Qubit version 2.0 fluorometer.

Gut microbiome analysis using 16S ribosomal RNA (rRNA) gene sequencing. The 16S rRNA gene was amplified using a 341F/806R primer set targeting the V3–V4 hypervariable region. DNA was sequenced using an Illumina MiSeq platform. Bioinformatics analysis of the gut microbiome was performed using a QIIME 2 2019.10 platform (https://qiime2.org). Raw sequence data were demultiplexed and quality filtered using a q2-demux plugin, followed by denoising with DADA2 (via q2-dada2).

University, Changsha, China; [8]Chao Zeng, MD, PhD, Guanghua Lei, MD, PhD: Department of Orthopaedics, Xiangya Hospital, Central South University, Changsha, National Clinical Research Center of Geriatric Disorders, Xiangya Hospital, Central South University, Changsha, and Hunan Key Laboratory of Joint Degeneration and Injury, Changsha, China.

No potential conflicts of interest relevant to this article were reported.

Address correspondence to Guanghua Lei, MD, PhD, or Chao Zeng, MD, PhD, Department of Orthopaedics, Xiangya Hospital, Central South University, 87 Xiangya Road, Changsha, Hunan, China 410008. Email: lei_guanghua@csu.edu.cn or zengchao@csu.edu.cn.

Submitted for publication October 29, 2020; accepted in revised form March 9, 2021.

All amplicon sequence variants (ASVs) were aligned with mafft (via q2-alignment) and used to construct a phylogeny with fasttree2 (via q2-phylogeny). Metrics for α-diversity and β-diversity and data from principal coordinates analysis (PCoA) were estimated using q2-diversity after samples were rarefied (subsampled without replacement) to the minimal number of reads per sample. Taxonomy was assigned to ASVs using a q2-feature-classifier, classify-sklearn naive Bayes taxonomy classifier, against the Greengenes 13_8 99% operational taxonomic units (OTUs) from reference sequences. All 16S rRNA sequencing data obtained in this study are available for download from the European Nucleotide Archive (project no. PRJEB33926; https://www.ebi.ac.uk/ena/browser/home).

Statistical analysis. Similarities in the composition of the gut microbiome between participants with symptomatic hand OA (i.e., the symptomatic hand OA group) and those without symptomatic hand OA (i.e., the control group) were compared using α-diversity as measured by the Shannon diversity index, and β-diversity as measured by the unweighted Unifrac distance. We used a Wilcoxon's rank sum test to determine the differences in α-diversity between groups, and a permutation multivariate analysis of variance test to determine the differences in β-diversity between groups.

To gain more insight into which gut microbiome taxonomies drive the association with symptomatic hand OA, we performed multivariate linear regression analyses at the phylum, family, and genus levels, with adjustments for age, sex, body mass index (BMI), alcohol consumption, and frequency of dietary intake of meat/eggs, dairy, and vegetables. Specifically, we removed from the analyses any microbiome taxa that were present in <20% of samples, and then compared the difference in relative abundance of taxa at the phylum, family, and genus levels between the symptomatic hand OA and control groups. Bacterial metagenomes were imputed from 16S rRNA sequencing–based microbial DNA data using the Phylogenetic Investigation of Communities by Reconstruction of Unobserved States (PICRUSt) software package. Functional annotation was applied using the annotated pathways from the KEGG catalog (http://www.genome.ad.jp/kegg). We performed multivariate linear regression analyses to assess differences in KEGG level 3 pathways (i.e., those present in more than 20% of samples) between participants with and those without symptomatic hand OA, with adjustments for age, sex, BMI, alcohol consumption, and frequency of dietary intake of meat/eggs, dairy, and vegetables. Significant differences were assessed using *P* values corrected for multiple testing with the Benjamin and Hochberg false discovery rate method; corrected *P* values (and Q values) less than 0.1 were considered statistically significant.

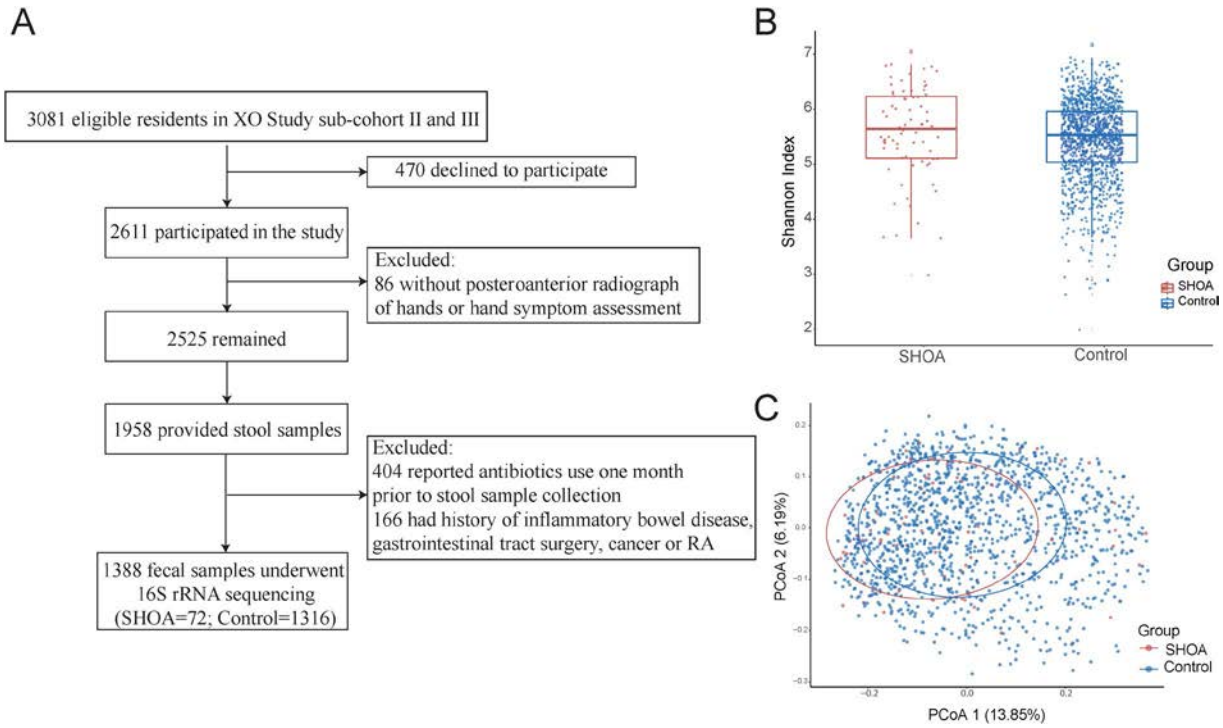

Figure 1. Profiling of the gut microbiome using 16S ribosomal RNA (rRNA) sequencing in subjects from the Xiangya Osteoarthritis (XO) Study cohort. **A**, Selection process of study subjects with symptomatic hand osteoarthritis (SHOA) and those without symptomatic hand OA (controls). **B**, Shannon index of microbial diversity (α-diversity) in each group. Results are shown as box plots, in which symbols represent individual subjects, the horizontal line inside the box represents the median, each box represents the 25th to 75th percentiles, and the lines outside the box represent the smallest and largest value of 1.5 × the interquartile range. **C**, Principle coordinates analysis (PCoA) plots of β-diversity in each group, constructed using the unweighted Unifrac distance. RA = rheumatoid arthritis.

In addition, 3 sensitivity analyses were performed to assess the robustness of our study findings. First, to minimize the potential residual effect of antibiotic use, we compared the differences in relative abundance of microbiota at the genus level between the symptomatic hand OA group and the control group, after exclusion of individuals who reported having received antibiotics within 2 or 3 months prior to the stool sample collection. Second, we conducted a matched case–control study in which up to 4 controls were matched to each case by age, sex, and BMI. We compared the difference in relative abundance of the microbiome genera and KEGG level 3 pathways between the case and control groups using multivariate linear regression analyses adjusted for alcohol consumption and frequency of dietary intake of meat/eggs, dairy, and vegetables. Third, we performed a sex-specific analysis to explore the potential sex interaction between the microbiome and symptomatic hand OA. Detailed information on the methods and analysis codes used are provided in the Supplementary Methods (available on the *Arthritis & Rheumatology* website at http://onlinelibrary.wiley.com/doi/10.1002/art.41729/abstract).

RESULTS

A flow chart depicting the participant selection process is shown in Figure 1A. Baseline characteristics of the 1,388 included study participants are shown in Supplementary Table 1 (available on the *Arthritis & Rheumatology* website at http://onlinelibrary.wiley.com/doi/10.1002/art.41729/abstract). Participants with symptomatic hand OA (n = 72) were older than participants without symptomatic hand OA (n = 1,316) (age 70.9 years versus 62.8 years; $P < 0.001$), and those with symptomatic hand OA were more likely to be women (75% versus 57%; $P = 0.003$).

A total of 90,608,388 raw sequence reads (mean reads per sample 65,279) were generated from all stool samples obtained from eligible participants. After quality filtering and removal of contaminants, there were 61,294,662 high-quality reads that were used for analysis (mean reads per sample 44,160). Among all samples, 31,355 different ASVs were discovered.

The Shannon index of microbial α-diversity was not significantly different between patients with symptomatic hand OA and

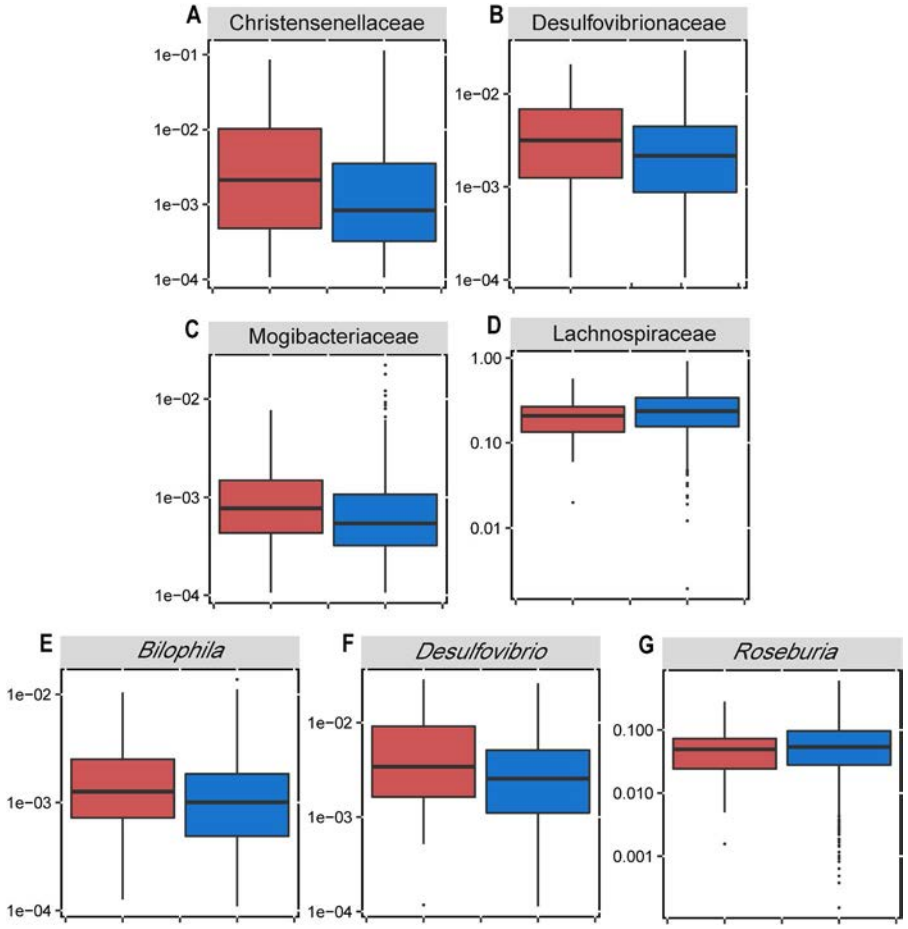

Figure 2. Differences in the composition (relative abundance) of the gut microbiota at the family level (**A–D**) and genus level (**E–G**) between individuals with symptomatic hand osteoarthritis (OA) (n = 72) (red) and individuals without symptomatic hand OA (controls) (n = 1,316) (blue), after adjustments for age, sex, body mass index, alcohol consumption, and frequency of dietary intake of meat/eggs, dairy, and vegetables. Data are shown as box plots, in which the horizontal line inside the box represents the median, each box represents the 25th to 75th percentiles, and the lines outside the box represent the smallest and largest value of 1.5 × the interquartile range. Circles represent individual outliers.

controls without symptomatic hand OA (P = 0.095) (Figure 1B). However, the PCoA plot constructed using unweighted UniFrac distances showed that the structure and composition of the gut microbiome differed significantly between the 2 groups (P = 0.003) (Figure 1C). In both groups, the profile of the gut microbiome appeared to be dominated by Firmicutes and Bacteroidetes at the phylum level, by Lachnospiraceae, Bacteroidaceae, Prevotellaceae, and Ruminococcaceae at the family level, and by *Bacteroides*, *Prevotella*, *Faecalibacterium*, and *Roseburia* at the genus level (for details, see Supplementary Figures 1, 2, and 3, available on the *Arthritis & Rheumatology* website at http://onlinelibrary.wiley.com/doi/10.1002/art.41729/abstract), consistent with the usual composition of the human gut microbiome.

The associations between microbiome taxonomies and symptomatic hand OA are shown in Figure 2. After adjustment for age, sex, BMI, alcohol consumption, and frequency of dietary intake of meat/eggs, dairy, and vegetables, there was no apparent difference in microbiome taxa at the phylum level between subjects with and those without symptomatic hand OA. However, at the family level, individuals with symptomatic hand OA had a higher relative abundance of Christensenellaceae (P < 0.001, Q < 0.001) (Figure 2A), Desulfovibrionaceae (P = 0.001, Q = 0.008) (Figure 2B), and Mogibacteriaceae (P = 0.01, Q = 0.053) (Figure 2C), but a lower relative abundance of Lachnospiraceae (P = 0.02, Q = 0.092) (Figure 2D) compared to those without symptomatic hand OA. Statistically significant differences in the gut microbiome were also observed at the genus level. Individuals with symptomatic hand OA had higher relative abundances of *Bilophila* (P = 0.001, Q = 0.006) (Figure 2E) and *Desulfovibrio* (P = 0.012, Q = 0.064) (Figure 2F) but a lower relative abundance of *Roseburia* (P = 0.011, Q = 0.062) (Figure 2G) compared to those without symptomatic hand OA. Full summary statistics of the associations of microbiome taxonomies with symptomatic hand OA adjusted for age, sex, BMI, alcohol consumption, and frequency of dietary intake of meat/eggs, dairy, and vegetables, determined using multivariate linear regression analyses, are presented in Supplementary Tables 2–4 (available on the *Arthritis & Rheumatology* website at http://onlinelibrary.wiley.com/doi/10.1002/art.41729/abstract). After exclusion of individuals who reported having received antibiotic treatment within 2 months or 3 months prior to the stool sample collection, the associations remained statistically significant (Supplementary Tables 5 and 6; http://onlinelibrary.wiley.com/doi/10.1002/art.41729/abstract).

Sensitivity analyses conducted in case–control studies, with matching for age, sex, and BMI (68 participants with symptomatic

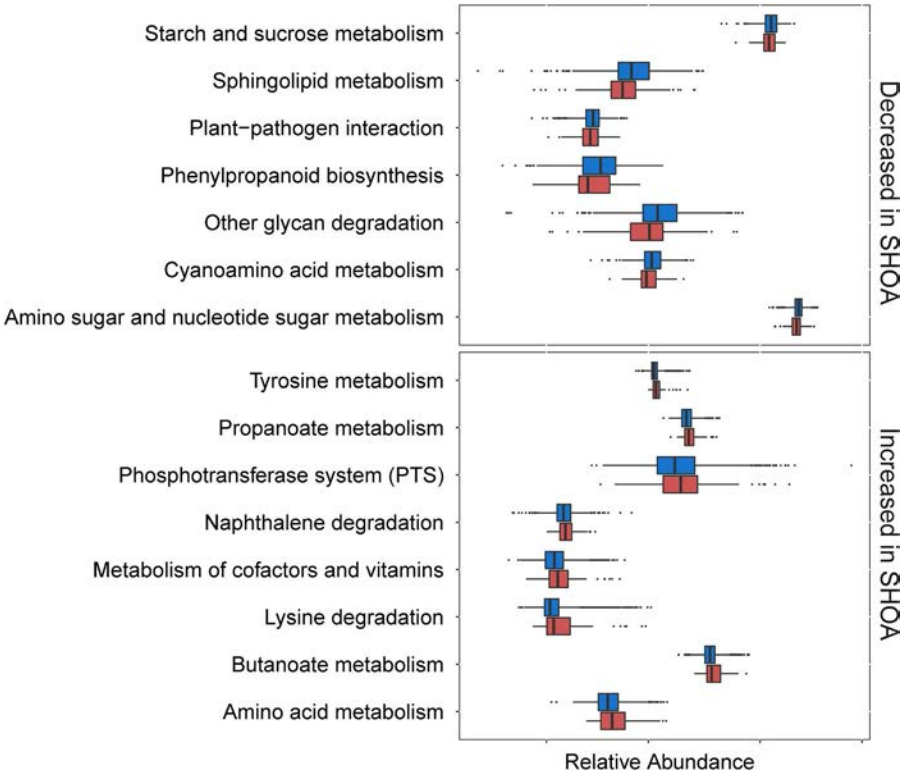

Figure 3. Differences in the relative abundance of predicted functions (third level of the KEGG Ortholog hierarchy), expressed as either a decrease or increase in the relative abundance of each level 3 functional pathway in individuals with symptomatic hand osteoarthritis (SHOA) (n = 72) (red) compared to individuals without symptomatic hand OA (controls) (n = 1,316) (blue), based on the Phylogenetic Investigation of Communities by Reconstruction of Unobserved States (PICRUSt) data set. Data are shown as box plots, in which the line inside the box represents the median, each box represents the 25th to 75th percentiles, and the lines outside the box represent the smallest and largest value of 1.5 × the interquartile range. Circles represent individual outliers.

hand OA versus 234 matched controls without symptomatic hand OA) showed similar results (Supplementary Table 7; http://onlinelibrary.wiley.com/doi/10.1002/art.41729/abstract). The sex-specific analysis undertaken in the 54 women with symptomatic hand OA yielded results consistent with the primary analysis in terms of taxonomic associations with symptomatic hand OA (i.e., for *Bilophila*, $\beta = 0.008$, $P = 0.003$, Q = 0.031; for *Desulfovibrio*, $\beta = 0.011$, $P = 0.026$, Q = 0.148; for *Roseburia*, $\beta = -0.046$, $P = 0.006$, Q = 0.049). However, taxonomic associations in the 18 men with symptomatic hand OA were not statistically significant, although the findings were similar to that in women (i.e., relative abundance of the genera *Bilophila* and *Desulfovibrio* increased, and relative abundance of the genus *Roseburia* decreased in men with symptomatic hand OA).

The functional analysis, performed by reconstructing metagenomes using PICRUSt software, identified 15 KEGG level 3 pathways that were altered in association with symptomatic hand OA (Figure 3). Most KEGG pathways that were related to amino acids (metabolism of amino acids, tyrosine and lysine degradation, and cyano–amino acid metabolism), carbohydrates (metabolism of starch, sucrose, amino sugar and nucleotide sugar, and butanoate and propanoate), and lipids (sphingolipid metabolism) were significantly altered in individuals with symptomatic hand OA compared to controls. Full summary statistics of the associations of KEGG level 3 pathways with symptomatic hand OA adjusted for age, sex, BMI, alcohol consumption, and frequency of dietary intake of meat/eggs, dairy, and vegetables, determined using multivariate linear regression analyses, are presented in Supplementary Table 8 (available on the *Arthritis & Rheumatology* website at http://onlinelibrary.wiley.com/doi/10.1002/art.41729/abstract). Similar results were observed in the case–control study with matching for age, sex, and BMI (Supplementary Table 9; http://onlinelibrary.wiley.com/doi/10.1002/art.41729/abstract).

DISCUSSION

Several studies have demonstrated that patients with inflammatory arthritis have a decreased relative abundance of the genus *Roseburia* (8), and there was a strong positive correlation between the relative abundance of the genus *Desulfovibrio* and inflammatory blood biomarkers in the general population (9). In accord with those findings, our results suggest that a high relative abundance of the genus *Desulfovibrio* but low relative abundance of the genus *Roseburia* may play a role in symptomatic hand OA. Furthermore, previous work has shown that metabolic pathways, namely those affecting metabolism of the branched-chain amino acids, from arginine and phosphatidylcholine to lysophosphatidylcholine, were significantly associated with the pathogenesis of OA (10). Similarly, our results based on reconstruction of metagenomes using PICRUSt software also identified altered KEGG pathways related to metabolism of amino acids, lipids, and carbohydrates in association with symptomatic hand OA. Taken together, our findings suggest that metabolic dysfunction of the gut microbiome may play a key role in the state of systemic inflammation in patients with symptomatic hand OA by affecting the host metabolite levels, a concept that warrants further investigation.

Several biologic mechanisms linking the gut microbiome to systemic inflammation have been proposed. *Bilophila* member species have been shown to produce lipopolysaccharides that promote intestinal barrier dysfunction, bile acid dysmetabolism, and inflammation in mouse models (11). In addition, in in vitro experiments, a species belonging to *Bilophila* was able to convert taurine to the toxic metabolite hydrogen sulfide (H_2S), which plays an important role in systemic inflammation (12). OTUs in *Desulfovibrio* have been shown to have a strong correlation with systemic and chronic inflammation in models of mice fed a high-fat diet, suggesting that OTUs in *Desulfovibrio* might influence chronic inflammation in the host in a way that relates to weight gain and glucose tolerance (13). Several species included in *Roseburia* have been reported to serve an antiinflammatory function by producing butyrate, which is the main source of energy for colonic epithelial cells and which inhibits messenger RNA expression of proinflammatory cytokines in the mucosa by inhibiting NF-κB activation (14).

Several strengths of our study are noteworthy. This was a population-based study, and thus the findings may be generalizable to the entire Chinese population, among subjects with similar characteristics. This is supported by the prevalence of symptomatic hand OA in our study (5.2%), which was similar to that reported in other parts of China (15). In addition, our results provided novel evidence linking the gut microbiome composition to the prevalence of symptomatic hand OA. The significant associations of several genera with symptomatic hand OA parallel previous observations in inflammatory arthritis studies, supporting the validity of our findings. Furthermore, we demonstrated that several altered KEGG metabolism pathways were associated with symptomatic hand OA. This information may contribute to translational opportunities for the identification and treatment of individuals with symptomatic hand OA, and warrants further studies in independent populations.

There are several limitations of our study. First, the gut microbiomes were profiled by 16S rRNA gene sequencing. Although this technology can identify microbial taxonomies and composition, it has limitations in identifying genetically specific species and strains. Future studies using metagenomic approaches are needed to evaluate the relationship of a specific bacterial gene(s) and its function to symptomatic hand OA. Second, the current study was a cross-sectional study; thus, we could not assess the temporal sequence between the gut microbiome and occurrence of symptomatic hand OA. Third, the present results were not validated and reproduced in an independent cohort. Changes in specific microbiome genera may not be replicable in other populations, given the heterogeneity of the gut microbiome in different geographic locations. Finally, although the main findings

were shown to be similar in women with symptomatic hand OA, there may have been insufficient power to detect an association in sex-specific analyses due to the relatively small number of men in the study, particularly in terms of fully exploring the potential sex interaction between the gut microbiome and symptomatic hand OA; this warrants further study.

This large population-based study provides the first evidence that alterations in the gut microbiome composition are present in individuals with symptomatic hand OA, and a low relative abundance of *Roseburia* but high relative abundance of *Bilophila* and *Desulfovibrio* at the genus level were associated with prevalent symptomatic hand OA in this population. Our findings may help investigators understand the role of the microbiome in the development of symptomatic hand OA, and could contribute to potential translational opportunities.

ACKNOWLEDGMENTS

We thank Sally A. Doherty and Piran Aliabadi for their assistance with radiograph readings, and we acknowledge Yilun Wang, Jiatian Li, Xiaoxiao Li, Dongxing Xie, Jing Wu, Bei Xu, Jian Tian, Yuqing Wang, Zhenglei Zhu, Fan Wu, Ke He, Haochen Wang, Hongyi He, Xing Huang, Ning Wang, Ziying Wu, Hui Li, Xiang Ding, Bin Zhou, Ye Yang, Ruijun Bai, Zhichen Liu, Kun Li, Junyu Zhu, Xinjia Deng, Manli Chen, Li Zhang, Ying Pan, Zikun Xie, and Renpeng Fang for their contribution to this study.

AUTHOR CONTRIBUTIONS

All authors were involved in drafting the article or revising it critically for important intellectual content, and all authors approved the final version to be published. Drs. Lei and Zeng had full access to all of the data in the study and take responsibility for the integrity of the data and the accuracy of the data analysis.

Study conception and design. Wei, C. Zhang, Y. Zhang, W. Zhang, Doherty, Zeng, Lei.

Acquisition of data. Wei, Yang.

Analysis and interpretation of data. Wei, Y. Zhang, W. Zhang, Zhai, Obotiba, Lyu, Zeng.

REFERENCES

1. Marshall M, Watt FE, Vincent TL, Dziedzic K. Hand osteoarthritis: clinical phenotypes, molecular mechanisms and disease management [review]. Nat Rev Rheumatol 2018;14:641–56.
2. Michon M, Maheu E, Berenbaum F. Assessing health-related quality of life in hand osteoarthritis: a literature review. Ann Rheum Dis 2011;70:921–8.
3. Conaghan PG, Cook AD, Hamilton JA, Tak PP. Therapeutic options for targeting inflammatory osteoarthritis pain [review]. Nat Rev Rheumatol 2019;15:355–63.
4. Clemente JC, Manasson J, Scher JU. The role of the gut microbiome in systemic inflammatory disease [review]. BMJ 2018;360:j5145.
5. Zeng C, Wei J, Terkeltaub R, Yang T, Choi HK, Wang YL, et al. Dose-response relationship between lower serum magnesium level and higher prevalence of knee chondrocalcinosis. Arthritis Res Ther 2017;19:236.
6. Kellgren JH, Lawrence JS. Radiological assessment of osteo-arthrosis. Ann Rheum Dis 1957;16:494–502.
7. Snyder EA, Alvarez C, Golightly YM, Renner JB, Jordan JM, Nelson AE. Incidence and progression of hand osteoarthritis in a large community-based cohort: the Johnston County Osteoarthritis Project. Osteoarthritis Cartilage 2020;28:446–52.
8. Forbes JD, Chen CY, Knox NC, Marrie RA, El-Gabalawy H, de Kievit T, et al. A comparative study of the gut microbiota in immune-mediated inflammatory diseases—does a common dysbiosis exist? Microbiome 2018;6:221.
9. Fu BC, Hullar MA, Randolph TW, Franke AA, Monroe KR, Cheng I, et al. Associations of plasma trimethylamine N-oxide, choline, carnitine, and betaine with inflammatory and cardiometabolic risk biomarkers and the fecal microbiome in the Multiethnic Cohort Adiposity Phenotype Study. Am J Clin Nutr 2020;111:1226–34.
10. Zhai G, Randell EW, Rahman P. Metabolomics of osteoarthritis: emerging novel markers and their potential clinical utility. Rheumatology (Oxford) 2018;57:2087–95.
11. Natividad JM, Lamas B, Pham HP, Michel ML, Rainteau D, Bridonneau C, et al. Bilophila wadsworthia aggravates high fat diet induced metabolic dysfunctions in mice. Nat Commun 2018;9:2802.
12. Peck SC, Denger K, Burrichter A, Irwin SM, Balskus EP, Schleheck D. A glycyl radical enzyme enables hydrogen sulfide production by the human intestinal bacterium Bilophila wadsworthia. Proc Natl Acad Sci U S A 2019;116:3171–6.
13. Zhang C, Zhang M, Pang X, Zhao Y, Wang L, Zhao L. Structural resilience of the gut microbiota in adult mice under high-fat dietary perturbations. ISME J 2012;6:1848–57.
14. Tamanai-Shacoori Z, Smida I, Bousarghin L, Loreal O, Meuric V, Fong SB, et al. Roseburia spp.: a marker of health? [review]. Future Microbiol 2017;12:157–70.
15. Zhang Y, Xu L, Nevitt MC, Niu J, Goggins JP, Aliabadi P, et al. Lower prevalence of hand osteoarthritis among Chinese subjects in Beijing compared with white subjects in the United States: the Beijing Osteoarthritis Study. Arthritis Rheum 2003;48:1034–40.

Arthritis & Rheumatology
Vol. 73, No. 9, September 2021, pp 1663–1672
DOI 10.1002/art.41716

American College of Rheumatology
Empowering Rheumatology Professionals

Withdrawing Ixekizumab in Patients With Psoriatic Arthritis Who Achieved Minimal Disease Activity: Results From a Randomized, Double-Blind Withdrawal Study

Laura C. Coates,[1] Sreekumar G. Pillai,[2] Hasan Tahir,[3] Ivo Valter,[4] Vinod Chandran,[5] Hideto Kameda,[6] Masato Okada,[7] Lisa Kerr,[2] Denise Alves,[2] So Young Park,[2] David H. Adams,[2] Gaia Gallo,[2] Matthew M. Hufford,[2] Maja Hojnik,[2] Philip J. Mease,[8] and Arthur Kavanaugh,[9] for the SPIRIT-P3 Study Group

Objective. To evaluate the effect of withdrawing ixekizumab in patients with psoriatic arthritis (PsA) in whom minimal disease activity (MDA) has been achieved after open-label ixekizumab treatment.

Methods. SPIRIT-P3 was a multicenter, randomized, double-blind withdrawal study of biologic treatment–naive adult patients with PsA who were treated with open-label ixekizumab for 36 weeks (160 mg at week 0, then 80 mg every 2 weeks). Patients in whom MDA was sustained for >3 consecutive months were randomized 1:1, between weeks 36 and 64, to undergo blinded withdrawal of ixekizumab treatment (placebo) or to continue ixekizumab treatment every 2 weeks up to week 104. The primary efficacy end point was time to relapse (loss of MDA) for randomized patients. Patients who experienced a relapse were re-treated with ixekizumab every 2 weeks up to week 104.

Results. A total of 394 patients were enrolled and received open-label ixekizumab every 2 weeks. Of those patients, 158 (40%) achieved sustained MDA and were randomized to undergo withdrawal of ixekizumab treatment (placebo every 2 weeks; n = 79) or to continue ixekizumab treatment every 2 weeks (n = 79). Disease relapse occurred more rapidly with treatment withdrawal (median 22.3 weeks [95% confidence interval (95% CI) 16.1–28.3]) compared to those who continued treatment with ixekizumab (median not estimable; $P < 0.0001$). Sixty-seven patients (85%) compared to 30 patients (38%) experienced relapse in the placebo group and the continued treatment group, respectively. Median time to achieving MDA again with re-treatment was 4.1 weeks (95% CI 4.1–4.3); in 64 of 67 patients (96%) who experienced relapse with treatment withdrawal, MDA was achieved again with re-treatment. Safety was consistent with the known safety profile for ixekizumab.

Conclusion. Continued ixekizumab therapy is superior to ixekizumab withdrawal in maintaining low disease activity in biologic treatment–naive patients with PsA. Re-treatment with ixekizumab following a relapse may restore disease control in cases of treatment interruption.

ClinicalTrials.gov identifier: NCT02584855.
Supported by Eli Lilly and Company.

[1]Laura C. Coates, MD: University of Oxford, Nuffield Department of Orthopaedics, Rheumatology and Musculoskeletal Sciences and Oxford University Hospitals NHS Foundation Trust, NIHR Oxford Biomedical Research Centre, Oxford, UK; [2]Sreekumar G. Pillai, PhD, Lisa Kerr, MSPH, Denise Alves, BPharm, So Young Park, PhD, David H. Adams, PhD, Gaia Gallo, MD, Matthew M. Hufford, PhD, Maja Hojnik, MD: Eli Lilly and Company, Indianapolis, Indiana; [3]Hasan Tahir, MD: Royal Free London NHS Trust and University College London, Division of Medicine, London, UK; [4]Ivo Valter, MD: Center for Clinical and Basic Research, Tallinn, Estonia; [5]Vinod Chandran, MD: University of Toronto and Krembil Research Institute, University Health Network, Toronto, Ontario, Canada, and Memorial University of Newfoundland, St. John's, Newfoundland, Canada; [6]Hideto Kameda, MD: Toho University, Tokyo, Japan; [7]Masato Okada, MD: Immuno-Rheumatology Center, St. Luke's International Hospital, Tokyo, Japan; [8]Philip J. Mease, MD: Swedish Medical Center/Providence St. Joseph Health and University of Washington, Seattle; [9]Arthur Kavanaugh, MD: University of California San Diego.

Dr. Coates has received consulting fees, speaking fees, and/or honoraria from AbbVie, Amgen, Biogen, Boehringer Ingelheim, Celgene, Gilead, Janssen, Eli Lilly and Company, Medac, Pfizer, and UCB (less than $10,000 each) and from Novartis (more than $10,000). Dr. Pillai, Ms Kerr, Ms Alves, and Drs. Park, Adams, Gallo, Hufford, and Hojnik are employees of Eli Lilly and Company and own stock or stock options in Eli Lilly and Company. Dr. Tahir has received speaking fees and contributed to advisory boards for Novartis, AbbVie, Eli Lilly and Company, and Gilead (less than $10,000 each). Dr. Chandran has received consulting fees, speaking fees, and/or honoraria from AbbVie, Amgen, Bristol Myers Squibb, Celgene, Eli Lilly and Company, Janssen, Novartis, Pfizer, and UCB (less than $10,000 each) and has a spouse who is an employee of Eli Lilly and Company. Dr. Kameda has received consulting fees, speaking fees, and/or honoraria from AbbVie, Astellas, Bristol Myers Squibb, Chugai, Eisai, Gilead, Janssen, Novartis, Pfizer, and UCB (less than $10,000 each) and from Asahi Kasei, Eli Lilly and Company, and Mitsubishi Tanabe (more than $10,000 each) and has received research support from AbbVie, Asahi Kasei, Astellas, Chugai, Eisai, Mitsubishi Tanabe, and Novartis. Dr. Okada has received consulting fees, speaking fees, and/or honoraria from Eli Lilly and Company (less than $10,000). Dr. Mease has received consulting fees, speaking fees, and/or honoraria from Amgen, Bristol Myers Squibb, Boehringer Ingelheim, Celgene, Galápagos, Genentech, Gilead, GlaxoSmithKline, Sun, and UCB (less than $10,000 each) and from AbbVie, Janssen, Eli Lilly and Company, Novartis, and Pfizer (more than $10,000 each). Dr. Kavanaugh has received consulting fees, speaking fees, and/or honoraria from Eli Lilly and Company, Novartis, Pfizer, Amgen, and

INTRODUCTION

Psoriatic arthritis (PsA) is a chronic, heterogeneous, inflammatory disease that may lead to serious disability if not appropriately treated (1–3). There are a number of disease-modifying antirheumatic drugs (DMARDs) available to patients with PsA, including conventional synthetic DMARDs (csDMARDs) and biologic DMARDs (bDMARDs) (4,5). These treatments can help patients achieve low disease activity or remission across the manifestations of PsA; however, it is unclear whether patients with long-term low disease activity or remission need to continue treatment to maintain this outcome. Dose tapering or treatment discontinuation may potentially be cost effective and could limit potential side effects associated with PsA treatments. Data on treatment withdrawal in PsA are limited and inconsistent, with a few small observational, uncontrolled studies available (6–10). These studies used various outcome measures to evaluate the effect of bDMARD treatment withdrawal (8,10) or to compare csDMARD and bDMARD withdrawal (6,7,9), or analyzed patients from a PsA registry (10), indicating that further assessment in a large, controlled withdrawal trial is warranted.

Ixekizumab, a high-affinity monoclonal antibody that selectively targets interleukin-17A (IL-17A) (11), has been demonstrated to improve the signs and symptoms of active PsA in 2 phase III trials with long-term extensions (SPIRIT-P1 [12–14] and SPIRIT-P2 [15–17]). The present study, SPIRIT-P3, is the first large, multicenter, randomized, double-blind, placebo-controlled withdrawal study in patients with PsA. The study evaluated the efficacy and safety of withdrawing ixekizumab treatment versus continued ixekizumab treatment in patients who had achieved stable minimal disease activity (MDA) (18) while receiving ixekizumab therapy, and the impact of re-treatment after relapse.

PATIENTS AND METHODS

Trial design. SPIRIT-P3 (ClinicalTrials.gov identifier NCT02584855; European Union Clinical Trials Register identifier 2015-002433-22) was a phase III, multicenter study with an initial open-label treatment period, followed by a randomized double-blind withdrawal period (Figure 1). The study was conducted at 86 sites in 12 countries (for a list of investigators, see Appendix A). During the initial 36-week open-label treatment period, all patients received a starting dose of 160 mg ixekizumab at week 0, followed by 80 mg ixekizumab every 2 weeks to week 36. Between weeks 36 and 64, patients who exhibited sustained MDA for ≥4 visits over 3 consecutive months were eligible for 1:1 blinded randomization to continue receiving ixekizumab every 2 weeks or to undergo ixekizumab withdrawal every 2 weeks (placebo) up to week 104. Patients whose disease relapsed following ixekizumab withdrawal (i.e., no longer meeting MDA criteria) (see below) received ixekizumab every 2 weeks in a blinded manner until week 104. Patients who did not meet randomization criteria by week 64 continued receiving open-label ixekizumab every 2 weeks uninterrupted up to week 104. Patients were discontinued from the study if ≥20% improvement in tender joint counts (TJCs) and swollen joint counts (SJCs) had not been achieved at week 24 or at any subsequent visit through week 104, except from the point of randomization until the visit following relapse in patients during the randomized withdrawal period.

All patients provided written informed consent before any study assessments, examinations, or procedures were performed. The study was approved by the ethical or institutional review boards at each participating study site and was conducted in accordance with the Declaration of Helsinki, the Council for International Organizations of Medical Sciences, the International Conference on Harmonisation Guidelines for Good Clinical Practice, and applicable laws and regulations.

Trial participants. SPIRIT-P3 enrolled adults age ≥18 years with a confirmed diagnosis of active PsA for ≥6 months and who fulfilled the criteria of the Classification of Psoriatic Arthritis Study Group (19). Active PsA was defined as the presence of ≥3 of 68 tender joints and ≥3 of 66 swollen joints at screening and baseline. Patients were required to have documented inadequate response or intolerance to ≥1 csDMARDs and active psoriatic skin lesions or a documented history of plaque psoriasis. Exclusion criteria included current use of >1 csDMARD, current or prior use of bDMARDs or small-molecule agents for treatment of psoriasis or PsA, active Crohn's disease or ulcerative colitis, or active uveitis.

During the initial open-label treatment period, alteration of csDMARD dosage and/or introduction of a new csDMARD were permitted. During the randomized withdrawal period, alteration of the csDMARD dosage and/or introduction of a new csDMARD in patients who were randomized was not permitted until the point of relapse. Patients who were not randomized could continue alteration of csDMARD dosage and/or introduction of a new csDMARD throughout the randomized withdrawal period.

Randomization and blinding. During the randomized withdrawal period, randomized treatment was assigned to eligible patients using an interactive web-response system. Patients who met the criteria for randomized withdrawal were assigned in a 1:1 ratio (stratified by geographic region and csDMARD use at the

AbbVie (less than $10,000 each). No other disclosures relevant to this article were reported.

Address correspondence to Laura C. Coates, MD, University of Oxford, Botnar Research Centre, Nuffield Department of Orthopaedics, Rheumatology and Musculoskeletal Sciences, Windmill Road, Oxford OX3 7LD, UK. Email: laura.coates@ndorms.ox.ac.uk.

Submitted for publication June 16, 2020; accepted in revised form February 25, 2021.

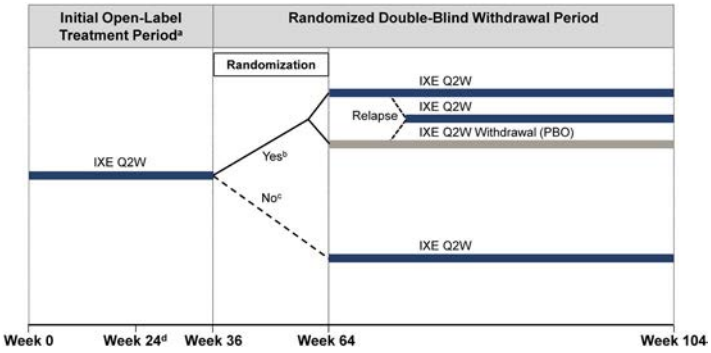

Figure 1. SPIRIT-P3 study design. [a] Encompassed week 0 (study baseline) up to week 36. [b] Between weeks 36 and 64 (inclusive), patients treated with ixekizumab (IXE) every 2 weeks (Q2W) in whom minimal disease activity (MDA) was achieved for 4 consecutive visits for at least 36 weeks were eligible for randomization at the visit at which these criteria were met. Patients were randomized 1:1 to the ixekizumab every 2 weeks group or the ixekizumab withdrawal group. Patients remained in their treatment groups up to week 104 or until relapse (no longer met MDA), at which point they received ixekizumab every 2 weeks up to week 104. [c] Patients who did not meet the randomization eligibility criteria by week 64 continued to receive ixekizumab every 2 weeks uninterrupted up to week 104. [d] Patients in whom ≥20% improvement in tender joint count and swollen joint count at week 24 or at any subsequent visit through week 104, except from the point of randomization until the visit after relapse for patients in the randomized double-blind withdrawal period, were discontinued from the study. PBO = placebo.

time of randomization) to receive blinded ixekizumab treatment every 2 weeks (1 80-mg subcutaneous injection or matching placebo every 2 weeks) from week 36 to week 104. Patients, study site personnel, and investigators remained blinded with regard to treatment assignment and dosage adjustments throughout the randomized withdrawal period from week 36 to week 104.

Procedures. Following open-label treatment with ixekizumab every 2 weeks, MDA was used to establish eligibility for entry into the randomized withdrawal period. Patients were assessed for MDA at each post-baseline visit, starting at week 2. MDA was considered to have been achieved if at least 5 of the following 7 disease activity measures were met: TJC ≤1, SJC ≤1, Psoriasis Area and Severity Index (PASI) (20) total score ≤1 or body surface area (BSA) affected by psoriasis ≤3%, patient pain visual analog scale (VAS) score ≤15 (of a maximum possible 100), patient global assessment of disease activity (PtGA) VAS score ≤20 (of a maximum possible 100), Health Assessment Questionnaire (HAQ) disability index (DI) (21) score ≤0.5, and number of tender entheseal points ≤1 (18). Patients in whom sustained MDA was exhibited at ≥4 visits over 3 consecutive months qualified for randomization to either continue ixekizumab treatment every 2 weeks or undergo withdrawal of ixekizumab treatment (placebo). The first opportunity for randomization at week 36 was based on 3 months of sustained MDA from week 24. Patients were considered to have experienced a relapse if their status could no longer be classified as MDA (i.e., <5 of 7 of the above criteria were met) at any point in the randomized withdrawal period up to week 104.

Efficacy and safety assessments. The primary efficacy end point was time to relapse (loss of MDA) during the randomized withdrawal period. Secondary efficacy end points included the cumulative relapse rate and time to loss of response for each individual MDA component. Median time to regain MDA and sustained MDA was evaluated in patients who experienced a relapse and were re-treated with ixekizumab every 2 weeks during the randomized withdrawal period. Post hoc efficacy analyses were performed for patients who experienced a relapse during the randomized withdrawal period, and were conducted to assess the number of MDA components lost at the time of relapse and to evaluate relapse rates in patients in whom very low disease activity (VLDA) was achieved (7 of 7 disease activity measures met) (22) and in patients in whom MDA was achieved but VLDA was not achieved. Safety assessments included treatment-emergent adverse events, serious adverse events, and adverse events of special interest.

Statistical analysis. Sample size was determined using the assumption that of ~400 patients who entered the initial open-label treatment period, 136 patients (34%) would meet the criteria for sustained MDA and qualify for entry into the randomized withdrawal period (68 per treatment group). It was further assumed that ~60% and ~20% of patients in the ixekizumab withdrawal group and the continued ixekizumab treatment every 2 weeks group, respectively, would experience a relapse by no longer meeting the MDA criteria. According to these assumptions, 39 patients were needed to meet relapse criteria in the combined treatment groups in order to achieve 95% power to test the superiority of ixekizumab treatment compared to withdrawal of ixekizumab treatment (placebo) for time to relapse with a 2-sided α significance level of 0.05.

The open-label population was defined as all patients who received at least 1 dose of open-label ixekizumab every 2 weeks during the open-label treatment period. The randomized withdrawal intent-to-treat (ITT) population included all randomized patients (those who achieved sustained MDA and 3 patients

Table 1. Demographic and baseline clinical characteristics of patients in the SPIRIT-P3 study*

	Open-label population (ixekizumab every 2 weeks) (n = 394)	Randomized withdrawal ITT population	
		Ixekizumab withdrawal (n = 79)	Ixekizumab every 2 weeks (n = 79)
Age, years	47 ± 11.4	43 ± 10.5	44 ± 10.8
Male, no. (%)	182 (46)	40 (51)	47 (60)
BMI, kg/m^2	29 ± 6.3	29 ± 7.2	28 ± 5.0
Time since PsA onset, years	7.9 ± 7.1	7.5 ± 7.5	7.1 ± 6.3
Current csDMARD use, no. (%)†	291 (74)	60 (76)	59 (75)
TJC, 68 joints	21 ± 14.3	16 ± 12.3	17 ± 11.5
SJC, 66 joints	10 ± 8.1	9.0 ± 5.6	9.4 ± 7.4
HAQ DI total score	1.2 ± 0.6	1.0 ± 0.5	1.1 ± 0.6
Pain VAS score (maximum possible 100)	61 ± 18.0	59 ± 18.9	60 ± 19.4
PtGA score (maximum possible 100)	62 ± 18.9	61 ± 19.5	59 ± 18.3
PASI total score‡	7.1 ± 9.5	7.6 ± 10.2	8.4 ± 8.2
BSA, %§	14 ± 17.6	14 ± 17.8	17 ± 18.2
LEI score >0, no. (%)	276 (70.1)	47 (59.5)	48 (60.8)
LEI total score¶	2.6 ± 1.5	2.5 ± 1.3	2.4 ± 1.3
Enthesitis SPARCC score >0, no. (%)	330 (83.8)	57 (72.2)	62 (78.5)
Enthesitis SPARCC score#	5.3 ± 3.7	4.4 ± 3.3	4.6 ± 3.1

* Except where indicated otherwise, values are the mean ± SD. ITT = intent-to-treat; BMI = body mass index; PsA = psoriatic arthritis; TJC = tender joint count; SJC = swollen joint count; HAQ DI = Health Assessment Questionnaire disability index; VAS = visual analog scale; PtGA = patient global assessment of disease activity.
† Current use of conventional synthetic disease-modifying antirheumatic drugs (csDMARDs) (methotrexate, sulfasalazine, leflunomide, hydroxychloroquine, or cyclosporine) reported in open-label population and at time of randomization.
‡ In patients with a baseline Psoriasis Area and Severity Index (PASI) >0.
§ In patients whose percentage of body surface area (BSA) affected by psoriasis was >0 at baseline.
¶ In patients with a baseline Leeds Enthesitis Index (LEI) >0.
# Based on 16-point entheseal point assessment in patients with a baseline Spondyloarthritis Research Consortium of Canada (SPARCC) enthesitis score >0.

who did not achieve sustained MDA who were inadvertently randomized). Patients in the randomized withdrawal ITT population were analyzed according to their treatment assignment (withdrawal of ixekizumab treatment [placebo] or continued ixekizumab treatment every 2 weeks). The relapse population was defined as all randomized patients who experienced relapse (i.e., no longer meeting MDA criteria) after randomization and received at least 1 dose of ixekizumab every 2 weeks after experiencing relapse.

The primary efficacy end point was time to relapse (loss of MDA) during the randomized withdrawal period for the randomized withdrawal ITT population. The Kaplan-Meier product limit method was used to estimate survival curves for time to variables. Treatment comparisons were performed using a log-rank test, with adjustment for geographic region and csDMARD use at the time of randomization. *P* values less than 0.05 were considered statistically significant. Time to relapse in weeks was defined as follows: ([date of relapse – date of first injection of randomized dose of study treatment in the randomized double-blind withdrawal period] + 1)/7. Patients completing the withdrawal period without meeting relapse criteria were censored at the date of completion (the date of the last scheduled visit in the withdrawal period). Patients without a date of completion or discontinuation were censored at the latest nonmissing date from the following dates: date of last injection of study treatment in the withdrawal period and date of last attended visit in the withdrawal period.

Cumulative proportion of relapse was analyzed using a logistic regression model, with treatment, geographic region, and csDMARD use at the time of randomization as factors. Since the first opportunity for randomization at week 36 was based on 3 months of sustained MDA from week 24 in a 104-week study, the cumulative proportion of relapse was analyzed up to the first 40 weeks of the randomized withdrawal period.

Safety data are presented for the randomized withdrawal ITT population and for the all-ixekizumab combined safety population, which comprised all patients who received at least 1 dose of ixekizumab during the study.

RESULTS

Patient disposition and baseline characteristics. Between November 18, 2015 and October 30, 2018, 511 patients were screened, of whom 100 (20%) did not pass the screening (see Supplementary Figure 1, available on the *Arthritis & Rheumatology* website at http://onlinelibrary.wiley.com/doi/10.1002/art.41716/abstract). Three hundred ninety-four patients were enrolled in the study and treated with open-label ixekizumab every 2 weeks. By week 36, 291 patients (74%) completed the open-label treatment period, and 103 patients (26%) discontinued the study. The main reason for discontinuation was lack of efficacy. Sustained MDA was achieved in a total of 158 of 394 patients (40%), and they

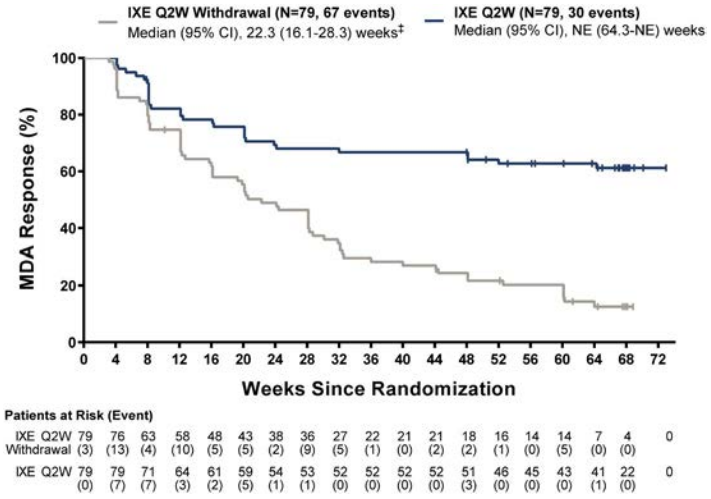

Figure 2. Time to relapse (loss of MDA) in the randomized withdrawal intent-to-treat population. ‡$P < 0.0001$ versus ixekizumab withdrawal. 95% CI = 95% confidence interval; NE = not estimable (see Figure 1 for other definitions).

qualified for double-blind randomization (79 patients were randomized to the withdrawal of ixekizumab group [placebo] and 79 were randomized to the continued ixekizumab treatment every 2 weeks group). Sustained MDA was not achieved in a total of 133 of the 394 patients (34%). These patients were not randomized and continued receiving open-label ixekizumab treatment every 2 weeks (Supplementary Figure 1, http://onlinelibrary.wiley.com/doi/10.1002/art.41716/abstract).

Patients enrolled in the open-label study had symptoms of PsA for an average of 8 years. The mean age of these patients was 47 years, and 54% were women. The majority of patients were taking concomitant csDMARDs (most commonly methotrexate) and had high disease activity at baseline, with a mean TJC of 21 and a mean SJC of 10; 70% and 84% had enthesitis according to the Leeds Enthesitis Index (23) and Spondyloarthritis Research Consortium of Canada index, respectively (24) (Table 1). In the randomized withdrawal ITT population, a higher proportion of the patients were male, and disease activity was numerically lower, compared to the open-label population. Within the randomized withdrawal ITT population, baseline demographic and disease characteristics were generally well balanced between the withdrawal of ixekizumab treatment group and the continued ixekizumab treatment every 2 weeks group (Table 1).

Clinical end points. Patients experienced relapse (lost MDA) more rapidly with treatment withdrawal compared to continued ixekizumab treatment every 2 weeks ($P < 0.0001$) (Figure 2). The median time to relapse for patients in the withdrawal of ixekizumab treatment group was 22.3 weeks (95% confidence interval [95% CI] 16.1–28.3), while the median time to relapse for patients in the continued ixekizumab treatment group was not estimable, as <50% of patients experienced relapse by the end of the study

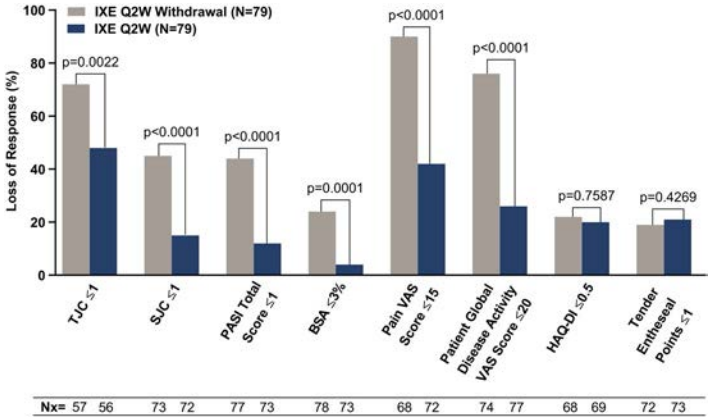

Figure 3. Loss of response for individual components of MDA in the randomized withdrawal intent-to-treat population. *P* values were determined by adjusted log rank test after stratification by geographic region and use of conventional synthetic disease-modifying antirheumatic drugs. TJC = tender joint count; SJC = swollen joint count; PASI = Psoriasis Area and Severity Index; BSA = body surface area affected by psoriasis; VAS = visual analog scale; HAQ DI = Health Assessment Questionnaire disability index; Nx = the number of patients who met the MDA component at randomization and subsequently lost the response (see Figure 1 for other definitions).

period. The cumulative relapse rate in the first 40 weeks of the randomized withdrawal period was significantly higher in the treatment withdrawal group (58 of 79 patients [73%]) compared to the continued ixekizumab treatment every 2 weeks group (27 of 79 patients [34%]) ($P < 0.0001$). The cumulative relapse rate from week 24 to week 104 was also significantly higher in the treatment withdrawal group (67 of 79 patients [85%]) compared to the continued ixekizumab treatment every 2 weeks group (30 of 79 patients [38%]) ($P < 0.0001$).

For individual components of MDA, relapse occurred more frequently and time to relapse was significantly shorter in patients in the treatment withdrawal group compared to those in the continued ixekizumab treatment every 2 weeks group among patients who met the MDA component at randomization. A total of 72% of patients lost TJC ≤1 (at a median of 22.3 weeks) in the treatment withdrawal group compared to 48% (at a median of 64.3 weeks) in the continued ixekizumab treatment group ($P = 0.0022$); 45% of patients lost SJC ≤1 (at a median of 28.7 weeks) in the treatment withdrawal group compared to 15% in the continued ixekizumab treatment group (median not estimable) ($P < 0.0001$); 44% of patients lost PASI total score ≤1 (at a median of 36.0 weeks) in the treatment withdrawal group compared to 12% in the continued ixekizumab treatment group (median not estimable) ($P < 0.0001$); 24% of patients lost BSA ≤3% in the treatment withdrawal group compared to 4% in the continued ixekizumab treatment group (medians not estimable) ($P = 0.0001$); 90% of patients lost patient pain VAS score ≤15 (at a median of 16.1 weeks) in the treatment withdrawal group compared to 42% in the continued ixekizumab treatment group (median not estimable) ($P < 0.0001$); and 76% of patients lost PtGA VAS score ≤20 (at a median of 20.6 weeks) in the treatment withdrawal group compared to 26% in the continued ixekizumab treatment group (median not estimable) ($P < 0.0001$). For loss of the HAQ DI and enthesitis components of the MDA criteria, the differences between treatment groups were not significant (Figure 3). Kaplan-Meier curves of time to loss of all individual components are shown in Supplementary Figures 2–9, on the *Arthritis & Rheumatology* website at http://onlinelibrary.wiley.com/doi/10.1002/art.41716/abstract.

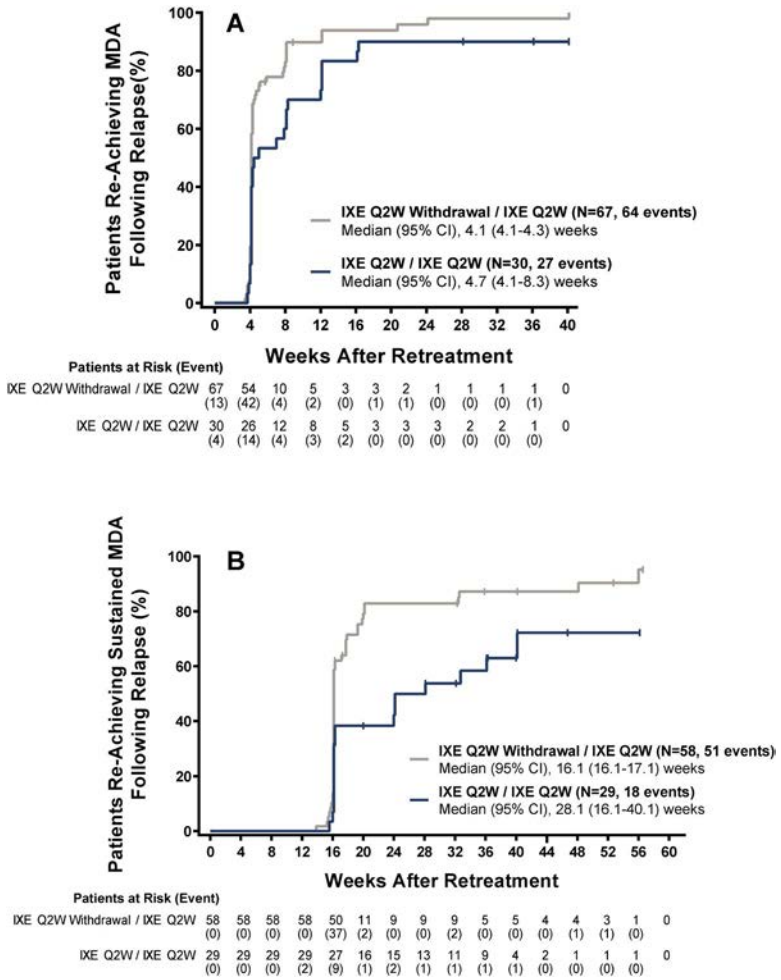

Figure 4. Time to reachievement of MDA following relapse (**A**) or reachievement of sustained MDA (≥4 visits over 3 consecutive months) following relapse (**B**). Week 0 represents re-treatment. Data were available through week 40 in **A** and through week 60 in **B**. 95% CI = 95% confidence interval (see Figure 1 for other definitions).

Median time to reachievement of MDA on re-treatment following relapse was 4.1 weeks (95% CI 4.1–4.3) in the ixekizumab withdrawal/ixekizumab re-treatment group and 4.7 weeks (95% CI 4.1–8.3) in the continued ixekizumab/ixekizumab re-treatment group, with week 0 representing the start of re-treatment (Figure 4A). MDA was reachieved during the re-treatment period in 64 of 67 patients (95.5%) in the ixekizumab withdrawal/ixekizumab re-treatment group and 27 of 30 patients (90.0%) in the continued ixekizumab/ixekizumab re-treatment group.

Median time to reachievement of sustained MDA (≥4 visits over 3 consecutive months) on re-treatment following relapse was 16.1 weeks (95% CI 16.1–17.1) in the ixekizumab withdrawal/ixekizumab re-treatment group and 28.1 weeks (95% CI 16.1–40.1) in the continued ixekizumab/ixekizumab re-treatment group, with week 0 representing the start of re-treatment (Figure 4B). Sustained MDA was reachieved during the re-treatment period in 51 of 58 patients (87.9%) in the ixekizumab withdrawal/ixekizumab re-treatment group and 18 of 29 patients (62.1%) in the continued ixekizumab/ixekizumab re-treatment group.

In the post hoc analysis of the randomized withdrawal ITT population, the proportion of patients in whom VLDA was achieved (7 of 7 disease activity measures met) was similar in the 2 treatment groups at the time of randomization (see Supplementary Figure 10, available on the *Arthritis & Rheumatology* website at http://onlinelibrary.wiley.com/doi/10.1002/art.41716/abstract). Of the 37 patients in whom VLDA had been achieved at randomization, 30 (81%) experienced a relapse (lost MDA) during the randomized withdrawal period; MDA was maintained in the other 7 patients. Of the 40 patients in the continued ixekizumab treatment every 2 weeks group in whom VLDA had been achieved at randomization, 10 (25%) experienced a relapse (lost MDA) during the randomized withdrawal period, and MDA was maintained in 30 patients.

In the same post hoc analysis, of the 40 patients in the treatment withdrawal group in whom MDA had been achieved but VLDA had not been achieved at randomization, 36 patients (90%) experienced a relapse during the randomized withdrawal period, and MDA was maintained in 4 patients (Supplementary Figure 10, http://onlinelibrary.wiley.com/doi/10.1002/art.41716/abstract).

Table 2. Safety results in patients in the SPIRIT-P3 study*

		Randomized withdrawal ITT population‡	
	All-ixekizumab combined (every 2 weeks) (n = 394)†	Ixekizumab withdrawal (n = 79)	Ixekizumab every 2 weeks (n = 79)
Exposure, no. of person-years	631.1	42.1	71.0
TEAEs	325 (82.5)	40 (50.6)	40 (50.6)
Mild	156 (39.6)	30 (38.0)	24 (30.4)
Moderate	144 (36.5)	9 (11.4)	14 (17.7)
Severe	25 (6.3)	1 (1.3)	2 (2.5)
Serious AE	28 (7.1)	2 (2.5)	1 (1.3)
Discontinuations due to AE	21 (5.3)	1 (1.3)	0 (0)
Deaths	2 (0.5)	0 (0)	0 (0)
Most frequent TEAEs§			
Nasopharyngitis	70 (17.8)	4 (5.1)	11 (13.9)
Upper respiratory tract infection	65 (16.5)	4 (5.1)	9 (11.4)
Injection site reaction	62 (15.7)	0 (0)	1 (1.3)
Bronchitis	34 (8.6)	1 (1.3)	4 (5.1)
Urinary tract infection	21 (5.3)	3 (3.8)	1 (1.3)
Sinusitis	20 (5.1)	1 (1.3)	0 (0)
AEs of special interest¶			
Infections	243 (61.7)	20 (25.3)	29 (36.7)
Serious infections	5 (1.3)	1 (1.3)	0 (0)
Injection site reactions	80 (20.3)	0 (0)	2 (2.5)
Hepatic events	37 (9.4)	3 (3.8)	6 (7.6)
Allergic reactions/hypersensitivity events#	25 (6.3)	0 (0)	3 (3.8)
Cytopenias	21 (5.3)	1 (1.3)	5 (6.3)
Depression	13 (3.3)	0 (0)	0 (0)
Cerebrocardiovascular events**	3 (0.8)	0 (0)	0 (0)
Malignancies	2 (0.5)	0 (0)	0 (0)
Inflammatory bowel disease**	1 (0.3)††	0 (0)	0 (0)

* Except where indicated otherwise, values are the number (%). ITT = intent-to-treat; TEAEs = treatment-emergent adverse events.
† Patients who had at least 1 dose of ixekizumab.
‡ Randomization to relapse or week 104.
§ Defined as >5% of TEAEs reported in the all-ixekizumab combined group.
¶ Reported as AEs according to the high-level term in Medical Dictionary for Regulatory Activities, v.21.1. Groups of AEs of special interest are shown. No events of interstitial lung disease were reported in any group.
# No allergic reactions/hypersensitivity events were anaphylaxis events.
** Adjudicated event.
†† Crohn's disease.

Of the 38 patients in the continued ixekizumab treatment group in whom MDA had been achieved but VLDA had not been achieved at randomization, 19 patients (50%) experienced a relapse during the randomized withdrawal period, and MDA was maintained in 19 patients.

Safety. Overall, safety data were consistent with the data obtained in previous studies regarding PsA treated with ixekizumab, with no unexpected safety signals (Table 2). Two deaths (0.5%) occurred during the open-label treatment period. One patient died due to an accidental drowning, which was not considered to be related to the study drug. The other patient died of pneumonia, which the investigator considered to be related to the study drug. One case of inflammatory bowel disease (0.3%) (adjudicated as Crohn's disease) was reported during the open-label treatment period. The patient had a previous history of irritable bowel syndrome, and the event resulted in study discontinuation.

DISCUSSION

In the SPIRIT-P3 study of biologic treatment–naive patients with active PsA in whom sustained MDA was achieved with open-label ixekizumab treatment every 2 weeks, continued ixekizumab therapy was superior to withdrawal in maintaining MDA. Ixekizumab withdrawal resulted in significantly earlier relapse and a higher proportion of patients experiencing a relapse compared to continued treatment. Further, ixekizumab withdrawal, compared to continued treatment, was associated with more and earlier relapses in the majority of individual components of MDA. Importantly, retreatment with ixekizumab resulted in a rapid return to MDA for the vast majority of patients who experienced a relapse following ixekizumab withdrawal. Overall safety findings were consistent with those observed in previous ixekizumab PsA studies (25).

The attainment of remission or, alternatively, a low disease activity status is a treatment goal in chronic inflammatory diseases, including PsA. MDA is a recommended and clinically relevant treat-to-target outcome in PsA (26), and is also increasingly being used as an end point in clinical trials due to its capacity to discriminate between different treatments (27). We used sustained achievement of MDA as a strict criterion to randomize patients and loss of MDA as the criterion for relapse.

In SPIRIT-P3, 73% of the patients in whom sustained MDA was achieved experienced a relapse in the first 40 weeks when ixekizumab treatment was withdrawn, while only 34% of the patients in the continued treatment group experienced a relapse. Relapse started as early as 4 weeks after ixekizumab withdrawal, which was the first time point of assessment after randomization. Treatment withdrawal impacted multiple components of MDA in PsA. TJC, PtGA, and pain scores were the most frequently lost components with ixekizumab withdrawal. In a smaller randomized withdrawal study in patients with PsA who experienced a relapse following discontinuation of tumor necrosis factor inhibitor (TNFi) therapy (6), PtGA and pain scores similarly worsened (10 of 12 treated). These observations imply that patient-reported outcomes are important indicators to assess fluctuations in disease activity, along with objective measures of disease activity such as SJC or skin scores.

Of note in the SPIRIT-P3 study, significantly more patients experienced a reemergence of psoriasis with treatment withdrawal compared to those who continued ixekizumab treatment. When re-treatment with ixekizumab every 2 weeks was instituted after a relapse, MDA was regained in 96% of patients in the ixekizumab withdrawal group. In many patients, MDA was regained as early as 4 weeks, which was the first time point of assessment after retreatment. Of the 30 patients assigned to the continued treatment group who lost MDA and continued to receive ixekizumab every 2 weeks, 27 patients (90%) regained MDA, and the median time to regain MDA was 4.7 weeks. The loss of MDA with continued ixekizumab treatment may partially be due to a nocebo effect, or reflective of temporal fluctuation in the signs and symptoms of the disease, which is supported by the rapid restoration of MDA even though the actual treatment was not changed. A small proportion of patients in the ixekizumab withdrawal group (12 of 79 [15%]) did not experience a relapse during the randomized withdrawal period. These patients represent drug-free remission, and elucidation of the characteristics of those patients in whom long-term remission was achieved with drug withdrawal will be of much value in clinical practice; however, the number of these patients was small, and the duration of follow-up in this study up to 104 weeks may not be long enough to reliably determine true long-term, drug-free remission status.

To date, SPIRIT-P3 is the first large, multicenter, randomized, double-blind withdrawal trial in PsA. There have been a few previous uncontrolled observational and open-label studies investigating the possibility of continued PsA remission/low disease activity following csDMARD and/or bDMARD withdrawal (6–10). These studies differed in patient population and in definition of remission/low disease activity and flare, and yielded conflicting results.

Two small studies (n = 26 and n = 17) (6,7) showed that disease control was quickly lost in the vast majority of patients with PsA after discontinuation of csDMARD or bDMARD treatment, while 2 somewhat larger studies (n = 47 and n = 236) (8,9) showed that up to 24% of patients may be able to maintain drug-free remission for up to 18–56 weeks. Finally, in an analysis of TNFi withdrawal in a cohort of 325 patients from the Corrona registry, low disease activity was lost in 45% of patients in a median of 29 months, indicating that in some patients with PsA, clinical benefit was maintained after TNFi discontinuation (10). In addition to several other important methodologic differences, the mean duration of prior TNF therapy in patients in the Corrona registry was 1.5 years, which is significantly longer than the maximum 36-week duration of open-label ixekizumab treatment prior to withdrawal in our study. While the duration of prior low disease activity among patients with PsA in the Corrona

study was not reported, the duration of prior remission/low disease activity was found to be a positive predictor for maintaining drug-free disease control in rheumatoid arthritis (28,29). Similar to our findings in PsA, withdrawal of biologic treatment (TNFi) has generally been shown to result in rapid flare in patients with axial spondyloarthritis, another subset of the spondyloarthritis group of diseases (30–33). It remains to be evaluated which patient and disease characteristics, including some potential biomarkers, may predict the outcome of treatment discontinuation in patients with PsA.

The SPIRIT-P3 study has limitations that should be considered. The approved dosage regimen for PsA treatment in the US and Europe is ixekizumab every 4 weeks, while the dosage used in this study was ixekizumab every 2 weeks. This study was started when the pivotal phase III studies in PsA (SPIRIT-P1 and SPIRIT-P2) were still ongoing, evaluating the safety and efficacy of ixekizumab in 2 dosage regimens: 80 mg every 2 weeks or every 4 weeks. The efficacy and safety of ixekizumab in the 2 dosage regimens are similar (12,15); thus, the results from this study are scientifically and clinically relevant. The study was designed to assess complete treatment discontinuation and did not assess dosage reduction. Approaches in clinical practice may differ, where treatment may be tapered or discontinued after longer periods of sustained remission/low disease activity than assessed in this study.

In conclusion, continued ixekizumab therapy was superior to withdrawal in maintaining MDA in biologic treatment–naive patients with PsA in whom sustained MDA was achieved via treatment with ixekizumab every 2 weeks. Among patients who experienced a relapse after ixekizumab withdrawal, the vast majority regained MDA after re-treatment with ixekizumab every 2 weeks. These results indicate that continuous ixekizumab treatment is optimal for maintaining good disease control in PsA. However, disease control can be regained after re-treatment with ixekizumab in cases of treatment interruption.

AUTHOR CONTRIBUTIONS

All authors were involved in drafting the article or revising it critically for important intellectual content, and all authors approved the final version to be published. Dr. Coates had full access to all of the data in the study and takes responsibility for the integrity of the data and the accuracy of the data analysis.

Study conception and design. Coates, Kerr, Adams.
Acquisition of data. Pillai, Tahir, Valter, Alves, Adams.
Analysis and interpretation of data. Coates, Pillai, Tahir, Valter, Chandran, Kameda, Okada, Kerr, Alves, Park, Adams, Gallo, Hufford, Hojnik, Mease, Kavanaugh.

ROLE OF THE STUDY SPONSOR

Eli Lilly and Company provided funding for the study. Eli Lilly and Company contributed to the study design, data collection, data analysis, data interpretation, preparation of the manuscript, and the decision to submit the paper for publication. All authors had full access to all of the data in the study and had final responsibility for the decision to submit for publication. All authors critically revised the manuscript. Medical writing support was provided by Melody Pupols, PhD of Syneos Health (support for this assistance was funded by Eli Lilly and Company) and Emily K. Blue, PhD (an employee of Eli Lilly and Company).

REFERENCES

1. Mease PJ, Armstrong AW. Managing patients with psoriatic disease: the diagnosis and pharmacologic treatment of psoriatic arthritis in patients with psoriasis [review]. Drugs 2014;74:423–41.
2. Zachariae H, Zachariae R, Blomqvist K, Davidsson S, Molin L, Mørk C, et al. Quality of life and prevalence of arthritis reported by 5,795 members of the Nordic Psoriasis Associations: data from the Nordic Quality of Life Study. Acta Derm Venereol 2002;82:108–13.
3. Boehncke WH, Menter A. Burden of disease: psoriasis and psoriatic arthritis [review]. Am J Clin Dermatol 2013;14:377–88.
4. Gossec L, Smolen JS, Ramiro S, de Wit M, Cutolo M, Dougados M, et al. European League Against Rheumatism (EULAR) recommendations for the management of psoriatic arthritis with pharmacological therapies: 2015 update. Ann Rheum Dis 2016;75:499–510.
5. Lee MP, Lii J, Jin Y, Desai RJ, Solomon DH, Merola JF, et al. Patterns of systemic treatment for psoriatic arthritis in the US: 2004–2015. Arthritis Care Res (Hoboken) 2018;70:791–6.
6. Araujo EG, Finzel S, Englbrecht M, Schreiber DA, Faustini F, Hueber A, et al. High incidence of disease recurrence after discontinuation of disease-modifying antirheumatic drug treatment in patients with psoriatic arthritis in remission. Ann Rheum Dis 2015;74:655–60.
7. Moverley A, Coates L, Marzo-Ortega H, Waxman R, Torgerson D, Cocks K, et al. A feasibility study for a randomised controlled trial of treatment withdrawal in psoriatic arthritis (REmoval of treatment for patients in REmission in psoriatic ArThritis (RETREAT (F)). Clin Rheumatol 2015;34:1407–12.
8. Chimenti MS, Esposito M, Giunta A, Graceffa D, Bobino G, Teoli M, et al. Remission of psoriatic arthritis after etanercept discontinuation: analysis of patients' clinical characteristics leading to disease relapse. Int J Immunopathol Pharmacol 2013;26:833–8.
9. Cantini F, Niccoli L, Nannini C, Cassarà E, Pasquetti P, Olivieri I, et al. Frequency and duration of clinical remission in patients with peripheral psoriatic arthritis requiring second-line drugs. Rheumatology (Oxford) 2008;47:872–6.
10. Huynh DH, Boyd TA, Etzel CJ, Cox V, Kremer J, Mease P, et al. Persistence of low disease activity after tumour necrosis factor inhibitor (TNFi) discontinuation in patients with psoriatic arthritis. RMD Open 2017;3:e000395.
11. Liu L, Lu J, Allan BW, Tang Y, Tetreault J, Chow C, et al. Generation and characterization of ixekizumab, a humanized monoclonal antibody that neutralizes interleukin-17A. J Inflamm Res 2016;9:39–50.
12. Mease PJ, van der Heijde D, Ritchlin CT, Okada M, Cuchacovich RS, Shuler CL, et al. Ixekizumab, an interleukin-17A specific monoclonal antibody, for the treatment of biologic-naive patients with active psoriatic arthritis: results from the 24-week randomised, double-blind, placebo-controlled and active (adalimumab)-controlled period of the phase III trial SPIRIT-P1. Ann Rheum Dis 2017;76:79–87.
13. Van der Heijde D, Gladman DD, Kishimoto M, Okada M, Rathmann SS, Moriarty SR, et al. Efficacy and safety of ixekizumab in patients with active psoriatic arthritis: 52-week results from a phase III study (SPIRIT-P1). J Rheumatol 2018;45:367–77.
14. Chandran V, van der Heijde D, Fleischmann RM, Lespessailles E, Helliwell PS, Kameda H, et al. Ixekizumab treatment of biologic-naive patients with active psoriatic arthritis: 3-year results from a phase III clinical trial (SPIRIT-P1). Rheumatology (Oxford) 2020;59:2774–84.
15. Nash P, Kirkham B, Okada M, Rahman P, Combe B, Burmester G, et al. Ixekizumab for the treatment of patients with active psoriatic arthritis and an inadequate response to tumour necrosis

factor inhibitors: results from the 24-week randomised, double-blind, placebo-controlled period of the SPIRIT-P2 phase 3 trial. Lancet 2017;389:2317–27.
16. Genovese MC, Combe B, Kremer JM, Tsai T, Behrens F, Adams DH, et al. Safety and efficacy of ixekizumab in patients with PsA and previous inadequate response to TNF inhibitors: week 52 results from SPIRIT-P2. Rheumatology (Oxford) 2018;57:2001–11.
17. Orbai AM, Gellett AM, Kerr L, Constantin A. Efficacy and safety of ixekizumab in patients with active psoriatic arthritis and previous inadequate response to TNF inhibitors: two-year follow-up from a phase 3 study [abstract]. Arthritis Rheumatol 2018;70 Suppl 10. URL: https://acrabstracts.org/abstract/efficacy-and-safety-of-ixekizumab-in-patients-with-active-psoriatic-arthritis-and-previous-inadequate-response-to-tnf-inhibitors-two-year-follow-up-from-a-phase-3-study/.
18. Coates LC, Fransen J, Helliwell PS. Defining minimal disease activity in psoriatic arthritis: a proposed objective target for treatment. Ann Rheum Dis 2010;69:48–53.
19. Taylor W, Gladman D, Helliwell P, Marchesoni A, Mease P, Mielants H, and the CASPAR Study Group. Classification criteria for psoriatic arthritis: development of new criteria from a large international study. Arthritis Rheum 2006;54:2665–73.
20. Fredriksson T, Pettersson U. Severe psoriasis—oral therapy with a new retinoid. Dermatologica 1978;157:238–44.
21. Fries JF, Spitz P, Kraines RG, Holman HR. Measurement of patient outcome in arthritis. Arthritis Rheum 1980;23:137–45.
22. Coates LC, Helliwell PS. Defining low disease activity states in psoriatic arthritis using novel composite disease instruments [letter]. J Rheumatol 2016;43:371–5.
23. Healy PJ, Helliwell PS. Measuring clinical enthesitis in psoriatic arthritis: assessment of existing measures and development of an instrument specific to psoriatic arthritis. Arthritis Rheum 2008;59:686–91.
24. Maksymowych WP, Mallon C, Morrow S, Shojania K, Olszynski WP, Wong RL, et al. Development and validation of the Spondyloarthritis Research Consortium of Canada (SPARCC) Enthesitis Index. Ann Rheum Dis 2009;68:948–53.
25. Mease P, Roussou E, Burmester GR, Goupille P, Gottlieb A, Moriarty S, et al. Safety of ixekizumab in patients with psoriatic arthritis: results from a pooled analysis of three clinical trials. Arthritis Care Res (Hoboken) 2019;71:367–78.
26. Coates LC, Helliwell PS. Treat to target in psoriatic arthritis: evidence, target, research agenda. Curr Rheumatol Rep 2015;17:517.
27. Coates LC, Strand V, Wilson H, Revicki D, Stolshek B, Samad A, et al. Measurement properties of the minimal disease activity criteria for psoriatic arthritis. RMD Open 2019;5:e001002.
28. Ajeganova S, Huizinga T. Sustained remission in rheumatoid arthritis: latest evidence and clinical considerations. Ther Adv Musculoskelet Dis 2017;9:249–62.
29. Tanaka Y, Takeuchi T, Mimori T, Saito K, Nawata M, Kameda H, et al. Discontinuation of infliximab after attaining low disease activity in patients with rheumatoid arthritis: RRR (remission induction by Remicade in RA) study. Ann Rheum Dis 2010;69:1286–91.
30. Baraliakos X, Listing J, Brandt J, Zink A, Alten R, Burmester G, et al. Clinical response to discontinuation of anti-TNF therapy in patients with ankylosing spondylitis after 3 years of continuous treatment with infliximab. Arthritis Res Ther 2005;7:R439–44.
31. Brandt J, Listing J, Haibel H, Sörensen H, Schwebig A, Rudwaleit M, et al. Long-term efficacy and safety of etanercept after readministration in patients with active ankylosing spondylitis. Rheumatology (Oxford) 2005;44:342–8.
32. Sebastian A, Wojtala P, Lubinski L, Mimier M, Chlebicki A, Wiland P. Disease activity in axial spondyloarthritis after discontinuation of TNF inhibitors therapy. Reumatologia 2017;55:157–62.
33. Song IH, Althoff CE, Haibel H, Hermann KG, Poddubnyy D, Listing J, et al. Frequency and duration of drug-free remission after 1 year of treatment with etanercept versus sulfasalazine in early axial spondyloarthritis: 2 year data of the ESTHER trial. Ann Rheum Dis 2012;71:1212–5.

APPENDIX A: MEMBERS OF THE SPIRIT-P3 STUDY GROUP

Members of the SPIRIT-P3 Study Group are as follows: Khalid Ahmed, Nicholas Barkham, Linda Belhorn, Daniela Bichovska, Michaela Blahova, Ladislav Bortlik, Johannes Breedt, Michael Brooks, Paul Caldron, Silvia Ciernik, Stefan Daniluk, Roger Diegel, Pavol Dobrovodsky, Eva Dokoupilova, Leobardo Teran Estrada, Francisco Javier Blanco Garcia, Olena Garmish, Iurii Gasanov, Mariela Geneva-Popova, David Goddard, Oleksandr Golovchenko, Katarzyna Gruszecka, Tomas Hala, Jolana Hejlova, Mary Howell, Elena Ilivanova, Ramina Jajoo, Ewa Kaliszuk-Kaminska, Nadezhda Kapandjieva, Steven Klein, Mariusz Korkosz, Milan Krpciar, Dolores Alonso Martinez, Nomawethu Matsiliza, Marcin Mazurek, Małgorzata Miakisz, Eric Mueller, Raili Müller, Leysan Myasoutova, Oleh Nadashkevych, Antonio Fernandez Nebro, Petr Nemec, Clark Neuwelt, Meera Oza, Margus Pail, Iris Colunga Pedraza, Dimitar Penev, Lucie Podrazilova, Jennifer-Anne Potts, Grazyna Pulka, Eve-Kai Raussi, Riteesha Reddy, Dmytro Rekalov, Maria Rell-Bakalarska, Juan Cruz Rizo Rodriguez, Euthalia Roussou, Anna Rychlewska-Hanczewska, Federico Navarro Sarabia, Liliana Sedova, Shadi Shahouri, Sergii Shevchuk, David Sikes, Lubomira Simova, Andrea Skublova, Małgorzata Socik-Pojawa, Sheldon Solomon, Catherine Spargo, Mykola Stanislavchuk, Helena Stehlikova, Zuzana Stejfova, Maria Stopinska-Polaszewska, Katarzyna Swierkocka, Hasan Tahir, Sandra Tälli, Gareth Tarr, Cesar Francisco Pacheco Tena, Erika Timanikova, Vira Tseluyko, Zuzana Urbanova, Ivo Valter, Edgar Hernandez Vargas, Viktoriia Vasylets, Federico Galvan Villegas, Petr Vitek, Monika Wronisz, and Hana Zelenkova.

Arthritis & Rheumatology
Vol. 73, No. 9, September 2021, pp 1673–1682
DOI 10.1002/art.41730

American College of Rheumatology
Empowering Rheumatology Professionals

Mycophenolate Mofetil Versus Cyclophosphamide for Remission Induction in Childhood Polyarteritis Nodosa: An Open-Label, Randomized, Bayesian Noninferiority Trial

Paul A. Brogan,[1] Barbara Arch,[2] Helen Hickey,[2] Jordi Anton,[3] Este Iglesias,[3] Eileen Baildam,[4] Kamran Mahmood,[4] Gavin Cleary,[4] Elena Moraitis,[5] Charalampia Papadopoulou,[5] Michael W. Beresford,[2] Phil Riley,[6] Selcan Demir,[7] Seza Ozen,[7] Giovanna Culeddu,[8] Dyfrig A. Hughes,[8] Pavla Dolezalova,[9] Lisa V. Hampson,[10] John Whitehead,[10] David Jayne,[11] Nicola Ruperto,[12] Catrin Tudur-Smith,[2] and Despina Eleftheriou[1]

Objective. Cyclophosphamide (CYC) is used in clinical practice off-label for the induction of remission in childhood polyarteritis nodosa (PAN). Mycophenolate mofetil (MMF) might offer a less toxic alternative. This study was undertaken to explore the relative effectiveness of CYC and MMF treatment in a randomized controlled trial (RCT).

Methods. This was an international, open-label, Bayesian RCT to investigate the relative effectiveness of CYC and MMF for remission induction in childhood PAN. Eleven patients with newly diagnosed childhood PAN were randomized (1:1) to receive MMF or intravenous CYC; all patients received the same glucocorticoid regimen. The primary end point was remission within 6 months while compliant with glucocorticoid taper. Bayesian distributions for remission rates were established a priori for MMF and CYC by experienced clinicians and updated to posterior distributions on trial completion.

Results. Baseline disease activity and features were similar between the 2 treatment groups. The primary end point was met in 4 of 6 patients (67%) in the MMF group and 4 of 5 patients (80%) in the CYC group. Time to remission was shorter in the MMF group compared to the CYC group (median 7.1 weeks versus 17.6 weeks). No relapses occurred in either group within 18 months. Two serious infections were found to be likely linked to MMF treatment. Physical and psychosocial quality-of-life scores were superior in the MMF group compared to the CYC group at 6 months and 18 months. Combining the prior expert opinion with results from the present study provided posterior estimates of remission of 71% for MMF (90% credibility interval [90% CrI] 51, 83) and 75% for CYC (90% CrI 57, 86).

Conclusion. The present results, taken together with prior opinion, indicate that rates of remission induction in childhood PAN are similar with MMF treatment and CYC treatment, and MMF treatment might be associated with better health-related quality of life than CYC treatment.

INTRODUCTION

Polyarteritis nodosa (PAN) is a necrotizing vasculitis that causes aneurysmal nodules of medium-sized arteries (1,2). Childhood PAN is exceptionally rare, with a prevalence of ~1 per 1 million children (1,3). Peak onset of childhood PAN is at age 7–11 years, with no sex bias (4,5). Features of childhood PAN include constitutional symptoms, vasculitis rash, myalgia, abdominal pain,

EudraCT database no. 2013-004668-71 and ISRCTN: 75434563.

Supported by Versus Arthritis (grant 20094), Vasculitis UK, the Lauren Currie Twilight Foundation, the Paediatric Rheumatology International Trial Organisation (PRINTO), the Great Ormond St Hospital Charity, and the Hacettepe University Research Fund (grant TK-2017-15782).

[1]Paul A. Brogan, MBChB, PhD, Despina Eleftheriou, MD, PhD: University College London Great Ormond Street Institute of Child Health and Great Ormond Street Hospital for Children NHS Foundation Trust, London, UK; [2]Barbara Arch, MSc, Helen Hickey, BSc, Michael W. Beresford, MBChB, PhD, Catrin Tudur-Smith, PhD: University of Liverpool, Liverpool, UK; [3]Jordi Anton, MD, PhD, Este Iglesias, MD: St. Joan de Déu Hospital, Barcelona, Spain; [4]Eileen Baildam, MD, Kamran Mahmood, FRCPCH, Gavin Cleary, MBChB: Alder Hey Children's NHS Foundation Trust, Liverpool, UK; [5]Elena Moraitis, MD, PhD, Charalampia Papadopoulou, MD, PhD: Great Ormond Street Hospital for Children NHS Foundation Trust, London, UK; [6]Phil Riley, MBChB: Royal Manchester Children's Hospital, Manchester, UK; [7]Selcan Demir, MD, Seza Ozen, MD: Hacettepe University, Ankara, Turkey; [8]Giovanna Culeddu, MSc, Dyfrig A. Hughes, PhD: Bangor University, Bangor, UK; [9]Pavla Dolezalova, PhD: General University Hospital in Prague and Charles University, Prague, Czech Republic; [10]Lisa V. Hampson, PhD, John Whitehead, PhD: Lancaster University, Lancaster, UK; [11]David Jayne, MD, FMedSci: University of Cambridge, Cambridge, UK; [12]Nicola Ruperto, MD, MPH: Instituto Giannina Gaslini, IRCCS, UOSID Centro Trial, Genoa, Italy.

Dr. Brogan has received consulting fees from Sobi, Novartis, UCB, and Roche (less than $10,000 each). Dr. Cleary has received speaking fees

and arthropathy; however, any organ system can be affected (2,4,5). The etiology of childhood PAN remains unknown (6,7). In 2014, a monogenetic form of childhood PAN caused by deficiency of adenosine deaminase 2 (DADA2) was described (8–11).

If left untreated, the mortality rate of childhood PAN was historically close to 100% within months of disease onset (12,13); with aggressive immunosuppression, the mortality rate is as low as 4% (4). Cyclophosphamide (CYC) has been used off-label for over 40 years in the treatment of PAN (14–17) and is still recommended for induction of remission in childhood PAN, though this has never been studied in a pediatric randomized controlled trial (RCT) (12). If alternative treatment exists, it is desirable that CYC treatment in children be avoided, since adverse reactions associated with CYC include infertility and malignancy (18).

Mycophenolate mofetil (MMF) is an alternative immunosuppressant with lymphocyte selective suppressive effects, which is associated with remission rates similar to those observed with CYC in the treatment of lupus nephritis (19) and antineutrophil cytoplasmic antibody (ANCA)–associated vasculitis (AAV) (20). MMF is not associated with urothelial malignancy or infertility and is used off-label in pediatric patients.

We hypothesized that MMF may be noninferior to CYC for induction of remission in childhood PAN and may be a less toxic alternative. Therefore, the purpose of the present study was to investigate the relative effectiveness of MMF and CYC for remission induction in childhood PAN. It is infeasible to conduct a conventional, definitive phase III study of childhood PAN due to its rarity. We therefore opted for a Bayesian approach to assess the relative efficacy of MMF and CYC. This was a 2-stage process. Stage 1 consisted of a robust 2-day elicitation process conducted to quantify clinical opinion in light of results from a trial in adults (mycophenolate mofetil versus cyclophosphamide for remission induction in ANCA-associated vasculitis [MYCYC]) (20). The results from this trial were previously published (21). Stage 2 was a multicenter, open-label RCT of mycophenolate mofetil versus cyclophosphamide for the induction of remission of childhood PAN (the MYPAN trial; http://www.mypan.org.uk), and these data were used to further quantify the relative effectiveness of each treatment for remission induction in patients with newly diagnosed childhood PAN.

PATIENTS AND METHODS

Study design and patients. MYPAN was an international multicenter, open-label, randomized controlled prospective trial comparing MMF treatment with intravenous (IV) CYC treatment for the remission of childhood PAN (Figure 1). The trial was sponsored by University College London, and the trial was coordinated and data were stored by the Liverpool Clinical Trials Centre (LCTC) at the University of Liverpool. Centers were identified among members of the Paediatric Rheumatology International Trials Organisation (PRINTO) (www.printo.it) (22).The trial was conducted using a Bayesian noninferiority design (noninferiority margin 10%). Children were randomized 1:1 to receive either MMF (1,200 mg/m^2/day, maximum 1 gm twice daily) (12,23) or a standard IV CYC regimen (12). Randomization was achieved using a secure web-based tool generated centrally by the LCTC. Minimization variables for randomization were planned additional therapy with methylprednisolone >15 mg/kg at trial entry (yes/no) and plasma exchange at trial entry (yes/no). Treatment allocation prior to randomization was concealed from recruiting clinicians. Both trial groups received the same glucocorticoid treatment regimen per study protocol. The full protocol is available in Supplementary MYPAN protocol V4.0 (available on the *Arthritis & Rheumatology* website at http://onlinelibrary.wiley.com/doi/10.1002/art.41730/abstract).

Inclusion criteria were age at screening ≥4 years and ≤18 years, new-onset childhood PAN (within 3 months of screening) classified in accordance with the European Alliance of Associations for Rheumatology/PRINTO/Paediatric Rheumatology European Society criteria (2,24), active vasculitis of any major organ, or meeting ≥3 minor components of the Pediatric Vasculitis Activity Score (PVAS) criteria (25) (see Supplementary Table 1, available on the *Arthritis & Rheumatology* website at http://onlinelibrary.wiley.com/doi/10.1002/art.41730/abstract).

Children were excluded if they did not meet the classification criteria for childhood PAN, if they received alternative diagnoses, if they had chronic infection, if they experienced previous reactions to one of the study medications, or if they had immunodeficiency or malignancy. Genetic screening for ADA-2 was administered as part of the routine evaluation of the patients (i.e., outside the protocol).

Ethics approval. The protocol was approved by the Multicentre Research Ethics Committee in the UK and from relevant ethics committees for each participating center internationally. The study was conducted in accordance with the ethics principles of the Declaration of Helsinki. Patient and public involvement informed the design of the protocol and patient-facing trial documents. All participants provided written informed consent.

from AbbVie (less than $10,000). Dr. Ozen has received consulting fees from Novartis and Sobi (less than $10,000). Dr. Hampson owns stock or stock options in Novartis. Dr. Jayne has received consulting fees from AstraZeneca, Chemocentryx, GlaxoSmithKline, Genentech, InflaRx, Takeda, and Vifor (less than $10,000 each). Dr. Ruperto has received consulting fees, speaking fees, and/or honoraria from Ablynx, AstraZeneca, MedImmune, Bayer, Biogen, Boehringer, Bristol Myers Squibb, Celgene, Eli Lilly, EMD Serono, GlaxoSmithKline, Hoffmann-La Roche, Janssen, Merck, Novartis, Pfizer, R-Pharm, Synergie, Sobi, and UCB (less than $10,000 each). No other disclosures relevant to this article were reported.

Address correspondence to Paul A. Brogan, MBChB, PhD, 30 Guilfor Street, London, UK. Email: p.brogan@ucl.ac.uk.

Submitted for publication July 9, 2020; accepted in revised form March 11, 2021.

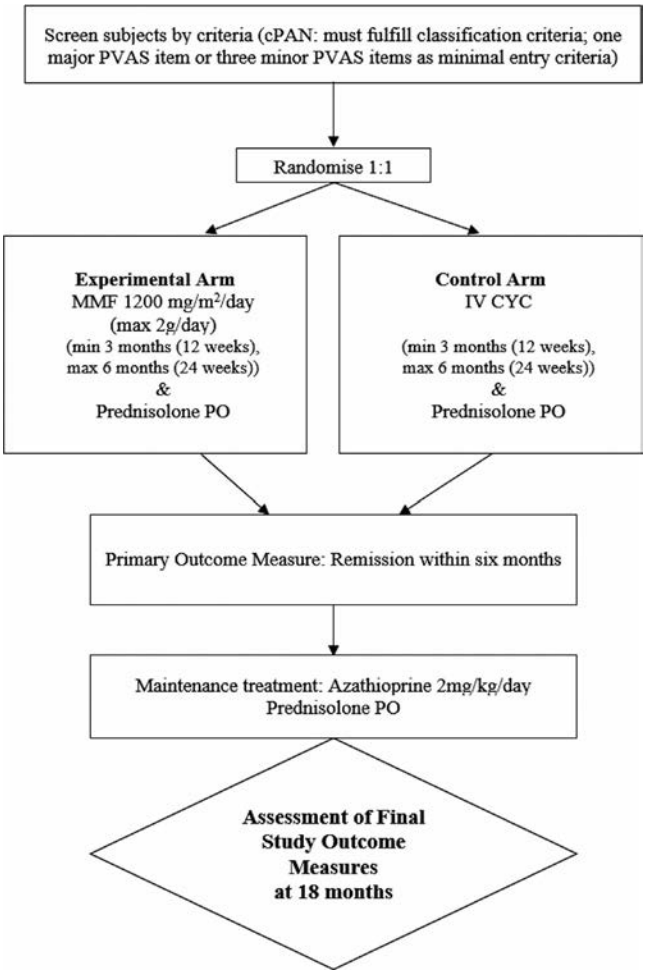

Figure 1. Overview of mycophenolate mofetil (MMF) versus cyclophosphamide (CYC) for the induction of remission of childhood polyarteritis nodosa (cPAN) (the MYPAN trial). PVAS = Pediatric Vasculitis Activity Score; PO = by mouth; IV = intravenous.

Treatments. Participants received oral MMF or IV CYC treatment for 18 months, which comprised 3–6 months of induction therapy (1:1 randomization); followed by 12–15 months of oral azathioprine (AZA) maintenance therapy (Figure 1). Both groups in the trial received tapering glucocorticoids (see below). Unless participants had an allergy, prophylaxis with trimethoprim/sulfamethoxazole was required until week 24. Trial treatment ended after 18 months.

MMF was administered to patients until disease remission was achieved at 3–6 months. The starting dose was 600 mg/m²/day (maximum 1 gm/day) for the first week, followed by 1,200 mg/m²/day (maximum 2 gm/day) in 2 divided doses (12,23,26).

CYC was administered at weeks 0, 2, and 4 and then every 3 weeks until remission was achieved (maximum 10 IV doses and minimum 6 doses) (Supplementary Table 2, available on the *Arthritis & Rheumatology* website at http://onlinelibrary.wiley.com/doi/10.1002/art.41730/abstract). The first dose was 500 mg/m^2/day, followed by 750 mg/m^2/day (maximum dose 1.2 gm) (12). Mesna and IV fluids were administered, as per local practice. CYC could be discontinued after a minimum of 6 doses if disease was in remission. Patients were administered oral AZA (2 mg/kg/day, maximum 200 mg/day) (12,26) the day following discontinuation of MMF treatment or 10–14 days after the last dose of IV CYC.

All patients received prednisolone starting at 1 mg/kg/day (maximum 80 mg dose), which was decreased to 0.1 mg/kg/day by 6 months and to 0.05–0.075 mg/kg by 9 months (Supplementary Table 3, available on the *Arthritis & Rheumatology* website at http://onlinelibrary.wiley.com/doi/10.1002/art.41730/abstract). Intravenous methylprednisolone could also be administered at trial entry (maximum 30 mg/kg for 3 doses or 3 gm total) at the investigator's discretion.

Principal investigators recorded medications received by the patient on a medication clinical research form during protocol face-to-face follow-up trial visits as specified below. In addition, patients completed a diary listing the medications taken as an outpatient, which allowed careful cross-checking of the accuracy of medications taken on a daily basis.

Assessments. Assessments were performed at weeks 0, 4, 10, 16, and 24 when the primary end point of remission was evaluated. Thereafter, assessments occurred at weeks 36, 48, 60, and 72. A final follow-up visit also took place on the date of the last patient's last visit, which varied considerably among the patients. Therefore, only results up to and including week 72 are reported here.

Disease activity was determined using the PVAS (25). Briefly, the PVAS ranges from 0 to 63, with higher scores denoting active clinical disease activity within 9 organ systems and a score of 0 indicating the absence of disease activity. Safety events were coded using The Medical Dictionary for Regulatory Activities version 19.

Primary outcome measure. The primary outcome measure was remission within 6 months, which was defined as the absence of disease activity (PVAS 0 [of a maximum 63]) on 2 consecutive visits at least 1 month apart, with adherence to glucocorticoid taper protocol (20,21,25). The primary end point was assessed at 6 months because this reflects the typical time point to assess the effectiveness of remission induction in routine clinical practice (12) and is therefore used in most vasculitis trials (20). Secondary end points assessed over the full 18-month trial were as follows: remission within 6 months regardless of glucocorticoid taper; time to remission; pediatric vasculitis damage index (PVDI) score (27,28); mycophenolic acid 12-hour trough levels; the cross-culturally adapted and validated version of the Childhood Health Assessment Questionnaire (C-HAQ) for disability and the Child Health Questionnaire (CHQ) for quality of life (29); cost-effectiveness using the UK NHS costs and quality-adjusted life-years (QALYs) measurement based on the Child Health Utility-9D (CHU-9D) (30) and EuroQol-5D-3L (EQ-5D-3L) questionnaires

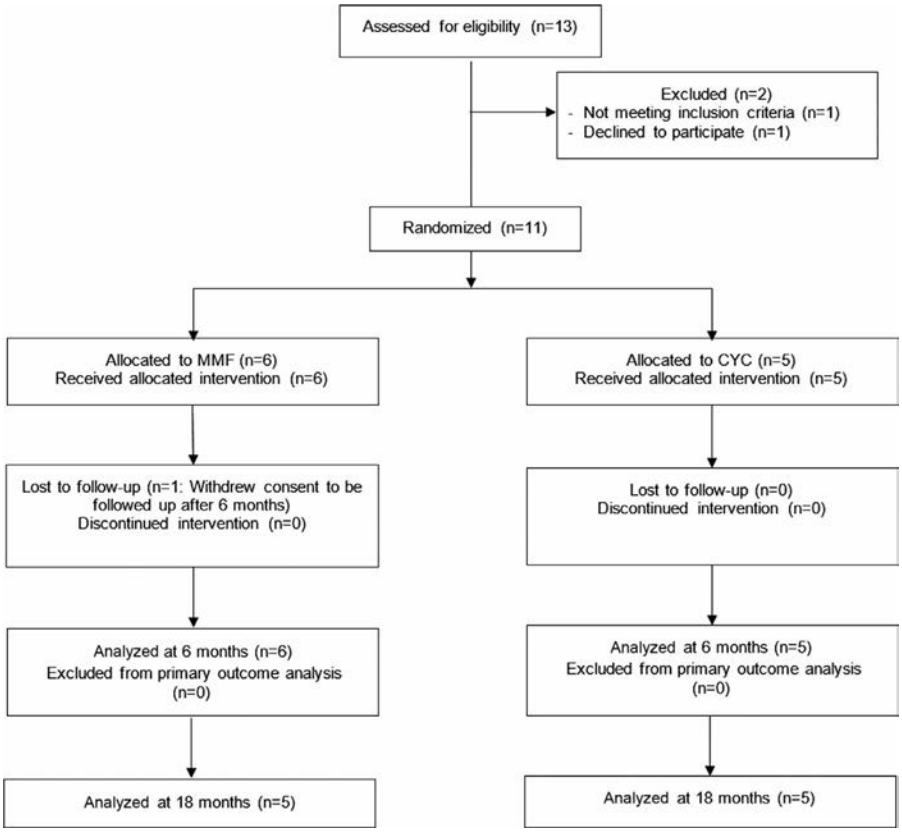

Figure 2. Flow chart of patient recruitment, treatment allocation, and patient follow-up in patients receiving mycophenolate mofetil (MMF) versus cyclophosphamide (CYC) for the induction of remission of childhood polyarteritis nodosa (MYPAN trial).

(31); cumulative glucocorticoid dose; growth; disease relapse within 18 months; adverse events; withdrawal from trial due to drug intolerance; and mortality.

Statistical analysis. *Sample size.* A maximum target sample size of 40 was chosen pragmatically, as this was the largest number feasible to recruit among PRINTO sites. A Bayesian approach is not restricted by small sample sizes and allows data to be combined with existing evidence. The larger the recruitment, the greater the contribution of trial results to the totality of evidence, post–MYPAN trial. Bayesian sample-size calculations suggested that this would yield a power of 62% to ascertain noninferiority of the primary end point (32). The MYPAN trial was conducted using a Bayesian design due to the challenge of low participant numbers, given that childhood PAN is extremely rare. Bayesian power was therefore also calculated for smaller sample sizes (8 patients [41% power], 10 patients [52% power], and 12 patients [53% power]).

Data analyses. Per the recommendation in the Consolidated Standards of Reporting Trials statement (33), reported results are from the intent-to-treat (ITT) population. Missing data were not imputed. The date at which the primary outcome was achieved was the first of the 2 consecutive visits in which the PVAS was 0. The primary outcome was examined using a Bayesian analysis. Bayes theorem was used to combine expert prior opinion with the MYPAN data to obtain posterior distributions for remission rates with CYC treatment (pC), remission rates with MMF treatment (pM), and the log odds ratio of remission with MMF compared to CYC (θ).

Full details of the primary outcome measure analysis methods were previously published (21,32). Briefly, noninferiority of MMF was defined as a Bayesian posterior probability of obtaining remission within 6 months, within 10% (absolute difference) of CYC. Quantities of interest were pC, pM, and θ. Bayesian prior distributions for pC and pM were established during a prior elicitation workshop in September 2013 (before recruitment for the MYPAN trial began), using expert opinion and evidence presented from the MYCYC trial (20,21,32). The posterior distributions for pC, pM, and θ were calculated and summarized by their modes, which reflected the most likely values for these quantities, and by 90% credibility intervals (90% CrIs), which quantified our certainty. We also calculated 2 posterior probabilities, i.e., that the 6-month remission rate among patients taking MMF is noninferior to the 6-month remission rate among patients taking CYC ($pM \geq pC - 0.10$) and that achievement of remission within 6 months is more likely to occur among patients taking MMF than among those taking CYC ($pM > pC$). All secondary outcome measures were analyzed descriptively

Table 1. Characteristics of the patients in the MMF group and the CYC group at trial entry*

Characteristic	MMF group (n = 6)	CYC group (n = 5)	All patients (n = 11)
Age at randomization, median (IQR) years	10.8 (7.0, 12.1)	7.9 (6.7, 9.4)	12.1 (4.6, 15.5)
Male	3	2	5
Female	3	3	6
Ethnicity			
White	6	4	10
Mixed	0	1	1
Height Z score, median (IQR)	−0.7 (−1.2, 1.0)	0.2 (−0.1, 0.2)	−0.1 (−0.7, 1.0)
Weight Z score, median (IQR)	−1.3 (−2.7, −0.3)	1.3 (0.7, 2.3)	-0.2 (−1.5, 1.3)
eGFR (mL/min/1.73 m^2), median (IQR)	128.4 (125.8, 152.0)	101.3 (99.6, 101.9)	113.0 (101.3, 129.0)
PVAS (maximum 63), median (IQR)	8.5 (7.0, 12.0)	7.0 (6.0, 9.0)	7.0 (6.0, 12.0)
Affected organ system†			
General/constitutional	6	4	10
Cutaneous	3	3	6
Eyes	1	0	1
Abdominal	5	4	9
Renal	0	1	1
Nervous	2	2	4
CRP (mg/liter; RR <5 mg/liter), median (IQR)	14.7 (4.0, 47.4)	4.0 (4.0, 38.0)	8.0 (4.0, 47.4)
ESR (mm/hour; 0–10 mm/hour), median (IQR)	28.5 (7.0, 63.0)	16.0 (14.0, 28.0)	16.0 (7.0, 63.0)
C-HAQ disability index, median (IQR)	1.5 (0.6, 1.8)	1.5 (0.3, 1.5)	1.5 (0.6, 1.8)
Total dose of IV methylprednisolone pre-randomization, mg/kg	4	3	7
Median (IQR)	59.7 (45.6, 291.6)	87.2 (17.3, 222.2)	73.2 (45.0, 222.2)
Plasma exchange pre-randomization	0	0	0
ADA-2 genetic screening‡	5	2	7

* Except where indicated otherwise, values are the number of patients. MMF = mycophenolate mofetil; CYC = cyclophosphamide; IQR = interquartile range; eGFR = estimated glomerular filtration rate; PVAS = Pediatric Vasculitis Activity Score; CRP = C-reactive protein; ESR = erythrocyte sedimentation rate; C-HAQ = Childhood Health Assessment Questionnaire; IV = intravenous; ADA-2 = adenosine deaminase 2.
† A full breakdown list of all PVAS items is provided in Supplementary Table 4 (http://onlinelibrary.wiley.com/doi/10.1002/art.41730/abstract).
‡ Four patients declined genetic testing for deficiency of adenosine deaminase 2 (DADA2) (1 in the MMF group and 3 in the CYC group). DADA2 was excluded in all 7 patients in the MMF and CYC groups.

using frequentist statistics (i.e., number, median, and interquartile range [IQR]), unless otherwise stated. Results were summarized graphically using Kaplan-Meier curves, patient profile plots, and radar plots.

For each participant, total NHS costs associated with primary care, secondary care, and community care services, and medication use were measured over 18 months. This was based on resource use questionnaires completed by trial participants or their parents or guardians during clinic appointments, and via information from case report forms. Unit costs were obtained from standard NHS sources (https://improvement.nhs.uk/resources/national-tariff/). The estimation of preference weights for each health state was generated from patient responses to CHU-9D questionnaires (30). QALYs were then computed by applying the trapezium rule to estimate the area under the curve. Second-year costs and QALYs were discounted at 3.5%. Differences between the MMF and CYC treatment groups in costs and QALYs were estimated by linear regression, with the per-patient cost (or per QALY) as the dependent variable and the treatment group as the only independent predictor. A nonparametric bootstrap analysis using 10,000 replicates was performed to assess the joint uncertainty in mean costs and QALYs. The probability of each treatment being cost-effective was determined at the threshold of £20,000 per QALY, which operates within the NHS (34) and in accordance with the National Institute for Health and Care Excellence guidance (https://www.nice.org.uk/process/pmg9/). Analyses were performed using R version 3.6.1 or SAS version 9.4.

RESULTS

Patients. Eleven patients with childhood PAN were enrolled from January 2014 to June 2018 from 5 of 13 international centers (Great Ormond Street Hospital [n = 3], Alder Hey Children's NHS Foundation Trust [n = 3], Hacettepe University Children's Hospital [n = 3], Royal Manchester Children's Hospital [n = 1], and Hospital Sant Joan de Déu [n = 1]). The randomized treatment allocation is summarized in Figure 2. Six patients were randomized to receive MMF, and 5 patients were randomized to receive CYC. All 11 patients received their allocated treatment and were retained for the primary analysis; 1 patient withdrew from follow-up at 26 weeks. Baseline characteristics of the patients are provided in Table 1 and Supplementary Table 4 (available on the *Arthritis & Rheumatology* website at http://onlinelibrary.wiley.com/doi/10.1002/art.41730/abstract).

Prior and Posterior Beliefs			
Parameter		**Mode**	**90% Credibility Interval**
pM	*Probability of remission within 6 months of randomization, given that the treatment was MMF*		
	Prior	71%	(45%, 85%)
	Posterior	71%	(51%, 83%)
pC	*Probability of remission within 6 months of randomization, given that the treatment was CYC*		
	Prior	74%	(51%, 86%)
	Posterior	75%	(57%, 86%)
θ	*Log-odds ratio of being in remission within 6 months, if given MMF compared with CYC*		
	Prior	-0.17	(-0.91, 0.58)
	Posterior	-0.21	(-0.91, 0.50)
Exp (θ)	*Odds ratio of being in remission within 6 months, if given MMF compared with CYC*		
	Prior	0.84	(0.40, 1.79)
	Posterior	0.81	(0.40, 1.65)
Hypotheses		**Probability**	
Noninferiority	*Probability MMF is noninferior to CYC within a margin of 10%*		
	Prior	0.766	
	Posterior	0.755	
Superiority	*Probability of superiority of MMF over CYC*		
	Prior	0.356	
	Posterior	0.313	

Figure 3. Bayesian primary outcome analysis results. MMF = mycophenolate mofetil; CYC = cyclophosphamide.

Findings for the primary outcome measure. Remission within 6 months of randomization occurred in 4 of 6 patients (67%) in the MMF group and 4 of 5 patients (80%) in the CYC group. The Bayesian posterior distributions for remission rates (modes) were 71% (90% CrI 51, 83) for MMF and 75% (90% CrI 57, 86) for CYC, and the odds ratio of remission within 6 months with MMF compared to CYC was 0.81 (90% CrI 0.40, 1.65) (Figures 3 and 4). The posterior probability that MMF is noninferior to CYC was 0.76, indicating that noninferiority is likely. Also, the posterior probability that the 6-month remission rate is higher in MMF than in CYC was 0.31, indicating that MMF superiority is unlikely (Figure 3).

Findings for the secondary efficacy outcome measures. *Remission and relapses.* All patients adhered to the protocol for glucocorticoids; hence, remission within 6 months regardless of glucocorticoid taper was the same as that for the primary end point. Five patients in the MMF group exhibited remission within 18 months, at a median of 7.1 weeks (IQR 4.0, 10.3; full range 4–25.6). Remission was achieved in all patients in the CYC group within 18 months, at median of 17.6 weeks (IQR 6.0, 18.9; full range 4.4–35.3) (Supplementary Figure 1, available on the *Arthritis & Rheumatology* website at http://onlinelibrary.wiley.com/doi/10.1002/art.41730/abstract). No relapses occurred in either group.

Vasculitis damage, glucocorticoid exposure, and mortality. The median PVDI score was 0 (of a maximum 72) for both groups at trial entry. The median PVDI score at trial end (18 months) was 0 (IQR 0, 1) in the MMF group and 2 (IQR 0, 3) in the CYC group (Supplementary Table 5, available on the *Arthritis & Rheumatology* website at http://onlinelibrary.wiley.com/doi/10.1002/art.41730/abstract). There was no major growth disturbance in either group. At 18 months, the median height Z score was –1.0

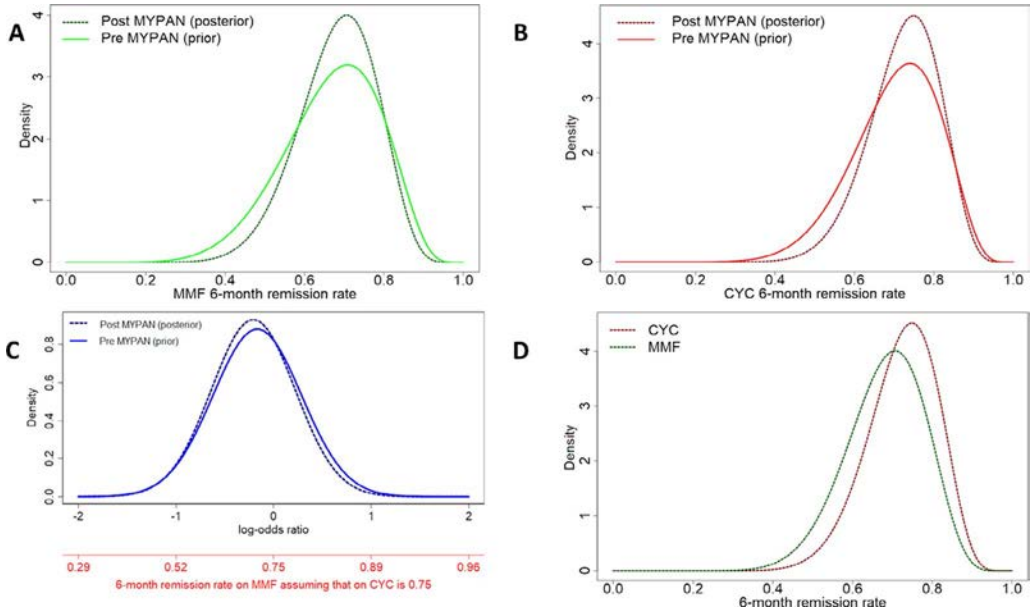

Figure 4. Graphs showing prior and posterior distributions for mycophenolate mofetil (MMF) 6-month remission rate (**A**), cyclophosphamide (CYC) 6-month remission rate (**B**), and log odds ratio of 6-month remission if given MMF compared to CYC (**C**), and posterior distributions for MMF and CYC 6-month remission rates (**D**). MYPAN = mycophenolate mofetil versus cyclophosphamide for the induction of remission of childhood polyarteritis nodosa (trial).

(IQR –1.1, 1.0) in the MMF group and 0.0 (IQR –0.2, 0.1) in the CYC group, which were similar to heights at baseline. Cumulative oral prednisolone doses at 6 and 18 months were similar between the 2 groups (Supplementary Table 6, available on the *Arthritis & Rheumatology* website at http://onlinelibrary.wiley.com/doi/10.1002/art.41730/abstract). Three patients received IV methylprednisolone after randomization (1 patient in the CYC group and 2 in the MMF group). No patients died in either group.

Disability. Patients in both groups had moderate disability at baseline, but patients with moderate disability in the MMF group improved over time (Supplementary Table 7, available on the *Arthritis & Rheumatology* website at http://onlinelibrary.wiley.com/doi/10.1002/art.41730/abstract). The median disability score (C-HAQ) at 18 months among patients with childhood PAN was 0 (of a maximum 3) (IQR 0, 0) in the MMF group and 1.0 (IQR 0.2,1.8) in the CYC group. C-HAQ pain scores decreased more rapidly in the MMF group compared to the CYC group (Supplementary Table 8, available on the *Arthritis & Rheumatology* website at http://onlinelibrary.wiley.com/doi/10.1002/art.41730/abstract). Similarly, C-HAQ general assessment scores also improved more rapidly in the MMF group compared to the CYC group (Supplementary Table 9, available on the *Arthritis & Rheumatology* website at http://onlinelibrary.wiley.com/doi/10.1002/art.41730/abstract).

Quality of life. Results from the CHQ showed that quality of life was overall better in patients treated with MMF compared to those treated with CYC (Supplementary Table 10 and Supplementary Figures 2–4, available on the *Arthritis & Rheumatology* website at http://onlinelibrary.wiley.com/doi/10.1002/art.41730/abstract). At baseline, median CHQ physical summary scores reflected severe impairment in both groups, ~5 SD below the normal for a healthy control (8.3 [IQR –0.4, 18] in the MMF group and 9.0 [IQR 1.8, 14.0] in the CYC group). Similarly, median psychosocial summary scores reflected impairment in both groups, though to a lesser degree than the physical summary scores (34.9 [IQR 32.5, 48.1] in the MMF group and 28.9 [IQR 25.0, 32.7] in the CYC group). Physical summary scores and psychosocial summary scores improved more rapidly and to an overall greater level in the MMF group compared to the CYC group (Supplementary Table 10 and Supplementary Figures 2–4, available on the *Arthritis & Rheumatology* website at http://onlinelibrary.wiley.com/doi/10.1002/art.41730/abstract).

Health economics. The mean total discounted costs were £4,725 (95% confidence interval [95% CI] 1,480, 7,157) in the CYC group and £6,071 (95% CI 640, 15,555) in the MMF group. Participants in the CYC group experienced discounted QALYs of 1.18 (95% CI 1.07, 1.48), compared to 1.13 (95% CI 0.58, 1.44) in the MMF group. Therefore, MMF was more costly (£1,346 [95% CI –4709, 11,175]) and was associated with fewer QALYs (0.047 [–0.5749, 0.4798]) compared to CYC. The probability of MMF being cost-effective at a threshold of £20,000 per QALY was 0.32, which was evaluated in the 7 patients from the UK only.

Safety outcome measures. Total adverse events were similar between the 2 groups. Thirty-eight events (63% mild severity and 37% moderate severity) occurred in 5 of 6 patients treated with MMF, and 31 events (97% mild and 3% moderate) occurred

Table 2. Summary of adverse events in the MMF group compared to the CYC group*

	MMF group (n = 6)		CYC group (n = 5)		All patients (n = 11)	
	Events, no.	Patients, no. (%)	Events, no.	Patients, no. (%)	Events, no.	Patients, no. (%)
Adverse events, no.						
All	38	5 (83.3)	31	5 (100)	69	10 (90.9)
Mild	24	2 (33.3)	30	4 (80)	54	6 (54.5)
Moderate	14	3 (50)	1	1 (20)	15	4 (36.4)
All SAEs, no.	4	3 (50)	0	0 (0)	4	3 (27)

* MMF = mycophenolate mofetil; CYC = cyclophosphamide; SAEs = serious adverse events.

in all 5 patients treated with CYC (Table 2 and Supplementary Table 11, available on the *Arthritis & Rheumatology* website at http://onlinelibrary.wiley.com/doi/10.1002/art.41730/abstract). A total of 4 serious adverse events, including 2 infections, occurred in 3 of 6 patients in the MMF group. One patient had abdominal pain (deemed not related to MMF) and a lower respiratory tract infection (possibly related to MMF), which fully resolved with treatment. One patient had colitis (deemed not related to MMF) ongoing at trial end, and 1 patient had herpes zoster (possibly related to MMF), which fully resolved with treatment. No serious adverse events were observed in the CYC group (Supplementary Table 12, available on the *Arthritis & Rheumatology* website at http://onlinelibrary.wiley.com/doi/10.1002/art.41730/abstract). No patients withdrew from the trial due to drug intolerance.

DISCUSSION

A major challenge in the study of rare diseases is conducting a clinical trial with sufficient power to inform best clinical practice when the anticipated sample size is small. Historically, this has been an insurmountable barrier in the study of rare pediatric autoimmune diseases, and explains why a clinical trial of childhood PAN had never been undertaken until now (21). We adopted a Bayesian clinical trial design with the objective of quantifying disease remission rates with CYC and MMF treatment, combining a robust elicitation of prior opinion and evidence with our trial data. Six-month remission rates observed in the MYPAN trial were consistent with prior opinions, and since we could only recruit 11 patients, the totality of evidence is heavily influenced by those prior distributions. We calculated a Bayesian posterior probability of 76% for noninferiority of MMF compared to CYC for remission within 6 months. This observation, while not definitive, is still clinically useful, particularly since conducting a confirmatory frequentist trial is impossible (21). Further clinical face validity for the noninferiority of MMF compared to CYC is suggested by the fact that glucocorticoid use could be successfully tapered in all patients and all patients had nearly identical cumulative glucocorticoid exposure. Therefore, our results suggest that MMF might represent a viable alternative to CYC for remission induction in childhood PAN. Moreover, these results will inform prior opinions for any future trials in childhood PAN (e.g., the Biologics in Refractory Vasculitis Study [https://www.isrctn.com/ISRCTN16502655]).

The MYPAN data are consistent with data from studies in AAV, most notably the MYCYC study (20) (though not completely independently, as the MYCYC data helped inform the prior opinion used in MYPAN), which included adults and children and showed that MMF was noninferior to CYC for inducing remission. Following remission, all patients in our trial received AZA and glucocorticoid maintenance therapy, with no relapses. This observation contrasts with findings in the MYCYC trial which showed that relapses occurred earlier and more frequently among patients in the MMF group (33%) compared to among those in the CYC group (19%) (20). Thus, the previous suggestion that relapses in childhood PAN are less common than in childhood AAV is supported by our results (1).

Other secondary end points are also potentially clinically relevant, though the results are purely descriptive. Remission was exhibited at a median of 7.1 weeks among patients in the MMF group, compared to a median of 17.6 weeks in the CYC group. PVDI scores were lower in the MMF group, implying less damage, although our trial was not powered to demonstrate statistical significance of this observation. PVDI scores (and in adults, VDI scores) are not weighted; hence, overall low numerical scores can still indicate severe damage in patients. Therefore, future studies are needed to further examine the potential clinical importance of this preliminary observation.

C-HAQ disability scores and pain scores at trial end were comparable among patients in both groups, though scores were numerically lower among patients in the MMF group. While we must be careful not to overinterpret this purely descriptive observation, a possible obvious explanation is that the C-HAQ score reflected a more rapid resolution of disease activity among patients in the MMF group, resulting in faster resolution of disability and pain. Similarly, and in accordance with this suggestion, quality of life improved more rapidly and to a greater extent among patients in the MMF group compared to the CYC group, particularly in regard to the physical summary score. The health economic analysis in the UK suggested that MMF may generate fewer QALYs and may be more expensive than CYC, though

with a significant element of uncertainty. No patients died in either trial group. Lastly, remission was achieved in all the patients in the MMF group who completed follow-up.

There were no new safety signals for MMF or CYC. Notably, 2 infections were considered to be possibly linked to MMF. Improved short-term safety with MMF was thus not demonstrated. However, long-term safety issues are probably of more importance and are not captured in our trial. The use of MMF along with a standard dose of glucocorticoids offers clear advantages over CYC in terms of fertility preservation in younger patients, and potentially lower malignancy rates later in life, which is of particular concern among pediatric patients (18,20).

Our trial has several notable strengths. To our knowledge, it is the first randomized trial in childhood PAN. Patients were recruited from regional tertiary centers; thus, the trial cohort was fully representative of the spectrum of disease in childhood PAN, as indicated by the extent of organ involvement observed. The study also included the use of standardized tools developed specifically for children with vasculitis to allow accurate classification of childhood PAN (35), and of disease activity and remission (using the PVAS) (24). Our study was also the first to record vasculitis damage prospectively using the PVDI, which to date has been only preliminarily used in retrospective studies (27,28).

The strengths of this trial should be viewed against its limitations, notably, that the clinical trial evidence is based on a small sample size, augmented by a distillation of clinical experience in the form of prior distributions. However, the fact that the posterior distributions we observed are largely consistent with prior expert opinions adds important clinical face validity to the conclusion, which must be based on the final Bayesian posterior distributions and may provide the prior distributions for future cumulative research of childhood PAN. In addition, MYPAN was not blinded, for purely practical reasons. Although glucocorticoid exposure was documented, glucocorticoid toxicity was not systematically captured using the glucocorticoid toxicity index (36). Only 7 of 11 patients were screened for DADA2 as part of their routine evaluation, which might have important implications for determining the efficacy of both MMF and CYC in childhood PAN (10,11). Health economic analyses were based on UK costs, and therefore may not apply uniformly in other countries (e.g., in Turkey, where MMF is more expensive than CYC). Our trial also did not address the possibility that higher doses of MMF might be even more efficacious. Regulatory approval for dose escalation was initially requested in the MYPAN trial, but not granted by competent authority since it was suggested that adverse effects might also increase with higher doses. Finally, generalizability to other ethnic groups was limited as 10 of 11 patients in our trial were White.

In summary, MMF is probably noninferior to CYC for induction of remission in childhood PAN when combined with glucocorticoids. MMF may also be associated with better quality of life compared to CYC.

ACKNOWLEDGMENTS

This was a fully investigator-led trial. Sponsorship was provided by University College London. Funding was provided by Versus Arthritis (grant 20094), Vasculitis UK, and the Lauren Currie Twilight Foundation. The lead clinical trial unit was the Liverpool Clinical Trials Centre (LCTC). We also acknowledge support from the Pediatric Rheumatology International Trial Organisation (PRINTO), particularly Elisa Patrone and Marco Garrone; and Hacettepe University Research Fund (TK-2017-15782). We are grateful to all the trial investigators, subinvestigators, research nurses, and all of the patients who participated in this study. Centers that opened for recruitment in the MYPAN trial were as follows: Hospital Sant Joan de Déu (Barcelona); University Hospital Centre Zagreb, University School of Medicine; Azienda Ospedalario Meyer (Florence); IRCCS Gaslini (Genoa); Hacettepe University Children's Hospital, Ankara; Alder Hey Children's NHS Foundation Trust, Liverpool; Great Ormond Street Hospital NHS Foundation Trust, London; Royal Victoria Hospital, Newcastle Hospitals NHS Foundation Trust; Royal Hospital for Sick Children, Glasgow; Royal Manchester Children's Hospital; Sheffield Children's Hospital; Addenbrookes Hospital, Cambridge; and University College London Hospital. Authors Brogan and Elitheriou acknowledge support from the Great Ormond St Hospital Clinical Research Facility and Great Ormond St Hospital Children's Charity.

AUTHOR CONTRIBUTIONS

All authors were involved in drafting the article or revising it critically for important intellectual content, and all authors approved the final version to be published. Dr. Brogan had full access to all of the data in the study and takes responsibility for the integrity of the data and the accuracy of the data analysis.

Study conception and design. Brogan, Hickey, Beresford, Ozen, Hughes, Dolezalova, Hampson, Whitehead, Jayne, Tudur-Smith, Eleftheriou.

Acquisition of data. Brogan, Arch, Hickey, Anton, Iglesias, Baildam, Mahmood, Cleary, Moraitis, Papadopoulou, Riley, Demir, Ozen, Ruperto, Tudur-Smith, Eleftheriou.

Analysis and interpretation of data. Brogan, Arch, Hickey, Ozen, Culeddu, Hughes, Hampson, Tudur-Smith, Eleftheriou.

REFERENCES

1. Dillon MJ, Eleftheriou D, Brogan PA. Medium-size-vessel vasculitis. Pediatr Nephrol 2010;25:1641–52.
2. Ozen S, Pistorio A, Iusan SM, Bakkaloglu A, Herlin T, Brik R, et al. EULAR/PRINTO/PRES criteria for Henoch–Schonlein purpura, childhood polyarteritis nodosa, childhood Wegener granulomatosis and childhood Takayasu arteritis: Ankara 2008. Part II. Final classification criteria. Ann Rheum Dis 2010;69:798–806.
3. Gardner-Medwin JM, Dolezalova P, Cummins C, Southwood TR. Incidence of Henoch-Schonlein purpura, Kawasaki disease, and rare vasculitides in children of different ethnic origins. Lancet 2002;360:1197–202.
4. Eleftheriou D, Dillon MJ, Tullus K, Marks SD, Pilkington CA, Roebuck DJ, et al. Systemic polyarteritis nodosa in the young: a single-center experience over thirty-two years. Arthritis Rheum 2013;65:2476–85.
5. Ozen S, Anton J, Arisoy N, Bakkalogly A, Besbas N, Brogan P, et al. Juvenile polyarteritis: results of a multicenter survey of 110 children. J Pediatr 2004;145:517–22.
6. Brogan PA, Shah V, Bagga A, Klein N, Dillon MJ. T cell Vβ repertoires in childhood vasculitides. Clin Exp Immunol 2003;131:517–27.
7. Brogan PA, Shah V, Dillon MJ. Polyarteritis nodosa in children. Clev Clin J Med 2002;69 Suppl 2:Sii168–9.
8. Elkan PN, Pierce SB, Segel R, Walsh T, Barash J, Padeh S, et al. Mutant adenosine deaminase 2 in a polyarteritis nodosa vasculopathy. N Engl J Med 2014;370:921–31.

9. Zhou Q, Yang D, Ombrello AK, Zavialov AV, Toro C, Zavialov AV, et al. Early-onset stroke and vasculopathy associated with mutations in ADA2. N Engl J Med 2014;370:911–20.
10. Ombrello AK, Qin J, Hoffmann PM, Kumar P, Stone D, Jones A, et al. Treatment strategies for deficiency of adenosine deaminase 2 [letter]. N Engl J Med 2019;380:1582–4.
11. Nanthapisal S, Murphy C, Omoyinmi E, Hong Y, Standing A, Berg S, et al. Deficiency of adenosine deaminase type 2: a description of phenotype and genotype in 15 cases. Arthritis Rheumatol 2016;68:2314–22.
12. De Graeff N, Groot N, Brogan P, Ozen S, Avcin T, Bader-Meunier B, et al. European consensus-based recommendations for the diagnosis and treatment of rare paediatric vasculitides: the SHARE initiative. Rheumatology (Oxford) 2019;58:656–71.
13. Baggenstoss AH, Shick RM, Polley HF. The effect of cortisone on the lesions of periarteritis nodosa. Am J Pathol 1951;27:537–59.
14. Gayraud M, Guillevin L, Cohen P, Lhote F, Cacoub P, Deblois P, et al, on behalf of the French Cooperative Study Group for Vasculitides. Treatment of good-prognosis polyarteritis nodosa and Churg-Strauss syndrome: comparison of steroids and oral or pulse cyclophosphamide in 25 patients. Br J Rheumatol 1997;36:1290–7.
15. Guillevin L, Lhote F, Cohen P, Jarrousse B, Lortholary O, Généreau T, et al. Corticosteroids plus pulse cyclophosphamide and plasma exchanges versus corticosteroids plus pulse cyclophosphamide alone in the treatment of polyarteritis nodosa and Churg-Strauss syndrome patients with factors predicting poor prognosis: a prospective, randomized trial in sixty-two patients. Arthritis Rheum 1995;38:1638–45.
16. Guillevin L, Cohen P, Mahr A, Arène JP, Mouthon L, Puéchal X, et al. Treatment of polyarteritis nodosa and microscopic polyangiitis with poor prognosis factors: a prospective trial comparing glucocorticoids and six or twelve cyclophosphamide pulses in sixty-five patients. Arthritis Rheum 2003;49:93–100.
17. Ribi C, Cohen P, Pagnoux C, Mahr A, Arène JP, Puéchal X, et al. Treatment of polyarteritis nodosa and microscopic polyangiitis without poor-prognosis factors: a prospective randomized study of one hundred twenty-four patients. Arthritis Rheum 2010;62:1186–97.
18. Langford CA. Cyclophosphamide as induction therapy for Wegener's granulomatosis and microscopic polyangiitis. Clin Exp Immunol 2011;164 Suppl 1:31–4.
19. Appel GB, Contreras G, Dooley MA, Ginzler EM, Isenberg D, Jayne D, et al. Mycophenolate mofetil versus cyclophosphamide for induction treatment of lupus nephritis. J Am Soc Nephrol 2009;20:1103–12.
20. Jones RB, Hiemstra TF, Ballarin J, Blockmans DE, Brogan P, Bruchfeld A, et al. Mycophenolate mofetil versus cyclophosphamide for remission induction in ANCA-associated vasculitis: a randomised, non-inferiority trial. Ann Rheum Dis 2019;78:399–405.
21. Hampson LV, Whitehead J, Eleftheriou D, Tudur-Smith C, Jones R, Jayne D, et al. Elicitation of expert prior opinion: application to the MYPAN trial in childhood polyarteritis nodosa. PLoS One 2015;10:e0120981.
22. Ruperto N, Martini A. Networking in paediatrics: the example of the Paediatric Rheumatology International Trials Organisation (PRINTO). Arch Dis Child 2011;96:596–601.
23. Downing HJ, Pirmohamed M, Beresford MW, Smyth RL. Paediatric use of mycophenolate mofetil [review]. Br J Clin Pharmacol 2013;75:45–59.
24. Ruperto N, Ozen S, Pistorio A, Dolezalova P, Brigan P, Cabral DA, et al. EULAR/PRINTO/PRES criteria for Henoch-Schonlein purpura, childhood polyarteritis nodosa, childhood Wegener granulomatosis and childhood Takayasu arteritis: Ankara 2008. Part I. Overall methodology and clinical characterisation. Ann Rheum Dis 2010;69:790–7.
25. Dolezalova P, Price-Kuehne FE, Özen S, Benseler SM, Cabral DA, Anton J, et al. Disease activity assessment in childhood vasculitis: development and preliminary validation of the Paediatric Vasculitis Activity Score (PVAS). Ann Rheum Dis 2013;72:1628–33.
26. Jones R, Harper L, Ballarin J, Blockmans D, Brogan P, Bruchfeld A, et al, on behalf of the European Vasculitis Study Group. A randomized trial of mycophenolate mofetil versus cyclophosphamide for remission induction of ANCA-associated vasculitis:"MYCYC" [abstract]. Presse Med 2013;42:678–9.
27. Eleftheriou D, Varnier G, Dolezalova P, McMahon AM, Al-Obaidi M, Brogan PA. Takayasu arteritis in childhood: retrospective experience from a tertiary referral centre in the UK. Arthritis Res Ther 2015;17:545.
28. Eleftheriou D, Gale H, Pilkington C, Fenton M, Sebire NJ, Brogan PA. Eosinophilic granulomatosis with polyangiitis in childhood: retrospective experience from a tertiary referral centre in the UK. Rheumatology (Oxford) 2016;55:1263–72.
29. Ruperto N, Ravelli A, Pistorio A, Malattia C, Cavuto S, Gado-West L, et al. Cross-cultural adaptation and psychometric evaluation of the Childhood Health Assessment Questionnaire (CHAQ) and the Child Health Questionnaire (CHQ) in 32 countries: review of the general methodology. Clin Exp Rheumatol 2001;19 Suppl 23:S1–9.
30. Stevens K. Valuation of the Child Health Utility 9D index. Pharmacoeconomics 2012;30:729–47.
31. Brooks R. EuroQol: the current state of play. Health Policy 1996;37:53–72.
32. Hampson LV, Whitehead J, Eleftheriou D, Brogan P. Bayesian methods for the design and interpretation of clinical trials in very rare diseases. Stat Med 2014;33:4186–201.
33. Schulz KF, Altman DG, Moher D, Fergusson D. CONSORT 2010 changes and testing blindness in RCTs. Lancet 2010;37:1144–6.
34. Fenwick E, Claxton K, Sculpher M. Representing uncertainty: the role of cost-effectiveness acceptability curves. Health Econ 2001;10:779–87.
35. Ozen S, Pistorio A, Iusan SM, Bakkaloglu A, Herlin T, Brik R, et al. EULAR/PRINTO/PRES criteria for Henoch-Schönlein purpura, childhood polyarteritis nodosa, childhood Wegener granulomatosis and childhood Takayasu arteritis: Ankara 2008. Part II: Final classification criteria. Ann Rheum Dis 2010;69:798-806.
36. Miloslavsky EM, Naden RP, Bijlsma JW, Brogan PA, Brown ES, Brunetta P, et al. Development of a Glucocorticoid Toxicity Index (GTI) using multicriteria decision analysis. Ann Rheum Dis 2017;76:543–6.

Arthritis & Rheumatology
Vol. 73, No. 9, September 2021, pp 1683–1693
DOI 10.1002/art.41727

American College of Rheumatology
Empowering Rheumatology Professionals

Eosinophil ETosis–Mediated Release of Galectin-10 in Eosinophilic Granulomatosis With Polyangiitis

Mineyo Fukuchi,[1] Yosuke Kamide,[2] Shigeharu Ueki,[1] Yui Miyabe,[1] Yasunori Konno,[1] Nobuyuki Oka,[3] Hiroki Takeuchi,[4] Souichi Koyota,[1] Makoto Hirokawa,[1] Takechiyo Yamada,[1] Rossana C. N. Melo,[5] Peter F. Weller,[6] and Masami Taniguchi[2]

Objective. Eosinophils are tissue-dwelling immune cells. Accumulating evidence indicates that a type of cell death termed ETosis is an important cell fate involved in the pathophysiology of inflammatory diseases. Although the critical role of eosinophils in eosinophilic granulomatosis with polyangiitis (EGPA; formerly Churg-Strauss syndrome) is well established, the presence of eosinophil ETosis (EETosis) is poorly understood. We undertook this study to better understand the characteristics of EETosis.

Methods. In vitro studies using blood-derived eosinophils were conducted to characterize EETosis. The occurrence of EETosis in tissues from patients with EGPA was studied by immunostaining and electron microscopy. Serum concentrations of eosinophil-derived proteins in healthy controls, patients with asthma, and EGPA patients with active disease or with disease in remission (n = 15 per group) were examined.

Results. EETosis was reliant on reactive oxygen species and peptidylarginine deiminase type 4–dependent histone citrullination, resulting in the cytolytic release of net-like eosinophil extracellular traps, free galectin-10, and membrane-bound intact granules. The signature of EETosis, including loss of cytoplasmic galectin-10 and deposition of granules, was observed in eosinophils infiltrating various tissues from EGPA patients. Serum eosinophil granule proteins and galectin-10 levels were increased in EGPA and positively correlated with disease activity as assessed by the Birmingham Vasculitis Activity Score (r = 0.8531, $P < 0.0001$ for galectin-10). When normalized to blood eosinophil counts, this correlation remained for galectin-10 (r = 0.7168, $P < 0.0001$) but not for granule proteins. Galectin-10 levels in active EGPA positively correlated with serum interleukin-5 levels.

Conclusion. Eosinophils infiltrating diseased tissues in EGPA undergo EETosis. Considering the exclusive expression and large pool of cytoplasmic galectin-10 in eosinophils, elevated serum galectin-10 levels in patients with EGPA might reflect the systemic occurrence of cytolytic EETosis.

INTRODUCTION

Eosinophils are tissue-dwelling immune cells that play an important role in type 2 inflammation. As end-stage effector cells, eosinophils may mediate cytotoxic effects on parasites or allergic tissue. The pleiotropic effects of recruited eosinophils were recently reported to affect immunomodulation, as well as tissue homeostasis and repair (1,2). Many of these functions rely on

Supported in part by the Japan Agency for Medical Research and Development (Allergic Disease and Immunology grant JP20ek0410055 to Dr. Ueki), the Japan Society for the Promotion of Science (Kakenhi Grant-in-Aid 19K17898 to Dr. Kamide and Kakenhi Grants-in-Aid 16K08926, 15KK0329, and 20K08794 to Dr. Ueki), the Conselho Nacional de Desenvolvimento Científico e Tecnológico (grants 309734/2018-5 and 434914/2018-5 to Dr. Melo), the Fundação de Amparo à Pesquisa do Estado de Minas Gerais (grant CBB-APQ-03647-16 to Dr. Melo), and the NIH (grant R37-AI-020241 to Dr. Weller). Dr. Ueki's work was supported in part by the Mochida Memorial Foundation for Medical and Pharmaceutical Research and the Japanese Society of Laboratory Medicine Fund for Promotion of Scientific Research.

[1]Mineyo Fukuchi, DDS, Shigeharu Ueki, MD, PhD, Yui Miyabe, MD, Yasunori Konno, DDS, PhD, Souichi Koyota, PhD, Makoto Hirokawa, MD, PhD, Takechiyo Yamada, MD, PhD: Akita University, Akita, Japan; [2]Yosuke Kamide, MD, PhD, Masami Taniguchi, MD, PhD: Sagamihara National Hospital, Kanagawa, Japan; [3]Nobuyuki Oka, MD, PhD: Kyoto Konoe Rehabilitation Hospital, Kyoto, Japan; [4]Hiroki Takeuchi, MD, PhD: Kyoto Minami Hospital, Kyoto, Japan; [5]Rossana C. N. Melo, PhD: Federal University of Juiz de Fora, Juiz de Fora, Brazil, and Beth Israel Deaconess Medical Center and Harvard Medical School, Boston, Massachusetts; [6]Peter F. Weller, MD: Beth Israel Deaconess Medical Center and Harvard Medical School, Boston, Massachusetts.

Drs. Fukuchi and Kamide contributed equally to this work.

Dr. Fukuchi has received research grants from GlaxoSmithKline. Dr. Kamide has received honoraria from AstraZeneca (less than $10,000). Dr. Ueki has received honoraria from AstraZeneca (less than $10,000) and research grants from GlaxoSmithKline, Novartis, Sanofi, and Maruho. Dr. Konno has received research grants from GlaxoSmithKline. Dr. Oka has received honoraria from AstraZeneca (less than $10,000). Dr. Takeuchi has received research grants from Teijin. Dr. Weller has received honoraria from GlaxoSmithKline (less than $10,000). Dr. Taniguchi has received research grants from AstraZeneca and GlaxoSmithKline. No other disclosures relevant to this article were reported.

Address correspondence to Shigeharu Ueki, MD, PhD, Akita University Graduate School of Medicine, Department of General Internal Medicine and Clinical Laboratory Medicine, 1-1-1 Hondo, Akita 010-8543, Japan. Email: shigeharu.ueki@gmail.com.

Submitted for publication June 3, 2020; accepted in revised form March 4, 2021.

the capacity of eosinophils to release a group of granule-derived proteins, including major basic protein (MBP), eosinophil peroxidase, eosinophil cationic protein (ECP), and eosinophil-derived neurotoxin (EDN) (1,3). Understanding eosinophil activation and the process of degranulation remains one of the central research questions related to the pathophysiology of eosinophilic diseases.

Detailed transmission electron microscopy (TEM) studies have demonstrated that eosinophils have multiple degranulation mechanisms. Preformed, granule-stored proteins can be released by 3 main secretory processes: exocytosis, piecemeal degranulation, and cytolysis (1,4,5). Exocytosis is the release of whole granule contents as individual granules that fuse with the cell membrane, although this has rarely been observed in vivo. Secretory vesicle–mediated release of granule contents, known as piecemeal degranulation, is important for the selective secretion of various proteins contained in the granules. Cytolysis, or lytic degranulation, releases cytoplasmic proteins and intact eosinophil granules. This process has been reported in numerous pathologic conditions, ranging from 10% to 80% of all degranulation modes in vivo (1,6–8).

Recent findings revealed that lytic degranulation represents a process of active cell death, referred to as eosinophil ETosis (EETosis) (3,9), which is characterized by the release of filamentous chromatin structures called eosinophil extracellular traps (EETs) (10). EETs, mediators of eosinophil innate immune function, may capture pathogens; however, in excess, they can be pathogenic. EETs form stable aggregates that contribute to the viscosity of secretions observed in eosinophilic chronic rhinosinusitis (11), eosinophilic otitis (12), and allergic bronchopulmonary aspergillosis (13). EETosis is also associated with the crystallization of galectin-10 (also known as Charcot-Leyden protein or lysophospholipase) to form Charcot-Leyden crystals, a classic hallmark of eosinophilic inflammation (14,15). EETosis is the cell fate of lytic "whole-cell degranulation" and therefore is crucial to understanding the pathophysiology of allergic diseases.

Eosinophilic granulomatosis with polyangiitis (EGPA; formerly Churg-Strauss syndrome) is a rare form of antineutrophil cytoplasmic antibody–associated vasculitis that affects multiple organs. Clinical features of EGPA include various combinations of neuropathy, pulmonary infiltrates, myocarditis, skin, gastrointestinal, renal, and ear, nose, and throat involvement (16). Eosinophil-rich granulomatous inflammation and small- to medium-sized vessel vasculitis characterize the pathologic findings of EGPA. The critical role of eosinophils in EGPA is well established, as demonstrated by the clinical benefit of eosinophil-targeted anti–interleukin-5 (anti–IL-5) antibody therapy (3,17). A recent study indicated that isolated eosinophils are prone to undergo EETosis in response to autoimmune antibodies (18). Several studies indicated that neutrophil extracellular traps (NETs) might contribute to the pathogenesis of EGPA (16,19), although the presence of EETs/EETosis is less well understood.

Because there is no gold standard for detecting EETs and EETosis in vivo, we performed a series of in vitro studies to better understand the characteristics of EETosis. We studied the occurrence of EETosis in various organ tissues obtained from EGPA patients. Finally, we measured serum concentrations of eosinophil-derived proteins from healthy controls, patients with stable asthma, and EGPA patients with active disease or with disease in remission.

PATIENTS AND METHODS

Study subjects and ethics approval. Written informed consent was obtained from all participants in accordance with the principles laid out in the Declaration of Helsinki. The study used institutional review board–approved protocols (Akita University, permission no. 994; National Hospital Organization Sagamihara, approval no. 2017-048). Experimental protocols requiring purified blood eosinophils used samples obtained from patients with mild eosinophilia. Biopsy tissues and blood samples were obtained from EGPA patients treated at the Clinical Research Center for Allergy and Rheumatology, National Hospital Organization, Sagamihara. Collected blood was left for 30 minutes at room temperature, centrifuged (1,700*g* for 10 minutes), and then serum was stored at –30°C. All biopsy specimens were fixed in 10% formaldehyde and embedded in paraffin.

The control group and group of patients with asthma comprised 15 subjects per group who were matched to patients in the EGPA group by sex, age, and body mass index. The patients with asthma were assessed as having well-controlled disease, based on the Global Initiative for Asthma guidelines (20), with exclusion criteria of nonsteroidal antiinflammatory drug–exacerbated respiratory disease and allergic bronchopulmonary mycosis. EGPA patients were diagnosed using the American College of Rheumatology 1990 criteria for the classification of Churg-Strauss syndrome with reference to the International Chapel Hill Consensus Conferences systems (21,22). Active EGPA was characterized by increased eosinophil counts (>10% eosinophils or >1,000 eosinophils/μl) and by symptoms listed in the Birmingham Vasculitis Activity Score (BVAS; version 3) (23) in ≥1 involved organ as shown by histologic, clinical, or laboratory data. All patients with active EGPA were newly diagnosed and had not been receiving systemic steroids except for the purpose of treating asthma. Patients with active EGPA whose symptoms flared during treatment were not included. Remission was defined as the absence of any clinical signs or symptoms of active vasculitis for ≥3 months after these treatments. Persistent and unchanged symptoms were not defined as vasculitis in this study. The BVAS (version 3) was used to capture all current symptoms, meaning a combination of active disease and previous damage. Disease features that had been present for >1 month were counted as "persistent" scores. Receipt of antibody-based therapy was a criterion for exclusion from the study.

Eosinophil isolation. Human eosinophils were purified by CD16-negative selection as previously described (24). Briefly, venous blood was collected in tubes containing 0.1*M* EDTA–dextran solution to sediment erythrocytes. Supernatants were collected, layered onto 1.085 gm/ml Percoll (P1644; Sigma) density gradients, and centrifuged (740*g* for 30 minutes at 20°C) to separate mononuclear cells. We collected the cell pellet and added ice-cold distilled water to lyse erythrocytes. The remaining granulocytes were incubated with anti-CD16 microbeads (no. 130-045-701; Miltenyi Biotec) for 40 minutes at 4–8°C. The cell suspension was applied to a magnetic column at 4°C to remove neutrophils. Eosinophil purity was >98%, and viability assessed by trypan blue exclusion was >99%.

Induction of cell death. EETosis was induced as previously described (11). Briefly, eosinophils were stimulated with 10 ng/ml phorbol 12-myristate 13-acetate (PMA) (no. P1585; Sigma), 1 mg/ml immobilized IgG and IgA (Sigma) (coated on plates for 3 hours), or 1 μ*M* platelet-activating factor (Enzo Life Sciences) and 10 ng/ml IL-5 (205-IL; R&D Systems) in phenol red–free RPMI 1640 medium containing 0.3% bovine serum albumin (BSA; Sigma) at 37°C for 180 minutes. Necrotic cell death was induced by brief heating in medium containing 0.3% BSA (60°C for 7 minutes followed by 37°C for 60 minutes). Apoptosis was induced using an anti-Fas antibody (100 ng/ml in medium containing 10% fetal bovine serum) (clone CH11; Millipore) for the indicated times. To quantify cell death, Sytox green in a 1:5,000 dilution (no. S7020; Life Technologies) was added to the medium. Brightfield and fluorescence images were randomly obtained, and Sytox-positive cells were counted among ≥200 cells in a blinded manner. In some experiments, 20 μ*M* diphenyleneiodonium chloride (DPI; Sigma) was added to the culture medium. Indicated concentrations of Cl-amidine (Cayman Chemical) were added 15 minutes prior to each stimulus.

TEM. For conventional TEM, eosinophils isolated from peripheral blood (treated to induce cell death as described above) and nerve tissues obtained from 6 EGPA patients at the Kyoto Konoe Rehabilitation Hospital were fixed and prepared as previously described (24,25). Details are included in Supplementary Methods (available on the *Arthritis & Rheumatology* website at http://onlinelibrary.wiley.com/doi/10.1002/art.41727/abstract).

Immunofluorescence staining. Human eosinophils (1×10^6/ml) were seeded in 8-well Lab-Tek II chamber slides (Nunc), stimulated for the indicated durations, and then fixed with 4% paraformaldehyde for 10 minutes. Cells were blocked with phosphate buffered saline (PBS) containing 3% BSA at 4°C overnight and then permeabilized with PBS containing 10% BSA and 0.1% saponin. For pathologic tissue analyses, samples were fixed with 10% formalin and embedded in paraffin. For MBP and galectin-10 staining, deparaffinized sections were treated for antigen retrieval with 0.1% proteinase K at room temperature for 6 minutes. The samples were incubated with the following primary antibodies: 10 μg/ml rabbit anti-human MBP (a kind gift from Dr. Hirohito Kita, Mayo Clinic, Scottsdale, AZ) for 30 minutes at 37°C, and mouse anti–galectin-10 antibody in a 1:50 dilution (B-F42) (ab27417; Abcam) for 90 minutes at room temperature. Subsequently, the samples were incubated in Alexa Fluor 488–conjugated goat anti-mouse IgG with a 1:200 dilution (A11001; Life Technologies), Alexa Fluor 594–conjugated goat anti-rabbit IgG antibody in a 1:200 dilution (A11072; Life Technologies), and Hoechst 33342 in a 1:5,000 dilution (H3570; Invitrogen) for 30 minutes at room temperature.

The cytolysis index was calculated from images immunostained for galectin-10 and MBP: a greater loss of intracellular galectin-10 compared to cell-retained MBP yielded an elevated cytolysis index. Assessment of the cytolysis index was conducted as described in Supplementary Figure 1 (http://onlinelibrary.wiley.com/doi/10.1002/art.41727/abstract). The non-cytolytic control value was set at 0.7. For staining with galectin-10 and MBP, 23 tissue samples were obtained from 16 EGPA patients (Supplementary Table 1, http://onlinelibrary.wiley.com/doi/10.1002/art.41727/abstract).

For citrullinated histone H3 (CitH3) staining, antigen retrieval of human eosinophil samples was performed by incubation for 15 minutes in Tris–EDTA buffer in a microwave oven. The slides were subsequently incubated with 10 μg/ml primary rabbit anti-CitH3 monoclonal antibody (90 minutes at room temperature; Abcam). Alexa Fluor 488–conjugated secondary antibodies (Life Technologies) were then added for 30 minutes at room temperature. Isotype-matched control antibodies and Hoechst 33342 were used in each experiment. Samples were mounted using Prolong Diamond (Life Technologies), and images were obtained using an LSM 780 confocal microscope (Carl Zeiss). In some experiments, coverslips were removed and samples were stained with hematoxylin and eosin (H&E) (22). For CitH3 staining, 14 tissue samples were obtained from 10 EGPA patients (lung, n = 3; skin, n = 6; upper digestive tract, n = 4; lower digestive tract, n = 1). Tissue samples with nonspecific staining were excluded.

Details regarding Western blotting and the measurement of galectin-10, EDN, ECP, lactate dehydrogenase (LDH), and IL-5 levels are described in Supplementary Methods (http://onlinelibrary.wiley.com/doi/10.1002/art.41727/abstract).

Statistical analysis. Data were analyzed using GraphPad Prism, version 5.04. Differences between groups were assessed using unpaired *t*-tests and one-way analysis of variance (ANOVA) followed by the Newman-Keuls test. Blood sample data were analyzed using the Kruskal-Wallis test with Dunn's multiple comparison post hoc test. One-way ANOVA with post hoc Tukey's test was used for normally distributed data. Correlation was analyzed using Spearman's correlation analysis. *P* values less than 0.05 were considered significant.

RESULTS

Characterization of EETosis by reactive oxygen species (ROS)–dependent histone citrullination and release of EETs. To better characterize the different types of eosinophil cell death, we assessed the ultrastructural morphologies of EETosis, apoptosis, and necrosis in vitro (Figures 1A–C). Each type of cell death was induced in purified human eosinophils using previously established conditions (9). Anti-Fas antibody–stimulated eosinophils showed the classic morphology of apoptosis, including cytoplasmic and nuclear condensation (Figure 1B). Heat-treated eosinophils showed morphology typical of necrosis, including bleb formation and organ swelling. Notably, most electron-dense granular contents remained in apoptotic cells but were lost from necrotic cells (Figure 1C). PMA-stimulated EETotic cells showed chromatolysis and plasma membrane disintegration (Figure 1A). Consistent with findings from previous studies (9,14), membrane-bound cell-free granules filled with granular contents were associated with the originating EETotic cells. Similar morphologies were observed using other known physiologic EETosis stimuli (Supplementary Figure 2, http://onlinelibrary.wiley.com/doi/10.1002/art.41727/abstract).

In neutrophils, peptidylarginine deiminase type 4 (PAD4)–mediated histone hypercitrullination was reported to have an essential role in the formation of NETs by relaxing the chromatin structure (26,27). We assessed the presence of CitH3 in each type of cell death using immunostaining. As expected, EETotic cells released CitH3-stained net-like EETs (Figure 1D). CitH3-positive EETs were observed regardless of the EETosis stimulus (Supplementary Figure 2). CitH3 was also detected in apoptotic cells, although EETs were not observed (Figure 1E). Necrotic cells did not show any CitH3 (Figure 1F). These results were confirmed by Western blotting for CitH3 and total histone H3 (Supplementary Figure 3, http://onlinelibrary.wiley.com/doi/10.1002/art.41727/abstract).

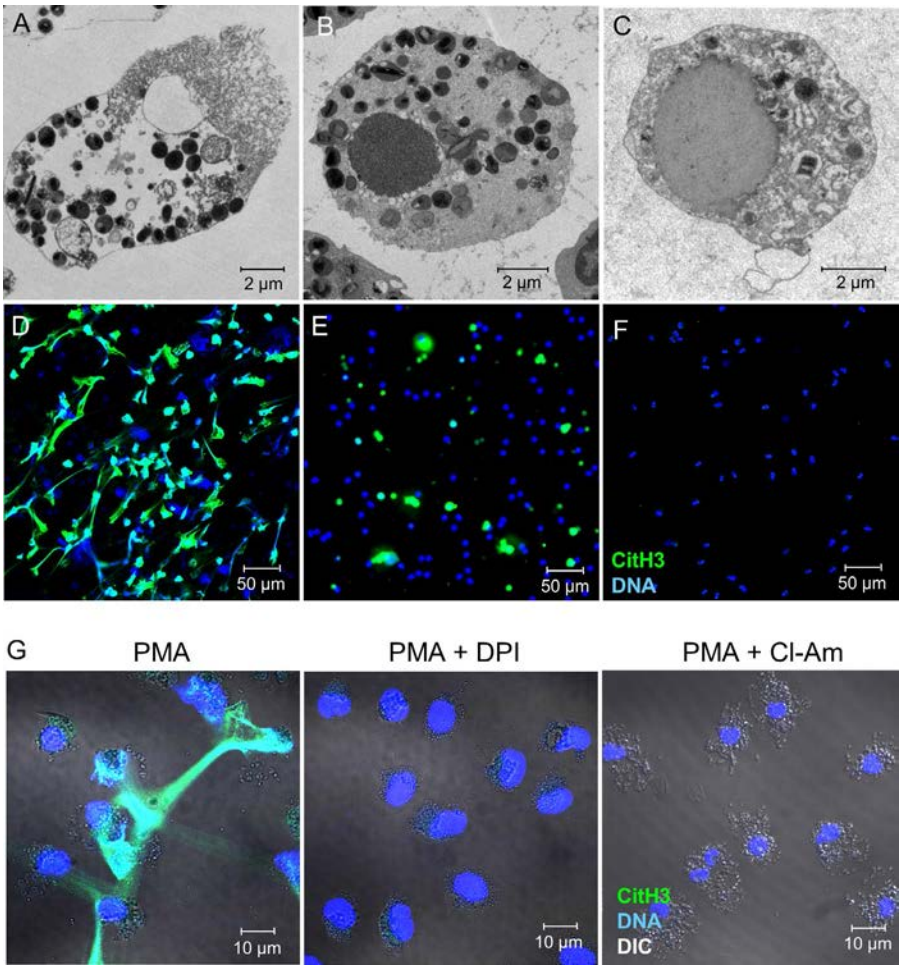

Figure 1. Citrullinated histone H3 (CitH3)–loaded eosinophil extracellular traps (EETs) are released during eosinophil ETosis (EETosis). **A–F**, Using purified human eosinophils, EETosis was induced by stimulation with phorbol 12-myristate 13-acetate (PMA) for 180 minutes (**A** and **D**), apoptosis was induced by treatment with anti-Fas antibody for 48 hours (**B** and **E**), and necrosis was induced by heat treatment for 7 minutes followed by incubation at 37°C for 60 minutes (**C** and **F**). Cells were assessed by transmission electron microscopy (**A–C**), and immunofluorescence staining of CitH3 and DNA (**D–F**) was visualized by confocal microscopy. Original magnification × 20. **G**, Eosinophils were stimulated with PMA for 3 hours in the presence of vehicle, diphenyleneiodonium chloride (DPI), or Cl-amidine (Cl-Am) and assessed by immunofluorescence staining. Differential interference contrast (DIC) images were merged.

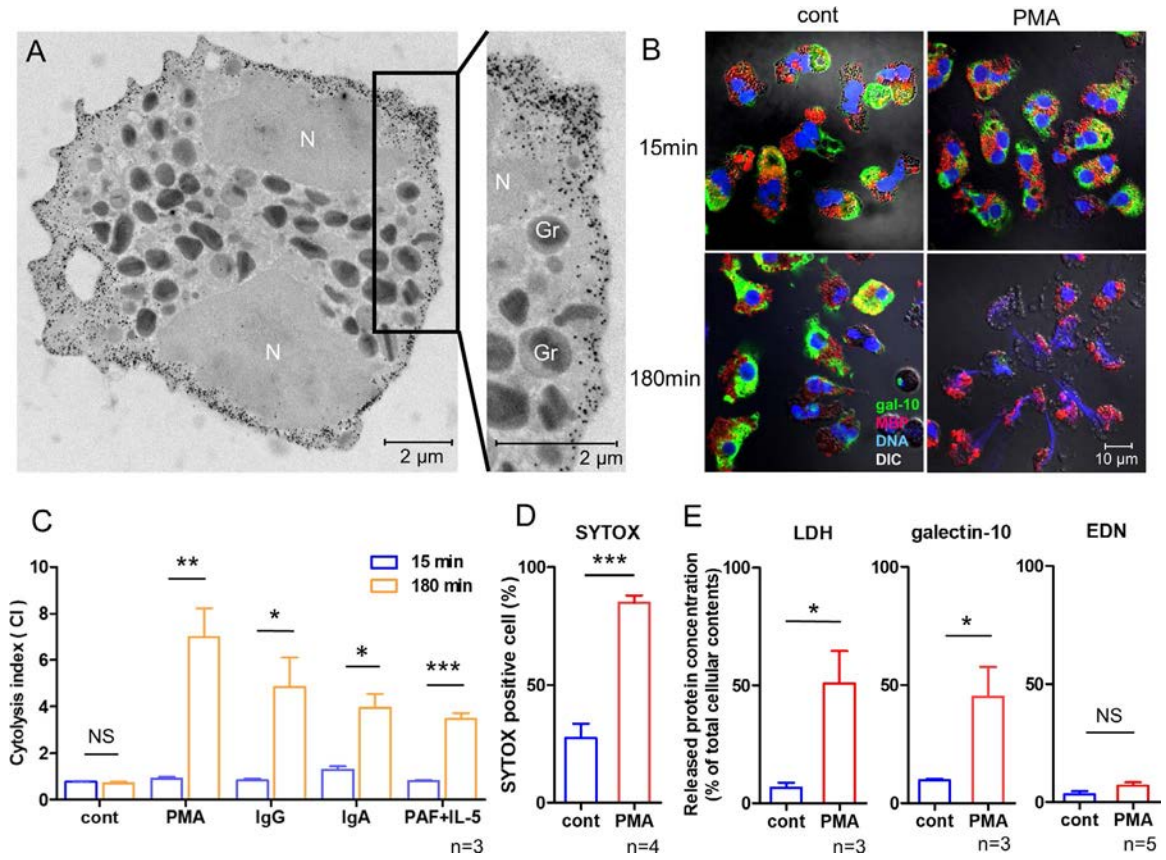

Figure 2. Release of cytoplasmic galectin-10 (gal-10), but not granule proteins, during EETosis. **A**, Ultrastructural immunolabeling of galectin-10 in unstimulated eosinophils is shown. Black dots indicate nanogold-conjugated antibody. Secretory granules (**Gr**) show typical morphology (an electron-dense core surrounded by an electron-lucent matrix). **N** = nucleus. **B**, Merged immunofluorescence staining of galectin-10, major basic protein (MBP), and DNA, and DIC images obtained by confocal microscopy are shown. Original magnification × 100. **C**, Cytolysis index (ratio of intracellular MBP-stained and galectin-10–stained areas) was assessed as described in Supplementary Figure 1 (http://onlinelibrary.wiley.com/doi/10.1002/art.41727/abstract). **D**, EETosis was induced by treatment with PMA for 180 minutes. Membrane permeability was assessed using Sytox. **E**, Following induction of EETosis (PMA, 180 minutes), culture supernatants were obtained by centrifugation at 10,000*g* for 10 minutes. Concentrations of lactate dehydrogenase (LDH), galectin-10, and eosinophil-derived neurotoxin (EDN) were measured and assessed as a percentage of the total cell lysate (set at 100%). In **C–E**, bars show the mean ± SD; n = 3–5 samples from different donors. * = $P < 0.05$; ** = $P < 0.01$; *** = $P < 0.005$. Cont = control; PAF = platelet-activating factor; IL-5 = interleukin-5; NS = not significant (see Figure 1 for other definitions).

Taken together, these data suggest that EETosis is characterized by the cytolytic release of CitH3-positive EETs and cell-free granules.

EETosis involves the NADPH oxidase (NOX)–dependent production of ROS (9). To examine the role of ROS in histone hypercitrullination, eosinophils were left unstimulated or were stimulated with DPI, a NOX inhibitor. As shown in Figure 1G and Supplementary Figures 3 and 4 (http://onlinelibrary.wiley.com/doi/10.1002/art.41727/abstract), EETosis-mediated cytolysis and CitH3-positive EETs were completely inhibited by DPI. We also confirmed PAD4-mediated histone hypercitrullination using Cl-amidine, a pharmacologic PAD4 inhibitor. Histone citrullination and formation of EETs were completely inhibited by Cl-amidine (Figure 1G and Supplementary Figures 3 and 4). Interestingly, varying concentrations of Cl-amidine did not inhibit cell death, even at higher concentrations (Supplementary Figure 5, http://onlinelibrary.wiley.com/doi/10.1002/art.41727/abstract). These findings indicate that cytolytic cell death was mediated by enzymatic activation of NOX, but release of net-like EETs was dependent on the NOX/PAD4 pathway.

Cytolytic release of cytoplasmic galectin-10 and intact granules. Human eosinophils contain a large pool of galectin-10, an S-type lectin that comprises 10% of total eosinophil cytoplasmic protein (25). During EETosis, cytoplasmic galectin-10 is released extracellularly (14). To assess the precise subcellular localization of galectin-10, we used a nanogold-conjugated antibody and TEM (28). In blood eosinophils, galectin-10 was consistently localized in the peripheral cytoplasm but not within granules (Figure 2A). We stimulated eosinophils to induce EETosis, fixed them at 15 and 180 minutes, and then immunostained for galectin-10 and MBP (Figure 2B and Supplementary Figure 6, http://onlinelibrary.wiley.com/doi/10.1002/art.41727/abstract). In unstimulated cells, galectin-10 and MBP

were localized in the cytoplasm and in the granules, respectively. Cells undergoing EETosis and releasing net-like DNA stained with MBP only, indicating that the cytolytic loss of galectin-10 was not accompanied by loss of granular contents. We quantified the immunostaining images further using ImageJ software. The ratio of MBP:galectin-10 was considered to reflect the cytolysis index, whereby the greater loss of intracellular galectin-10 over that of cell-retained MBP yielded an elevated cytolysis index (Supplementary Figure 1, http://onlinelibrary.wiley.com/doi/10.1002/art.41727/abstract). The cytolysis index was comparable following stimulation for 15 minutes but was significantly increased by stimulation for 180 minutes with various EETosis-inducing stimuli (Figure 2C).

The cell-impermeable DNA-specific dye, Sytox, can reveal cells whose plasma and nuclear membranes have been compromised. Following induction of EETosis by treatment with PMA for 180 minutes, ~85% of eosinophils were Sytox-positive (Figure 2D). To quantify the proteins released by EETosis, levels of LDH (a cytoplasmic protein), galectin-10, and EDN (a granular protein) in culture medium were measured (Figure 2E). Culture medium was centrifuged at 10,000*g* to remove contaminating cellular components including major free vesicles and granules. EETosis resulted in the release of 51% total cellular LDH and 45% galectin-10, but only 7% EDN. These findings suggest that the release of intracellular galectin-10 was closely associated with cytolysis rather than the classic secretory mechanisms of degranulation, in accordance with recent studies (14,25).

Eosinophil infiltration into various tissues shows EETosis signature in EGPA patients. We studied affected tissues from patients with active EGPA to confirm our in vitro results. H&E staining showed the infiltration of intact eosinophils as well as chromatolytic cells and free eosinophil granules (Figure 3A and Supplementary Figure 7, http://onlinelibrary.wiley.com/doi/10.1002/art.41727/abstract). Immunostaining of identical fields indicated these lytic eosinophils contained net-like CitH3 and DNA (Figure 3B and Supplementary Figure 7). CitH3-stained lytic eosinophils were detected in 12 of 14 biopsy samples from 10 patients with EGPA. The characteristic ultrastructural morphology of EETosis was also confirmed by TEM (Figure 3C). We did not observe eosinophils with apoptotic or necrotic morphology.

Next, biopsy samples were immunostained for galectin-10 and MBP. Low-magnification images were typical of inflamed tissues and showed diffuse staining of MBP and cellular staining of galectin-10 (Figures 3D and E). High-magnification images showed intact eosinophils positive for galectin-10 and MBP,

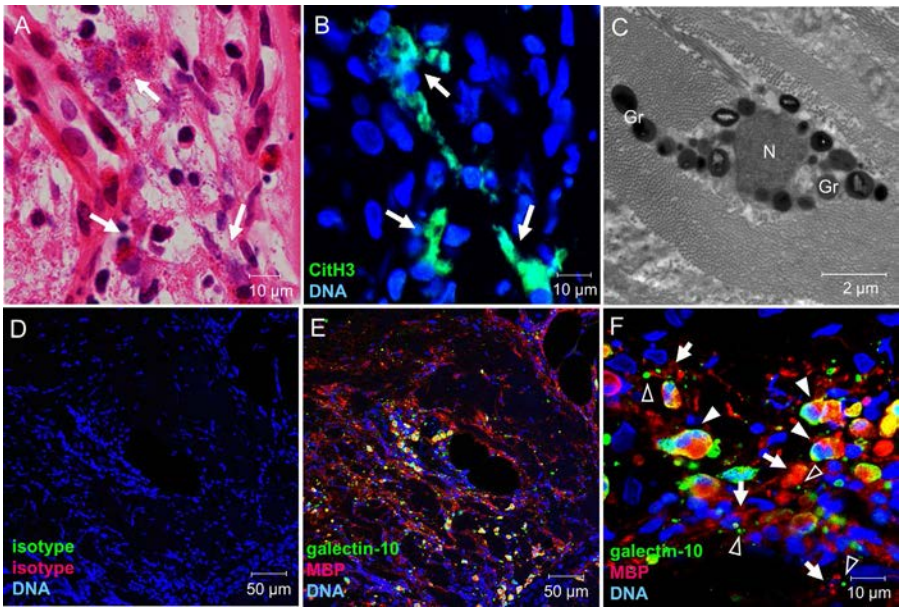

Figure 3. Presence of eosinophil ETosis (EETosis) in affected tissues in patients with eosinophilic granulomatosis with polyangiitis (EGPA). **A**, Hematoxylin and eosin staining shows chromatolytic eosinophils and adjacent cell-free granules (**arrows**) in lung biopsy tissue from a patient with EGPA. **B**, Immunostaining image (identical field to **A**) for citrullinated histone H3 (CitH3) and DNA (Hoechst 33342) indicates mesh-like extracellular traps (**arrows**). Note that most intact cells are not stained with CitH3. Original magnification × 100. **C**, Typical EETosis morphology, characterized by plasma/nuclear membrane disintegration and chromatin decondensation, was present in the nerve tissue from an EGPA patient, observed by transmission electron microscopy. Chromatolytic nucleus (**N**) and free granules (**Gr**) were observed in nerve tissue. **D**, Skin biopsy tissue from a patient with EGPA was stained with 2 isotype-matched control antibodies and assessed by confocal microscopy, showing absence of fluorescence. Original magnification × 100. **E**, Serial sections of skin biopsy tissue from an EGPA patient were stained for galectin-10, major basic protein (MBP), and DNA and assessed using confocal microscopy. **F**, Higher magnification of the image shown in **E** (original magnification × 100) shows that intact eosinophils retained MBP and galectin-10 (**solid arrowheads**). Separate distinct and focal areas of staining for extracellular punctate MBP (**arrows**) and galectin-10 (**open arrowheads**) are indicative of free extracellular granules and vesicles, respectively. Cytolytic eosinophils were observed in 21 samples from 16 patients.

whereas lytic cells and free granules were only positive for MBP (Figure 3F). Cytolytic eosinophils were detected in 21 of 23 samples from 15 patients and were often associated with small punctate galectin-10 labeling (Figure 3F), which were probably eosinophil extracellular vesicles released from EETotic cells (9,14). No cells were positively stained for cytoplasmic galectin-10 alone. Additional representative images are shown in Supplementary Figure 8 (http://onlinelibrary.wiley.com/doi/10.1002/art.41727/abstract). A summary of detailed clinical data obtained from EGPA patient biopsy samples is shown in Supplementary Table 1 (http://onlinelibrary.wiley.com/doi/10.1002/art.41727/abstract). The cytolysis index of affected tissue from EGPA patients exceeded 0.7 (the control value obtained from intact cells) except in 1 of 23 samples. These results show, for the first time, that eosinophils infiltrating various tissues undergo EETosis in EGPA patients.

Association of serum galectin-10 levels in EGPA with disease activity. Given the difference in the release of cytoplasmic galectin-10 and granule proteins, we investigated their serum concentrations in healthy individuals, patients with stable asthma, EGPA patients whose disease was active, and EGPA patients whose disease was in remission (Figure 4). Clinical characteristics are shown in Table 1, and the treatment history of the patients with EGPA is shown in Supplementary Table 2 (http://onlinelibrary.wiley.com/doi/10.1002/art.41727/abstract). Elevated galectin-10 (cutoff 0.312 ng/ml) was detected in all EGPA patients with active disease but in only 7 of 15 EGPA patients with disease in remission. Levels of galectin-10 and granule proteins (EDN and ECP) were significantly higher in patients with active EGPA compared to all of the other groups (Figure 4A). To exclude the possibility that blood eosinophil

Table 1. Patient characteristics and laboratory data*

	Patients with active EGPA (n = 15)	Patients with EGPA in remission (n = 15)	Patients with asthma (n = 15)	Healthy controls (n = 15)	*P*
Age, median (IQR) years	50 (46.5–65.5)	59.5 (48.5–66.5)	49 (42.0–57.0)	50 (41.5–59.5)	0.5264
Male sex	8 (53.3)	6 (40.0)	7 (46.7)	6 (40.0)	0.8636
BMI, median (IQR) kg/m^2	21.4 (18.0–23.6)	21.4 (18.5–23.9)	23.7 (20.8–25.4)	21.1 (20.3–22.2)	0.3367
Atopy	10 (66.7)	8 (53.3)	11 (73.3)	5 (33.3)	0.1271
GINA step					0.0548
1	2 (13.3)	0	0	–	
2	1 (6.7)	1 (6.7)	1 (6.7)	–	
3	0	0	3 (20.0)	–	
4	5 (33.3)	4 (26.7)	8 (53.3)	–	
5	7 (46.7)	10 (66.7)	3 (20.0)	–	
Smoking status					0.8066
Never smoker	10 (66.7)	12 (80.0)	11 (73.3)	12 (80.0)	
Former smoker	5 (33.3)	3 (20.0)	4 (26.7)	3 (20.0)	
Current smoker	0	0	0	0	
Basic laboratory tests					
WBC count, median (IQR) 10^3/μl	12.6 (11.1–24.5)	8.1 (6.5–8.5)	5.4 (4.67–6.34)	6.0 (5.1–7.0)	<0.0001
Blood eosinophilia, median (IQR) 10^3/μl	5.0 (3.4–15.5)	0.5 (0.4–0.7)	0.39 (0.34–0.54)	0.2 (0.1–0.3)	<0.0001
Blood platelet count, median (IQR) 10^3/μl	299 (236–394)	245 (214–261)	237 (186–267)	212 (195–249)	0.03
IgE, median (IQR) IU/ml	1,060 (702–2,530)	134 (68–375)	341 (199–574)	–	0.0002
MPO-ANCA positive	5 (33.3)	6 (40.0)	–	–	>0.9999
BVAS, median (IQR)	12.0 (10.0–30.0)	4.0 (4.0–5.0)	–	–	<0.0001
Diagnostic disease characteristics at EGPA onset					
Asthma with eosinophilia	15 (100)	15 (100)	–	–	>0.9999
Biopsy evidence†	8 (53.3)	12 (80.0)	–	–	0.2451
Neuropathy	13 (86.7)	15 (100)	–	–	0.4828
Pulmonary infiltrates	7 (46.7)	6 (40.0)	–	–	>0.9999
Sinonasal abnormality	14 (93.3)	13 (86.7)	–	–	>0.9999
Cardiomyopathy	1 (6.7)	4 (26.7)	–	–	0.3295
Palpable purpura	5 (33.3)	4 (26.7)	–	–	>0.9999

* Except where indicated otherwise, values are the number (%) of subjects. For diagnostic disease characteristics at the onset of eosinophilic granulomatosis with polyangiitis (EGPA), we referred to the Birmingham Vasculitis Activity Score (BVAS); for more details about the BVAS, see Patients and Methods. IQR = interquartile range; BMI = body mass index; GINA = Global Initiative for Asthma; WBC = white blood cell; MPO-ANCA = myeloperoxidase–antineutrophil cytoplasmic antibody.

† Biopsy evidence was defined as a biopsy specimen showing histopathologic evidence of eosinophilic vasculitis, perivascular eosinophilic infiltration, or eosinophil-rich granulomatous inflammation.

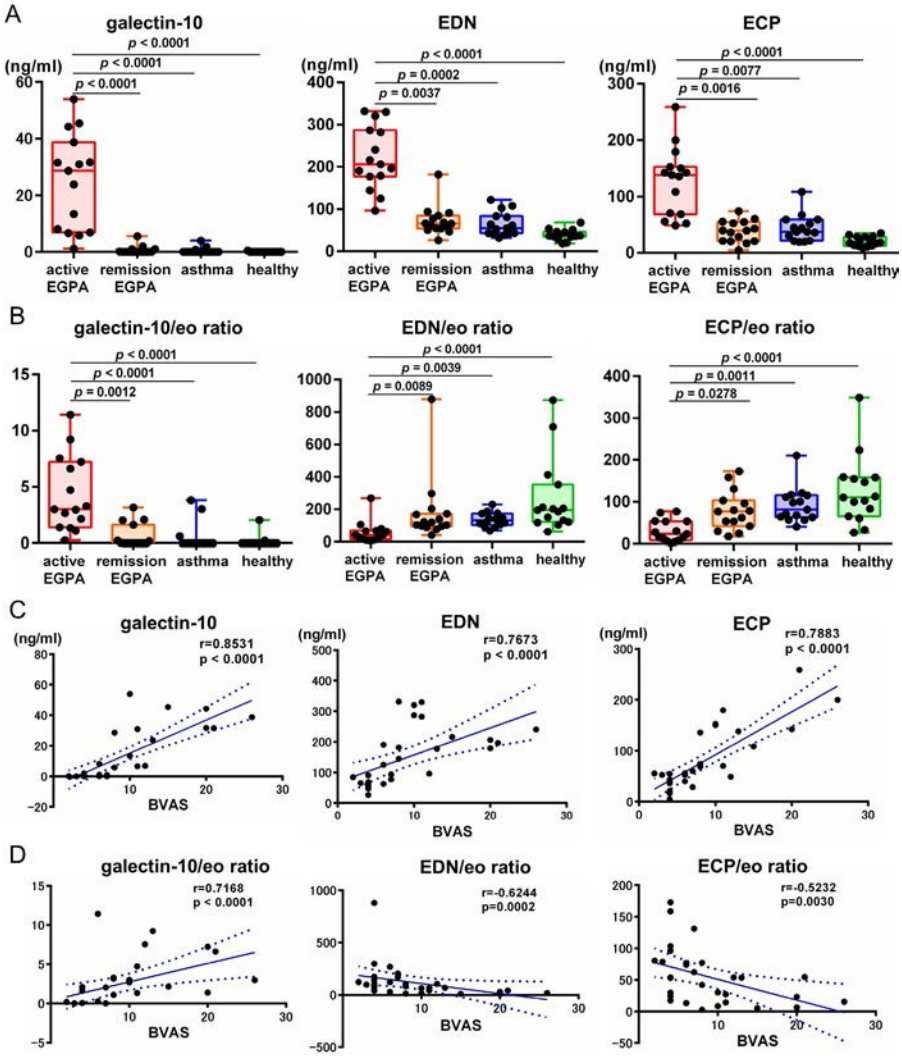

Figure 4. Increased serum galectin-10 levels in patients with eosinophilic granulomatosis with polyangiitis (EGPA). **A** and **B**, Serum levels of the eosinophil-derived proteins galectin-10, eosinophil-derived neurotoxin (EDN), and eosinophil cationic protein (ECP) were measured by enzyme-linked immunosorbent assay (**A**), and the ratio of each protein to blood eosinophil counts (eo) was determined (**B**). Data are presented as box plots, with lines inside the boxes showing the median, boxes showing the interquartile range, and bars outside the boxes showing the minimum and maximum values. Fifteen samples were analyzed for each group. **C** and **D**, Serum levels of eosinophil-derived proteins (**C**) and the ratio of each protein to blood eosinophil counts (**D**) were assessed for correlations with the Birmingham Vasculitis Activity Score (BVAS) in patients with EGPA (n = 30). For more details about the BVAS, see Patients and Methods.

density affected these results (29,30), we compared serum concentrations of these proteins normalized to blood eosinophil counts (Figure 4B). Normalized levels of galectin-10, but not of granule proteins, were significantly elevated in patients with active EGPA. Detailed correlations with eosinophil counts in each group are shown in Supplementary Table 3 (http://onlinelibrary.wiley.com/doi/10.1002/art.41727/abstract).

We then investigated whether the clinical symptoms of EGPA were associated with levels of galectin-10 and granule proteins. Disease activity was characterized using the BVAS scoring system. As expected, there was a positive correlation between BVAS score and serum eosinophil–derived proteins (Figure 4C). When serum concentrations were normalized to blood eosinophil counts, galectin-10 was positively correlated with BVAS score, but granule proteins showed a negative correlation (Figure 4D). These findings indicate that galectin-10 is a unique biomarker for EGPA.

Association of serum IL-5 levels with galectin-10 in active EGPA. Since the IL-5/eosinophil axis plays a critical role in the pathogenesis of EGPA (3,16,17), we measured serum IL-5 in all subjects. As expected, serum IL-5 levels were significantly increased in patients with active EGPA compared to other subjects (Figure 5A). In addition, a positive correlation between galectin-10 and IL-5 was observed (Figure 5B), indicating the causal role of IL-5 in increased galectin-10 levels. We further assessed the relationship between IL-5 and blood eosinophil count, galectin-10, ECP, and EDN in each group (Supplementary Table 4,

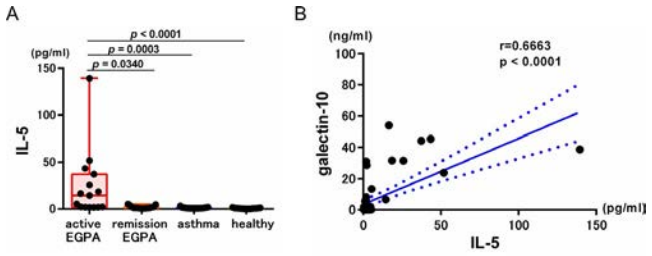

Figure 5. Serum levels of interleukin-5 (IL-5) and galectin-10 in patients with eosinophilic granulomatosis with polyangiitis (EGPA) (active disease or in remission) compared to patients with asthma and healthy controls. **A**, Serum IL-5 levels were measured by enzyme-linked immunosorbent assay. Data are presented as box plots, with lines inside the boxes showing the median, boxes showing the interquartile range, and bars outside the boxes showing the minimum and maximum values. **B**, Correlation between serum levels of IL-5 and serum levels of galectin-10 in all subjects (n = 60) is shown.

http://onlinelibrary.wiley.com/doi/10.1002/art.41727/abstract). Of note, a positive correlation was observed only with galectin-10 in the group with active EGPA.

DISCUSSION

ETosis, the controlled release of chromatin from inflammatory cells, is considered an evolutionarily conserved mechanism of the innate immune system (31). Accumulating studies of neutrophils have indicated that uncontrolled ETosis can lead to end-organ dysfunction; however, the relationship with eosinophils is less clear. Similar to neutrophils, eosinophils terminally differentiate in the bone marrow and are nondividing cells. Evaluation of eosinophil cell death is therefore essential to our understanding of eosinophilic inflammatory diseases. Eosinophils are the major cells responsible for EGPA, as opposed to neutrophils in other vasculitides including microscopic polyangiitis and granulomatosis with polyangiitis (32). The present study is the first to demonstrate that EETosis occurs in patients with EGPA. Galectin-10, a nonsecreted, lectin-like protein that is highly abundant in the cytoplasm of human (and not other animal) eosinophils (33), was detected in the serum of EGPA patients and was associated with disease activity. Our findings suggest that galectin-10 might be a novel biomarker for systemic eosinophilic inflammation.

Using isolated human eosinophils, we found several characteristics of EETosis that were clearly different from apoptosis and necrosis. EETosis does not cause DNA fragmentation but disintegrates the plasma and nuclear membranes through NOX activation (9,24) and eventually releases PAD4-mediated CitH3-positive EETs. Indeed, patients with chronic granulomatosis diseases lacking ROS production in phagocytes and PAD4-deficient mice were susceptible to bacterial infection related to a lack of NET formation (27,34). PAD4 is a calcium-dependent enzyme responsible for histone hypercitrullination (26), and calcium ionophore is a potent EETosis inducer (9). Conversely, physiologic stimulus–induced EETosis was completely inhibited by the calcium chelator EDTA (9,11). These signaling pathways might have an important role in future therapeutic modalities by regulating EETs.

Lytic eosinophils in inflamed tissue are not caused by necrosis or related to artifacts caused by sample handling and preparation (35). We did not observe morphologically identifiable apoptotic or necrotic eosinophils in EGPA tissues using TEM. In contrast, EETotic cells were consistently observed in diseased tissues. This is likely because of the rapid process of EETosis (0.5–3 hours in vitro) and the lack of surface phosphatidylserine redistribution typical during apoptosis (9). Phosphatidylserine is recognized by macrophages as a "find me" signal (36); however, extracellular traps remain in the tissue without macrophage processing. Apoptotic eosinophils are rapidly engulfed by phagocytes, protecting tissues from harmful exposure to the inflammatory contents (37). A previous electron microscopic study revealed that the occurrence of apoptosis in eosinophils in allergic airway tissues was rare (6).

Nuclear histones and DNA have been known to act as alarmins (8,38). To identify EETs/EETosis in tissue samples, we utilized multiple methods including TEM, conventional H&E staining, and immunofluorescence confocal microscopy targeting relevant indicators of EETs/EETosis. Detecting EETs only in conventional thin sections of solid tissues is challenging, because limited cross-sectional planes of view preclude the recognition of eosinophils and EETs extending into contiguous but unexamined sections (37). Because NETs contain neutrophil elastase and myeloperoxidase, double immunostaining techniques for DNA (histones) and these neutrophil-specific granule proteins can be utilized to identify NETs (27). In contrast, eosinophil granule proteins were not uniformly colocalized with EETs, because EETosis releases intact granules but not free granule–derived proteins (9,24). A recent electron microscopy study demonstrated the ongoing release of free eosinophil granules in a sural nerve biopsy specimen from an EGPA patient (39). The extracellular granules remained in the tissues and secreted their contents (9,37,40).

Eosinophil granule proteins have marked potential toxicity for host tissues and significant functions relevant to the mechanisms of pathogenesis in EGPA. For example, MBP contributed to increased epithelial permeability, smooth muscle contraction, and liberation of molecules related to tissue remodeling and fibrosis (41). EDN can recruit dendritic cells and enhance antigen-specific immune responses (42). Consistent with our data, the deposition of extracellular eosinophil granule proteins was prominently associated with lesional tissues from patients with EGPA (43). The cationic nature of granule proteins suggests they are adsorbed to negatively charged tissues and likely contribute to the local inflammatory response (2,44). Previous studies have shown increased serum eosinophil granule proteins in patients with EGPA: higher concentrations of serum ECP (45), MBP (43,46), and EDN (43,46)

were observed in those with active EGPA compared to healthy controls.

To the best of our knowledge, there have been no reports of the clinical significance of serum galectin-10. Eosinophils contain large amounts of galectin-10 in the cytoplasm, which is not secreted by piecemeal degranulation (14,25). Our current data indicate that galectin-10 is a unique marker with different characteristics compared to granule-derived proteins. Cationic eosinophil granule proteins bind strongly to tissue elements and aggregate with long half-lives, and thus may fail to readily enter the peripheral circulation (2,47). The rapid release of extracellular galectin-10 and membrane-bound, cell-free intact eosinophil granules (with their contained cationic granule proteins) from human eosinophils might be associated with differing serum concentrations of galectin-10 and eosinophil granule proteins.

A proposed mechanism of increased galectin-10 levels in EGPA is shown in Supplementary Figure 9 (http://onlinelibrary.wiley.com/doi/10.1002/art.41727/abstract). In patients with EGPA, serum IL-5 has been shown to be associated with disease severity (48,49), and anti–IL-5 treatment is an important therapeutic modality (17). Taken together with the fact that IL-5 induces EETosis in the presence of additional stimuli (9), IL-5–elicited eosinophil activation cascades might lead to the induction of EETosis and the release of galectin-10. Unlike patients with stable asthma, increased serum galectin-10 levels were observed in patients with active EGPA, likely due to systemic occurrence of EETosis.

Although our findings suggest that serum galectin-10 is a surrogate marker for EETosis, there are limitations to this study. Galectin-10 levels could be affected by various factors including eosinophil production, distribution, and activation status, as well as by blood half-life of galectin-10. Galectin-10 may also be expressed by basophils and some T cell subsets (33). We speculate that these cells were not contributory because galectin-10–positive cells consistently stained for eosinophil-specific MBP in our histologic analysis. Elevated galectin-10 levels might not be specific to EGPA, since the occurrence of EETosis has been observed in other diseases (8,50). Future studies on galectin-10 levels from various eosinophilic diseases under different conditions are required to provide cogent evidence regarding the association between EETosis and galectin-10.

Eosinophils, granulocytes of the innate immune system, contain distinct proteins in their granules and cytoplasm. Proteomic analysis of human peripheral blood revealed that galectin-10 was the fifth most abundant human eosinophil protein (after actin, a nonsecretory ribonuclease and histones) (51). Another earlier proteomic study showed that galectin-10 was the second most prevalent protein in eosinophil cytoplasmic subcellular fractions (52). Considering the exclusive expression and large pool of galectin-10 in eosinophils, elevated serum galectin-10 levels in EGPA patients likely reflect systemic eosinophil cytolysis/EETosis.

ACKNOWLEDGMENTS

The authors are grateful to Noriko Tan for outstanding technical assistance and Satomi Misawa for outstanding assistance in drawing the figure. We thank Ludovic Croxford and Dr. Gillian Campbell from the Edanz Group for editing a draft of the manuscript.

AUTHOR CONTRIBUTIONS

All authors were involved in drafting the article or revising it critically for important intellectual content, and all authors approved the final version to be published. Drs. Fukuchi and Kamide had full access to all of the data in the study and takes responsibility for the integrity of the data and the accuracy of the data analysis.

Study conception and design. Fukuchi, Kamide, Ueki.

Acquisition of data. Fukuchi, Kamide, Ueki, Miyabe, Konno, Oka, Takeuchi, Koyota, Melo.

Analysis and interpretation of data. Fukuchi, Kamide, Ueki, Hirokawa, Yamada, Weller, Taniguchi.

REFERENCES

1. Melo RC, Liu L, Xenakis JJ, Spencer LA. Eosinophil-derived cytokines in health and disease: unraveling novel mechanisms of selective secretion. Allergy 2013;68:274–84.
2. Klion AD, Ackerman SJ, Bochner BS. Contributions of eosinophils to human health and disease [review]. Annu Rev Pathol 2020;15:179–209.
3. Nagase H, Ueki S, Fujieda S. The roles of IL-5 and anti-IL-5 treatment in eosinophilic diseases: asthma, eosinophilic granulomatosis with polyangiitis, and eosinophilic chronic rhinosinusitis. Allergol Int 2020;69:178–86.
4. Weller PF, Spencer LA. Functions of tissue-resident eosinophils [review]. Nat Rev Immunol 2017;17:746–60.
5. Melo RC, Weller PF. Contemporary understanding of the secretory granules in human eosinophils. J Leukoc Biol 2018;104:85–93.
6. Erjefalt JS, Persson CG. New aspects of degranulation and fates of airway mucosal eosinophils. Am J Respir Crit Care Med 2000;161:2074–85.
7. Saffari H, Hoffman LH, Peterson KA, Fang JC, Leiferman KM, Pease LF III, et al. Electron microscopy elucidates eosinophil degranulation patterns in patients with eosinophilic esophagitis. J Allergy Clin Immunol 2014;133:1728–34.
8. Mukherjee M, Lacy P, Ueki S. Eosinophil extracellular traps and inflammatory pathologies—untangling the web! [review]. Front Immunol 2018;9:2763.
9. Ueki S, Melo RC, Ghiran I, Spencer LA, Dvorak AM, Weller PF. Eosinophil extracellular DNA trap cell death mediates lytic release of free secretion-competent eosinophil granules in humans. Blood 2013;121:2074–83.
10. Wartha F, Henriques-Normark B. ETosis: a novel cell death pathway. Sci Signal 2008;1:pe25.
11. Ueki S, Konno Y, Takeda M, Moritoki Y, Hirokawa M, Matsuwaki Y, et al. Eosinophil extracellular trap cell death-derived DNA traps: their presence in secretions and functional attributes. J Allergy Clin Immunol 2016;137:258–67.
12. Ohta N, Ueki S, Konno Y, Hirokawa M, Kubota T, Tomioka-Matsutani S, et al. ETosis-derived DNA trap production in middle ear effusion is a common feature of eosinophilic otitis media [letter]. Allergol Int 2018;67:414–6.
13. Muniz VS, Silva JC, Braga YA, Melo RC, Ueki S, Takeda M, et al. Eosinophils release extracellular DNA traps in response to Aspergillus fumigatus. J Allergy Clin Immunol 2018;141:571–85.

14. Ueki S, Tokunaga T, Melo RC, Saito H, Honda K, Fukuchi M, et al. Charcot-Leyden crystal formation is closely associated with eosinophil extracellular trap cell death. Blood 2018;132:2183–7.
15. Persson EK, Verstraete K, Heyndrickx I, Gevaert E, Aegerter H, Percier JM, et al. Protein crystallization promotes type 2 immunity and is reversible by antibody treatment. Science 2019;364:eaaw4295.
16. Furuta S, Iwamoto T, Nakajima H. Update on eosinophilic granulomatosis with polyangiitis. Allergol Int 2019;68:430–6.
17. Wechsler ME, Akuthota P, Jayne D, Khoury P, Klion A, Langford CA, et al. Mepolizumab or placebo for eosinophilic granulomatosis with polyangiitis. N Engl J Med 2017;376:1921–32.
18. Hellmark T, Ohlsson S, Pettersson A, Hansson M, Johansson AC. Eosinophils in anti-neutrophil cytoplasmic antibody associated vasculitis. BMC Rheumatol 2019;3:9.
19. Natorska J, Zabczyk M, Siudut J, Krawiec P, Mastalerz L, Undas A. Neutrophil extracellular traps formation in patients with eosinophilic granulomatosis with polyangiitis: association with eosinophilic inflammation. Clin Exp Rheumatol 2017;35 Suppl 103:27–32.
20. Global Initiative for Asthma. Global strategy for asthma management and prevention, 2021. URL: http://www.ginasthma.org.
21. Masi AT, Hunder GG, Lie JT, Michel BA, Bloch DA, Arend WP, et al. The American College of Rheumatology 1990 criteria for the classification of Churg-Strauss syndrome (allergic granulomatosis and angiitis). Arthritis Rheum 1990;33:1094–100.
22. Jennette JC, Falk RJ, Bacon PA, Basu N, Cid MC, Ferrario F, et al. 2012 revised International Chapel Hill Consensus Conference nomenclature of vasculitides. Arthritis Rheum 2013;65:1–11.
23. Mukhtyar C, Lee R, Brown D, Carruthers D, Dasgupta B, Dubey S, et al. Modification and validation of the Birmingham Vasculitis Activity Score (version 3). Ann Rheum Dis 2009;68:1827–32.
24. Ueki S, Konno Y, Takeda M, Moritoki Y, Hirokawa M, Matsuwaki Y, et al. Eosinophil extracellular trap cell death-derived DNA traps: their presence in secretions and functional attributes. J Allergy Clin Immunol 2016;137:258–67.
25. Melo RC, Wang H, Silva TP, Imoto Y, Fujieda S, Fukuchi M, et al. Galectin-10, the protein that forms Charcot-Leyden crystals, is not stored in granules but resides in the peripheral cytoplasm of human eosinophils. J Leukoc Biol 2020;108:139–49.
26. Rohrbach AS, Slade DJ, Thompson PR, Mowen KA. Activation of PAD4 in NET formation [review]. Front Immunol 2012;3:360.
27. Brinkmann V, Zychlinsky A. Neutrophil extracellular traps: is immunity the second function of chromatin? J Cell Biol 2012;198:773–83.
28. Melo RC, Morgan E, Monahan-Earley R, Dvorak AM, Weller PF. Pre-embedding immunogold labeling to optimize protein localization at subcellular compartments and membrane microdomains of leukocytes. Nat Protoc 2014;9:2382–94.
29. Imai C, Yamazaki H, Tanaka Y, Matsunaga M, Numata O, Torigoe K. Ratio of eosinophil cationic protein/eosinophil count as a new marker in children with acute asthma. Pediatr Int 1999;41: 142–6.
30. Koh YY, Kang H, Kim CK. Ratio of serum eosinophil cationic protein/blood eosinophil counts in children with asthma: comparison between acute exacerbation and clinical remission. Allergy Asthma Proc 2003;24:269–74.
31. Robb CT, Dyrynda EA, Gray RD, Rossi AG, Smith VJ. Invertebrate extracellular phagocyte traps show that chromatin is an ancient defence weapon. Nat Commun 2014;5:4627.
32. Chaigne B, Guillevin L. Vasculitis for the internist: focus on ANCA-associated vasculitis. Intern Emerg Med 2017;12:577–85.
33. Weller PF, Wang H, Melo RC. The Charcot-Leyden crystal protein revisited: a lysopalmitoylphospholipase and more. J Leukoc Biol 2020;108:105–12.
34. Li P, Li M, Lindberg MR, Kennett MJ, Xiong N, Wang Y. PAD4 is essential for antibacterial innate immunity mediated by neutrophil extracellular traps. J Exp Med 2010;207:1853–62.
35. Persson CG, Erjefalt JS. "Ultimate activation" of eosinophils in vivo: lysis and release of clusters of free eosinophil granules (Cfegs). Thorax 1997;52:569–74.
36. Nagata S. Apoptosis and clearance of apoptotic cells [review]. Annu Rev Immunol 2018;36:489–517.
37. Ueki S, Tokunaga T, Fujieda S, Honda K, Hirokawa M, Spencer LA, et al. Eosinophil ETosis and DNA traps: a new look at eosinophilic inflammation. Curr Allergy Asthma Rep 2016;16:54.
38. Semeraro F, Ammollo CT, Morrissey JH, Dale GL, Friese P, Esmon NL, et al. Extracellular histones promote thrombin generation through platelet-dependent mechanisms: involvement of platelet TLR2 and TLR4. Blood 2011;118:1952–61.
39. Nishi R, Koike H, Ohyama K, Fukami Y, Ikeda S, Kawagashira Y, et al. Differential clinicopathologic features of EGPA-associated neuropathy with and without ANCA. Neurology 2020;94:e1726–37.
40. Neves JS, Perez SA, Spencer LA, Melo RC, Reynolds L, Ghiran I, et al. Eosinophil granules function extracellularly as receptor-mediated secretory organelles. Proc Natl Acad Sci U S A 2008;105:18478–83.
41. Furuta GT, Kagalwalla AF, Lee JJ, Alumkal P, Maybruck BT, Fillon S, et al. The oesophageal string test: a novel, minimally invasive method measures mucosal inflammation in eosinophilic oesophagitis. Gut 2013;62:1395–405.
42. Yang D, Chen Q, Su SB, Zhang P, Kurosaka K, Caspi RR, et al. Eosinophil-derived neurotoxin acts as an alarmin to activate the TLR2-MyD88 signal pathway in dendritic cells and enhances Th2 immune responses. J Exp Med 2008;205:79–90.
43. Peen E, Hahn P, Lauwers G, Williams RC Jr, Gleich G, Kephart GM. Churg-Strauss syndrome: localization of eosinophil major basic protein in damaged tissues. Arthritis Rheum 2000;43:1897–900.
44. Adamko DJ, Wu Y, Ajamian F, Ilarraza R, Moqbel R, Gleich GJ. The effect of cationic charge on release of eosinophil mediators. J Allergy Clin Immunol 2008;122:383–90.
45. Guilpain P, Auclair JF, Tamby MC, Servettaz A, Mahr A, Weill B, et al. Serum eosinophil cationic protein: a marker of disease activity in Churg-Strauss syndrome. Ann N Y Acad Sci 2007;1107:392–9.
46. Drage LA, Davis MD, de Castro F, van Keulen V, Weiss EA, Gleich GJ, et al. Evidence for pathogenic involvement of eosinophils and neutrophils in Churg-Strauss syndrome. J Am Acad Dermatol 2002;47:209–16.
47. Soragni A, Yousefi S, Stoeckle C, Soriaga AB, Sawaya MR, Kozlowski E, et al. Toxicity of eosinophil MBP is repressed by intracellular crystallization and promoted by extracellular aggregation. Mol Cell 2015;57:1011–21.
48. Kataoka H, Tomita T, Kondo M, Mukai M. Presence of purpura is related to active inflammation in association with IL-5 in eosinophilic granulomatosis with polyangiitis. Rheumatol Int 2021;41:449–54.
49. Hellmich B, Csernok E, Gross WL. Proinflammatory cytokines and autoimmunity in Churg-Strauss syndrome. Ann N Y Acad Sci 2005;1051:121–31.
50. Fukuchi M, Miyabe Y, Furutani C, Saga T, Moritoki Y, Yamada T, et al. How to detect eosinophil ETosis (EETosis) and extracellular traps. Allergol Int 2021;70:19–29.
51. Wilkerson EM, Johansson MW, Hebert AS, Westphall MS, Mathur SK, Jarjour NN, et al. The peripheral blood eosinophil proteome. J Proteome Res 2016;15:1524–33.
52. Straub C, Pazdrak K, Young TW, Stafford SJ, Wu Z, Wiktorowicz JE, et al. Toward the proteome of the human peripheral blood eosinophil. Proteomics Clin Appl 2009;3:1151–73.

American College of Rheumatology
Empowering Rheumatology Professionals

Arthritis & Rheumatology
Vol. 73, No. 9, September 2021, pp 1694–1702
DOI 10.1002/art.41722

Occupational Exposures and Smoking in Eosinophilic Granulomatosis With Polyangiitis: A Case–Control Study

Federica Maritati,[1] Francesco Peyronel,[2] Paride Fenaroli,[2] Francesco Pegoraro,[3] Vieri Lastrucci,[4] Giuseppe D. Benigno,[2] Alessandra Palmisano,[2] Giovanni M. Rossi,[2] Maria L. Urban,[5] Federico Alberici,[6] Paolo Fraticelli,[1] Giacomo Emmi,[4] Massimo Corradi,[7] and Augusto Vaglio[8]

Objective. Eosinophilic granulomatosis with polyangiitis (EGPA) is a rare antineutrophil cytoplasmic antibody (ANCA)–associated vasculitis. Environmental agents and occupational exposures may confer susceptibility to EGPA, but data are scarce. This study was undertaken to investigate the association between occupational exposures (e.g., silica, farming, asbestos, and organic solvents) and other environmental agents (e.g., smoking) and the risk of EGPA.

Methods. Patients with newly diagnosed EGPA (n = 111) and general population controls (n = 333) who were matched for age, sex, and geographic area of origin were recruited at a national referral center for EGPA. Exposures were assessed using a dedicated questionnaire administered by a specialist in occupational medicine, under blinded conditions. Odds ratios (ORs) and 95% confidence intervals (95% CIs) were calculated.

Results. Exposures to silica (OR 2.79 [95% CI 1.55–5.01], $P = 0.001$), organic solvents (OR 3.19 [95% CI 1.91–5.34], $P < 0.001$), and farming (OR 2.71 [95% CI 1.71–4.29], $P < 0.001$) were associated with an increased risk of EGPA. Co-exposure to silica and farming yielded an OR of 9.12 (95% CI 3.06–27.19, $P < 0.001$), suggesting a multiplicative effect between these 2 exposures. Smoking (current and former smokers combined) was significantly less frequent among patients with EGPA compared to controls (OR 0.49 [95% CI 0.29–0.70], $P < 0.001$). The pack-year index was also lower among patients with EGPA (OR 0.96 [95% CI 0.94–0.98], $P < 0.001$). The association of silica and farming was primarily aligned with ANCA-positive EGPA, while the association of smoking status and organic solvents was primarily aligned with ANCA-negative EGPA.

Conclusion. The environment can influence susceptibility to EGPA. Exposure to silica, farming, or organic solvents is associated with an increased risk of EGPA, while smoking is associated with a lower risk. These exposures seem to have distinct effects on different EGPA subsets.

INTRODUCTION

Eosinophilic granulomatosis with polyangiitis (EGPA) is a rare form of antineutrophil cytoplasmic antibody (ANCA)–associated vasculitis (AAV) (1), characterized by adult-onset asthma, blood and tissue eosinophilia, eosinophil-rich granulomas, and small vessel vasculitis (2). After a prodromal phase hallmarked by asthma and rhino-sinusitis, EGPA patients develop the distinctive clinical manifestations of the disease, which are primarily eosinophilic (e.g., eosinophilic cardiomyopathy, and gastroenteritis) or vasculitic (e.g., peripheral neuropathy, purpura, and glomerulonephritis) (3). Although EGPA is included in the spectrum of AAV, only 30–40% of EGPA patients are positive for ANCA, usually with specificity for myeloperoxidase (MPO) (4). ANCA status distinguishes 2 main disease subsets, with features of vasculitis being more common in ANCA-positive patients and eosinophilic features being more common in ANCA-negative patients (4).

The pathogenesis of EGPA is still unclear. Immunogenetic factors confer susceptibility to the disease and shape its phenotypes. A recent genome-wide association study revealed several genetic

[1]Federica Maritati, MD, PhD, Paolo Fraticelli, MD, PhD: University Hospital of Ospedali Riuniti, Ancona, Italy; [2]Francesco Peyronel, MD, Paride Fenaroli, MD, Giuseppe D. Benigno, MD, Alessandra Palmisano, MD, PhD, Giovanni M. Rossi, MD: Parma University Hospital, Parma, Italy; [3]Francesco Pegoraro, MD: Meyer Children's Hospital, Florence, Italy; [4]Vieri Lastrucci, MD, Giacomo Emmi, MD, PhD: University of Florence and Meyer Children's University Hospital, Florence, Italy; [5]Maria L. Urban, MD: University of Florence, Florence, Italy; [6]Federico Alberici, MD: Spedali Civili Hospital, Brescia, and University of Brescia, Brescia, Italy; [7]Massimo Corradi, MD: University of Parma, Parma, Italy; [8]Augusto Vaglio, MD, PhD: University of Florence, Florence, Italy.

No potential conflicts of interest relevant to this article were reported.

Address correspondence to Augusto Vaglio, MD, PhD, Università di Firenze, Dipartimento di Scienze Biomediche Sperimentali e Cliniche "Mario Serio", Viale Pieraccini, 6 50139 Firenze, Italy. Email: augusto.vaglio@unifi.it.

Submitted for publication September 30, 2020; accepted in revised form March 2, 2021.

associations with EGPA and showed that the ANCA-based clinical dichotomy is reflected by distinct genetic signatures. While ANCA-positive EGPA is associated with the HLA–DQ locus (as MPO-ANCA–positive AAV), ANCA-negative EGPA is associated with variants of genes encoding barrier proteins such as GPA33, suggesting that this subset involves a mucosal/barrier dysfunction rather than an autoimmune pathogenesis (5).

In complex diseases, environmental agents contribute to disease susceptibility. In AAV, particularly granulomatosis with polyangiitis (GPA) and microscopic polyangiitis (MPA), some occupational exposures or activities (e.g., silica and farming) have been found to be associated with an increased risk of disease. However, most of these studies were underpowered and included very few, if any, patients with EGPA (6–11).

In this present study, we investigated the association between environmental and occupational agents and EGPA. Additionally, we analyzed other traditional risk factors associated with vascular diseases (e.g., smoking).

PATIENTS AND METHODS

In this case–control study, each patient was matched with 3 controls from the general population. A questionnaire was administered by a specialist in occupational medicine who was not part of the team of physicians that monitored the patients and was blinded with regard to the subject's study group status (case or control). Cases and controls were identified by the physicians and received an appointment for the interview. In order to limit recall bias (an overestimation of exposures by patients), neither the questionnaire nor the informed consent form disclosed the purpose of the study. The study was presented to the participants as an epidemiologic survey aimed at assessing various occupational and non-occupational exposures in different Italian regions. EGPA patients were not informed of the possible association between the different risk factors and EGPA during their routine visits. All patients had newly diagnosed EGPA and were interviewed within 3 months of the diagnosis. This study was conducted in accordance with the Declaration of Helsinki and was approved by the local ethics committee. All patients and controls provided written informed consent. Privacy was preserved through the adoption of alphanumeric codes as identifiers.

Cases and controls. All EGPA patients who were referred to or received a diagnosis at the Vasculitis Clinic of Parma University Hospital between December 2010 and October 2018 were invited to participate. EGPA was diagnosed according to the American College of Rheumatology criteria (12) and the Chapel Hill Consensus Conference definition (1). Disease activity was assessed by the Birmingham Vasculitis Activity Score (BVAS) (13), and prognosis was assessed using the revised Five-Factors Score (FFS) (14). Patients age <18 years at time of diagnosis, those with other vasculitides, and patients with cognitive impairment or severe illness that could potentially enable them from completing the questionnaire were excluded.

We identified 130 patients with EGPA, of whom 19 were excluded (1 died, 11 were lost to follow-up before the interview, 3 were age <18 years at time of diagnosis, 2 declined participation, 1 had dementia, and 1 never resided or worked in Italy). We also identified 340 controls, of whom 7 were excluded (3 declined participation and 4 did not attend the appointment to be interviewed). The controls were case-matched for age (±5 years), sex, and geographic origin (North versus Central/Southern Italy) and were recruited from among relatives or friends of patients from all over Italy who were admitted to Parma University Hospital for kidney transplantation. The recruitment of controls occurred in parallel with that of the patients.

Data collection and exposure assessment. We developed a structured questionnaire (see Supplementary Questionnaire, available on the *Arthritis & Rheumatology* website at http://onlinelibrary.wiley.com/doi/10.1002/art.41722/abstract) to collect data regarding medical history and exposures. This was based on a questionnaire we previously used for a study on idiopathic retroperitoneal fibrosis (15), which was adapted to AAV with the inclusion of additional questions. The main exposures analyzed were cigarette smoking and occupational exposure to silica, asbestos, farming, organic solvents, metals, other industrial chemicals, pesticides, and textile fibers. All exposures had to have taken place prior to the diagnosis of EGPA among the cases or the date on which the controls were interviewed.

The questionnaire comprised 3 main sections. Section 1 addressed demographic data, level of education, lifestyle-related risk factors, and comorbidities such as smoking, cardiovascular disease, or other autoimmune diseases. Tobacco smoking was evaluated both as a categorical variable (presence or absence) and a continuous variable (pack-years). Persons who had abstained from smoking for at least 6 months were classified as former smokers. Hypertension was identified when at least 1 of the following criteria was met: physician diagnosis of hypertension, self-reported use of antihypertensive drugs, or reported values of systolic blood pressure ≥140 mm Hg and/or diastolic blood pressure ≥90 mm Hg. Obesity was defined as a body mass index (BMI) >30 kg/m^2. Data on established ischemic heart disease, cerebrovascular disease, and cancer were also obtained (no physical examination or laboratory tests were conducted as part of the study). Ischemic heart disease was recorded as present if there was a history of myocardial infarction, revascularization procedures, or a clinical diagnosis of angina. Cerebrovascular disease was recorded as present if the subject had a history of stroke confirmed by computed tomography or magnetic resonance imaging, or a transient ischemic attack. A diagnosis of cancer was recorded if the subject had a history of any malignant neoplasm for which they underwent surgery, chemotherapy, or radiotherapy.

Section 2 of the questionnaire focused on exposure to asbestos, silica, and farming. Questions regarding asbestos exposure were derived from an ad hoc questionnaire developed and validated by the Italian National Mesothelioma Register (ReNaM) (16). Asbestos exposure was classified as occupational or extra-occupational. Occupational asbestos exposure was further classified as the following: documented, if individuals worked using asbestos; probable, if individuals worked in industrial settings where asbestos was present but exposure could not be documented; and possible, if asbestos was probably present but not reported in the work environment. Extra-occupational asbestos exposure included familial contact (individuals who lived with a worker assigned to the documented/possible exposure group) and environmental contact (individuals who presently lived or had lived near industrial sites where asbestos was used). We eventually only analyzed occupational asbestos exposure because this could be ascertained more reliably. Direct questions were asked to determine whether individuals had a work history that involved exposure to silica, such as coal or mine workers, sandblasters, bakers, dental workers, or construction workers. The questions related to farming generally included farm exposure, participation in harvesting, and exposure to animals, although no specific questions were asked on the different types of farming activities or the different animal species to which the subjects were exposed.

Section 3 of the questionnaire focused on other occupational exposures. The assessment of occupational exposure to organic solvents, metals, other industrial chemicals, and pesticides was based on the Geoparkinson questionnaire, which was used in a previous European study on exposures in Parkinson's disease (17). In addition, the evaluation of exposure to textile fibers was based on the questionnaire used in the ICARE study, which investigated this type of exposure in patients with lung cancer (18).

Sample size calculation. In a meta-analysis investigating the association between AAV and silica exposure, an overall odds ratio (OR) of 2.56 was reported (8). The CAREX database identified a prevalence of silica exposure among Italian workers of 7% (19). We hypothesized that the correlation coefficient (r) for exposures between cases and controls in a matched case–control study with a 1:3 design would be 0.2. Using a chi-square test with a 0.05 significance level, 90% power to detect an OR of 3.00 compared to the alternative of equal odds would be achieved with a sample size of 100 cases and 300 controls. To detect an OR of 2.63, 80% power would be achieved with the same sample size.

Statistical analysis. Continuous variables are reported as the median and interquartile range (IQR), and categorical variables are reported as the number and percent. Student's *t*-test was used to assess differences between continuous variables. Differences between categorical variables were analyzed by chi-square test. Correlation analyses were performed by computing Spearman's correlation coefficients. Univariable and multivariable matched logistic regression models were used to assess the impact of exposure to risk factors on the development of EGPA. ORs expressed by exp(B) values were reported with 95% confidence intervals (95% CIs). In the multivariable matched logistic regression model, independent variables were entered using a forward selection method. Two-sided *P* values less than or equal to 0.05 were considered significant. Statistical analyses were performed using IBM SPSS Statistics version 25.0.

RESULTS

The main characteristics of EGPA patients and controls are summarized in Supplementary Table 1 (available on the *Arthritis & Rheumatology* website at http://onlinelibrary.wiley.com/doi/10.1002/art.41722/abstract). The 2 groups were well matched for age, sex, and geographic origin. In addition, no significant differences between EGPA patients and controls were observed with respect to levels of education.

Non-occupational risk factors. Prevalence comparisons of non-occupational risk factors are shown in Table 1. Patients with EGPA had a lower median BMI (24 kg/m^2 [IQR 22–26]) compared to controls (25 kg/m^2 [IQR 23–28]) ($P = 0.001$), although the prevalence of obesity did not differ between the 2 groups (6% versus 11%; $P = 0.128$). No statistically significant differences were observed in the prevalence of other clinical variables such as hypertension, diabetes, cerebrovascular disease, ischemic heart disease, or malignancies.

The analysis of smoking status showed a significantly lower proportion of current and former smokers combined among cases compared to controls (34% versus 54%) (OR 0.49 [95% CI 0.29–0.70], $P < 0.001$). The proportion of current and former smokers observed in the control group is consistent with the national prevalence of smoking among subjects within the age range of the study in Italy during the past 2 decades (20). The cumulative exposure to smoking showed a lower pack-year index among cases compared to controls (OR 0.96 [95% CI 0.94–0.98], $P < 0.001$). Notably, the difference in pack-years among cases compared to controls was also significant when assessed only in ever-smokers (median 10 pack-years [IQR 5–20] versus median 17 pack-years [IQR 9–30]; $P = 0.006$) (Table 1).

To exclude the possibility that the lower proportion of ever-smokers (current and former smokers) among EGPA patients compared to controls was attributable to disease-related respiratory symptoms (mainly asthma), we analyzed smoking exposure among patients before asthma onset (median age 43 years [IQR 36–52]) and in 222 controls from the control cohort after matching with the cases for age at asthma onset (or for the age at diagnosis in those without asthma). Again, the proportion of current and former smokers combined was significantly lower among EGPA patients compared to controls (Table 1). Despite these considerations, it cannot be excluded with certainty that respiratory

Table 1. Prevalence of comorbidities and non-occupational risk factors in cases and controls*

Risk factor	Cases (n = 111)	Controls (n = 333)	Crude OR (95% CI)	*P*
BMI, median (IQR) kg/m^2	24 (22–26)	25 (23–28)	0.90 (0.84–0.96)	0.001
Overweight (BMI ≥25 kg/m^2)	50 (45)	191 (57)	0.61 (0.40–0.94)	0.025
Obese (BMI ≥30 kg/m^2)	7 (6)	38 (11)	0.52 (0.23–1.21)	0.128
Comorbidities				
Hypertension	28 (25)	133 (40)	0.66 (0.41–1.07)	0.089
Diabetes	5 (5)	20 (6)	0.74 (0.27–2.02)	0.554
Ischemic heart disease	3 (3)	28 (8)	0.30 (0.09–1.01)	0.051
Cerebrovascular disease	1 (1)	6 (2)	0.50 (0.06–4.16)	0.518
Cancer	7 (6)	13 (4)	1.66 (0.64–4.26)	0.296
Smoking at diagnosis				
Non-smokers	73 (66)	154 (46)	1.0	–
Former smokers	36 (32)	83 (25)	0.92 (0.57–1.48)	0.717
Current smokers	2 (2)	96 (29)	0.04 (0.01–0.18)	<0.001
Former and current smokers	38 (34)	179 (54)	0.49 (0.29–0.70)	<0.001
Ever-smokers, median (IQR) pack-years	10 (5–20)	17 (9–30)	–	0.006
All study subjects, median (IQR) pack-years	0 (0–5)	3 (0–20)	0.96 (0.94–0.98)	<0.001
Smoking at asthma onset†				
Age, median (IQR) years	43 (36–52)	49 (41–53)	–	0.106
Non-smokers	75 (67)	93 (42)	1.0	–
Former and current smokers	36 (32)	129 (58)	0.34 (0.21–0.56)	<0.001

* Except where indicated otherwise, values are the number (%). OR = odds ratio; 95% CI = 95% confidence interval; BMI = body mass index; IQR = interquartile range.
† These 222 controls were matched (1:2) with the cases for age at asthma onset or at time of diagnosis in patients without asthma.

symptoms preceding EGPA diagnosis had influenced the patients' smoking behavior.

Occupational risk factors. Table 2 shows the results of univariable logistic regression analysis of associations between occupational risk factors and EGPA. Silica exposure was strongly associated with EGPA (OR 2.79 [95% CI 1.55–5.01], $P = 0.001$). To assess whether this association was influenced by the duration of exposure, we analyzed the proportion of subjects who were not exposed versus the proportion of subjects who were exposed below or above the median exposure duration (i.e., 20 years). The OR among subjects whose exposure was above the median was 5.09 (95% CI 2.11–12.32, $P < 0.001$), while it was 2.28 (95% CI 1.03–5.06, $P = 0.06$) among those whose exposure was below the median.

Exposure to organic solvents was also associated with a significant risk of EGPA (OR 3.19 [95% CI 1.91–5.34], $P < 0.001$). However, the duration of exposure did not seem to influence the risk (data not shown).

We also found a significant association between EGPA and exposure to chemical agents, although this was of borderline statistical significance (OR 1.84 [95% CI 1.12–3.03], $P = 0.016$). However, we detected a dose effect for chemicals, since an exposure above the median of 20 years was strongly associated with EGPA, with an OR of 3.30 (95% CI 1.62–6.70, $P = 0.001$); no association was identified when exposures below the median were considered (OR 1.34 [95% CI 0.70–2.57], $P = 0.38$).

Farming was also associated with EGPA risk (OR 2.71 [95% CI 1.71–4.29], $P < 0.001$). Farming entails different types

Table 2. Prevalence of occupational exposures in cases and controls*

Risk factor	Cases (n = 111)	Controls (n = 333)	Crude OR (95% CI)	*P*
Chemicals	32 (29)	60 (18)	1.84 (1.12–3.03)	0.016
Metals	13 (12)	42 (25)	0.92 (0.47–1.78)	0.803
Pesticides	11 (10)	28 (8)	1.20 (0.58–2.49)	0.629
Silica	24 (22)	30 (9)	2.79 (1.55–5.01)	0.001
Organic solvents	35 (32)	42 (25)	3.19 (1.91–5.34)	<0.001
Asbestos exposure				
Non-exposed	56 (50)	227 (68)	1.0	–
Documented (occupational)	3 (3)	13 (4)	0.94 (0.26–3.40)	0.919
Possible/probable (occupational)	17 (15)	29 (9)	2.38 (1.22–4.63)	0.011
Any occupational exposure	20 (18)	42 (25)	1.93 (1.05–3.54)	0.034
Textile fibers	21 (19)	38 (11)	1.81 (0.99–3.24)	0.062
Farming	47 (42)	71 (21)	2.71 (1.71–4.29)	<0.001

* OR = odds ratio; 95% CI = 95% confidence interval.

Table 3. Association between exposure to risk factors and eosinophilic granulomatosis with polyangiitis (matched logistic regression multivariable analysis)*

Variable	OR (95% CI)	*P*
Smoke exposure (former and current smokers)	0.39 (0.22–0.69)	0.001
Silica	2.26 (1.10–4.62)	0.026
Organic solvents	2.20 (1.14–4.25)	0.018
Farming	2.10 (1.19–3.73)	0.011

* OR = odds ratio; 95% CI = 95% confidence interval.

of exposure, but we could not distinguish between exposure to crops, livestock, or specific animal species. We could only assess exposure to pesticides, which showed no significant association (OR 1.20 [95% CI 0.58–2.49], $P = 0.62$).

We evaluated exposure to asbestos, distinguishing between documented and possible/probable occupational exposure. Documented occupational exposure to asbestos was not associated with EGPA (OR 0.94 [95% CI 0.26–3.40], $P = 0.919$), while a statistically significant, although weak, association with EGPA was identified with possible/probable exposure (OR 2.38 [95% CI 1.22–4.63], $P = 0.011$). Finally, there was no significant association between EGPA and exposure to metals or textile fibers (Table 2).

Multivariable logistic regression analysis showed that exposures to silica, organic solvents, and farming were independently associated with an increased risk of EGPA (OR 2.26 [95% CI 1.10–4.62], $P = 0.026$; OR 2.20 [95% CI 1.14–4.25)], $P = 0.018$; and OR 2.10 [95% CI 1.19–3.73], $P = 0.011$, respectively), whereas tobacco smoking was independently associated with a lower risk (OR 0.39 [95% CI 0.22–0.69], $P = 0.001$) (Table 3). The results of the multivariable analysis, including the matching variables, are shown in Supplementary Table 2 (available on the *Arthritis & Rheumatology* website at http://onlinelibrary.wiley.com/doi/10.1002/art.41722/abstract).

We next investigated co-exposures to >1 of the agents which were shown to be independent risk factors in the multivariable analysis. To this end, we investigated co-exposures to farming and silica, farming and organic solvents, and organic solvents and silica, comparing co-exposed subjects to non-exposed subjects. Interestingly, co-exposure to silica and farming yielded the highest OR (9.12 [95% CI 3.06–27.19], $P < 0.001$). This OR was much greater than the sum of the ORs associated with exposure to either silica alone (OR 3.04 [95% CI 1.07–8.62], $P = 0.04$) or farming alone [OR 2.75 [95% CI 1.53–4.98], $P = 0.001$), suggesting a multiplicative effect between these 2 exposures (Figure 1). Co-exposures to silica and organic solvents and to farming and organic solvents were also significantly associated with EGPA, but they only slightly enhanced the risk associated with either factor.

Associations between exposures and disease manifestations or ANCA status. We performed a sub-analysis aimed at investigating the associations between ANCA, major disease manifestations, and exposures that reached statistical significance in the multivariable analysis. The results are summarized in Table 4. Most of these sub-analyses, however, were underpowered, and the resulting associations were largely influenced by the size of the subsets considered.

All of the exposures that proved to be associated with EGPA in the multivariable analysis of the overall cohort remained significant when we considered patient subsets with highly prevalent manifestations such as asthma, ear, nose, and throat involvement, or peripheral neuropathy. The associations of the studied exposures with other manifestations of EGPA varied widely. The most intriguing associations were those with ANCA; in particular, smoking and organic solvents were more strongly associated with MPO-ANCA–negative EGPA than with MPO-ANCA–positive EGPA. Conversely, the associations with silica and farming were highly significant among MPO-ANCA–positive patients and only of borderline significance among MPO-ANCA–negative patients (Table 4).

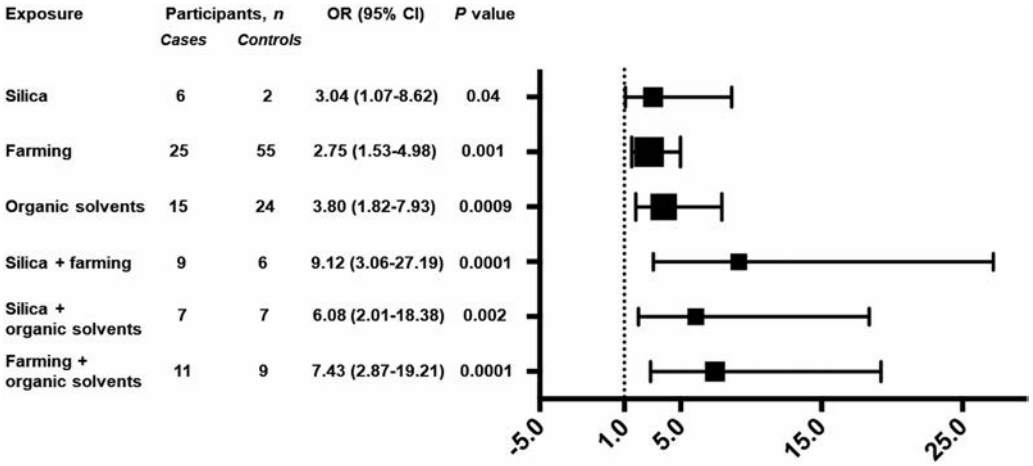

Figure 1. Effects on risk of eosinophilic granulomatosis with polyangiitis following single or co-exposures to silica, organic solvents, and farming in cases and controls. The baseline for comparison was participants who were not exposed to silica, organic solvents, or farming (219 controls and 36 cases) (odds ratio [OR] 1.00). 95% CI = 95% confidence interval.

Table 4. Associations between exposures and either ANCA status or disease manifestations in patients with eosinophilic granulomatosis with polyangiitis*

	Smoking		Silica		Farming		Organic solvents	
	OR (95% CI)	*P*	OR (95% CI)	*P*	OR (95% CI)	*P*	OR (95% CI)	*P*
All patients (n = 111)	0.49 (0.29–0.70)	<0.001	2.79 (1.55–5.01)	0.001	2.71 (1.71–4.29)	<0.001	3.19 (1.91–5.34)	<0.001
MPO-ANCA positive (n = 46)	0.66 (0.35–1.23)	0.210	3.98 (1.89–8.37)	<0.001	2.59 (1.36–4.93)	0.005	2.44 (1.17–5.09)	0.022
MPO-ANCA negative (n = 46)	0.34 (0.17–0.66)	0.002	2.45 (1.08–5.57)	0.037	2.37 (1.24–4.53)	0.014	4.87 (2.49–9.53)	<0.001
Asthma (n = 106)	0.47 (0.29–0.74)	0.001	2.55 (1.37–4.74)	0.003	2.61 (1.61–4.20)	0.001	3.15 (1.85–5.38)	<0.001
ENT involvement (n = 92)	0.46 (0.28–0.74)	0.001	2.46 (1.29–4.65)	0.008	2.26 (1.38–3.72)	0.001	3.18 (1.84–5.50)	<0.001
Pulmonary involvement (n = 62)	0.47 (0.27–0.83)	0.009	3.51 (1.77–6.95)	<0.001	2.66 (1.50–4.70)	0.001	1.80 (0.88–3.68)	0.103
Gastrointestinal involvement (n = 16)	0.29 (0.09–0.91)	0.038	2.33 (0.63–8.64)	0.184	1.23 (0.38–3.93)	0.756	1.15 (0.13–9.83)	1.000
Cardiac involvement (n = 22)	0.32 (0.12–0.84)	0.026	4.71 (1.78–12.47)	0.004	1.08 (0.38–3.04)	0.794	2.04 (0.71–5.81)	0.190
Peripheral neuropathy (n = 78)	0.38 (0.22–0.64)	<0.001	2.60 (1.34–5.07)	0.008	2.43 (1.44–4.11)	0.001	2.89 (1.61–5.19)	<0.001
Skin involvement (n = 35)	0.34 (0.16–0.73)	0.007	2.52 (1.02–6.27)	0.068	4.38 (2.14–8.96)	<0.001	2.39 (1.05–5.47)	0.041
Kidney involvement (n = 12)	0.17 (0.04–0.79)	0.016	3.36 (0.86–13.11)	0.096	2.63 (0.81–8.55)	0.146	3.46 (0.99–12.01)	0.061

* OR = odds ratio; 95% CI = 95% confidence interval; MPO-ANCA = myeloperoxidase–antineutrophil cytoplasmic antibody; ENT = ear, nose, and throat.

DISCUSSION

The pathogenesis of EGPA is multifactorial. Genetic determinants contribute to disease susceptibility and to the dichotomy between ANCA-positive and ANCA-negative subsets, while the role of environmental agents is unknown. In this study, we demonstrated an association of occupational exposures to organic solvents, silica, and farming with an increased risk of EGPA, while cigarette smoking was associated with a lower risk. Silica and farming were primarily associated with ANCA-positive EGPA, while smoking and organic solvents were associated with ANCA-negative EGPA.

Smoking is a risk factor for autoimmune diseases such as systemic lupus erythematosus and rheumatoid arthritis (21). However, our findings show smoking to be associated with a reduced risk of EGPA. Although surprising, this association was consistent across different analyses. We observed that the proportions of current and former smokers were lower among cases than among controls. Additionally, the pack-year index, which reflects cumulative exposure to smoking, was lower among cases, and this difference was statistically significant when assessed both in all of the study participants and in the subgroup of ever-smokers. Smoking behavior can be influenced by asthma, although the prevalence of smokers among individuals with asthma is similar to or slightly lower than that observed in the general population (22). To control for the possible influence of asthma, we evaluated the smoking behavior of patients before asthma onset and selected a matched control group for age at asthma onset. In this analysis, we also determined that the proportion of current and former smokers was significantly lower among patients.

The relationship between smoking and the other AAVs is controversial. While a recent study performed in the US identified smoking as a risk factor for AAV (23), findings from previous European studies identified a protective effect (24), or no effect at all (6,25). Interestingly, the prevalence of smoking is extremely low among patients with chronic eosinophilic lung disorders such as chronic eosinophilic pneumonia (prevalence in ever-smokers is 10–30%) (26), which may be considered a forme fruste of EGPA. Biologic mechanisms that may account for the association between smoking and a lower risk of EGPA can be postulated. Smoking has suppressive effects on mucosal immunity, particularly on T cells (27), and can also modify the local microbiota (28) in a way that limits the development of immune responses. These and other mechanisms have been hypothesized in other mucosal inflammatory disorders such as ulcerative colitis, where smoking seems to protect against severe disease and relapses (29). In our study, the association of EGPA with smoking was confined to the ANCA-negative subset, a finding that is consistent with the hypothesis of a mucosal/barrier dysfunction (5).

Organic solvents are compounds commonly used for painting, decoration, and dry cleaning. We found that occupational exposure to organic solvents was strongly associated with an increased risk of EGPA. In a previous study of 75 patients with AAV, including 16 with EGPA, solvent exposure predisposed to AAV (particularly

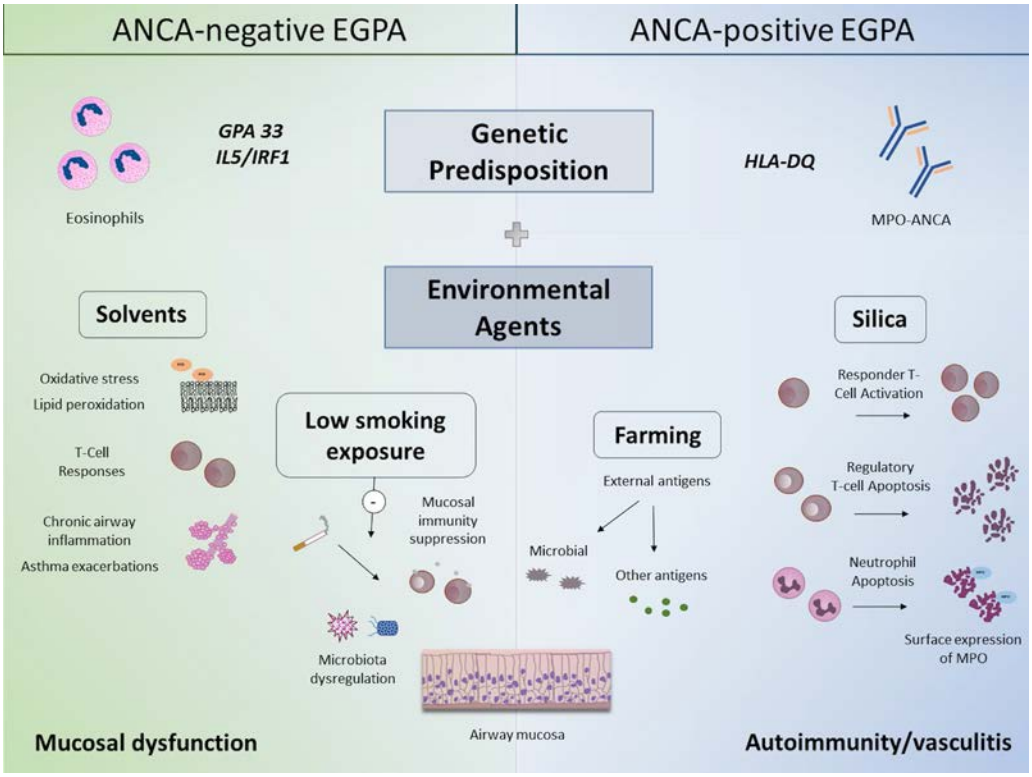

Figure 2. Proposed scheme of the influence of the different exposures on eosinophilic granulomatosis with polyangiitis (EGPA) subsets. ANCA = antineutrophil cytoplasmic antibody; IL5 = interleukin-5; IRF1 = interferon regulatory factor 1; MPO = myeloperoxidase.

GPA). No association with EGPA was reported, but the subgroup size was clearly too small (6). Remarkably, solvents have also been associated with other autoimmune diseases, particularly systemic sclerosis and multiple sclerosis (30). Different mechanisms are probably involved, namely solvent-induced oxidative stress, lipid peroxidation with subsequent modification of autoantigens, and enhancement of T cell responses (31,32). In addition, inhaled volatile compounds can induce chronic airway inflammation and exacerbate asthma (33). In our subset analysis, the effect of solvents was particularly strong in the ANCA-negative subset.

Silica and farming are established risk factors for AAV, and silica in particular predisposes to a wide range of autoimmune diseases (6–8). Silica and farming are also interconnected, as some farming activities (e.g., harvesting of crops) can result in silica exposure. We found that both silica and farming were significantly associated with an increased risk of EGPA. Interestingly, both showed a stronger association with the ANCA-positive subset.

Several studies have investigated silica in AAV, but EGPA patients were either excluded or there were too few included to detect significant associations (6–8,25). Overall, these studies indicated that silica predisposes to AAV. Notably, most patients with AAV following silica exposure were MPO-ANCA positive (34), which is consistent with our finding of a stronger association between silica and MPO-ANCA–positive EGPA. We also found a dose effect for silica (patients with longer duration of exposure were at greater risk), which was also observed in other studies on AAV (25,35). Silica may promote autoimmunity, particularly in AAV, by different mechanisms. It acts as a nonspecific immune adjuvant, especially for effector T cells, and favors early apoptosis of Treg cells, but it can also activate autoantigens such as MPO following the induction of neutrophil activation, apoptosis, or necrosis. An amplification of autoreactive B cell responses has also been proposed (36).

In our study, farming also showed a strong association with EGPA. Two previous studies on farming and AAV included EGPA patients, but again the numbers were too small (6,11). Given the structure of our questionnaire, we were unable to distinguish between the various farming exposures and could only exclude an association between EGPA and pesticides. No single agent or mechanism can therefore fully explain the link between farming and EGPA. However, farming can indeed be linked to exposure to an excess of foreign antigens (e.g., agents infecting animals), and to other compounds such as animal feeds and antibiotics (6). The hypothesis of an antigen-driven mechanism matches our finding of a stronger effect of farming on the ANCA-positive EGPA subset, which is genetically linked to HLA–DQ (5). Furthermore, the observed multiplicative interaction between farming and silica suggests that farming activities other than those exposing subjects to silica may also contribute to disease risk.

Taken together, our findings suggest that environmental factors contribute to identifying the 2 main sub-phenotypes of EGPA, as demonstrated in genetic determinants. Organic solvents and low exposure to smoking are involved in mucosal dysfunction, particularly in ANCA-negative EGPA, which is linked to genetic variants involved in mucosal responses (Figure 2). However, by enhancing autoimmunity and MPO-ANCA generation and through exposure to an excessive antigen load, silica and farming may boost autoimmunity and systemic vasculitis particularly in ANCA-positive EGPA, which is linked to HLA–DQ. These findings, however, must be considered with caution since the study was not designed to investigate differences in exposures between ANCA-positive patients and ANCA-negative patients.

Our study has limitations, namely those inherent to the questionnaire-based ascertainment of exposures and the small size of the EGPA sub-phenotype groups. However, the overall cohort was quite large considering the rarity of the disease, the patients were enrolled by a multidisciplinary team, and the controls were carefully case-matched. Also, since asthma is an almost universal feature of EGPA, the inclusion of a control group of patients with asthma and without EGPA would have allowed us to explore which environmental exposures differentiate asthma from EGPA. This was beyond the scope of our work; however, other studies showed that some of the factors we found to be associated with EGPA (e.g., organic solvents, and farming) were also triggers for asthma (33,37–39). In contrast, other risk factors for asthma (e.g., chemicals, metals, pesticides, and textile fibers) showed no effect on EGPA or even a protective effect (i.e., smoking) (37,40,41). Finally, agents such as silica, which is strongly associated with EGPA and AAV overall, do not seem to predispose to asthma in these patients (6–8,42). Further studies addressing differences in environmental exposures between asthma and EGPA may shed light on the different pathogenic mechanisms involved in these 2 conditions.

In conclusion, susceptibility to EGPA is influenced by exposure to organic solvents, silica, and farming, which are associated with an increased risk, and to smoking, which is associated with a lower risk. Such exposures appear to have distinct effects in different EGPA subsets.

AUTHOR CONTRIBUTIONS

All authors were involved in drafting the article or revising it critically for important intellectual content, and all authors approved the final version to be published. Dr. Maritati had full access to all of the data in the study and takes responsibility for the integrity of the data and the accuracy of the data analysis.

Study conception and design. Maritati, Peyronel, Fenaroli, Pegoraro, Emmi, Vaglio.

Acquisition of data. Maritati, Peyronel, Fenaroli, Benigno, Palmisano, Rossi, Urban, Alberici, Fraticelli, Emmi, Corradi, Vaglio.

Analysis and interpretation of data. Maritati, Peyronel, Pegoraro, Lastrucci, Vaglio.

REFERENCES

1. Jennette JC, Falk RJ, Bacon PA, Basu N, Cid MC, Ferrario F, et al. 2012 revised International Chapel Hill Consensus Conference nomenclature of vasculitides. Arthritis Rheum 2013;65:1–11.
2. Churg J, Strauss L. Allergic granulomatosis, allergic angiitis, and periarteritis nodosa. Am J Pathol 1951;27:277–301.

3. Vaglio A, Buzio C, Zwerina J. Eosinophilic granulomatosis with polyangiitis (Churg-Strauss): state of the art [review]. Allergy 2013;68:261–73.
4. Sinico RA, Di Toma L, Maggiore U, Bottero P, Radice A, Tosoni C, et al. Prevalence and clinical significance of antineutrophil cytoplasmic antibodies in Churg-Strauss syndrome. Arthritis Rheum 2005;52:2926–35.
5. Lyons PA, Peters JE, Alberici F, Liley J, Coulson RM, Astle W, et al. Genome-wide association study of eosinophilic granulomatosis with polyangiitis reveals genomic loci stratified by ANCA status. Nat Commun 2019;10:5120.
6. Lane SE, Watts RA, Bentham G, Innes NJ, Scott DG. Are environmental factors important in primary systemic vasculitis? A case–control study. Arthritis Rheum 2003;48:814–23.
7. Hogan SL, Cooper GS, Savitz DA, Nylander-French LA, Parks CG, Chin H, et al. Association of silica exposure with anti-neutrophil cytoplasmic autoantibody small-vessel vasculitis: a population-based, case-control study. Clin J Am Soc Nephrol 2007;2:290–9.
8. Gomez-Puerta JA, Gedmintas L, Costenbader KH. The association between silica exposure and development of ANCA-associated vasculitis: systematic review and meta-analysis. Autoimmun Rev 2013;12:1129–35.
9. Pai P, Bone JM, Bell GM. Hydrocarbon exposure and glomerulonephritis due to systemic vasculitis [letter]. Nephrol Dial Transplant 1998;13:1321–3.
10. Duna GF, Cotch MF, Galperin C, Hoffman DB, Hoffman GS. Wegener's granulomatosis: role of environmental exposures. Clin Exp Rheumatol 1998;16:669–74.
11. Willeke P, Schlüter B, Sauerland C, Becker H, Reuter S, Jacobi A, et al. Farm exposure as a differential risk factor in ANCA-associated vasculitis. PLoS One 2015;10:e0137196.
12. Masi AT, Hunder GG, Lie JT, Michel BA, Bloch DA, Arend WP, et al. The American College of Rheumatology 1990 criteria for the classification of Churg-Strauss syndrome (allergic granulomatosis and angiitis). Arthritis Rheum 1990;33:1094–100.
13. Mukhtyar C, Lee R, Brown D, Carruthers D, Dasgupta B, Dubey S, et al. Modification and validation of the Birmingham Vasculitis Activity Score (version 3). Ann Rheum Dis 2009;68:1827–32. doi: 10.1136/ard.2008.101279.
14. Guillevin L, Pagnoux C, Seror R, Mahr A, Mouthon L, Le Toumelin P, et al. The Five-Factor Score revisited: assessment of prognoses of systemic necrotizing vasculitides based on the French Vasculitis Study Group (FVSG) cohort. Medicine (Baltimore) 2011;90:19–27.
15. Goldoni M, Bonini S, Urban ML, Palmisano A, De Palma G, Galletti E, et al. Asbestos and smoking as risk factors for idiopathic retroperitoneal fibrosis: a case-control study. Ann Intern Med 2014;161:181–8.
16. Nesti M, Marinaccio A, Chellini E. Malignant mesothelioma in Italy, 1997. Am J Ind Med 2004;45:55–62.
17. Semple SE, Dick F, Cherri JW, on behalf of the Geoparkinson Study Group. Exposure assessment for a population-based case-control study combining a job-exposure matrix with interview data. Scand J Work Environ Health 2004;30:241–8.
18. Ben Khedher S, Neri M, Guida F, Matrat M, Cenée S, Sanchez M, et al. Occupational exposure to textile dust and lung cancer risk: results from the ICARE Study. Am J Ind Med 2018;61:216–28.
19. Kauppinen T, Toikkanen J, Pedersen D, Young R, Ahrens W, Boffetta P, et al. Occupational exposure to carcinogens in the European Union. Occup Environ Med 2000;57:10–8.
20. I.Stat. Aspects of daily life: smoking habit–age, educational level. URL: http://dati.istat.it/Index.aspx?QueryId=15513.
21. Hoovestol RA, Mikuls TR. Environmental exposures and rheumatoid arthritis risk [review]. Curr Rheumatol Rep 2011;13:431–9.
22. Kogevinas M, Zock JP, Jarvis D, Kromhout H, Lillienberg L, Plana E, et al. Exposure to substances in the workplace and new-onset asthma: an international prospective population-based study (ECRHS-II). Lancet 2007;370:336–41.
23. McDermott G, Fu X, Stone JH, Wallwork R, Zhang Y, Choi HK, et al. Association of cigarette smoking with antineutrophil cytoplasmic antibody-associated vasculitis. JAMA Intern Med 2020;180:1–7.
24. Haubitz M, Woywodt A, de Groot K, Haller H, Goebel U. Smoking habits in patients diagnosed with ANCA associated small vessel vasculitis. Ann Rheum Dis 2005;64:1500–2.
25. Beaudreuil S, Lasfargues G, Lauériere L, El Ghoul Z, Fourquet F, Longuet C, et al. Occupational exposure in ANCA-positive patients: a case-control study. Kidney Int 2005;67:1961–6.
26. Suzuki Y, Suda T. Eosinophilic pneumonia: a review of the previous literature, causes, diagnosis, and management. Allergol Int 2019;68:413–9.
27. Suzuki N, Wakisaka S, Takeba Y, Mihara S, Sakane T. Effects of cigarette smoking on Fas/Fas ligand expression of human lymphocytes. Cell Immunol 1999;192:48–53.
28. Huang C, Shi G. Smoking and microbiome in oral, airway, gut and some systemic diseases [review]. J Transl Med 2019;17:225.
29. Papoutsopoulou S, Satsangi J, Campbell BJ, Probert CS. Review article: impact of cigarette smoking on intestinal inflammation-direct and indirect mechanisms. Aliment Pharmacol Ther 2020;51:1268–85.
30. Barragán-Martínez C, Speck-Hernández CA, Montoya-Ortiz G, Mantilla RD, Anaya JM, Rojas-Villarraga A. Organic solvents as risk factor for autoimmune diseases: a systematic review and meta-analysis. PLoS One 2012;7:e51506.
31. Wang G, Cai P, Ansari GA, Khan MF. Oxidative and nitrosative stress in trichloroethene-mediated autoimmune response. Toxicology 2007;229:186–93.
32. Cai P, König R, Boor PJ, Kondraganti S, Kaphalia BS, Khan MF, et al. Chronic exposure to trichloroethene causes early onset of SLE-like disease in female MRL +/+ mice. Toxicol Appl Pharmacol 2008;228:68–75.
33. Nurmatov UB, Tagiyeva N, Semple S, Debereux G, Sheikh A. Volatile organic compounds and risk of asthma and allergy: a systematic review. Eur Respir Rev 2015;24:92–101.
34. Chen M, Kallenberg CG. The environment, geoepidemiology and ANCA-associated vasculitides [review]. Autoimmun Rev 2010;9:A293–8.
35. Hogan SL, Satterly KK, Dooley MA, Nachman PH, Jennette JC, Falk RJ, et al. Silica exposure in anti-neutrophil cytoplasmic autoantibody-associated glomerulonephritis and lupus nephritis. J Am Soc Nephrol 2001;12:134–42.
36. Lee S, Matsuzaki H, Kumagai-Takei N, Yoshitome K, Maeda M, Chen Y, et al. Silica exposure and altered regulation of autoimmunity [review]. Environ Health Prev Med 2014;19:322–9.
37. Karjalainen A, Kurppa K, Martikainen R, Klaukka T, Karjalainen J. Work is related to a substantial portion of adult-onset asthma incidence in the Finnish population. Am J Respir Crit Care Med 2001;164:565–8.
38. Kogevinas M, Antó JM, Sunyer J, Tobias A, Kromhout H, Burney P, on behalf of the European Community Respiratory Health Survey Study Group. Occupational asthma in Europe and other industrialised areas: a population-based study. Lancet 1999;353:1750–4.
39. Arif AA, Shah SM. Association between personal exposure to volatile organic compounds and asthma among US adult population. Int Arch Occup Environ Health 2007;80:711–9.
40. Chan-Yeung M, Malo JL. Aetiological agents in occupational asthma [review]. Eur Respir J 1994;7:346–71.
41. Baur X. A compendium of causative agents of occupational asthma [review]. J Occup Med Toxicol 2013;8:15.
42. Scott J, Hartnett J, Mockler D, Little MA. Environmental risk factors associated with ANCA associated vasculitis: a systematic mapping review. Autoimmun Rev 2020;19:102660.

Arthritis & Rheumatology
Vol. 73, No. 9, September 2021, pp 1703–1712
DOI 10.1002/art.41723

American College of Rheumatology
Empowering Rheumatology Professionals

Dynamic Changes in the Nasal Microbiome Associated With Disease Activity in Patients With Granulomatosis With Polyangiitis

Rennie L. Rhee,[1] Jiarui Lu,[1] Kyle Bittinger,[2] Jung-Jin Lee,[2] Lisa M. Mattei,[2] Antoine G. Sreih,[1] Sherry Chou,[1] Jonathan J. Miner,[3] Noam A. Cohen,[1] Brendan J. Kelly,[1] Hongzhe Lee,[1] Peter C. Grayson,[4] Ronald G. Collman,[1] and Peter A. Merkel[1]

Objective. Little is known about temporal changes in nasal bacteria in granulomatosis with polyangiitis (GPA). This study was undertaken to examine longitudinal changes in the nasal microbiome in association with relapse in GPA patients.

Methods. Bacterial 16S ribosomal RNA gene sequencing was performed on nasal swabs from 19 patients with GPA who were followed up longitudinally for a total of 78 visits, including 9 patients who experienced a relapse and 10 patients who remained in remission. Relative abundance of bacteria and ratios between bacteria were examined. Generalized estimating equation models were used to evaluate the association between bacterial composition and 1) disease activity and 2) levels of antineutrophil cytoplasmic antibody (ANCA) with specificity for proteinase 3 (PR3), adjusted for medication.

Results. *Corynebacterium* and *Staphylococcus* were the most abundant bacterial genera across all nasal samples. Patients with quiescent disease maintained a stable ratio of *Corynebacterium* to *Staphylococcus* across visits. In contrast, in patients who experienced a relapse, a significantly lower ratio was observed at the visit prior to relapse, followed by a higher ratio at the time of relapse (adjusted $P < 0.01$). Species-level analysis identified an association between a higher abundance of nasal *Corynebacterium tuberculostearicum* and 1) relapse (adjusted $P = 0.04$) and 2) higher PR3-ANCA levels (adjusted $P = 0.02$).

Conclusion. In GPA, significant changes occur in the nasal microbiome over time and are associated with disease activity. The occurrence of these changes months prior to the onset of relapse supports a pathogenic role of nasal bacteria in GPA. Our results uphold existing hypotheses implicating *Staphylococcus* as an instigator of disease and have generated a novel finding involving *Corynebacterium* as a potential mediator of disease in GPA.

INTRODUCTION

Granulomatosis with polyangiitis (GPA) is a life- and organ-threatening systemic vasculitis characterized by granulomatosis inflammation and frequent relapses. Rhinosinusitis occurs in up to 90% of patients with GPA and is associated with a higher risk of relapse (1). While our understanding of the immunopathogenesis of GPA has advanced, little is known about the triggers of disease activity.

Mechanistic and epidemiologic studies suggest that microbes, in particular nasal microbiota, may be an important environmental activator of GPA. Cross-reactivity between host and bacterial peptides may lead to the formation of pathogenic antineutrophil cytoplasmic antibodies (ANCAs), which are associated with GPA (2,3). Low-grade infections may also evoke inflammatory cytokines that prime neutrophils for activation by ANCA or stimulate neutrophils to release neutrophil extracellular traps embedded with ANCA antigens, further breaking immune tolerance and generating autoantibodies (4,5). Nasal colonization with *Staphylococcus aureus* is associated with a higher risk of relapse in GPA, an observation that led to a randomized, placebo-controlled trial of cotrimoxazole (an antistaphylococcal antibiotic), which was found

Supported by the National Institute of Arthritis and Musculoskeletal and Skin Diseases, NIH (grant K23-AR-071514).

[1]Rennie L. Rhee, MD, MSCE, Jiarui Lu, PhD, Antoine G. Sreih, MD, Sherry Chou, BS, Noam A. Cohen, MD, PhD, Brendan J. Kelly, MD, MSCE, Hongzhe Lee, PhD, Ronald G. Collman, MD, Peter A. Merkel, MD, MPH: University of Pennsylvania, Philadelphia; [2]Kyle Bittinger, PhD, Jung-Jin Lee, PhD, Lisa M. Mattei, PhD: The Children's Hospital of Philadelphia, Philadelphia, Pennsylvania; [3]Jonathan J. Miner, MD, PhD: Washington University School of Medicine, St. Louis, Missouri; [4]Peter C. Grayson, MD, MS: National Institute of Arthritis and Musculoskeletal and Skin Diseases, NIH, Bethesda, Maryland.

No potential conflicts of interest relevant to this article were reported.

Address correspondence to Rennie L. Rhee, MD, MSCE, Rheumatology, White Building, 5th Floor, 3400 Spruce Street, Philadelphia, PA 19104. Email: rennie.rhee@pennmedicine.upenn.edu.

Submitted for publication August 24, 2020; accepted in revised form March 2, 2021.

to significantly reduce the risk of relapse in GPA (6,7). These initial culture-dependent studies were limited due to the lack of profiling of the whole community of microbes and the lack of evaluation of temporally dynamic changes within an individual over time. Furthermore, the mechanism through which *S aureus* may instigate relapse in GPA remains unclear (8–12).

Advances in culture-independent techniques have enhanced the ability to examine the diversity of microbial species that colonize host sites, known as the human microbiome. While culture-dependent approaches view disease states as exclusively due to a single pathogenic microbe, studies now demonstrate that the overall composition of the microbiota strongly influences the behavior of a specific species. In prior work using high-throughput sequencing, our group profiled the entire community of nasal microbiota in GPA patients and healthy controls using 16S ribosomal RNA (16S rRNA) gene sequencing (13). We found a lower abundance of "healthy" commensals in patients with GPA and that patients with GPA who were not receiving immunosuppressive therapy had the greatest dysbiosis (imbalance in microbiota). However, what changes occur in the nasal microbiome longitudinally within an individual and how these changes relate temporally to disease activity remain unknown. This knowledge is needed to better understand potentially causal relationships between dysbiosis and disease. The objective of this study was to apply culture-independent sequencing methods to examine longitudinal changes in the nasal microbiome and their association with disease activity in GPA.

PATIENTS AND METHODS

Study design and participants. We performed a prospective cohort study at the University of Pennsylvania. Participants were recruited through the Penn Vasculitis Center. Participants with GPA were eligible if they met the modified American College of Rheumatology classification criteria for GPA (14,15). Participants were excluded if they had another systemic inflammatory disorder, known history of HIV infection, primary immunodeficiency, lymphoma, or other malignancy that mimics GPA. This study was approved by the Institutional Review Board of the University of Pennsylvania, and written informed consent was obtained from all participants.

Procedures. Nasal mucosa was sampled by swabbing the middle meatus with a sterile flocked specimen collection swab (Copan Diagnostics) which was then transferred to a –80°C freezer. To control for environmental contamination, negative controls (swab exposed to ambient air) were obtained with each participant sampling, and a randomly chosen subsample of these controls was processed in parallel. Sampling occurred at every office visit, usually with 3–6-month time intervals. Detailed clinical data were also collected at each visit, including data on disease activity and symptoms, infections, topical nasal therapies, and medications. All patients who had received rituximab in the past 6 months were considered to be receiving rituximab at the study visit. Serial serum samples were collected in a subset of patients (11 patients with a total of 29 visits), and ANCA levels were tested by direct enzyme-linked immunosorbent assay at a single institutional clinical laboratory. Disease activity was measured using the Birmingham Vasculitis Activity Score for Wegener's Granulomatosis (BVAS/WG; a BVAS/WG of >0 indicates active disease and a BVAS/WG of 0 indicates disease remission) (16).

Microbial DNA sequencing and taxonomic assignment. Nasal swab samples were sequenced and analyzed at the PennCHOP (University of Pennsylvania/Children's Hospital of Philadelphia) Microbiome Center. Bacterial DNA was extracted from swabs using a DNeasy PowerSoil Kit (Qiagen). The V1–V2 variable regions of the bacterial 16S rRNA gene, which has superior taxonomic resolution for the nasal cavity and sinuses (17), were amplified by polymerase chain reaction (PCR) using the 27F (5′-AGAGTTTGATCCTGGCTCAG-3′) and 338R (5′-TGCTGCCTCCCGTAGGAGT-3′) primers. Each sample was amplified in quadruplicate PCR reactions that consisted of 0.5 μ*M* of each primer, 0.34 units Q5 Pol, 1X Buffer, 0.2 m*M* dNTPs, and 5 μl DNA in a total volume of 25 μl. PCR cycling conditions were as follows: 98°C for 1 minute; 25 cycles of 98°C for 10 seconds, 56°C for 20 seconds, and 72°C for 20 seconds; and 72°C for 8 minutes. The quadruplicate reactions were pooled together, cleaned using SPRI beads (GE Healthcare), and quantified using a Quant-iT PicoGreen dsDNA Assay Kit (ThermoFisher). Samples were pooled in equimolar amounts and then sequenced on an Illumina MiSeq instrument using a 500-cycle v2 sequencing kit, yielding 250-bp paired-end sequence reads. Environmental and reagent control samples, consisting of air-exposed swabs, DNA-free water, and empty wells, and positive control samples were processed and sequenced alongside participant samples.

Sequencing data were processed and analyzed using the QIIME2 pipeline (18). The QIIME2 plug-in implementation of DADA2 was used to create a set of amplicon sequence variants (ASVs) from the raw sequence reads (19). Taxonomic assignment was performed using a naive Bayes classifier trained on the reference sequences from GreenGenes 13_8. For diversity metrics including UniFrac distances, a multiple sequence alignment was performed using MAFFT (20) and a phylogenetic tree was generated using FastTree (21). ASVs were evaluated for consistency with named bacterial species by aligning to the reference sequence from bacterial type strains, and estimating the probability that the full-length 16S rRNA gene similarity diverged by >2.5%. The software implementing this algorithm is available at https://github.com/kylebittinger/unassigner. Data are accessible via the NCBI Sequence Read Archive.

Statistical analysis. To evaluate bacterial communities, alpha and beta diversity were assessed and compared between patients with relapsing GPA and those with nonrelapsing GPA. Alpha diversity (within-sample diversity) was measured by the Shannon diversity index, which accounts for the evenness and richness (number) of ASVs within a sample. Beta diversity (between-sample diversity) was calculated using the weighted UniFrac distance, which estimates the fraction of a sample's phylogenetic tree that differs from another sample, accounting for the relative abundance of ASVs (22,23). UniFrac distances were visualized on a multidimensional scaling plot. Wilcoxon's rank sum test was used to compare continuous variables, and chi-square test was used for categorical variables.

To account for repeated measures, we applied generalized estimating equations (GEEs) to explore the association between bacterial composition and disease activity, adjusting for antibiotics, immunosuppressive drugs, and nasal irrigation. The GEE approach is a semiparametric model that accounts for the unknown correlations between the longitudinal repeated measurements. We grouped visits based on disease status (stable remission, prerelapse, relapse, and postrelapse), using stable remission as a reference. We analyzed the data at the genus level and normalized the read counts into compositions. Genera with a median relative abundance of >1% were included in the analysis. Relative abundance of individual genera as well as log ratios between 2 genera were used as outcomes to address the compositional nature of the microbiome data. Because of the unit-sum constraint on the data, the bacteria components cannot vary freely such that changes in one bacterium must result in changes in another. Using a log ratio transformation accounts for the unit-sum constraint and is a well-established approach for relative abundance data (24). False discovery rate controlling procedure was used to adjust for multiple comparisons of all pairs of bacterial genera and was set to 10% as the cutoff.

Secondary analyses included exploration of the consistency between ASVs and named bacterial species and were limited to taxa with a mean relative abundance of >2% across all samples. Test for trend was used to evaluate for linear associations between relative abundance and disease status (stable remission, preprerelapse, prerelapse, relapse, and postrelapse). Analyses were conducted using R V.3.4.1, and code is available upon request.

RESULTS

Participant characteristics. Nineteen patients with GPA who attended a total of 78 visits were included in this study (Table 1). The median total follow-up time was 13.8 months. The median time between visits for all visits was 3.9 months, and the median time between the prerelapse and relapse visits was 3.7 months. As expected, most of the participants were positive for ANCA with specificity for proteinase 3 (PR3-ANCA) and had sinonasal involvement at some point during their disease course. Nine of the 19 patients developed a relapse of disease during follow-up, and the other 10 patients remained in remission. Medications that patients were receiving at the first visit, typically when disease was in remission, are listed in Table 1. Prednisone was being used at 24 (31%) of all patient visits, with a median dose of 6 mg.

Table 1. Characteristics of the patients with GPA*

	Relapsing GPA (n = 9)	Nonrelapsing GPA (n = 10)
Number of visits per patient	4 (3–5)	4 (3–5)
Time between visits, months	3.3 (2.9–4.9)	4.1 (3.2–5.9)
Age at enrollment, years	58 (49–67)	64 (54–69)
Sex, % female	44	40
Race, % White	100	90
Hispanic, Latino, or Spanish origin, %	0	20†
ANCA type, %		
PR3-ANCA	78	70
MPO-ANCA	11	30
Negative ANCA	11	0
History of relapse prior to enrollment, %	67	50
Sinonasal involvement prior to enrollment, %	67	80
Sino-Nasal Outcome Test 22 score at first visit	23 (22–35)	29 (8–41)
Medications at first visit, no. (%)		
Systemic immunosuppressive drugs	6 (67)	10 (100)‡
Oral prednisone	3 (33)	5 (50)
Rituximab	2 (22)	4 (40)
Azathioprine	2 (22)	4 (40)
Methotrexate	1 (11)	1 (10)
Topical nasal therapies		
Nasal saline irrigation	5 (56)	5 (50)
Topical nasal steroid	1 (11)	2 (20)
Nasal mupirocin	0 (0)	1 (10)
Systemic antibiotics	1 (11)	3 (30)
TMP/SMX, full dose	0 (0)	0 (0)
TMP/SMX, low dose	1 (11)	2 (20)

* Except where indicated otherwise, values are the median (interquartile range). ANCA = antineutrophil cytoplasmic antibody; PR3 = proteinase 3; MPO = myeloperoxidase; TMP/SMX = trimethoprim/sulfamethoxazole.
† $P = 0.02$ versus relapsing granulomatosis with polyangiitis (GPA).
‡ $P = 0.04$ versus relapsing GPA.

The 9 patients with relapsing GPA had a total of 12 visits at which they had active disease. Of these 12 visits, 10 visits included manifestations outside of the upper respiratory tract, and at 8 visits patients had sinonasal inflammation. At 9 of the 12 visits, patients were receiving immunosuppressive therapy: at 6 visits, patients were receiving oral prednisone (3 receiving a stable prednisone dose of 5 mg and 3 had initiated a higher dose of prednisone 1–3 weeks prior due to concern for relapse), 4 were receiving rituximab, 1 was receiving azathioprine, 1 was receiving methotrexate, and 2 were receiving leflunomide. Patients were performing home nasal saline irrigation prior to 7 of the 12 active disease visits, and 2 patients were taking nasal antibiotics (mupirocin and gentamicin). Notably, only 2 patients

were receiving a systemic antibiotic at the time of the relapse visit: 1 patient was receiving full-dose trimethoprim/sulfamethoxazole and the other patient was receiving azithromycin. All patients responded to escalation of systemic immunosuppression, except for 1 patient who received only topical nasal steroids for sinonasal symptoms; this patient initially improved but later developed a multisystem relapse requiring oral prednisone and rituximab.

Common nasal bacteria identified in patients with GPA. The heatmap in Figure 1A depicts the 20 most abundant bacteria found in the samples, grouped by disease status (remission, prerelapse, relapse, and postrelapse visit) and outcome (relapse versus no relapse). The most abundant bacteria at the genus level (in decreasing order of abundance) were *Corynebacterium*, *Staphylococcus*, *Propionibacterium*, *Alloiococcus*, and *Streptococcus* (Figure 1A). These 5 bacteria made up a large majority of the composition of the samples (mean ± SD total combined abundance 86 ± 13% in the relapsing group and 83 ± 18% in the nonrelapsing group) (Figure 1B). No significant differences were found in the Shannon diversity (Figure 1C) or weighted UniFrac (data not shown) between patients with relapsing disease versus those with nonrelapsing disease; no difference was seen in these diversity measures when comparing disease status (remission, prerelapse, relapse, and postrelapse visits).

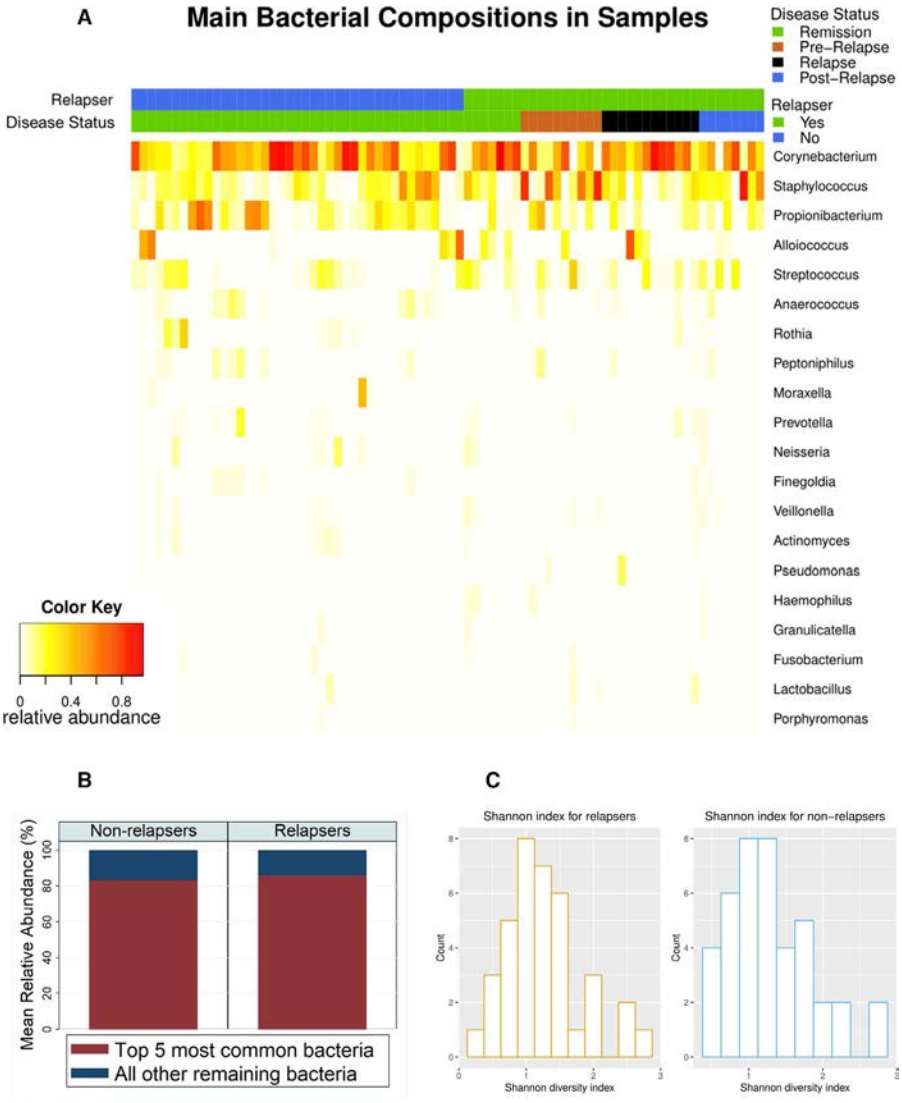

Figure 1. Bacterial composition of nasal samples from patients with granulomatosis with polyangiitis (GPA). **A**, Heatmap illustrating the relative abundance of the top 20 most abundant bacterial genera across all samples (n = 78), grouped by outcome (relapsing versus nonrelapsing GPA) and disease status (remission, prerelapse, relapse, and postrelapse). The samples primarily comprised 5 bacteria (in descending order of abundance): *Corynebacterium*, *Staphylococcus*, *Propionibacterium*, *Alloiococcus*, and *Streptococcus*. **B**, Mean relative abundance of the 5 most abundant bacteria versus all other remaining bacteria in patients with relapsing GPA versus patients with nonrelapsing GPA. Over 80% of the bacteria in the samples were represented by the 5 most abundant bacteria. **C**, Comparison of α-diversity, as measured by the Shannon diversity index, among all visits for patients with relapsing GPA versus patients with nonrelapsing GPA ($P = 0.78$). The y-axis shows the number of samples with the indicated Shannon diversity index.

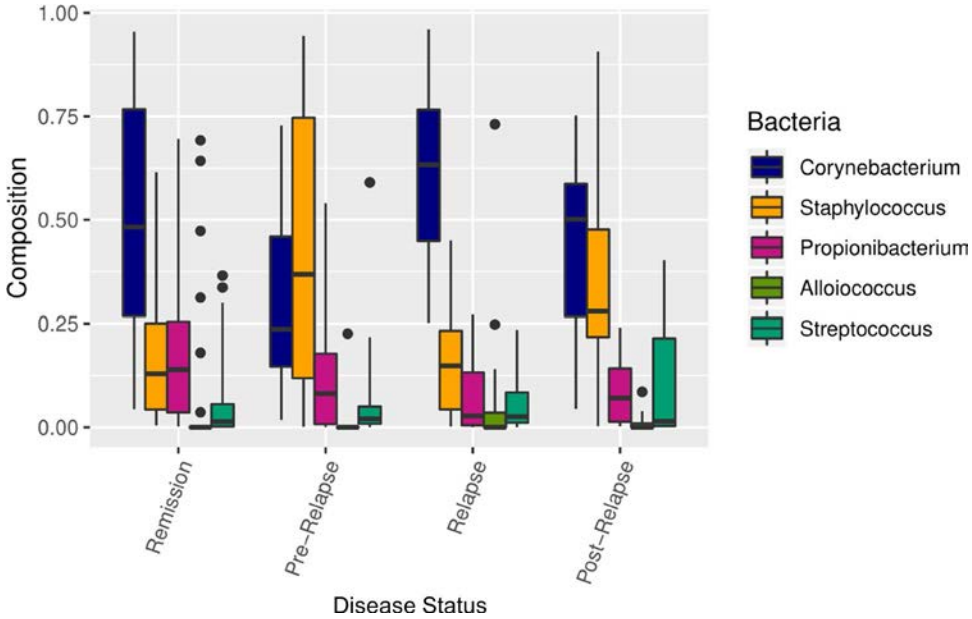

Figure 2. Relative abundance of the 5 most abundant bacteria in nasal samples from patients with granulomatosis with polyangiitis (GPA) grouped by disease status. Differences in relative abundance associated with disease status are shown, with the most pronounced variations seen in the abundance of *Corynebacterium* and *Staphylococcus*. Data are shown as box plots. Each box represents the first to the third quartile. Lines inside the boxes represent the median. Whiskers represent the maximum and minimum values. Circles represent outliers.

Dynamic changes in *Corynebacterium* and *Staphylococcus* beginning prior to the onset of relapse in GPA. Since most of the bacteria had very low abundance, we focused on the top 5 most abundant bacteria genera (the only genera with a median relative abundance of >1%) and recalculated the relative abundance of these 5 bacteria. Temporally dynamic changes in the relative abundance of the 5 bacteria were observed with change in disease status (remission, prerelapse, relapse, and postrelapse). Specifically, there was a greater abundance of *Staphylococcus* at the prerelapse visit followed by an increase in the abundance of *Corynebacterium* at the time of relapse (Figure 2). This is best demonstrated when examining the log ratio of *Corynebacterium* to *Staphylococcus*, which was significantly lower at the prerelapse visit even after adjusting for antibiotics, immunosuppressive drugs, and nasal irrigation (adjusted $P < 0.01$) (Figure 3). This log ratio subsequently increased at the relapse visit (adjusted $P < 0.01$), similar to remission levels ($P > 0.05$ versus remission visits). No significant changes were observed at prerelapse or relapse visits among the ratios of the other bacteria (data not shown). A sensitivity analysis excluding patients with >1 active disease visit yielded similar results (data not shown).

Associations between nasal *Corynebacterium tuberculostearicum* and relapse in GPA in species-level analysis. We further analyzed the 16S rRNA marker gene sequences to assess whether the partial gene sequences observed in our study were compatible with named bacterial species. Although we were not able to conclusively determine that the observed sequences arose from a particular named species, we were in many cases able to rule out all potential species assignments but one. When this occurred, we used the observed sequence, representing a fraction of the 16S gene, to compute the probability that the full-length 16S gene sequence would be compatible with the named bacterial species.

We found that 16S sequences compatible with *C tuberculostearicum* featured prominently in this cohort. *C tuberculostearicum*, which has previously been shown to have a pathogenic role in chronic rhinosinusitis (25), had the highest mean relative abundance in all of the samples (relative abundance 12.7%) followed by *C propinquum* (relative abundance 11.9%) and *Cutibacterium acnes* (formerly known as *Propionibacterium acnes*; relative abundance 10.6%). *C tuberculostearicum*, *Cutibacterium acnes*, and *Staphylococcus epidermidis* were the only 3 bacterial species detected in all 78 samples. *S aureus* was present in 33 of the samples (42%) and had a mean relative abundance of 3.5%.

When we evaluated associations between nasal bacteria and relapse in GPA, we found that an increasing relative abundance of *C tuberculostearicum* was associated with disease status, categorized as stable remission, pre-prerelapse, prerelapse, relapse, and postrelapse visits, even after adjusting for medications (adjusted $P = 0.04$ by test for trend) (Figure 4). Given the historical interest in *S aureus* in GPA and prior studies demonstrating interactions between *S aureus* and *Corynebacterium* species, we also adjusted for the presence of *S aureus* in the sample and found that the presence of *S aureus* was independently associated with a higher abundance of *C tuberculostearicum* (adjusted $P = 0.02$). We found similar results involving *C tuberculostearicum* when examining only relapses with sinonasal involvement (adjusted

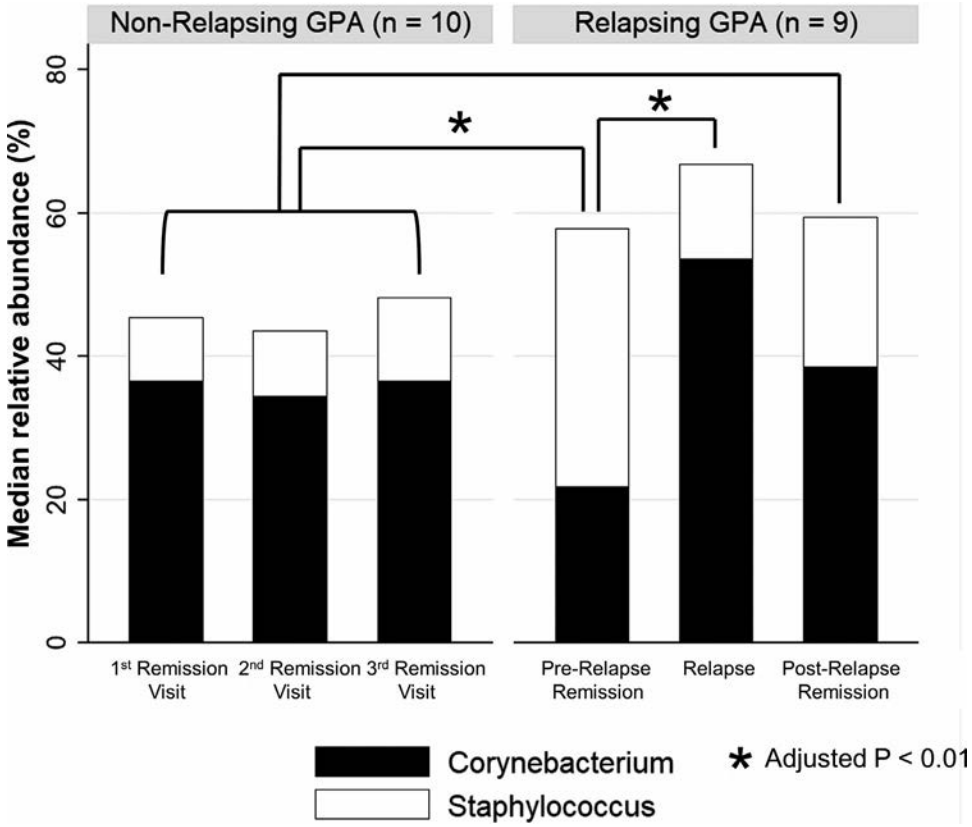

Figure 3. Dynamic changes in the ratio of *Corynebacterium* to *Staphylococcus* across visits in nasal samples from patients with relapsing granulomatosis with polyangiitis (GPA). Bars show the median relative abundance of *Corynebacterium* and *Staphylococcus* in patients with nonrelapsing GPA and those with relapsing GPA. Consecutive visits are shown separately to display temporal shifts. Patients with nonrelapsing GPA had a relatively stable ratio of *Corynebacterium* to *Staphylococcus* across 3 consecutive visits (all $P > 0.05$); in contrast, patients with relapsing GPA had a significantly lower ratio at the prerelapse visit (adjusted $P < 0.01$ versus patients with nonrelapsing GPA) followed by an increase in the ratio at relapse (adjusted $P < 0.01$ versus patients with relapsing GPA at the prerelapse visit), even after adjusting for antibiotics, immunosuppressive drugs, and nasal irrigation.

$P < 0.01$ by test for trend). No significant associations were found between individual bacteria and patient-reported symptoms of rhinosinusitis (the Sino-Nasal Outcome Test 22 [SNOT-22] score).

To investigate relationships between bacteria, we examined the association between ratios of bacterial abundance and clinical outcomes. An increasing ratio of *C tuberculostearicum* to *S caprae* was associated with disease status (stable remission, pre-prerelapse, prerelapse, relapse, and postrelapse visits) when examining any relapse (adjusted $P < 0.01$ by test for trend) as well as only relapses including the sinonasal area (adjusted $P < 0.01$ by test for trend). Disease status was also associated with an increasing ratio of *C pseudodiphtheriticum* to *S caprae* (adjusted $P < 0.01$ by test for trend). No bacterial ratios were associated with patient-reported symptoms of rhinosinusitis (SNOT-22 score).

Association of nasal *Corynebacterium tuberculostearicum* with higher PR3-ANCA levels. Due to the potential pathogenicity of PR3-ANCA in GPA (26,27), we assessed the association between nasal bacteria and PR3-ANCA levels in a subgroup of 11 patients with 29 visits with available ANCA levels. The median PR3-ANCA level was 19 units (interquartile range 6–56). No significant association between PR3-ANCA and the abundance of bacterial genera or ratios of bacterial genera were found. When examining bacterial species, we found that an increasing abundance of nasal *C tuberculostearicum* was associated with higher levels of PR3-ANCA even after adjusting for immunosuppressive drugs, antibiotics, and nasal rinse (adjusted $P = 0.02$) (Figure 5). No other nasal bacterial species were associated with PR3-ANCA levels, including *S aureus*.

DISCUSSION

Using unbiased molecular methods, we examined temporal changes in the nasal bacterial community in patients with GPA over multiple consecutive visits. At the genus level, we found that dynamic changes in the relative abundance of 2 common nasal commensals, *Corynebacterium* and *Staphylococcus*, precedes the development of relapse in GPA, whereas the abundance of these 2 bacteria remains stable in patients with quiescent disease. At the species level, an increasing abundance of nasal *C tuberculostearicum*, a bacterium previously found to be a potential pathogenic mediator of chronic rhinosinusitis (25), was associated with

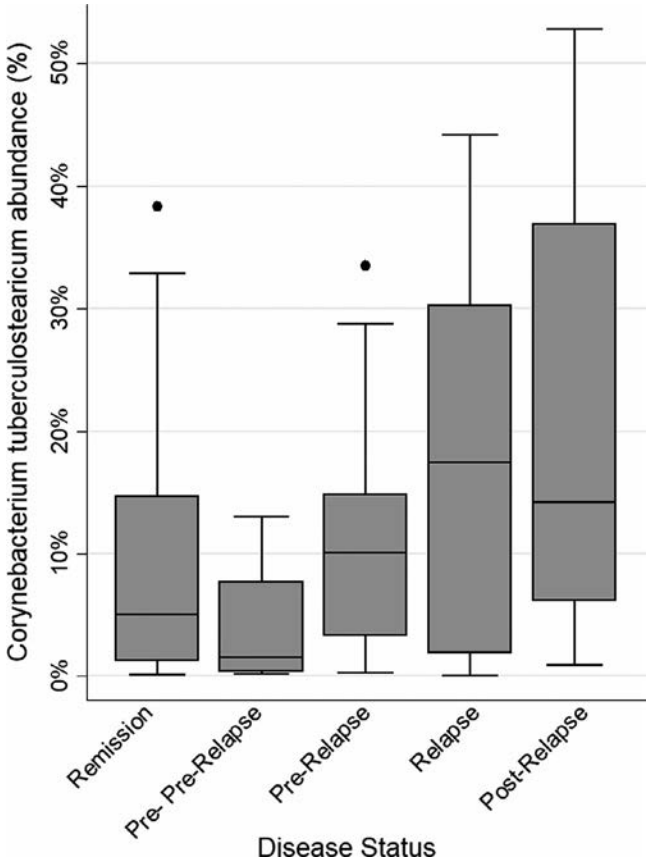

Figure 4. Association of increasing abundance of nasal *Corynebacterium tuberculostearicum* with relapse in patients with granulomatosis with polyangiitis (GPA). Relative abundance of *C tuberculostearicum* by disease status (stable remission, pre-prerelapse, prerelapse, relapse, and postrelapse) is shown. Data are shown as box plots. Each box represents the first to the third quartile. Lines inside the boxes represent the median. Whiskers represent the maximum and minimum values. Circles represent outliers. Test for trend detected a significant linear increase in nasal *C tuberculostearicum* abundance across visits even after adjusting for antibiotics, immunosuppressive drugs, nasal irrigation, and the presence of *Staphylococcus aureus* (adjusted $P = 0.04$).

both relapse as well as PR3-ANCA levels in GPA. Our results are consistent with prior interest in *Staphylococcus* species in GPA and additionally suggest that 1) the totality of the microbiome, not just individual bacteria, may be critical; 2) the composition at time points preceding disease activity may have a role in inciting disease; and 3) another nasal commensal bacteria that has not been previously studied in GPA may be an important mediator of disease.

The possibility that microbes are instigators of the immune response has been a longstanding theory for GPA as well as other autoimmune diseases. We chose to study the nasal cavity for 2 primary reasons: 1) the nasal mucosa is an active site of immunity (28), and 2) sinonasal inflammation is a destructive feature of GPA and associated with relapse. The overall bacterial composition in our cohort is similar to the nasal microbiome described in other non-GPA populations (17,29,30) as well as other cohorts of GPA (8,13,31) and is consistent with previous studies in demonstrating that the nasal cavity is colonized by a restricted number of microbes in contrast to other mucosal surfaces such as the intestine (29,32). The longitudinal design of our study offers the added advantage of assessing intraindividual changes temporally over time.

Prior studies of the nasal microbiota in GPA largely focused on *S aureus*, a pathogenic bacterium with a well-known predilection for the nasal cavity. *S aureus* has been found in a greater proportion of patients with relapsing GPA (6), but the potential mechanism of *S aureus* pathogenicity in GPA is unknown. *Staphylococcus* superantigens have been proposed as a link between *S aureus* and relapse in GPA (12) but this finding has not been replicated by subsequent studies (8–10). Differences in *S aureus* strains and genetic loci have been found between PR3-ANCA and myeloperoxidase (MPO)–ANCA vasculitis, although no direct mechanistic links between strain heterogeneity and disease have been shown (10). A prior study showed a potential role for complementary PR3 peptide in the formation of PR3-ANCA and identified sequence homology between complementary PR3 peptide and several microbes, including *S aureus* (3). However, there still remains no direct evidence demonstrating that *S aureus* colonization or infection leads to PR3-ANCA formation in GPA. More recently, an *S aureus* plasmid that has homology to an MPO T cell epitope was shown to induce MPO-ANCA formation and glomerulonephritis in mice (11); whether this explains ANCA formation in all patients with GPA including those with PR3-ANCA still remains unclear.

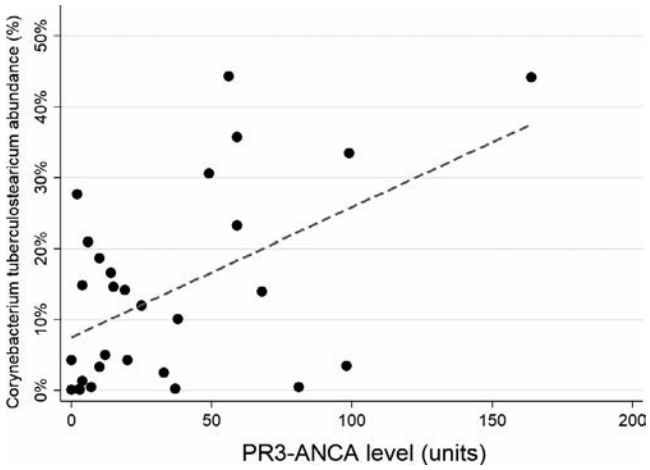

Figure 5. Association of the relative abundance of nasal *Corynebacterium tuberculostearicum* with proteinase 3 antineutrophil cytoplasmic antibody (PR3-ANCA) level in patients with granulomatosis with polyangiitis (GPA). The scatterplot demonstrates the association between the abundance of nasal *C tuberculostearicum* and serum PR3-ANCA levels in 11 patients who attended a total of 29 visits (unadjusted $P < 0.01$). The association remained significant even after adjusting for use of antibiotics, immunosuppressive drugs, and nasal irrigation (adjusted $P = 0.02$). PR3-ANCA levels of <20 units were considered normal.

In this study, we found a significant increase in the abundance of the genus *Staphylococcus* prior to onset of a relapse; however, interrogation of species-level identity of bacteria did not show any relationship between *S aureus* and relapse. The lack of an association between *S aureus* and relapse in GPA may be due to constraints of 16S gene sequencing, which is limited in resolving species-level classification. Differences in methodology may also explain disparate results compared to prior studies that relied on repeated nasal cultures to define chronic carriers (6,33). We chose to use sequence-based culture-independent methods which, compared to culture-dependent methods, have the added advantage of comprehensively evaluating all nasal microbes, including unculturable or difficult-to-culture organisms. Lastly, we sampled the middle meatus, which is lined by mucosa with ciliated pseudostratified columnar epithelium, closer in proximity to sinuses, and a site of active inflammation in GPA; prior studies sampled the anterior nares which is lined by skin-like squamous epithelium and the main reservoir for *S aureus*, but not typically an area of active disease in GPA. Differences in sampling site may also account for differences in results between this study and prior studies.

Unexpectedly, we identified a novel finding involving a lesser known and poorly studied nasal commensal, corynebacteria. Corynebacteria are aerobic, gram-positive bacilli that populate the human nose and skin and were previously thought to be harmless commensals. However, emerging evidence implicates *Corynebacterium* in diseases of the lower respiratory tract (such as asthma), upper respiratory tract (such as chronic rhinosinusitis), and skin (such as atopic dermatitis) as well as granulomatous diseases (25,34–37). In both our cohort and others, corynebacteria are often among the most abundant genera in the nasal cavity, and prior studies have shown it is also the most species-rich taxon with one study reporting at least 23 different species of corynebacteria in the nose of almost every patient sampled (38).

Corynebacteria typically have a complex cell wall with an outer layer of mycolic acids which is similar to the cell wall of mycobacteria (another granuloma-forming pathogen) and functionally equivalent to the outer layer of gram-negative bacteria with respect to its permeability barrier and host–pathogen interactions (39). While the immunogenicity of the *Corynebacterium* cell wall has not been well-studied, the mycolic acid–containing cell wall of *Mycobacterium tuberculosis* is known to contribute to its pathogenicity (40). For example, trehalose dimycolate (TDM), which is a constituent of the mycolic acid layer in *M tuberculosis*, induces inflammatory responses and granuloma formation (41). Trehalose 6,6′-dicorynomycolate (TDCM) in corynebacteria is comparable to TDM in mycobacteria; TDCM has been shown to activate murine macrophages and induce inflammatory cytokines such as tumor necrosis factor (42). Therefore, it is plausible that corynebacteria may play a role in the granulomatous inflammation characteristic of GPA. Interestingly, most species of *Corynebacterium* are susceptible to trimethoprim/sulfamethoxazole, an antibiotic found to prevent relapses in GPA.

At the species level, we found associations between nasal *C tuberculostearicum* abundance and both GPA disease relapse and PR3-ANCA levels. *C tuberculostearicum* has been implicated in the pathogenesis of chronic rhinosinusitis (25). That study found that only nasal *C tuberculostearicum* was significantly increased in abundance in patients with chronic rhinosinusitis compared to healthy subjects, and inoculating the nasal cavity of antibiotic-treated mice with *C tuberculostearicum* induced pathologic features of chronic rhinosinusitis. In GPA, studies have shown evidence for induction of PR3-ANCA by autoreactive B cells in granulomatous lesions and chronic B cell activation in inflamed mucosa of patients with GPA, indicating a local antigen-driven process that promotes formation of autoantibodies that are associated with the life-threatening systemic features of GPA (43,44). We postulate that *Corynebacterium* (and more specifically, *C tuberculostearicum*) may contribute to the initiation of local granulomatous lesions and PR3-ANCA formation in sinonasal mucosa of patients with GPA. Our use of unbiased profiling methods has identified the potential role of this previously disregarded bacteria in the pathogenesis of GPA.

We propose two possible explanations for the dynamic changes observed between *Corynebacterium* and *Staphylococcus* in this study. One potential hypothesis is that *Corynebacterium* regulates *Staphylococcus* through interspecies interactions, consistent with the findings of prior studies, but when this balance is lost an outgrowth in *Staphylococcus* incites host inflammation. By the time of the relapse visit, the balance between these 2 bacteria may be restored but ongoing inflammation ensues due to a dysregulated immune response in the host. Alternatively, *Staphylococcus* may promote the outgrowth of a pathogenic strain of *Corynebacterium* which promotes inflammation. It is notable that the relative abundance of *Staphylococcus*, which had significantly increased at the prerelapse visit, returned to baseline at the relapse visit, which was contrary to what we had expected to find.

While our data do not show direct interactions between *Corynebacterium* and *Staphylococcus*, many prior studies have demonstrated species-specific interactions between these 2 bacteria (29,45–47). In the context of GPA, this may involve a type of 3-way relationship that has been previously described in the nasal cavity (48,49). In this process, referred to as within-host competition, negative competition between bacteria is mediated by the host. The median time interval between the prerelapse visit (in which *Staphylococcus* predominated) and the relapse visit (in which *Corynebacterium* predominated) was 3.7 months; this relatively long time interval supports the possibility that *Corynebacterium* may be a more important mediator of disease than *Staphylococcus*. Furthermore, aberrant immune responses in patients with GPA may explain why these ubiquitous commensals are associated with disease in only a small fraction of the general population.

There are several limitations of this study to consider. While these novel findings raise new questions about the pathogenesis of GPA, they are associative and do not demonstrate causality. It is possible that disruption of the nasal microbiota is occurring

secondary to mucosal inflammation; however, identification of changes in nasal bacteria 3 months prior to the onset of disease relapse makes this less likely. Similarly, other confounders such as unmeasured environmental or medication exposures not accounted for in the analyses may explain these results. While sequencing of the highly conserved 16S bacterial gene is a commonly used initial approach to evaluating the microbiome, this sequencing method is limited in its ability to determine species identity (50). Additionally, 16S rRNA gene sequencing allows taxonomic identification but not enumeration of functional content; it is possible that metabolic pathways and virulence-related genes are the key to understanding the pathogenesis of disease (32). Additional studies are needed to investigate mechanisms mediating microbe–microbe and host–microbial relationships, and the present study suggests that greater attention should be paid to both *Corynebacterium* and *Staphylococcus*. Lastly, results of this study may not be generalizable to other populations of GPA including patients residing in different geographic regions or with different genetic predisposition for disease.

In conclusion, this longitudinal study of the nasal microbiome in GPA identified changes in the nasal commensal bacteria several months prior to disease relapse. In addition to supporting the possibility that *Staphylococcus* is an instigator of disease activity, this study has identified a novel finding implicating *Corynebacterium* as a potential mediator of host–microbial interactions, and specifically *C tuberculostearicum* as a species of particular interest. These findings support the longstanding theory that overgrowth of pathogenic bacteria is potentially involved in the disease process of GPA and identify specific new targets for mechanistic investigation. Understanding how nasal bacteria activate disease in GPA may potentially lead to novel therapeutic targets, new measures to predict relapse, and better precision medicine approaches in GPA.

ACKNOWLEDGMENT

We thank all participants for their involvement in the study.

AUTHOR CONTRIBUTIONS

All authors were involved in drafting the article or revising it critically for important intellectual content, and all authors approved the final version to be published. Dr. Rhee had full access to all of the data in the study and takes responsibility for the integrity of the data and the accuracy of the data analysis.

Study conception and design. Rhee, Bittinger, Grayson, Collman, Merkel.
Acquisition of data. Rhee, Mattei, Sreih, Chou, Merkel.
Analysis and interpretation of data. Rhee, Lu, Bittinger, Lee, Miner, Cohen, Kelly, Lee, Grayson, Collman, Merkel.

REFERENCES

1. Hoffman GS, Kerr GS, Leavitt RY, Hallahan CW, Lebovics RS, Travis WD, et al. Wegener granulomatosis: an analysis of 158 patients. Ann Intern Med 1992;116:488–98.
2. Kain R, Exner M, Brandes R, Ziebermayr R, Cunningham D, Alderson CA, et al. Molecular mimicry in pauci-immune focal necrotizing glomerulonephritis. Nat Med 2008;14:1088–96.
3. Pendergraft WF III, Preston GA, Shah RR, Tropsha A, Carter CW Jr, Jennette JC, et al. Autoimmunity is triggered by cPR-3(105–201), a protein complementary to human autoantigen proteinase-3. Nat Med 2004;10:72–9.
4. Van Dam LS, Kraaij T, Kamerling SW, Bakker JA, Scherer UH, Rabelink TJ, et al. Intrinsically distinct role of neutrophil extracellular trap formation in antineutrophil cytoplasmic antibody–associated vasculitis compared to systemic lupus erythematosus. Arthritis Rheumatol 2019;71:2047–58.
5. Tadema H, Abdulahad WH, Lepse N, Stegeman CA, Kallenberg CG, Heeringa P. Bacterial DNA motifs trigger ANCA production in ANCA-associated vasculitis in remission. Rheumatology (Oxford) 2011;50:689–96.
6. Stegeman CA, Tervaert JW, Sluiter WJ, Manson WL, de Jong PE, Kallenberg CG. Association of chronic nasal carriage of Staphylococcus aureus and higher relapse rates in Wegener granulomatosis. Ann Intern Med 1994;120:12–7.
7. Stegeman CA, Tervaert JW, de Jong PE, Kallenberg CG, for the Dutch Co-trimoxazole Wegener Study Group. Trimethoprim-sulfamethoxazole (co-trimoxazole) for the prevention of relapses of Wegener's granulomatosis. N Engl J Med 1996;335:16–20.
8. Wagner J, Harrison EM, Del Pero MM, Blane B, Mayer G, Leierer J, et al. The composition and functional protein subsystems of the human nasal microbiome in granulomatosis with polyangiitis: a pilot study. Microbiome 2019;7:137.
9. Fijołek J, Wiatr E, Petroniec V, Augustynowicz-Kopec E, Bednarek M, Gawryluk D, et al. The presence of staphylococcal superantigens in nasal swabs and correlation with activity of granulomatosis with polyangiitis in own material. Clin Exp Rheumatol 2018;36 Suppl 111:40–5.
10. Glasner C, de Goffau MC, van Timmeren MM, Schulze ML, Jansen B, Tavakol M, et al. Genetic loci of Staphylococcus aureus associated with anti-neutrophil cytoplasmic autoantibody (ANCA)-associated vasculitides. Sci Rep 2017;7:12211.
11. Ooi JD, Jiang JH, Eggenhuizen PJ, Chua LL, van Timmeren M, Loh KL, et al. A plasmid-encoded peptide from Staphylococcus aureus induces anti-myeloperoxidase nephritogenic autoimmunity. Nat Commun 2019;10:3392.
12. Popa ER, Stegeman CA, Abdulahad WH, van der Meer B, Arends J, Manson WM, et al. Staphylococcal toxic-shock-syndrome-toxin-1 as a risk factor for disease relapse in Wegener's granulomatosis. Rheumatology (Oxford) 2007;46:1029–33.
13. Rhee RL, Sreih AG, Najem CE, Grayson PC, Zhao C, Bittinger K, et al. Characterisation of the nasal microbiota in granulomatosis with polyangiitis. Ann Rheum Dis 2018;77:1448–53.
14. Leavitt RY, Fauci AS, Bloch DA, Michel BA, Hunder GG, Arend WP, et al. The American College of Rheumatology 1990 criteria for the classification of Wegener's granulomatosis. Arthritis Rheum 1990;33:1101–7.
15. The Wegener's Granulomatosis Etanercept Trial (WGET) Research Group. Etanercept plus standard therapy for Wegener's granulomatosis. N Engl J Med 2005;352:351–61.
16. Stone JH, Hoffman GS, Merkel PA, Min YI, Uhlfelder ML, Hellmann DB, et al, for the International Network for the Study of the Systemic Vasculitides (INSSYS). A disease-specific activity index for Wegener's granulomatosis: modification of the Birmingham Vasculitis Activity Score. Arthritis Rheum 2001;44:912–20.
17. Escapa IF, Chen T, Huang Y, Gajare P, Dewhirst FE, Lemon KP. New insights into human nostril microbiome from the expanded Human Oral Microbiome Database (eHOMD): a resource for the microbiome of the human aerodigestive tract. mSystems 2018;3:e00187-18.
18. Bolyen E, Rideout JR, Dillon MR, Bokulich NA, Abnet CC, Al-Ghalith GA, et al. Reproducible, interactive, scalable and extensible microbiome data science using QIIME 2 [letter]. Nat Biotechnol 2019;37:852–7.

19. Callahan BJ, McMurdie PJ, Rosen MJ, Han AW, Johnson AJ, Holmes SP. DADA2: high-resolution sample inference from Illumina amplicon data. Nat Methods 2016;13:581–3.
20. Katoh K, Standley DM. MAFFT multiple sequence alignment software version 7: improvements in performance and usability. Mol Biol Evol 2013;30:772–80.
21. Price MN, Dehal PS, Arkin AP. FastTree 2: approximately maximum-likelihood trees for large alignments. PLoS One 2010;5:e9490.
22. Lozupone C, Knight R. UniFrac: a new phylogenetic method for comparing microbial communities. Appl Environ Microbiol 2005; 71:8228–35.
23. Lozupone CA, Hamady M, Kelley ST, Knight R. Quantitative and qualitative β diversity measures lead to different insights into factors that structure microbial communities. Appl Environ Microbiol 2007;73:1576–85.
24. Aitchison J. The statistical analysis of compositional data. J R Stat Soc Series B Methodol 1982;44:139–60.
25. Abreu NA, Nagalingam NA, Song Y, Roediger FC, Pletcher SD, Goldberg AN, et al. Sinus microbiome diversity depletion and Corynebacterium tuberculostearicum enrichment mediates rhinosinusitis. Sci Transl Med 2012;4:151ra24.
26. Primo VC, Marusic S, Franklin CC, Goldmann WH, Achaval CG, Smith RN, et al. Anti-PR3 immune responses induce segmental and necrotizing glomerulonephritis. Clin Exp Immunol 2010;159:327–37.
27. Millet A, Martin KR, Bonnefoy F, Saas P, Mocek J, Alkan M, et al. Proteinase 3 on apoptotic cells disrupts immune silencing in autoimmune vasculitis. J Clin Invest 2015;125:4107–21.
28. Riese P, Sakthivel P, Trittel S, Guzmán CA. Intranasal formulations: promising strategy to deliver vaccines. Expert Opin Drug Deliv 2014;11:1619–34.
29. Yan M, Pamp SJ, Fukuyama J, Hwang PH, Cho DY, Holmes S, et al. Nasal microenvironments and interspecific interactions influence nasal microbiota complexity and S. aureus carriage. Cell Host Microbe 2013;14:631–40.
30. Rom D, Bassiouni A, Eykman E, Liu Z, Paramasivan S, Alvarado R, et al. The association between disease severity and microbiome in chronic rhinosinusitis. Laryngoscope 2019;129:1265–73.
31. Lamprecht P, Fischer N, Huang J, Burkhardt L, Lütgehetmann M, Arndt F, et al. Changes in the composition of the upper respiratory tract microbial community in granulomatosis with polyangiitis. J Autoimmun 2019;97:29–39.
32. The Human Microbiome Project Consortium. Structure, function and diversity of the healthy human microbiome. Nature 2012;486:207–14.
33. Salmela A, Rasmussen N, Tervaert JW, Jayne DR, Ekstrand A. Chronic nasal Staphylococcus aureus carriage identifies a subset of newly diagnosed granulomatosis with polyangiitis patients with high relapse rate. Rheumatology (Oxford) 2017;56:965–72.
34. Kobayashi T, Glatz M, Horiuchi K, Kawasaki H, Akiyama H, Kaplan DH, et al. Dysbiosis and Staphylococcus aureus colonization drives inflammation in atopic dermatitis. Immunity 2015;42:756–66.
35. Ridaura VK, Bouladoux N, Claesen J, Chen YE, Byrd AL, Constantinides MG, et al. Contextual control of skin immunity and inflammation by Corynebacterium. J Exp Med 2018;215:785–99.
36. Zhou Y, Jackson D, Bacharier LB, Mauger D, Boushey H, Castro M, et al. The upper-airway microbiota and loss of asthma control among asthmatic children. Nat Commun 2019;10:5714.
37. Co M, Cheng VC, Wei J, Wong SC, Chan SM, Shek T, et al. Idiopathic granulomatous mastitis: a 10-year study from a multicentre clinical database. Pathology 2018;50:742–7.
38. Kaspar U, Kriegeskorte A, Schubert T, Peters G, Rudack C, Pieper DH, et al. The culturome of the human nose habitats reveals individual bacterial fingerprint patterns. Environ Microbiol 2016;18: 2130–42.
39. Burkovski A. Cell envelope of corynebacteria: structure and influence on pathogenicity [review]. ISRN Microbiol 2013;2013:935736.
40. Indrigo J, Hunter RL, Actor JK. Cord factor trehalose 6,6′-dimycolate (TDM) mediates trafficking events during mycobacterial infection of murine macrophages. Microbiology (Reading) 2003;149:2049–59.
41. Shenderov K, Barber DL, Mayer-Barber KD, Gurcha SS, Jankovic D, Feng CG, et al. Cord factor and peptidoglycan recapitulate the Th17-promoting adjuvant activity of mycobacteria through mincle/CARD9 signaling and the inflammasome. J Immunol 2013;190:5722–30.
42. Chami M, Andréau K, Lemassu A, Petit JF, Houssin C, Puech V, et al. Priming and activation of mouse macrophages by trehalose 6,6′-dicorynomycolate vesicles from Corynebacterium glutamicum. FEMS Immunol Med Microbiol 2002;32:141–7.
43. Voswinkel J, Mueller A, Kraemer JA, Lamprecht P, Herlyn K, Holl-Ulrich K, et al. B lymphocyte maturation in Wegener's granulomatosis: a comparative analysis of VH genes from endonasal lesions. Ann Rheum Dis 2006;65:859–64.
44. Zhao Y, Odell E, Choong LM, Barone F, Fields P, Wilkins B, et al. Granulomatosis with polyangiitis involves sustained mucosal inflammation that is rich in B-cell survival factors and autoantigen. Rheumatology (Oxford) 2012;51:1580–6.
45. Ramsey MM, Freire MO, Gabrilska RA, Rumbaugh KP, Lemon KP. Staphylococcus aureus shifts toward commensalism in response to Corynebacterium species. Front Microbiol 2016;7:1230.
46. Hardy BL, Dickey SW, Plaut RD, Riggins DP, Stibitz S, Otto M, et al. Corynebacterium pseudodiphtheriticum exploits Staphylococcus aureus virulence components in a novel polymicrobial defense strategy. mBio 2019;10:e02491-18.
47. Lemon KP, Klepac-Ceraj V, Schiffer HK, Brodie EL, Lynch SV, Kolter R. Comparative analyses of the bacterial microbiota of the human nostril and oropharynx. mBio 2010;1:e00129-10.
48. Brown SP, Le Chat L, Taddei F. Evolution of virulence: triggering host inflammation allows invading pathogens to exclude competitors. Ecol Lett 2008;11:44–51.
49. Ratner AJ, Lysenko ES, Paul MN, Weiser JN. Synergistic proinflammatory responses induced by polymicrobial colonization of epithelial surfaces. Proc Natl Acad Sci U S A 2005;102:3429–34.
50. Poretsky R, Rodriguez RL, Luo C, Tsementzi D, Konstantinidis KT. Strengths and limitations of 16S rRNA gene amplicon sequencing in revealing temporal microbial community dynamics. PLoS One 2014;9:e93827.

Arthritis & Rheumatology
Vol. 73, No. 9, September 2021, pp 1713–1719
DOI 10.1002/art.41728

American College of Rheumatology
Empowering Rheumatology Professionals

Risk Factors for Severe Outcomes in Patients With Systemic Vasculitis and COVID-19: A Binational, Registry-Based Cohort Study

Matthew A. Rutherford,[1] Jennifer Scott,[2] Maira Karabayas,[3] Marilina Antonelou,[4] Seerapani Gopaluni,[5] David Gray,[6] Joe Barrett,[6] Silke R. Brix,[7] Neeraj Dhaun,[8] Stephen P. McAdoo,[9] Rona M. Smith,[5] Colin C. Geddes,[10] David Jayne,[5] Raashid Luqmani,[11] Alan D. Salama,[12] Mark A. Little,[2] and Neil Basu,[13] on behalf of the UK and Ireland Vasculitis Rare Disease Group (UKIVAS)

Objective. COVID-19 is a novel infectious disease with a broad spectrum of clinical severity. Patients with systemic vasculitis have an increased risk of serious infections and may be at risk of severe outcomes following COVID-19. We undertook this study to establish the risk factors for severe COVID-19 outcomes in these patients, including the impact of immunosuppressive therapies.

Methods. A multicenter cohort was developed through the participation of centers affiliated with national UK and Ireland vasculitis registries. Clinical characteristics and outcomes are described. Logistic regression was used to evaluate associations between potential risk factors and a severe COVID-19 outcome, defined as a requirement for advanced oxygen therapy, a requirement for invasive ventilation, or death.

Results. The cohort included 65 patients with systemic vasculitis who developed COVID-19 (median age 70 years, 49% women), of whom 25 patients (38%) experienced a severe outcome. Most patients (55 of 65 [85%]) had antineutrophil cytoplasmic antibody–associated vasculitis (AAV). Almost all patients required hospitalization (59 of 65 [91%]), 7 patients (11%) were admitted to intensive care, and 18 patients (28%) died. Background glucocorticoid therapy was associated with severe outcomes (adjusted odds ratio [OR] 3.7 [95% confidence interval 1.1–14.9]; $P = 0.047$), as was comorbid respiratory disease (adjusted OR 7.5 [95% confidence interval 1.9–38.2]; $P = 0.006$). Vasculitis disease activity and nonglucocorticoid immunosuppressive therapy were not associated with severe outcomes.

Conclusion. In patients with systemic vasculitis, glucocorticoid use at presentation and comorbid respiratory disease were associated with severe outcomes in COVID-19. These data can inform clinical decision-making relating to the risk of severe COVID-19 in this vulnerable patient group.

INTRODUCTION

COVID-19 is a novel, multisystem infectious disease caused by SARS–CoV-2. COVID-19 is associated with a broad spectrum of clinical severity (1), ranging from asymptomatic disease to severe respiratory failure and death. In March 2020, the World Health Organization (WHO) characterized COVID-19 as a global pandemic (2), prompting considerable concerns from health care systems worldwide about their resilience to manage this threat. Critical care service capacity was, and remains, a global priority.

Systemic vasculitis is a rare, multisystem autoimmune disorder. Compared to other rheumatic musculoskeletal diseases, it may result in major organ dysfunction and is therefore typically managed with more potent immunosuppressive therapy and

[1]Matthew A. Rutherford, MBChB, MRCP: University of Glasgow and Queen Elizabeth University Hospital, Glasgow, UK; [2]Jennifer Scott, MRCPI, Mark A. Little, PhD: Trinity College Dublin, Dublin, Ireland; [3]Maira Karabayas, MBChB, MRCP: NHS Grampian, Aberdeen, UK; [4]Marilina Antonelou, MBBS, PhD: University College London, London, UK; [5]Seerapani Gopaluni, MBBS, MRCP, Rona M. Smith, MD, MRCP, David Jayne, MD: University of Cambridge, Cambridge, UK; [6]David Gray, BSc, Joe Barrett, BA: University of Oxford, Oxford, UK; [7]Silke R. Brix, MD, MRCP: Manchester University NHS Foundation Trust and University of Manchester, Manchester, UK; [8]Neeraj Dhaun, MD, PhD: University of Edinburgh, Edinburgh, UK; [9]Stephen P. McAdoo, MBBS, PhD: Hammersmith Hospital and Imperial College London, London, UK; [10]Colin C. Geddes, FRCP: Queen Elizabeth University Hospital, Glasgow, UK; [11]Raashid Luqmani, DM, FRCP, FRCPE: Oxford University Hospitals NHS Foundation Trust, Oxford, UK; [12]Alan D. Salama, PhD, FRCP: University College London and Royal Free Hospital, London, UK; [13]Neil Basu, MD, PhD: University of Glasgow, Glasgow, UK.

Drs. Rutherford and Scott contributed equally to this work.

Dr. Rutherford has received research support from Vifor Pharma. No other disclosures relevant to this article were reported.

Address correspondence to Matthew A. Rutherford, MBChB, MRCP, University of Glasgow, Sir Graeme Davies Building, 120 University Place, Glasgow F12 8TA, UK. Email: matthew.rutherford@glasgow.ac.uk.

Submitted for publication October 29, 2020; accepted in revised form March 4, 2021.

higher doses of glucocorticoids in order to induce and maintain disease remission. While this therapeutic approach successfully manages vasculitis activity, glucocorticoid exposure contributes, in part, to the increased risk of infection in these patients (3,4). Thus, although risk factors associated with poor outcomes from COVID-19 in this population are unknown, there is an assumption that these patients are at a high risk.

The RECOVERY trial has demonstrated a benefit of moderate-dose glucocorticoids in hospitalized general population patients with COVID-19 who require supplemental oxygen or mechanical ventilation, but showed potential harm when used in milder disease (5). Given these paradoxical effects, it is unknown whether chronic background glucocorticoid exposure makes patients more susceptible to severe COVID-19 infection or whether it might be protective.

We report the results of a coordinated binational effort to identify the predictors of a severe outcome in the largest reported cohort of systemic vasculitis patients infected with COVID-19.

PATIENTS AND METHODS

Study design. A registry-based multicenter cohort was designed to facilitate rapid real-world data capture. Centers affiliated with the UK and Ireland Vasculitis Registry (UKIVAS; www.ukivas.org/) and the Irish Rare Kidney Disease Registry (RKD; www.tcd.ie/medicine/thkc/research/rare.php) were invited to contribute. UKIVAS covers 89 sites; RKD covers 8 sites across Ireland. Participating centers represent both secondary and tertiary centers across the UK and Ireland, resulting in a broad population sampling frame. A vasculitis-focused COVID-19 case report form was developed, underpinned by standardized BioPortal ontologies (e.g., SNOMED CT) (6) and interoperable with other emerging data sets, such as the COVID-19 Global Rheumatology Alliance (GRA) (7), thereby facilitating future international data linkage as the COVID-19 pandemic progresses. This enables compatibility of these data with the principles of the global GO-FAIR initiative (8). Additional modules of the UKIVAS and RKD web apps were developed to support data capture.

Study population. Patients were eligible for case submission if they had a diagnosis of systemic vasculitis and COVID-19 (laboratory, radiologic, or clinical). The diagnosis of vasculitis was determined by the local specialist clinician, according to the International Chapel Hill Consensus Conference nomenclature of vasculitides (9). Recruitment commenced on March 28, 2020 and is ongoing. For this analysis, the final case was submitted on July 31, 2020. The population sampling frame consisted of individuals under the clinical care of sites associated with the UKIVAS and RKD registries. At the end of July 2020, there were 795 patients in the RKD registry and ~7,400 patients in the UKIVAS registry, with 4 patients enrolled in both. In the UK, the Health Research Authority decision tool determined that ethics approval was not required, and the local sponsor confirmed the project as a service evaluation (R&D reference no. GN20RH165). RKD registry ethics approval was originally granted by the Tallaght University Hospital/St. James's Hospital Joint Research Ethics Committee (reference no. 2019-08 List 29 [07]). All RKD participants provided informed consent. Additional approvals were not required.

Study variables. Variables included potential predictors of severe outcomes. The selection of predictive variables was informed by emerging risk factors for COVID-19 disease severity in other populations (10,11). These included age, sex, ethnicity, smoking status, comorbid conditions, immunosuppressive treatment for vasculitis, and vasculitis disease activity. Among the comorbid conditions, respiratory disease refers to non–vasculitis-related lower respiratory tract disease, though it is possible that some patients had coexistent vasculitis-related respiratory disease. Intravenous immunosuppressive therapy was considered to be "current" if the assessing clinician determined that the therapy was likely to exert a biologic effect at the time of COVID-19 diagnosis; specific definitions were not provided.

Vasculitis disease activity was determined according to global clinician assessment. Outcome data included complications, such as acute kidney injury (AKI), respiratory failure and vasopressor requirement, and death. To enable interoperability, the standardized outcomes (grade range 1–8) from the COVID-19 GRA case reporting form were used (see Supplementary Table 1, available on the *Arthritis & Rheumatology* website at http://onlinelibrary.wiley.com/doi/10.1002/art.41728/abstract) (10). A severe outcome was defined as a composite of requirement for advanced oxygen therapy (such as noninvasive ventilation or high-flow oxygen device), requirement for invasive ventilation, or death. Dates of hospital and intensive care unit (ICU) admission and discharge were collected in order to derive length of stay. Other variables were collected to characterize the clinical features of COVID-19 in patients with vasculitis. These included symptoms, laboratory tests, and radiology results. Reporting clinicians were asked to indicate which of these variables contributed to diagnosis.

Statistical analysis. Continuous variables are described as the median and interquartile range (IQR). Categorical variables are described as the number and percentage of patients. Associations between various explanatory variables and the odds of severe outcomes were determined. Unadjusted and age/sex-adjusted logistic regression models were individually calculated for each explanatory variable and reported as odds ratios (ORs), *P* values, and 95% confidence intervals (95% CIs). The adjusted ORs for age and sex were derived from a single logistic regression model which included age and sex only. When a potential interaction could account for a positive finding, logistic regression modeling incorporating the explanatory and interacting variables was used. Sensitivity analyses were performed in the event that any effects may have been different in an important subgroup. Missing data were acknowledged in the relevant tables. *P* values less than

Table 1. Baseline characteristics of the study patients (n = 65)*

Characteristic	Value	Characteristic	Value
Age, median (IQR) years	70 (55–76)	Vasculitis, active disease	32 (49.2)
Female sex	32 (49.2)	Vasculitis disease duration, median (IQR) years	2.2 (0.76–6.8)
Ethnicity		Current immunosuppressive therapy	
Asian	7 (10.8)	Any immunosuppressive therapy	56 (86.2)
Black	1 (1.5)	Any immunosuppressive therapy and GCs	43 (66.2)
White	46 (70.8)	Azathioprine	12 (18.5)
Not stated	6 (9.2)	GCs (any dose)	45 (69.2)
Missing data	5 (7.7)	Prednisone 1.0–5.0 mg/day	19 (29.2)
Smoking status		Prednisone ≥5.1 mg/day	26 (40.0)
Current	3 (4.6)	Unknown/missing data	2 (3.1)
Former	15 (23.1)	CYC	10 (15.4)
Never	26 (40.0)	HCQ	4 (6.2)
Unknown/missing data	21 (32.3)	IVIG	1 (1.5)
Comorbidities		MMF	11 (16.9)
Vasculitis†		Rituximab	22 (33.8)
GPA (or PR3 AAV)	24 (36.9)	Tacrolimus	4 (6.2)
MPA (or MPO AAV)	25 (38.5)	Other medications	
EGPA	6 (9.2)	ACE inhibitors	9 (13.8)
LVV	2 (3.1)	ARB	8 (12.3)
Behçet's disease	1 (1.5)	NSAIDs	2 (3.1)
PAN	1 (1.5)	Unknown/missing data	5 (7.7)
Other	5 (7.7)	Laboratory tests, median (IQR)	
Unknown/missing data	1 (1.5)	Creatinine, μmoles/liter¶	127 (69–204)
Diabetes	13 (20.0)	CRP, mg/liter	99 (44–149)
Hypertension	25 (38.5)	Lymphocytes, $\times 10^9$/liter	0.7 (0.4–0.9)
CVD	17 (26.2)	Method used for COVID-19 diagnosis	
Respiratory disease‡	13 (20.0)	PCR	47 (72.3)
Renal disease	30 (46.2)	Radiologic	3 (4.6)
End-stage kidney disease§		Symptoms only	3 (4.6)
Yes	17 (26.2)	Unknown/missing data	12 (18.5)
No	46 (70.8)		
Unknown/missing data	2 (3.1)		
Organ transplant	3 (4.6)		

* Except where indicated otherwise, values are the number (%) of patients. IQR = interquartile range; GPA = granulomatosis with polyangiitis; PR3 = proteinase 3; AAV = antineutrophil cytoplasmic antibody–associated vasculitis; MPA = microscopic polyangiitis; MPO = myeloperoxidase; EGPA = eosinophilic granulomatosis with polyangiitis; LVV = large vessel vasculitis; PAN = polyarteritis nodosa; CVD = cardiovascular disease; GCs = glucocorticoids; CYC = cyclophosphamide; HCQ = hydroxychloroquine; IVIG = intravenous immunoglobulin; MMF = mycophenolate mofetil; ACE = angiotensin-converting enzyme; ARB = angiotensin II receptor blocker; NSAIDs = nonsteroidal antiinflammatory drugs; CRP = C-reactive protein; PCR = polymerase chain reaction.
† Other vasculitis diagnoses include IgA vasculitis, leukocytoclastic vasculitis, and unspecified vasculitis.
‡ Refers to non–vasculitis-related lower respiratory tract disease, though it is possible that some patients had coexistent vasculitis-related respiratory disease.
§ Includes 13 patients receiving hemodialysis, 3 kidney transplant recipients, and 1 patient with sustained stage 5 chronic kidney disease.
¶ Excludes patients receiving hemodialysis.

0.05 were considered significant. R (version 4.0.2) was used for data analysis with packages including tidyverse and finalfit.

RESULTS

In total, 65 patients with an established diagnosis of systemic vasculitis who developed COVID-19 were registered. Fifty-eight patients were submitted to the UKIVAS registry, and 7 were submitted to the RKD registry, with no duplicate submissions.

Baseline characteristics. The median age was 70 years (IQR 55–76 years) and 49% of the patients were female (Table 1). The majority of patients (55 of 65 [85%]) had antineutrophil cytoplasm antibody–associated vasculitis (AAV): of these, 24 patients (44%) had granulomatosis with polyangiitis, 25 patients (45%) had microscopic polyangiitis, and 6 patients (11%) had eosinophilic granulomatosis with polyangiitis. The characteristics of AAV patients were broadly similar to those of the full cohort (data not shown). Thirty-two patients (49%) were assessed as having concurrent active disease. Fifteen patients (23%) were suspected to have contracted COVID-19 through a health care setting; of these, 9 patients (60%) had some degree of active vasculitis. In one case, COVID-19 was considered to have increased disease activity. For the remaining patients, COVID-19 was not perceived to have altered or induced disease activity.

Forty-seven patients (72%) were diagnosed by polymerase chain reaction (PCR) testing, 3 patients (5%) did not have PCR-confirmed disease but had radiologic evidence of disease, and 3

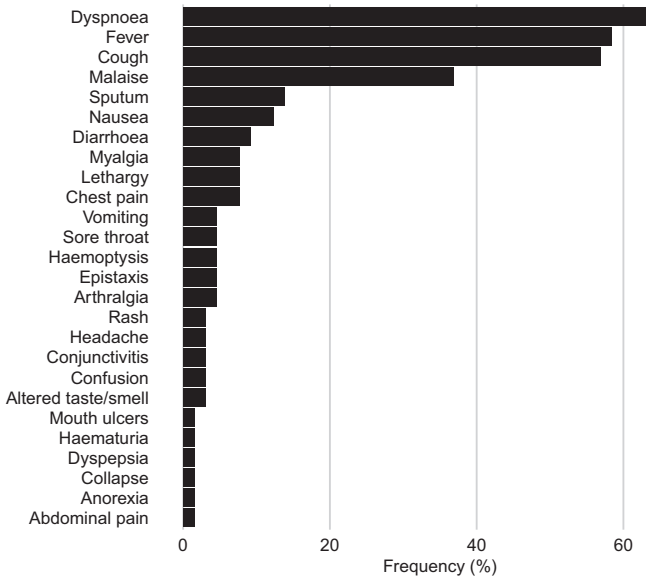

Figure 1. Frequency of patient symptoms at initial presentation.

patients (5%) were diagnosed by clinical presentation only (Table 1). Data on diagnostic testing were unknown/missing for 12 patients (19%). The characteristics of those diagnosed by PCR testing were broadly similar to the full cohort (data not shown).

Most patients were receiving background glucocorticoids (45 of 65 [69%]) at the time of COVID-19 diagnosis. Nineteen patients (29%) were receiving the equivalent of ≤5 mg prednisone, and 26 patients (40%) were receiving >5 mg. For those receiving background glucocorticoids, the median dose was the equivalent of 7.5 mg prednisone daily (IQR 5–25 mg). Twenty-two patients (34%) and 10 patients (15%) had recently been treated with rituximab and cyclophosphamide, respectively (Table 1).

Symptom frequency. The most common symptoms among the included patients were dyspnea (41 of 65 [63%]), fever (38 of 65 [58%]), and cough (37 of 65 [57%]) (Figure 1). Full data on symptoms were missing for 2 patients. Hemoptysis occurred in 3 patients (5%), and epistaxis occurred in 3 individuals (5%); of these, 1 patient had both epistaxis and hemoptysis. Of note, some of these patients had ongoing disease activity prior to COVID-19 diagnosis.

Complication frequency. Respiratory failure was the most commonly reported complication among patients (35 of 65 [54%]), followed by AKI (12 of 65 [18%]) and secondary infection (10 of 65 [15%]) (Figure 2). Full data on complications were missing for 10 patients.

Clinical outcomes. Almost all patients required hospitalization (59 of 65 [91%]); 7 patients (11%) were admitted to an ICU, and 18 patients (28%) died (Table 2). The median length of hospital stay for discharged patients was 11 days (IQR 5–27 days). A severe outcome was experienced by 25 of 65 patients (38%).

Predictors of severe outcomes. Patients with comorbid respiratory disease were more likely to experience a severe outcome than those without (adjusted OR 7.5 [95% CI 1.9–38.2]; $P = 0.006$), as were those who had been receiving glucocorticoids (adjusted OR 3.7 [95% CI 1.1–14.9]; $P = 0.047$) (Table 3). Glucocorticoid exposure remained a poor prognostic indicator even after adjusting for vasculitis disease activity (data not shown). A sensitivity analysis including only patients with a confirmed PCR diagnosis (n = 47) was performed, which demonstrated effect sizes consistent with these findings; this was statistically significant for comorbid respiratory disease but not for glucocorticoid exposure (data not shown). A sensitivity analysis was also performed for individuals with AAV (n = 55) with a similar result. There was insufficient power to assess the association between glucocorticoid dose and poor outcome. Similarly, there was insufficient power to assess for differences between common nonglucocorticoid immunosuppressive agents. Associations were not demonstrated for any demographics, other comorbid conditions, vasculitis diagnosis, vasculitis disease activity, or nonglucocorticoid immunosuppressant medication.

DISCUSSION

This multicenter study includes the largest cohort of patients with systemic vasculitis who have developed COVID-19 to date. It identifies comorbid respiratory disease and background glucocorticoid therapy as significant predictors of a severe outcome, defined as a need for advanced oxygen therapy or invasive ventilation, or death. Routinely used nonglucocorticoid immunosuppressants, such as rituximab and cyclophosphamide, were not associated with a severe outcome, nor was vasculitis disease activity.

Glucocorticoids have pleotropic immunologic effects and are generally considered risk factors for infections (12). Glucocorticoids at high doses have been associated with prolonged viral shedding, with a similar effect being observed in other coronaviruses (13,14). That glucocorticoids are associated with worse COVID-19 disease outcomes is consistent with findings from

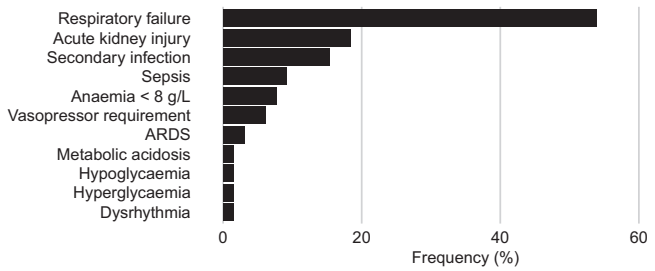

Figure 2. Frequency of patient complications. ARDS = acute respiratory distress syndrome.

Table 2. COVID-19 disease outcomes in the study patients (n = 65)*

Hospitalization	59 (90.8)
ICU admission	
Yes	7 (10.8)
No	49 (75.4)
Unknown/missing data	9 (13.8)
Graded outcome (grade no.)	
Not hospitalized, no limitations on activities (1)	2 (3.1)
Not hospitalized, limitation on activities (2)	3 (4.6)
Hospitalized, not requiring supplemental oxygen (3)	9 (13.8)
Hospitalized, requiring supplemental oxygen (4)	25 (38.5)
Hospitalized, on noninvasive ventilation or high-flow oxygen devices (5)	4 (6.2)
Hospitalized, on invasive mechanical ventilation or ECMO (6)	3 (4.6)
Death (7)	18 (27.7)
Unknown/missing data (8)	1 (1.5)
Length of hospital stay, median (IQR) days	11 (5–27)
Length of hospital stay, unknown/missing data	40 (61.5)

* Except where indicated otherwise, values are the number (%) of patients. ICU = intensive care unit; ECMO = extracorporeal membrane oxygenation.

across the rheumatic autoimmune spectrum, as demonstrated by the COVID-19 GRA study (10). Our point estimate for the association of any glucocorticoid dose with severe outcomes (OR 3.7 [95% CI 1.09–14.9]) was comparable to that of the COVID-19 GRA evaluation of steroids equivalent to ≥10 mg prednisone per day (OR 2.05 [95% CI 1.06–3.96). The confidence interval for this finding is relatively wide, and thus, it remains to be determined if there is a dose threshold at which risk commences.

The association between glucocorticoids and severe outcomes may appear to conflict with findings from the RECOVERY trial (5). This trial demonstrated that low-dose dexamethasone had a substantial survival benefit in patients hospitalized with COVID-19. However, the groups that benefited in RECOVERY were those requiring supplemental oxygen, with the greatest benefit derived in those requiring mechanical ventilation. In fact, the point estimate for patients not requiring oxygen suggested that glucocorticoids could be associated with increased mortality, though this was not a statistically significant finding (5). Therefore, prior to requiring oxygen, it may be that glucocorticoids are deleterious, as observed in this and other studies of autoimmune disease (15). Our finding that comorbid respiratory disease (most commonly chronic obstructive pulmonary disease, asthma, and interstitial lung disease) was associated with severe disease outcomes was consistent with a recent general population meta-analysis (16). Among some

Table 3. Unadjusted and adjusted ORs for potential risk factors and association with severe outcomes*

	No. of severe outcomes/ no. of cases (%)	Unadjusted OR (95% CI)	Adjusted OR (95% CI)
Female	13/26 (50)	1.04 (0.51–2.10)	1.05 (0.52–2.13)
Age	–	1.01 (0.98–1.05)	1.01 (0.98–1.05)
Vasculitis diagnosis			
GPA (referent: not GPA)	12/24 (50)	1.71 (0.62–4.81)	2.19 (0.68–7.63)
MPA (referent: not MPA)	7/25 (28)	0.53 (0.17–1.52)	0.43 (0.13–1.36)
Comorbidities (referent: individual comorbidity not present)			
Hypertension	12/25 (48)	1.46 (0.71–3.04)	1.39 (0.64–3.04)
CVD	8/17 (47)	1.32 (0.59–2.93)	1.08 (0.52–2.23)
Respiratory disease	10/13 (77)	7.50 (1.99–36.94)	7.53 (1.93–38.22)†
Diabetes	6/13 (46)	1.25 (0.51–2.99)	1.20 (0.48–2.92)
Renal disease	12/30 (40)	1.00 (0.49–2.03)	1.05 (0.52–2.14)
End-stage kidney disease	6/17 (35)	0.85 (0.25–2.65)	0.77 (0.22–2.48)
Smoking status			
Ever smoker (referent: never)	9/18 (50)	2.25 (0.65–8.05)	2.33 (0.62–9.28)
Immunosuppressive therapy			
Any immunosuppressive therapy (referent: not receiving immunosuppressive therapy)	24/55 (44)	3.10 (0.70–21.79)	3.66 (0.77–27.29)
GCs (referent: no prednisone)			
Prednisone (any dose)	22/45 (49)	3.35 (1.02–13.2)	3.66 (1.09–14.9)‡
Prednisone 1.0–5.0 mg/day	10/19 (53)	3.89 (0.98–17.93)	3.76 (0.91–18.02)
Prednisone ≥5.1 mg/day	12/26 (46)	3.00 (0.82–12.86)	3.32 (0.86–15.35)
Other immunosuppressive therapy			
Azathioprine (referent: not receiving azathioprine)	6/12 (50)	1.65 (0.46–5.97)	1.57 (0.42–5.85)
CYC (referent: not receiving CYC)	5/10 (50)	1.62 (0.41–6.48)	1.83 (0.44–7.76)
Rituximab (referent: not receiving rituximab)	9/22 (41)	1.06 (0.36–3.01)	1.25 (0.40–3.90)

* A severe outcome was defined as a composite of requirement for advanced oxygen therapy (such as noninvasive ventilation or high-flow oxygen device), requirement for invasive ventilation, or death. A separate logistic regression model including sex and age as a continuous variable was calculated for each explanatory variable. The adjusted models for age and sex were derived from a single logistic regression model which included sex and age as a continuous variable. OR = odds ratio; 95% CI = 95% confidence interval (see Table 1 for other definitions).
† $P < 0.00645$. Respiratory disease refers to non–vasculitis-related lower respiratory tract disease, though it is possible that some patients had coexistent vasculitis-related respiratory disease.
‡ $P < 0.047$.

patients with chronic lung disease, enhanced respiratory tract angiotensin-converting enzyme 2 expression, the principal binding site for COVID-19 cell entry, is a possible explanation for this association (10). Consistent with findings from the COVID-19 GRA study, we did not find an association of adverse disease outcomes with other immunosuppressive agents (17). This is reassuring, as current guidance emphasizes the importance of maintaining immunosuppressive therapy among uninfected patients due to concerns of destabilizing disease control (18).

This cohort represents a severely affected group, as reflected by the very high proportion of hospitalization (91%). The mortality rate of 28% is similar to that reported in the largest UK study of hospitalized patients carried out by the International Severe Acute Respiratory and emerging Infections Consortium (ISARIC) WHO Clinical Characterisation Protocol UK (CCP-UK) group, in which 26% of patients died (18). Age, sex, and symptom distribution were also broadly similar to the ISARIC WHO CCP-UK study. The most common symptoms, in that cohort and ours, were those that have been the most prominent in the case definition: breathlessness, fever, and cough. Both active pulmonary vasculitis and COVID-19 are recognized causes of hemoptysis (18,19). In the ISARIC WHO CCP-UK group, 3.5% of patients experienced this symptom, compared to 3 patients (4.8%) in our cohort. None were thought to have diffuse alveolar hemorrhage, as assessed by the responding clinician. Differentiating COVID-19 from active pulmonary vasculitis remains a challenge, and indeed these presentations may coexist. Ensuring that these diagnoses are considered when a patient with vasculitis presents with hemoptysis remains of high importance.

A large proportion of patients (49%) had concurrent active vasculitis. A considerable proportion of these patients were believed to have contracted COVID-19 from a health care setting. Notably, the onset of vasculitis disease activity preceded COVID-19 infection in almost all cases. However, it is unknown whether COVID-19 may trigger vasculitis activity in the longer term. The emergence of pediatric multisystem inflammatory syndrome temporally associated with SARS–CoV-2, a condition bearing strong similarities to Kawasaki disease, is a potential example of SARS–CoV-2 triggering autoimmune vasculitis, though the pathogenesis is not currently understood (20). We did not find evidence of vasculitis being triggered in the short term. Longitudinal studies will seek to address this question. The prevalence of active disease in this cohort was higher than expected—previous cross-sectional UK studies have shown disease activity prevalence at ~20% (21). Although disease activity was not associated with worse outcomes, it may be that patients with unstable disease are more vulnerable to contracting COVID-19. Physician or patient-led reduction in immunosuppressive treatment, in a bid to limit the impact of COVID-19, is another potential reason accounting for a high proportion of disease activity. Due to the study design, our data are limited in the extent to which they can answer this question.

Ascertainment bias is likely to have affected this study. Given that most patients were hospitalized, it is likely that patients with milder disease were not identified. The number of PCR-diagnosed COVID-19 patients in our study as a proportion of the combined UKIVAS and RKD populations was similar to the proportion of UK cases relative to the UK population for a comparable time period (22). However, due to the study design, it is not possible to derive incidence rates. Patients with vasculitis may have been more likely to contract COVID-19 due to risk factors such as immunosuppressive therapy and the need to attend health care facilities; therefore, ascertainment bias remains possible.

There was a high preponderance of small vessel vasculitis (SVV) in this study compared to giant cell arteritis (GCA). Although it is a more common condition, patients with GCA are typically older and may have adopted stricter self-isolation restrictions (according to national guidance). In addition, SVV may have predominated due to a disproportionate number of renal departments, compared to rheumatology centers, represented in the UKIVAS registry. Due to a large majority of patients in this study having SVV, the extent to which its findings can be generalized to other vasculitides is limited. Other limitations of this study include a relative lack of power. As a result, our analyses may not detect some clinically significant effects, and, conversely, the risk of spurious findings is higher. Similarly, due to the limited number of events, our ability to control for multiple potential confounding factors was limited. Due to the heterogeneous immunobiology, phenotypes, and management approaches of systemic vasculitis, it is possible that individual disorders may incur different risks; due to insufficient power, we were limited in the extent to which this could be examined.

This study is the first to describe a cohort of vasculitis patients with COVID-19. The clinical presentation of COVID-19 was similar to descriptions in large series of patients without autoimmune disease. Glucocorticoids were associated with an increased risk of severe outcomes, but other immunosuppressants were not. Patients with autoimmune disease have been considered vulnerable during the COVID-19 pandemic, and many governments have instructed that they adhere to exceptional social isolation restrictions. While patients with systemic vasculitis remain at a higher risk for severe outcomes, these data indicate that some patients may not need to face similar restrictions in the future if other known risk factors are absent. Conversely, patients who are receiving background glucocorticoids or have comorbid respiratory disease should be closely monitored when presenting with COVID-19, since their risk of progression to a severe state appears to be higher (11). This study primarily describes a cohort of hospitalized patients and is thus more likely to reflect severe COVID-19 disease. Future work should seek to establish risk factors for severe disease in a wider population. Comparisons with controls who did not contract COVID-19 would allow for assessment of incidence and risk factors for contracting COVID-19.

Taken together with findings from other cohorts exposed to immunosuppressant medication, these data could inform future public health guidance for patients with autoimmune disease.

These data were designed to be interoperable with other national data sets. Future work should seek to combine international efforts to allow for greater power to assess the factors that impact this potentially vulnerable group.

ACKNOWLEDGMENTS

The authors thank the following individuals who contributed data for this project: Jocelyn Berdeprado, Nina Brown, Chee Kay Cheung, Denise De Lord, Oliver Flossman, Venkat Gangaram, Sian Griffin, Alex Hamilton, Philip Ind, Vikki Jubb, Maria King, Sarah Logan, Alice Lorenzi, Ann Morgan, Dan Pugh, Ravindra Rajakariar, Saira Risdale, Michael Robson, Bhrigu Sood, Katie Vinen, and Zoe Wellbelove.

AUTHOR CONTRIBUTIONS

All authors were involved in drafting the article or revising it critically for important intellectual content, and all authors approved the final version to be published. Dr. Rutherford had full access to all of the data in the study and takes responsibility for the integrity of the data and the accuracy of the data analysis.

Study conception and design. Rutherford, Scott, Gray, Barrett, Brix, Dhaun, McAdoo, Jayne, Luqmani, Salama, Little, Basu.

Acquisition of data. Rutherford, Scott, Karabayas, Antonelou, Gray, Barrett, Brix, Dhaun, McAdoo, Geddes, Luqmani, Salama, Little, Basu.

Analysis and interpretation of data. Rutherford, Scott, Gopaluni, Brix, Dhaun, McAdoo, Smith, Geddes, Jayne, Luqmani, Salama, Little, Basu.

REFERENCES

1. Zhou F, Yu T, Du R, Fan G, Liu Y, Liu Z, et al. Clinical course and risk factors for mortality of adult inpatients with COVID-19 in Wuhan, China: a retrospective cohort study. Lancet 2020;395:1054–62.
2. World Health Organization. WHO Director-General's opening remarks at the media briefing on COVID-19–11 March 2020. URL: https://www.who.int/dg/speeches/detail/who-director-general-s-opening-remarks-at-the-media-briefing-on-covid-19---11-march-2020.
3. Neumann I. Immunosuppressive and glucocorticoid therapy for the treatment of ANCA-associated vasculitis [review]. Rheumatology (Oxford) 2020;59:iii60–7.
4. Walsh M, Merkel PA, Peh CA, Szpirt WM, Puéchal X, Fujimoto S, et al. Plasma exchange and glucocorticoids in severe ANCA-associated vasculitis. N Engl J Med 2020;382:622–31.
5. Horby P, Lim WS, Emberson JR, Mafham M, Bell JL, Linsell L, et al, for the RECOVERY Collaborative Group. Dexamethasone in hospitalized patients with Covid-19. N Engl J Med 2021; 384:693–704.
6. Musen MA, Noy NF, Shah NH, Whetzel PL, Chute CG, Story MA, et al. The National Center for Biomedical Ontology. J Am Med Inform Assoc 2012;19:190–5.
7. COVID-19 Global Rheumatology Alliance. URL: https://rheum-covid.org/.
8. Wilkinson MD, Dumontier M, Aalbersberg IJ, Appleton G, Axton M, Baak A, et al. The FAIR Guiding Principles for scientific data management and stewardship. Sci Data 2016;3:160018.
9. Jennette JC, Falk RJ, Bacon PA, Basu N, Cid MC, Ferrario F, et al. 2012 revised International Chapel Hill Consensus Conference nomenclature of vasculitides. Arthritis Rheum 2013;65:1–11.
10. Gianfrancesco M, Hyrich KL, Al-Adely S, Carmona L, Danila MI, Gossec L, et al. Characteristics associated with hospitalisation for COVID-19 in people with rheumatic disease: data from the COVID-19 Global Rheumatology Alliance physician-reported registry. Ann Rheum Dis 2020;79:859–66.
11. The OpenSAFELY Collaborative, Williamson E, Walker AJ, Bhaskaran KJ, Bacon S, Bates C, et al. OpenSAFELY: factors associated with COVID-19-related hospital death in the linked electronic health records of 17 million adult NHS patients [preprint]. medRxiv. May 2020. URL: https://doi.org/10.1101/2020.05.06.20092999.
12. Cain DW, Cidlowski JA. Immune regulation by glucocorticoids [reivew]. Nat Rev Immunol 2017;17:233–47.
13. Johnson RM, Vinetz JM. Dexamethasone in the management of covid-19 [editorial]. BMJ 2020;370:m2648.
14. Li S, Hu Z, Song X. High-dose but not low-dose corticosteroids potentially delay viral shedding of patients with COVID-19. Clin Infect Dis 2020 doi: https://doi.org/10.1093/cid/ciaa829. E-pub ahead of print.
15. Sanchez-Ramirez DC, Mackey D. Underlying respiratory diseases, specifically COPD, and smoking are associated with severe COVID-19 outcomes: a systematic review and meta-analysis. Respir Med 2020;171:106096.
16. Smith JC, Sausville EL, Girish V, Yuan ML, Vasudevan A, John KM, et al. Cigarette smoke exposure and inflammatory signaling increase the expression of the SARS-CoV-2 receptor ACE2 in the respiratory tract. Dev Cell 2020;53:514–29.
17. Landewé RB, Machado PM, Kroon F, Bijlsma HW, Burmester GR, Carmona L, et al. EULAR provisional recommendations for the management of rheumatic and musculoskeletal diseases in the context of SARS-CoV-2. Ann Rheum Dis 2020;79:851–8.
18. Docherty AB, Harrison EM, Green CA, Hardwick HE, Pius R, Norman L, et al. Features of 20 133 UK patients in hospital with covid-19 using the ISARIC WHO Clinical Characterisation Protocol: prospective observational cohort study. BMJ 2020;369:m1985.
19. Kitching AR, Anders HJ, Basu N, Brouwer E, Gordon J, Jayne DR, et al. ANCA-associated vasculitis [review]. Nat Rev Dis Primers 2020;6:71.
20. Pouletty M, Borocco C, Ouldali N, Caseris M, Basmaci R, Lachaume N, et al. Paediatric multisystem inflammatory syndrome temporally associated with SARS-CoV-2 mimicking Kawasaki disease (Kawa-COVID-19): a multicentre cohort. Ann Rheum Dis 2020;79:999–1006.
21. Basu N, McClean A, Harper L, Amft EN, Dhaun N, Luqmani RA, et al. The characterisation and determinants of quality of life in ANCA associated vasculitis. Ann Rheum Dis 2014;73:207–11.
22. Gov.UK Coronavirus (COVID-19) in the UK. URL: https://coronavirus.data.gov.uk/details/cases.

American College of Rheumatology
Empowering Rheumatology Professionals

Arthritis & Rheumatology
Vol. 73, No. 9, September 2021, pp 1720–1730
DOI 10.1002/art.41737

Regulation of Monocyte Adhesion and Type I Interferon Signaling by CD52 in Patients With Systemic Sclerosis

Michał Rudnik,[1] Filip Rolski,[2] Suzana Jordan,[1] Tonja Mertelj,[3] Mara Stellato,[1] Oliver Distler,[1] Przemysław Blyszczuk,[4] and Gabriela Kania[1]

Objective. Systemic sclerosis (SSc) is characterized by dysregulation of type I interferon (IFN) signaling. CD52 is known for its immunosuppressive functions in T cells. This study was undertaken to investigate the role of CD52 in monocyte adhesion and type I IFN signaling in patients with SSc.

Methods. Transcriptome profiles of circulating CD14+ monocytes from patients with limited cutaneous SSc (lcSSc), patients with diffuse cutaneous SSc (dcSSs), and healthy controls were analyzed by RNA sequencing. Levels of CD52, CD11b/integrin αM, and CD18/integrin β2 in whole blood were assessed by flow cytometry. CD52 expression was analyzed in relation to disease phenotype (early, lcSSc, dcSSc) and autoantibody profiles. The impact of overexpression, knockdown, and antibody blocking of CD52 was analyzed by gene and protein expression assays and functional assays.

Results. Pathway enrichment analysis indicated an increase in adhesion- and type I IFN–related genes in monocytes from SSc patients. These cells displayed up-regulated expression of CD11b/CD18, reduced expression of CD52, and enhanced adhesion to intercellular adhesion molecule 1 and endothelial cells. Changes in CD52 expression were consistent with the SSc subtypes, as well as with immunosuppressive treatments, autoantibody profiles, and monocyte adhesion properties in patients with SSc. Overexpression of CD52 led to decreased levels of CD18 and monocyte adhesion, while knockdown of CD52 increased monocyte adhesion. Experiments with the humanized anti-CD52 monoclonal antibody alemtuzumab in blood samples from healthy controls increased monocyte adhesion and CD11b/CD18 expression, and enhanced type I IFN responses. Monocytic CD52 expression was up-regulated by interleukin-4 (IL-4)/IL-13 via the STAT6 pathway, and was down-regulated by lipopolysaccharide and IFNs α, β, and γ in a JAK1 and histone deacetylase IIa (HDAC IIa)–dependent manner.

Conclusion. Down-regulation of the antiadhesion CD52 antigen in CD14+ monocytes represents a novel mechanism in the pathogenesis of SSc. Targeting of the IFN–HDAC–CD52 axis in monocytes might represent a new therapeutic option for patients with early SSc.

INTRODUCTION

Systemic sclerosis (SSc) is an autoimmune disorder with a severe and chronic phenotype. The primary characteristics include microvasculopathy, systemic inflammation, and multiple organ involvement. The etiology of the disease remains unknown; however, microvasculature damage followed by infiltration of immune cells, including monocytes, has been recognized as a primary pathogenic event (1,2).

Monocytes fundamentally contribute to tissue homeostasis, protection of organisms, and both promotion and resolution of inflammation. As a part of the innate immune response, they protect from infections in which inflammatory cytokines are produced, and they coordinate the adaptive immune response (3,4).

Dr. Kania's work was supported by the Swiss National Science Foundation (grants 310030_152876/1 and 310030_175663) and the Swiss Heart Foundation.

[1]Michał Rudnik, PhD, Suzana Jordan, PhD, Mara Stellato, PhD, Oliver Distler, MD, Gabriela Kania, PhD: University Hospital Zurich and University of Zurich, Zurich, Switzerland; [2]Filip Rolski, MSc: Jagiellonian University Medical College, Krakow, Poland; [3]Tonja Mertelj, MD: University Hospital Zurich and University of Zurich, Zurich, Switzerland, and University Medical Centre Ljubljana, Ljubljana, Slovenia; [4]Przemysław Blyszczuk, PhD: University Hospital Zurich and University of Zurich, Zurich, Switzerland, and Jagiellonian University Medical College, Krakow, Poland.

Dr. Distler has received consulting fees, speaking fees, and/or honoraria from Actelion, Acceleron, AnaMar, Bayer, Beacon Discovery, Blade Therapeutics, Boehringer, CSL Behring, Chemomab, Curzion, ErgoNex, Galápagos NV, GlaxoSmithKline, Glenmark, Inventiva, Italfarmaco, IQVIA, Medac, Medscape, Mitsubishi Tanabe Pharma, MSD, Roche, Sanofi, and UCB (less than $10,000 each), and research grants from Actelion, Bayer, Boehringer Ingelheim, Kymera, and Mitsubishi Tanabe Pharma, and holds a patent related to the use of miR-29 for the treatment of systemic sclerosis. No other disclosures relevant to this article were reported.

Address correspondence to Gabriela Kania, PhD, University Hospital Zurich, Center of Experimental Rheumatology, Wagistrasse 14, 8091 Zurich, Switzerland. Email: gabriela.kania@uzh.ch.

Submitted for publication September 14, 2020; accepted in revised form March 11, 2021.

Monocytes play a pivotal role in the pathogenesis of SSc by contributing to extracellular matrix deposition and by producing proinflammatory and profibrotic factors. In disease, monocytes migrate from the circulation through the endothelium, and differentiate into specialized cells such as monocyte-derived macrophages, dendritic cells, and fibroblast-like cells (5).

Transmigration of monocytes is a strictly regulated process requiring a series of interactions between the endothelium and monocytes. Initially, activated endothelial cells present adhesion molecules, including E-selectin, P-selectin, intercellular adhesion molecule 1 (ICAM-1), vascular cell adhesion molecule 1 (VCAM-1), and chemokines on the luminal surface of the vessel (6,7). Selectins interact with P-selectin glycoprotein ligand 1, which is expressed by monocytes, thus enabling the monocytes to roll on the endothelium. Firm adhesion to endothelium is dependent on CCL2 and CXCL8 chemokines and their receptors (CCR2, CXCR1, and CXCR2) (8). Monocytes then crawl toward favorable sites of extravasation via β2 integrins, mainly lymphocyte function–associated antigen 1 (αLβ2 integrin or CD11a/CD18) and Mac-1 (αMβ2 integrin or CD11b/CD18) (9). Eventually, monocytes need to migrate through a monolayer of endothelial cells, the basement membrane, and pericytes. β2 integrin forms complexes with 4 partners (CD11a–d), and these complexes are involved in adhesion and migration, phagocytosis, and cell–cell interactions in a variety of circumstances (10).

CD52 is a small glycosylphosphatidylinositol-anchored protein that is composed of a 12–amino acid scaffold peptide and an *N*-linked complex glycan. It is highly expressed on T cells and B cells and, to a lower extent, on monocytes, macrophages, and dendritic cells (11). The Fc fusion chimeric form of the CD52 protein (CD52-Fc) impairs phosphorylation of the T cell receptor–associated kinases Lck and Zap70, thereby limiting T cell activation (12). Moreover, recombinant CD52-Fc suppresses innate immunity by limiting Toll-like receptor–induced NF-κB activation, followed by reduced inflammatory cytokine production and apoptosis. CD52 was initially discovered as an antigen of a lymphocyte-depleting rat antibody (trade name Campath). The humanized form, alemtuzumab, has been approved as a monoclonal antibody treatment for lymphocytic leukemia, T cell lymphomas, and multiple sclerosis. Treatment with alemtuzumab depletes lymphocytes by antibody-dependent, cell-mediated cytotoxicity mechanisms (13), leading to beneficial reconstitution of the immune system (14), and yet this treatment can induce autoimmunity (15).

Similar to other autoimmune diseases, SSc is associated with an interferon (IFN) gene signature, which is characterized by higher expression of IFN-stimulated genes in response to IFNs (mainly, IFNα) (16). Both type I and type II IFNs interact with members of the JAK family, leading to the phosphorylation of STAT transcription factors and expression of target genes (17). It is suggested that type I IFNs have a pathogenic role in SSc by promoting antigen presentation, lymphocyte responses, and chemokine production (18).

Histone deacetylases (HDACs) are a family of epigenetic modifiers that have been implicated in regulation of the inflammatory responses of immune cells. HDACs mediate their biologic activity via diverse molecular mechanisms, including through the direct inhibition of gene transcription or, indirectly, through modulation of nuclear transcription factors such as NF-κB and STATs (19).

In the present study, we investigated the pro-adhesive phenotype of CD14+ monocytes in the blood of patients with SSc and described the role of CD52 in the regulation of adhesion and IFN responses in monocytes. Moreover, we explored the regulatory mechanisms of CD52 expression and identified the involvement of HDACs in that process.

PATIENTS AND METHODS

SSc patients and healthy controls. Collection of blood and skin biopsy samples from patients with SSc and healthy controls was approved by the local ethics committee of the Zurich Canton (approval nos. KEK-ZH 515, PB-2016-02014, and KEK-Nr. 2018-01873). All study subjects provided written informed consent.

SSc patients and healthy controls were recruited at the Department of Rheumatology of University Hospital Zurich. Patients were diagnosed as having SSc by rheumatologists. Patients who had Raynaud's syndrome and a least one other SSc characteristic, such as SSc-specific antibodies, capillaroscopy changes characteristic of SSc, and/or puffy fingers, but who did not fulfill the American College of Rheumatology/European Alliance of Associations for Rheumatology (ACR/EULAR) 2013 classification criteria for SSc, were grouped as having early SSc. Patients fulfilling the ACR/EULAR 2013 criteria for SSc (20) were further divided into those with limited cutaneous SSc (lcSSc) and those with diffuse cutaneous SSc (dcSSc), according to the definitions of Le Roy et al (21). Details on the demographic and clinical characteristics of the SSc patients are listed in Supplementary Table 1 (available on the *Arthritis & Rheumatology* website at http://onlinelibrary.wiley.com/doi/10.1002/art.41737/abstract). Healthy control subjects (n = 16) were subjects without SSc who were age- and sex-matched to the patients (mean ± SD age 46.2 ± 5.4 years, 12 women [75%]).

Blood samples were collected in EDTA tubes (BD Vacutainer) and processed within 24 hours. For flow cytometry analysis, red blood cell lysis with fixation was performed, and samples were cryopreserved until analyzed. Peripheral blood mononuclear cells were isolated by gradient centrifugation on cell separation medium (Lympholyte; Cedarlane), followed by magnetic-activated cell sorting for CD14 using human microbeads (Miltenyi Biotec). Monocytes were directly analyzed or further cultured in RPMI medium with 10% fetal bovine serum and 1% penicillin/streptomycin (Gibco).

Statistical analysis. Statistical analysis was performed using GraphPad Prism version 8 and SPSS software. Data distribution was calculated using the Shapiro-Wilk test. For normally distributed data, values are the mean ± SD, with unpaired 2-tailed parametric *t*-tests used for comparison between 2 groups. For non–normally distributed data, values are the median, with unpaired nonparametric Mann-Whitney U tests used for comparison between 2 groups. For comparisons of >2 groups, 2-way analysis of variance with testing for multiple comparisons (for normally distributed data) and Kruskal-Wallis test with testing for multiple comparisons (for non–normally distributed data) were used. Pearson's correlation analysis was used for assessing correlations between the expression of CD52 and adhesion of monocytes. Differences were considered statistically significant at *P* values less than 0.05. More detailed information on the materials and methods used for the study is provided in the Supplementary Methods (available on the *Arthritis & Rheumatology* website at http://onlinelibrary.wiley.com/doi/10.1002/art.41737/abstract).

Data availability statement. All data are available from the corresponding author upon request. The RNA-sequencing data sets for this study can be found in the Gene Expression Omnibus (accession no. GSE157840).

RESULTS

Wide range of changes in the transcriptome of peripheral blood monocytes in patients with SSc. For RNA-sequencing analyses, we sorted CD14+ monocytes from the peripheral blood of patients with lcSSc, patients with dcSSc, and healthy controls (Figure 1 and Supplementary Figure 1 [available on the *Arthritis & Rheumatology* website at http://onlinelibrary.wiley.com/doi/10.1002/art.41737/abstract]). The demographic and clinical characteristics of the SSc patients and healthy controls are shown in Supplementary Table 2 (http://onlinelibrary.wiley.com/doi/10.1002/art.41737/abstract).

Pairwise comparisons of the RNA transcriptome profiles between patients with SSc and healthy controls showed significant alterations in gene expression. Specifically, we detected 225 genes that were differentially expressed in patients with lcSSc (160 up-regulated and 65 down-regulated) and 1,440 genes that were differentially expressed in patients with dcSSc (1,076 up-regulated and 364 down-regulated) compared to healthy controls ($P \leq 0.01$, $\log_2 P \geq 0.5$) (see Supplementary Methods and Supplementary Figures 1A and B, http://onlinelibrary.wiley.com/doi/10.1002/art.41737/abstract).

To unravel which biologic processes are dysregulated in SSc monocytes, we performed pathway enrichment analyses. We observed a significant enrichment of functional pathways that are critical for the infiltration of monocytes into the tissue, such as the chemotaxis and adhesion pathways (Figure 1A and Supplementary Figure 2 [available on the *Arthritis & Rheumatology* website at http://onlinelibrary.wiley.com/doi/10.1002/art.41737/abstract]). Among the genes implicated in those processes, we observed higher expression of the chemokines CCL2 and CCL3, the chemokine receptors CXCR1 and CXCR2, the adhesion molecules SELPLG and integrin β2 (ITGB2, CD18), and the kinases MAPK11 and PTK2. Furthermore, the expression of CD52 was down-regulated in SSc monocytes (Figure 1B).

Correlation of monocytic CD52 expression with SSc disease subtype. Considering the prominent enrichment of adhesion pathways in SSc monocytes, we next assessed the protein levels of CD52 and the adhesion-related integrins CD11b and CD18 (Figure 1C and Supplementary Figure 3 [available on the *Arthritis & Rheumatology* website at http://onlinelibrary.wiley.com/doi/10.1002/art.41737/abstract]). Flow cytometry analysis of the whole blood from patients with SSc confirmed the down-regulation of CD52, and showed that the levels of CD11b and CD18 were elevated in CD14+ monocytes from patients with SSc.

In addition, the subdivision of SSc patients into early SSc, lcSSc, and dcSSc subgroups revealed a significant decrease in CD52 expression in those with early SSc and those with lcSSc (Supplementary Figure 4A, available on the *Arthritis & Rheumatology* website at http://onlinelibrary.wiley.com/doi/10.1002/art.41737/abstract), while the expression of CD11b and CD18 was higher in both the lcSSc and dcSSc subgroups compared to healthy controls.

Because patients with early SSc do not show skin fibrosis and major organ involvement, we assessed the correlation of monocytic CD52 expression with specific autoantibody profiles in these patients. Consistently, CD14+ monocytes from patients with early SSc who were positive for anticentromere autoantibodies were characterized by lower expression of CD52, while the presence of anti–topoisomerase I autoantibodies was associated with higher CD52 levels. No association with the presence of anti–RNA polymerase III autoantibodies was observed (Figure 1D).

Moreover, CD14+ monocytes from patients with early SSc who had not received immunosuppressive therapy showed lower CD52 levels in comparison to CD14+ monocytes obtained from healthy controls and patients with early SSc who had received immunosuppressive therapy (prednisone dosage ≥10 mg/day, any disease-modifying antirheumatic treatment, or any biologic treatment such as rituximab or tumor necrosis factor [TNF] inhibitors) (Supplementary Figure 4B, http://onlinelibrary.wiley.com/doi/10.1002/art.41737/abstract). CD52 expression on CD14+ monocytes was comparable between patients who had received immunosuppression and healthy controls.

Correlation of adhesion molecule expression with enhanced adhesion of monocytes in patients with SSc. We next examined the adhesion capabilities of blood CD14+ monocytes in terms of cell adhesion to ICAM-1–coated plates. The results showed increased adhesion of

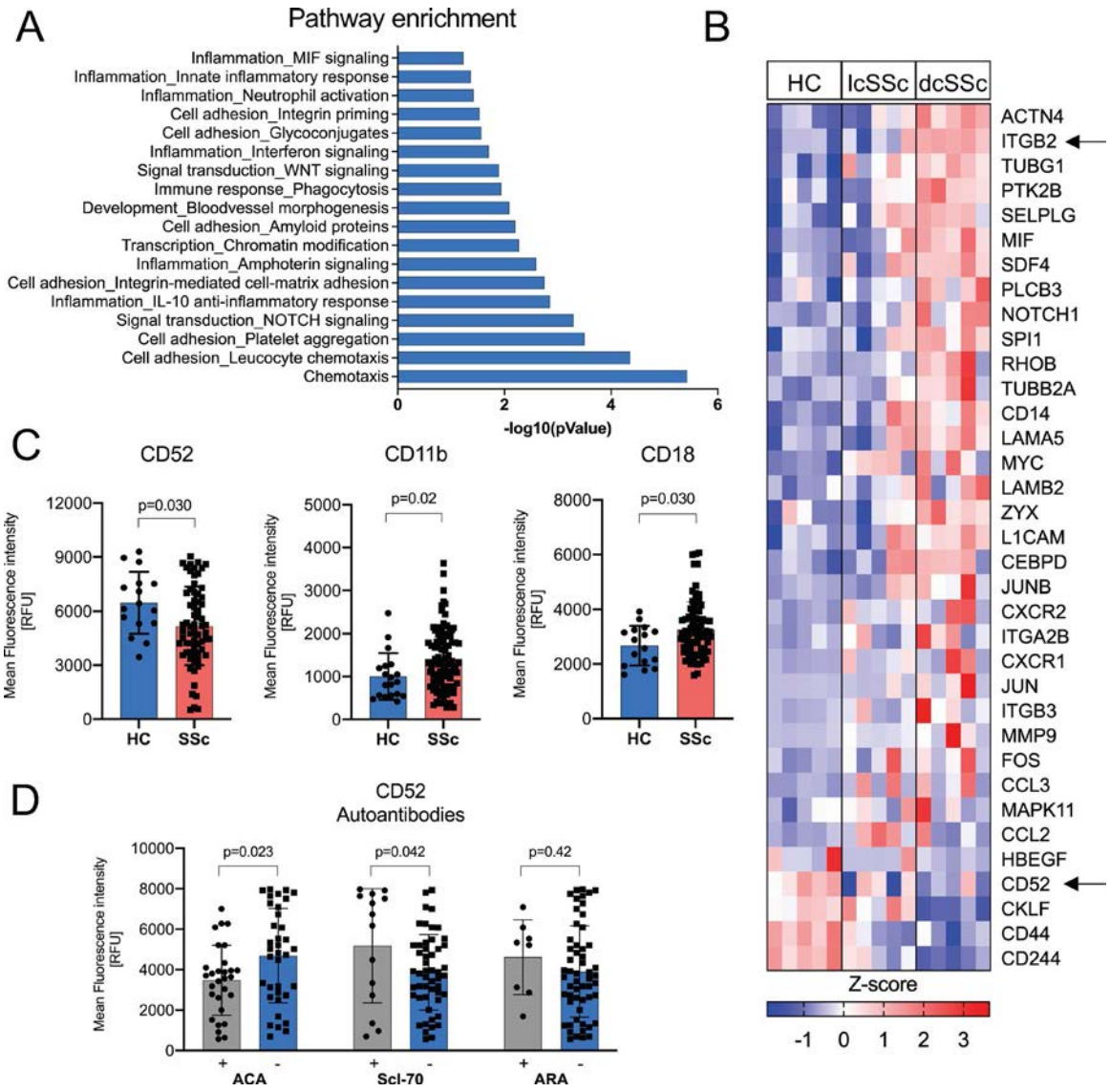

Figure 1. Transcriptomic analyses of CD14+ monocytes from patients with limited cutaneous systemic sclerosis (lcSSc), patients with diffuse cutaneous SSc (dcSSc), and healthy controls (HC) to assess alterations in adhesion molecule expression. **A**, Pathway enrichment analysis of related biologic processes based on differentially expressed gene sets, calculated using Metacore software. **B**, Differentially expressed genes identified by RNA-sequencing in the blood of patients with lcSSc or dcSSc compared to healthy controls. **Arrows** indicate genes involved in chemotaxis and monocyte adhesion. **C**, Flow cytometry analyses of CD52, CD11b, and CD18 expression in CD14+ monocytes from SSc patients and healthy controls. **D**, CD52 expression in SSc patients stratified according to the presence versus absence of anticentromere (ACA), anti–Scl-70, and anti–RNA polymerase III (ARA) autoantibodies. In **C** and **D**, symbols represent individual subjects; horizontal lines with bars show the mean ± SD. *P* values are based on unpaired 2-tailed *t*-tests. MIF = macrophage migration inhibitory factor; IL-10 = interleukin-10; RFU = relative fluorescence intensity units.

CD14+ monocytes from SSc patients (Figure 2A), consistent with the increased expression of adhesion molecules. SSc monocytes also demonstrated increased adhesion to TNFα-activated endothelial cells (Figure 2A), which led to increased infiltration of monocytes into the skin (Figure 2B). We observed a negative correlation between the expression levels of CD52 and the rates of adhesion (Figure 2C).

To evaluate whether CD52 could be implicated in cell adhesion, CD14+ monocytes from healthy controls were treated with alemtuzumab. Blocking of CD52 resulted in increased adhesion of the cells when compared to that of isotype control–treated cells (Figure 2D).

Effect of CD52 on cell rolling and adhesion of monocytes in an integrin-dependent manner. To investigate how CD52 affects monocyte responses, we generated a monocytic cell line, THP-1, and analyzed overexpression or knockdown of CD52 (Supplementary Figure 5, available on the *Arthritis & Rheumatology* website at http://onlinelibrary.wiley.com/doi/10.1002/art.41737/abstract). CD52-overexpressing monocytes exhibited

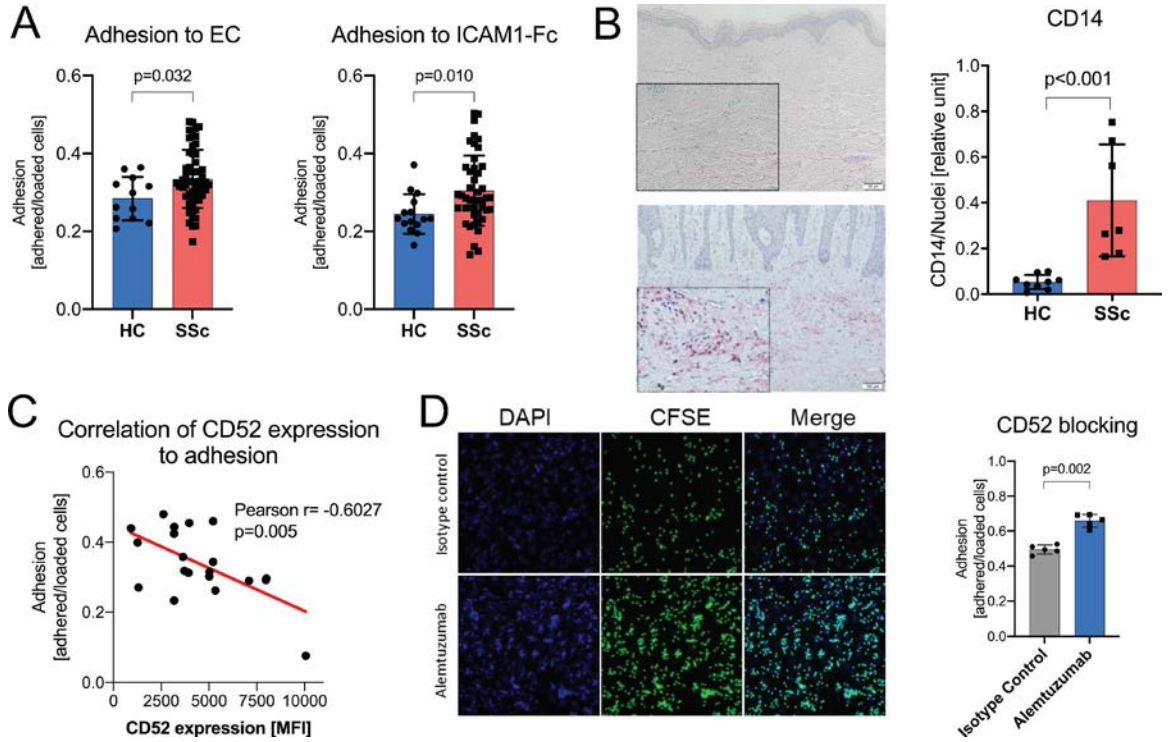

Figure 2. CD52-dependent elevation in adhesion levels of monocytes from patients with SSc. **A**, Adhesion of monocytes to tumor necrosis factor α–activated endothelial cells (ECs) (left) and intercellular adhesion molecule 1 (ICAM-1)–Fc–coated plates (right) was compared between SSc patients and healthy controls. *P* values are based on unpaired 2-tailed *t*-test (left) or Mann-Whitney U test (right). **B**, Left, Immunohistochemical staining was performed to assess infiltration of CD14+ cells into the skin of SSc patients. Images show representative paraffin-embedded skin sections from a healthy control (top) and SSc patient (bottom). Bars = 100 μm. **Insets** are higher-magnification views (original magnification × 12). Right, Results of immunohistochemical staining for CD14+ cells in skin sections from healthy controls and SSc patients were quantified. **C**, A negative correlation between CD52 expression on SSc monocytes and adhesion to ECs was observed. Correlations were assessed by Pearson's correlation test. **D**, Adhesion of healthy control CD14+ monocytes was assessed after 1 hour of blocking of CD52 function with alemtuzumab. Alemtuzumab-treated and isotype control–treated cells were analyzed by microscopy using DAPI and 5,6-carboxyfluorescein succinimidyl ester (CFSE) (left), and results were quantified in each group (right). In **A**, **B**, and **D**, symbols represent individual subjects; horizontal lines with bars show the mean ± SD. *P* values are based on paired *t*-test. MFI = mean fluorescence intensity (see Figure 1 for other definitions).

decreased levels of adhesion to ICAM-1–Fc–, ICAM-2–Fc–, and VCAM-1–Fc–coated plates and decreased adhesion to TNFα-activated endothelial cells, in comparison to control cells (Figures 3A and B). Accordingly, we observed an increased adhesion of THP-1 cells to endothelial cells when the expression of CD52 was silenced (see Supplementary Figure 6, available on the *Arthritis & Rheumatology* website at http://onlinelibrary.wiley.com/doi/10.1002/art.41737/abstract).

We then used a microcapillary shear flow system to analyze specific phases of monocyte adhesion to activated endothelial cells (see Supplementary Video 1, available on the *Arthritis & Rheumatology* website at http://onlinelibrary.wiley.com/doi/10.1002/art.41737/abstract). We observed no differences in the numbers of rolling cells and the rolling distance between cells transfected with a CD52-overexpressing plasmid and control cells transfected with an empty plasmid (Figure 3C). Nevertheless, CD52-overexpressing cells rolled for a shorter time and at a higher speed and, finally, adhered in a significantly lower number of cells, as compared to control cells (Figure 3D).

Results in previous reports have suggested that the molecular function of CD52 is dependent on the binding of *N*-linked glycan to sialic acid–binding Ig-like lectin 10 (Siglec-10) (22). We treated monocytes with peptide *N*-glycosidase F to remove the glycan. Although the digestion resulted in an increased adhesion of control cells, glycan removal in CD52-overexpressing cells did not change their adhesion (Supplementary Figure 7A, available on the *Arthritis & Rheumatology* website at http://onlinelibrary.wiley.com/doi/10.1002/art.41737/abstract). These data suggest that glycosylation of CD52 is not directly involved in monocyte adhesion.

We next evaluated Siglec-10–Fc binding to CD52-overexpressing cells. No differences in binding were observed between CD52-overexpressing cells and control cells (Supplementary Figure 7B [http://onlinelibrary.wiley.com/doi/10.1002/art.41737/abstract]). These results suggest that the mechanisms of CD52 functions in monocytes are independent of Siglec-10.

We then evaluated the expression of integrins CD11b and CD18 in CD52-overexpressing cells. Interestingly, the level of CD18 was reduced on cells overexpressing CD52, whereas the

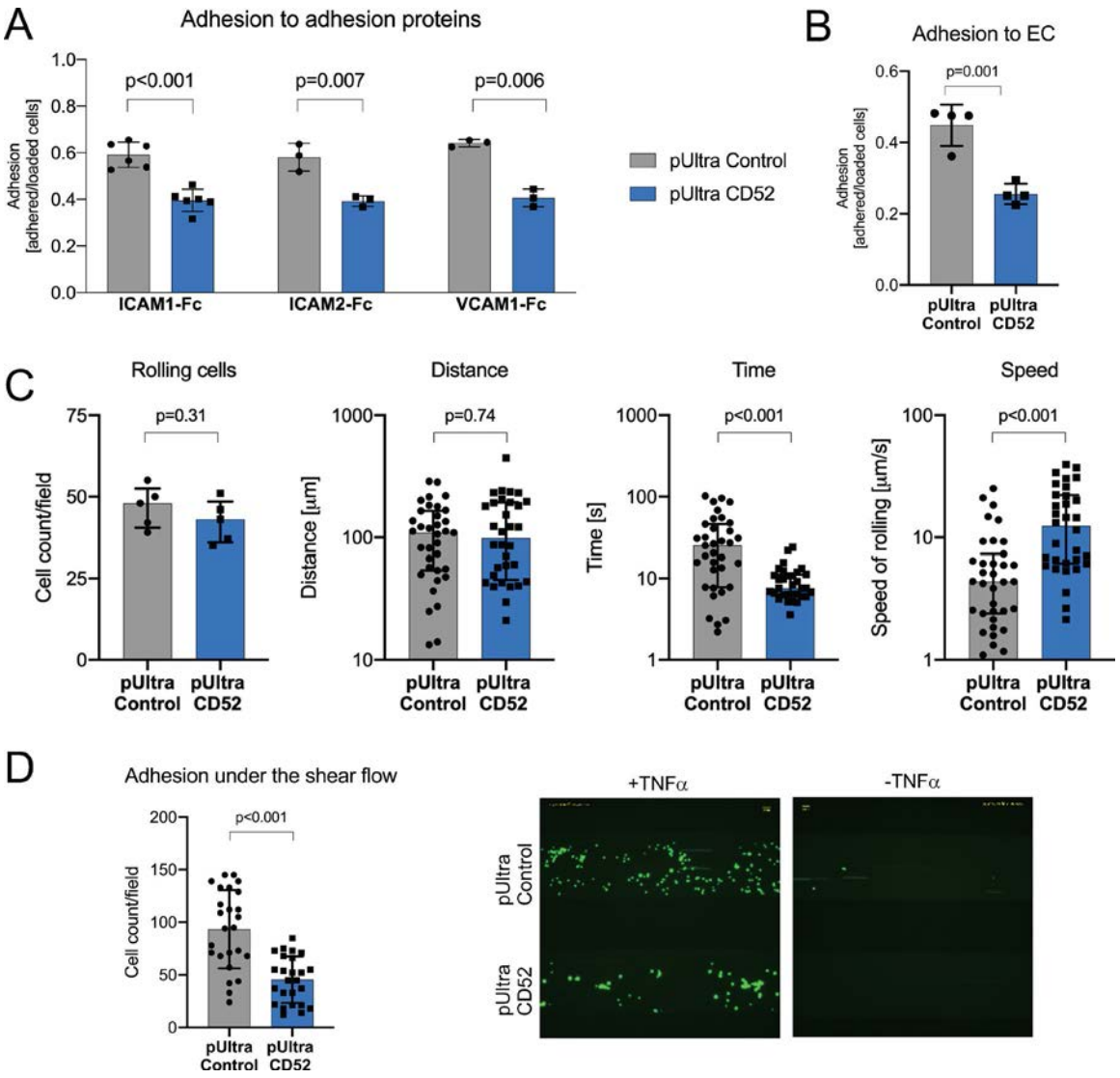

Figure 3. Modulation of the adhesive properties of THP-1 cell lines by CD52. **A** and **B**, THP-1 cells were transfected with pUltra CD52 plasmid to induce overexpression of CD52 or a pUltra empty vector as control. Adhesion of THP-1 cells to plates coated with intercellular adhesion molecule 1–Fc (ICAM-1–Fc), ICAM-2–Fc, and vascular cell adhesion molecule 1–Fc (VCAM-1–Fc) (**A**) and adhesion of THP-1 cells to endothelial cells (ECs) (**B**) were evaluated in static conditions. **C**, The number of rolling cells, rolling distance, time of rolling, and speed of rolling were compared between CD52-transfected and control-transfected cells. **D**, A microcapillary shear flow system was used to assess the number of cells showing adhesion under shear flow in each treatment group (left). Representative microscopy images depict cells showing adhesion in the presence or absence of tumor necrosis factor α (TNFα) activation in each treatment group (right). Symbols in **A–D** represent individual subjects; horizontal lines with bars show the mean ± SD. *P* values are based on unpaired 2-tailed *t*-test.

level of CD11b was elevated (Figure 4A). This may be a consequence of the dysregulation of other integrin-mediated functions such as phagocytosis. Blocking of CD52 with alemtuzumab caused an increase in the activated and total protein levels of CD11b and CD18 on CD14+ monocytes from healthy controls (Figure 4B).

Regulation of CD52 expression by IFN signaling via the HDAC IIa enzyme family in monocytes. The comparison of transcriptomes between monocytes from healthy controls and monoctyes from patients with SSc revealed a dysregulation in the inflammatory pathways, including the pathway for IFN signaling (Figure 1A and Supplementary Figure 8A, available on the *Arthritis & Rheumatology* website at http://onlinelibrary.wiley.com/doi/10.1002/art.41737/abstract). Previous studies demonstrated that the type I IFN signature was up-regulated in the peripheral blood of patients with SSc (23–25). Similarly, in our cohort, elevated serum levels of IFNα2 were observed (Supplementary Figure 8B [http://onlinelibrary.wiley.com/doi/10.1002/art.41737/abstract]). Moreover, monocytes from patients with SSc produced higher amounts of CXCL10, without any stimulation (Supplementary Figure S8C [http://onlinelibrary.wiley.com/doi/10.1002/art.41737/abstract]). Therefore, we hypothesized that CD52 expression might be regulated by IFNs.

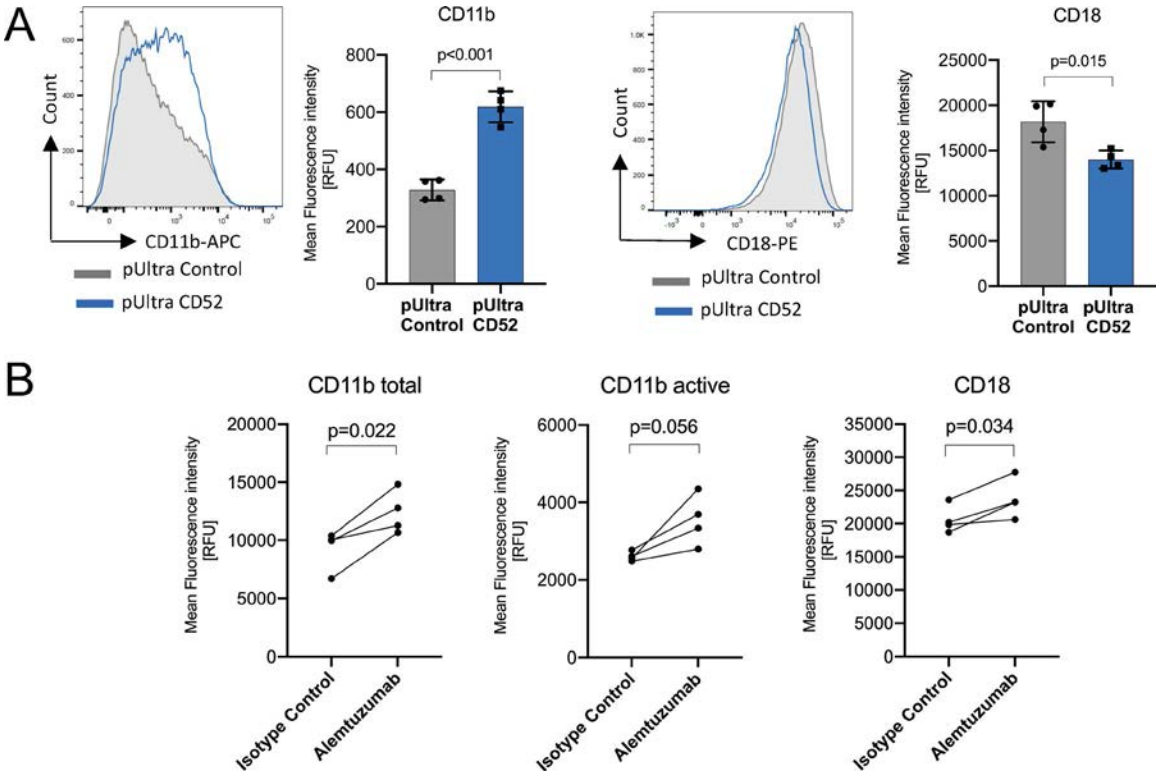

Figure 4. CD52 effects on adhesion occurring via changes in the integrin expression profile. **A**, Protein levels of CD11b and CD18 were assessed by flow cytometry (left panels) and quantified (right panels) in pUltra CD52–transfected THP-1 cells versus pUltra control–transfected THP-1 cells (for CD11b, $P < 0.001$; for CD18, $P = 0.015$). Symbols represent individual samples; horizontal lines with bars show the mean ± SD. **B**, Expression of total CD11b (ICRF44), active form of CD11b (CBRM1/5), and CD18 was assessed by flow cytometry in healthy control CD14+ monocytes after treatment with anti-CD52 antibody alemtuzumab (trade name Campath-1H) or an isotype control (n = 4 per group) for 24 hours. *P* values are based on unpaired 2-tailed *t*-test. APC = allophycocyanin; PE = phycoerythrin (see Figure 1 for other definitions).

Monocytes from healthy control subjects were stimulated with either type I or type II IFNs. Both type I and type II IFN–stimulated monocytes exhibited reduced levels of *CD52* (Figure 5A). Importantly, pharmacologic inhibition of JAK1 with the clinically used JAK1 inhibitor itacitinib resulted in partial restoration of *CD52* expression in monocytes (Figure 5B). In contrast, inhibition of JAK2 with the JAK2 inhibitor fedratinib resulted in a further decrease in the expression of *CD52* in monocytes. Furthermore, expression levels of *CD52* messenger RNA (mRNA) were decreased, in a dose-dependent manner, by lipopolysaccharide and IFNγ, while the addition of interleukin-4 (IL-4) and IL-13 to monocyte cultures resulted in up-regulation of *CD52* mRNA expression (Supplementary Figure 9A, available on the *Arthritis & Rheumatology* website at http://onlinelibrary.wiley.com/doi/10.1002/art.41737/abstract). The IL-4–induced up-regulation of *CD52* expression was diminished by pharmacologic inhibition of STAT6 with the STAT6 inhibitor AS1517499 (Supplementary Figure 9B [http://onlinelibrary.wiley.com/doi/10.1002/art.41737/abstract]).

To further investigate the IFN-dependent regulation of CD52 expression on monocytes, we analyzed the expression profiles of chromatin-modifying enzymes of the HDAC family (26). RNA-sequencing data pointed to a clear pattern in CD14+ monocytes from patients with SSc, with induced expression of class II and class IV HDACs and suppression of class I HDACs (Figure 5C).

In the next step, we used clinically used pharmacologic inhibitors to address the relevance of HDACs in monocytes. CD14+ monocytes from healthy controls were treated with the pan-HDAC inhibitor valproic acid and the HDAC class IIa–specific inhibitor TMP269. Both treatments resulted in reduced IFNγ-dependent phosphorylation of STAT1 (Figure 5D). Furthermore, treatment of monocytes with valproic acid or TMP269 led to up-regulation of *CD52* expression, and reduced expression of *CXCL9*, *CXCL10*, and *STAT1* (Figure 5E and Supplementary Figure 10, available on the *Arthritis & Rheumatology* website at http://onlinelibrary.wiley.com/doi/10.1002/art.41737/abstract). Of note, expression of these genes was not affected by pharmacologic inhibitors of class I, class IIb, and class IV HDACs (Supplementary Figure 10).

Modification of the monocyte response to type I IFN by CD52. We next investigated the effects of CD52 on IFN signaling pathways in more detail. We observed that CD52-overexpressing cells exhibited lower basal protein levels of STAT1, but exhibited

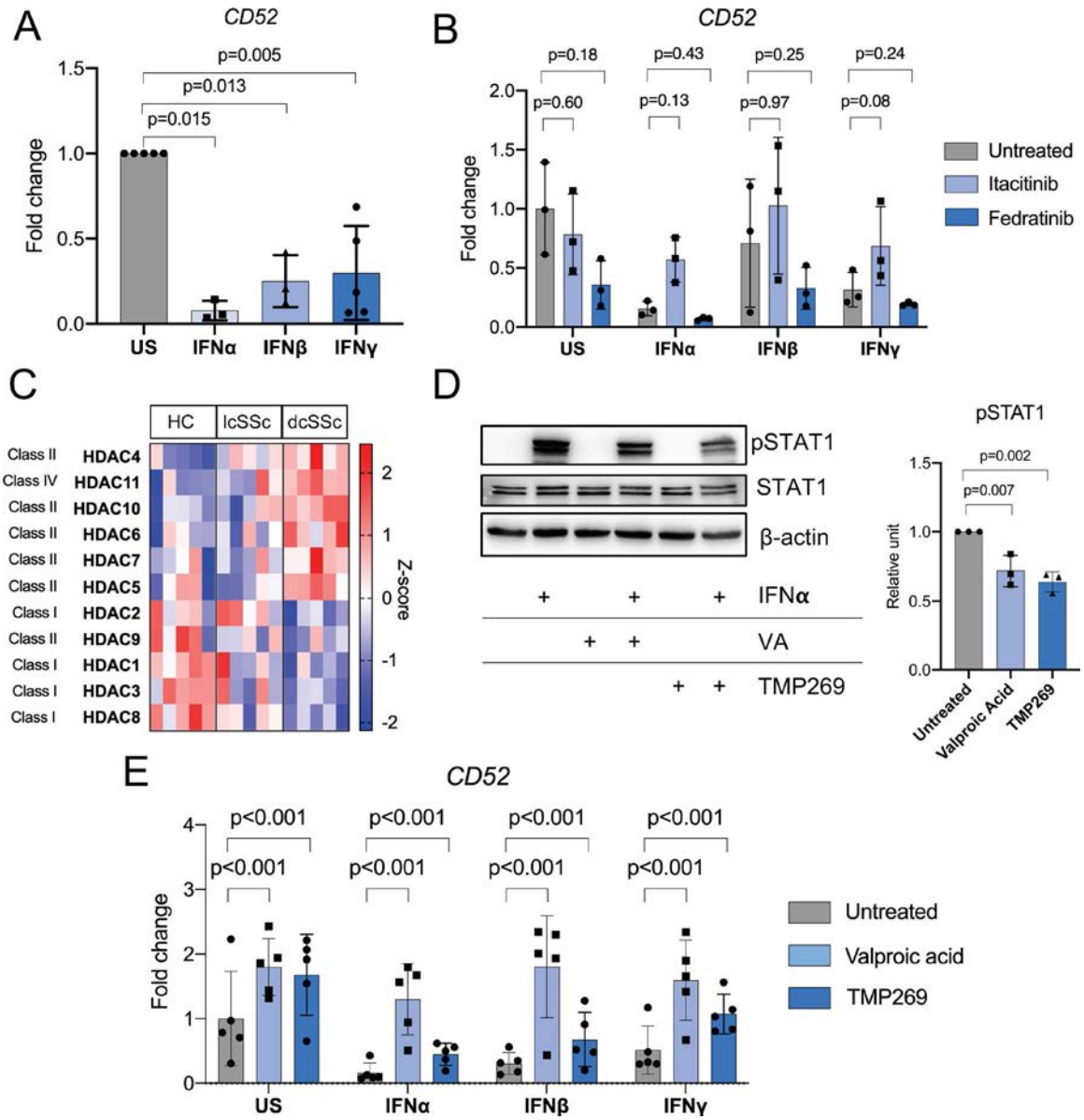

Figure 5. Regulation of CD52 expression in monocytes under different conditions. **A**, Fold change in *CD52* mRNA expression was assessed in healthy control monocytes stimulated with type I and type II interferons (IFNs), including IFNα, IFNβ, and IFNγ, relative to that in unstimulated (US) monocytes (set at 1.0). *P* values are based on Wilcoxon's signed rank test. **B**, Fold change in *CD52* mRNA expression was assessed in healthy control monocytes after treatment with the JAK1 selective inhibitor itacitinib (2.5 μ*M*) or JAK2 selective inhibitor fedratinib (2.5 μ*M*), relative to that in untreated, unstimulated monocytes (set at 1.0). **C**, Heatmap shows expression of histone deacetylases (HDACs) based on RNA-sequencing data in monocytes from healthy controls and patients with lcSSc or dcSSc. **D**, Western blot analysis was used to assess pSTAT1 expression in protein lysates of CD14+ monocytes from healthy controls treated with or without the pan-HDAC inhibitor valproic acid (VA) (20 m*M*) or HDAC class IIa inhibitor TMP269 (2.5 μ*M*), followed by stimulation with interferon-α (IFNα) (1 ng/ml) (left). Results in both treatment groups were quantified as the expression of pSTAT1 relative to that in untreated cells (set at 1.0) (right). *P* values are based on one-way analysis of variance. **E**, Fold change in *CD52* mRNA levels was assessed in healthy control CD14+ monocytes treated with valproic acid (20 m*M*) or TMP269 (2.5 μ*M*), followed by stimulation with IFNα, IFNβ, or IFNγ (each at 1 ng/ml), relative to that in untreated, unstimulated cells (set at 1). *P* values are based on two-way analysis of variance with Benjamini, Krieger, and Yekutieli post hoc test. In **A**, **B**, **D**, and **E**, symbols represent individual subjects; horizontal lines with bars show the mean ± SD. See Figure 1 for other definitions.

no change in STAT3 protein levels (Figure 6A and Supplementary Figure 11A, available on the *Arthritis & Rheumatology* website at http://onlinelibrary.wiley.com/doi/10.1002/art.41737/abstract). Interestingly, in response to type I IFNs, we observed stronger and faster phosphorylation of STAT1 (Figure 6B and Supplementary Figures 11B–E). Moreover, STAT3 phosphorylation was also increased after stimulation with IFNγ in CD52-overexpressing cells.

Consistent with these findings, experiments with alemtuzumab showed that, following stimulation of monocytes with IFNγ, blocking of CD52 expression resulted in increased mRNA

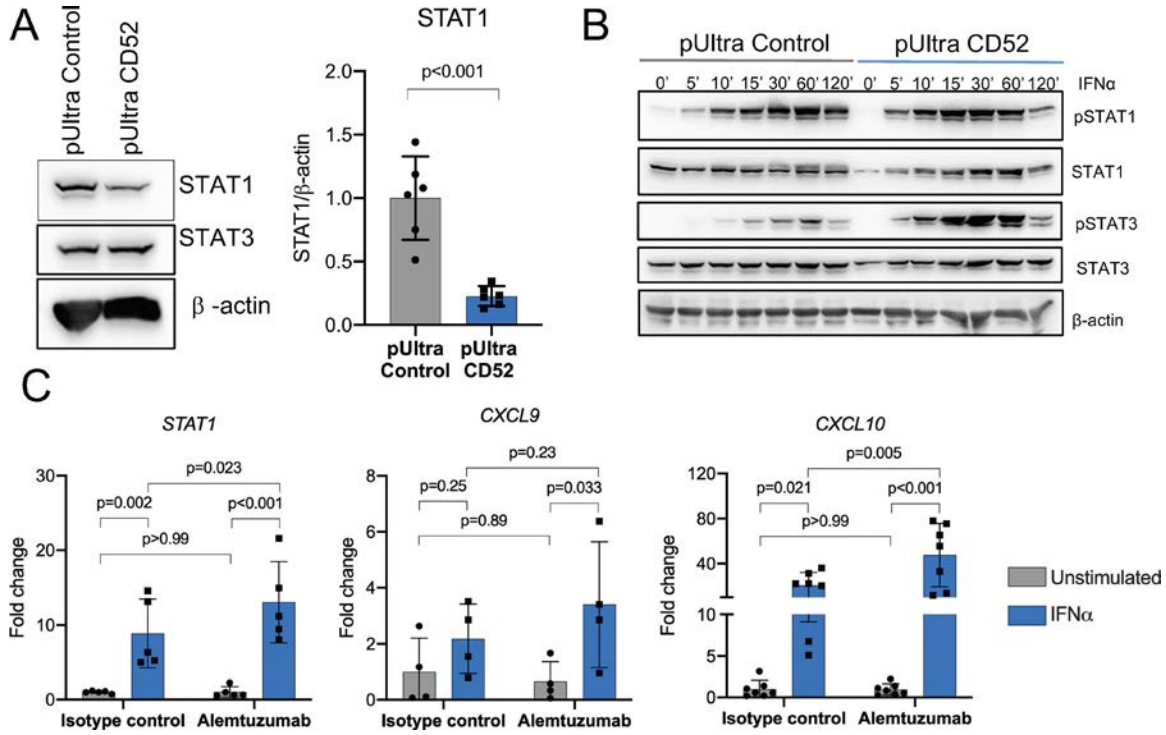

Figure 6. Effect of CD52 on type I interferon (IFN) signaling in monocytes. **A**, Left, Western blot analysis was used to assess expression of STAT1 ($P < 0.001$) and STAT3 ($P = 0.42$) in protein lysates from THP-1 cell lines transfected with pUltra CD52 for overexpression of CD52 versus pUltra empty vector as control (n = 6 per group). Right, Levels of STAT1 were quantified in each treatment group. *P* values are based on unpaired 2-tailed *t*-test. **B**, Western blot analysis was used to assess phosphorylation of STAT1 and STAT3 in THP-1 cell lines with overexpression of CD52 compared to empty vector control–transfected cells, after stimulation with IFNα (1 ng/ml) at the indicated time points (in minutes). **C**, Fold change in mRNA levels of the IFN-stimulated genes *STAT1*, *CXCL9*, and *CXCL10* was assessed in healthy control CD14+ monocytes treated with alemtuzumab or isotype control, followed by stimulation with IFNα (1 ng/ml). Values are the fold change relative to that in untreated, unstimulated cells. In **A** and **C**, symbols represent individual subjects; horizontal lines with bars show the mean ± SD.

levels of *CXCL9, CXCL10*, and *STAT1* (Figure 6C). In addition, increased protein levels of CXCL9 and CXCL10 were observed following blockade of CD52 (Supplementary Figure 11F [http://onlinelibrary.wiley.com/doi/10.1002/art.41737/abstract]).

DISCUSSION

Our data demonstrated that the adhesive properties of circulating CD14+ monocytes were increased in patients with SSc. Immune cell infiltration (including circulating CD14+ monocytes) into the tissue plays an essential role in the onset and activation of fibrotic processes in the skin and other organs (27–29) and contributes to the pathogenesis of SSc by modulating inflammatory and fibrotic responses (5). Previous studies pointed toward the important role of activation of endothelial cells during the pathogenesis of SSc (30,31). Complementary to those prior studies, our findings highlighted the development of pro-adhesive changes in monocytes as another pathogenic feature in early SSc. These 2 mechanisms seem to act synergistically to control tissue infiltration by CD14+ monocytes and thereby regulate disease progression.

The increased adhesive properties of monocytes were associated with reduced levels of the antiadhesive antigen CD52. Interestingly, we found particularly low CD52 levels in SSc patients at the early stage of the disease. Down-regulation of CD52 in monocytes may therefore be functionally involved in disease development. The antiadhesive properties of CD52 were previously hypothesized on the basis of its biochemical structure (i.e., extensive glycosylation and sialylation) in spermatozoa and T lymphocytes resulting from the negatively charged extracellular moiety of the antigen (32,33). However, this suggestion has not been supported by experimental data. Herein, the antiadhesive function of CD52 in monocytes was confirmed in gain-of-function and loss-of-function experiments, and was linked with the rolling phase and with firm adhesion. Of note, our findings suggested that glycosylation of CD52 does not play a pivotal role in monocyte adhesion; therefore, its antiadhesive properties in monocytes might not be limited to electrostatic interactions only.

In fact, our data suggested that CD52 could regulate membrane levels of the β2 integrin CD11b and CD18 complex, which plays an essential role in cell adhesion (7). Unlike in neutrophils (34), the role of the CD11b and CD18 integrins on CD14+ monocytes has not been extensively studied in patients with SSc; however, the importance of other integrins has been clearly postulated (35). Our data showed increased levels of CD11b and

CD18 in monocytes from patients with SSc, which is consistent with previous reports describing up-regulated levels of β2 integrins in monocytes in other autoimmune diseases, such as in patients with rheumatoid arthritis, Crohn's disease, or systemic lupus erythematosus (36–38). Regulation of β2 integrins by CD52 represents a novel mechanism involved in SSc. Previous data demonstrated that soluble CD52 could bind to Siglec-10 on T cells and thereby act as an immunosuppressor (39). However, we found no evidence of binding of Siglec-10 to CD52 on monocytes.

At the molecular level, we demonstrated that proinflammatory type I and type II IFNs down-regulated expression of the antiadhesive molecule CD52 in monocytes. Strikingly, SSc patients showed a dysregulated IFN gene signature at the early stage of the disease (16,40,41), and our data confirmed that the elevated serum levels of IFNα2 and IFN targeted CXCL10 in our SSc cohort. Of note, monocytes from patients receiving immunosuppressive treatment showed recovered CD52 levels. This observation further supports the crucial role of proinflammatory cytokines in the regulation of CD52 in SSc. Unlike fibroblasts, monocytes showed a clearly dysregulated expression pattern of the chromatin-modifying HDAC enzymes. Our data suggest that CD52 is regulated by IFN-dependent HDACs (mainly, class IIa HDACs). Notably, HDAC inhibitors have shown therapeutic efficacy in vitro, in animal models and in clinical studies of various immune-fibrotic disorders (42–47). Therefore, targeting CD52 expression by epigenetic modifiers may constitute an alternative therapeutic approach.

Moreover, in our experiments, CD52 negatively regulated the type I IFN–dependent STAT1 pathway, which suggested a feedback loop mechanism. Interestingly, JAK–STAT signaling, which interplays with proinflammatory IL-6 and profibrotic transforming growth factor β pathways, is intensively studied as a potential target for treatment in SSc (48,49). In contrast to IFNs, the profibrotic Th2 cytokines IL-4 and IL-13 up-regulated expression of CD52. Elevated levels of IL-4 and IL-13 are a typical feature in patients with dcSSc (50). This could explain the down-regulation of CD52 specifically in patients with early SSc, and might point to potential regulatory mechanisms preventing the exacerbated inflammatory response in SSc. It should, however, be noted that many SSc patients in our cohort were pharmacologically treated and showed long-lasting symptoms of the disease (in particular, in the dsSSc group), which is a major limiting factor of this study.

In summary, our results demonstrated the antiadhesive and antiinflammatory functions of CD52 in circulating CD14+ monocytes, and linked this with early SSc. Of note, CD52 is highly expressed in T lymphocytes; therefore, its role in these cells should also be addressed in patients with SSc in future studies. Furthermore, our findings demonstrated a new aspect of the disease, involving the role of proinflammatory type I IFN signaling in monocytes. Thus, the CD52–IFN–HDAC axis might serve as a novel therapeutic target in SSc, particularly for patients at the early stage of the disease.

ACKNOWLEDGMENT

We thank Maria Comazzi-Fornallaz for performing immunohistochemical analyses for the study.

AUTHOR CONTRIBUTIONS

All authors were involved in drafting the article or revising it critically for important intellectual content, and all authors approved the final version to be published. Dr. Kania had full access to all of the data in the study and takes responsibility for the integrity of the data and the accuracy of the data analysis.

Study conception and design. Rudnik, Distler, Blyszczuk, Kania.
Acquisition of data. Rudnik, Rolski, Stellato.
Analysis and interpretation of data. Rudnik, Rolski, Jordan, Mertelj, Stellato.

REFERENCES

1. Allanore Y, Simms R, Distler O, Trojanowska M, Pope J, Denton CP, et al. Systemic sclerosis [review]. Nat Rev Dis Primers 2015;1:15002.
2. Higashi-Kuwata N, Jinnin M, Makino T, Fukushima S, Inoue Y, Muchemwa FC, et al. Characterization of monocyte/macrophage subsets in the skin and peripheral blood derived from patients with systemic sclerosis. Arthritis Res Ther 2010;12:R128.
3. Yona S, Jung S. Monocytes: subsets, origins, fates and functions [review]. Curr Opin Hematol 2010;17:53–9.
4. Ginhoux F, Jung S. Monocytes and macrophages: developmental pathways and tissue homeostasis [review]. Nat Rev Immunol 2014;14:392–404.
5. Kania G, Rudnik M, Distler O. Involvement of the myeloid cell compartment in fibrogenesis and systemic sclerosis [review]. Nat Rev Rheumatol 2019;15:288–302.
6. Schnoor M, Alcaide P, Voisin MB, van Buul JD. Crossing the vascular wall: common and unique mechanisms exploited by different leukocyte subsets during extravasation [review]. Mediators Inflamm 2015;2015:946509.
7. Imhof BA, Aurrand-Lions M. Adhesion mechanisms regulating the migration of monocytes [review]. Nat Rev Immunol 2004;4:432–44.
8. Gerszten RE, Garcia-Zepeda EA, Lim YC, Yoshida M, Ding HA, Gimbrone MA Jr, et al. MCP-1 and IL-8 trigger firm adhesion of monocytes to vascular endothelium under flow conditions. Nature 1999;398:718–23.
9. Schenkel AR, Mamdouh Z, Muller WA. Locomotion of monocytes on endothelium is a critical step during extravasation. Nat Immunol 2004;5:393–400.
10. Arnaout MA. Biology and structure of leukocyte β2 integrins and their role in inflammation [review]. F1000Res 2016;5:2433.
11. Bandala-Sanchez E, Bediaga NG, Naselli G, Neale AM, Harrison LC. Siglec-10 expression is up-regulated in activated human $CD4^+$ T cells. Hum Immunol 2020;81:101–4.
12. Bandala-Sanchez E, Zhang Y, Reinwald S, Dromey JA, Lee BH, Qian J, et al. T cell regulation mediated by interaction of soluble CD52 with the inhibitory receptor Siglec-10. Nat Immunol 2013;14:741–8.
13. Hu Y, Turner MJ, Shields J, Gale MS, Hutto E, Roberts BL, et al. Investigation of the mechanism of action of alemtuzumab in a human CD52 transgenic mouse model. Immunology 2009;128:260–70.
14. Fox EJ. Alemtuzumab in the treatment of relapsing-remitting multiple sclerosis [review]. Expert Rev Neurother 2010;10:1789–97.
15. Von Kutzleben S, Pryce G, Giovannoni G, Baker D. Depletion of CD52-positive cells inhibits the development of central nervous system autoimmune disease, but deletes an immune-tolerance promoting CD8 T-cell population: implications for secondary

autoimmunity of alemtuzumab in multiple sclerosis. Immunology 2017;150:444–55.
16. Ronnblom L, Eloranta ML. The interferon signature in autoimmune diseases. Curr Opin Rheumatol 2013;25:248–53.
17. Platanias LC. Mechanisms of type-I- and type-II-interferon-mediated signalling [review]. Nat Rev Immunol 2005;5:375–86.
18. Hall JC, Rosen A. Type I interferons: crucial participants in disease amplification in autoimmunity [review]. Nat Rev Rheumatol 2010;6:40–9.
19. Shakespear MR, Halili MA, Irvine KM, Fairlie DP, Sweet MJ. Histone deacetylases as regulators of inflammation and immunity. Trends Immunol 2011;32:335–43.
20. Van den Hoogen F, Khanna D, Fransen J, Johnson SR, Baron M, Tyndall A, et al. 2013 classification criteria for systemic sclerosis: an American College of Rheumatology/European League Against Rheumatism collaborative initiative. Arthritis Rheum 2013;65:2737–47.
21. LeRoy EC, Black C, Fleischmajer R, Jablonska S, Krieg T, Medsger TA Jr, et al. Scleroderma (systemic sclerosis): classification, subsets and pathogenesis. J Rheumatol 1988;15:202–5.
22. Khanna D, Furst DE, Clements PJ, Allanore Y, Baron M, Czirjak L, et al. Standardization of the modified Rodnan skin score for use in clinical trials of systemic sclerosis. J Scleroderma Relat Disord 2017;2:11–8.
23. Skaug B, Assassi S. Type I interferon dysregulation in systemic sclerosis. Cytokine 2020;132:154635.
24. Wu M, Assassi S. The role of type 1 interferon in systemic sclerosis [review]. Front Immunol 2013;4:266.
25. Ciechomska M, Wojtas B, Swacha M, Olesinska M, Benes V, Maslinski W. Global miRNA and mRNA expression profiles identify miRNA-26a-2-3p-dependent repression of IFN signature in systemic sclerosis human monocytes. Eur J Immunol 2020;50:1057–66.
26. De Ruijter AJ, van Gennip AH, Caron HN, Kemp S, van Kuilenburg AB. Histone deacetylases (HDACs): characterization of the classical HDAC family. Biochem J 2003;370:737–49.
27. Gu YS, Kong J, Cheema GS, Keen CL, Wick G, Gershwin ME. The immunobiology of systemic sclerosis. Semin Arthritis Rheum 2008;38:132–60.
28. Bosello S, Angelucci C, Lama G, Alivernini S, Proietti G, Tolusso B, et al. Characterization of inflammatory cell infiltrate of scleroderma skin: B cells and skin score progression. Arthritis Res Ther 2018;20:75.
29. Whitfield ML, Finlay DR, Murray JI, Troyanskaya OG, Chi JT, Pergamenschikov A, et al. Systemic and cell type-specific gene expression patterns in scleroderma skin. Proc Natl Acad Sci U S A 2003;100:12319–24.
30. Asano Y, Sato S. Vasculopathy in scleroderma [review]. Semin Immunopathol 2015;37:489–500.
31. Kraling BM, Maul GG, Jimenez SA. Mononuclear cellular infiltrates in clinically involved skin from patients with systemic sclerosis of recent onset predominantly consist of monocytes/macrophages. Pathobiology 1995;63:48–56.
32. Schroter S, Derr P, Conradt HS, Nimtz M, Hale G, Kirchhoff C. Male-specific modification of human CD52. J Biol Chem 1999;274:29862–73.
33. Kirchhoff C, Schroter S. New insights into the origin, structure and role of CD52: a major component of the mammalian sperm glycocalyx. Cells Tissues Organs 2001;168:93–104.
34. Maugeri N, Rovere-Querini P, Baldini M, Baldissera E, Sabbadini MG, Bianchi ME, et al. Oxidative stress elicits platelet/leukocyte inflammatory interactions via HMGB1: a candidate for microvessel injury in sytemic sclerosis. Antioxid Redox Signal 2014;20:1060–74.
35. Conroy KP, Kitto LJ, Henderson NC. Alphav integrins: key regulators of tissue fibrosis [review]. Cell Tissue Res 2016;365:511–9.
36. Nath SK, Han S, Kim-Howard X, Kelly JA, Viswanathan P, Gilkeson GS, et al. A nonsynonymous functional variant in integrin-α(M) (encoded by ITGAM) is associated with systemic lupus erythematosus. Nat Genet 2008;40:152–4.
37. Takahashi H, Soderstrom K, Nilsson E, Kiessling R, Patarroyo M. Integrins and other adhesion molecules on lymphocytes from synovial fluid and peripheral blood of rheumatoid arthritis patients. Eur J Immunol 1992;22:2879–85.
38. Weisshof R, El Jurdi K, Zmeter N, Rubin DT. Emerging therapies for inflammatory bowel disease [review]. Adv Ther 2018; 35:1746–62.
39. Kivi E, Elima K, Aalto K, Nymalm Y, Auvinen K, Koivunen E, et al. Human Siglec-10 can bind to vascular adhesion protein-1 and serves as its substrate. Blood 2009;114:5385–92.
40. Assassi S, Mayes MD, Arnett FC, Gourh P, Agarwal SK, McNearney TA, et al. Systemic sclerosis and lupus: points in an interferon-mediated continuum. Arthritis Rheum 2010;62:589–98.
41. Tan FK, Zhou X, Mayes MD, Gourh P, Guo X, Marcum C, et al. Signatures of differentially regulated interferon gene expression and vasculotrophism in the peripheral blood cells of systemic sclerosis patients. Rheumatology (Oxford) 2006;45:694–702.
42. Yoon S, Kang G, Eom GH. HDAC inhibitors: therapeutic potential in fibrosis-associated human diseases [review]. Int J Mol Sci 2019;20:1329.
43. Lyu X, Hu M, Peng J, Zhang X, Sanders YY. HDAC inhibitors as antifibrotic drugs in cardiac and pulmonary fibrosis [review]. Ther Adv Chronic Dis 2019;10:2040622319862697.
44. Adcock IM. HDAC inhibitors as anti-inflammatory agents [editorial]. Br J Pharmacol 2007;150:829–31.
45. Hull EE, Montgomery MR, Leyva KJ. HDAC inhibitors as epigenetic regulators of the immune system: impacts on cancer therapy and inflammatory diseases [review]. Biomed Res Int 2016;2016: 8797206.
46. Hemmatazad H, Rodrigues HM, Maurer B, Brentano F, Pileckyte M, Distler JH, et al. Histone deacetylase 7, a potential target for the antifibrotic treatment of systemic sclerosis. Arthritis Rheum 2009;60:1519–29.
47. Huber LC, Distler JH, Moritz F, Hemmatazad H, Hauser T, Michel BA, et al. Trichostatin A prevents the accumulation of extracellular matrix in a mouse model of bleomycin-induced skin fibrosis. Arthritis Rheum 2007;56:2755–64.
48. Henderson J, O'Reilly S. A therapy for systemic sclerosis: STAT! [editorial]. Rheumatology (Oxford) 2018;57:1695–7.
49. Volkmann ER, Varga J. Emerging targets of disease-modifying therapy for systemic sclerosis [review]. Nat Rev Rheumatol 2019;15:208–24.
50. Huang XL, Wang YJ, Yan JW, Wan YN, Chen B, Li BZ, et al. Role of anti-inflammatory cytokines IL-4 and IL-13 in systemic sclerosis. Inflamm Res 2015;64:151–9.

Arthritis & Rheumatology
Vol. 73, No. 9, September 2021, pp 1731–1737
DOI 10.1002/art.41732

American College of Rheumatology
Empowering Rheumatology Professionals

BRIEF REPORT

Performance of the DETECT Algorithm for Pulmonary Hypertension Screening in a Systemic Sclerosis Cohort

Amber Young, Victor M. Moles, Sara Jaafar, Scott Visovatti, Suiyuan Huang, Dharshan Vummidi, Vivek Nagaraja, Vallerie McLaughlin, and Dinesh Khanna

Objective. Pulmonary arterial hypertension (PAH) is one of the leading causes of mortality in systemic sclerosis (SSc). This study was undertaken to assess predictive accuracies of the DETECT algorithm and the 2015 European Society of Cardiology/European Respiratory Society (ESC/ERS) guidelines in SSc patients who underwent right-sided heart catheterization (RHC) for pulmonary hypertension (PH) evaluation.

Methods. Patients with SSc who had diagnostic RHC, had no PH or had PAH, and had available data on variables to allow application of the DETECT and 2015 ESC/ERS guidelines were included for analysis. PH classification was based on hemodynamics using the 2018 revised criteria and extent of lung fibrosis shown on high-resolution computed tomography. Sensitivity and predictive accuracies of the DETECT algorithm and 2015 ESC/ERS guidelines were calculated, including analysis of subjects with a diffusing capacity for carbon monoxide (DLco) of ≥60% predicted.

Results. Sixty-eight patients with SSc had RHC, of whom 58 had no PH and 10 had PAH. The mean age was 60.0 years, and 58.8% had limited cutaneous SSc. The DETECT algorithm had a sensitivity of 1.00 (95% confidence interval [95% CI] 0.69–1.00) and a negative predictive value (NPV) of 1.00 (95% CI 0.80–1.00), whereas the 2015 ESC/ERS guidelines had a sensitivity of 0.80 (95% CI 0.44–0.97) and an NPV of 0.94 (95% CI 0.81–0.99). In patients with a DLco of ≥60% (n = 27), the DETECT algorithm had a sensitivity of 1.00 (95% CI 0.29–1.00) and an NPV of 1.00 (95% CI 0.59–1.00), whereas the 2015 ESC/ERS guidelines had a sensitivity of 0.67 (95% CI 0.09–0.99) and an NPV of 0.94 (95% CI 0.71–1.00).

Conclusion. The DETECT algorithm has high sensitivity and NPV for diagnosis of PAH, including among individuals with a DLco of ≥60%.

INTRODUCTION

Systemic sclerosis (SSc) is an autoimmune disease affecting multiple organ systems and characterized by fibrosis, inflammation, and vascular damage (1,2). Pulmonary arterial hypertension (PAH) is one of the leading causes of mortality in SSc, and in the past, SSc-associated PAH (SSc-PAH) had a significantly worse prognosis compared to other forms of PAH. PAH may go unrecognized in SSc patients until the disease has reached advanced stages, due to lack of or mild symptoms or attribution of symptoms to other comorbidities, such as interstitial lung disease (ILD) and/or myopathy.

PAH is present in 10–12% of patients with SSc and in 19% of those with a diffusing capacity for carbon monoxide (DLco) of <60% predicted (1,2). Over the last decade, treatment for PAH has evolved dramatically due to the addition of new therapies and

Dr. Khanna's work was supported by the NIH (National Institute of Arthritis and Musculoskeletal and Skin Diseases grants K24-AR-063120 and R01-AR-07047).

Amber Young, MD, Victor M. Moles, MD, Sara Jaafar, MD, Scott Visovatti, MD, Suiyuan Huang, MPH, Dharshan Vummidi, MD, Vivek Nagaraja, MBBS, Vallerie McLaughlin, MD, Dinesh Khanna, MD, MS: University of Michigan, Ann Arbor.

Dr. McLaughlin has received consulting fees, speaking fees, and/or honoraria from Altavant, Caremark, CiVi Biopharma, Gossamer Bio, Liquida, and United Therapeutics (less than $10,000 each) and from Actelion and Acceleron (more than $10,000 each) and research support from Acceleron, Actelion, Gilead, Reata, SoniVie, and United Therapeutics. Dr. Khanna has received consulting fees, speaking fees, and/or honoraria from Acceleron, Actelion, Amgen, Bayer, Blade Therapeutics, Boehringer Ingelheim, Bristol Myers Squibb, Corbus, Galápagos, Genentech/Roche, Merck, Mitsubishi Tanabe, Sanofi-Aventis, and United Therapeutics (less than $10,000 each) and from CSL Behring and Horizon (more than $10,000 each), research support from Bristol Myers Squibb, Bayer, and Pfizer, and owns stock or stock options in Eicos Sciences. No other disclosures relevant to this article were reported.

Address correspondence to Dinesh Khanna, MD, MSc, University of Michigan, Division of Rheumatology, Department of Internal Medicine, Suite 7C27, 300 North Ingalls Street, SPC 5422, Ann Arbor, MI 48109. Email: khannad@med.umich.edu.

Submitted for publication September 24, 2020; accepted in revised form March 9, 2021.

the transition from sequential to initial combination therapy. Outcomes have recently improved in SSc-PAH and are now similar to those with idiopathic PAH (2,3).

Previous observational studies have shown that screening for PAH may lead to better outcomes. Among patients in a French SSc-PAH registry, application of an active PAH screening program identified patients at a lower functional class with SSc-PAH, and patients had better survival (4). The PHAROS (Pulmonary Hypertension Assessment and Recognition of Outcomes in Scleroderma) registry, a large North American registry of SSc patients at risk for or with incident PAH that incorporated PAH screening, showed improved survival compared to historical cohorts (5).

There are various screening algorithms and guidelines for early detection of SSc-PAH. The European Society of Cardiology/European Respiratory Society (ESC/ERS) guidelines for identification of PAH on echocardiography were published in 2009 and were revised in 2015 to improve sensitivity during screening for PAH (6). These revisions included a combination of tricuspid regurgitation velocity (TRV), additional echocardiographic variables with assessment of the right ventricle (RV) size and pressure overload, the pattern of blood flow velocity out of the RV, the diameter of the pulmonary artery, and an estimate of right atrial pressure. The DETECT algorithm is an evidence-based screening algorithm created in 2013 as the result of a multicenter cross-sectional study that compared multiple clinical variables to the gold standard of right-sided heart catheterization (RHC), which resulted in the development of a 2-step PAH detection algorithm (7). Step 1 includes the combination of 6 clinical variables and step 2 includes echocardiographic variables. The DETECT algorithm has been recommended by a number of different societies, including the 2013 recommendations for screening and detection of connective tissue disease (CTD)–associated PAH (8), the 2015 ESC/ERS guidelines, and the 2018 6th World Symposium on Pulmonary Hypertension (WSPH) (9).

In the present study, we compared the predictive accuracies of the DETECT algorithm and the 2015 ESC/ERS guidelines in a cohort of SSc patients who underwent RHC for pulmonary hypertension (PH) evaluation. In this analysis, we applied the 2018 6th WSPH Task Force revised hemodynamic definition of group I PH (PAH) (9).

PATIENTS AND METHODS

Study design and subjects. This was a cross-sectional study of a cohort of SSc patients at the University of Michigan (UM) who had a diagnostic RHC prior to March 14, 2019. All patients were at least 18 years of age and met the 2013 American College of Rheumatology/European Alliance of Associations for Rheumatology classification criteria for SSc (10). The study was approved by the UM Institutional Review Board, and a waiver of consent was approved as this was a retrospective analysis. The study was carried out in compliance with the Declaration of Helsinki.

The initial cohort included 261 patients who underwent RHC between December 2004 and March 2019. One hundred fourteen of these patients did not have PH, 63 had PAH, 30 had group II PH, 35 had group III PH, and 19 had group IV PH based on the 2018 hemodynamic classification (9). One hundred nine subjects were excluded as they did not have available data on variables required to calculate a DETECT score and/or did not have a transthoracic echocardiogram (TTE) available for review at UM to apply the 2015 ESC/ERS guidelines. Of the remaining subjects, we focused on the 68 who had PAH or no PH and had data available for application of the DETECT algorithm and the 2015 ESC/ERS guidelines. Data on demographic characteristics and additional clinical variables were obtained for each of the 68 subjects. Additional analyses were performed by applying the DETECT algorithm and the 2015 ESC/ERS guidelines to the 2009 hemodynamic definition of PAH (mean pulmonary arterial pressure [mPAP] ≥25 mm Hg and pulmonary arterial wedge pressure [PAWP] ≤15 mm Hg with no-to-minimal ILD), as incorporated in the original DETECT publication (7,11). We also explored the performance of the DETECT algorithm for screening of group II and group III PH.

PAH screening. All SSc patients at UM undergo PAH screening at the time of SSc diagnosis and annually thereafter, based on the 2013 CTD-PAH recommendations, which include clinical signs/symptoms, N-terminal pro–brain natriuretic peptide (NT-proBNP), pulmonary function tests (PFTs), TTE variables, and the DETECT algorithm (8). In clinical practice, we routinely apply the DETECT algorithm to patients with SSc regardless of their DL_{CO}. Patients who had a diagnostic RHC with variables available for application of the DETECT algorithm and had TTE imaging at UM prior to RHC were included for analysis. Every TTE was reanalyzed by a cardiologist (VMM) using the TTE variables included in the 2015 ESC/ERS guidelines (6). The data for this study were primarily derived after the 2013 e-publication of the DETECT algorithm and the 2013 CTD-PAH recommendations.

PAH classification. PAH classification was based on the 2018 WSPH Task Force revised hemodynamic definition of group I PH (PAH), i.e., mPAP >20 mm Hg, PAWP ≤15 mm Hg, pulmonary vascular resistance (PVR) ≥3 Wood units (WU) (9), and extent of ILD <20% on high-resolution computed tomography (HRCT). Patients classified as having postcapillary PH or group II PH had an mPAP of >20 mm Hg, PAWP of >15 mm Hg, and PVR of <3 WU. Those classified as having group III PH had precapillary PH due to chronic lung disease, i.e., 1) HRCT demonstrating >20% total lung involvement due to ILD, or 2) total lung involvement due to ILD 10–20% with concomitant moderate-to-severe emphysema, or 3) if HRCT was not available, then forced vital capacity (FVC) of <70% predicted within a median of 2 months of the RHC.

Statistical analysis. Descriptive statistics for demographic and clinical characteristics of SSc patients without PH and those with PAH were calculated using the mean and SD for continuous variables and the percentage for categorical variables. For continuous variables, the significance of the differences between groups was assessed by Student's *t*-test for normally distributed variables and by Wilcoxon's rank sum test for non-normally distributed variables. For categorical variables, Fisher's exact test was used due to small, expected counts. Predictive accuracies were calculated, and 95% confidence intervals (95% CIs) were obtained via a binomial method for comparisons between non-PH and groups I, II, and III PH. *P* values less than 0.05 were considered significant. Missing data, if any, were not imputed. Analyses were conducted with SAS 9.4 (SAS Institute).

RESULTS

Baseline demographic characteristics of the patients. Of the 261 patients in this cohort who had undergone RHC, 63 had PAH and 114 had no PH. Of these 177 patients, 68 had available data on variables needed to calculate a DETECT score and TTE data available to apply the 2015 ESC/ERS guidelines; these

Table 1. Characteristics of the study patients*

Characteristic†	Total (n = 68)	No PH (n = 58)	PAH (n = 10)	*P*‡
Age at RHC, years	60.0 ± 11.7	59.4 ± 12.0	63.2 ± 9.6	0.39
Age at initial non-RP sign/symptom, years	50.5 ± 12.8	49.8 ± 13.1	54.4 ± 10.7	0.34
Female sex, no. (%)	58 (85.3)	49 (84.5)	9 (90.0)	1.00
Race, no. (%)				1.00
White	58 (85.3)	49 (84.5)	9 (90.0)	
African American	5 (7.4)	4 (6.9)	1 (10.0)	
Asian	2 (2.9)	2 (3.4)	0 (0.0)	
Other	3 (4.4)	3 (5.2)	0 (0.0)	
SSc subtype, no. (%)				0.77
Limited cutaneous SSc	40 (58.8)	33 (56.9)	7 (70.0)	
Diffuse cutaneous SSc	27 (39.7)	24 (41.4)	3 (30.0)	
Sine scleroderma	1 (1.5)	1 (1.7)	0 (0.0)	
Disease duration, years	9.5 ± 7.6	9.6 ± 7.8	8.8 ± 6.8	0.87
Autoantibodies, no. (%)				
ANA (n = 64)	59 (92.2)	50 (90.9)	9 (100.0)	1.00
ANA pattern (n = 59)				0.0355
Nucleolar	13 (22.0)	10 (20.0)	3 (33.3)	
Centromere	12 (20.3)	8 (16.0)	4 (44.4)	
Other	34 (57.6)	32 (64.0)	2 (22.2)	
Anti–Scl-70 (n = 60)	11 (18.3)	11 (21.2)	0 (0.0)	0.33
Anti–RNA polymerase III (n = 31)	6 (19.4)	6 (21.4)	0 (0.0)	1.00
Anticentromere (n = 54)	10 (18.5)	7 (14.9)	3 (42.9)	0.11
HRCT with ILD near time of RHC, no. (%) (n = 59)	43 (72.9)	40 (76.9)	3 (42.9)	0.078
PFTs near time of RHC				
Time from PFT to RHC, months	4.5 ± 7.3	4.0 ± 5.4	7.4 ± 14.1	0.82
FVC, % predicted	79.8 ± 19.5	78.6 ± 19.4	86.5 ± 19.5	0.26
DLco, % predicted (n = 67)	53.6 ± 18.8	54.6 ± 18.6	47.8 ± 20.2	0.29
FVC % predicted:DLco % predicted (n = 67)	1.6 ± 0.6	1.6 ± 0.6	2.0 ± 0.7	0.03
TTE near time of RHC				
Time from TTE to RHC, months	4.0 ± 7.8	3.6 ± 6.9	6.1 ± 12.0	0.76
RA area, cm^2	15.7 ± 4.3	15.3 ± 4.2	17.7 ± 4.5	0.10
TRV, meters/second (n = 54)	2.8 ± 0.5	2.7 ± 0.4	3.3 ± 0.4	<0.0001
RVSP, mm Hg (n = 54)	37.3 ± 11.8	34.4 ± 9.0	52.0 ± 13.7	0.0006
RHC				
mPAP, mm Hg	23.5 ± 7.0	21.6 ± 5.4	34.2 ± 6.1	<0.0001
mPAWP, mm Hg	10.9 ± 3.0	10.8 ± 3.2	11.2 ± 2.1	0.81
CO (TD), liters/minute	5.7 ± 1.5	5.8 ± 1.5	5.1 ± 1.3	0.0999
PVR, Wood units	2.3 ± 1.4	1.9 ± 0.6	4.8 ± 2.0	<0.0001

* Except where indicated otherwise, values are the mean ± SD. PH = pulmonary hypertension; PAH = pulmonary arterial hypertension; RHC = right-sided heart catheterization; RP = Raynaud's phenomenon; SSc = systemic sclerosis; ANA = antinuclear antibody; HRCT = high-resolution computed tomography; ILD = interstitial lung disease; PFTs = pulmonary function tests; FVC = forced vital capacity; DLco = diffusing capacity for carbon monoxide; TTE = transthoracic echocardiography; RA = right atrial; TRV = tricuspid regurgitation velocity; RVSP = right ventricular systolic pressure; mPAP = mean pulmonary arterial pressure; mPAWP = mean pulmonary arterial wedge pressure; CO (TD) = cardiac output (thermodilution); PVR = pulmonary vascular resistance.
† For some characteristics, data were not available for all 68 patients; n values represent the total number with available data.
‡ By Wilcoxon's rank sum test; Fisher's exact test, or Student's *t*-test as appropriate.

Table 2. Predictive accuracies of the DETECT algorithm and the 2015 ESC/ERS guidelines in screening for PAH as classified using the 2018 revised hemodynamic definition*

	DETECT (95% CI)	2015 ESC/ERS guidelines (95% CI)
2018 revised hemodynamic PAH definition and all DLco values (n = 68)		
Sensitivity	1.00 (0.69–1.00)	0.80 (0.44–0.97)
Specificity	0.29 (0.18–0.43)	0.57 (0.43–0.70)
PPV	0.20 (0.10–0.33)	0.24 (0.11–0.42)
NPV	1.00 (0.80–1.00)	0.94 (0.81–0.99)
2018 revised hemodynamic PAH definition and DLco ≥60% predicted (n = 27)		
Sensitivity	1.00 (0.29–1.00)	0.67 (0.09–0.99)
Specificity	0.29 (0.13–0.51)	0.67 (0.45–0.84)
PPV	0.15 (0.03–0.38)	0.2 (0.03–0.56)
NPV	1.00 (0.59–1.00)	0.94 (0.71–1.00)

* ESC/ERS = European Society of Cardiology/European Respiratory Society; PAH = pulmonary arterial hypertension; 95% CI = 95% confidence interval; DLco = diffusing capacity for carbon monoxide; PPV = positive predictive value; NPV = negative predictive value.

individuals were the subjects of the present study. When comparing these 68 patients to the 109 patients who had missing data, we found that patients with missing data were more likely to have limited cutaneous SSc (lcSSc) (70.6% versus 58.8%) and to have higher TRV (3.2 meters/second versus 2.8 meters/second), mPAP (31.7 mm Hg versus 23.5 mm Hg), and PVR (4.4 WU versus 2.3 WU) (all $P < 0.05$).

Of the 68 patients included in the study, 58 did not have PH and 10 had PAH. The mean ± SD age in the overall cohort was 60.0 ± 11.7 years, age at initial non–Raynaud's phenomenon sign/symptom was 50.5 ± 12.8 years, and disease duration was 9.5 ± 7.6 years. The cohort was mainly composed of patients who were female (85.3%), White (85.3%), and had lcSSc (58.8%) (Table 1).

Cardiopulmonary characteristics of the patients. Among the patients with PAH, 42.9% were anticentromere antibody positive. Compared to the patients without PH, the prevalence of ILD in those with PAH was lower, though the difference was not statistically significant (42.9% versus 76.9%; $P = 0.08$), and the patients with PAH had a lower mean DLco % predicted (47.8 versus 54.6; $P = 0.29$) and a significantly higher FVC % predicted:DLco % predicted (2.0 versus 1.6; $P = 0.03$) (Table 1).

TTE variables in the patients with PAH compared to those without PH indicated a higher mean TRV (3.3 meters/second versus 2.7 meters/second; $P < 0.0001$) and estimated right ventricular systolic pressure (52.0 mm Hg versus 34.4 mm Hg; $P = 0.0006$). On RHC, the mPAP in the PAH group was 34.2 mm Hg, cardiac output was 5.1 liters/minute, and PVR was 4.8 WU (Table 1).

Predictive accuracies of the DETECT algorithm and 2015 ESC/ERS guidelines for diagnosing SSc-PAH. Using the 2018 revised hemodynamic definition of group I PH (PAH), the DETECT algorithm performed better as a PAH screening tool compared to the 2015 ESC/ERS guidelines. The sensitivity of the DETECT algorithm was 1.00 (95% CI 0.69–1.00) and its negative predictive value (NPV) was 1.00 (95% CI 0.80–1.00), whereas the 2015 ESC/ERS guidelines yielded false-negative results in 2 patients (sensitivity 0.80 [95% CI 0.44–0.97], NPV 0.94 [95% CI 0.81–0.99]) (Table 2). As expected for a screening tool, specificity and positive predictive value (PPV) of the DETECT algorithm were low at 0.29 (95% CI 0.18–0.43) and 0.20 (95% CI 0.10–0.33),

Table 3. Predictive accuracies of the DETECT algorithm and 2015 ESC/ERS guidelines in screening for PAH as classified using the 2009 hemodynamic definition*

	DETECT (95% CI)	2015 ESC/ERS guidelines (95% CI)
2009 hemodynamic PAH definition from original DETECT study and all DLco values (n = 70)		
Sensitivity	1.00 (0.82–1.00)	0.74 (0.49–0.91)
Specificity	0.33 (0.21–0.48)	0.61 (0.46–0.74)
PPV	0.36 (0.23–0.50)	0.41 (0.25–0.59)
NPV	1.00 (0.80– 1.00)	0.86 (0.71–0.95)
2009 hemodynamic PAH definition from original DETECT study and DLco ≥60% predicted (n = 28)		
Sensitivity	1.00 (0.48–1.00)	0.60 (0.15–0.95)
Specificity	0.30 (0.13–0.53)	0.70 (0.47–0.87)
PPV	0.24 (0.08–0.47)	0.30 (0.07–0.65)
NPV	1.00 (0.59–1.00)	0.89 (0.65–0.99)

* ESC/ERS = European Society of Cardiology/European Respiratory Society; PAH = pulmonary arterial hypertension; 95% CI = 95% confidence interval; DLco = diffusing capacity for carbon monoxide; PPV = positive predictive value; NPV = negative predictive value.

respectively, and specificity and PPV of the 2015 ESC/ERS guidelines were 0.57 (95% CI 0.43–0.70) and 0.24 (95% CI 0.11–0.42), respectively (Table 2). The 2009 hemodynamic definition of PAH (mPAP ≥25 mm Hg and PAWP ≤15mm Hg with no-to-minimal ILD), as incorporated in the original DETECT publication, was also evaluated in 70 subjects in the cohort who had no PH or PAH and had available data on variables needed to apply the DETECT algorithm and 2015 ESC/ERS guidelines, with the DETECT algorithm showing higher sensitivity and NPV compared to the 2015 ESC/ERS guidelines (Table 3).

At our institution, we apply the DETECT algorithm to all patients with SSc including those with a DLCO of ≥60% predicted. Within this cohort, there were 27 patients with a DLCO of ≥60% predicted who had no PH (n = 24) or had PAH (n = 3) according to the 2018 revised hemodynamic definition of PAH and had both DETECT scores and a TTE to review for the 2015 ESC/ERS guidelines. The DETECT algorithm had a sensitivity of 1.00 (95% CI 0.29–1.00) and an NPV of 1.00 (95% CI 0.59–1.00), whereas the 2015 ESC/ERS guidelines had a sensitivity of 0.67 (95% CI 0.09–0.99) and an NPV of 0.94 (95% CI 0.71–1.00) (Table 2). The results were similar in patients with a DLCO of ≥60% predicted who had PAH or no PH when using the 2009 hemodynamic definition of PAH described in the original DETECT publication (Table 3).

Application of the DETECT algorithm and 2015 ESC/ERS guidelines for group II PH and group III PH screening. Additionally, we evaluated the performance of the DETECT algorithm and the 2015 ESC/ERS guidelines in patients with group II PH (n = 12) and group III PH (n = 12), using the 2018 revised hemodynamic definitions. The performance of the DETECT algorithm was overall similar to that of the 2015 ESC/ERS guidelines in patients with group II PH (NPV 0.94 [95% CI 0.71–1.00] and NPV 0.92 [95% CI 0.76–0.98], respectively) and in patients with group III PH (NPV 0.94 [95% CI 0.71–1.00] and NPV 0.97 [95% CI 0.85–1.00], respectively).

DISCUSSION

We compared predictive accuracies of the DETECT algorithm and the 2015 ESC/ERS guidelines in a cohort of SSc patients who underwent RHC for PH evaluation, using the 2018 WSPH Task Force revised hemodynamic definition of group I PH (PAH). Our results demonstrate that the DETECT algorithm works well as a screening tool for PAH with 100% NPV and 100% sensitivity, and it was effective in patients with a DLCO of ≥60% predicted. We also evaluated the DETECT algorithm using the 2009 PAH definition that was used in the original DETECT study, and again found high sensitivity and NPV.

The performance of the DETECT algorithm in the present study using both the 2009 and 2018 revised hemodynamic definitions of PAH was similar to that in previous studies using the 2009 hemodynamic definition of PAH. In the original DETECT derivation study by Coghlan et al, the DETECT algorithm had a sensitivity of 96%, NPV of 98%, specificity of 48%, and PPV of 35% (7). Guillén-Del Castillo and colleagues studied 63 SSc patients who had PAH or no PH and found that the sensitivity of the DETECT algorithm was 100%, NPV was 100%, specificity was 42.9%, and PPV was 68.6% (12). In a study by Hao et al in a prospective cohort of 61 SSc patients with PAH or no PH, the DETECT algorithm had a sensitivity and NPV of 100%, specificity of 35.3%, and PPV of 55.1% (13). In a prospective SSc cohort studied by Vandecasteele and colleagues, the DETECT algorithm demonstrated a PPV of 6% (95% CI 2–17%); sensitivity and NPV were not reported (14).

The World Health Organization defines a screening test as the presumptive identification of an unrecognized disease in a patient who is asymptomatic (https://apps.who.int/iris/bitstream/handle/10665/330829/9789289054782-eng.pdf). TTE has been advocated by different societies and is included as part of screening and diagnostic algorithms. In the original DETECT study, TTE (according to the 2009 ESC/ERS guidelines) missed 29% of patients who had PAH on RHC (7). Most published studies regarding the detection of PAH through routine screening of SSc patients based on TTE used the 2009 ESC/ERS guidelines, which are based on symptoms and TRV (15). In the previously published studies by Guillén-Del Castillo et al, Hao et al, and Coghlan et al, the 2009 ESC/ERS guidelines had lower sensitivity (ranging from 71.0% to 96.3%) and NPV (ranging from 88.9% to 90.9%) (7,12,13). One report discussed the application of the 2015 ESC/ERS guidelines for detection of asymptomatic SSc-PAH, but data on sensitivity and NPV were not provided (14).

During the development of the DETECT algorithm, the key inclusion criteria included a disease duration of >3 years and a DLCO of <60% predicted, largely to account for patients at higher risk of PAH. However, this should not be interpreted to mean that SSc patients whose DLCO is ≥60% predicted are not at risk for development of PAH. Previously published data from the UK showed that ~10% of SSc patients with PH had a DLCO of ≥60% (16), and in the study by Hao and colleagues, DLCO was >60% in 6.5% of patients (n = 4) with PAH (13). If a strict criterion of DLCO <60% predicted was enforced to apply the DETECT algorithm, 3 patients with PAH would have been missed in our current analysis using the 2018 revised hemodynamic definition, and 5 patients with PAH would have been missed using the 2009 PAH hemodynamic definition. Our data using DLCO ≥60% predicted provide evidence in support of the 2018 WSPH recommendations that proposed the DETECT algorithm, along with the 2015 ESC/ERS guidelines or an FVC:DLCO ratio of >1.6 (assuming no-to-mild ILD) and an NT-proBNP level >2 times the upper limit of normal among those with an uncorrected DLCO of <80% predicted.

The DETECT algorithm is being increasingly incorporated into clinical practice and was developed to discriminate between PAH and non-PH. In our cohort, the performance of the DETECT algorithm was similar to that of the 2015 ESC/ERS guidelines in

patients with group II and group III PH, and we do not advocate incorporating DETECT into clinical practice to distinguish between group II or III PH and non-PH.

It should also be kept in mind that the DETECT algorithm is a screening tool with high sensitivity and NPV that provides guidance regarding whether a patient should undergo RHC. High sensitivity is preferred in a screening tool, but the tradeoffs include an increased number of RHCs to exclude PAH, as seen in the original DETECT cohort (7). Since PAH is the leading cause of mortality in SSc and a recent meta-analysis suggests better outcomes with utilization of screening algorithms and early initiation of combination therapy (2), we believe a higher rate of RHC to rule out PAH is justified. In patients who do not meet the criteria for RHC at a single time point according to the DETECT algorithm (i.e., the DETECT score does not indicate that the patient should be referred for RHC), we continue to incorporate the DETECT algorithm on an annual basis during clinic visits, with spirometry with DLco to assess the FVC:DLco ratio and with measurement of serum uric acid and NT-proBNP levels. If TTE is recommended, it is performed as part of the screening algorithm. In patients for whom RHC is recommended based on the DETECT score but are not found to have PH on RHC (53% of patients in our cohort), DETECT is no longer a valid tool in screening for PH. In this scenario, we follow the 6th WSPH recommendations with annual screening with TTE, incorporate the 2015 ESC/ERS guidelines, and assess for worsening of DLco and an FVC:DLco ratio of >1.6 (assuming no-to-mild ILD) and for an NT-proBNP level >2 times the upper limit of normal. In addition, new signs/symptoms suggestive of PH should lead to a clinical evaluation for PH.

We uniformly screen SSc patients according to published recommendations for CTD-PAH (8). Although our cohort included 261 patients who had RHC, of whom 114 did not have PH and 63 had PAH, our analysis focused on only 68 patients, in whom a screening algorithm was largely applied prospectively and TTE was available for reassessment using 2015 ESC/ERS guidelines highlighting an inherent limitation of cohort studies. The more severe hemodynamic findings in members of the cohort with missing data may reflect a lack of uniform screening in the patient population prior to 2013–2014, which was when DETECT and the CTD-PAH recommendations were published (7,8). This was a single-center study with small numbers of patients, and the findings need to be validated in a prospective study in the future. In addition, we did not exclude patients in the non-PH group with moderate-to-severe ILD, which may impact the diagnostic accuracy of our analysis.

In conclusion, early detection of PAH in SSc is necessary to implement early treatment, which can improve outcomes (2). To our knowledge, this is the first cohort study to assess the performance of the DETECT algorithm and 2015 ESC/ERS guidelines using the 2018 revised hemodynamic definition of PAH. The DETECT algorithm is a better screening tool for SSc-PAH than TTE. Although the original derivation study for the DETECT excluded patients with higher DLco values, our present results suggest that those whose DLco is ≥60% predicted can have PAH, and the DETECT algorithm performs well in this group.

AUTHOR CONTRIBUTIONS

All authors were involved in drafting the article or revising it critically for important intellectual content, and all authors approved the final version to be published. Dr. Khanna had full access to all of the data in the study and takes responsibility for the integrity of the data and the accuracy of the data analysis.

Study conception and design. Young, Jaafar, Huang, Nagaraja, McLaughlin, Khanna.

Acquisition of data. Young, Moles, Jaafar, Visovatti, Vummidi, Nagaraja, McLaughlin, Khanna.

Analysis and interpretation of data. Young, Jaafar, Huang, Nagaraja, McLaughlin, Khanna.

REFERENCES

1. Denton CP, Khanna D. Systemic sclerosis [review]. Lancet 2017; 390:1685–99.
2. Khanna D, Zhao C, Saggar R, Mathai SC, Chung L, Coghlan JG, et al. Long-term outcomes in patients with connective tissue disease–associated pulmonary arterial hypertension in the modern treatment era: meta-analyses of randomized, controlled trials and observational registries. Arthritis Rheumatol 2021;73:837–47.
3. Galie N, Channick RN, Frantz RP, Grunig E, Jing ZC, Moiseeva O, et al. Risk stratification and medical therapy of pulmonary arterial hypertension. Eur Respir J 2019;53:1801889.
4. Humbert M, Yaici A, de Groote P, Montani D, Sitbon O, Launay D, et al. Screening for pulmonary arterial hypertension in patients with systemic sclerosis: clinical characteristics at diagnosis and long-term survival. Arthritis Rheum 2011;63:3522–30.
5. Chung L, Domsic RT, Lingala B, Alkassab F, Bolster M, Csuka ME, et al. Survival and predictors of mortality in systemic sclerosis-associated pulmonary arterial hypertension: outcomes from the pulmonary hypertension assessment and recognition of outcomes in scleroderma registry. Arthritis Care Res (Hoboken) 2014;66:489–95.
6. Galie N, Humbert M, Vachiery JL, Gibbs S, Lang I, Torbicki A, et al, on behalf of the Joint Task Force for the Diagnosis and Treatment of Pulmonary Hypertension of the European Society of Cardiology (ESC) and the European Respiratory Society (ERS). 2015 ESC/ERS guidelines for the diagnosis and treatment of pulmonary hypertension. Eur Respir J 2015;46:903–75.
7. Coghlan JG, Denton CP, Grunig E, Bonderman D, Distler O, Khanna D, et al. Evidence-based detection of pulmonary arterial hypertension in systemic sclerosis: the DETECT study. Ann Rheum Dis 2014;73:1340–9.
8. Khanna D, Gladue H, Channick R, Chung L, Distler O, Furst DE, et al. Recommendations for screening and detection of connective tissue disease–associated pulmonary arterial hypertension. Arthritis Rheum 2013;65:3194–201.
9. Simonneau G, Montani D, Celermajer DS, Denton CP, Gatzoulis MA, Krowka M, et al. Haemodynamic definitions and updated clinical classification of pulmonary hypertension. Eur Respir J 2019;53:1801913.
10. Van den Hoogen F, Khanna D, Fransen J, Johnson SR, Baron M, Tyndall A, et al. 2013 classification criteria for systemic sclerosis: an American College of Rheumatology/European League Against Rheumatism collaborative initiative. Arthritis Rheum 2013;65:2737–47.
11. Badesch DB, Champion HC, Sanchez MA, Hoeper MM, Loyd JE, Manes A, et al. Diagnosis and assessment of pulmonary arterial hypertension. J Am Coll Cardiol 2009;54:S55–66.
12. Guillén-Del Castillo A, Callejas-Moraga EL, Garcia G, Rodriguez-Palomares JF, Roman A, Berastegui C, et al. High sensitivity and negative predictive value of the DETECT algorithm for an early

diagnosis of pulmonary arterial hypertension in systemic sclerosis: application in a single center. Arthritis Res Ther 2017;19:135.
13. Hao Y, Thakkar V, Stevens W, Morrisroe K, Prior D, Rabusa C, et al. A comparison of the predictive accuracy of three screening models for pulmonary arterial hypertension in systemic sclerosis. Arthritis Res Ther 2015;17:7.
14. Vandecasteele E, Drieghe B, Melsens K, Thevissen K, De Pauw M, Deschepper E, et al. Screening for pulmonary arterial hypertension in an unselected prospective systemic sclerosis cohort. Eur Respir J 2017;49:1602275.
15. Galie N, Hoeper MM, Humbert M, Torbicki A, Vachiery JL, Barbera JA, et al. Guidelines for the diagnosis and treatment of pulmonary hypertension: the Task Force for the Diagnosis and Treatment of Pulmonary Hypertension of the European Society of Cardiology (ESC) and the European Respiratory Society (ERS), endorsed by the International Society of Heart and Lung Transplantation (ISHLT). Eur Heart J 2009;30:2493–537.
16. Schwaiger JP, Khanna D, Coghlan JG. Screening patients with scleroderma for pulmonary arterial hypertension and implications for other at-risk populations. Eur Respir Rev 2013;22:515–25.

DOI 10.1002/art.41759

Clinical Images: Multiple pulmonary artery aneurysms in Hughes-Stovin syndrome

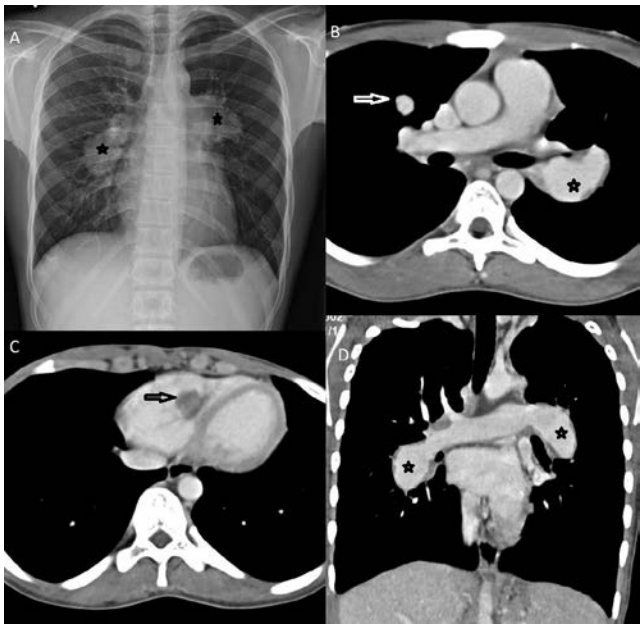

The patient, an 18-year-old man, presented with fever of 1 month's duration and intermittent hemoptysis, dry cough, joint pain, and myalgia. There were no oral or genital ulcers. His erythrocyte sedimentation rate was elevated (117 mm/hour) a with microcytic, hypochromic anemia. Results of a complete blood cell count with differential cell count and laboratory test results were otherwise normal. Plain posteroanterior radiography of the chest showed enlarged hila (**asterisks** in **A**). Contrast-enhanced computed tomography (CE-CT) of the chest showed saccular and fusiform pulmonary artery aneurysms involving the main pulmonary arteries, extending into lobar and segmental branches. CE-CT (**B** and **C**) and imaging of coronal reformation (**D**) showed pulmonary artery aneurysms (**asterisks** in **B** and **D**) involving main, lobar, and segmental branches (**arrow** in **B**) along with a right ventricular thrombus (**arrow** in **C**). The CT window showed normal findings in all lung fields. The right ventricle showed a mural thrombus close to the interventricular septum, consistent with a diagnosis of Hughes-Stovin syndrome. Hughes and Stovin described the syndrome as being characterized by multiple pulmonary artery aneurysms and systemic venous thromboses, including thromboses in the right side of the heart (1). Cases of Hughes-Stovin syndrome have been found predominantly in male patients with Behçet's syndrome. With routine use of CT pulmonary angiography, the need for catheter pulmonary angiography is reduced (2,3). Treatment approaches involving immunomodulator therapy have been shown to reverse many of the changes occurring in Hughes-Stovin syndrome.

1. Hughes JP, Stovin PG. Segmental pulmonary artery aneurysms with peripheral venous thrombosis. Br J Dis Chest 1959;53:1927.
2. Ketchum ES, Zamanian RT, Fleischmann D. CT angiography of pulmonary artery aneurysms in Hughes-Stovin syndrome. AJR Am J Roentgenol 2005;185:330–2.
3. Emad Y, Ragab Y, Ibrahim O, Saad A, Rasker JJ. Pattern of pulmonary vasculitis and major vascular involvement in Hughes-Stovin syndrome (HSS): brief report of eight cases. Clin Rheumatol 2020;39:1223–8.

Nichanametla Sravani, MD
Krishnan Nagarajan, MD, DM
Veer S. Negi, MD, DM
Jawaharlal Institute of Postgraduate Medical Education & Research
Pondicherry, India

American College of Rheumatology
Empowering Rheumatology Professionals

Arthritis & Rheumatology
Vol. 73, No. 9, September 2021, pp 1738–1748
DOI 10.1002/art.41733

Serum Metabolomics Identifies Dysregulated Pathways and Potential Metabolic Biomarkers for Hyperuricemia and Gout

Xia Shen,[1] Can Wang,[2] Ningning Liang,[3] Zhen Liu,[2] Xinde Li,[2] Zheng-Jiang Zhu,[4] Tony R. Merriman,[5] Nicola Dalbeth,[6] Robert Terkeltaub,[7] Changgui Li,[2] and Huiyong Yin[1]

Objective. To systematically profile metabolic alterations and dysregulated metabolic pathways in hyperuricemia and gout, and to identify potential metabolite biomarkers to discriminate gout from asymptomatic hyperuricemia.

Methods. Serum samples from 330 participants, including 109 with gout, 102 with asymptomatic hyperuricemia, and 119 normouricemic controls, were analyzed by high-resolution mass spectrometry–based metabolomics. Multivariate principal components analysis and orthogonal partial least squares discriminant analysis were performed to explore differential metabolites and pathways. A multivariate methods with Unbiased Variable selection in R (MUVR) algorithm was performed to identify potential biomarkers and build multivariate diagnostic models using 3 machine learning algorithms: random forest, support vector machine, and logistic regression.

Results. Univariate analysis demonstrated that there was a greater difference between the metabolic profiles of patients with gout and normouricemic controls than between the metabolic profiles of individuals with hyperuricemia and normouricemic controls, while gout and hyperuricemia showed clear metabolomic differences. Pathway enrichment analysis found diverse significantly dysregulated pathways in individuals with hyperuricemia and patients with gout compared to normouricemic controls, among which arginine metabolism appeared to play a critical role. The multivariate diagnostic model using MUVR found 13 metabolites as potential biomarkers to differentiate hyperuricemia and gout from normouricemia. Two-thirds of the samples were randomly selected as a training set, and the remainder were used as a validation set. Receiver operating characteristic analysis of 7 metabolites yielded an area under the curve of 0.83–0.87 in the training set and 0.78–0.84 in the validation set for distinguishing gout from asymptomatic hyperuricemia by 3 machine learning algorithms.

Conclusion. Gout and hyperuricemia have distinct serum metabolomic signatures. This diagnostic model has the potential to improve current gout care through early detection or prediction of progression to gout from hyperuricemia.

INTRODUCTION

As the most common inflammatory arthritis, affecting up to 6.8% of the population worldwide, gout usually presents as a flare triggered by monosodium urate (MSU) crystals in the joints (1,2). Hyperuricemia, a condition of high serum urate concentration, is diagnosed when the fasting serum urate level is >420 μmoles/liter (~7 mg/dl) on 2 different days (3). Hyperuricemia significantly increases the incident gout risk, and serum urate levels represent a strong predictor of incident gout (3). In the Normative Aging Study, the annual incidence rate of gout was 4.9% in those with a prior serum urate level of ≥9 mg/dl compared to 0.1% in those with urate levels of <7 mg/dl (4). In the Malmö Preventive Project Study, the absolute risk of incident gout during 30 years of follow-up was only 3.8% but increased to 14–20% in association with hyperuricemia (5). A recent study of 9,371 Chinese

Supported by the National Key Research and Development Program of China administered by the Chinese Ministry of Science and Technology (MOST; grant 2016YFC0903403) and by an open grant from the CAS Key Laboratory of Nutrition, Metabolism, and Food Safety. Dr. Terkeltaub's work was supported by the NIH (grants AR-060772 and AR-075990) and the VA Office of Research and Development.

[1]Xia Shen, BS, Huiyong Yin, PhD: ShanghaiTech University, CAS Key Laboratory of Nutrition, Metabolism, and Food Safety, Shanghai Institute of Nutrition and Health, Chinese Academy of Sciences, Shanghai, China, and University of Chinese Academy of Sciences, Beijing, China; [2]Can Wang, MD, Zhen Liu, MD, Xinde Li, MS, Changgui Li, MD: Shandong Provincial Key Laboratory of Metabolic Diseases, Qingdao Key Laboratory of Gout, Affiliated Hospital of Qingdao University Medical College, and Institute of Metabolic Diseases, Qingdao University, Qingdao, China; [3]Ningning Liang, BS: CAS Key Laboratory of Nutrition, Metabolism, and Food Safety, Shanghai Institute of Nutrition and Health, Chinese Academy of Sciences, Shanghai, China, and University of Chinese Academy of Sciences, Beijing, China; [4]Zheng-Jiang Zhu, PhD: Interdisciplinary Research Center on Biology and Chemistry, Shanghai Institute of Organic Chemistry, Chinese Academy of Sciences, Shanghai, China; [5]Tony R. Merriman, PhD: Institute of Metabolic Diseases, Qingdao University, Qingdao, China, University of Alabama at Birmingham, and University of Otago, Dunedin, New Zealand; [6]Nicola Dalbeth, MD, FRACP:

adolescents ages 13–19 years found that the prevalence of hyperuricemia was 42.3% in male subjects and 8.0% in female subjects (6). For the Chinese adult population, the prevalence of hyperuricemia and gout is ~13.3% and 1.1%, respectively (2,7). Although hyperuricemia significantly increases the incident gout risk, a majority of individuals with hyperuricemia remain asymptomatic (1,3). Thus, predicting who will develop gout in the future is clinically challenging.

Hyperuricemia is associated with many comorbidities, such as chronic kidney disease, diabetes mellitus, hypertension, hyperlipidemia, nonalcoholic fatty liver disease, and cardiovascular diseases (1,8). In these metabolic diseases, systematic metabolic alterations have often been observed (9,10). As such, metabolomic analysis of biologic fluids may provide an organism-wide view at a systems biology level of the dysregulated metabolic pathways and identify potential biomarkers for the progression from hyperuricemia to gout. Although such metabolomic approaches have been increasingly explored in rheumatic diseases (11–14), studies in hyperuricemia and gout are limited (15). Early metabolomics studies have primarily focused on investigating mechanisms and therapeutic effects using rodent models of hyperuricemia and gout even though each animal model has its limitations with regard to mimicking human pathology (16,17).

Metabolic profiling in humans identified pathways and metabolites that play an important role in regulating serum urate levels (15). A urinary metabolomics study in 35 gout patients and 29 healthy controls found 30 metabolites that were significantly different, including amino acids, carbohydrates, and organic acids (18). ^{1}H nuclear magnetic resonance–based metabolomic profiling revealed some differential metabolites in a relatively small cohort of 50 individuals with asymptomatic hyperuricemia and 49 gout patients (19). To date, studies have not systematically profiled the serum metabolome in large cohorts to identify potential biomarkers to differentiate or predict the progression from asymptomatic hyperuricemia to gout.

In this study, we recruited 330 participants, including normouricemic controls, individuals with asymptomatic hyperuricemia, and patients with gout, for the identification of diagnostic biomarkers using high-resolution mass spectrometry (MS)–based metabolomics. Univariate analysis, multivariate analysis, and 3 machine learning algorithms, including random forest, support vector machine, and logistic regression, were applied to identify dysregulated pathways between hyperuricemia, gout, and normouricemia and to develop prediction models based on potential metabolic biomarkers for the discrimination of asymptomatic hyperuricemia from gout. Such an approach may have a tremendous impact not only on understanding the molecular basis of hyperuricemia and gout, but also on improving current clinical practice in hyperuricemia and gout (1,20).

MATERIALS AND METHODS

Study participants. Three hundred thirty male participants (109 patients with gout, 102 individuals with hyperuricemia, and 119 normouricemic controls) were enrolled at the dedicated Gout Clinic of the Affiliated Hospital of Qingdao University. The enrolled participants included outpatients and participants in a general survey on lifestyle factors and hyperuricemia and gout that was carried out at the same clinic. Gout and hyperuricemia were diagnosed based on the 2015 American College of Rheumatology/European Alliance of Associations for Rheumatology gout classification criteria (21) and the Guideline for the Diagnosis and Management of Hyperuricemia and Gout in China 2019 from the Chinese Society of Endocrinology, Chinese Medical Association (7). The deposition of MSU crystals in the joint tissues was assessed by dual-energy computed tomography and ultrasound, whereas polarized light microscopy was not routinely performed. All participants with hyperuricemia had fasting serum urate levels of >420 μmoles/liter on 2 different days without any current or prior gout symptoms (7,22).

Participants were not permitted to take any urate-lowering drugs or other medicine affecting the serum urate level in the 2 weeks prior to enrollment. The duration of the 2-week washout period was based on the pharmacokinetics of common urate-lowering medications. Patients were given immediate medical treatment and excluded from this study if a gout flare occurred during this 2-week washout period. Participants in any of the 3 groups (normouricemic controls, hyperuricemia, and gout) were excluded if they had other known metabolic diseases, such as diabetes mellitus, kidney or liver diseases, hyperthyroidism, hyperlipidemia, hypertension, alcohol abuse, obesity, rheumatoid arthritis, or cancer.

Venous blood samples were obtained from participants who had not taken any medication after overnight fasting. Blood was allowed to clot for 30 minutes at room temperature and then centrifuged at 3,000 revolutions per minute for 10 minutes before supernatants were removed. The serum samples were aliquoted

University of Auckland, Auckland, New Zealand; [7]Robert Terkeltaub, MD: VA San Diego Healthcare System and University of California, San Diego.

Ms Shen and Dr. Wang contributed equally to this work.

Ms Shen, Ms Liang, and Dr. Yin are inventors on a pending patent in China for a mass spectrometry–based prediction model of gout from asymptomatic hyperuricemia. Dr. Merriman has received consulting fees, speaking fees, and/or honoraria from Ardea Biosciences and AstraZeneca (less than $10,000 each). Dr. Dalbeth has received consulting fees, speaking fees, and/or honoraria from AstraZeneca, Dyve Biosciences, Hengrui, Pfizer, Selecta, Arthrosi, Janssen, AbbVie, and Horizon (less than $10,000 each). Dr. Terkeltaub has received consulting fees from Ardea/AstraZeneca, Sobi, Horizon, and Acquist (less than $10,000 each) and from Selecta (more than $10,000) and has received research support from AstraZeneca. No other disclosures relevant to this article were reported.

Address correspondence to Changgui Li, MD, Shandong Provincial Key Laboratory of Metabolic Diseases, The Affiliated Hospital of Qingdao University, Qingdao 266003, China (email: changguili@vip.163.com); or to Huiyong Yin, PhD, Shanghai Institute of Nutrition and Health, Chinese Academy of Sciences, 320 Yueyang Road, Shanghai 200031, China (email: hyyin@sibs.ac.cn).

Submitted for publication November 12, 2020; accepted in revised form March 9, 2021.

and stored immediately at –80°C prior to further sample preparation and liquid chromatography mass spectrometry (LC-MS) analysis. The study was approved by the Ethics Committee of Qingdao University, and written informed consent was obtained from all participants. The LC-MS analysis procedure is described in the Supplementary Methods, available on the *Arthritis & Rheumatology* website at http://onlinelibrary.wiley.com/doi/10.1002/art.41733/abstract.

Data processing and normalization. MS raw data (.wiff) were converted to the mzXML format using ProteoWizard software (http://proteowizard.sourceforge.net). R package XCMS was used to extract peaks (23). The main parameters of XCMS processing were set as follows: mass accuracy in peak detection = 25 ppm; peak width = (5, 30); snthresh = 3; bw = 5; and minfrac = 0.5. A data matrix consisting of retention time, mass-to-charge ratio, and peak intensity was generated by XCMS. All metabolic peaks with a value of <80% in all quality control (QC) samples were excluded. The support vector regression normalization method based on QC samples (24) was used to normalize the original data. Peaks with a relative standard deviation of >30% in QC samples were removed from the peak table.

Statistical analysis. The study design and data analysis workflow are illustrated in Figure 1. We performed Wilcoxon's test to compare gout with hyperuricemia, gout with normouricemia, and hyperuricemia with normouricemia. Unsupervised analysis, principal components analysis (PCA; R package MixOmics), and hierarchical clustering analysis (pheatmap; R package pheatmap) were performed to explore the global metabolic variations among each group (Supplementary Figure 1A, available on the *Arthritis & Rheumatology* website at http://onlinelibrary.wiley.com/doi/10.1002/art.41733/abstract). The supervised analysis orthogonal partial least squares discriminant analysis (OPLS-DA; R package MetaboAnalystR) (25) was used to maximize the global metabolic variations among groups. The orthogonal signal correction technique was used to decompose matrix information into response-related and irrelevant information. We performed a test with 200 permutations to assess the validity of the discriminant models to avoid overfitting (Supplementary Figures 1B–D). Pathway enrichment analysis was conducted using the R package MetaboAnalystR. Metabolites with a false discovery rate (FDR) of <0.05 between 2 groups were considered to be significantly different. Then the metabolites were mapped into the KEGG database with the hypergeometric test to calculate significantly perturbed pathways. The pathway impact is the sum of the importance of the matched metabolites normalized to the sum of the importance of all of the metabolites in each metabolic pathway.

In univariate analysis, metabolites with an FDR of <0.05 and fold changes of >4/3 or <3/4 were considered to be significant metabolites, which were used for hierarchical clustering analysis. For biomarker discovery, we used multivariate methods with Unbiased Variable selection in R package (MUVR) to select potential biomarkers (26). We randomly selected two-thirds of the samples as a training set and used the remaining one-third as a validation set in each group. Subsequently, the prediction models were established according to 3 machine learning models: random forest (R package randomForest), support vector machine (R package e1071), and logistic regression (R function glm).

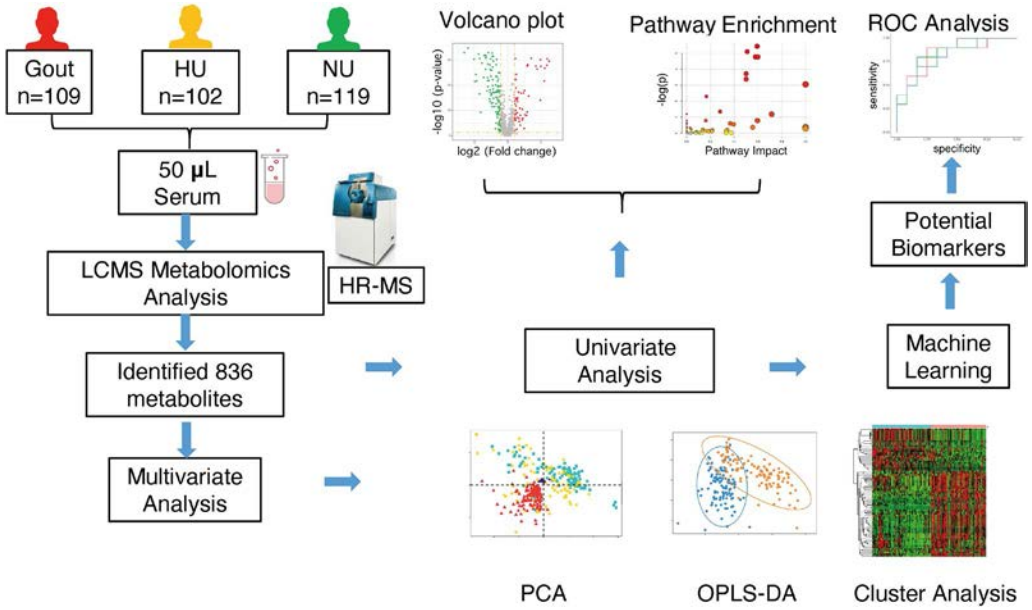

Figure 1. Study design and data analysis workflow. HU = hyperuricemia; NU = normouricemia; LC-MS = liquid chromatography mass spectrometry; HR-MS = high-resolution mass spectrometry; PCA = principal components analysis; OPLS-DA = orthogonal partial least squares discriminant analysis; ROC = receiver operating characteristic.

These machine learning algorithms have been shown to decrease the bias of prediction models.

The bootstrap method was used to improve the precision of prediction and dilute the selection bias (27). Notably, no overlap between the discovery and validation data sets was observed. The area under the receiver operating characteristic (ROC) curve (AUC) (R package pROC) was applied to evaluate the performance of the statistical model. We used the bootstrap method to calculate the AUC 1,001 times, then chose the median value of AUC corresponding to the data split as the final statistical model. The 0.25th and 99.75th percentiles were used to calculate the 95% confidence interval (95% CI). All statistical analyses were performed using R software (version 3.6.1) (28).

RESULTS

Clinical characteristics of the enrolled participants. The clinical characteristics of the participants are shown in Table 1. The serum urate levels in the hyperuricemia group (mean ± SD 516 ± 99.28 μmoles/liter) and gout group (mean ± SD 498 ± 91.48 μmoles/liter) were significantly higher than those in the normouricemic control group (mean ± SD 238 ± 35.82 μmoles/liter). Notably, serum urate levels in the hyperuricemia and gout groups were similar. Although we excluded participants with other metabolic diseases to minimize confounding factors, age, body mass index (BMI), aspartate aminotransferase/alanine aminotransferase, glucose, triglycerides, total cholesterol, creatinine, systolic blood pressure, and diastolic blood pressure in the hyperuricemia and gout groups were significantly different from those in the normouricemic control group. However, a majority of these parameters were not significantly different between the hyperuricemia and gout groups, except for age, glucose, and blood urea nitrogen. Notably, although the mean BMI in the hyperuricemia and gout groups was significantly larger than that in the normouricemic control group, most participants were of normal weight to slightly overweight.

Serum metabolomic profiles of the normouricemic controls, participants with hyperuricemia, and patients with gout. We performed an untargeted metabolomic analysis using high-resolution MS and detected 20,666 peaks in positive and negative ionization modes. After excluding the natural isotopic peaks in a database search, 320 and 516 metabolites were identified in positive and negative modes, respectively. An unsupervised PCA was used to evaluate the intrinsic metabolic variations and data quality in the metabolic analysis. Metabolites from gout patients had better separation from normouricemic controls, whereas individuals with hyperuricemia and gout patients showed less obvious separation, suggesting a smaller metabolic alteration between hyperuricemia and gout compared with that between gout and normouricemia (Supplementary Figure 1A). A tight clustering of the QC samples indicated a good reproducibility across all samples. To gain further insights into the metabolomic profiles, we performed a supervised OPLS-DA analysis, which is widely used to maximize the variations between groups in metabolomics analysis and detect metabolites with a significant contribution to the variation (29–31). Volcano plots were visualized using metabolites with an FDR of <0.05 and fold changes of >4/3 or <3/4. The significantly different metabolites were used for clustering analysis in a heatmap, followed by a pathway enrichment analysis with metabolites with an FDR of <0.05.

Comparison of the metabolic profiles of the hyperuricemia and normouricemic control groups. Compared with the PCA analysis, the OPLS-DA analysis showed a better separation of all metabolites in the hyperuricemia and normouricemic control groups (Figure 2A). Next, we performed a univariate nonparametric Wilcoxon's analysis based on the fold changes of metabolites in these 2 groups and found 328 metabolites with an FDR of <0.05. As shown in the volcano plot in Figure 2B and in Supplementary Table 1 (available on the *Arthritis & Rheumatology* website at http://onlinelibrary.wiley.com/doi/10.1002/art.41733/abstract), 22 metabolites were significantly up-regulated, whereas

Table 1. Clinical and demographic characteristics of the study participants*

	Normouricemic controls (n = 119)	Participants with hyperuricemia (n = 102)	Patients with gout (n = 109)
Age, years	46.77 ± 10.14	32.67 ± 12.57†	43.94 ± 11.88‡
BMI, kg/m^2	23.42 ± 3.43	26.94 ± 4.44†	26.67 ± 3.56†
AST/ALT, units/liter	1.10 ± 0.32	0.87 ± 0.37†	0.81 ± 0.24†
Glucose, mmoles/liter	4.34 ± 0.59	4.95 ± 1.07†	5.66 ± 1.28†‡
Triglycerides, mmoles/liter	1.17 ± 0.61	1.95 ± 1.31†	1.97 ± 1.12†
Total cholesterol, mmoles/liter	4.28 ± 0.74	4.60 ± 0.93	4.84 ± 0.95†
BUN, mmoles/liter	5.49 ± 1.55	5.22 ± 1.56	4.35 ± 0.92†‡
Creatinine, mmoles/liter	61.50 ± 9.56	82.77 ± 16.33†	83.06 ± 12.32†
Serum urate, μmoles/liter	238.17 ± 35.82	516.99 ± 99.28†	498.2 ± 91.48†
Systolic BP, mm Hg	118.75 ± 11.77	129.82 ± 11.49†	130.2 ± 14.48†
Diastolic BP, mm Hg	73.40 ± 8.31	80.09 ± 8.86†	80.91 ± 11.30†

* Values are the mean ± SD. BMI = body mass index; AST = aspartate aminotransferase; ALT = alanine aminotransferase; BUN = blood urea nitrogen; BP = blood pressure.
† $P < 0.01$ versus normouricemic controls.
‡ $P < 0.01$ versus participants with hyperuricemia.

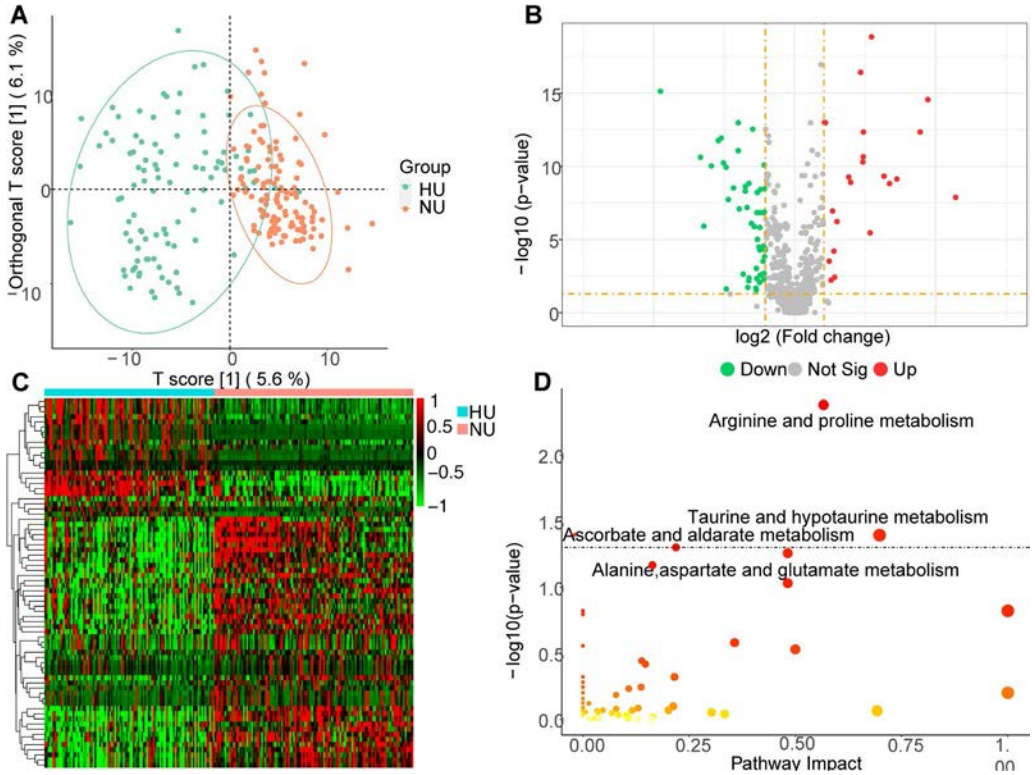

Figure 2. Metabolic profiles discriminating participants with hyperuricemia (HU) from normouricemic (NU) controls. **A**, Plot of orthogonal partial least squares discriminant analysis scores. Samples in the encircled areas are within the 95% confidence interval. **B**, Volcano plot of differential metabolites. Metabolites with a fold change of <3/4 and a false discovery rate (FDR) of <0.05 were considered significantly down-regulated. Metabolites with a fold change of >4/3 and an FDR of <0.05 were considered significantly up-regulated. Changes in other metabolites were not significant (Not Sig). **C**, Heatmap of differential metabolites. Red indicates metabolites that were up-regulated and green indicates metabolites that were down-regulated in individuals with hyperuricemia compared to normouricemic controls. **D**, Pathway enrichment plot. Colors represent the relative degree of the impact of each pathway (x-axis) and statistical significance (y-axis). Dotted line represents a *P* value of 0.05.

50 metabolites were significantly down-regulated, in the hyperuricemia group compared to the normouricemic control group. In addition to purine metabolism, these differential metabolites fell into diverse metabolic pathways.

Next, clustering analysis of these 72 significantly altered metabolites showed a clear separation in the heatmap (Figure 2C). Pathway enrichment analysis demonstrated that these metabolites primarily belonged to 4 pathways: arginine and proline metabolism; ascorbate and aldarate metabolism; taurine and hypotaurine metabolism; and alanine, aspartate, and glutamate metabolism (Figure 2D). These 4 metabolic pathways are interconnected primarily through amino acids, among which arginine and proline metabolism appears to be the key node (Supplementary Figure 2, available on the *Arthritis & Rheumatology* website at http://onlinelibrary.wiley.com/doi/10.1002/art.41733/abstract).

Comparison of the metabolic profiles of the gout and normouricemic control groups. To examine the metabolic profiles of gout patients compared to normouricemic controls, we performed OPLS-DA analysis. We observed a large overall metabolic separation between the groups (Figure 3A), consistent with the PCA plots (Supplementary Figure 1A). The volcano plots showed that 501 metabolites had an FDR of <0.05, among which 62 metabolites were up-regulated and 112 metabolites were down-regulated (Figure 3B and Supplementary Table 2, available on the *Arthritis & Rheumatology* website at http://onlinelibrary.wiley.com/doi/10.1002/art.41733/abstract). Consistently, these significantly altered metabolites clustered in the heatmap (Figure 3C) with a clear separation between the groups.

We found 7 pathways perturbed significantly between patients with gout and normouricemic controls, including glycine, serine, and threonine metabolism; arginine and proline metabolism; arginine biosynthesis; ascorbate and aldarate metabolism; D-glutamine and D-glutamate metabolism; alanine, aspartate, and glutamate metabolism; and phenylalanine, tyrosine and tryptophan biosynthesis (Figure 3D and Supplementary Figure 3, available on the *Arthritis & Rheumatology* website at http://onlinelibrary.wiley.com/doi/10.1002/art.41733/abstract). Interestingly, of the 4 significantly perturbed pathways between individuals with hyperuricemia and normouricemic controls, 3 pathways were also significantly altered between patients with gout and normouricemic controls, with the exception of taurine and hypotaurine metabolism.

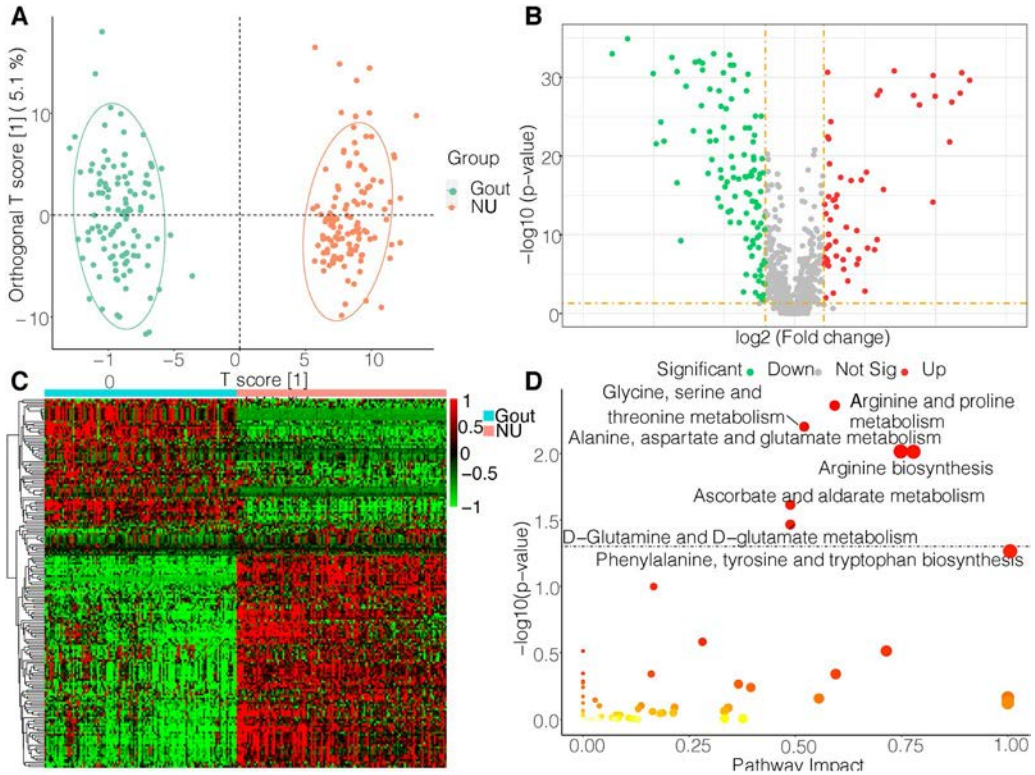

Figure 3. Metabolic profiles discriminating patients with gout from normouricemic (NU) controls. **A**, Plot of orthogonal partial least squares discriminant analysis scores. Samples in the encircled areas are within the 95% confidence interval. **B**, Volcano plot of differential metabolites. Metabolites with a fold change of <3/4 and a false discovery rate (FDR) of <0.05 were considered significantly down-regulated. Metabolites with a fold change of >4/3 and an FDR of <0.05 were considered significantly up-regulated. Changes in other metabolites were not significant (Not Sig). **C**, Heatmap of differential metabolites. Red indicates metabolites that were up-regulated and green indicates metabolites that were down-regulated in patients with gout compared to normouricemic controls. **D**, Pathway enrichment plot. Colors represent the relative degree of the impact of each pathway (x-axis) and statistical significance (y-axis). Dotted line represents a *P* value of 0.05.

Moreover, amino acid metabolism was also predominantly altered between patients with gout and normouricemic controls.

Comparison of the metabolic profiles of the hyperuricemia and gout groups. We observed a clear overall separation between the hyperuricemia and gout groups in the OPLS-DA analysis (Figure 4A), suggesting that these 2 disease stages had distinct metabolic profiles at the molecular level. These observations prompted us to explore metabolites that could be used to differentiate these 2 stages (as described below). In the volcano plot (Figure 4B), there were 321 metabolites with an FDR of <0.05, among which 37 were up-regulated and 58 were down-regulated (Supplementary Table 3, available on the *Arthritis & Rheumatology* website at http://onlinelibrary.wiley.com/doi/10.1002/art.41733/abstract). All of these significantly altered metabolites clustered well in the heatmap (Figure 4C). Surprisingly, however, these differential metabolites were only enriched in 2 pathways: arginine biosynthesis; and glycine, serine, and threonine metabolism (Figure 4D and Supplementary Figure 4, available on the *Arthritis & Rheumatology* website at http://onlinelibrary.wiley.com/doi/10.1002/art.41733/abstract).

Prediction models to differentiate the hyperuricemia, gout, and normouricemic control groups. After systematically defining the metabolomic profiles and pathways associated with hyperuricemia and gout, we set out to develop prediction models by selecting metabolites that could be used to differentiate individuals with hyperuricemia and patients with gout from normouricemic controls. We randomly selected two-thirds of the samples in each group as the training set and the remaining one-third as the validation set. To improve predictive performance and avoid overfitting and false positives, we performed multivariate modeling using a random forest–based MUVR algorithm that could simultaneously identify minimal-optimal and all-relevant variables for regression analysis (26). To increase the confidence and reproducibility of the potential biomarkers, we chose only the metabolites with grade 1 identification based on MetDNA criteria and further validated the structural identities of these potential biomarkers by using the commercial standards with the identical LC-MS method.

A total of 13 metabolites were selected and structurally validated (Supplementary Table 4 and Supplementary Figure 5, available on the *Arthritis & Rheumatology* website at http://onlinelibrary.wiley.com/doi/10.1002/art.41733/abstract). Relative MS

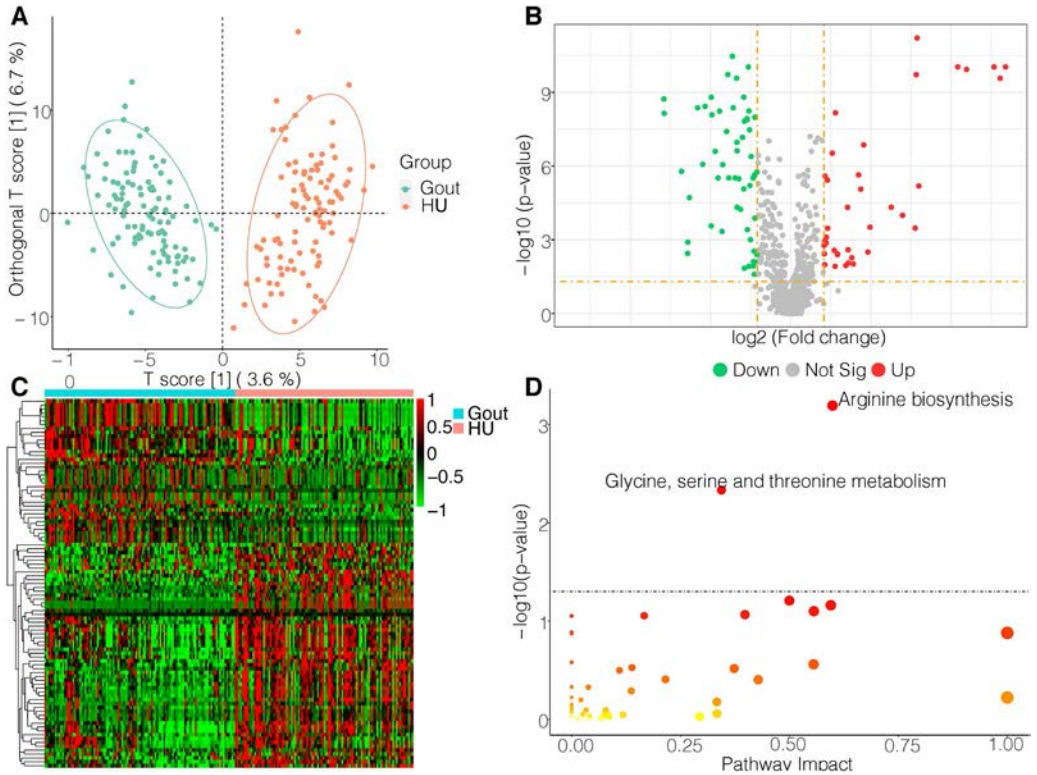

Figure 4. Metabolic profiles discriminating patients with gout from individuals with hyperuricemia (HU). **A**, Plot of orthogonal partial least squares discriminant analysis scores. Samples in the encircled areas are within the 95% confidence interval. **B**, Volcano plot of differential metabolites. Metabolites with a fold change of <3/4 and a false discovery rate (FDR) of <0.05 were considered significantly down-regulated. Metabolites with a fold change of >4/3 and an FDR of <0.05 were considered significantly up-regulated. Changes in other metabolites were not significant (Not Sig). **C**, Heatmap of differential metabolites. Red indicates metabolites that were up-regulated and green indicates metabolites that were down-regulated in patients with gout compared to individuals with hyperuricemia. **D**, Pathway enrichment plot. Colors represent the relative degree of the impact of each pathway (x-axis) and statistical significance (y-axis). Dotted line represents a *P* value of 0.05.

abundances of these metabolites showed statistical significance (Supplementary Figure 6, available on the *Arthritis & Rheumatology* website at http://onlinelibrary.wiley.com/doi/10.1002/art.41733/abstract), highlighting the potential of these metabolites as biomarkers to distinguish individuals with hyperuricemia and patients with gout from normouricemic controls. Subsequently, we performed an ROC analysis with random forest, support vector machine, and logistic regression to construct prediction models. Importantly, we selected only the metabolites and prediction models that had similar performance in all 3 methods.

To discriminate individuals with hyperuricemia from normouricemic controls, 7 metabolites were selected, including sphingomyelin, trigonelline, pyroglutamic acid, citrulline, inositol, arachidonate, and glycocholate (Supplementary Figures 7A and B, available on the *Arthritis & Rheumatology* website at http://onlinelibrary.wiley.com/doi/10.1002/art.41733/abstract). The following prediction formula was deduced to classify individuals with hyperuricemia and normouricemic controls. Notably, the prediction score is not the probability for the disease but is used for classification purposes. We calculated the prediction score as follows: Prediction score = $e^{logit(P)}/(1 + e^{logit(P)})$, where Logit (P) = $25.11 + 2.29 \times 10^{-6} \times M_{pyroglutamic\ acid} - 2.58 \times 10^{-4} \times M_{inositol} - 3.33 \times 10^{-5} \times M_{glycocholate} + 4.65 \times 10^{-6} \times M_{trigonelline} - 1.77 \times 10^{-3} \times M_{Citrulline} + 7.48 \times 10^{-6} \times M_{Sphingomyelin} - 2.45 \times 10^{-6} \times M_{arachidonate}$, and where M stands for the normalized MS intensity of each metabolite.

The cutoff for the prediction score was set at 0.5, with individuals with a score of >0.5 diagnosed as having hyperuricemia, while those with a score of <0.5 are classified as normouricemic. This cutoff value is derived from the 3 models to ensure the lowest false-positive and false-negative values in the classifications. Further analysis showed that AUCs ranged from 0.87 to 0.94 in the training set, and from 0.80 to 0.82 in the validation set (Supplementary Figures 7C and D).

Similarly, only 4 metabolites (glutamate, pyroglutamic acid, glycocholate, and lactic acid) were needed to distinguish patients with gout from normouricemic controls. We calculated the prediction score as follows: Prediction score = $e^{logit(P)}/(1 + e^{logit(P)})$, where Logit (P) = $144.9 - 4.06 \times 10^{-5} \times M_{pyroglutamic\ acid} - 4.67 \times 10^{-4} \times M_{glycocholate} - 3.98 \times 10^{-5} \times M_{lactic\ acid} - 2.58 \times 10^{-3} \times M_{Glutamate}$.

The cutoff for the prediction score was set at 0.5, with individuals with a score of >0.5 diagnosed as having gout, and those with a score of <0.5 classified as normouricemic. Interestingly, the maximum AUC (AUC_{max}) was close to 1 in both the training and validation sets (Supplementary Figures 8A–D, available on the

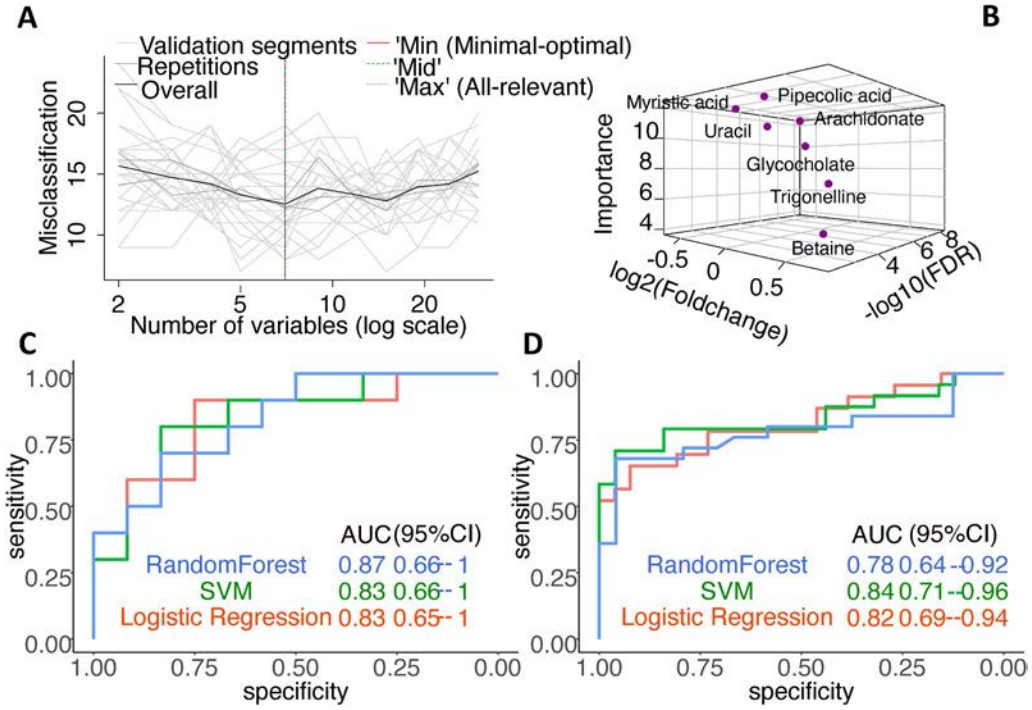

Figure 5. Selection of potential metabolic biomarkers discriminating patients with gout from individuals with hyperuricemia. **A**, Variable selection based on a Multivariate methods with Unbiased Variable selection in R (MUVR) algorithm. MUVR was used to simultaneously identify minimal-optimal and all-relevant variables for regression analysis. **B**, Statistical parameters of the 7 metabolites identified as potential biomarkers discriminating patients with gout from individuals with hyperuricemia. **C** and **D**, Receiver operating characteristic area under the curve (AUC) for sensitivity and specificity of the predictive model in the training set (**C**) and in the validation set (**D**), determined using 3 machine learning algorithms: random forest, support vector machine (SVM), and logistic regression. FDR = false discovery rate; 95% CI = 95% confidence interval.

Arthritis & Rheumatology website at http://onlinelibrary.wiley.com/doi/10.1002/art.41733/abstract), consistent with a large metabolomic difference between these 2 groups.

More importantly, 7 metabolites were successfully identified as the potential biomarkers to discriminate patients with gout from individuals with hyperuricemia: uracil, trigonelline, betaine, pipecolic acid, myristic acid, arachidonate, and glycocholate (Figures 5A and B). The prediction formula and a cutoff value of 0.51 were determined from the prediction model, i.e., individuals with a score of >0.51 are classified as having gout, whereas those with a prediction score of <0.51 are classified as having hyperuricemia. The formula for the prediction score was as follows: Prediction score = $e^{logit(P)}/(1 + e^{logit(P)})$, where Logit(P) = $-12.03 + 2.57 \times 10^{-6} \times M_{betaine} + 5.77 \times 10^{-5} \times M_{trigonelline} - 4.03 \times 10^{-5} \times M_{glycocholate} - 2.45 \times 10^{-5} \times M_{uracil} + 2.97 \times 10^{-4} \times M_{pipecolic\ acid} + 6.04 \times 10^{-7} \times M_{myristic\ acid} + 1.81 \times 10^{-6} \times M_{arachidonate}$.

The AUCs in the training set ranged from 0.83 to 0.87 (Figure 5C), whereas AUCs in the validation set ranged from 0.78 to 0.84 using the 3 different machine learning algorithms (Figure 5D).

DISCUSSION

Despite extensive research focused on understanding gout pathogenesis, the quality of current gout care and management remains far from optimal worldwide (1). Among the key steps in a proposed roadmap to improve global outcomes, developing novel prognostic markers and gout-specific disease activity indices beyond serum urate levels may help refine the disease stages of gout as well as improve care for the comorbidities of hyperuricemia and gout (20). Although hyperuricemia represents the major risk factor for gout, most individuals with hyperuricemia remain asymptomatic (3). Thus, it poses a tremendous clinical challenge to differentiate or predict which individuals with asymptomatic hyperuricemia will progress to gout.

We carried out a state-of-the-art metabolomics study to systematically define the metabolic profiles and related pathways in participants with hyperuricemia, patients with gout, and normouricemic controls. We further selected and structurally validated a panel of 13 metabolites using 3 machine learning algorithms to distinguish patients with gout and individuals with hyperuricemia from normouricemic controls (Supplementary Table 4 and Supplementary Figure 5). More importantly, we developed a prediction model based on 7 metabolites to distinguish patients with gout from individuals with asymptomatic hyperuricemia, with good sensitivity and specificity: AUCs in the training and validation sets ranged from 0.83 to 0.87 and from 0.78 to 0.84, respectively (Figure 5).

The metabolomic profile analysis showed that diverse pathways are significantly dysregulated in individuals with hyperuricemia

and patients with gout compared to normouricemic controls, among which arginine metabolism emerges as the most significantly altered. In individuals with hyperuricemia, metabolites that are involved in amino acid metabolism, arachidonic acid metabolism, and carbohydrate metabolism, in addition to purine and pyrimidine metabolism, were significantly up-regulated compared to normouricemic controls, while different metabolites in similar pathways were significantly down-regulated (Supplementary Table 1). Consistent with these results, pathway enrichment analysis showed that significantly altered pathways include arginine and proline metabolism; taurine and hypotaurine metabolism; ascorbate and aldarate metabolism; and alanine, aspartate, and glutamate metabolism (Figure 2D and Supplementary Figure 2).

Interestingly, these 4 metabolic pathways are interconnected primarily through amino acids, among which arginine and proline metabolism appears to be the key node: it connects with taurine and hypotaurine metabolism via glutamate; with glycine, serine, and threonine metabolism via creatine; and with ascorbate and aldarate metabolism via proline. Although arginine levels have been closely associated with inflammation in several human diseases, our study suggests that arginine and proline metabolism locate at the key node linking 3 other metabolic pathways differentiating individuals with hyperuricemia from normouricemic controls (Supplementary Figure 2). Even though there is no direct evidence linking arginine to hyperuricemia, arginine and urate were among the 6 metabolites recently identified in a rat model of acute heart failure using untargeted metabolomics (32). Furthermore, ascorbate and aldarate metabolism has previously been linked to urate metabolism (33). Peng et al found that ascorbic acid significantly reduces high-altitude hyperuricemia in young men initially migrated to high altitude (34). Alanine, aspartate, and glutamate metabolism is correlated with urate metabolism (19,35). Taurine significantly reduces the level of urate in rats with hyperuricemia and alleviates kidney damage (36). Furthermore, taurine and hypotaurine metabolism is also involved in inflammation (37) and oxidative stress (38), two factors that have been associated with gout and urate levels (39).

Interestingly, compared to the normouricemic control group, the top 4 significantly up-regulated metabolites in the gout group were the same as those in the hyperuricemia group (Supplementary Table 2), albeit to a greater extent. Furthermore, 2 pathways appear to play a key role in the progression from hyperuricemia to gout: arginine biosynthesis; and glycine, serine, and threonine metabolism (Figure 4D and Supplementary Figure 4). A previous study correlated the synthesis of arginine with inflammatory reactions (40), which may serve as potential indicators differentiating gout from hyperuricemia (41,42). Glycine, serine, and threonine are essential precursors of protein synthesis, nucleic acids, and lipids, among which glycine and serine are precursors of urate (40). Notably, the biosynthesis of phenylalanine, tyrosine, and tryptophan has been associated with acute inflammatory diseases such as severe malaria and sepsis (40). Previous evidence has linked glutamate and glutamine with asymptomatic hyperuricemia and gout (19,43,44). In addition to being a major metabolite in the tricarboxylic acid cycles in energy metabolism and precursor for urate synthesis (41), glutamate inhibits the glutamate–cystine reverse transport system, leading to a significant decrease in intracellular glutathione levels and an increase in reactive oxygen species and oxidative stress. Taken together, the findings of our metabolomics study have revealed diverse metabolic pathways that are significantly altered in gout and asymptomatic hyperuricemia, among which amino acid metabolism pathways (especially arginine) appear to play a critical role.

After systematically profiling the metabolic alterations in hyperuricemia and gout, we successfully selected potential metabolites to discriminate between hyperuricemia and gout using machine learning algorithms, which are increasingly recognized as an effective method to evaluate and predict disease states (24,27,28,45–47). Using a similar approach, a recent study identified potential biomarkers from serum metabolomics and lipidomics to discriminate between seronegative rheumatoid arthritis and psoriatic arthritis (9). In our study, 13 metabolites were successfully identified as potential biomarkers for discriminating the gout and hyperuricemia groups from the normouricemic control group (Supplementary Table 4). Among them, 7 metabolites were identified for discrimination of the hyperuricemia group from the normouricemic control group, with an AUC_{max} of 0.94 and 0.82 in the training set and validation set, respectively, whereas 4 metabolites were identified to discriminate the gout group from the normouricemic control group, with an AUC_{max} close to 1 in both the training and validation sets. More importantly, we identified 7 metabolites as potential biomarkers to discriminate between gout and asymptomatic hyperuricemia, with an AUC_{max} of 0.87 and 0.84 in the training and validation sets, respectively.

There are several limitations of the present study. First, to minimize the confounding factors that may affect the metabolomic differences, we included only a "pure" population of patients with gout or hyperuricemia, without the common comorbidities linked to hyperuricemia, in this cross-sectional study, which may limit generalizability to the general gout population. Among the different factors that may influence systemic metabolism, age and BMI were not matched in this study. Although BMI may have limited impact because most participants were of normal weight to slightly overweight, the average age in the hyperuricemia group was much younger than in the normouricemic control and gout groups (Table 1). When we matched the 3 groups for age in a subgroup analysis, we found that >90% of the significantly differential metabolites remained; most importantly, all of the metabolites included in the diagnostic models were retained (data not shown).

Second, our cohort had quite different genetic and environmental characteristics from other national/ethnic cohorts (1). For example, the average age of the participants in the gout group in the present study was 44 years, which is comparable to the

average age of 42 years at onset of gout in Chinese patients, but much younger than in the populations of Western countries (48).

Third, some conclusions using serum remain hypothesis generating, since the altered metabolites in serum can reflect, for example, inflammatory and metabolic changes in the liver, gut, and kidney, in leukocytes, and in the large "organ mass" of the synovial joint, vascular system, and bone. As such, future longitudinal studies are warranted to validate our findings in larger multinational/ethnic cohorts, combining serum or plasma metabolomics with other omics, including genomics, epigenomics, and proteomics. Such an approach could shed light on the relationships of the differentially abundant metabolites identified with purine metabolism, urate transport, inflammatory processes, and MSU crystal deposition.

In summary, our study has exemplified the power of combining metabolomics and machine learning algorithms for identifying potential metabolic biomarkers to distinguish gout from asymptomatic hyperuricemia. If validated in separate cohorts, these biomarkers may have the potential to discriminate gout from hyperuricemia, and even predict the development of gout and other comorbidities. These prediction models may also be applied in epidemiologic settings to predict the percentage of individuals with hyperuricemia who are at high risk of gout. Such a novel approach may have a profound impact on the clinical assessment and management of hyperuricemia and gout.

AUTHOR CONTRIBUTIONS

All authors were involved in drafting the article or revising it critically for important intellectual content, and all authors approved the final version to be published. Dr. Yin had full access to all of the data in the study and takes responsibility for the integrity of the data and the accuracy of the data analysis.

Study conception and design. Shen, C. Li, Yin.

Acquisition of data. Shen, Wang, Liang, Liu, C. Li.

Analysis and interpretation of data. Shen, Wang, Liu, X. Li, Zhu, Merriman, Dalbeth, Terkeltaub, Yin.

REFERENCES

1. Dehlin M, Jacobsson L, Roddy E. Global epidemiology of gout: prevalence, incidence, treatment patterns and risk factors [review]. Nat Rev Rheumatol 2020;16:380–90.
2. Liu R, Han C, Wu D, Xia X, Gu J, Guan H, et al. Prevalence of hyperuricemia and gout in mainland China from 2000 to 2014: a systematic review and meta-analysis. Biomed Res Int 2015;2015:762820.
3. Dalbeth N, Phipps-Green A, Frampton C, Neogi T, Taylor WJ, Merriman TR. Relationship between serum urate concentration and clinically evident incident gout: an individual participant data analysis. Ann Rheum Dis 2018;77:1048–52.
4. Campion EW, Glynn RJ, DeLabry LO. Asymptomatic hyperuricemia: risks and consequences in the Normative Aging Study. Am J Med 1987;82:421–6.
5. Kapetanovic MC, Nilsson P, Turesson C, Englund M, Dalbeth N, Jacobsson L. The risk of clinically diagnosed gout by serum urate levels: results from 30 years follow-up of the Malmö Preventive Project cohort in southern Sweden. Arthritis Res Ther 2018;20:190.
6. Lu J, Sun W, Cui L, Li X, He Y, Liu Z, et al. A cross-sectional study on uric acid levels among Chinese adolescents. Pediatr Nephrol 2020;35:441–6.
7. Chinese Society of Endocrinology. Guideline for the diagnosis and management of hyperuricemia and gout in China (2019). Chinese J Endocrinol Metabol 2020;36:1–13.
8. Zhu Y, Pandya BJ, Choi HK. Prevalence of gout and hyperuricemia in the US general population: the National Health and Nutrition Examination Survey 2007–2008. Arthritis Rheum 2011;63:3136–41.
9. Souto-Carneiro M, Tóth L, Behnisch R, Urbach K, Klika KD, Carvalho RA, et al. Differences in the serum metabolome and lipidome identify potential biomarkers for seronegative rheumatoid arthritis versus psoriatic arthritis. Ann Rheum Dis 2020;79:499–506.
10. Holers VM. Challenges and opportunities: using omics to generate testable insights into pathogenic mechanisms in preclinical seropositive rheumatoid arthritis. Arthritis Rheumatol 2021;73:1–4.
11. Guma M, Tiziani S, Firestein GS. Metabolomics in rheumatic diseases: desperately seeking biomarkers [review]. Nat Rev Rheumatol 2016;12:269–81.
12. Kapoor SR, Filer A, Fitzpatrick MA, Fisher BA, Taylor PC, Buckley CD, et al. Metabolic profiling predicts response to anti–tumor necrosis factor α therapy in patients with rheumatoid arthritis. Arthritis Rheum 2013;65:1448–56.
13. Menni C, Zierer J, Valdes AM, Spector TD. Mixing omics: combining genetics and metabolomics to study rheumatic diseases [review]. Nature Rev Rheumatol 2017;13:174–81.
14. Chandran V, Rahman P. Predicting therapeutic response through biomarker analysis in psoriatic arthritis, an example of precision medicine [review]. Expert Rev Precis Med Drug Dev 2020;5:35–42.
15. Albrecht E, Waldenberger M, Krumsiek J, Evans AM, Jeratsch U, Breier M, et al. Metabolite profiling reveals new insights into the regulation of serum urate in humans. Metabolomics 2014;10:141–51.
16. Luo Y, Wang L, Peng A, Liu JY. Metabolic profiling of human plasma reveals the activation of 5-lipoxygenase in the acute attack of gouty arthritis. Rheumatology (Oxford) 2019;58:345–51.
17. Lu J, Dalbeth N, Yin H, Li C, Merriman TR, Wei WH. Mouse models for human hyperuricaemia: a critical review [review]. Nature Rev Rheumatol 2019;15:413–26.
18. Li Q, Wei S, Wu D, Wen C, Zhou J. Urinary metabolomics study of patients with gout using gas chromatography-mass spectrometry. Biomed Res Int 2018;2018:3461572.
19. Zhang Y, Zhang H, Chang D, Guo F, Pan H, Yang Y. Metabolomics approach by 1H NMR spectroscopy of serum reveals progression axes for asymptomatic hyperuricemia and gout. Arthritis Res Ther 2018;20:111.
20. Dalbeth N, Choi HK, Terkeltaub R. Gout: a roadmap to approaches for improving global outcomes [review]. Arthritis Rheumatol 2017;69:22–34.
21. Neogi T, Jansen TL, Dalbeth N, Fransen J, Schumacher HR, Berendsen D, et al. 2015 gout classification criteria: an American College of Rheumatology/European League Against Rheumatism collaborative initiative. Arthritis Rheumatol 2015;74:2557–68.
22. Bursill D, Taylor WJ, Terkeltaub R, Abhishek A, So AK, Vargas-Santos AB, et al. Gout, Hyperuricaemia and Crystal-Associated Disease Network (G-CAN) consensus statement regarding labels and definitions of disease states of gout. Ann Rheum Dis 2019;78:1592–600.
23. Smith CA, Want EJ, O'Maille G, Abagyan R, Siuzdak G. XCMS: processing mass spectrometry data for metabolite profiling using nonlinear peak alignment, matching, and identification. Anal Chem 2006;78:779–87.
24. Shen X, Gong X, Cai Y, Guo Y, Tu J, Li H, et al. Normalization and integration of large-scale metabolomics data using support vector regression. Metabolomics 2016;12:89.

25. Chong J, Xia J. MetaboAnalystR: an R package for flexible and reproducible analysis of metabolomics data. Bioinformatics 2018; 34:4313–4.
26. Shi L, Westerhuis JA, Rosén J, Landberg R, Brunius C. Variable selection and validation in multivariate modelling. Bioinformatics 2019;35:972–80.
27. Costa C, Maraschin M, Rocha M. An R package for the integrated analysis of metabolomics and spectral data. Comput Methods Programs Biomed 2016;129:117–24.
28. Al-Akwaa FM, Yunits B, Huang S, Alhajaji H, Garmire LX. Lilikoi: an R package for personalized pathway-based classification modeling using metabolomics data. Gigascience 2018;7:giy136.
29. Triba MN, Le Moyec L, Amathieu R, Goossens C, Bouchemal N, Nahon P, et al. PLS/OPLS models in metabolomics: the impact of permutation of dataset rows on the K-fold cross-validation quality parameters. Mol Biosyst 2015;11:13–9.
30. Silva AF, Sarraguca MC, Ribeiro PR, Santos AO, De Beer T, Lopes JA. Statistical process control of cocrystallization processes: a comparison between OPLS and PLS. Int J Pharm 2017;520:29–38.
21. Worley B, Powers R. PCA as a practical indicator of OPLS-DA model reliability. Curr Metabolomics 2016;4:97–103.
32. Liu M, Li Y, Tang Y, Zheng L, Peng C. Synergistic effect of Aconiti Lateralis Radix Praeparata water-soluble alkaloids and Ginseng Radix et Rhizoma total ginsenosides compatibility on acute heart failure rats. J Chromatogr B Analyt Technol Biomed Life Sci 2020;1137:121935.
33. Esteve C, Jones EA, Kell DB, Boutin H, McDonnell LA. Mass spectrometry imaging shows major derangements in neurogranin and in purine metabolism in the triple-knockout 3xTg Alzheimer mouse model. Biochim Biophys Acta Proteins Proteom 2017;1865:747–54.
34. Peng H, Feng D, Wang Y, Dong Z, Chen Q, Zhang L, et al. Effect of oral vitamin C supplementation on high-altitude hyperuricemia in young men initially migrating to high altitude: a pilot study. High Alt Med Biol 2018;19:373–81.
35. Mossa AH, Swelam ES, Mohafrash SM. Sub-chronic exposure to fipronil induced oxidative stress, biochemical and histopathological changes in the liver and kidney of male albino rats. Toxicol Rep 2015;2:775–84.
36. Feng Y, Sun F, Gao Y, Yang J, Wu G, Lin S, et al. Taurine decreased uric acid levels in hyperuricemic rats and alleviated kidney injury. Biochem Biophys Res Commun 2017;489:312–8.
37. Zhou J, Yao N, Wang S, An D, Cao K, Wei J, et al. Fructus Gardeniae-induced gastrointestinal injury was associated with the inflammatory response mediated by the disturbance of vitamin B6, phenylalanine, arachidonic acid, taurine and hypotaurine metabolism. J Ethnopharmacol 2019;235:47–55.
38. Pandya KG, Budhram R, Clark GJ, Lau-Cam CA. Taurine can enhance the protective actions of metformin against diabetes-induced alterations adversely affecting renal function. Adv Exp Med Biol 2015;803:227–50.
39. Wu SH, Shu XO, Milne G, Xiang YB, Zhang X, Cai Q, et al. Uric acid correlates to oxidation and inflammation in opposite directions in women. Biomarkers 2015;20:225–31.
40. Wang H, McNeil YR, Yeo TW, Anstey NM. Simultaneous determination of multiple amino acids in plasma in critical illness by high performance liquid chromatography with ultraviolet and fluorescence detection. J Chromatogr B Analyt Technol Biomed Life Sci 2013;940:53–8.
41. Yu TF, Adler M, Bobrow E, Gutman AB. Plasma and urinary amino acids in primary gout, with special reference to glutamine. J Clin Invest 1969;48:885–94.
42. Humer E, Khol-Parisini A, Metzler-Zebeli BU, Gruber L, Zebeli Q. Alterations of the lipid metabolome in dairy cows experiencing excessive lipolysis early postpartum. PLoS One 2016;11:e0158633.
43. Yü T, Kaung C. The natural history of hyperuricemia among asymptomatic relatives of patients with gout. Adv Exp Med Biol 1980;122A:1–7.
44. Pagliara AS, Goodman AD. Elevation of plasma glutamate in gout: its possible role in the pathogenesis of hyperuricemia. N Engl J Med 1969;281:767–70.
45. Toubiana D, Puzis R, Wen L, Sikron N, Kurmanbayeva A, Soltabayeva A, et al. Combined network analysis and machine learning allows the prediction of metabolic pathways from tomato metabolomics data. Commun Biol 2019;2:214.
46. Xia J, Broadhurst DI, Wilson M, Wishart DS. Translational biomarker discovery in clinical metabolomics: an introductory tutorial. Metabolomics 2013;9:280–99.
47. Smith JS, Nebgen BT, Zubatyuk R, Lubbers N, Devereux C, Barros K, et al. Approaching coupled cluster accuracy with a general-purpose neural network potential through transfer learning. Nat Commun 2019;10:2903.
48. Gao Q, Cheng X, Merriman TR, Wang C, Cui L, Zhang H, et al. Trends in the manifestations of 9754 gout patients in a Chinese clinical center: a 10-year observational study. Joint Bone Spine 2020 doi: https://doi.org/10.1016/j.jbspin.2020.09.010. E-pub ahead of print.

Arthritis & Rheumatology
Vol. 73, No. 9, September 2021, pp 1749–1757
DOI 10.1002/art.41710

American College of Rheumatology
Empowering Rheumatology Professionals

Effectiveness of Allopurinol in Reducing Mortality: Time-Related Biases in Observational Studies

Samy Suissa,[1] Karine Suissa,[2] and Marie Hudson[1]

Objective. The treatment of gout with allopurinol is effective at reducing urate levels and the frequency of flares. Several observational studies have shown important reductions in mortality with allopurinol use, with wide variations in results. We undertook this review to assess the extent of bias in these studies, particularly time-related biases such as immortal time bias.

Methods. We searched the literature to identify all observational studies describing the effect of allopurinol use versus nonuse on all-cause mortality.

Results. We identified 12 observational studies, of which 3 were affected by immortal time bias and 3 by immeasurable time bias, while the remaining 6 studies avoided these time-related biases. Reductions in all-cause mortality with allopurinol use were observed among the studies with immortal time bias, with a pooled hazard ratio (HR) of death associated with allopurinol of 0.71 (95% confidence interval [95% CI] 0.50–1.01), as well as in those with immeasurable time bias (pooled HR 0.62 [95% CI 0.56–0.67]). The 6 studies that avoided these biases demonstrated a null effect of allopurinol on mortality (pooled HR 0.99 [95% CI 0.87–1.11]), though the lack of an analysis based on treatment adherence may have attenuated the effect.

Conclusion. Observational studies are important to provide real-world data on medication effects. The observational studies showing significantly decreased mortality with allopurinol treatment cannot be used as evidence, however, mainly due to time-related biases that tend to greatly exaggerate the potential benefit of treatments. The ALL-HEART randomized trial, which is currently underway and evaluates the effect of adding allopurinol to usual care (compared to no added treatment), will provide reliable evidence on mortality.

INTRODUCTION

Gout, the most common type of inflammatory arthritis, has been associated with increased risk of cardiovascular events and related mortality (1,2). Moreover, gout has been associated with increases of 10% to 237% in the risk of all-cause mortality, with mortality increasing with higher serum urate levels (3,4).

Treatment with allopurinol is highly effective at reducing urate levels and the frequency of flares in patients with gout (5). Consequently, the hypothesis that allopurinol could, based on its effectiveness, also reduce the higher mortality of patients with gout has received considerable attention. A meta-analysis of randomized controlled trials reporting on the comparison of allopurinol or oxypurinol to placebo found an odds ratio (OR) of all-cause mortality of 0.94 (95% confidence interval [95% CI] 0.62–1.44), although it included trials with patients who had other conditions (aside from gout) (6). Currently underway is the ALL-HEART study, a large placebo-controlled randomized trial comparing allopurinol therapy to usual care, which will provide some data on all-cause mortality (7).

On the other hand, several observational studies have assessed this association, with hazard ratios (HRs) of all-cause mortality with allopurinol use compared to nonuse ranging widely between 0.39 and 1.46 (8,9). A meta-analysis of 4 observational studies demonstrated a numerically nonsignificant reduction in mortality with allopurinol use versus nonuse (pooled HR 0.80 [95% CI 0.60–1.05]) (10).

Time-related biases, such as immortal and immeasurable time biases, have been shown to affect many observational studies conducted using computerized health care databases (11).

[1]Samy Suissa, PhD, Marie Hudson, MD: Jewish General Hospital and McGill University, Montreal, Quebec, Canada; [2]Karine Suissa, PhD: Brigham and Women's Hospital and Harvard Medical School, Boston, Massachusetts.

Dr. S. Suissa has received consulting fees, speaking fees, and/or honoraria from Atara Bio, Bristol Myers Squibb, Merck, Pfizer, Seqirus, Boehringer Ingelheim, and Novartis (less than $10,000 each). Dr. Hudson has received consulting fees from Boehringer Ingelheim, Alexion, and Octapharma (less than $10,000 each). No other disclosures relevant to this article were reported.

Address correspondence to Samy Suissa, PhD, Jewish General Hospital, Centre for Clinical Epidemiology, 3755 Cote St. Catherine, Montreal, Quebec H3T 1E2, Canada. Email: samy.suissa@mcgill.ca.

Submitted for publication January 5, 2021; accepted in revised form February 24, 2021.

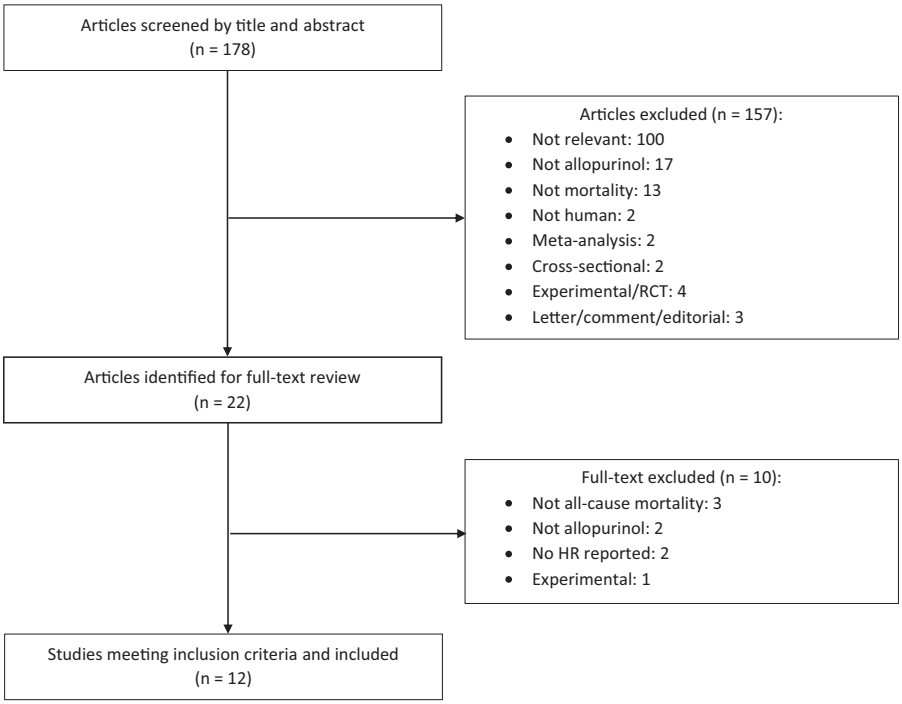

Figure 1. Selection of reviewed observational studies. RCT = randomized controlled trial; HR = hazard ratio.

Immortal time bias arises in cohort studies as a result of misclassifying as "exposed", rather than "unexposed", a period of follow-up in which, by design, the study outcome cannot occur. Immortal time is typically introduced when a patient's exposure/treatment status is determined after the start of the follow-up period. Immeasurable time bias results from periods of time in cohorts or case–control studies during which a subject cannot be recognized as being exposed to a drug because prescription records were not available. For example, if exposure is based on outpatient prescription records, data will be missing during hospitalizations, thus making the patient appear unexposed. These time-related biases tend to exaggerate the apparent benefit of drugs (11).

The inconsistent findings of the effect of allopurinol on mortality among observational studies and meta-analyses warrants a methodologic examination of these data. In this study, we review the observational studies of the effect of allopurinol on mortality in gout in order to assess potential sources of time-related bias that could explain these differences.

METHODS

We searched the literature for all publications of observational studies investigating the effectiveness of allopurinol use versus nonuse on the outcome of mortality. We searched PubMed on January 2, 2021 for keywords "allopurinol" and "mortality" and ("cohort" or "observational") with no restriction on publication date or time. We excluded comparative studies of allopurinol versus another urate-lowering therapy (ULT). The titles and abstracts of identified publications were independently screened in Endnote by 2 authors (KS and SS), with those deemed relevant by at least 1 author identified for full-text review. In addition, to find studies that were not identified in our PubMed search, we scanned the references of other reviews on allopurinol and mortality. Those included were observational studies that examined allopurinol monotherapy as an exposure and all-cause mortality as an outcome. We excluded studies that had nonhuman subjects, pediatric populations, studies that were not observational (randomized controlled trials, reviews, meta-analyses, letters, comments, and editorials), and studies with a cross-sectional design. The full texts of the remaining studies were reviewed, and studies meeting inclusion criteria were identified. The final

Table 1. Observational studies on the risk of death associated with allopurinol use

Author, year (ref.)	Patient population	Data source region
Struthers et al, 2002 (14)	Chronic heart failure	Scotland
Luk et al, 2009 (22)	Hyperuricemia	US
Wei et al, 2009 (9)	Chronic heart failure	Scotland
Thanassoulis et al, 2010 (19)	Heart failure*	Quebec, Canada
Gotsman et al, 2012 (15)	Chronic heart failure*	Israel
Tsuruta et al, 2014 (23)	Hemodialysis	Japan
Dubreuil et al, 2015 (24)	Hyperuricemia	UK
Kuo et al, 2015 (25)	Gout	UK
Chen et al, 2015 (8)	General population*	Taiwan
Larsen et al, 2016 (20)	Hyperuricemia	Denmark
Weisman et al, 2018 (21)	Diabetes and allopurinol use	Ontario, Canada
Ju et al, 2020 (26)	Gout	Hong Kong

* Data available for the subgroups with gout or hyperuricemia.

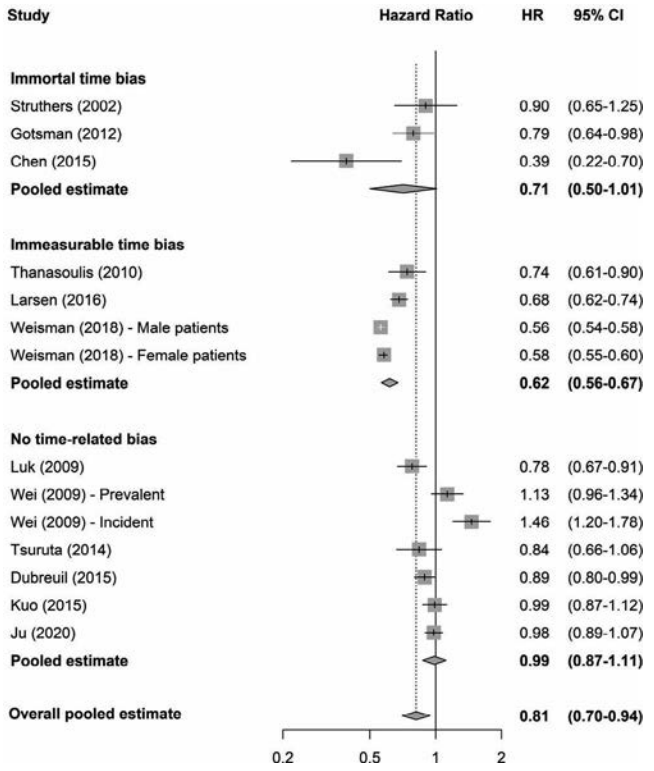

Figure 2. Forest plot of hazard ratios (HRs) of mortality associated with allopurinol use in the observational studies listed in Table 1, with pooled estimates from a random-effects model, according to studies affected by immortal time bias, those affected by immeasurable time bias, and those unaffected by time-related biases. 95% CI = 95% confidence interval.

selection of studies was classified according to potential time-related biases induced by the study design, including immortal time bias and immeasurable time bias (12,13). The HR of all-cause mortality with allopurinol use versus nonuse was extracted from each study, and, when available, the estimated HR among patients with gout was selected. Study-specific HRs were pooled using random-effect models and stratified by studies according to the type of time-related bias.

RESULTS

Study selection. We identified 178 potential studies, of which we found the majority to be reviews, editorials or opinion pieces, meta-analyses, observational studies comparing allopurinol to another ULT, or those in which allopurinol was not analyzed alone among ULTs (Figure 1). We therefore reviewed the full text of 12 studies that had findings on the effects of allopurinol on mortality in different patient populations (Table 1). Of the included studies, we identified 6 studies that were affected by time-related biases: 3 by immortal time bias, with a pooled HR of all-cause mortality with allopurinol use of 0.71 (95% CI 0.50–1.01), and 3 by immeasurable time bias (pooled HR 0.62 [95% CI 0.56–0.67]), while the remaining 6 studies avoided these biases (pooled HR 0.99 [95% CI 0.87–1.11]), with the results demonstrating wide variations (Figure 2).

Immortal time bias. Immortal time bias was identified in 3 of the studies (8,14,15). Immortal time refers to a period of follow-up during which the outcome under study cannot occur, usually because it involves the time from cohort entry to the start of the treatment under study (16). Misclassifying or excluding this period when defining treatment exposure will introduce immortal time bias (12).

An observational study by Gotsman et al, showing a 21% reduction in all-cause mortality associated with the use of allopurinol, is an example of immortal time bias from exposure misclassification (15). The study used electronic medical records from a health maintenance organization to identify a cohort of 6,201 patients with chronic heart failure with a median follow-up period of 16 months. The overall adjusted HR of death was 0.79 (95% CI 0.64–0.98). Immortal time bias was introduced in this study by classifying patients as exposed to allopurinol from the day of cohort entry, even if they only filled their first prescription during follow-up. The period between cohort entry and the first allopurinol prescription during follow-up is considered immortal time, as the patient must survive to receive this prescription. Moreover, the patient was unexposed to allopurinol during this immortal period, with the misclassification of this unexposed period resulting in immortal time bias (12). Figure 3 depicts this bias by comparing the survival times between 2 typical cohort patients, 1 "user" of allopurinol and 1 nonuser. Clearly, allopurinol users will necessarily have a longer survival, artificially created by this added immortal time. Such immortal time bias from exposure misclassification will result in an exaggerated protective effect of allopurinol exposure.

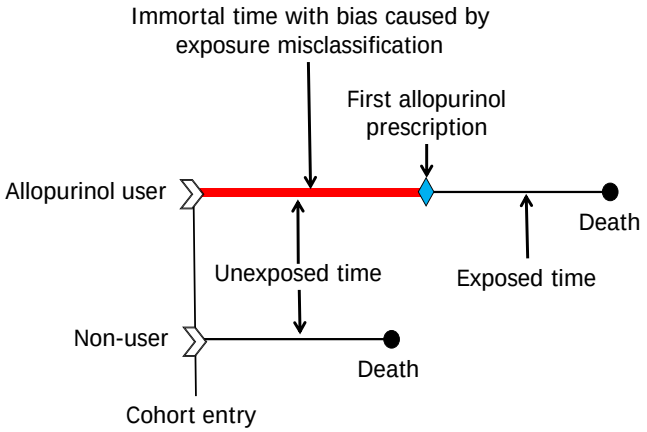

Figure 3. Immortal time bias in cohort studies classifying patients as users and nonusers of allopurinol. In the users group, the immortal time period between cohort entry and the first allopurinol prescription was misclassified as "exposed to allopurinol," when in fact the patient was unexposed. This immortal time should be counted as unexposed and added to the nonuser group person-time, while only the subsequent time should be counted as exposed to allopurinol treatment.

To illustrate the impact of the bias, we used data reported in the article and estimated necessary data that were not provided (15). We restricted this to patients with hyperuricemia (uric acid level >7.7 mg/dl), which included 305 allopurinol users and to 1,263 nonusers who were followed for up to 18 months. As the mean follow-up duration was not provided in the study, we used the Kaplan-Meier curves from one of the figures in the study to approximate the mean follow-up period for mortality at 526 and 511 days for allopurinol users and nonusers, respectively. For the purposes of illustrating the bias, we assumed a mean delay of 4 months between cohort entry and the first allopurinol prescription among users, as this was not provided in the study. There were 49 deaths among the 305 allopurinol users (439 person-years) and 278 deaths among the 1,263 nonusers (1,767 person-years). The 439 person-years of follow-up in the patients who received allopurinol include the immortal and unexposed person-time between cohort entry and the first allopurinol prescription, which should be added to the nonuser person-time (Figure 3).

Assuming a mean delay of 4 months between cohort entry and the first allopurinol prescription, a total of 101 immortal person-years would be misclassified as exposed. This 4-month delay is conservative, as suggested by a study from the UK that showed a median time from diagnosis of gout to initiation of allopurinol of 8 months (17). As shown in Table 2, by correctly reclassifying this person-time that is in fact unexposed, the rate of the unexposed group was 278/(1,767 + 101) = 14.9 per 100 person-years instead of 15.7 per 100 person-years. The rate in the allopurinol-exposed group was 49/(439 – 101) = 14.5 per 100 person-years instead of 11.2 per 100 person-years, resulting in a corrected crude rate ratio (RR) of 0.97, instead of a significant crude RR of 0.71 affected by immortal time bias. Table 2 also illustrates these calculations using a mean delay of 2 months and 6 months after cohort entry before allopurinol treatment initiation. It shows that the gap between the biased RR of 0.71 and the corrected RRs increased with longer immortal time periods.

An intriguing example of this bias is in the study by Chen et al, which demonstrates an HR of death of 0.39 (95% CI 0.22–0.70) with allopurinol and in which the authors claim that "matching for the index date of ULT prescription was performed to remove the immortal time bias between treatment and no treatment" (8).

Table 2. Comparison between biased time–fixed data analysis and corrected time–dependent data analysis of a cohort study of the effect of allopurinol on mortality*

	Allopurinol users (n = 305)			Allopurinol nonusers (n = 1,263)			
	Deaths	Person-years	Rate per 1,000 person-years	Deaths	Person-years	Rate per 1,000 person-years	Crude rate ratio (95% CI)
Assuming 2-month delay to allopurinol initiation							
Biased time–fixed analysis							
Immortal and unexposed person-time	0	51	–	0	0	–	–
At-risk person-time	49	388	–	278	1,767	–	–
Total	49	439	11.2	278	1,767	15.7	0.71 (0.52–0.96)
Corrected time–dependent analysis							
Immortal and unexposed person-time	0	0	–	0	51	–	–
At risk person-time	49	388	–	278	1,767	–	–
Total	49	388	12.6	278	1,818	15.3	0.80 (0.58–1.11)
Assuming 4-month delay to allopurinol initiation							
Biased time–fixed analysis							
Immortal and unexposed person-time	0	101	–	0	0	–	–
At risk person-time	49	338	–	278	1,767	–	–
Total	49	439	11.2	278	1,767	15.7	0.71 (0.52–0.96)
Corrected time–dependent analysis							
Immortal and unexposed person-time	0	0	–	0	101	–	–
At risk person-time	49	338	–	278	1,767	–	–
Total	49	338	14.5	278	1,868	14.9	0.97 (0.72–1.32)
Assuming 6-month delay to allopurinol initiation							
Biased time–fixed analysis							
Immortal and unexposed person-time	0	151	–	0	0	–	
At risk person-time	49	288	–	278	1,767	–	–
Total	49	439	11.2	278	1,767	15.7	0.71 (0.52–0.96)
Corrected time–dependent analysis							
Immortal and unexposed person-time	0	0	–	0	151	–	
At risk person-time	49	288	–	278	1,767	–	–
Total	49	288	17.0	278	1,918	14.5	1.21 (0.87–1.69)

* Based on data from a study of patients with heart failure and a uric acid level of >7.7 mg/dl, assuming a mean delay of 2, 4, and 6 months between cohort entry and allopurinol treatment initiation (see ref. 15). 95% CI = 95% confidence interval.

The methods, however, do not support this claim. The study used a cohort of 2,632 patients with gout, including 286 patients initiating allopurinol treatment who were propensity score–matched to 286 untreated patients with up to 7 years of follow-up for mortality. While the study matched patients according to the index date of allopurinol prescription, the data analysis started at the time of the gout diagnosis (8). Therefore, using the date of gout diagnosis as the start of follow-up in the data analysis rather than the date of the first allopurinol prescription can lead to immortal time bias.

Finally, the study by Struthers et al included a cohort of 1,760 patients with chronic heart failure, showing an HR of death of 0.90 (95% CI 0.65–1.25) with "recent low-dose" allopurinol (14). This analysis compared patients who received no allopurinol before cohort entry but who started to receive low-dose allopurinol at some point during the study follow-up (referred to as recent low-dose allopurinol) to patients who never received allopurinol. Clearly, the time between cohort entry and the first low-dose allopurinol prescription during follow-up was immortal and unexposed, thus introducing immortal time bias.

The solution to avoid immortal time bias is to use a time-dependent definition of exposure that includes and properly classifies exposure, as was illustrated in our recalculations using simple rates and proper reclassification of person-time (12). There are more refined ways to estimate the RR to account for these types of time-varying exposures, such as the Cox proportional hazards model with time-dependent factors (12). Alternatively, one could use approaches such as the prevalent new-user design which matches allopurinol users and nonusers at the same time point in the disease course, thus avoiding immortal time bias (18).

Immeasurable time bias. Immeasurable time bias affected 3 of the identified studies (19–21). It refers to a period of time during follow-up (for a cohort study) or prior to the index date (for a case–control study) during which a subject cannot be recognized as being exposed to the treatment (13). This problem is a consequence of the nature of some databases, in which exposure to the study drugs is typically assessed from outpatient prescription records, but is not available from inpatient sources. This can have an impact on studies in which the outcome is death. Indeed, several deaths may occur during hospitalization, so that patients hospitalized prior to death will appear to have received no prescriptions during this time, making exposure during this time period immeasurable. In studying serious chronic diseases that lead to frequent and lengthy hospitalizations, we know that deaths can be preceded by hospitalizations that span a portion of the exposure time period of interest.

In a case–control study on the use of a particular drug, patient deaths are compared to controls from the same disease population, usually around the index date defined as the date of death for the patient and the corresponding date for the controls. Most studies are generally interested in the effect of current drug treatment on mortality. Thus, patients and controls will be considered exposed to a drug if the subjects received a prescription for that drug that covers the index date or within a few days of it. Figure 4A illustrates this phenomenon in 2 subjects from a case–control study that uses an outpatient prescription of allopurinol in the 30-day period prior to the index date as the exposure definition. In a cohort approach, continuous exposure to the drug is generally defined by consecutive prescriptions during follow-up. Cohort follow-up stops at the end of continuous exposure or at death. Thus, hospitalizations occurring during follow-up can interrupt the continuity of exposure, so that subsequent deaths would not have been captured as exposed. Figure 4B illustrates this phenomenon in 2 subjects from a cohort study with exposure and hospitalizations occurring throughout follow-up.

A result of such immeasurable time in a case–control study is that exposed deaths will be misclassified as unexposed, while in a cohort study, a patient at the end of continuous treatment will appear to be alive, leading to bias from misclassification. This

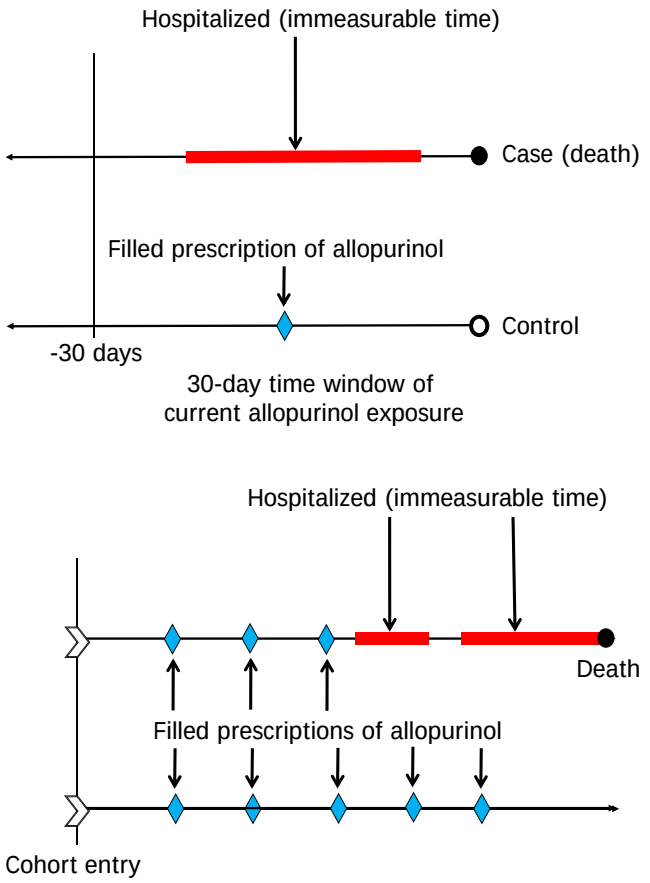

Figure 4. Immeasurable time bias from 2 studies. Top, A case–control study with a 30-day exposure time period prior to the index date, in which treatment exposure during time in hospital was immeasurable in databases (e.g., only outpatient prescriptions that defined treatment exposure could be identified). Bottom, A cohort study, in which 1 subject was hospitalized more frequently during the follow-up period, with immeasurable time periods for outpatient prescriptions that defined continuous treatment exposure.

immeasurable time phenomenon is especially pronounced in serious chronic diseases where hospitalizations preceding death are numerous and prolonged. The key reason for immeasurable time bias is that multiple hospitalizations preceding death, while likely associated with an increased risk of death, lead to an artificially lower probability of drug exposure, thus resulting in an underestimation of the rate or ORs.

An example of this bias in a case–control design is in the study by Thanassoulis et al that identified, within a cohort of patients hospitalized for heart failure and with a history of gout, all 1,053 deaths (cases) and 6,631 matched controls (19). Current allopurinol exposure was defined based on prescriptions dispensed at the time of the event date, i.e., if a filled prescription overlapped the event date, namely the date of death or the corresponding matched date for the controls. The resulting HR of death was 0.74 (95% CI 0.61–0.90) with current allopurinol use. While patients with heart failure often die while in the hospital after a lengthy hospitalization or are hospitalized just prior to death, no data on hospitalization during this period were provided. During these hospitalization episodes, the patient could not receive any outpatient prescriptions for allopurinol, as shown in Figure 4A. The time spent in hospital just prior to death, defining current exposure, is thus immeasurable due to the unavailability of information on prescriptions dispensed during hospitalizations in the database. If the cases had more immeasurable time than the controls (differentially among those who were exposed and those who were unexposed), immeasurable time bias would have occurred and resulted in the estimated RR underestimating the true OR.

The study by Weisman et al provides an example of this bias within a cohort design (21). The researchers identified a cohort of 38,416 new users of allopurinol, comparing mortality during exposed versus unexposed periods. Subjects were considered exposed during the time allopurinol was prescribed and for an additional 14 days beyond that to account for suboptimal adherence; otherwise, they were considered unexposed to treatment. The cohort generated 136,000 person-years of allopurinol-exposed time and 65,500 person-years of unexposed time, during which 22,012 deaths occurred. For allopurinol exposure versus no exposure, the HRs of death were 0.56 (95% CI 0.54–0.58) and 0.58 (95% CI 0.55–0.60), respectively, for male and female subjects. This study is subject to immeasurable time bias, since the end of allopurinol exposure could have been the result of a patient being hospitalized at that time. This is quite likely as 22% of the patients in the cohort had been hospitalized in the year prior to cohort entry, predicting an elevated rate of hospitalization during the follow-up period. Such informative censoring, particularly if a hospitalization ends in death, results in an underestimation of the true HR, since this exposed subject would have been classified as alive at the time of allopurinol "discontinuation." Consequently, immeasurable time bias makes allopurinol exposure appear protective for mortality (13).

An important clue regarding this bias is the difference in the effect of the drug on fatal and nonfatal outcomes. For example, the study by Larsen et al showed a highly significant HR of 0.68 (95% CI 0.62–0.74) for all-cause death associated with allopurinol use, but the HR of nonfatal myocardial infarction was not significant (0.89 [95% CI 0.73–1.08]) (20). Indeed, unlike death, the first hospitalization for myocardial infarction during follow-up is less likely to be preceded by multiple hospitalizations, resulting in less important immeasurable time and smaller bias. This bias was specifically mentioned by the authors as a possible explanation for the remarkable reduction in mortality (20).

Evidently, this bias does not apply to studies using complete integrated health care databases that capture both outpatient and inpatient drug use. However, all studies identified with this bias only captured outpatient prescriptions. The solution to avoid immeasurable time bias is to first identify all hospitalizations during follow-up. The timing and duration of these immeasurable time periods can then be taken into account by either defining exposure accordingly or using a weighted approach based on measurable time (13).

Studies avoiding time-related biases. We found 6 studies that addressed these 2 time-related biases (9,22–26). Four of the studies used a design that began follow-up at or after initiation of allopurinol exposure, with a comparable time point for nonusers that removed immortal time equally in both groups. For example, the study by Luk et al used a cohort of 9,924 subjects from Veterans Affairs databases, namely 2,483 allopurinol users and 7,441 nonusers, with a study design that avoided immortal time bias (22). Indeed, allopurinol users had to be recorded as having hyperuricemia (serum urate level >7.0 mg/dl) within 1 year prior to allopurinol initiation, while the nonusers were identified among those in the database who were alive at the time the user initiated allopurinol (index date) and also had hyperuricemia in the previous year.

On the other hand, 2 studies properly classified the immortal time as unexposed (9,26). For example, the study by Wei et al avoided immortal time bias at the data analysis stage by using a Cox proportional hazard model with a time-dependent variable for allopurinol use in the model, whereby the patients were considered unexposed until they started allopurinol treatment and were subsequently exposed (9). In the study by Ju et al "to address the issue of potential immortal time bias, the patient-years of xanthine oxidase inhibitor users between the diagnosis of gout and the start of xanthine oxidase inhibitor treatment were included in the xanthine oxidase inhibitor nonuser cohort for any analyses" (26). Thus, these authors correctly classified the unexposed immortal time, removing it from the xanthine oxidase inhibitor users group and adding it to the nonusers group.

Nevertheless, all 6 studies used an intent-to-treat approach for the data analysis, which does not consider adherence to allopurinol use. Thus, a single prescription of allopurinol was sufficient to establish exposure in most of these studies, which complicates the interpretation of results if adherence to allopurinol is poor.

Indeed, studies from different populations suggest that a minority of patients who initiate treatment with allopurinol continue to use it regularly (27–30). Another important issue in these studies is the control for confounding by indication, which should restrict studies to patients with gout and control for the level hyperuricemia prior to the initiation of allopurinol, as well as for comorbidity, which are all associated with mortality.

DISCUSSION

Observational studies are now used extensively to evaluate the real-world effectiveness of drugs, particularly with respect to major outcomes rarely available in randomized controlled trials (31). In this study, we evaluated methodologic aspects of 12 observational studies of the effects of allopurinol, used to treat gout and hyperuricemia, on all-cause mortality. When combined, the data from the 12 studies result in a pooled HR of all-cause mortality of 0.81 (95% CI 0.70–0.94) with allopurinol use. However, we found that 6 studies were subject to major time-related biases, particularly from immortal time (pooled HR 0.71 [95% CI 0.50–1.01]) and immeasurable time (pooled HR 0.62 [95% CI 0.56–0.67]), 2 types of bias that tend to overestimate the benefit of a drug. The 6 studies that avoided these biases in their design or data analysis found a null effect of allopurinol on mortality (pooled HR 0.99 [95% CI 0.87–1.11]).

Of the 2 sources of time-related bias identified in 6 studies, we found that immeasurable time bias results in a more pronounced distortion of results and a stronger impact on bias. For example, a case–control study of patients with ischemic heart disease, affected by this bias, suggested that a combination of statins, aspirin, and beta-blockers reduced all-cause mortality by a remarkable 83% (RR 0.17 [95% CI 0.12–0.73]) and that statins alone reduced all-cause mortality by 47% (RR 0.53 [95% CI 0.33–0.86]) (32). A cohort study of patients with congestive heart failure, also subject to this bias, showed that continuous use of statins was associated with reduced all-cause mortality (HR 0.67 [95% CI 0.57–0.78]) (33). These findings are quite dissimilar in magnitude from meta-analyses of large randomized trials that showed statins to be associated with a reduction in all-cause mortality of 16% (RR 0.84 [95% CI 0.79–0.89]) in similar patients with coronary heart disease (34). Correcting for immeasurable time bias can lead to major readjustments. For example, a case–control analysis of patients with chronic obstructive pulmonary disease showed an RR of death of 0.60 (95% CI 0.50–0.73) with inhaled glucocorticoids. However, after weighting with the measurable time to account for the timing and duration of hospitalizations, the RR increased to 0.98 (95% CI 0.83–1.17) (13). These examples confirm that the magnitude of immeasurable time bias can be substantial.

Immortal time bias, arising from the misclassification of exposure to allopurinol and the exclusion of subjects, was also present in 3 studies. Unlike immeasurable bias that depends on more intricate weighted analyses, immortal time bias is easily corrected. It does not require any additional data but rather a proper approach to study design or a data analysis that correctly classifies exposure over time. This bias was recently identified in several observational studies that showed important protective effects of statins on mortality in patients with various rheumatic diseases (35). The study by Wei et al is an interesting example of the impact of this bias (9). The crude rate of death for the incident allopurinol users was 97 per 1,000 person-years compared to 146 for nonusers, resulting in a "protective" RR of 0.66, which changed to 1.46 after properly classifying the immortal time prior to allopurinol initiation in the users (9). In contrast, 6 of the 12 studies avoided immortal time bias by using a proper study design or data analysis.

Bias from confounding by indication should be an important consideration in these observational studies, since allopurinol is indicated for gout, especially in patients with significant hyperuricemia, both of which are associated with increased mortality. However, some studies did not control for this important factor. Indeed, some studies did not consider gout at all, while others considered the condition but did not control for the level of uric acid (9,14). For example, the study by Wei and colleagues included patients with congestive heart failure, but comparing users of allopurinol to nonusers inherently included more patients with gout in the users group, which can confound the risk estimate (9). The resulting adjusted HR of 1.46 (95% CI 1.20–1.78), estimated after avoiding immortal time bias, could thus be subject to residual confounding by the absence of adjustment for gout and its severity. It is essential to account for such confounding by restricting studies of these drugs to patients with indications of gout.

Moreover, studies conducted in patients with gout should match or control for the level of uric acid measured prior to the initiation of allopurinol treatment. One should avoid adjusting for a uric acid level measured after allopurinol exposure, as was done in the study by Tsuruta et al (23). In that study, the Dialysis Outcomes and Practice Patterns Study registry of patients with dialysis collected data on uric acid level and allopurinol at baseline, which does not ensure the timing of uric acid level preceding allopurinol initiation. Finally, the 2 studies that avoided time-related biases and included extensive data to adjust for gout severity, including adjustment for uric acid level prior to allopurinol initiation, suggest a potential modest benefit on mortality, although they could not rule out residual confounding (22,24).

Time-related biases, especially immortal time bias, are particularly a concern in studies in which a comparison is made to nonusers, rather than to active comparators (11). Indeed, comparing patients receiving allopurinol to those not receiving allopurinol presents a challenge regarding where to start follow-up for the latter group. Therefore, such studies with nonuser comparators should raise a red flag with respect to the presence of immortal time bias, particularly if the results suggest a remarkable benefit for the study drug. Study designs such as the prevalent new-user

design or a marginal structural approach that emulates randomized trials avoid immortal time bias (18,36). Moreover, these study designs allow for treatment adherence to be addressed and can reduce confounding, although such studies require rich data sources with available and accurate information on medications, clinical diagnoses, and laboratory measures.

In conclusion, while observational studies are important to assess the real-world effects of medications on major outcomes, proper design and analysis are essential to minimize bias. The observational studies demonstrating significantly decreased mortality with allopurinol use cannot be used as evidence, mainly due to immortal and immeasurable time biases. These time-related biases, which tend to greatly exaggerate the benefit of drugs and are prevalent in observational studies of allopurinol on mortality, are correctable. The studies that avoided these biases found a null effect of allopurinol on mortality. The ALL-HEART randomized controlled trial comparing allopurinol to placebo, which is currently underway with results expected in 2021, will provide evidence on the outcome of mortality (7).

AUTHOR CONTRIBUTIONS

All authors were involved in drafting the article or revising it critically for important intellectual content, and all authors approved the final version to be published. Dr. S. Suissa had full access to all of the data in the study and takes responsibility for the integrity of the data and the accuracy of the data analysis.

Study conception and design. S. Suissa, K. Suissa, Hudson.
Acquisition of data. S. Suissa, K. Suissa.
Analysis and interpretation of data. S. Suissa, K. Suissa, Hudson.

REFERENCES

1. Clarson LE, Chandratre P, Hider SL, Belcher J, Heneghan C, Roddy E, et al. Increased cardiovascular mortality associated with gout: a systematic review and meta-analysis. Eur J Prev Cardiol 2015;22:335–43.
2. Gupta MK, Singh JA. Cardiovascular disease in gout and the protective effect of treatments including urate-lowering therapy [review]. Drugs 2019;79:531–41.
3. Fisher MC, Rai SK, Lu N, Zhang Y, Choi HK. The unclosing premature mortality gap in gout: a general population-based study. Ann Rheum Dis 2017;76:1289–94.
4. Mitchell S, Liedgens H, Johannes E. THU0462 Mortality in patients with gout: a systematic review [poster]. Ann Rheum Dis 2017;76:382.
5. FitzGerald JD, Dalbeth N, Mikuls T, Brignardello-Petersen R, Guyatt G, Abeles AM, et al. 2020 American College of Rheumatology guideline for the management of gout. Arthritis Rheumatol 2020; 72:879–95.
6. Bredemeier M, Lopes LM, Eisenreich MA, Hickmann S, Bongiorno GK, d'Avila R, et al. Xanthine oxidase inhibitors for prevention of cardiovascular events: a systematic review and meta-analysis of randomized controlled trials. BMC Cardiovasc Disord 2018;18:24.
7. Mackenzie IS, Ford I, Walker A, Hawkey C, Begg A, Avery A, et al. Multicentre, prospective, randomised, open-label, blinded end point trial of the efficacy of allopurinol therapy in improving cardiovascular outcomes in patients with ischaemic heart disease: protocol of the ALL-HEART study. BMJ Open 2016;6:e013774.
8. Chen JH, Lan JL, Cheng CF, Liang WM, Lin HY, Tsay GJ, et al. Effect of urate-lowering therapy on the risk of cardiovascular disease and all-cause mortality in patients with gout: a case-matched cohort study. J Rheumatol 2015;42:1694–701.
9. Wei L, Fahey T, Struthers AD, MacDonald TM. Association between allopurinol and mortality in heart failure patients: a long-term follow-up study. Int J Clin Pract 2009;63:1327–33.
10. Hay CA, Prior JA, Belcher J, Mallen CD, Roddy E. Mortality in patients with gout treated with allopurinol: a systematic review and meta-analysis. Arthritis Care Res (Hoboken) 2020 doi: https://onlinelibrary.wiley.com/doi/10.1002/acr.24205. E-pub ahead of print.
11. Suissa S, Dell'Aniello S. Time-related biases in pharmacoepidemiology. Pharmacoepidemiol Drug Saf 2020;29:1101–10.
12. Suissa S. Immortal time bias in pharmacoepidemiology. Am J Epidemiol 2008;167:492–9.
13. Suissa S. Immeasurable time bias in observational studies of drug effects on mortality. Am J Epidemiol 2008;168:329–35.
14. Struthers AD, Donnan PT, Lindsay P, McNaughton D, Broomhall J, MacDonald TM. Effect of allopurinol on mortality and hospitalisations in chronic heart failure: a retrospective cohort study. Heart 2002;87:229–34.
15. Gotsman I, Keren A, Lotan C, Zwas DR. Changes in uric acid levels and allopurinol use in chronic heart failure: association with improved survival. J Card Fail 2012;18:694–701.
16. Suissa S. Immortal time bias in observational studies of drug effects. Pharmacoepidemiol Drug Saf 2007;16:241–9.
17. Clarson LE, Hider SL, Belcher J, Roddy E, Mallen CD. Factors influencing allopurinol initiation in primary care. Ann Fam Med 2017;15:557–60.
18. Suissa S, Moodie EE, Dell'Aniello S. Prevalent new-user cohort designs for comparative drug effect studies by time-conditional propensity scores. Pharmacoepidemiol Drug Saf 2017;26:459–68.
19. Thanassoulis G, Brophy JM, Richard H, Pilote L. Gout, allopurinol use, and heart failure outcomes. Arch Intern Med 2010;170: 1358–64.
20. Larsen KS, Pottegård A, Lindegaard HM, Hallas J. Effect of allopurinol on cardiovascular outcomes in hyperuricemic patients: a cohort study. Am J Med 2016;129:299–306.
21. Weisman A, Tomlinson GA, Lipscombe LL, Perkins BA, Hawker GA. Association between allopurinol and cardiovascular outcomes and all-cause mortality in diabetes: a retrospective, population-based cohort study. Diabetes Obes Metab 2019;21:1322–9.
22. Luk AJ, Levin GP, Moore EE, Zhou XH, Kestenbaum BR, Choi HK. Allopurinol and mortality in hyperuricaemic patients. Rheumatology (Oxford) 2009;48:804–6.
23. Tsuruta Y, Nitta K, Akizawa T, Fukuhara S, Saito A, Karaboyas A, et al. Association between allopurinol and mortality among Japanese hemodialysis patients: results from the DOPPS. Int Urol Nephrol 2014;46:1833–41.
24. Dubreuil M, Zhu Y, Zhang Y, Seeger JD, Lu N, Rho YH, et al. Allopurinol initiation and all-cause mortality in the general population. Ann Rheum Dis 2015;74:1368–72.
25. Kuo CF, Grainge MJ, Mallen C, Zhang W, Doherty M. Effect of allopurinol on all-cause mortality in adults with incident gout: propensity score-matched landmark analysis. Rheumatology (Oxford) 2015;54:2145–50.
26. Ju C, Lai RW, Li KH, Hung JK, Lai JC, Ho J, et al. Comparative cardiovascular risk in users versus non-users of xanthine oxidase

inhibitors and febuxostat versus allopurinol users. Rheumatology (Oxford) 2020;59:2340–9.

27. Zandman-Goddard G, Amital H, Shamrayevsky N, Raz R, Shalev V, Chodick G. Rates of adherence and persistence with allopurinol therapy among gout patients in Israel. Rheumatology (Oxford) 2013; 52:1126–31.
28. Singh JA, Richman J, Yang S, Bridges SL, Saag K. Allopurinol adherence and its predictors in gout: a national cohort study in US veterans. Lancet Rheumatol 2020;2:e281–91.
29. Scheepers L, van Onna M, Stehouwer CD, Singh JA, Arts IC, Boonen A. Medication adherence among patients with gout: a systematic review and meta-analysis. Semin Arthritis Rheum 2018; 47:689–702.
30. Scheepers L, Burden AM, Arts IC, Spaetgens B, Souverein P, de Vries F, et al. Medication adherence among gout patients initiated allopurinol: a retrospective cohort study in the Clinical Practice Research Datalink (CPRD). Rheumatology (Oxford) 2018;57:1641–50.
31. Sherman RE, Anderson SA, Dal Pan GJ, Gray GW, Gross T, Hunter NL, et al. Real-world evidence—what is it and what can it tell us? N Engl J Med 2016;375:2293–7.
32. Hippisley-Cox J, Coupland C. Effect of combinations of drugs on all cause mortality in patients with ischaemic heart disease: nested case-control analysis. BMJ 2005;330:1059–63.
33. Ray JG, Gong Y, Sykora K, Tu JV. Statin use and survival outcomes in elderly patients with heart failure. Arch Intern Med 2005;165:62–7.
34. Wilt TJ, Bloomfield HE, MacDonald R, Nelson D, Rutks I, Ho M, et al. Effectiveness of statin therapy in adults with coronary heart disease. Arch Intern Med 2004;164:1427–36.
35. Abrahami D, Hudson M, Suissa S. Statins and lower mortality in rheumatic diseases: an effect of immortal time bias? Semin Arthritis Rheum 2021;51:211–8.
36. Hernán MA, Sauer BC, Hernández-Díaz S, Platt R, Shrier I. Specifying a target trial prevents immortal time bias and other self-inflicted injuries in observational analyses. J Clin Epidemiol 2016;79:70–5.

American College of Rheumatology
Empowering Rheumatology Professionals

Arthritis & Rheumatology
Vol. 73, No. 9, September 2021, pp 1758–1764
DOI 10.1002/art.41691

Elevated Urate Levels Do Not Alter Bone Turnover Markers: Randomized Controlled Trial of Inosine Supplementation in Postmenopausal Women

Nicola Dalbeth,[1] Anne Horne,[1] Borislav Mihov,[1] Angela Stewart,[1] Gregory D. Gamble,[1] Tony R. Merriman,[2] Lisa K. Stamp,[3] and Ian R. Reid[1]

Objective. Observational studies have consistently demonstrated that serum urate level positively correlates with bone mineral density (BMD). We undertook this study to determine whether moderate hyperuricemia induced by inosine supplements influences bone turnover markers in postmenopausal women over a 6-month period.

Methods. One hundred twenty postmenopausal women were recruited for a 6-month randomized, double-blind, placebo-controlled trial. Key exclusion criteria were osteoporosis, previous fragility fracture, bisphosphonate therapy, gout, kidney stones, and a urine pH level of ≤5.0. Participants were randomized in a 1:1 ratio to receive placebo or inosine. The coprimary end points were change in levels of N-propeptide of type I procollagen (PINP) and change in levels of β-C-telopeptide of type I collagen (β-CTX). Change in BMD, as measured by dual x-ray absorptiometry, was an exploratory end point.

Results. Administration of inosine led to a significant increase in serum urate concentration over the study period ($P < 0.0001$ for all follow-up time points). At week 26, the mean change in serum urate concentration was +0.13 mmoles/liter (+2.2 mg/dl) in the inosine group and 0.00 mmoles/liter (0 mg/dl) in the placebo group. There was no difference in PINP or β-CTX levels between groups over the 6 months. There were no significant changes in bone density between groups over the 6 months. Adverse events and serious adverse events were similar between the 2 groups.

Conclusion. This clinical trial shows that although inosine supplementation leads to sustained increases in serum urate levels over a 6-month period, it does not alter markers of bone turnover in postmenopausal women. These findings do not support the concept that urate has direct biologic effects on bone turnover.

INTRODUCTION

Observational studies have consistently shown that hyperuricemia is protective against the development of osteoporosis (1). In many populations, serum urate concentrations positively correlate with bone mineral density (BMD) (2–8). Furthermore, higher serum urate concentrations have been associated with reduced risk of fragility fractures (4,9,10). Some laboratory data have supported the hypothesis that urate, a potent antioxidant, has a direct effect on bone to increase BMD. In rat bone marrow osteoclastogenesis assays, soluble urate reduced osteoclast formation (3). Additionally, an analysis of human bone mesenchymal stem cells demonstrated that culture with soluble urate promoted proliferation, increased osteogenic differentiation, and inhibited adipogenic differentiation of these cells (11). Collectively, these data suggest that urate has an anabolic effect on bone.

Despite these positive results, it remains uncertain whether urate has a clinically significant direct effect on bone. Although a strong association between serum urate level and BMD was observed in the third generation cohort in the Framingham Heart Study, in a Mendelian randomization analysis of the same cohort, there was no evidence that urate had a causal effect on BMD (6).

Supported by Auckland Medical Research Foundation Project grant 1118012.

[1]Nicola Dalbeth, MD, FRACP, Anne Horne, MBChB, Borislav Mihov, BPhty, Angela Stewart, RN, Gregory D. Gamble, MSc, Ian R. Reid, MD, FRACP: University of Auckland, Auckland, New Zealand; [2]Tony R. Merriman, PhD: University of Otago, Dunedin, New Zealand, and University of Alabama at Birmingham; [3]Lisa K. Stamp, PhD, FRACP: University of Otago, Christchurch, New Zealand.

Dr. Dalbeth has received consulting fees, speaking fees, and/or honoraria from AstraZeneca, Horizon, Amgen, Selecta, Arthrosi, Dyve BioSciences, Hengrui, AbbVie, and Janssen (less than $10,000 each). Dr. Reid has received consulting fees, speaking fees, and/or honoraria from Novartis, Eli Lilly, Amgen, and Merck (less than $10,000 each). No other disclosures relevant to this article were reported.

Address correspondence to Nicola Dalbeth, MD, FRACP, University of Auckland, Faculty of Medical and Health Sciences, Department of Medicine, 85 Park Road, Grafton, Auckland, New Zealand. Email: n.dalbeth@auckland.ac.nz.

Submitted for publication December 8, 2020; accepted in revised form February 9, 2021.

Furthermore, a series of in vitro assays did not show evidence of direct anabolic interaction between soluble urate and bone cells (12), and in a rat model of inducible mild hyperuricemia, no alterations were observed in BMD, bone volume density, or bone biomechanical properties (13).

Inosine is a purine nucleoside, available as an over-the-counter nutritional supplement, that increases serum urate concentrations. Inosine is metabolized in vivo from AMP as part of the purine salvage metabolic pathway. It is degraded to hypoxanthine, which is, in turn, metabolized to xanthine and then urate in the purine degradation pathway. Oral supplementation of inosine is currently under clinical investigation for neuroprotection against multiple sclerosis and Parkinson's disease (14–16), due to its ability to increase serum urate concentrations.

Given the numerous observational studies demonstrating a positive association between serum urate concentrations and both BMD and fracture risk, as well as the ability of inosine supplements to increase serum urate concentrations, we undertook a randomized placebo-controlled trial in healthy postmenopausal women to determine the efficacy and safety of inosine-induced moderate hyperuricemia on bone turnover markers.

PATIENTS AND METHODS

This study was a randomized, double-blind, placebo-controlled trial of 120 postmenopausal female participants that lasted 6 months. The study was approved by the New Zealand Ministry of Health Southern Health and Disability Ethics Committee (no. 17/STH/102), and all participants provided written informed consent. The trial was prospectively registered with the Australia and New Zealand Clinical Trials Registry (no. ACTRN12617000940370). The study was undertaken at a single study site (Clinical Research Centre, University of Auckland) in Auckland, New Zealand. The first study visit occurred on April 17, 2018, and the final study visit occurred on September 30, 2019.

The hypothesis of this study was that moderate hyperuricemia (serum urate level <0.48 mmoles/liter [8.0 mg/dl]) caused by inosine supplements would result in a change in bone turnover markers during a 6-month period. Participants were randomized in a 1:1 ratio to receive either placebo or inosine. The coprimary end points included change in serum N-propeptide of type I procollagen (PINP) levels and change in serum β-C-telopeptide of type I collagen (β-CTX) levels.

Recruitment and inclusion criteria. Letters of invitation were sent to women ages 55 years and older, randomly selected from the New Zealand parliamentary electoral roll. Inclusion criteria were as follows: age ≥55 years; postmenopausal; female; estimated glomerular filtration rate >60 ml/minute; serum urate level <0.42 mmoles/liter (7 mg/dl); and ability to provide written informed consent and attend study visits. Exclusion criteria were as follows: BMD T score <−2.5 at the total hip, femoral neck, or lumbar spine; previous fragility fracture of the hip or clinical spine fracture; current or past use (within 12 months) of medications that can affect bone turnover markers, including bisphosphonate therapy and hormone replacement therapy, or any past zoledronate use; history of gout; history of kidney stones; history of diabetes mellitus; current use of diuretic medications; urine pH level ≤5.0 (risk factor for uric acid urolithiasis); and/or current use of inosine as a nutritional supplement.

Interventions. Participants were randomized to 1 of 2 groups: placebo or inosine (n = 60 participants per group). Treatment assignment was allocated randomly within blocks of varying size using random numbers drawn from a pseudorandom number generator (Excel 2010).

Participants were asked to take study medication in the morning and evening (before 7:00 PM). All participants were advised to drink 2 liters of fluids per day. Placebo tablets consisted of lactose, microcrystalline cellulose, and magnesium stearate. Inosine and placebo tablets were the same color and had identical packaging.

The initial inosine dose was based on our prior study in which acute increases in serum urate levels were induced using a commercially produced inosine supplement (Source Naturals) (17). Based on that study, we estimated that 1.5 gm of inosine (2 × 500 mg tablets in the morning and 1 × 500 mg tablet in the evening) would increase the serum urate concentration by 0.10 mmoles/liter. However, we were unable to purchase sufficient tablets from the commercial manufacturer for use in the current trial. Therefore, inosine supplements were compounded by Optimus Healthcare, a registered pharmacy that specializes in compounding for pharmaceutical formulations. Given the change in compounding, a preplanned blinded review of serum urate concentrations at the week 6 visit was undertaken for the first 10 participants. This blinded review demonstrated increases in serum urate concentrations of 0.20 mmoles/liter (3.3 mg/dl) in some participants. This change was higher than in our previous study and likely reflected differences in compounded inosine compared to the commercially available inosine supplement used in our previous study. To ensure a state of moderate hyperuricemia (<0.48 mmoles/liter [<8.0 mg/dl]) in the inosine group, the following changes were made to the study protocol after the blinded review: all 10 participants were advised to reduce their study medication to 1 tablet (500 mg inosine or placebo) twice daily, and the starting inosine (and matched placebo) dose was reduced to 1 tablet twice daily for all subsequent participants.

Prelabeling of tablet bottles was performed by staff members who had no contact with the study participants and no role in study procedures such as assessments of end points. All personnel who had contact with study participants and the participants themselves were blinded with regard to treatment allocation and serum urate concentrations during the study. Serum urate was checked at each study visit, using the Roche/Hitachi Modular P analyzer. If a participant's serum urate level was ≥0.48 mmoles/liter

(≥8 mg/dl), the inosine dose was reduced by 500 mg. To maintain blinding for study participants and staff, serum urate measurements were visible only to staff members who had no contact with study participants. In the event of dose reduction in a participant from the inosine group, that participant was matched by the study statistician (GDG) to a participant in the placebo group who had placebo dose reduction at the same study visit. At the end of the study, participants completed a questionnaire to assess study blinding, with options of "active treatment," "placebo," and "don't know." Completed study blinding questionnaires were available for 54 participants in each group at the final study visit; 13 participants (24%) in the placebo group and 16 participants (30%) in the inosine correctly identified their allocation.

Visit schedules. Participants had a screening visit within a month of the baseline study visit, a clinic visit with randomization at 0 weeks, and a study visit at 6 weeks, 13 weeks, 19 weeks, and 26 weeks. Adherence was assessed using counts of returned tablets. Any adverse events (AEs) and serious AEs (SAEs) were recorded at all follow-up visits. AEs were monitored by an independent safety monitor blinded with regard to treatment allocation.

Study end points. The coprimary end points were detection of change in a serum marker of bone formation (PINP) and a marker of bone resorption (β-CTX). PINP and β-CTX are recommended as reference markers in intervention studies by the International Osteoporosis Foundation and International Federation of Clinical Chemistry and Laboratory Medicine (18). Fasting blood samples were collected at each study visit, and serum was stored at –80°C until analysis. PINP and β-CTX were assessed in batches at the completion of the study using the Roche Elecsys 2010 platform. Coefficients of variation of these markers were 5.1% for β-CTX and 1.9% for PINP.

Change in BMD was an exploratory end point. BMD was measured at baseline and after 6 months at the total body, lumbar spine (L1–L4), and proximal femur, using a GE Prodigy dual x-ray absorptiometer.

Sample size calculation. We calculated 60 participants per group, with a potential 15% loss to follow-up over the 6-month period. Estimates of the SD of the change in bone turnover markers β-CTX (0.195) and PINP (15.2) to 6 months were obtained from a clinical trial of low-dose zoledronate (19). Fifty-one subjects per group would be needed in order to yield 90% power at the 2.5% significance level for a 2-tailed test to detect differences of 0.14 ng/ml and 10.5 ng/ml in the change in β-CTX and PINP, respectively, to 6 months. These differences represent 30% and 20% of the baseline values of β-CTX and PINP, respectively, and were considered clinically relevant. The significance level was equally divided between these 2 coprimary end points. Sample size calculations were made using PASS 2002 (www.ncss.com).

Statistical analysis. Data are presented as the mean ± SD or the median (IQR) for descriptive purposes. Measures of effect are presented with the appropriate 95% confidence intervals (95% CIs). The primary analysis was a comparison of the change in PINP and β-CTX levels, based on treatment allocation (placebo versus inosine) over the 6-month period. Data were analyzed on an intent-to-treat basis, using a mixed-model approach to repeated measures. False detection rate–protected pairwise comparisons were performed at each time point using the mixed-model variances. All analyses were performed using SAS (version 9.4). As there were 2 coprimary end points, *P* values less than 0.025 were considered significant, and all tests were 2-tailed. Two sensitivity analyses were performed: a per-protocol analysis and an analysis in which missing data were imputed. The per-protocol analysis only included participants

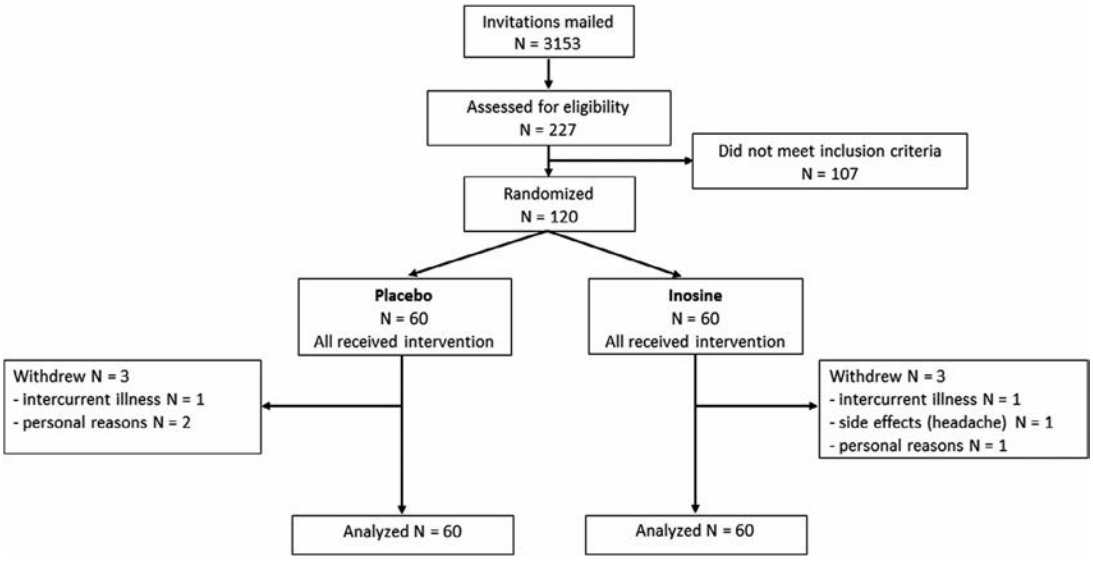

Figure 1. Flow chart of the included study participants.

Table 1. Baseline characteristics of the study participants*

	Placebo (n = 60)	Inosine (n = 60)
Age, years	68.8 ± 1.9	68.2 ± 2.3
Ethnicity, no. (%)		
NZ European	59 (98)	58 (97)
NZ Māori	1 (2)	0
NZ Asian	0	2 (3)
Weight, kg	72.4 ± 12.6	67.5 ± 10.9
BMI, kg/m^2	27.3 ± 4.7	26.1 ± 4.2
Previous fracture, no. (%)†	29 (48)	24 (40)
Creatinine (μmoles/liter)	63.3 ± 8.6	62.5 ± 8.7
Serum urate		
mmoles/liter	0.28 ± 0.06	0.27 ± 0.06
mg/dl	4.7 ± 1.0	4.5 ± 1.0
PINP, μg/liter	62.0 ± 16.9	59.9 ± 18.3
β-CTX, ng/ml	0.49 ± 0.16	0.45 ± 0.13
Total body BMD, gm/cm^2	1.11 ± 0.08	1.09 ± 0.09
Lumbar spine (L1–L4) BMD, gm/cm^2	1.13 ± 0.15	1.09 ± 0.15
Neck of femur BMD, gm/cm^2	0.91 ± 0.11	0.88 ± 0.10
Total hip BMD, gm/cm^2	0.97 ± 0.12	0.92 ± 0.10

* Except were indicated otherwise, values are the mean ± SD. NZ = New Zealand; BMI = body mass index; PINP = N-propeptide of type I procollagen; β-CTX = β-C-telopeptide of type I collagen; BMD = bone mineral density.
† During lifetime.

with >80% adherence to the study medication. For the imputed analysis, replacement data for missing values were imputed using a standard Markov chain Monte Carlo approach. Five separate data sets were created, and the MIANALYZE procedure in SAS was used to appropriately create multivariate inferences from these imputed data sets.

RESULTS

The flow chart of participants included in this study is shown in Figure 1. There were 227 women assessed for eligibility, and 120 participants were randomized to treatment groups. Of these, 3 participants from each group withdrew from the study. Data from all participants were included in the primary (intent-to-treat) analysis.

Selected participant characteristics are shown in Table 1. The average age was 68 years, and most participants were of New Zealand European ethnicity. The mean baseline serum urate level was 0.28 mmoles/liter (4.7 mg/dl) in the placebo group and 0.27 mmoles/liter (4.5 mg/dl) in the inosine group.

Administration of inosine supplements led to a significant increase in serum urate concentration during the study period ($P < 0.0001$ for all follow-up time points) (Figure 2A and Supplementary Table 1, available on the *Arthritis & Rheumatology* website at http://onlinelibrary.wiley.com/doi/10.1002/art.41691/abstract). At week 26, the mean change in serum urate level was 0.00 mmoles/liter (0 mg/dl) in the placebo group and +0.13 mmoles/liter (+2.2 mg/dl) in the inosine group (Supplementary Table 2, http://onlinelibrary.wiley.com/doi/10.1002/art.41691/abstract). For participants in the inosine group, the mean ± SD dose of inosine was 517 ± 91 mg/day at week 26.

There was no significant difference in PINP or β-CTX values between groups during the 6-month study period ($P > 0.61$ for

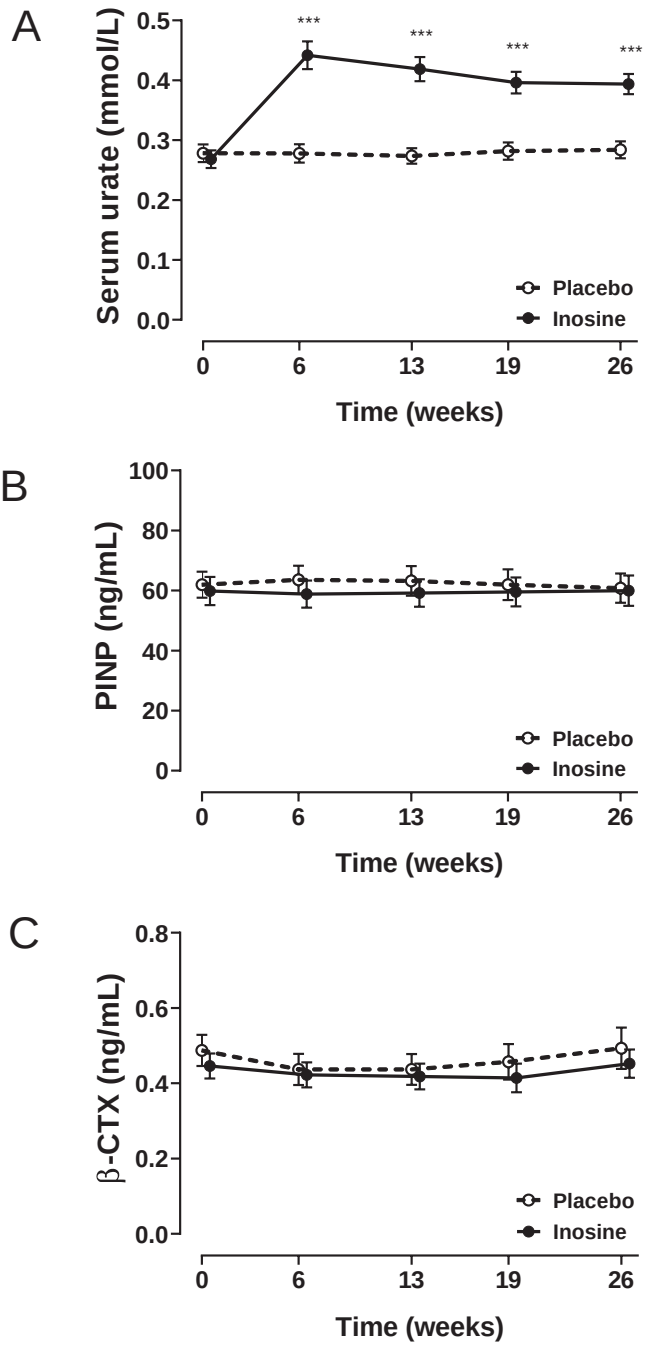

Figure 2. Serum urate concentrations and bone turnover markers during the study period. **A**, Serum urate. **B**, N-propeptide of type I procollagen (PINP). **C**, β-C-telopeptide of type I collagen (β-CTX). Data are presented as the mean (95% confidence interval). *** = $P < 0.0001$ for false detection rate–protected pairwise comparisons at each time point.

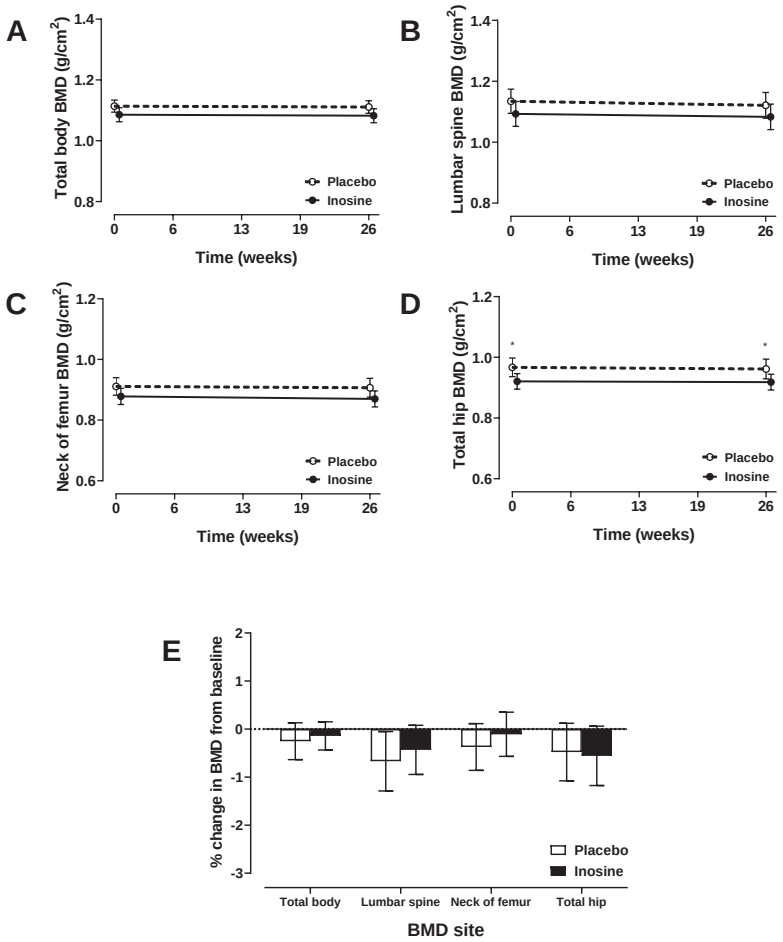

Figure 3. Bone mineral density (BMD) measurements during the study period. **A**, Total body BMD. **B**, Lumbar spine (L1–L4) BMD. **C**, Neck of femur BMD. **D**, Total hip BMD. **E**, Percentage change in BMD from baseline to week 26 at each site. Data are presented as the mean (95% confidence interval). * = $P < 0.05$ for false detection rate–protected pairwise comparisons at each time point.

PINP; $P > 0.37$ for β-CTX for all time points) (Figures 2B and C and Supplementary Tables 1 and 2). Furthermore, there were no significant between-group differences in total body, lumbar spine, or neck of femur BMD during the study period (Figure 3 and Supplementary Tables 1 and 2). Total femur BMD values were lower in the inosine group at baseline and 6 months ($P = 0.033$ at both time points), but there was no between-group difference over time (P for treatment × time interaction = 0.48 by analysis of variance).

Adherence data were available for 116 participants (4 participants did not return any tablets, so adherence data was missing for these participants). Of the 116 who returned tablets, the median adherence was 97% (IQR 90.9–99.5%): 97.1% in the placebo group and 97.2% in inosine group. Adherence of ≥80% was observed in 55 of 60 participants in each group. Sensitivity analyses for both the per-protocol data set and the imputed data set showed similar findings to the intent-to-treat analysis (data not shown).

AEs and SAEs were similar between the 2 groups (Table 2 and Supplementary Table 3, http://onlinelibrary.wiley.com/doi/10.1002/art.41691/abstract). There was 1 SAE in the placebo group and 4 SAEs in the inosine group. None of the SAEs were considered to be due to the study medication. No participant died during the study.

Table 2. Number of serious adverse events and adverse events during the study period

	Placebo (n = 60)	Inosine (n = 60)
Serious adverse events		
Cancer	0	2
Gastrointestinal	0	1
Infection	0	1
Miscellaneous*	1	0
Total	1	4
Adverse events		
Allergy	0	1
Cardiovascular	1	1
Fracture†	4	0
Gastrointestinal	6	10
Infection	13	11
Injury	6	2
Miscellaneous	6	8
Musculoskeletal	8	9
Total	44	42

* Hospital admission with femoral hernia.
† Fracture sites included tibial plateau (n = 1), distal fibula (n = 2), and metatarsal (n = 2).

DISCUSSION

In this randomized, double-blind, placebo-controlled trial of postmenopausal women, inosine supplementation led to sustained increases in serum urate concentrations over a 6-month period. However, there were no convincing effects of elevated urate levels on bone turnover markers or BMD in an exploratory analysis.

The results of this study are consistent with the following findings: previous clinical trial data on urate-lowering therapy that did not demonstrate between-group differences in BMD (12), Mendelian randomization data that did not demonstrate a causal effect of urate on BMD (6), data from a rat model that did not demonstrate changes in BMD in the setting of inducible hyperuricemia (13), and in vitro studies that did not show direct effects of soluble urate on osteoclast, osteoblast, or osteocyte function (12). These findings contrast with findings from numerous observational studies that have shown an association between elevated urate levels and BMD (2–8). It is conceivable that exposure to elevated urate levels over a longer duration or before menopause might have a biologic effect. However, discordance between results from observational studies and clinical trials is not unusual in bone research (20). It is possible that associations in observational studies demonstrating elevated urate and BMD represent residual confounding, potentially related to body mass index, visceral fat mass, or total body fat, which are associated with higher BMD as well as elevated urate levels (21). It is also theoretically possible that urate could affect bone density or strength without impacting bone turnover markers, but there is no evidence of any other factor having a clinically significant effect on bone health without some change in marker being detectable. Therefore, such a scenario seems improbable.

In human purine metabolism, inosine conversion to hypoxanthine is an essential step in purine degradation, which ultimately leads to urate production. It is possible that oral administration of inosine may also lead to purine salvaging and non–urate-mediated effects, as would be the case following a purine-containing meal in nonexperimental settings. Serum urate levels are also regulated by a suite of transporters that mediate urate excretion in the gut and kidney (22). While inhibition of urate excretion would theoretically provide a mechanism to increase urate levels without effects on other purines, specific inhibitors of urate excretion are not available for human use. For this reason, oral inosine was used as a method to increase serum urate concentrations in a standardized manner.

This study has some limitations. The coprimary end points were bone turnover markers rather than BMD, or the clinically relevant end point of fracture. At a population level, there is a modest but significant association between these turnover markers and future fracture (23). More importantly, these markers were responsive to change following treatment with antiresorptive and anabolic therapies (24). In drug development studies, early changes in bone turnover markers predicted changes in BMD and antifracture efficacy (25–27). Testing of bone turnover markers allows for efficient analysis of bone-active agents in human clinical trials and provides insights about the likely mechanism of action of any observed effects. The timeframe for BMD assessment was short, and change in BMD was an exploratory outcome. Although it is not standard practice to measure changes in BMD over 6-month studies, our group has done this previously and found significant effects, both positive and negative (19,28). The absence of any suggestion of change in bone density is entirely consistent with the absence of changes in bone turnover markers. Taken together, these findings indicate that inosine is very unlikely to have a clinically significant effect on bone metabolism.

In summary, despite a sustained increase in serum urate concentrations over a 6-month period, inosine supplementation did not alter markers of bone turnover in postmenopausal women. While urate may be a marker of BMD, these findings do not support the concept that urate has direct biologic effects on bone turnover.

ACKNOWLEDGMENTS

We thank Dr. Ravi Suppiah and Dr. Mark Bolland for data safety monitoring.

AUTHOR CONTRIBUTIONS

All authors were involved in drafting the article or revising it critically for important intellectual content, and all authors approved the final version to be published. Dr. Dalbeth had full access to all of the data in the study and takes responsibility for the integrity of the data and the accuracy of the data analysis.

Study conception and design. Dalbeth, Gamble, Merriman, Stamp, Reid.

Acquisition of data. Horne, Mihov, Stewart.

Analysis and interpretation of data. Dalbeth, Gamble, Stamp, Reid.

REFERENCES

1. Veronese N, Carraro S, Bano G, Trevisan C, Solmi M, Luchini C, et al. Hyperuricemia protects against low bone mineral density, osteoporosis and fractures: a systematic review and meta-analysis. Eur J Clin Invest 2016;46:920–30.
2. Dong XW, Tian HY, He J, Wang C, Qiu R, Chen YM. Elevated serum uric acid is associated with greater bone mineral density and skeletal muscle mass in middle-aged and older adults. PLoS One 2016;11:e0154692.
3. Ahn SH, Lee SH, Kim BJ, Lim KH, Bae SJ, Kim EH, et al. Higher serum uric acid is associated with higher bone mass, lower bone turnover, and lower prevalence of vertebral fracture in healthy postmenopausal women. Osteoporos Int 2013;24:2961–70.
4. Nabipour I, Sambrook PN, Blyth FM, Janu MR, Waite LM, Naganathan V, et al. Serum uric acid is associated with bone health in older men: a cross-sectional population-based study. J Bone Miner Res 2011;26:955–64.
5. Makovey J, Macara M, Chen JS, Hayward CS, March L, Seibel MJ, et al. Serum uric acid plays a protective role for bone loss in peri- and postmenopausal women: a longitudinal study. Bone 2013;52:400–6.
6. Dalbeth N, Topless R, Flynn T, Cadzow M, Bolland MJ, Merriman TR. Mendelian randomization analysis to examine for a causal effect of urate on bone mineral density. J Bone Miner Res 2015;30:985–91.

7. Ishii S, Miyao M, Mizuno Y, Tanaka-Ishikawa M, Akishita M, Ouchi Y. Association between serum uric acid and lumbar spine bone mineral density in peri- and postmenopausal Japanese women. Osteoporos Int 2014;25:1099–105.
8. Sritara C, Ongphiphadhanakul B, Chailurkit L, Yamwong S, Ratanachaiwong W, Sritara P. Serum uric acid levels in relation to bone-related phenotypes in men and women. J Clin Densitom 2013;16:336–40.
9. Lane NE, Parimi N, Lui LY, Wise BL, Yao W, Lay YA, et al. Association of serum uric acid and incident nonspine fractures in elderly men: the Osteoporotic Fractures in Men (MrOS) study. J Bone Miner Res 2014;29:1701–7.
10. Iki M, Yura A, Fujita Y, Kouda K, Tachiki T, Tamaki J, et al. Relationships between serum uric acid concentrations, uric acid lowering medications, and vertebral fracture in community-dwelling elderly Japanese men: Fujiwara-kyo Osteoporosis Risk in Men (FORMEN) Cohort Study. Bone 2020;139:115519.
11. Li HZ, Chen Z, Hou CL, Tang YX, Wang F, Fu QG. Uric acid promotes osteogenic differentiation and inhibits adipogenic differentiation of human bone mesenchymal stem cells. J Biochem Mol Toxicol 2015;29:382–7.
12. Dalbeth N, Pool B, Chhana A, Lin JM, Tay ML, Tan P, et al. Lack of evidence that soluble urate directly influences bone remodelling: a laboratory and clinical study. Calcif Tissue Int 2018;102:73–84.
13. Zhang D, Bobulescu IA, Maalouf NM, Adams-Huet B, Poindexter J, Park S, et al. Relationship between serum uric acid and bone mineral density in the general population and in rats with experimental hyperuricemia. J Bone Miner Res 2015;30:992–9.
14. The Parkinson Study Group SURE-PD Investigators. Inosine to increase serum and cerebrospinal fluid urate in Parkinson disease: a randomized clinical trial. JAMA Neurol 2014;71:141–50.
15. Markowitz CE, Spitsin S, Zimmerman V, Jacobs D, Udupa JK, Hooper DC, et al. The treatment of multiple sclerosis with inosine. J Altern Complement Med 2009;15:619–25.
16. Gonsette RE, Sindic C, D'Hooghe MB, De Deyn PP, Medaer R, Michotte A, et al. Boosting endogenous neuroprotection in multiple sclerosis: the ASsociation of Inosine and Interferon β in relapsing- remitting Multiple Sclerosis (ASIIMS) trial. Mult Scler 2010;16:455–62.
17. Hoque KM, Dixon EE, Lewis RM, Allan J, Gamble GD, Phipps-Green AJ, et al. The ABCG2 Q141K hyperuricemia and gout associated variant illuminates the physiology of human urate excretion. Nat Commun 2020;11:2767.
18. Vasikaran S, Cooper C, Eastell R, Griesmacher A, Morris HA, Trenti T, et al. International Osteoporosis Foundation and International Federation of Clinical Chemistry and Laboratory Medicine position on bone marker standards in osteoporosis. Clin Chem Lab Med 2011;49:1271–4.
19. Grey A, Bolland M, Wong S, Horne A, Gamble G, Reid IR. Low-dose zoledronate in osteopenic postmenopausal women: a randomized controlled trial. J Clin Endocrinol Metab 2012;97:286–92.
20. Tai V, Grey A, Bolland MJ. Results of observational studies: analysis of findings from the Nurses' Health Study. PLoS One 2014;9:e110403.
21. Pirro M, Mannarino MR, Bianconi V, De Vuono S, Sahebkar A, Bagaglia F, et al. Uric acid and bone mineral density in postmenopausal osteoporotic women: the link lies within the fat. Osteoporos Int 2017;28:973–81.
22. Mandal AK, Mount DB. The molecular physiology of uric acid homeostasis [review]. Annu Rev Physiol 2015;77:323–45.
23. Johansson H, Oden A, Kanis JA, McCloskey EV, Morris HA, Cooper C, et al. A meta-analysis of reference markers of bone turnover for prediction of fracture. Calcif Tissue Int 2014;94:560–7.
24. Eastell R, Szulc P. Use of bone turnover markers in postmenopausal osteoporosis. Lancet Diabetes Endocrinol 2017;5:908–23.
25. Bauer DC, Black DM, Garnero P, Hochberg M, Ott S, Orloff J, et al. Change in bone turnover and hip, non-spine, and vertebral fracture in alendronate-treated women: the fracture intervention trial. J Bone Miner Res 2004;19:1250–8.
26. Reginster JY, Sarkar S, Zegels B, Henrotin Y, Bruyere O, Agnusdei D, et al. Reduction in PINP, a marker of bone metabolism, with raloxifene treatment and its relationship with vertebral fracture risk. Bone 2004;34:344–51.
27. Eastell R, Black D, Bouxsein M, Lui LY, Cauley J, Khosla S, et al. Treatment-related changes in bone turnover and fracture risk reduction in clinical trials of anti-resorptive drugs: the FNIH bone quality study. J Bone Mineral Res 2017;32 Suppl:S173.
28. Grey A, Bolland M, Gamble G, Wattie D, Horne A, Davidson J, et al. The peroxisome proliferator-activated receptor-γ agonist rosiglitazone decreases bone formation and bone mineral density in healthy postmenopausal women: a randomized, controlled trial. J Clin Endocrinol Metab 2007;92:1305–10.

Arthritis & Rheumatology
Vol. 73, No. 9, September 2021, pp 1765–1772

American College of Rheumatology
Empowering Rheumatology Professionals

LETTERS

DOI 10.1002/art.41742

Prophylaxis against COVID-19 with hydroxychloroquine and chloroquine: comment on the article by Putman et al

To the Editor:

We read with great interest the article by Dr. Putman and colleagues, which reviews data from 45 studies evaluating hydroxychloroquine (HCQ), chloroquine (CQ), anakinra, and interleukin-6 (IL-6) inhibitor therapies in the treatment of COVID-19 (1). Except anakinra, none of the other therapies decreased the risk of death in hospitalized COVID-19 patients. We would like to discuss the evidence evaluating the role of HCQ as prophylaxis against SARS–CoV-2 infections. The in vitro antiviral effect of antimalarials suggested a role in preventing disease progression (2). A meta-analysis of 5,577 participants from 5 randomized controlled trials suggested that outpatient treatment with HCQ (as opposed to treatment in hospitalized patients) reduced the incidence of the composite outcome of SARS–CoV-2 infection, hospitalization, and death; serious adverse events were not reported and cardiac arrhythmias were rare (3). Several studies suggested that HCQ had no benefit in the prophylaxis against SARS–CoV-2 (4–8) (Table 1). Only 1 open-label, controlled trial showed lower incidence of COVID-19 in the HCQ group; however, imperfect methodology raises concerns over its validity (9). The bulk of the evidence suggests that HCQ has limited or no utility in the prophylaxis for SARS–CoV-2 infections.

Sixteen clinical studies investigating the preventive role of CQ or HCQ in the setting of COVID-19 have been registered around the world; 5 studies were completed and others were terminated, suspended, or withdrawn (10). Of note, our own double-blind, placebo-controlled, randomized trial to determine the efficacy of CQ in preventing symptomatic COVID-19 among New York–Presbyterian Hospital health care workers was terminated early because of lack of enrollment. CQ-naive health care workers with moderate or high risk of exposure to COVID-19 were randomized to receive placebo or CQ (500 mg daily for 1 week followed by 500 mg weekly). Study participants were followed up for 3 months to record SARS–CoV-2 infections and safety events. The primary end point was the percentage of patients with COVID-19 infections. The study started in April 2020 but progressed at a glacial pace due to safety concerns and loss of interest in prophylactic use of CQ and HCQ as the number of COVID-19 infections decreased in New York City over the summer. We enrolled 9 participants and terminated the study early. An additional double-blind, placebo-controlled, randomized trial of HCQ (800 mg on day 1 followed by 400 mg for 4 additional days) for post–COVID-19 exposure prophylaxis in asymptomatic household contacts was halted in early May 2020. This study was designed to have no contact between COVID-19–exposed participants and study staff. Based on our Institutional Review Board requirement that prolongation of the QTc interval be ruled out prior to enrollment, the trial was effectively terminated before even 20 of the planned 1,600 participants were enrolled.

As vaccination of the health care force is almost complete in the US, the prophylactic roles of CQ and HCQ have clearly become less relevant. Most treatment data on HCQ in COVID-19 to date have not shown clinical benefit, and final prevention data from the HERO-HCQ trial (11), which remains active, will hopefully elucidate the role of HCQ in the prophylaxis against the development of SARS–CoV-2 infections and conclude this chapter.

The authors acknowledge the support of Rising Pharma for the donation of the chloroquine used in one of the studies discussed in this publication.

Wei Tang, MD
Yevgeniya Gartshteyn, MD
Cathy Guo, MS
Tommy Chen, MS
Jon Giles, MD, MPH
Anca Askanase, MD, MPH
New York–Presbyterian Hospital and Columbia University Medical Center
New York, NY

1. Putman M, Chock YP, Tam H, Kim AH, Sattui SE, Berenbaum F, et al. Antirheumatic disease therapies for the treatment of COVID-19: a systematic review and meta-analysis. Arthritis Rheumatol 2021;73:36–47.
2. Wang M, Cao R, Zhang L, Yang X, Liu J, Xu M, et al. Remdesivir and chloroquine effectively inhibit the recently emerged novel coronavirus (2019-nCoV) in vitro. Cell Res 2020;30:269–71.
3. Ladapo JA, McKinnon JE, McCullough PA, Risch HA. Randomized controlled trials of early ambulatory hydroxychloroquine in the prevention of COVID-19 infection, hospitalization, and death: meta-analysis [preprint]. medRxiv 2020. E-pub ahead of print.
4. Abella BS, Jolkovsky EL, Biney BT, Uspal JE, Hyman MC, Frank I, et al. Efficacy and safety of hydroxychloroquine vs placebo for pre-exposure SARS-CoV-2 prophylaxis among health care workers: a randomized clinical trial. JAMA Intern Med 2021;181:195–202.
5. Rajasingham R, Bangdiwala AS, Nicol MR, Skipper CP, Pastick KA, Axelrod ML, et al. Hydroxychloroquine as pre-exposure prophylaxis for COVID-19 in healthcare workers: a randomized trial. Clin Infect Dis 2021;72:e835–43.

Table 1. Studies of CQ and HCQ as prophylaxis against SARS–CoV-2*

Author (ref.), date of publication, country	Methods	Population	Group	Dosage	Outcome measures	Results
Boulware et al (6), June 3, 2020, US and Canada	Double-blind, placebo-controlled, randomized	821 exposed within 4 days	HCQ (n = 414); placebo (n = 407)	800 mg/day; 600 mg/day for 4 days	Incidence of laboratory-confirmed or symptomatic illness	Symptomatic COVID-19 in 49 (11.8%) of 414 receiving HCQ vs. 58 (14.3%) of 407 receiving placebo (P = 0.35)
Salvarani et al (8), August 6, 2020, Italy	Population-based study	2,251,903 residents of Bologna, Modena, and Reggio Emilia	CQ/HCQ (n = 4,408); general population (n = 2,112,319)	≥1 prescription of CQ or HCQ for approved indications	Incidence of testing; incidence of positive result; probability of being found positive once tested	OR for testing 1.09 (95% CI 0.94–1.28); OR for Dx 0.94 (95% CI 0.66–1.34); OR for positive result 0.83 (95% CI 0.56–1.23)
Rajasingham et al (5), September 18, 2020, US and Canada	Double-blind, placebo-controlled, randomized	1,483 HCWs	Once weekly HCQ (n = 494); twice weekly HCQ (n = 495); placebo (n = 494)	400 mg in 2 doses; 400 mg once weekly; 400 mg twice weekly for 12 weeks	Incidence of COVID-19–free survival	COVID-19–free survival in 39 (7.9%) of 494 receiving placebo vs. 29 (5.9%) of 494 receiving HCQ once weekly (HR 0.72, 95% CI 0.44–1.16) vs. 29 (5.8%) of 495 receiving HCQ twice weekly (HR 0.74, 95% CI 0.46–1.19)
Abella et al (4), September 30, 2020, US	Double-blind, placebo-controlled, randomized	132 HCWs	HCQ (n = 66); placebo (n = 66)	600 mg/day for 8 weeks	SARS-CoV-2 positive by nasopharyngeal swab within 8 weeks	Terminated early for futility; COVID-19 in 4 (6.3%) of 64 receiving HCQ vs. 4 (6.9%) of 61 receiving placebo
Dhibar et al (9), November 6, 2020, India	Open-label, controlled	317 contacts of confirmed cases	HCQ (n = 132); control (n = 185)	800 mg for 1 day; 400 mg once/week for 3 weeks	Incidence of laboratory-confirmed or symptomatic illness	COVID-19 in 14 (10.6%) of 132 receiving HCQ vs. 36 (19.5%) of 185 controls (RR 0.50, 95% CI 0.25–0.99)
Mitjà et al (7), November 24, 2020, Spain	Open-label, cluster-randomized	2,314 contacts of index case patients	HCQ (n = 1,116); control (n = 1,198)	800 mg for 1 day; 400 mg/day for 6 days	PCR-confirmed symptomatic COVID-19 within 14 days	COVID-19 in 64 (5.7%) of 1,116 receiving HCQ vs. 74 (6.2%) of 1,198 controls (RR 0.86, 95% CI 0.52–1.42)

* CQ = chloroquine; HCQ = hydroxychloroquine; OR = odds ratio; 95% CI = 95% confidence interval; Dx = diagnosis; HCWs = health care workers; HR = hazard ratio; RR = relative risk; PCR = polymerase chain reaction.

6. Boulware DR, Pullen MF, Bangdiwala AS, Pastick KA, Lofgren SM, Okafor EC, et al. A randomized trial of hydroxychloroquine as postexposure prophylaxis for Covid-19. N Engl J Med 2020;383: 517–25.
7. Mitjà O, Corbacho-Monné M, Ubals M, Alemany A, Suñer C, Tebé C, et al. A cluster-randomized trial of hydroxychloroquine for prevention of Covid-19. N Engl J Med 2021;384:417–27.
8. Salvarani C, Mancuso P, Gradellini F, Viani N, Pandolfi P, Reta M, et al. Susceptibility to COVID-19 in patients treated with antimalarials: a population based study in Emilia-Romagna, Northern Italy. Arthritis Rheumatol 2021;73:48–52.
9. Dhibar DP, Arora N, Kakkar A, Singla N, Mohindra R, Suri V, et al. Post-exposure prophylaxis with hydroxychloroquine for the prevention of COVID-19, a myth or a reality? The PEP-CQ Study. Int J Antimicrob Agents 2020;56:106224.
10. Tan DH, Agrawal R, Barnabas RV, Giles JT, Dull P. Moving fast but going slow: coordination challenges for trials of COVID-19 post-exposure prophylaxis. Trials 2020;21:815.
11. Adrian Hernandez, sponsor. Healthcare Worker Exposure Response and Outcomes of Hydroxychloroquine (HERO-HCQ). ClinicalTrials.gov identifier: NCT04334148; 2020.

DOI 10.1002/art.41745

Reply

To the Editor:

We thank Dr. Tang and colleagues for their interest in our study and for their correspondence on an important clinical question. In May of 2020, when our literature search was last updated, we did not identify any case series, cohort studies, or randomized controlled trials (RCTs) that evaluated the role of HCQ as prophylaxis for COVID-19. Consequently, our analysis was unable to address this issue. The authors should be commended for their efforts to conduct an RCT during the early phases of the pandemic when there was widespread misinformation about antimalarials. We empathize with the difficulties they encountered, which highlight broader issues impacting the COVID-19 research agenda.

As noted in our analysis, early observational studies frequently had a high risk of bias, which could be attributed to small sample sizes, inappropriate or inadequate comparator groups, and issues related to confounding by indication. Overinterpretation of the preliminary evidence led to off-label HCQ use months before the first randomized trial was finished. An "infodemic" began, fueled by anecdotal reports of encouraging benefits and concerning harms (1). A seemingly contradictory situation arose, in which enrollment slowed because of overconfidence in HCQ's purported benefit, and trials were paused or terminated in response to potential safety signals. The typical regulatory and logistic hurdles to initiating RCTs compounded delays, resulting in many RCTs beginning after COVID-19 peaks had passed. Perhaps most importantly, aside from notable exceptions like the RECOVERY trials, few large-scale coordinated RCTs of HCQ were performed (2).

The importance of conducting large-scale, adequately powered RCTs and the consequences of relying on suboptimal evidence when they are absent will be one of the enduring legacies of the COVID-19 pandemic (3,4). Performing such trials will require greater collaboration between centers and a regulatory environment that encourages their execution. It will also require investigators like Dr. Tang and colleagues, who were willing to expend time and effort in this worthy endeavor.

The views expressed here are those of the authors and participating members of the COVID-19 Global Rheumatology Alliance and do not necessarily represent the views of the American College of Rheumatology, the European Alliance of Associations for Rheumatology (EULAR), or any other organization. Dr. Putman is recipient of a Scientist Development award from the Rheumatology Research Foundation. Dr. Sattui's work was supported by the Vasculitis Clinical Research Consortium and by a Vasculitis Foundation fellowship award. Dr. Sparks' work was supported by the NIH (National Institute of Arthritis and Musculoskeletal and Skin Disease grants K23-AR-069688, R03-AR-075886, L30-AR-066953, P30-AR-070253, and P30-AR-072577), the Rheumatology Research Foundation R Bridge award, the Brigham Research Institute, and the R. Bruce and Joan M. Mickey Research Scholar Fund. Dr. Duarte-García's work was supported by the CDC (grant U01-U01DP006491), the Rheumatology Research Foundation Scientist Development award, the Robert D. and Patricia E. Kern Center for the Science of Health Care Delivery, the Women's Health Career Enhancement award, and the Eaton Family Career Development award. Dr. Sparks has received consulting fees, speaking fees, and/or honoraria from Bristol Myers Squibb, Gilead, Inova, Janssen, and Optum (less than $10,000 each) and research grants from Bristol Myers Squibb and Amgen. Dr. Liew has received research support from Pfizer.

Michael Putman, MD, MSci
Medical College of Wisconsin
Wauwatosa, WI
Sebastian E. Sattui, MD, MS
Hospital for Special Surgery
New York, NY
Jeffrey A. Sparks, MD, MMSc
Brigham and Women's Hospital and Harvard Medical School
Jean W. Liew, MD, MS
Boston University School of Medicine
Boston, MA
Rebecca Grainger, MBChB, PhD
University of Otago
Wellington, New Zealand
Alí Duarte-García, MD, MSc
Mayo Clinic
Rochester, MN

1. The Lancet Infectious Diseases. The COVID-19 infodemic [editorial]. Lancet Infect Dis 2020;20:875.
2. Anon. Effect of hydroxychloroquine in hospitalized patients with Covid-19. N Engl J Med 2020;383:2030–40.

3. Berwanger O. Azithromycin, RECOVERY, and the power of large, simple trials. Lancet 2021;397:559–60.
4. Collins R, Bowman L, Landray M, Peto R. The magic of randomization versus the myth of real-world evidence. N Engl J Med 2020;382:674–8.

DOI 10.1002/art.41806

Use of tofacitinib in the context of COVID-19 vaccination: comment on the American College of Rheumatology clinical guidance for COVID-19 vaccination in patients with rheumatic and musculoskeletal diseases

To the Editor:

We read with great interest the American College of Rheumatology (ACR) clinical guidance for COVID-19 vaccination in patients with rheumatic and musculoskeletal diseases (1). We commend the Task Force's emphasis on the importance of immunization in this population and for providing guidance to the rheumatology community. Regarding their recommendation to withhold JAK inhibitors for 1 week after each COVID-19 vaccine dose (1), we propose the following available tofacitinib data for consideration in this context.

Tofacitinib is a reversible JAK inhibitor characterized by rapid absorption and elimination and a short half-life (2). The impact of tofacitinib on lymphocyte subsets consists of small and variable changes in T cell counts, increases in B cell counts, and decreases in natural killer (NK) cell counts. After drug discontinuation, B and NK cell counts can take from 2 to 6 weeks to return to baseline levels (2), which suggests that the impact of a 1-week hold of tofacitinib on immune cell counts would likely be small.

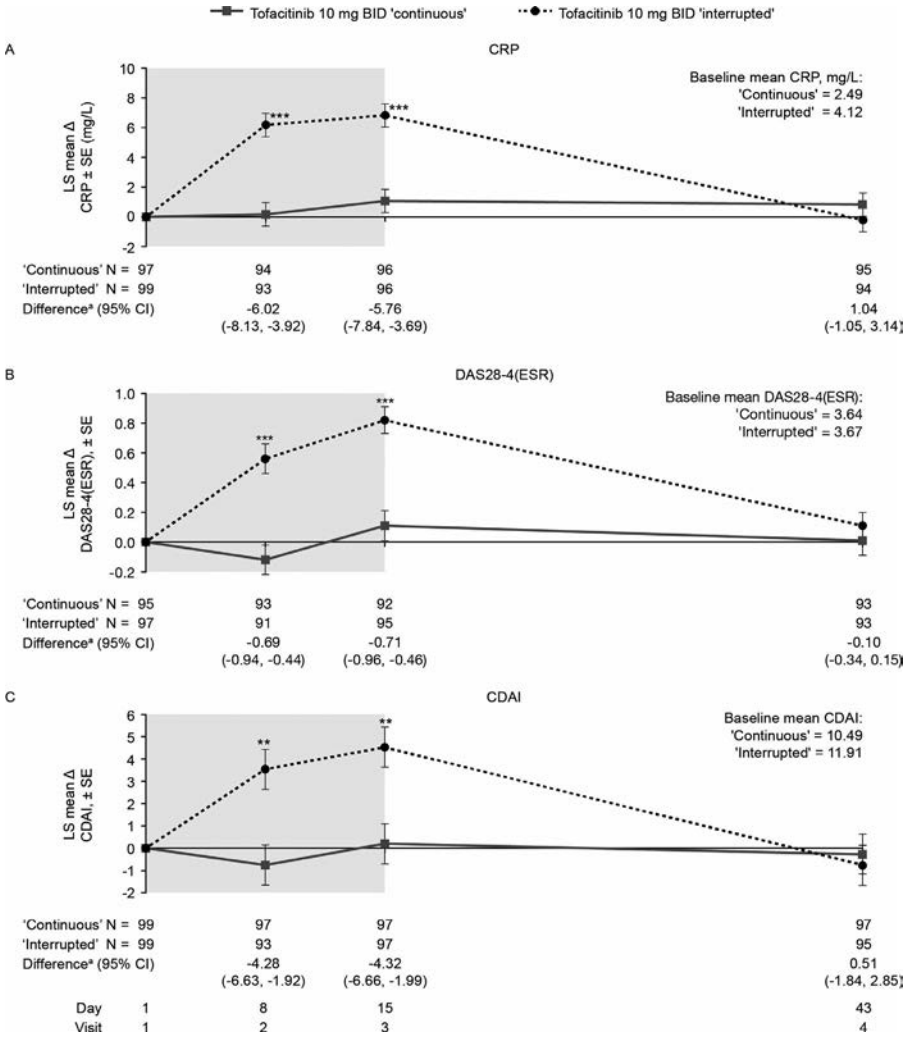

Figure 1. Least squares (LS) mean changes from baseline in C-reactive protein (CRP) levels (**A**), Disease Activity Score in 28 joints (4-variable) using the erythrocyte sedimentation rate (DAS28-4[ESR]) (**B**), and Clinical Disease Activity Index (CDAI) (**C**) over time during the sub-study of the long-term extension study, ORAL Sequel. Shaded areas indicate the dose-interruption period. Baseline was defined as visit 1 of the sub-study. [a]LS mean change (Δ) in continuous treatment group minus LS mean change in interrupted treatment group. bid = twice a day; 95% CI = 95% confidence interval. ** = $P < 0.001$; *** = $P < 0.0001$ for interrupted versus continuous treatment. Adapted from Figure 3 in Kaine et al (5) (available at https://link.springer.com/article/10.1007%2Fs10067-020-04956-1) by removing the original panel B from the figure; used under Creative Commons attribution 4.0 International (CC BY 4.0) at https://creativecommons.org/licenses/by/4.0/.

Studies have also shown that T cell–dependent and T cell–independent vaccine responses are unaffected by tofacitinib (3,4). In one study, patients with rheumatoid arthritis receiving treatment with tofacitinib 10 mg twice a day (with or without methotrexate) were randomized to continue or to stop tofacitinib treatment 1 week prior and 1 week following immunization with the pneumococcal polyvalent-23 vaccine (PPV23) or the trivalent influenza vaccine (3). Antibody titers measured 35 days postimmunization were satisfactory in both the continue and hold groups for the PPV23 (75.0% and 84.6%, respectively [T cell–independent response]) and the influenza vaccine (66.3% and 63.7%, respectively [T cell–dependent response]) (3). In another study, patients with psoriasis receiving treatment with tofacitinib 10 mg twice a day demonstrated a robust vaccine response to T cell–dependent tetanus toxoid (88%) and T cell–dependent 13-valent conjugate pneumococcal vaccines (80%) (4).

As with any clinical decision, risk–benefit analysis for each patient includes consideration of the potential for disease flares. In the aforementioned study, tofacitinib treatment interruption led to a steady increase in disease activity scores compared with continuous treatment (Figure 1) (5). Therefore, in addition to the ACR guidelines, we encourage clinicians to consider the above data during shared decision-making with patients when advising on medication management in the context of COVID vaccination.

Editorial support, under the guidance of the authors, was provided by Tanya Guha, PhD, CMC Connect, McCann Health Medical Communications and was funded by Pfizer Inc, New York, New York, USA, in accordance with Good Publication Practice (GPP3) guidelines (Ann Intern Med 2015;163:461–4). Drs. Mortezavi, Menon, Lee, and Rivas are employees and shareholders of Pfizer Inc.

Mahta Mortezavi, MD
Pfizer Inc
New York, NY
Sujatha Menon, PhD
Pfizer Inc
Groton, CT
Kristen Lee, MD
Pfizer Inc
New York, NY
Jose Rivas, MD
Pfizer SLU
Madrid, Spain

1. Curtis JR, Johnson SR, Anthony DD, Arasaratnam RJ, Baden LR, Bass AR, et al. American College of Rheumatology guidance for COVID-19 vaccination in patients with rheumatic and musculoskeletal diseases: version 1. Arthritis Rheumatol 2021;73:1093–107.
2. Hodge JA, Kawabata TT, Krishnaswami S, Clark JD, Telliez JB, Dowty ME, et al. The mechanism of action of tofacitinib: an oral Janus kinase inhibitor for the treatment of rheumatoid arthritis. Clin Exp Rheumatol 2016;34:318–28.
3. Winthrop KL, Silverfield J, Racewicz A, Neal J, Lee EB, Hrycaj P, et al. The effect of tofacitinib on pneumococcal and influenza vaccine responses in rheumatoid arthritis. Ann Rheum Dis 2016;75:687–95.
4. Winthrop KL, Korman N, Abramovits W, Rottinghaus ST, Tan H, Gardner A, et al. T cell-mediated immune response to pneumococcal conjugate vaccine (PCV-13) and tetanus toxoid vaccine in patients with moderate-to-severe psoriasis during tofacitinib treatment. J Am Acad Dermatol 2017;78:1149–55.e1.
5. Kaine J, Tesser J, Takiya L, DeMasi R, Wang L, Snyder M, et al. Re-establishment of efficacy of tofacitinib, an oral JAK inhibitor, after temporary discontinuation in patients with rheumatoid arthritis. Clin Rheumatol 2020;39:2127–37.

DOI 10.1002/art.41805

Reply

To the Editor:

We appreciate the comment by Dr. Mortezavi and colleagues describing COVID-19 vaccine response and the frequency of disease worsening in patients receiving tofacitinib. The ACR COVID-19 Vaccine Clinical Guidance Task Force was aware of the 2 studies cited and appreciate their summary of the results. We would point out that in the rheumatoid arthritis study by Winthrop et al (1), patients receiving tofacitinib in Study A had a lower likelihood of a satisfactory response to pneumococcal vaccination (45.1%) compared to placebo-treated patients (68.4%), a difference of 23.3% (95% confidence interval [95% CI] −36.6, −9.6). The differences were numerically even larger for patients receiving concomitant tofacitinib and methotrexate (31.6% of patients with a satisfactory response, difference of −30.2% [95% CI] −47.3, −11.4) compared to methotrexate monotherapy. Our challenge was in considering the appropriateness of extrapolating results from vaccine studies of influenza, pneumococcal, and tetanus toxoid vaccines to make inferences regarding the anticipated response to vaccination against SARS–CoV-2, a novel antigen to which most individuals have not previously been exposed.

The Task Force recognized that infection rates, and perhaps response to vaccinations against those infections, might be heterogeneous according to pathogen. For example, JAK inhibitors approximately double the incidence of herpes zoster compared to biologics such as tumor necrosis factor inhibitors, yet they do not meaningfully increase rates of other infections (e.g., pneumonia) (1–3). We noted that in the Oral Strategy study, adalimumab-treated patients receiving vaccination with the live herpes zoster vaccine had lower incidence rates of herpes zoster (0.0 per 100 patient-years) compared to nonvaccinated patients (incidence rate 2.1 per 100 patient-years) (4). In contrast, and recognizing that numbers were small, tofacitinib-treated patients had similar rates of herpes zoster regardless of vaccination (incidence rate 3.0 per 100 patient-years in vaccinated versus 2.2 per 100 patient-years in nonvaccinated patients).

We also appreciate the data provided by Dr. Mortezavi and colleagues regarding the rate of disease worsening in patients whose treatment with tofacitinib was briefly interrupted. At ~2 weeks, the mean worsening in the 4-variable DAS28 of 0.7 units was of smaller magnitude than typically considered the minimum clinically important difference (MCID) for the DAS28 (i.e., >1.2

units) (5). The MCID for defining disease worsening using the Clinical Disease Activity Index (CDAI) in patients who had moderate disease activity at the start of treatment is undefined, although a 1-unit change in each of the 4 CDAI components (tender joint count, swollen joint count, patient global assessment, and physician global assessment) is often considered to be the measurement error for each of these (6). Taken together, the mean amount of disease worsening associated with brief interruptions in therapy seems small and likely not of clinical importance for most patients, especially in light of the guidance recommending that JAK inhibitors be withheld for 1 week at the time of each vaccine administration, rather than for 2 consecutive weeks.

Ultimately, we await prospective data regarding the influence of JAK inhibitors and other immunomodulatory therapies used at the time of COVID-19 vaccination on immunogenicity and correlates of serologic protection. Since the ACR COVID-19 Vaccine Guidance is a living document, our plan is to rapidly update it and incorporate new evidence as it accumulates.

Jeffrey R. Curtis, MD, MS, MPH
University of Alabama at Birmingham
Sindhu R. Johnson, MD, PhD
Toronto Western Hospital Mount Sinai Hospital and University of Toronto
Toronto, Ontario, Canada
Donald D. Anthony, MD, PhD
VA Medical Center, MetroHealth Medical Center and Case Western Reserve
Cleveland, OH
Reuben J. Arasaratnam, MD
VA North Texas Health Care System and University of Texas Southwestern Medical Center
Dallas, TX
Lindsey R. Baden, MD, MSc
Ellen M. Gravallese, MD
Brigham and Women's Hospital
Boston, MA
Anne R. Bass, MD
Hospital for Special Surgery and Weill Cornell Medicine
New York, NY
Cassandra Calabrese, DO
Cleveland Clinic Foundation
Cleveland, OH
Rafael Harpaz, MD
Harpaz Herman Consultants, LLC
Atlanta, GA
Andrew Kroger, MD, MPH
Centers for Disease Control and Prevention
Atlanta, GA
Rebecca E. Sadun, MD, PhD
Duke University
Durham, NC
Amy S. Turner
American College of Rheumatology
Atlanta, GA
Eleanor Anderson Williams, MD
The Permanente Medical Group
Union City, CA
Ted R. Mikuls, MD, MSPH
University of Nebraska Medical Center and VA Nebraska–Western Iowa Health Care System
Omaha, NE

1. Winthrop KL, Curtis JR, Lindsey S, Tanaka Y, Yamaoka K, Valdez H, et al. Herpes zoster and tofacitinib: clinical outcomes and the risk of concomitant therapy. Arthritis Rheumatol 2017;69:1960–8.
2. Bechman K, Subesinghe S, Norton S, Atzeni F, Galli M, Cope AP, et al. A systematic review and meta-analysis of infection risk with small molecule JAK inhibitors in rheumatoid arthritis. Rheumatology (Oxford) 2019;58:1755–66.
3. Curtis JR, Xie F, Yun H, Bernatsky S, Winthrop KL. Real-world comparative risks of herpes virus infections in tofacitinib and biologic-treated patients with rheumatoid arthritis. Ann Rheum Dis 2016;75:1843–7.
4. Calabrese LH, Abud-Mendoza C, Lindsey SM, Lee SH, Tatulych S, Takiya L, et al. Live zoster vaccine in patients with rheumatoid arthritis treated with tofacitinib with or without methotrexate, or adalimumab with methotrexate: a post hoc analysis of data from a phase IIIb/IV randomized study. Arthritis Care Res (Hoboken) 2020;72:353–9.
5. Uhlig T, Kvien TK, Pincus T. Test-retest reliability of disease activity core set measures and indices in rheumatoid arthritis. Ann Rheum Dis 2009;68:972–5.
6. Curtis JR, Yang S, Chen L, Pope JE, Keystone EC, Haraoui B, et al. Determining the minimally important difference in the Clinical Disease Activity Index for improvement and worsening in early rheumatoid arthritis patients. Arthritis Care Res (Hoboken) 2015;67:1345–53.

DOI 10.1002/art.41721

Are there thresholds of conflict of interest with gifts from industry? Comment on the article by Wayant et al

To the Editor:

I would like to thank Dr. Wayant and colleagues for their analysis of financial conflicts of interest among physician-authors of American College of Rheumatology clinical practice guidelines (1). Given the known challenges with the Open Payments Database, as was described in their evaluation, I am curious if the data show a natural demarcation between small gifts and significantly larger gifts. While there are not defined levels of conflict of interest, I would like to know if the data suggested that there may be a threshold for authors with small gifts (for example, <$200 for smaller gifts and ≥$500 for larger gifts). The data may better define thresholds of conflict of interest. A gift with an estimated value of <$200 on a $200,000 physician salary would likely carry less influence than a $10,000 gift. A scatterplot with linear or logged y-axis for gift amount may be instructive. I would be grateful if Dr. Wayant and colleagues could provide this analysis to supplement their article.

John D. FitzGerald, MD, PhD
University of California, Los Angeles

1. Wayant C, Walters C, Zaaza Z, Gilstrap C, Combs T, Crow H, et al. Evaluation of financial conflicts of interest among physician-authors of American College of Rheumatology clinical practice guidelines. Arthritis Rheumatol 2020;72:1427–34.

DOI 10.1002/art.41719

Etanercept or methotrexate withdrawal in rheumatoid arthritis patients receiving combination therapy: comment on the article by Curtis et al

Rashmi Roongta, MD
Sumantro Mondal, DM
Alakendu Ghosh, FRCP
Institute of Postgraduate Medical Education and Research
Kolkata, India

To the Editor:

We read with great interest the article by Dr. Curtis and colleagues on etanercept or methotrexate withdrawal in rheumatoid arthritis (1). They identified patients whose RA was in sustained and deep remission according to the stringent Simplified Disease Activity Index (SDAI) criteria (2) and simulated near-ideal conditions, before withdrawing either methotrexate or etanercept from the treatment regimen. They then observed the proportion of patients in whom SDAI remission was maintained at week 48. However, a few matters need to be addressed.

First, the eligibility criteria state that patients should have an SDAI score of ≤3.3 at screening and at the end of the run-in period. However, Curtis and colleagues report that disease in 95%, 92.1%, and 96.1% of the patients in the methotrexate monotherapy arm, the etanercept monotherapy arm, and the combination arm, respectively, was in SDAI-defined remission at baseline (see Table 1 in Curtis et al [1]). Considering the eligibility criteria, these values should be 100% in each arm.

Second, we noticed the discrepancy between the percentage of patients at baseline whose disease was in SDAI-defined remission (>90%) as compared to Boolean-defined remission (33–45%). As both the SDAI definition of remission and the Boolean-based definition of remission are recommended by the American College of Rheumatology and the European Alliance of Associations for Rheumatology, both should be consistent (3). A recent report states that raising the cutoff score for patient global assessment of disease activity to 1.5 instead of 1 would lead to better agreement between the two indices (4). It would be of interest to know whether this was the reason for the grossly discordant values between the two indices in the study by Curtis and colleagues.

Third, among those who received rescue therapy in the combination arm, remission was recaptured in nearly 80% of patients, while low disease activity was seen in 100%. Further clarity on whether this improvement was achieved by merely continuing the same therapy or by treating the patients with steroids or analgesics would be helpful for extrapolation to daily clinical practice.

Last, we would like to bring to the authors' attention a possible misprint in the Discussion, where it is written that a difference in the proportion of radiographic nonprogression was observed between the combination arm and the etanercept monotherapy arm in the COMET trial (5). However, in the COMET trial, the combination arm was compared to methotrexate and not etanercept.

We appreciate the work done by the authors and are looking forward to their response.

1. Curtis JR, Emery P, Karis E, Haraoui B, Bykerk V, Yen PK, et al. Etanercept or methotrexate withdrawal in rheumatoid arthritis patients in sustained remission on combination therapy. Arthritis Rheumatol 2021;73:759–68.
2. Smolen JS, Breedveld FC, Schiff MH, Kalden JR, Emery P, Eberl G, et al. A Simplified Disease Activity Index for rheumatoid arthritis for use in clinical practice. Rheumatology (Oxford) 2003;42:244–57.
3. Felson DT, Smolen JS, Wells G, Zhang B, van Tuyl LH, Funovits J, et al. American College of Rheumatology/European League Against Rheumatism provisional definition of remission in rheumatoid arthritis for clinical trials. Arthritis Rheum 2011;63:573–86.
4. Studenic P, Felson D, de Wit M, Alasti F, Stamm TA, Smolen JS, et al. Testing different thresholds for patient global assessment in defining remission for rheumatoid arthritis: are the current ACR/EULAR Boolean criteria optimal? Ann Rheum Dis 2020;79:445–52.
5. Emery P, Breedveld FC, Hall S, Durez P, Chang DJ, Robertson D, et al. Comparison of methotrexate monotherapy with a combination of methotrexate and etanercept in active, early, moderate to severe rheumatoid arthritis (COMET): a randomised, double-blind, parallel treatment trial. Lancet 2008;372:375–82.

DOI 10.1002/art.41718

Reply

To the Editor:

We thank Dr. Roongta and colleagues for their interest in our report and for their comments on the initial online version of the article. We have addressed their points as detailed below. Clarifications or corrections were made, where relevant, during the copyediting phase and are now resolved.

First, the third and final run-in visit of this study required that the patient's rheumatoid arthritis (RA) be in SDAI remission at that time, but the subsequent randomization of the patient into the double-blind treatment period occurred at a separate visit ~1 week later, at which time the baseline disease activity score was remeasured. As expected, there were some minor fluctuations in disease activity during this interval, and in a small number of patients RA was not in SDAI-defined remission at the time of the baseline visit, and yet was found to be in SDAI-defined remission at the third run-in visit. Among those whose disease was not in SDAI-defined remission at the baseline visit, the range of SDAI scores remained close to the cutoff score representing remission and did not exceed the SDAI-defined low disease activity range. We have updated the Patients and Methods section in the final version of our article to provide greater clarity.

Second, although the discrepancy between patients whose disease was in SDAI-defined remission and the lower percentage whose disease was in Boolean-defined remission was expected, we agree that the magnitude of the difference was greater than

previously reported. Boolean-defined remission represents a stricter definition of remission, and the patient global assessment of disease activity has been identified as the most common variable accounting for the discrepancy between the two outcome measures (1,2). In addressing Roongta and colleagues' comment, we found an error in the calculation of Boolean-defined remission (using the 0–100 scale, rather than 0–10 scale in the formula). This error was limited to the calculation of Boolean-defined remission and did not apply to other outcome measures utilizing patient global assessment of disease activity, including SDAI. The updated Boolean-defined remission rates at baseline for the methotrexate monotherapy, etanercept monotherapy, and combination groups were 82.2%, 83.2%, and 80.4%, respectively. If the Boolean remission definition allowed for a patient global assessment score of ≤1.5 units (rather than ≤1.0 units), RA in 87.1%, 86.1%, and 84.3% of the patients would have been in Boolean-defined remission. Table 1 of the article has been updated with the corrected data.

Third, we found it interesting, though seen previously, that merely continuing combination therapy after rescue therapy led to recapturing low disease activity for those patients previously receiving combination therapy whose disease worsened (3). Across the 3 treatment groups, there was low use of glucocorticoids in patients who experienced disease worsening and received rescue therapy. Approximately 15% of patients overall were treated with glucocorticoids at any time after initiation of rescue therapy, and glucocorticoid usage was approximately twice as common in the methotrexate monotherapy group compared with the etanercept monotherapy group. In the combination therapy group, only 2 patients among those who received rescue therapy received low-dose steroids, and 1 patient received a nonsteroidal antiinflammatory drug for documented worsening of RA.

Roongta and colleagues are correct to point out that the COMET trial radiographic results referenced in the Discussion section of our article compare the combination therapy group and the methotrexate monotherapy group. It was an error, and the intended reference was for the 2-year follow-up report from the COMET trial, which describes the 2-year clinical and radiographic results and compares the radiographic data between patients who started on the combination of etanercept and methotrexate and continued this combination treatment, and those who then discontinued methotrexate and continued to receive etanercept as monotherapy as in the SEAM-RA trial (4). We have made the appropriate correction in the final version of the article.

Jeffrey R. Curtis, MD
University of Alabama at Birmingham
Elaine Karis, MD
Priscilla K. Yen, PhD
Greg Kricorian, MD
James B. Chung, MD, PhD
Amgen, Inc.
Thousand Oaks, CA

1. Studenic P, Smolen JS, Aletaha D. Near misses of ACR/EULAR criteria for remission: effects of patient global assessment in Boolean and index-based definitions. Ann Rheum Dis 2012;71:1702–5.
2. Aletaha D, Wang X, Zhong S, Florentinus S, Monastiriakos K, Smolen JS. Differences in disease activity measures in patients with rheumatoid arthritis who achieved DAS, SDAI, or CDAI remission but not Boolean remission. Semin Arthritis Rheum 2020;50:276–84.
3. Van Vollenhoven RF, Østergaard M, Leirisalo-Repo M, Uhlig T, Jansson M, Larsson E, et al. Full dose, reduced dose or discontinuation of etanercept in rheumatoid arthritis. Ann Rheum Dis 2016;75:52–8.
4. Emery P, Breedveld F, van der Heijde D, Ferraccioli G, Dougados M, Robertson D, et al. Two-year clinical and radiographic results with combination etanercept–methotrexate therapy versus monotherapy in early rheumatoid arthritis: a two-year, double-blind, randomized study. Arthritis Rheum 2010;62:674–82.